Optimal Allocation of Static and Dynamic VAR Resources

Final Project Report

Power Systems Engineering Research Center

A National Science Foundation
Industry/University Cooperative Research Center
since 1996



Power Systems Engineering Research Center

Optimal Allocation of Static and Dynamic VAR Resources

Final Project Report

Project Team

A.P. Sakis Meliopoulos, Project Leader
Georgia Institute of Technology

Vijay Vittal, Arizona State University

James McCalley and V. Ajjarapu, Iowa State University

Ian Hiskens, University of Wisconsin-Madison

PSERC Publication 08-06

March 2008

Information about this project

For information about this project contact:

A. P. Meliopoulos, Project Leader
Georgia Power Distinguished Professor
Department of Electrical & Computer Engineering
Georgia Institute of Technology
Van Leer Electrical Engineering Building
777 Atlantic Drive NW
Atlanta, GA 30332-0250
Phone: 404-894-2926
Fax: 404-894-4641
sakis.meliopoulos@ee.gatech.edu

Power Systems Engineering Research Center

This is a project report from the Power Systems Engineering Research Center (PSERC). PSERC is a multi-university Center conducting research on challenges facing the electric power industry and educating the next generation of power engineers. More information about PSERC can be found at the Center's website: http://www.pserc.org.

For additional information, contact:

Power Systems Engineering Research Center
Arizona State University
577 Engineering Research Center
Box 878606
Tempe, AZ 85287-8606
Phone: 480-965-1643
FAX: 480-965-0745

Notice Concerning Copyright Material

PSERC members are given permission to copy without fee all or part of this publication for internal use if appropriate attribution is given to this document as the source material. This report is available for downloading from the PSERC website.

© 2008 Georgia Institute of Technology, Arizona State University, Iowa State University, and the Board of Regents of the University of Wisconsin System. All rights reserved.

Acknowledgements

This is the final report for the Power Systems Engineering Research Center (PSERC) research project S-24 titled "Optimal Allocation of Static and Dynamic VAR Resources." We express our appreciation for the support provided by PSERC's industrial members and by the National Science Foundation's Industry / University Cooperative Research Center program under the grants NSF EEC-0080012 at Georgia Institute of Technology, EEC-0001880 at Arizona State University, NSF EEC-0002917 at Iowa State University and EEC-0119230 at the University of Wisconsin at Madison.

The authors wish to acknowledge and thank the following companies and individuals for providing supplemental funding for this project:

- Entergy (Floyd Galvan and Sharma Kolluri)
- TVA (Lisa Beard and Mike Ingram)
- American Transmission Company (Don Morrow)
- ABB (Le Tang and Jiuping Pan).

The authors wish to recognize their postdoctoral researchers and graduate students that contributed to the research and creation of the reports:

Georgia Institute of Technology

- Dr. Salman Mohagheghi
- George Stefopoulos, GRA
- Hua Fan, GRA

Arizona State University

- Dr. Arturo Messina
- Muhammad Randhawa

Iowa State University

- Ashutosh Tiwari
- Dan Yang
- Venkat Kumar Krishnan
- Haifeng Liu

Wisconsin University at Madison

- Jonathan Rose
- Joel Berry

The authors thank PSERC members for their technical advice on the project, particularly:

Sharma Kolluri, Sujit Mandal and Floyd Galvan – Entergy Corporation

Mike Ingram, Lisa Beard, DeJim Lowe and Russ Patterson – TVA

Jiuping Pan Le Tang and David Lubkeman – ABB

Don Morrow, Joel M. Berry, L Hillier and Sasan Jalali – American Transmission Company

Ed Ernst and Anthony C. Williams – Duke Power

Raymond Vice – Southern Co.

Baj Agrawal – Arizona Public Service

Ali Chowdhury – MidAmerican Energy

Mahendra Patel – PJM

Aty Edris – EPRI

David.Schooley – Exelon Corporation

Navin Bhatt and Dale Krummen – AEP

Executive Summary

In recent years, new attention has been given to use of volt-amperes reactive (VAR) resources to support power system operation. In part, this attention has been motivated by the voltage problems experienced during the hours and minutes before the U.S – Canada blackout of 2003. An additional motivation arises from the evolution toward decentralized decision-making in power system markets. Of interest, from a market design perspective, is how to provide economic incentives for investment in and operational commitment of VAR resources. The engineering questions are how much VAR resources are needed, where should they be located, and what should the allocation be between static VARs that provide constant VARs and dynamic VARs that can be controlled in real-time. The engineering questions cannot be addressed separately, thus suggesting the need for an integrated assessment of optimal selection and placement of static and dynamic VAR resources in a power system.

The project's objectives were

(a) to develop realistic models that accurately model system dynamics and capture voltage recovery phenomena,
(b) to develop criteria for selection of the optimal mix and placement of static and dynamic VAR resources in large power systems based on modeling results using the tools developed part (a),
(c) to create a unified optimization model for minimizing the deployment of static and dynamic VAR resources while meeting the criteria.

Examples of the criteria are:

- speed of voltage recovery
- avoidance of unnecessary relay operations
- avoidance of motor stalling and
- avoidance of voltage collapse.

The project was accomplished in five integrated steps described in the four volumes of this report. A fifth volume is still being prepared and will be distributed separately. A test system provided by Entergy was used as a common platform to test the tools.

Volume 1: Vijay Vittal, Arizona State University

Work at Arizona State University focused on the use of conventional production grade tools:

- for the identification of critical, voltage-stability prone areas and the associated critical contingencies (such as line outages, branch outages, and generator outages) that result in voltage instability, and
- the development of analytical procedures to monitor and increase reactive power margins and the distance to voltage instability for critical contingencies.

In addition, the method to calculate analytical sensitivities to various model parameter changes was also implemented and delivered to support the grazing approach being developed at the University of Wisconsin - Madison.

All analytical procedures were implemented and tested on the software packages VSAT and TSAT which are components of the suite of software tools called DSA^{Tools} developed by Powertech Labs.

The results demonstrate the feasibility of using existing production grade software in identifying voltage stability prone areas in a realistic system. However, the available tools lack the ability to optimize the allocation of VAR resources between the static and dynamic sources necessary to stabilize a system.

Volume 2: V. Ajjarapu, Iowa State University

Work at Iowa State University concentrated on:

- how to identify contingencies that can lead to violation of voltage dip and short term voltage stability criteria, and
- the optimal location and amount of dynamic VARs to maintain short-term voltage stability and satisfy NERC voltage sag criteria.

The analytical steps were:

1. Label the contingencies that result in violation of the NERC criteria as "dangerous."
2. Rank dangerous contingencies with respect to their severity.
3. Assess the dangerous contingencies to finding the optimal allocation of VAR resources.

The results demonstrated the accomplishment of the following methodologies:

- A decoupled time domain algorithm for faster time domain simulations
- A general approach to contingency filtering, ranking and assessment (FRA)
- An efficient filter to identify dangerous contingencies from a list of credible contingencies.
- A tool for the optimal location and amount of dynamic VARs to maintain short-term voltage stability while satisfying NERC voltage sag criteria.

Volume 3: Jim McCalley, Iowa State University

Long-term allocation of static and dynamic VAR resources is done when planning system investments. A mixed-integer optimization procedure was developed to identify minimum cost combination of static and dynamic reactive resources using switched shunts (static) and Static Var Compensators (dynamic) to mitigate voltage instability and transient voltage sags. In this procedure, a backward/forward search algorithm with linear complexity was developed to select candidate locations of reactive power resources while satisfying power system performance requirements. The results were used in a mixed-integer program to allocate static and dynamic reactive resources to restore equilibrium under contingencies while preventing unacceptable transient voltage sags. A second mixed-integer program identified minimum-cost, post-contingency reactive static resources to satisfy voltage instability margin requirements.

The optimization algorithms were implemented in CPLEX. They require (a) linear sensitivities of loading margin to static reactive resource and (b) linear sensitivities of transient voltage sag to dynamic reactive resources. All algorithms were tested on the New England 39-bus system and on a portion of the Entergy test system. Results indicate that the developed approach can be used to effectively plan reactive power control devices for transmission system enhancement.

The results provide the following specific contributions:

1. Development of a backward/forward search algorithm to select candidate locations of reactive power controls while satisfying power system performance requirements.
2. Development of a mixed-integer programming based algorithm of reactive power control planning to restore equilibrium under a set of severe contingencies.
3. Development of an algorithm using mixed-integer programming for reactive power control planning to increase voltage stability margin under a set of contingencies.
4. Development of a systematic algorithm of coordinated planning of static and dynamic VAR resources while satisfying the performance requirements of voltage stability margin and transient voltage sag.

This work resulted in the first optimization-based method for determination of the optimal balance between selected static and dynamic VAR resources in transmission planning. This is also the first work to propose the use of transient voltage sag sensitivities for dynamic VAR planning. Simulation results indicate that the proposed algorithm is effective. The proposed simultaneous optimization formulation would enable transmission planners to find solutions that reduce the system-wide investment cost of reactive power control devices.

Volume 4: Sakis Meliopoulos, Georgia Institute of Technology

Work at Georgia Tech focused on developing an integrated optimization method capable of selecting the optimal mix of static and dynamic VAR resources for achieving fast voltage recovery under adverse system conditions.. The method models load dynamics while selecting critical contingencies as an integral part of the optimization procedure. The new methodology more accurately represents the dynamic behavior of loads and their impact on voltage recovery phenomena than previous work. The optimization methodology is based on successive dynamic programming.

Dynamic load models of induction motor loads were developed for various designs of induction motors. The dynamic load models were incorporated into a three-phase breaker-oriented model that accurately predicts the rate of voltage recovery for any specific contingency. In addition, specific design criteria were developed by imposing the requirements that voltage recovery phenomena will not cause load disruption using modern protective relaying practices for motors and for general electric loads.

Next Steps

The tools developed in this project demonstrate the proof of concept of comprehensive approaches addressing transient recovery voltage phenomena and computing the optimal mix of static and dynamic VAR resources to meet specific performance criteria. The criteria are based on alleviating load interruptions and motor stalling. Further efforts should be focused on commercialization of these tools. Such work will significantly enhance the developed tools and lead to their evolution into production-grade tools.

Optimal Allocation of Static and Dynamic VAR Resources

Volume 1

Prepared by

Vijay Vittal
Arizona State University

Information about this project

For information about this volume contact:

Vijay Vittal
Ira A. Fulton Chair Professor
Department of Electrical Engineering
Arizona State University
PO Box 875706
Tempe, AZ 85287-5706
Tel: 480-965-1879
Fax: 480-965-0745
Email: vijay.vittal@asu.edu

Power Systems Engineering Research Center

This is a project report from the Power Systems Engineering Research Center (PSERC). PSERC is a multi-university Center conducting research on challenges facing the electric power industry and educating the next generation of power engineers. More information about PSERC can be found at the Center's website: http://www.pserc.org.

For additional information, contact:

Power Systems Engineering Research Center
Arizona State University
577 Engineering Research Center
Box 878606
Tempe, AZ 85287-8606
Phone: 480-965-1643
FAX: 480-965-0745

Notice Concerning Copyright Material

PSERC members are given permission to copy without fee all or part of this publication for internal use if appropriate attribution is given to this document as the source material. This report is available for downloading from the PSERC website.

© 2008 Georgia Institute of Technology, Arizona State University, Iowa State University, and the Board of Regents of the University of Wisconsin System. All rights reserved.

Table of Contents

1. Introduction 1
   - 1.1 Power system stability 2
   - 1.2 Voltage stability 3
   - 1.3 Voltage collapse 3
   - 1.4 Proximity to instability 4
   - 1.5 Objective of this work 6
   - 1.6 Organization 6
2. Modal Analysis and Reactive Reserve Margin 8
   - 2.1 Modal analysis 8
   - 2.2 Formulation of modal analysis 8
     - 2.2.1 Reduced Jacobian matrix 9
     - 2.2.2 Modes 10
     - 2.2.3 Eigenvalue and eigenvectors of J_R 11
   - 2.3 Participation factors 12
     - 2.3.1 Bus participation factor 12
     - 2.3.2 Branch and generator participation factors 13
   - 2.4 Reactive reserve margin 13
3. Modal Analysis 15
   - 3.1 Overview 15
   - 3.2 VSAT studies 17
   - 3.3 Q increase in the EES – Loading scenario I 18
   - 3.4 Load increase in the EES with a constant power factor – Loading scenario II 22
   - 3.5 Critical Contingencies 25
   - 3.6 Conclusion 27
4. Reactive Reserve Margin Analysis 28
   - 4.1 Overview 28
   - 4.2 VSAT studies 28
   - 4.3 Critical contingencies identified by Entergy in the western area 33
     - 4.3.1 Comparison between critical contingencies 34
     - 4.3.2 Common contingencies in other areas of EES 35
     - 4.3.3 Contingencies sharing the same bus 36
   - 4.4 Summary 36
   - 4.5 Identification of critical zones 37
   - 4.6 Time response of voltages for critical contingencies 37
   - 4.7 Sensitivity analysis and critical zones 38
     - 4.7.1 Comparison between peak-peak variation value and modal analysis 40
   - 4.8 Time domain analysis 41
5. Summary, conclusions, and future research directions 45
   - 5.1 Summary 45
   - 5.2 Conclusion and observation 46
   - 5.3 Future research directions 48

References 49

Appendix 1: Complete results of the modal analysis and reactive reserve margin studies conducted on the Entergy energy system 51

List of Figures

Figure 1.1 Classification of power system stability [1] 2
Figure 2.1 Modal voltages versus system load 11
Figure 3.1 Entergy footprint 16
Figure 3.2 Southwestern part of the Entergy Energy System 19
Figure 3.3 Eigenvalues as Q is increased as a percentage of critical load 21
Figure 3.4 Critical modes of loading scenario I 21
Figure 3.5 Critical modes of loading scenario II 24
Figure 4.1 Voltage magnitude difference observed in the time domain for 3 % change in the load (difference of voltage in case 1 and case 2) for bus 98085 39
Figure 4.3 Voltage response in time domain after the 7Grimes – Grmxf line contingency 42
Figure 4.4 Voltage response of the buses in time domain after the Grimes-Crockett line contingency for load 30070 MW 43
Figure 5.1 Critical zones in Entergy footprint 46

List of Tables

Table 3.1 Composition of Entergy Energy System 15
Table 3.2 Loading scenarios used in the analysis 17
Table 3.3 Mode 1 with eigenvalue = 0.0615 – Loading Scenario I 20
Table 3.4 Mode 1 with eigenvalue = 0.05218 – Loading Scenario II 23
Table 3.5 Critical contingencies in the Entergy Energy System 26
Table 4.1 Reactive power reserves in base case – Case I 29
Table 4.2 Voltage magnitude in p.u. after 7% load increase – Case I 30
Table 4.3 Reactive power reserves in base case – Case II 30
Table 4.4 Generators outages – Case II 31
Table 4.5 Single line outages – Case II 31
Table 4.6 Double line outages – Case II 31
Table 4.7 Reactive power reserves in base case – Case III 32
Table 4.8 Voltage magnitude in p.u. after 7% load increase – Case III 33
Table 4.9 Generators outages – Case III 33
Table 4.10 Single line Outages – Case III 33
Table 4.11 Critical contingencies identified by Entergy [12] 34
Table 4.12 Common contingencies 34
Table 4.13 Other common contingencies 35
Table 4.14 Common contingencies in other regions 35
Table 4.15 Common double line contingencies 36
Table 4.16 Contingencies sharing same bus 36
Table 4.17 Critical zones 37
Table 4.18 Buses affected the most after the Lewis generator outage 38
Table 4.19 Buses with maximum peak-peak voltage Variation 41
Table 4.20 Critical contingencies in time domain 42
Table A.1 Mode 2 with eigenvalue = 0.12727 – Loading Scenario I 51
Table A.2 Mode 5 with eigenvalue = 0.17387 – Loading Scenario I 52
Table A.3 Mode 4 with eigenvalue = 0.18724 – Loading Scenario II 53
Table A.4 Mode 5 with eigenvalue = 0.2010 – Loading Scenario II 54
Table A.5 Mode 6 with eigenvalue = 0.2227 – Loading Scenario II 55
Table A.6 Mode 7 with eigenvalue = 0.2381 – Loading Scenario II 55

Table B.1 Reactive power reserves in base case – 11220 MW 56
Table B.2 Reactive power reserves in base case – 12000 MW 56
Table B.3 Reactive power reserves in base case – 13000 MW 56
Table B.4 Single line outages – 13000 MW 56
Table B.5 Double line outages – 13000 MW 57
Table B.6 Reactive power reserves in base case – 14000 MW 57
Table B.7 Reactive power reserves in base case – 15000 MW 57
Table B.8 Reactive power reserves in base case – 16000 MW 58
Table B.9 Reactive power reserves in base case – 17000 MW 58
TableB.10 Single line outages – 17000 MW 58
Table B.11 Double line outages – 17000 MW 58
Table B.12 Reactive power reserves in base case – 19000 MW 59
Table B.13 Generators outages – 19000 MW 59
Table B.14 Single line outages – 19000 MW 59
Table B.15 Double line outages – 19000 MW 59
Table B.16 Reactive power reserves in base case – 20000 MW 60
Table B.17 Generators outages – 20000 MW 60
Table B.18 Single line outages – 20000 MW 60
Table B.19 Reactive power reserves in base case – 21000 MW 60
Table B.20 Generators outages – 21000 MW 61
Table B.21 Single line outages – 21000 MW 61
Table B.22 Double line outages – 21000 MW 61
Table B.23 Reactive power reserves in base case – 22000 MW 61
Table B.24 Generators outages – 22000 MW 62
Table B.25 Single line outages – 22000 MW 62
Table B.26 Double line outages – 22000 MW 62
Table B.27 Reactive power reserves in base case – 23000 MW 62
Table B.28 Generators outages – 23000 MW 63
Table B.29 Single line outages – 23000 MW 63
Table B.30 Double line outages – 23000 MW 63
Table B.31 Reactive power reserves in base case – 24000 MW 63
Table B.32 Generators outages – 24000 MW 63
Table B.33 Single line outages – 24000 MW 64

Table B.34 Double line outages – 24000 MW 64
Table B.35 Reactive power reserves in base case – 25000 MW 64
Table B.36 Generators outages – 25000 MW 64
Table B.37 Single line outages – 25000 MW 64
Table B.38 Double line outages – 25000 MW 65
Table B.39 Reactive power reserves in base case – 26000 MW 65
Table B.40 Generators outages – 26000 MW 65
Table B.41 Single line outages – 26000 MW 65
Table B.42 Double line outages – 26000 MW 65
Table B.43 Reactive power reserves in base case – 27000 MW 66
Table B.44 Generators outages – 27000 MW 66
Table B.45 Single line outages – 27000 MW 66
Table B.46 Double line outages – 27000 MW 66
Table B.47 Reactive power reserves in base case – 28000 MW 67
Table B.48 Generators outages – 28000 MW 67
Table B.49 Single line outages – 28000 MW 67
Table B.50 Double line outages – 28000 MW 67
Table B.51 Reactive power reserves in base case – 29000 MW 68
Table B.52 Single line outages – 29000 MW 68

NOMENCLATURE

A	Matrix
α	Eigenvalue of the system
α_i	Eigenvalue of the mode i^{th}
b	Vector of constants
B	Imaginary part of admittance value
B_{ik}	Imaginary part of the admittance matrix element Y_{ik}
ΔP	Real power mismatch vector
ΔQ	Reactive power mismatch vector
ΔQ_{mi}	Modal reactive power variation of the ith mode
ΔV	Voltage magnitude mismatch vector
ΔV_{mi}	Modal voltage variation of the ith mode
EES	Entergy Electrical System
G	Real part of admittance value
G_{ik}	Real part of the admittance matrix element Y_{ik}
J	Jacobian matrix
J_R	Reduced Jacobian matrix
Γ	Left eigenvector matrix of J_R
Γ_{ij}	Left eigenvector of bus j in mode i
Nc	Number of the most severe contingencies
P	Active power
P_i	Active power injection at bus i

P_{ji}	Participation factor of bus *j* in mode *i*
P_m	Nose point on PV curve
P_o	Initial operating point on PV curve
ϕ	Right eigenvector matrix of J_R
ϕ_{ji}	Right eigenvector of bus *j* in mode *i*
Q	Reactive power
Q_i	Reactive power injection at bus *i*
Q_{max}	Maximum reactive power available in the zone
Q_z	Sum of reactive power output of generators, adjustable and fixed shunts
S_i	Complex power injection at bus *i*
θ	Voltage phase angle
TSAT	Transient security assessment tool
V_i	Voltage at bus *i*
VS	Voltage stability
VSAT	Voltage stability assessment tool
V	Voltage magnitudes vector
x	Vector of unknowns
Y_{ik}	$_{ik}^{th}$ entry of the admittance matrix
Λ	Diagonal eigenvalue matrix of J_R

1. Introduction

This volume of the report details the work done at Arizona State University in details the use of conventional commercially available tools in the DSA[Tools] software package developed by Powertech Labs in identifying areas within a power system prone to voltage magnitude and voltage stability problems and to evaluate the effectiveness of these tools in quantifying a suitable measure of the voltage stability margin. The tools specifically used in the studies included VSAT and TSAT.

These tools were applied to a planning case provided by Entergy Corporation. The planning case represented a significant portion of the Southeastern portion of the US and consisted of 2778 generators, 16174 buses, and 20251 lines. Within this model the Entergy Electrical System (EES) was represented by 168 generators, 2070 buses, and 2145 lines. A detailed analysis was conducted to determine the voltage stability prone areas in the system. This was primarily done using the VSAT tool which is capable of identifying both voltage magnitude problems and voltage collapse problems. VSAT has the capability to examine the performance of the system under a range of contingencies which can be specified by the user. These include single contingencies, multiple contingencies and generator outages.

VSAT also has the capabilities of detailed analysis of cases prone to voltage collapse. This is done using a modal analysis approach and identifies specific buses which could be used to provide remedial control. This information could be especially useful in this project to work done in other aspects of the project to identify bus location to site the need VAr sources. The modal analysis feature in VSAT is used in the EES to identify critical buses in the voltage stability prone areas of the system.

Another useful feature of VSAT is an automated feature to evaluate the distance to the voltage stability boundary using a reactive reserve margin approach. This feature has also been applied to the EES to identify critical contingencies and the extent to which additional VAr resources are required.

As a final step the critical contingencies identified by the VSAT tool which is essentially a static analysis tool is further examined using TSAT which is time domain simulation tool. It is observed that a good correspondence between the static tools and time domain simulation tool is obtained in terms of identifying the critical contingencies. The time domain tool is also used to derive numerical sensitivities on the EES to support the work to be done in another aspect of this project.

A brief review of the salient aspects of power system stability and voltage stability is now provided.

1.1 Power system stability

Maintaining and supplying reliable power has been the main concern of power system engineers from the day electric power systems were invented. In the early days, transient stability was the main problem, but increased loads and implementation of new technologies in the network have resulted in different kind of instabilities including voltage instability [1].

Stability of the power system can be defined as the ability of the power system to regain an operating equilibrium after being subjected to some disturbance, such that the entire system remains intact.

Many other definitions had been proposed by CIGRE and IEEE task force reports [1] to define power system stability, but these definitions did not cover all the aspects of power system stability. Therefore, to formulate a precise definition which covers all the forms of instability in power systems, CIGRE and IEEE came up with a new classification of power system stability in a report published in 2004 [1]. In this report the stability phenomenon is divided into three main categories, which are

1) Rotor angle stability
2) Frequency stability
3) Voltage stability

These are further divided into different categories, depending on the nature of the disturbance and the timeframe for which the disturbances are being studied. The complete classification can be seen in Figure 1.1 (Taken directly from [1])..

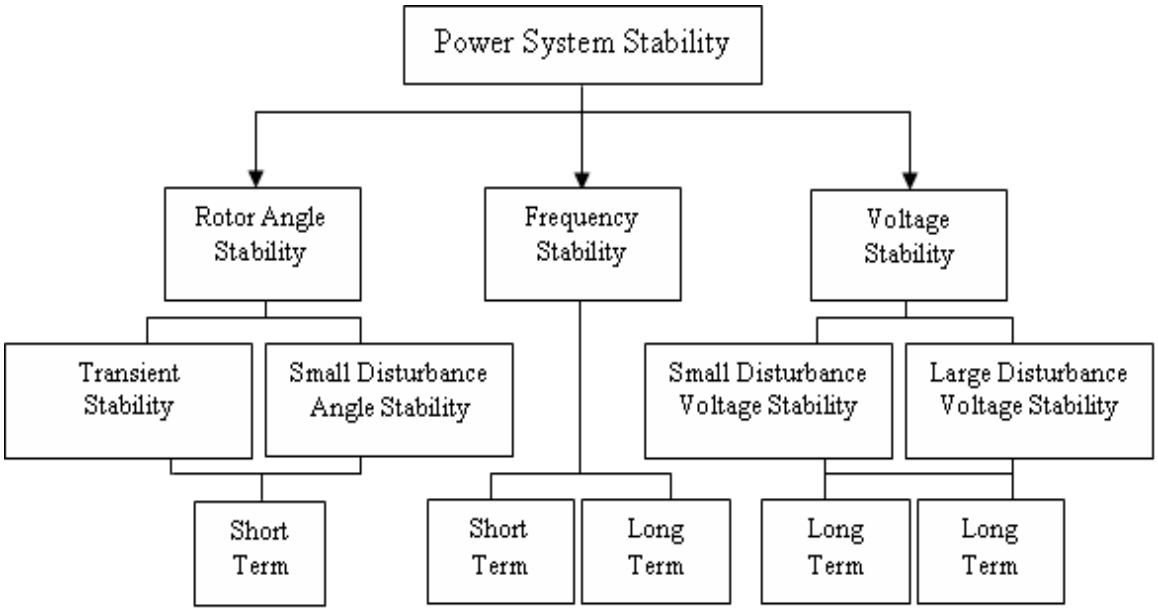


Figure 1.1 Classification of power system stability [1]

Rotor angle stability is defined as the ability of the synchronous machines which are interconnected in the power system to remain synchronized with each other after being subjected to a disturbance. When the rotor angles of some of the generators lose synchronism i.e. angular swings increase after some disturbance, stability is lost and the instability is referred to as rotor angle instability.

Frequency stability is the ability of the power system to maintain steady frequency after being subjected to a severe disturbance that results in large imbalance in generation and load. Frequency instability may occur in the form of sustained frequency swings which may result in the tripping of generators and loads.

Of the three stabilities i.e. rotor angle stability, frequency stability and voltage stability, the last topic will be discussed in greater detail as it is the main focus of this report.

1.2 Voltage stability

The focus of power system engineers for some time has been the voltage instability problem, because of the increased number of failures and blackouts not only in the USA but all over the world. Voltage stability can be defined as the ability of a power system to maintain acceptable voltages at all the buses in the system under normal conditions and after being subjected to a disturbance [2].

Instability may occur in the form of abnormal increase or decrease in the voltage(s) of buses, which could result in the loss of load, or tripping of lines by the protective devices resulting in cascading events. These events may trigger loss of synchronism between generators, thereby pushing the system further towards instability.

Voltage instability is also referred to as voltage collapse by many engineers but the voltage collapse problem is more complex than voltage instability and occurs in a power system when the change or disturbance causes rapid drop in voltage.

1.3 Voltage collapse

When voltages in an area are significantly low or blackout occurs due to the cascading events accompanying voltage instability, the problem is considered to be a voltage collapse phenomenon. Voltage collapse normally takes place when a power system is heavily loaded and/or has limited reactive power to support the load. The limiting factor could be the lack of reactive power (SVC and generators hit limits) production or the inability to transmit reactive power through the transmission lines [3]. The main limitation in the transmission lines is the loss of large amounts of reactive power and also line outages, which limit the transfer capacity of reactive power through the system.

In the early stages of analysis, voltage collapse was viewed as a static problem but it is now considered to be a non linear dynamic phenomenon. The dynamics in power systems involve the loads, and voltage stability is directly related to the loads. Hence, voltage stability is also referred to as load stability.

There are other factors which also contribute to voltage collapse, and are given below

1) Increase in load
2) Action of tap changing transformers
3) Load recovery dynamics

All these factors play a significant part in voltage collapse as they effect the transmission, consumption, and generation of reactive power.

As seen in figure 1.1, voltage stability is categorized into two parts

1) Large disturbance voltage stability
2) Small disturbance voltage stability

When a large disturbance occurs, the ability of the system to maintain acceptable voltages falls due to the impact of the disturbance. Ability to maintain voltages is dependent on the system and load characteristics, and the interactions of both the continuous and the discrete controls and protections. Similarly, the ability of the system to maintain voltages after a small perturbation i.e. incremental change in load is referred to as small disturbance voltage stability. It is influenced by the load characteristics, continuous control and discrete controls at a given instant of time.

Voltage stability studies can be performed for short and long time periods. When stability studies are conducted for a span of few seconds, the dynamics of fast acting components such as induction motors and HVDC converters are of great concern. For long term studies the response of the system is monitored for several minutes and it involves the slower acting equipments such as tap changing transformers, generator current limiters, and thermostatically controlled loads.

1.4 Proximity to instability

Voltage stability analysis can be broadly classified into two categories

1) Static voltage stability analysis
2) Dynamic voltage stability analysis

Most of the researchers have considered voltage stability as a static phenomenon [4] and have linked it to the maximum loadability of the system. Static analysis using the conventional power flow model is viable due to the fact that the voltage collapse, in most of the incidences, has been observed as a slow process, thus, being primarily considered as a small signal phenomenon [5].

Power engineers and operators are always interested in knowing how far the system is operating from voltage collapse or voltage instability, so that appropriate

actions could be taken. There are several indices that determine the distance to instability of the current operating point of the system. Some of the voltage instability indices are discussed briefly in the following paragraphs [6, 7].

Sensitivity analysis is one of the earliest methods used to find voltage stability problems. Sensitivities were first used to find voltage problems by using QV curves. However, this approach does not always give correct predictions especially in large power systems because sensitivity factors fail to account for large changes in system parameters.

Singular values of the Jacobian matrix have been used as a measure of the proximity to voltage instability and this method takes advantage of the orthogonal decomposition of the matrix [6]. The orthogonal decomposition is used to determine the smallest singular value which gives an indication of how far the system is from voltage instability. Singular values of the Jacobian matrix decrease when the power system is stressed. When any singular value is close to zero, it means that system is very close to voltage instability or voltage collapse.

Eigenvalue analysis or modal analysis determines the proximity to voltage instability in a manner similar to singular values. Eigenvalue decomposition is usually performed assuming that the Jacobian matrix is diagonalizable [6, 7]. The eigenvectors associated with the eigenvalue nearest to zero have the same properties near the collapse point as singular vectors. . Details and formulation of eigenvalue analysis are discussed in Section 2 of this report.

Loading margin is another very common index. It is very effective in identifying problem situations and is simple to implement. In evaluating this index, the load is increased from the present operating point of the power system until voltage collapse occurs. The amount of load increase from the base case until voltage collapse occurs is called the loading margin. It can be visualized as the distance between the operating point and the nose of the PV curve. For PV curve computation, the system load is increased step by step and at each step the power flow is solved. The voltage stability critical point is reached at the load level beyond which power flow solution does not exist. The increase in the system load from the initial operating point to the voltage stability critical point (nose of the PV curve) is the voltage stability (VS) margin of the system [3]. VQ curves are also commonly used to determine the critical buses in power systems. VQ relationship shows the sensitivity and variation of bus voltages with respected to the reactive power injection or absorption. VQ curves can be computed at various buses by successive power flow calculation with a variable reactive power source at the selected bus and recording its value required to hold different scheduled bus voltages [2].

Reactive power reserves can be used as an indicator of voltage instability. In this method, the reactive power is observed for the group of VAr sources (generators, SVCs, and shunt reactors) that exhaust their reserves in the process of meeting the load in the power system.

V/V_o ratio has been used as an index to voltage collapse where V is the known voltage of the bus under load. V_o is the voltage of the same bus under no load conditions. This index provides the location of the weak areas. This method was first implemented in Belgium in 1982 using off line studies, and since 1995 it has been implemented online [3].

The continuation power flow method [8] is used to find the proximity to voltage collapse. It obtains the power flow solution for the base case and computes the voltage profile for successive power flows by increasing loads and generation in the same proportion until the PV curve nose point is reached and this loading level is the static voltage limit.

Various methods have been discussed in this section to find the proximity to voltage instability. Every method has its merits and demerits, and it is difficult to recommend a particular method to evaluate voltage stability of a power system. In this report, modal analysis and reactive margin methods are used separately and the results from both studies are compared to find the voltage instability problems in Entergy's transmission system.

1.5 Objective of this work

The main objective of this research is to apply existing tools in the literature to determine the critical areas in Entergy's transmission system which are prone to voltage instability.

The voltage security assessment tool (VSAT) [9] is used to determine the voltage security as well as the security limit of the Entergy system. It is also used to identify critical contingencies and the type and location of insecurities for the system.

1.6 Organization

Section 1 gives an overview of stability problems in power systems with an emphasis on voltage instability. Different types of voltage stability problems are discussed, along with the methods which are currently being used to predict voltage instability in power systems.

Section 2 discusses modal analysis and reactive reserve margin methods in detail. These methods are used to predict proximity of voltage instability of power systems, with the identification of the critical areas which are prone to voltage instability.

In Section 3, critical contingencies are identified in the Entergy system. Modal analysis techniques are applied to the Entergy transmission system to obtain the critical areas which are prone to voltage instability by using the bus participation factor for different modes.

Section 4 includes a detailed study of the reactive reserve margin of the Entergy transmission system. Reactive reserves are monitored for generator outages, single line and double line outages. The results obtained by modal analysis and reactive reserve margin are compared and critical zones are identified. Time domain study is also conducted and response of the bus voltages of the Entergy energy system is discussed.

Section 5 provides conclusions and directions for future work.

2. Modal Analysis and Reactive Reserve Margin

2.1 Modal analysis

The modal analysis technique is used in steady state studies as a voltage stability index for power systems. This method computes eigenvalues and the associated eigenvectors of a reduced steady state Jacobian matrix which characterizes the QV relationship of the network [11]. Modal analysis is very similar to sensitivity analysis as it examines the relationship between the incremental change in bus voltage and the incremental change in bus reactive power injection. However, identification of different modes provides more insight into the system. Different modes are identified by the eigenvalues of the reduced Jacobian matrix, due to which the system could become unstable. The reduced Jacobian matrix is obtained from the Jacobian matrix when the power flow equations are solved using the Newton-Raphson technique. The Jacobian matrix can be transformed to a symmetric matrix by dividing the voltage magnitude mismatch vector ΔV with the corresponding bus voltage V i.e. $\Delta V_n / |V_n|$ and multiplying partial derivative terms with respect to V ($\partial / \partial V$) in the Jacobian matrix by V_n. Equation (2.1) given below shows this relationship.

$$\begin{bmatrix} \Delta P \\ \Delta Q \end{bmatrix} = \begin{bmatrix} \dfrac{\partial P}{\partial \theta} & |V_n| \dfrac{\partial P}{\partial V} \\ \dfrac{\partial Q}{\partial \theta} & |V_n| \dfrac{\partial Q}{\partial V} \end{bmatrix} \begin{bmatrix} \Delta \theta \\ \Delta V / |V_n| \end{bmatrix} \tag{2.1}$$

In practical power systems, V_n is approximately equal to 1 p.u. and if the step in equation (2.1) is not followed, the Jacobian matrix can be considered as an approximately symmetric matrix if not purely symmetrical and therefore the eigenvalues of the reduced Jacobian are close to being purely real [11]. Proximity to instability is determined by the size of the eigenvalue. If the size of the of an eigenvalue is large and positive, the system is considered to be secure, but if the eigenvalue is small or close to zero, the system is considered to be close to voltage instability or voltage collapse.

2.2 Formulation of modal analysis

The power flow equations of a power system can be written as

$$S_i = P_i + jQ_i = V_i I_i^* \tag{2.2}$$

where S_i is the complex power injection at bus i, P_i is the real power injection and Q_i is the reactive power injection.

$$P_i = V_i \sum_{k=1}^{n} (G_{ik} V_k \cos\theta_{ik} + B_{ik} V_k \sin\theta_{ik}) \tag{2.3}$$

$$Q_i = V_i \sum_{k=1}^{n} (G_{ik} V_m \sin\theta_{ik} - B_{ik} V_k \cos\theta_{ik}) \tag{2.4}$$

P and Q at each bus are functions of voltage magnitude V and angle θ of all buses. G and B are real and imaginary parts of the admittance values [10]. The only unknowns in the above equations are V and θ. It can be seen from equations (2.3) and (2.4) that the power flow equations are non-linear as they contain trigonometric functions. Because of the non-linear nature of the power flow equations, we can not put them in a matrix form of $Ax = b$, where A is a matrix, x is a vector of unknowns, and b is a vector of constants [10].

Therefore, equations (2.3) and (2.4) are linearized using Taylor's theorem to obtain.

$$\begin{bmatrix} \Delta P \\ \Delta Q \end{bmatrix} = \begin{bmatrix} \frac{\partial P}{\partial \theta} & \frac{\partial P}{\partial V} \\ \frac{\partial Q}{\partial \theta} & \frac{\partial Q}{\partial V} \end{bmatrix} \begin{bmatrix} \Delta \theta \\ \Delta V \end{bmatrix} \tag{2.5}$$

$$J = \begin{bmatrix} \frac{\partial P}{\partial \theta} & \frac{\partial P}{\partial V} \\ \frac{\partial Q}{\partial \theta} & \frac{\partial Q}{\partial V} \end{bmatrix} = \begin{bmatrix} J_{P\theta} & J_{PV} \\ J_{Q\theta} & J_{QV} \end{bmatrix} \tag{2.6}$$

where J is called the Jacobian matrix

2.2.1 Reduced Jacobian matrix

The power flow equations can be linearized as discussed above.

$$\begin{bmatrix} \Delta P \\ \Delta Q \end{bmatrix} = \begin{bmatrix} J_{P\theta} & J_{PV} \\ J_{Q\theta} & J_{QV} \end{bmatrix} \begin{bmatrix} \Delta \theta \\ \Delta V \end{bmatrix} \tag{2.7}$$

where

ΔP = incremental change in real power injection

ΔQ = incremental change in reactive power injection

$\Delta \theta$ = incremental change in voltage angle

ΔV = incremental change in voltage magnitude at the bus

Equation (2.7) can be divided into two equations i.e. (2.8) and (2.9)

$$\Delta P = J_{P\theta} \Delta \theta + J_{PV} \Delta V \tag{2.8}$$

$$\Delta Q = J_{Q\theta} \Delta \theta + J_{QV} \Delta V \tag{2.9}$$

Setting $\Delta P = 0$ in (2.8), and substituting the solution for $\Delta \theta$ in (2.9) gives (2.10)

$$\Delta Q = \left[J_{QV} - J_{Q\theta} J_{PQ}^{-1} J_{PV} \right] \Delta V \tag{2.10}$$

$$\Delta Q = J_R \Delta V \tag{2.11}$$

$$\Delta V = J_R^{-1} \Delta Q \tag{2.12}$$

J_R is a reduced Jacobian matrix of the system. J_R directly relates the bus voltage magnitude and bus reactive power injection [11].

To gain a better understanding of modal analysis, consider a single bus load in a power system. The relationship between the load voltage and load reactive power can be linearized as

$$\alpha \Delta V = \Delta Q \qquad (2.13)$$

where α is an eigenvalue of the system and can also be seen to be the *VQ* sensitivity. Equation (2.13) can also be rewritten as

$$\Delta V = \frac{\Delta Q}{\alpha} \qquad (2.14)$$

If alpha is greater than zero, the mode voltage and modal reactive variation are along the same directions. This indicates the system is voltage stable while if alpha is less than zero the modal voltage and the modal reactive power are along the opposite direction indicating that the system is voltage unstable [6]. If alpha is equal to zero then any change in modal reactive power causes infinite change in modal voltage indicating that voltage collapse occurs.

2.2.2 Modes

To comprehend the meaning of modes in modal analysis, consider an ideal scenario of a 4 bus system, where the Jacobian matrix is a diagonal matrix. If α_1 in (2.15) is close to zero, a small change in load will result in a large change in the voltage of the same bus i.e. bus 2. Similarly, if α_1 is very close to zero, a small change at bus 1 will result in a large change in the voltage at bus 1. This means that only bus 1 is responsible for voltage collapse, while other buses do not participate in the voltage collapse.

$$\begin{bmatrix} \alpha_1 & 0 & 0 & 0 \\ 0 & \alpha_2 & 0 & 0 \\ 0 & 0 & \alpha_3 & 0 \\ 0 & 0 & 0 & \alpha_4 \end{bmatrix} \begin{bmatrix} \Delta V_1 \\ \Delta V_2 \\ \Delta V_3 \\ \Delta V_4 \end{bmatrix} = \begin{bmatrix} \Delta Q_1 \\ \Delta Q_2 \\ \Delta Q_3 \\ \Delta Q_4 \end{bmatrix} \qquad (2.15)$$

But in real power systems, the Jacobian matrix is not diagonal. Therefore, we have to diagonalize the Jacobian matrix in order to take advantage of modal analysis. The Jacobian matrix can be diagonalized by using modal analysis techniques and the transformed voltage and reactive power relationship is given below in equation (2.16).

$$\begin{bmatrix} \alpha_1 & 0 & 0 & 0 \\ 0 & \alpha_2 & 0 & 0 \\ 0 & 0 & \alpha_3 & 0 \\ 0 & 0 & 0 & \alpha_4 \end{bmatrix} \begin{bmatrix} \Delta v_1 \\ \Delta v_2 \\ \Delta v_3 \\ \Delta v_4 \end{bmatrix} = \begin{bmatrix} \Delta q_1 \\ \Delta q_2 \\ \Delta q_3 \\ \Delta q_4 \end{bmatrix} \qquad (2.16)$$

where

$[\Delta v] = [\Gamma][\Delta V]$

$[\Delta q] = [\Gamma][\Delta Q]$

$[\Gamma] =$ eigenvector of the Jacobian matrix

Now if we assume that α_1 is very close to zero and the value of α for other modes is much greater than zero, then only mode 1 becomes very sensitive to a small change in reactive load and the other modes remain stable. This shows voltage collapse is a local phenomenon. Therefore, it can be concluded that voltage collapse occurs due to the voltage collapse of a mode. This phenomenon is shown graphically in Figure 2.1, where modal voltages are plotted against system load. It can be observed that mode 1 reaches the nose point much before the other modes, which reach the nose point at different stress levels.

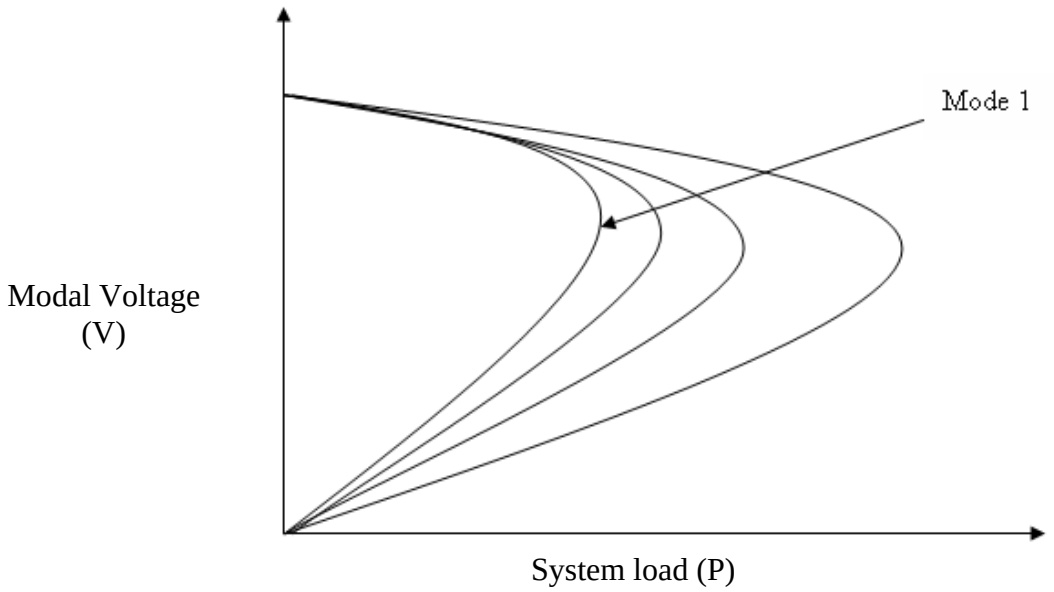


Figure 2.1 Modal voltages versus system load

2.2.3 Eigenvalue and eigenvectors of J_R

The Jacobian matrix J_R is a symmetric matrix and therefore, the eigenvalues of J_R are purely real. If all the eigenvalues are positive, *V-Q* sensitivities are also positive indicating that the system is voltage stable. As the system is stressed, the eigenvalues of J_R become smaller until, at the critical point of system voltage stability, at least one of the eigenvalues of J_R becomes zero. If one or more of the eigenvalues of J_R are negative, the system has passed the critical point of voltage stability because the eigenvalues of J_R change from positive to zero to negative as the system is stressed [6, 11].

For a large system which consists of thousands of buses, it becomes impractical to calculate all the eigenvalues, however it is also not reasonable to calculate only the smallest eigenvalue of Jacobian matrix. This is because, if there is more than one weak mode present in different areas of the power system the mode associated with the minimum eigenvalue may not remain critical as the load is increased.

The Jacobian matrix can be expressed in terms of the right eigenvector and left eigenvector as

$$J_R = \phi \Lambda^{-1} \Gamma \qquad (2.17)$$

where

$\phi =$ right eigenvector matrix of J_R

$\Gamma =$ left eigenvector matrix of J_R

$\Lambda =$ diagonal eigenvalue matrix of J_R

Eigenvalues and the corresponding eigenvectors of J_R define the ith mode of the system and the vector of modal reactive power variation is defined as

$$\Delta Q_{mi} = \Gamma_i \Delta Q \qquad (2.18)$$

$$\Delta V_{mi} = \Gamma_i \Delta V \qquad (2.19)$$

The consequent i^{th} modal voltage variation is

$$\Delta V_{mi} = \frac{1}{\alpha_i} \Delta Q_{mi} \qquad (2.20)$$

2.3 Participation factors

Eigenvalues of the reduced Jacobian matrix indicate whether the system is stable or unstable. In stability analysis it is important to know which physical elements in the power system are responsible for instability, so that suitable remedial actions can be taken. The most important system elements are buses, branches and generators, and the participation factors of each of these elements in each mode can be calculated using the right and left eigenvectors of the Jacobian matrix. The higher the participation factor of the element, the greater the association of that element in a given mode.

2.3.1 Bus participation factor

Bus participation factor determines the area or areas close to voltage instability by providing the association of the buses with the critical modes. Buses with large participation factor for a critical mode contribute more towards voltage instability than other buses with a lower participation factor. Therefore, by finding these critical buses, we can find the critical area in the power system.

The participation factor of bus *j* in mode *i* is defined as

$$P_{ji} = \phi_{ji} \Gamma_{ij} \qquad (2.21)$$

The value of the participation factor is very important in a given mode. Greater the value of bus participation, the more important is the relevance of the bus with regard to the stability of the mode. The participation value is also an indication of the effectiveness of a remedial action in stabilizing the mode.

Depending on the bus participation in a given mode, it can be categorized as localized and non-localized. The mode is considered localized when there are few buses with large participation factors and the remaining buses with little or no participation at all. Similarly, a mode is considered non-localized if there are many buses with similar participations and remaining buses with little or no participation.

2.3.2 Branch and generator participation factors

Branch and generator participation factors for each mode can also be calculated in modal analysis. Branch participation factors indicate the branches which are absorbing the most reactive power. This provides more insight by indicating the branches which are vital for the stability of the power and hence the critical area in the system. Branch participation factors can be used as a criterion of critical contingencies which may result in loss of voltage instability.

Generator or SVC participation factors indicate which generators are supplying the most reactive output in response to an incremental change in reactive load. This provides further insight by indicating the generators which should have reactive reserves to ensure voltage stability.

2.4 Reactive reserve margin

As discussed in Section 1, voltage collapse normally occurs when sources producing reactive power reach their limits i.e. generators, SVCs or shunt reactors, and there is not much reactive power to support the load. As reactive power is directly related to voltage collapse, it can be used as a measure of voltage stability margin. The voltage stability margin can be defined as a measure of how close the system is to voltage instability, and by monitoring the reactive reserves in the power system proximity to voltage collapse can be monitored.

The voltage stability margin should be sufficient at the operating point and under all likely contingencies which could occur in the power system. In case of reactive reserve criteria, the reactive power reserve of an individual or group of VAr sources must be greater than some specified percentage (x %) of their reactive power output under all contingencies. An operating point is considered voltage stable if the reactive reserves of the VAr sources meet the specified criteria before and after the contingencies.

Critical contingencies and areas can be identified by this method. The contingencies which diminish reactive power reserves below the specified value would

be identified as critical contingencies and the regions where reactive power reserves were exhausted would be identified as critical areas.

Methods discussed in this section i.e. modal analysis technique and reactive reserve margin are implemented on the EES and results obtained are given in Sections 3 and 4 of this report.

3. Modal Analysis

3.1 Overview

The EES is divided into five operating regions i.e. WOTAB, Amite South, Central, Dell and Sheridan North. Each region is compromised of many zones. Table 3.1 shows the composition of each region in terms of zones and buses. The Entergy footprint with the location of the regions is shown in Fig. 3.1.

Table 3.1 Composition of Entergy Energy System

Region	Zones Included
WOTAB	Zones: 100, 101, 102, 103, 104, 105, 106, 108, 109, 111, 112, 155, 221
Amite South	Zones: 110, 120, 121, 122, 123, 124, 130
Central	Zones: 140, 150 (Excluded bus 99680), 151, 152, 161 (Only buses 99225-99311)
Dell	Zones: 150 (Only bus 99680), 160 (Only bus 99697), 162 (Only buses 99695 and 99698), 163
Sheridan North	Zones: 160 (Excluded bus 99697), 161 (Excluded buses 99225-99311) and 162 (Excluded buses 99695 and 99698)

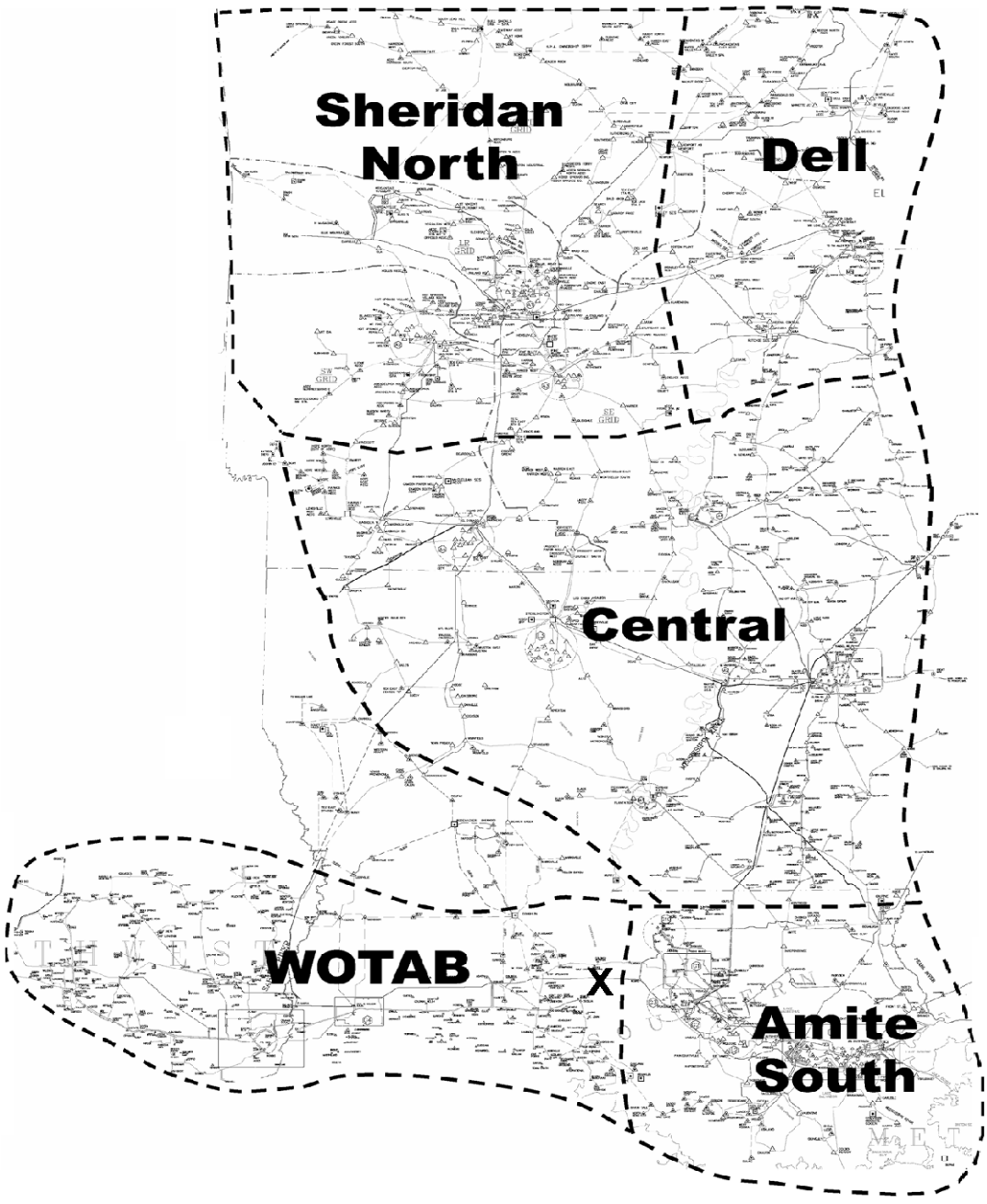


Figure 3.1 Entergy footprint

The modal analysis technique discussed in Section 2 is applied to the EES to determine the buses which participate in voltage instability or voltage collapse. Attention is focused on two main aspects, namely the identification of critical zones prone to voltage instability, and the associated contingencies leading to voltage instability. Voltage stability assessment tool (VSAT) [9] is used to determine the weak zones and to determine the critical contingencies. The procedure applied and the results obtained are explained in the following paragraphs.

3.2 VSAT studies

This section summarizes the main studies conducted to assess voltage instability in the EES. VSAT studies were performed to determine critical voltage stability modes which are responsible for the voltage collapse and the buses which participated in the modes. As discussed in Section 2, voltage collapse is actually a collapse of the modal voltage. If the modal voltages are plotted against the system load, then only one modal voltage curve would have a nose point [6]. VSAT ranks the modes in order of severity therefore the most critical mode (smallest eigenvalue) computed at the voltage stability limit will be labeled as mode 1 and similarly the next severe mode will be labeled as mode 2. The critical contingencies resulting in the smallest stability margins are also computed, and are ranked in the order of severity.

The power flow base case was provided by Entergy, and from the base case two loading scenarios were created. In the first scenario, only the reactive power portion of the load was increased in steps until the nose point was reached. Similarly, for the second scenario, the total load at each bus was increased with constant power factor until the solution diverged. These two loading scenarios were considered for voltage stability assessment. In the first loading scenario only the reactive power portion of the load of the system was increased and studied to see how much reactive support is available in the Entergy transmission system and also to observe how the modes and buses which participate in the voltage instability of the system would vary when compared to the second loading scenario as it is more practical.

It can be seen in Table 3.2 that the reactive power portion of the load was increased by approximately 44% from the base case value, and the load with constant power factor was increased by approximately 13% from the base case before the power flow diverged. In both cases the demand for reactive and real power was met by the EES generators and shunts and not by the swing bus.

Table 3.2 Loading scenarios used in the analysis

Loading Strategy	Case description	Base case load	Critical load	% Load Increase
Loading scenario I	Q increased at EES	9069.5 MVAr	13062.0 MVAr	44.02
Loading scenario II	P,Q increased at EES	30070.2 MW	34000.3 MW	13.06

Three operating points were derived for each of the loading scenarios described in Table 3.2. These are:

1) A base case condition provided by Entergy (Case A)
2) A stressed operating condition in the vicinity of the critical loading condition (Case B)
3) A critical operating condition in which the eigenvalue of a critical mode i.e. mode 1 is close to zero (Case C)

Mode 1 is the most critical mode with regard to voltage collapse of the power system as it reaches the nose point before the other modes. Modal analysis at the critical condition is used to determine the main buses involved in voltage collapse. The analysis is based on constant PQ load models and no time-dependent control actions are included in this analysis.

3.3 Q increase in the EES – Loading scenario I

In this scenario, the reactive load power was increased gradually in the EES and the demand for reactive power was met by excitation control in the generators and shunt compensation in EES. At each loading condition, the critical modes were obtained from the Jacobian of the power flow equations. The critical condition was obtained from the last loading condition for which a power flow solution exists as the loading was increased.

Table 3.3 shows the highest bus voltage magnitude participation factors for the critical voltage stability modes. For clarity, the zones associated with these modes are listed along with the bus names. Only participation factors larger than 10% are included in Table 3.3.

Figure 3.3 shows the behavior of the critical mode as the system is stressed and the results were obtained for three cases A, B and C. Cases A and B are utilized to assess the effect of critical system conditions on system instability, whereas case C is used to determine the weakest areas and the buses associated with the critical modes.

Figure 3.4 shows a schematic representation of the approximated locations of the critical zones in the EES obtained for case C. It is observed that these areas largely coincide with the critical areas determined for cases A and B showing that the initial condition is actually a stressed condition.

Analysis of mode 1 in Table 3.3 shows that it is localized mode as it has few buses with large participation factors and the remaining buses with small participation factor. These buses are present in the zones of the western region of the EES i.e. WOTAB. In this mode, a pocket of 69 kV buses in zones 100 and 101 has the highest participation. Calvert bus (69 kV) of zone 100 shows the largest participation followed by Sinhern (69 kV), Hearne (69 kV), and Texas Hearn (69 kV) buses also of zone 100. These buses are directly connected to each other as can be seen in figure 3.2 and are located at the southwestern border of the EES.

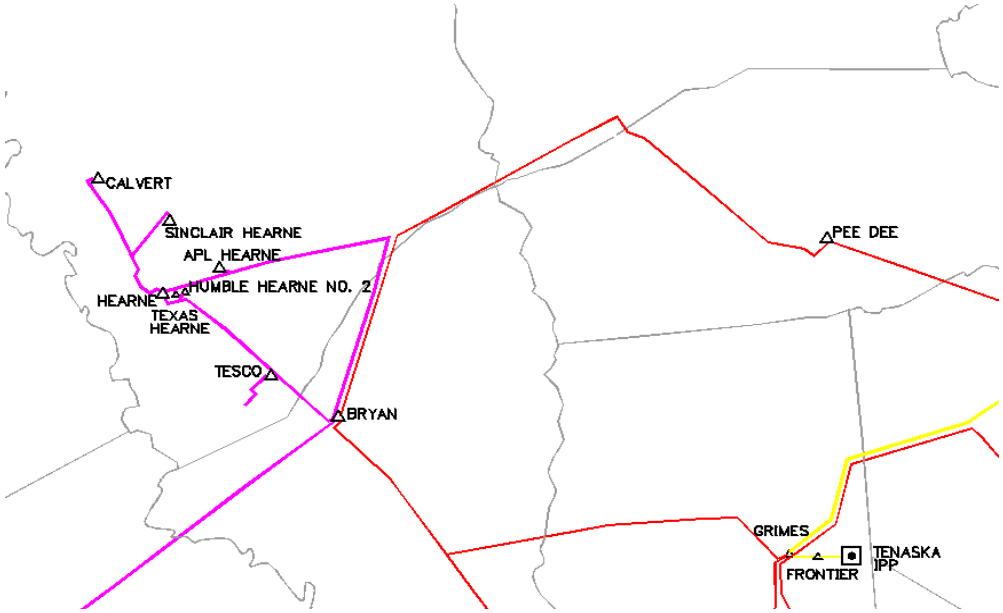


Figure 3.2 Southwestern part of the Entergy Energy System

The critical mode of the system may not necessarily be the one with the minimum eigenvalue, therefore other modes are also inspected. Mode 2 given in the appendix appears to be related to the loss of voltage control capability in zone 140 of the EES and also includes 115 kV buses from zone 152 with a significant contribution. These zones are next to each other as can be seen in Figure 3.4. The critical bus is Murrla (115 kV) in zone 140 followed by units #1-8 at Murru station which is connected to Murrla bus of zone 140 by a transformer.

Mode 3 and 4 are associated with areas not in EES and are not discussed here. Mode 5, given in the appendix, involves zone 112 which is also present in the WOTAB region. In this mode, buses with voltages 13.8 kV and 18.0 kV are involved in the voltage instability of the system. The stability problem appears to be related to the loss of voltage control capability at generators PPG in zone 112 which has the highest participation factor in mode 5.

Table 3.3 Mode 1 with eigenvalue = 0.0615 – Loading Scenario I

Bus No.	Bus Name	Area	Zone	Participation Factor
97515	2CALVERT	EES	100	1.0000
97527	2SINHERN	EES	100	0.7986
97516	2HEARNE	EES	100	0.6274
97517	2TXHEARN	EES	100	0.6140
97525	2HUMBHRN	EES	100	0.5906
97523	2APLHERN	EES	100	0.5707
97511	2TESCO	EES	100	0.4240
97501	2CALDWEL	EES	100	0.3281
97504	2BRYAN B	EES	100	0.3225
97503	2SOMERVL	EES	100	0.3140
97500	2INDEPEN	EES	100	0.2851
97505	2BRYAN A	EES	100	0.2794
97524	2IN.AT$T	EES	100	0.2599
97502	2ANAVSOT	EES	100	0.1924
97506	4BRYAN	EES	100	0.1865
97507	4COLSTTA	EES	100	0.1565
97512	4PEE DEE	EES	101	0.1549
97555	4BISHOP	EES	101	0.1433
97481	4CEDAR	EES	101	0.1302
97509	4SPEEDWY	EES	100	0.1244
97508	4NAVSOTA	EES	100	0.1335
97522	4TUBULAR	EES	100	0.1228
97510	4SOTA 1	EES	100	0.1168
97482	4CINCINT	EES	101	0.1137
97530	4WALKER	EES	100	0.1103

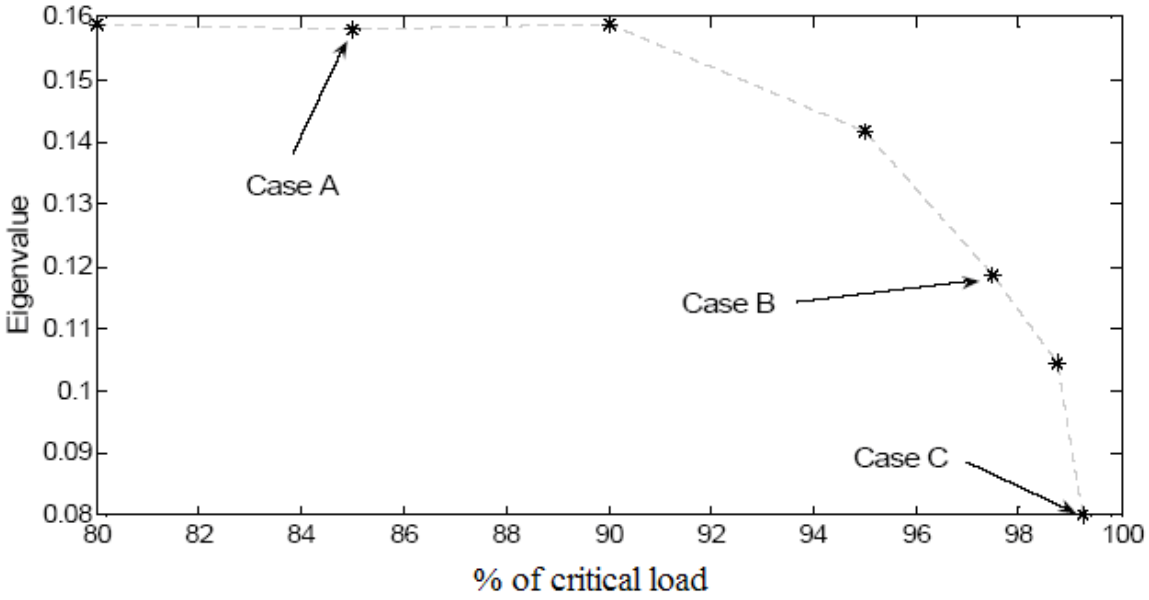


Figure 3.3 Eigenvalues as Q is increased as a percentage of critical load

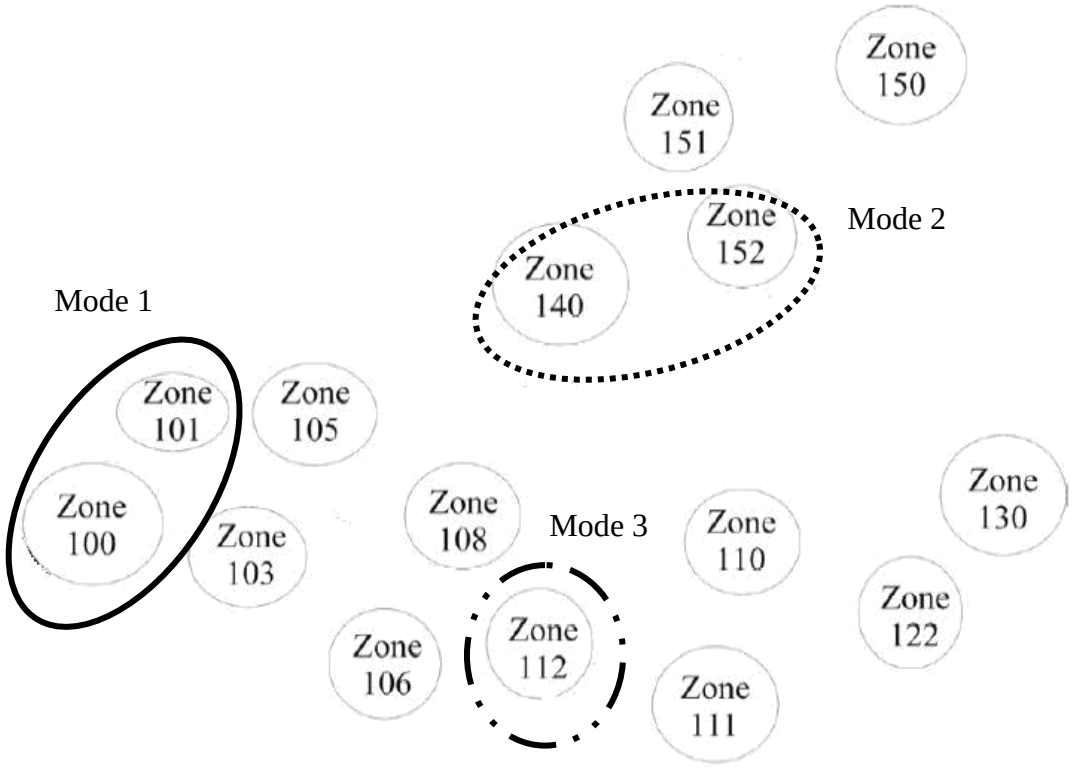


Figure 3.4 Critical modes of loading scenario I

3.4 Load increase in the EES with a constant power factor – Loading scenario II

In this scenario, the system was stressed gradually by increasing the load in EES while maintaining a constant power factor. The load increase was met by increasing the generation in EES.

Results for cases B and C are found to be largely consistent with those of loading scenario I where only reactive load power is increased in the EES. Table 3.4 provides the information regarding the critical mode (mode 1). Analysis shows that it is localized mode similar to the critical mode of the loading scenario I as it has few buses with large participation factors and the remaining buses with small participation factor. All the buses which are present in the critical mode of loading scenario I are also present in the critical mode of loading scenario II with almost the same participation factor towards the mode. Calvert bus (69 kV) of zone 100 shows the largest participation followed by Sinhern (69 kV), Hearne (69 kV), and Texas Hearn (69 kV) buses also of zone 100. These buses are present in the zones of the western region of the EES i.e. WOTAB.

Next critical mode with eigenvalue of 0.18724 also has the Calvert bus with the largest participation followed by Sinhern, Hearne, and Texas Hearn buses of zone 100. Buses of zone 105 also show a participation in this mode. Next mode with eigenvalue 0.201 is a non-localized mode as it has many buses with a large bus participation factor from zone 112 of WOTAB region. Complete results are attached in the appendix.

Table 3.4 Mode 1 with eigenvalue = 0.05218 – Loading Scenario II

Bus No.	Bus Name	Area	Zone	Participation Factor
97515	2CALVERT	EES	100	1.0000
97527	2SINHERN	EES	100	0.8167
97516	2HEARNE	EES	100	0.65696
97517	2TXHEARN	EES	100	0.64467
97525	2HUMBHRN	EES	100	0.62331
97523	2APLHERN	EES	100	0.60495
97511	2TESCO	EES	100	0.46721
97501	2CALDWEL	EES	100	0.37699
97504	2BRYAN B	EES	100	0.36870
97503	2SOMERVL	EES	100	0.36484
97500	2INDEPEN	EES	100	0.33581
97505	2BRYAN A	EES	100	0.32724
97524	2IN.AT$T	EES	100	0.31028
97502	2ANAVSOT	EES	100	0.24084
97506	4BRYAN	EES	100	0.23348
97507	4COLSTTA	EES	100	0.20115
97512	4PEE DEE	EES	101	0.20099
97555	4BISHOP	EES	101	0.18835
97481	4CEDAR	EES	101	0.17374
97509	4SPEEDWY	EES	100	0.16920
97508	4NAVSOTA	EES	100	0.16820
97522	4TUBULAR	EES	100	0.16737
97510	4SOTA 1	EES	100	0.16062
97482	4CINCINT	EES	101	0.15506
97530	4WALKER	EES	100	0.15114
97453	4DOBBIN	EES	100	0.14746
97546	4MAG AND	EES	100	0.14513

The main differences between the two loading scenarios were examined. It was observed that the number of critical modes participating in the voltages collapse in EES area are greater in scenario II than scenario I. There are three critical modes for loading scenario I and five critical modes for loading scenario II. Secondly, zones (zone 140 and zone 152) present in the second mode of loading scenario I did not appear in any of the modes of loading scenario II. In addition, two additional zones (zone 105 and zone 111) emerged in the loading scenario II which participated in the voltage instability of the EES.

Mode 1 and mode 3 contain the same buses which participated in the voltage instability of the EES in scenario II. Mode 1 is comprised of buses of zone 100 and zone 101 with voltage levels of 69 kV and 138 kV. Calvert bus (69 kV) of zone 100 has the highest bus participation in mode 1 followed by Sinhern (69 kV), Hearne (69 kV), and

Texas Hearn (69 kV) buses also of zone 100. Mode 3 contains low voltage level buses of zone 112 with 13.8 kV and 69 kV, where bus PPG (13.8 kV) has the highest bus participation in the mode.

Mode 2 contains buses of zone 100 and zone 105 with voltage levels of 69 kV and 138 kV. Calvert (69 kV) has the highest bus participation towards voltage instability in this mode. Zone 100 appears in two modes (mode 1 and mode 2). In both of these modes, Calvert (69 kV) bus has the greatest participation, indicating that zones 100 is the weakest zone of the EES.

Zone 105 also appeared in two modes (mode 2 and mode 4). In both modes, Weirgat (69 kV) is the weakest bus from zone 105 while in mode 4 it has the highest participation. Figure 3.5 shows a schematic representation of the approximated locations of the critical zones in the system obtained for case C of loading scenario II.

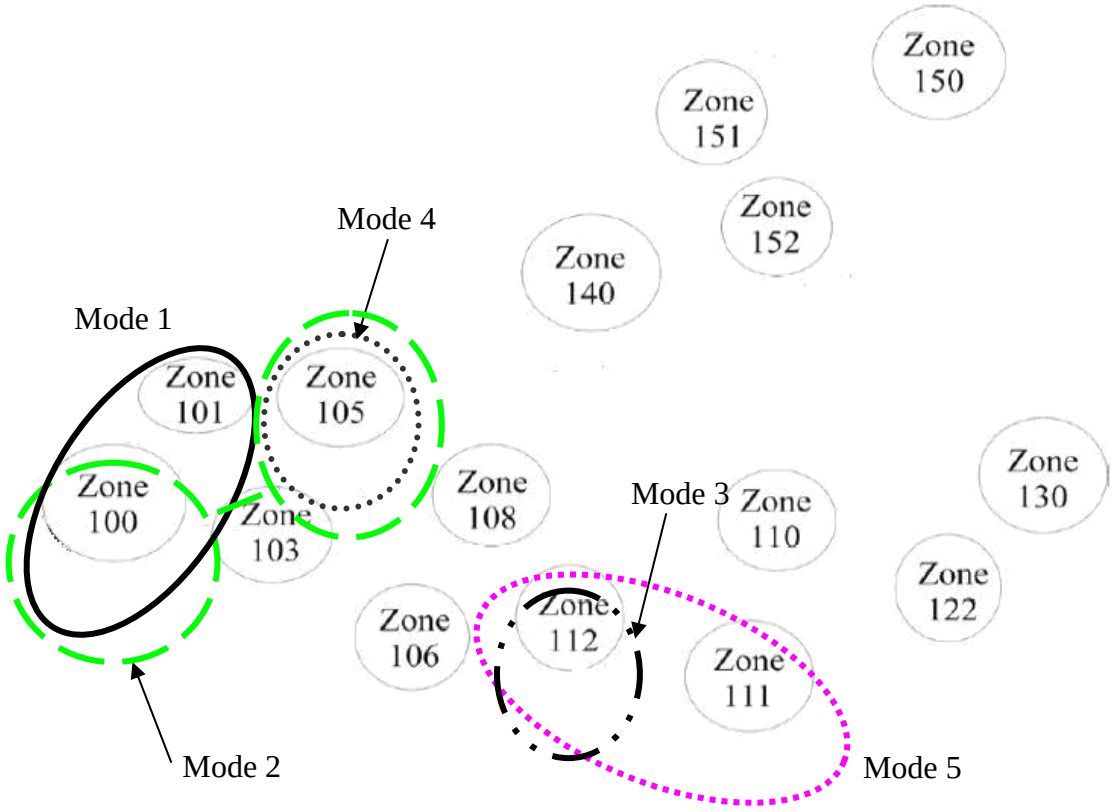


Figure 3.5 Critical modes of loading scenario II

3.5 Critical Contingencies

In a large system such as EES (which consists of 2070 buses, 2145 transmission lines, 168 generators), out of a large number of possible contingencies, only a few contingencies will be critical with regard to the voltage stability problem. Therefore, the aim of this study is to find the most critical contingencies which are important with regard to the stability of the EES.

The contingency screening in VSAT is designed to identify the critical contingencies. The screening of critical contingencies does not use any approximation i.e. linearization or extrapolation, and accurately classifies the contingencies based on their exact voltage stability (VS) margin. The VS margin of each contingency is defined as the difference between the pre-contingency transfer at the initial operating point (current operating point), and the last point where the post-contingency solution exists.

The process of finding the N_c most severe contingencies among the full list of contingencies is the following.

1) Starting from the initial point (P_0), compute only the pre-contingency *PV* curve, in the direction of the power transfer, to find the nose point (P_m = maximum power transfer level). *PV* curves are obtained for all the buses in the system.
2) Reduce the transfer from the nose point by S_1 MW. Name this point as P_1.
3) Solve all the contingencies at P_1 and find N_1 contingencies for which the post disturbance power flow does not solve.
4) If $N_1 = N_c$, stop.
5) Set the counter $i = 1$.
6) If $N_i > N_c$, reduce the transfer to $P_{i+1} = \frac{(P_0 + P_i)}{2}$, and find N_{i+1} contingencies, among the N_i unsolved contingencies identified at P_i. Else, increase the transfer to $P_{i+1} = \frac{(P_i + P_m)}{2}$, and find N_{i+1} contingencies among all the contingencies for which the post disturbance power flow does not solve at this point and these include the N_i contingencies identified at P_i which do not need to be resolved.
7) If $N_{i+1} = N_c$, stop.
8) If $N_i > N_c$ replace P_m by P_i, else, replace P_o by P_i, increase the counter *i* by 1, and go to step 6.

The process stops if the step $P_{i+1} - P_i$ becomes smaller than a limit, or number of search points (*i*) exceeds a limit e.g. if list has 100 contingencies whose voltage stability margins are almost the same, searching for the 10 most severe contingencies among 100 would reach a very small search step and also too many steps which makes the contingencies pointless because of numerical inaccuracies [9].

All the $N-1$ contingencies for the EES were assessed for voltage stability i.e. single line and generator outages. The 20 most severe contingencies were selected. Table 3.5 shows the top 20 critical contingencies which participate in the voltage instability of the system.

All the 20 contingencies are analyzed and the location of each contingency and the zone it is associated with is also noted. It was observed that 12 of the 20 most critical contingencies are located in the southwestern region of the EES i.e. WOTAB region. This region also contains all of the zones which are identified as a problem zones by modal analysis.

Table 3.5 Critical contingencies in the Entergy Energy System

Rank	Type	Name	Name	kV	Zone
1	Line	7GRIMES	GRMXF	345	100
2	Line	3GRNVIL	3SE-GRM	115	151
3	Line	3ELTON	3JAX-SW	115	150
4	Line	3B.WLSN	3VKSB-S	115	151
5	Transformer	6TITLTOB	RTILTOB	230/115	151
6	Line	3ELTON	3BYRAM	115	151
7	Line	3ALTO	3SWARTZ	115	140
8	Transformer	6PPG 23	2 PPC NO	230/69	112
9	Line	WATER V5	5WV-APL	161	999/163
10	Line	COCKET7	7GRIMES	345	999/100
11	Line	4LEWIS	4PANORAM	138	103/100
12	Line	3TILTOB	3GRNADA	115	150
13	Line	3STERL	3IPCO 1	115	140
14	Transformer	G1LEWIS	4LEWIS	22/138	103
15	Transformer	G2LEWIS	4LEWIS	22/138	103
16	Transformer	2PCG913	1PPG C1	69/13.8	112
17	Transformer	2PCG914	1PPG C2	69/13.8	112
18	Generator	G1LEWIS	-	22	103
19	Generator	G2LEWIS	-	22	103
20	Line	8CYPRESS	8HARTBRG	500	105/111

Critical contingencies are then compared to the modal analysis study of loading scenario II in which the load was increased by a constant power factor. This is performed to find if there is a relationship between the buses which participate in the critical modes and the critical contingencies of the Entergy system. It was observed that contingencies 1, 10, 11, 14, 15, 18, and 19 are associated (common bus) with mode 1 while contingencies 2, 3, 4, 5 and 6 are associated with mode 2 and contingencies 16 and 17 are related to mode 5. Out of the 20 critical contingencies, 14 of them are related to the critical modes identified by the modal analysis technique.

The agreement between the two studies show that the findings are valid and the zones in the southwestern region of the EES are most prone to voltage instability.

3.6 Conclusion

After comparing the two loading scenarios of the EES, it was concluded that the southwestern part of the Entergy transmission system with zones 100, 101, 105, 111 and 112 are the most critical to voltage stability.

Most of the critical contingencies identified are also located in the southwestern zones of the Entergy energy system.

4. Reactive Reserve Margin Analysis

4.1 Overview

Voltage collapse normally occurs when sources producing reactive power reach their limits i.e. generators, SVCs or shunt reactors, and there is not much reactive power to support the load. Therefore, the reactive reserve margin is used as a voltage stability indicator as discussed in chapter 2, and is implemented on the Entergy system to locate the zones which are vital for the system's security. Reactive reserve criteria specify that the reactive reserve of individual or group of VAr resources must remain above some percentage of their reactive power capability under all contingencies. Therefore, single line outages, generator outages and double line outages were conducted and reactive reserves were monitored for each contingency. Details of the procedure followed for this study are provided in the flowing sections of this chapter.

4.2 VSAT studies

The EES is a very large system (which consists of 2070 buses, 2145 transmission lines, and 168 generators). Measuring the reactive reserves of individual components such as generators or adjustable shunts of such a large system becomes meaningless. Therefore instead of monitoring the reserves of individual generators or adjustable shunts, reactive reserves of the zones were observed for single line outages, double line outages and generator outages.

Two power flow profiles were used for the EES, one was a peak load (30070 MW) case and the other one was an off-peak load (10110 MW) case. Twenty power flow profiles were generated by varying the load in the range of 10110 MW to 30070 MW with increments of 1000 MW. In generating the power flow profiles, generators were turned on using a priority list provided by Entergy as the load varied.

Before proceeding with the VSAT analysis, a study was done to determine the impact of load increase at each case and also determine which areas are affected in terms of voltage performance due to the load increase and whether these areas had sufficient reactive reserves in the base case. This step was performed to determine the existing situation in the base case. In several base cases it was seen that some zones already had zero reactive reserves; therefore for each base case considered, the load at each bus was increased by 7% and a power flow solution was obtained to examine the sensitivity of the base case. The voltages at all the buses were monitored to see which area or zone is more susceptible to voltage problems and whether any particular zone has sufficient reactive power reserves in the base case. Steps followed to find critical zones are given below:

1) Reactive reserves were observed for each base case and zones with reserves less than 20% of their reactive power limit were listed for each base case.

The load was increased by 7% in the Entergy area with constant power factor to see the zones which are affected the most by the load increase in terms of voltage.

Affected zones in step 2 were compared with zones of step 1 to see if the affected zone or zones have sufficient reserves to support the voltage. If a particular zone does not have sufficient reserves to support the voltage that zone is considered as a weak zone.
Generator outages were carried out and zones where the reactive reserves were reduced below 10% of their reactive power limit for each contingency were noted. The zone of the outaged generator was also noted to see if the generator is in the same zone or in the neighboring zone where the reserves were reduced below 10%.

2) Similarly for single and double outages, zones were noted where the reactive reserves were reduced below 10% and the zones of the contingencies were also noted to see if the contingency is in the same zone where there is a shortage of reactive reserves.

The reactive power reserve for each zone is calculated using (4.1)

$$\text{Reactive power reserve} = 100 * \frac{Q_{\max} - Q_Z}{Q_Z} \tag{4.1}$$

where

Q_Z = Sum of reactive power output of generators, adjustable and fixed shunts

$Q_{\max}$ = Maximum reactive power available in the zone

Three load cases are discussed in this section. Case I is an off-peak case with a total load of 10110 MW, case II is a stressed case with a load of 18000 MW and case III is a peak case with a load of 30070 MW. Results of the remaining power flow profiles are provided in the appendix.

Case I. Load = 10110 MW

Reactive power reserves were observed for each zone in a base case. It was noticed that zones 108 and 120 had already exhausted their reactive power reserves. Table 4.1 shows the base case information.

Table 4.1 Reactive power reserves in base case – Case I

Zone	**MVAr Output**	**Reserve**
120	212.94	0.0 %
108	54.41	0.0 %

The load was then increased by 7% in the EES to see which zones are affected the most by the load increase in terms of voltage. Table 4.2 shows that zone 112 is affected the most, but voltage can be improved in zone 112 because there is sufficient reactive power available in this zone and also in the surrounding zones.

Table 4.2 Voltage magnitude in p.u. after 7% load increase – Case I

Bus Number	Zone Number	Voltage Magnitude
98062	112	0.9021
98059	112	0.9026
98063	112	0.9026
98064	112	0.9026
98061	112	0.9026
98060	112	0.9026
98074	112	0.9159
98073	112	0.9162
98072	112	0.9175

For the generator, single line and double line outages no additional zones exhausted their reactive reserves below 10% of their limit. This demonstrates that in the off peak load case there is sufficient reactive power available in all the other zones of EES.

Case II. Load = 18000 MW

Case II was a stressed load case in which there was not much generation available to support the change in load. Table 4.3 shows that reactive power for most of the zones present in southwestern part of EES is already exhausted in the base case. When the load was increased by 7% to see the affect in terms of voltages, the solution diverged.

Of the nine zones shown in Table 4.3, six of them are located in the WOTAB region of the EES. All of these zones are physically next to each other and the exhaustion of the reactive power in the zones make this region very prone to voltage instability.

Table 4.3 Reactive power reserves in base case – Case II

Zone	MVAr Output	Reserve
105	486.10	9.1%
120	212.25	0.0%
102	169.66	0.0%
101	144.71	0.0%
160	110.92	0.0%
106	95.10	0.0%
130	346.23	19.5%
109	74.88	0.0%
108	53.01	0.0%

Tables 4.4, 4.5 and 4.6 show the response of the reactive reserves of EES for the generator, single line, and double line contingencies.

Table 4.4 Generators outages – Case II

Bus	Zone	MVAr Output	Reserve
97451 (Zone 103)	112	274.78	0.0 %
97911 (Zone 112)	112	274.78	0.0 %
97781 (Zone 105)	112	274.78	0.0 %
97912 (Zone 112)	112	274.78	0.0 %
98061 (Zone 112)	112	274.78	0.0 %
99489 (Zone 162)	162	428.21	7.5 %

Table 4.5 Single line outages – Case II

Line	Zone	MVAr Output	Reserve
97684-97689 (Zone 105-106)	112	232.87	0.6 %
97684-97713 (Zone 105-105)	112	233.37	0.2 %
97689-97714 (Zone 106-105)	112	232.87	0.7 %
97690-97792 (Zone 105-105)	112	217.37	7.9 %
97696-97769 (Zone 105-108)	112	232.61	0.7 %
97700-97792 (Zone 105-105)	112	217.53	7.8 %
97715-97718 (Zone 105-105)	112	233.60	0.0 %
98937-99203 (Zone 112-140)	112	229.32	2.0 %
99148-99295 (Zone 140-161)	112	217.95	7.4 %
99162-99295 (Zone 140-161)	112	222.24	5.3 %
97451-97461 (Zone 103-103)	112	227.54	0.0 %
97452-97461 (Zone 103-103)	112	228.37	0.0 %
97715-97717 (Zone 105-105)	112	233.24	0.0 %
97775-97781 (Zone 105-105)	112	233.45	0.1 %
99486-99489 (Zone 162-162)	162	422.23	9.1 %

Table 4.6 Double line outages – Case II

Contingency	Zone	MVAr Output	Reserve
98097-98108 '1' (Zone 111-111) 98097-98108 '2'	112	226.84	4.0 %
99148-99203 '1' (Zone 140-140) 99148-99203 '2'	112	227.97	0.0 %

It was observed that zone 112 which had sufficient reactive power reserves in the base case was affected the most because of the outages. This is because, there isn't sufficient reactive power available in the neighboring zones i.e. zone 106, 108 and most of the reactive power is provided by zone 112 after the disturbance, resulting in the exhaustion of reactive power reserves in zone 112.

Case III. Load = 30070 MW

Case III is a peak load case. Table 4.7 given below provides the information regarding the zones with reactive power reserves less than 20% in the base case.

Table 4.7 Reactive power reserves in base case – Case III

Zone	MVAr Output	Reserve
162	1013.35	17.8 %
120	233.20	0.0 %
103	413.04	14.2 %
102	151.41	0.0 %
101	131.49	0.0 %
160	127.59	3.0 %
109	74.85	0.0 %

Zones 101, 102 and 109 from the WOTAB region and zone 120 from the Amite South region had no reactive power reserves in the base case. In addition four out of seven zones shown in Table 4.7 are from WOTAB region, two zones (zones 160 and 162) are from Sheridan North and one zone (zone120) is from Amite South. The Sheridan North region consists of only three zones and occurrence of two of these zones (Zones 160 and 162) in Table 4.7 could make some portion of the region vulnerable to voltage instability.

Buses which are affected the most in terms of voltage after 7% load increase are shown in Table 4.8. All of these buses are located in the WOTAB region and the weakest bus identified is the Calvert bus from zone 100. The Calvert bus is also identified as the weakest bus in modal analysis studies.

The generator outages and single line outage which diminished the reactive power reserves in the zones are shown in Tables 4.9 and 410 respectively. Both types of outages i.e. generator outages (in zone 108) and line outages (in zone 108) diminish reactive power reserves in zone 106 of the WOTAB region.

Table 4.8 Voltage magnitude in p.u. after 7% load increase – Case III

Bus Number	Zone Number	Voltage Magnitude
97515	100	0.8766
97527	100	0.9021
97640	105	0.9046
97761	105	0.9104
98021	112	0.9152
98038	112	0.9166
98220	110	0.9179
98219	110	0.9198
98221	110	0.9198

Table 4.9 Generators outages – Case III

Bus	Zone	MVAr Output	Reserve
97773 (Zone 108)	106	113.49	10.2 %

Table 4.10 Single line Outages – Case III

Line	Zone	MVAr Output	Reserve
97757-97828 (Zone 106-106)	106	113.49	10.2 %

It can be observed from the data shown for the three cases that zones 100, 102, 103, 105, 106, 108, 100 and 112 have exhausted their reactive power reserves and these zones are located in the southwestern part of EES i.e. WOTAB region.

Critical contingencies can also be identified by this method. The contingencies which diminish reactive power reserves would be identified as critical contingencies. In the following sections a comparison is made between the critical contingencies identified by EES [13] with the critical contingencies identified by this study.

4.3 Critical contingencies identified by Entergy in the western area

Contingencies that were identified as critical by the transmission planning group at Entergy [12] are compared with the contingencies which diminish the reactive reserves of the zones in the analysis conducted.

First, contingencies in the western part of EES are compared, as this area is identified as critical for voltage stability by EES. There are two Lewis Creek generation units (97451 and 97452) in zone 103 and both are critical with regard to the stability of the system. Loss of any one of these two generators, followed by a fault and trip of one transmission line given in Table 4.11 are the critical contingencies identified by EES.

Table 4.11 Critical contingencies identified by Entergy [12]

Line	Names
97714-97478 (Zone 105-104)	China – Jacinto 230 kV
97714-97567 (Zone 105-104)	China – Porter 230 kV
97513-53526 (Zone 100-999)	Grimes – Crockett 345 kV
97463-97467 (Zone 102-104)	Oakridge – Porter 138 kV

4.3.1 Comparison between critical contingencies

A comparison of the contingencies identified as critical by Entergy and the contingencies identified as critical by the analysis performed using the reactive reserve margin approach is presented.

When the load is 18000 MW, the loss of the Lewis Creek unit 1 forced the reactive reserves of zone 112 to drop dramatically to 0 %. Similarly the loss of Lewis Creek unit 1 or unit 2 reduces the reactive reserves to 3.1 % when the load is 21000 MW.

Of the four line outages identified by Entergy [12] and listed in Table 4.11 shown above, the last three outages are also identified as critical outages in the study conducted using the reactive reserve margin approach. The difference between the two studies is that the Entergy study [12] was done with one generator out of service and a fault applied at one end of the line which is then tripped. In this study only the removal of line was considered without the fault and the generator out of service.

Table 4.12 Common contingencies

Bus	Zone	MVAr Output	Reserve
97451 (Zone 103) Gen. Lewis#1	112	274.78	0.0 %
97451 (Zone 103) Gen. Lewis#1 and 97452 (Zone 103) Gen. Lewis#2	112 112	338.72 338.72	3.1 % 3.1 %

Other common critical line outages for different operating conditions are shown in Table 4.13.

Table 4.13 Other common contingencies

Line	Zone	MVAr Output	Reserve
97513-53526 (Zone 100-999) (Grimes-Crockett) Load = 17000 MW	112	200.55	4.0 %
97714-97567 (Zone 105-104) (China-Porter) Load = 29000 MW	103	433.07	8.4 %
97714-97567 (Zone 105-104) (China-Porter) Load = 29000 MW	103	433.07	8.4 %

4.3.2 Common contingencies in other areas of EES

Common critical contingencies in the Entergy system other than the western part are given below in Table 4.14 and these contingencies are identified at different load levels.

Table 4.14 Common contingencies in other regions

Line	Zone	MVAr Output	Reserve
99162-97717 (Zone 140-105) (Mount Olive-Hartburg) Load = 17000 MW	112	203.33	4.0 %
99203-98937 (Zone 140-112) (Perry Ville - Baxter Wilson) Load = 18000 MW	112	229.32	2.0 %
99162-97717 (Zone 105-140) (Mount Olive-Hartburg) Load = 20000 MW	112	283.22	2.5 %
Generator	**Zone**	**MVAr Output**	**Reserve**
99489 (Zone 162) (ANO#2) Load = 18000 MW	162	428.21	7.5 %

The following double line outages in Table 4.15 are identified as critical contingencies in the reactive reserve analysis conducted, while in the Entergy study [12] for N-1 contingencies, the single line outage between the same two buses is critical.

Table 4.15 Common double line contingencies

Line	Zone	MVAr Output	Reserve
99203-99148 '1' (Zone 140-140) 99203-99148 '2' (Sterlington-Perry Ville) Load = 18000 MW	112	227.97	0.0 %
99203-99148 '1' (Zone 140-140) 99203-99148 '2' (Sterlington-Perry Ville) Load = 19000 MW	112	282.12	0.6 %

4.3.3 Contingencies sharing the same bus

There are some contingencies identified as critical in the analysis conducted in this study that share the same bus (not the same line) with the critical contingencies identified by Entergy [12]. The common buses are shown in bold letters in Table 4.16.

Table 4.16 Contingencies sharing same bus

Entergy Study	Analysis conducted	Zone	MVAr Output	Reserve
97714–97478 (China-Jacinto)	97689–**97714** (Load = 18000 MW)	112	232.87	0.7 %
	97567–**97714** (Load = 29000 MW)	103	433.07	8.4 %
98107-98109 (Richard-Wells)	97916-**98107** (Load = 24000 MW)	105 112	919.50 500.72	10.5 % 6.7 %
99162-97717 (Mount Olive-Hartburg)	**99162**-99295 (Load = 18000 MW)	112	222.24	5.3 %
99486-**99565** (ANO-Mabeville)	**99565**-99566 '1' **99565**-99566 '2' (Load = 19000 MW)	160	112.86	0.0 %
	99565-99566 (Load = 22000 MW)	120 120	238.98 120.94	1.7 % 3.4 %
	99565-99566 '1' **99565 -** 99566 '2' (Load = 25000 MW)	160	118.64	0.0 %

4.4 Summary

The weak zones identified by the analysis conducted were not same for all the cases as the operating conditions for the cases analyzed were different. Different generators were turned on as load was increased and also adjustable shunts were changed accordingly. It was noticed that at a load of 10110 MW zone120 and zone 108 have zero reactive reserves and zone 112 was affected the most in terms of voltage magnitudes but

as the load was increased to 30070 MW zones 101, 102, 109 and 120 have zero reactive reserves and zones 100, 105, 110, and 112 were affected the most in terms of voltage magnitudes after the 7% load increase to study the sensitivity. It was also noticed that most of the zones which do not have enough reactive reserves before and after the outages are in the southwestern part of EES. Contingencies which are identified as critical are also located in the south and western part of EES.

The following section will compare the results obtained by the modal analysis technique and the reactive reserve margin method.

4.5 Identification of critical zones

Zones which are critical to the stability of the system are identified by monitoring the participation factor of the buses using modal analysis. Buses which participated the most in the critical modes are noted along with their zones. Zones which are considered critical using modal analysis method are given below along with the zones identified by reactive reserve margin approach. Zones which are common to both studies are shown in bold in table 4.17.

Table 4.17 Critical zones

Zones identified using reactive reserve	Zones identified using modal analysis
101	100
102	**101**
103	**103**
106	105
109	111
120	112
160	

4.6 Time response of voltages for critical contingencies

The outage of the Lewis generator in zone 103 is carried out in a base case with a load of 30070 MW to examine the time response of the voltages in the system using Powertech Lab's TSAT analysis package [9]. The voltages of the buses before the contingency (pre contingency) and the minimum voltages of the buses in the time domain after the contingency (post contingency) are shown in Table 4.18. This outage is selected because it is identified as a critical outage in both static studies conducted in this thesis i.e. modal analysis and reactive reserve margin analysis. The outcome of this outage verified that results obtained in this study indeed locate the weak zones of the system which are prone to voltage instability as all the buses which are affected by this outage are present in the zones which are identified as weak zones i.e. Zones 100, 102, 105 and 112.

Table 4.18 Buses affected the most after the Lewis generator outage

Bus Number	Pre contingency voltage in p.u.	Post contingency voltage in p.u.	Zone
97515	0.9351	0.8462	100
97527	0.9565	0.8710	100
98059	0.9962	0.8930	112
97516	0.9766	0.8943	100
97517	0.9778	0.8957	100
97525	0.9793	0.8977	100
97523	0.9812	0.9000	100
97544	0.9838	0.9025	102
97640	0.9375	0.9029	105
97453	0.9931	0.9034	100

4.7 Sensitivity analysis and critical zones

Sensitivity analysis is also performed to gain further insight into the performance of the EES. Two load cases were considered in this study with total loads of 10110 MW and 30070 MW. The system is perturbed by increasing the total load in both cases so that the voltage response of the buses can be compared. Details of the procedure are explained below.

Transient Security Assessment Tool (TSAT) is used to observe the response of bus voltages in time domain after the perturbation of the total load. The simulation was run for 10 seconds to get the complete response of the system after the disturbance. The system is perturbed by increasing the load of a system with a constant power factor. The load is increased linearly by 25% and 22 % respectively from the base load in 0.1 second (ramp increase). The steps followed are given below.

1) Load is increased by 25% in the base case with constant power factor
2) Step 1 was repeated but with a load increase of 22%
3) For each parameter monitored in the simulations the results obtained from step 1 are subtracted from the results obtained in step 2. The change in the bus voltages divided by the change in the system load gives the sensitivity. The current analysis has been performed for one level of change in the load (3%), therefore the results obtained are not divided by 3 as it will only change the scale of the sensitivity factor.

The current analysis has been performed for one level of change in the load (3%), therefore the results obtained are not divided by change in load as it will only change the scale of the sensitivity factor. Buses present in the zones which are identified as critical zones in the earlier methods show high sensitivities compared to the buses from other zones. The sensitivities of two specific buses are shown in Figure 4.1 and Figure 4.2. Bus 98085 (in zone 112) shows little increase in sensitivity, whereas the sensitivity increases significantly at bus 97515 (in zone 100). Large peak-to-peak values of the sensitivities

indicate underlying system weakness. Bus 97515 present in zone 100 is identified as the weakest bus in the sensitivity studies.

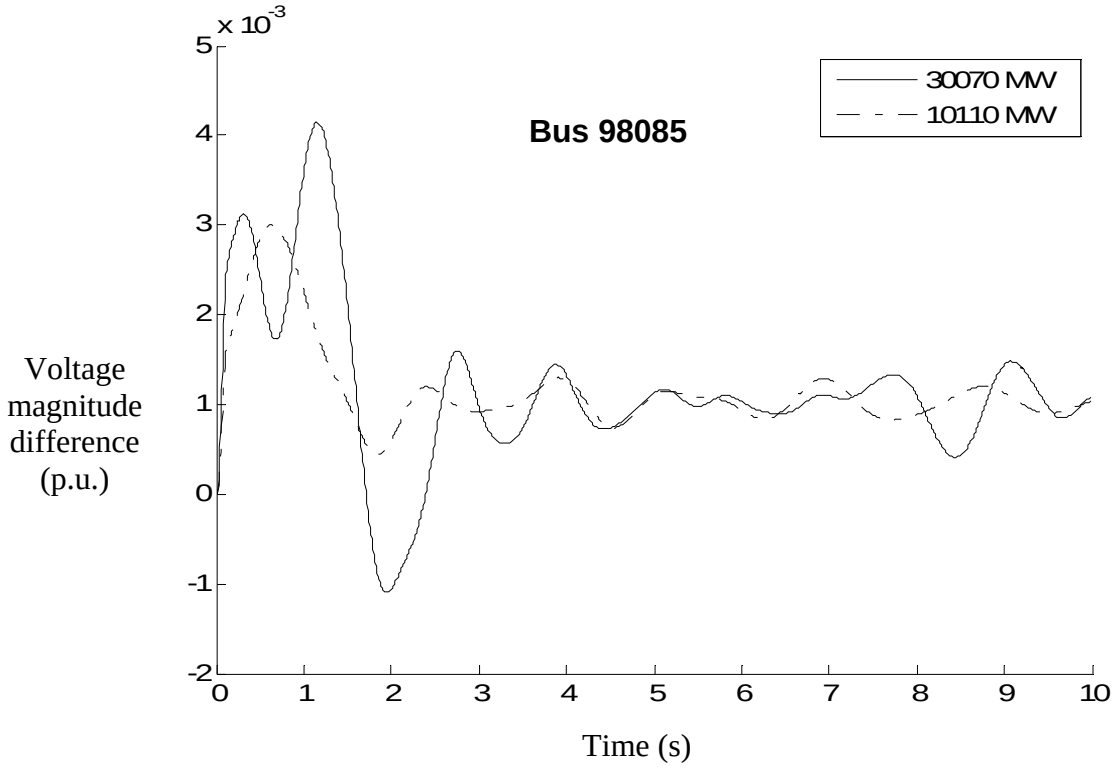


Figure 4.1 Voltage magnitude difference observed in the time domain for 3 % change in the load (difference of voltage in case 1 and case 2) for bus 98085

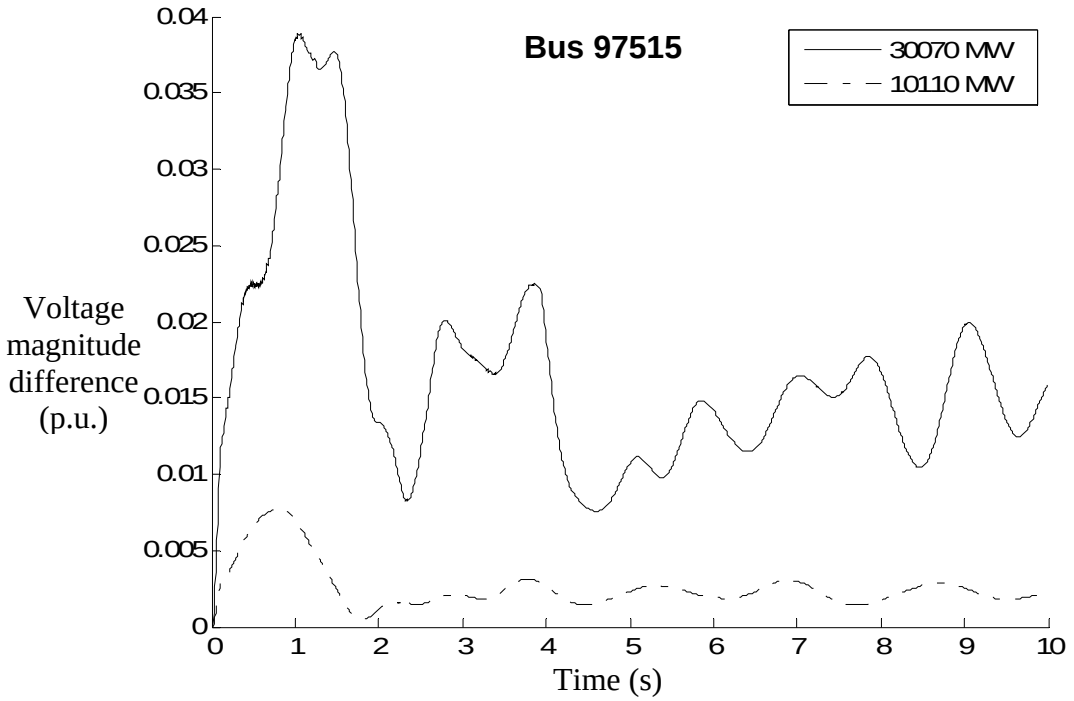


Figure 4.2 Voltage magnitude difference observed in the time domain for 3 % change in load (difference of voltage in case 1 and case 2) for bus 97515

4.7.1 Comparison between peak-peak variation value and modal analysis

A Comparison was made between the peak-peak values of the sensitivities performed and the modal analysis at the maximum load (30070 MW). The most severe peak-peak variation values are given in table 4.19. Few buses with the highest participation factor were chosen from mode 1 (most critical mode) of the modal analysis. The bolded buses in Table 4.19 show the buses which were found common to both the studies.

It was found out that all the buses which have the highest participation factor for mode 1 at the maximum load also have the maximum peak-peak variation values, which can be seen in Table 4.19.

The comparison between the trajectory sensitivities and modal analysis showed very interesting results as there is good agreement between the buses with largest peak-to-peak sensitivities and those associated with the critical mode at the maximum load.

From the above analysis and results, it is verified that the weakest region of the EES is WOTAB and the weakest zone present in WOTAB is zone 100.

Table 4.19 Buses with maximum peak-peak voltage Variation

Bus #	Bus Name	Zone	Peak-Peak Difference (p.u.)
97515	**2CALVERT69.0**	100	0.0321
97547	FRNTR 1 18.0	100	0.0318
97527	**2SINHERN69.0**	100	0.0316
97516	**2HEARNE 69.0**	100	0.0312
97517	**2TXHEARN69.0**	100	0.0312
97506	**4BRYAN 138.**	100	0.0312
97507	**4COLSTTA138.**	100	0.0312
97523	**2APLHERN69.0**	100	0.0311
97501	**2CALDWEL69.0**	100	0.0311
97525	**2HUMBHRN69.0**	100	0.0311
97511	**2TESCO 69.0**	100	0.0306
97503	**2SOMERVL69.0**	100	0.0305
97505	**2BRYAN A69.0**	100	0.0304
97504	**2BRYAN B69.0**	100	0.0303
97500	**2INDEPEN69.0**	100	0.0301
97514	4GRIMES 138.	100	0.0301
97524	**2IN.AT$T69.0**	100	0.0299
97526	4MAG AND138.	100	0.0299
97502	**2ANAVSOT69.0**	100	0.0292
97510	4SOTA 1138.	100	0.0292

4.8 Time domain analysis

TSAT is used to find the critical contingencies affecting the EES in the time domain. This step is performed to make a comparison between the contingencies identified as critical in steady state analysis using VSAT and also to monitor the location of the contingencies and the buses affected by the critical contingencies in time domain. The criteria used to determine the weak buses in the time domain study is given below.

After the line contingency, bus voltage is below 0.92 p.u at any instant during the simulation and the voltage difference between initial and minimum value of voltage is greater than 0.05 p.u.

All the single line outages (2145 lines) present in the EES were analyzed and the five most critical contingencies identified are shown in Table 4.20. Of the five contingencies, four of them are also identified as critical contingencies in steady state analysis, as shown in Table 3.5. All the buses shown in Table 4.20 (other than Crocket which is not in the EES area) are present in the western part of the WOTAB region of the

EES and the results are in complete agreement with the modal analysis as the buses which get affected the most in time domain also have a large bus participation in the critical modes of modal analysis study.

The voltage responses of the two buses (Calvert and Sinhern) which are affected the most by the line contingency (7Grimes – Grmxf) are shown in figure 4.3. Both buses are present in zone 100 of the EES and also have the highest bus participation factor in the critical mode of modal analysis. Time domain study provides a positive feedback of the results obtained earlier in this report.

Table 4.20 Critical contingencies in time domain

No.	Line	Zones
1	Crocket – 7Grimes	999-100
2	7Grimes – Grmxf	100-111
3	G1Lewis – 4Lewis	103-103
4	G2Lewis – 4Lewis	103-103
5	Wells – Webre	111-110

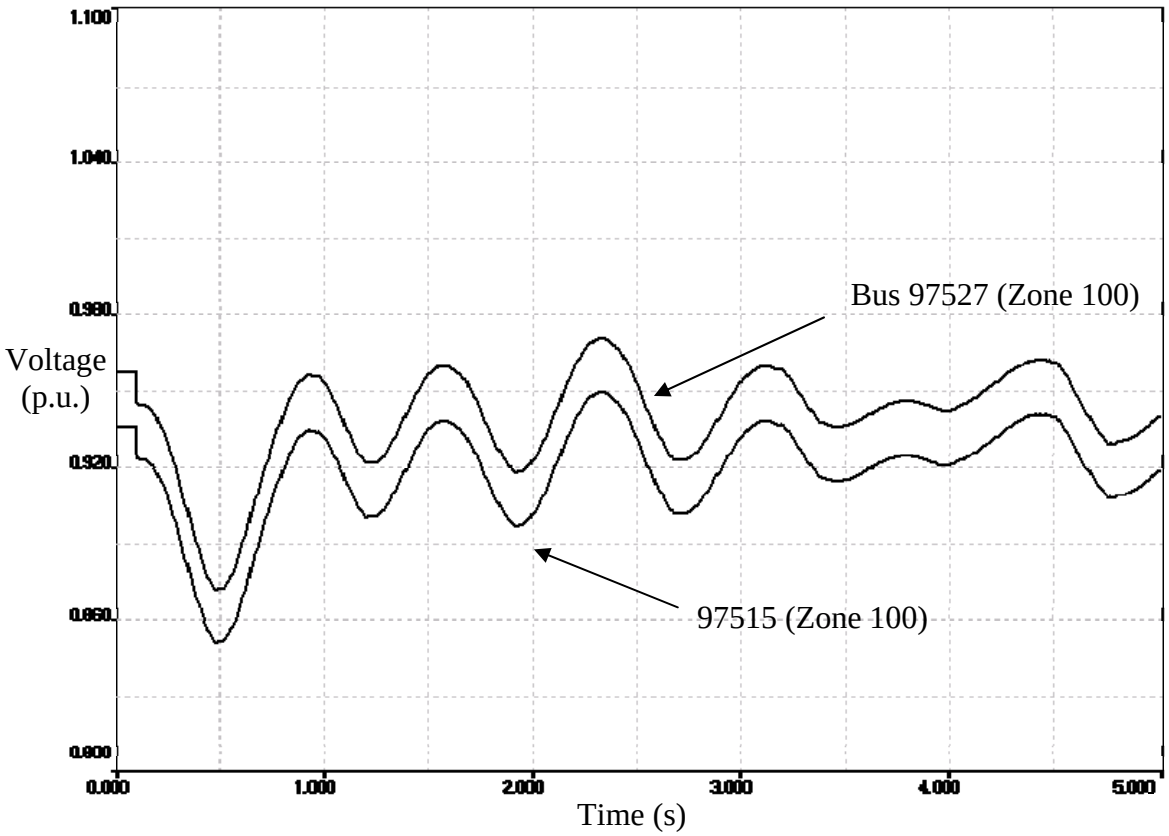
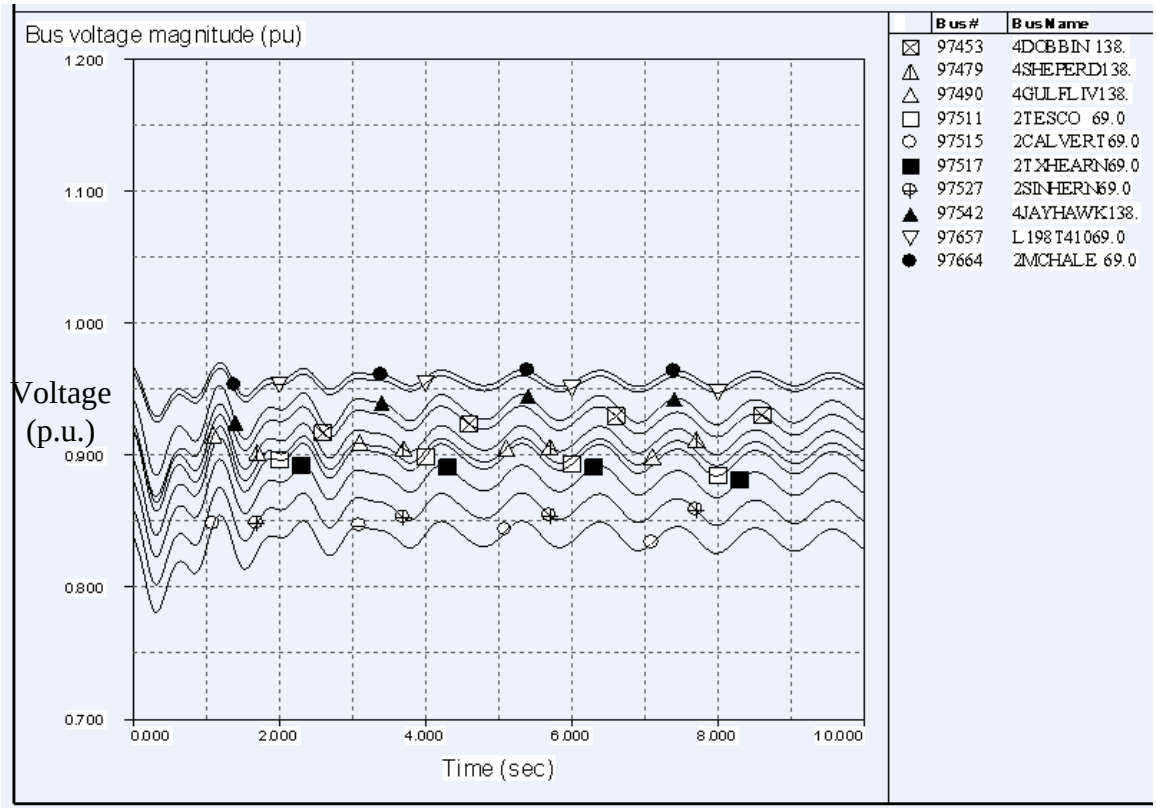


Figure 4.3 Voltage response in time domain after the 7Grimes – Grmxf line contingency

To further investigate the behavior of the Entergy system in time domain, contingencies which resulted in voltage instability in steady state analysis were also examined in TSAT.

The voltage responses of the buses were observed for a long period of time (10 seconds). The same power flow profiles were used in time domain analysis as were used in a steady state studies. After running the different scenarios in TSAT, most of the contingencies were found to have a huge impact on the voltages of the buses. Results of the different scenarios showed that the impact of some contingencies were severe and almost the whole system was affected in terms of low voltages. Even after 10 seconds of the occurrence of contingencies, the voltage of the buses were oscillating and it appeared that if the simulation time was increased, voltages would continue to behave in the same manner and would never come to a stable level.

The voltage response of one of the scenarios, in which the load is 30070 MW and the line outage considered is Grimes-Crockett (97513-53526) is shown in Figure 4.4. It was noticed that the whole system got affected by the contingency and the voltage responses of only a few buses are shown in the Figure 4.4 so that the figure is legible.



Time (s)

Figure 4.4 Voltage response of the buses in time domain after the Grimes-Crockett line contingency for load 30070 MW

The results obtained for this study shows that the contingencies which resulted in voltage instability in steady state analysis are also deemed critical by the time domain analysis and show significant voltage oscillations. These contingencies have a great impact on most of the EES system in terms of voltage, and the impact is so strong that the voltages of the buses oscillate for a long period of time showing the system is not voltage stable.

5. Summary, conclusions, and future research directions

5.1 Summary

The aim of this research is to use commercially available analysis tools to identify the weak zones or areas of the Entergy energy system (EES) which are prone to voltage instability. Two different static methods i.e. modal analysis technique and reactive reserve margin approach available in the software package VSAT are implemented to find the zones which push the EES into voltage instability or result in voltage magnitude problems. In the modal analysis method weak zones are identified by monitoring the participation factor of the buses in the critical modes. Zones which are identified as critical to voltage stability are zones 100, 101, 103, 105, 111 and 112. All of these zones are present in the same geographical neighborhood in the WOTAB region of EES.

In the reactive reserve margin method, reactive power reserves of the zones are used as an indictor of voltage instability. Single line outages, generator outages and double line outages are conducted and reactive power reserves of zones are monitored for each contingency. Contingencies which exhausted the reactive power reserves in the zone are identified as critical contingencies and the zone where the reactive reserve gets exhausted are identified as critical zones. Zones which are identified as critical by this method are 101, 102, 103, 106, 109, 120 and 160. Most of the zones are located in the WOTAB region of EES.

All the zones identified as critical are located in WOTAB region except zone 120 which is in the Amite South region and zone 160 which is in the Sheridan North region. The locations of the critical zones are indicated in the EES footprint in figure 5.1 below.

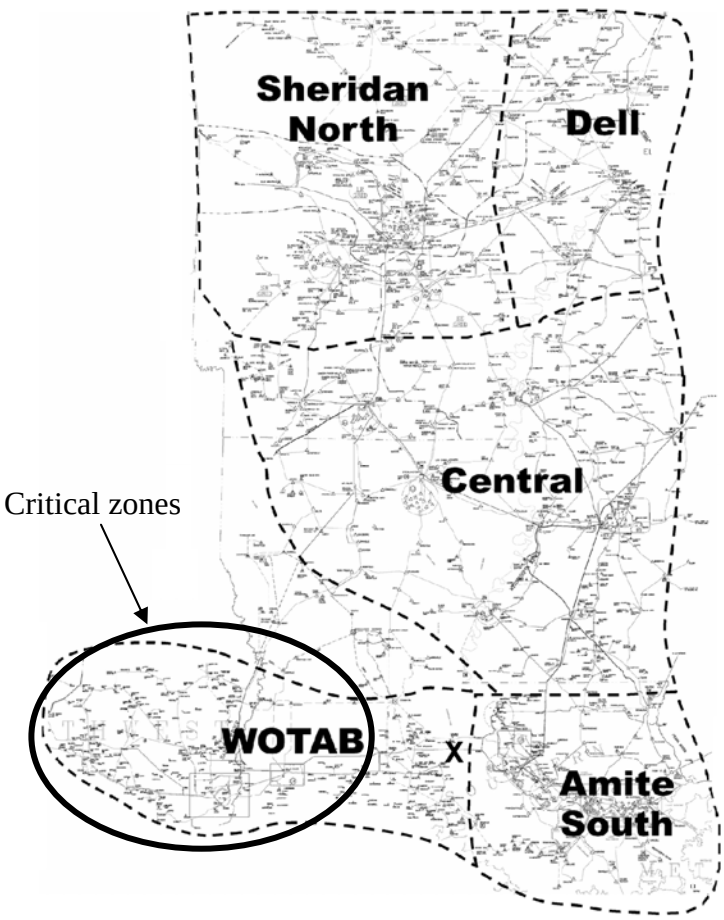


Figure 5.1 Critical zones in Entergy footprint

Sensitivity analyses are also performed and results are compared with the findings of the two methods discussed above. After comparing all the results, zone 100 of the southwestern EES region is identified as the most critical zone of the Entergy energy system.

5.2 Conclusion and observation

Several tools are available in the industry to assess the voltage stability of large and complex power systems. VSAT is one of these tools provided by Powertech Labs Inc., which analyzes voltage and reactive power flow problems using static power flow based methods.

VSAT uses modal analysis computation to pinpoint the buses which are responsible for the instability of the system by computing the bus participations from the eigenvectors of the reduced Jacobian matrix at the collapse point. VSAT also provides an

option of computing critical modes at different transfer levels as a system is stressed. This option provides the user the ability to observe and study how the critical modes of a power system are changing as a system is stressed. But VSAT can only compute the ten most critical modes of a power system and does not provide the option to find the critical modes of a particular region or zone. In this study, power flow data provided by EES consists of 31 areas and EES is one of those areas. During the modal analysis study, some critical modes also appeared from other areas which were meaningless and ignored in this study as we were only interested in finding the critical modes of the EES area. Options for calculating the critical modes of a particular area instead of a whole system would have provided more in depth assessment and analysis of the EES.

After implementing the modal analysis technique on the EES using VSAT, weak buses were identified. Sensitivity analysis was performed to verify if the results obtained by modal analysis are reasonable and accurate. TSAT is then used to observe the response of the bus voltages in time domain after the perturbation of the total load. The comparison between the trajectory sensitivities and modal analysis discussed in chapter 5 showed good agreement with each other. The results obtained during the research showed that the modal analysis method of VSAT can be implemented in a large system to identify the regions prone to voltage instability.

Addition of an extra feature i.e. identification of modes in a particular region or area in VSAT also discussed above, would provide a better and in-depth voltage stability view point of a large power systems.

Another criterion which can be used by the user in VSAT is the measure of reactive power reserves at specified zones of a system pre and post contingency. This method is also implemented in the EES to find the zones prone to voltage instability. According to the results and observation, this method is not a very good indictor of voltage instability in a very large system such as EES. Large power systems consist of many zones e.g. EES consists of 28 zones and some zones are larger than other in terms of size. Reactive power is a local phenomenon and can not be transferred over a long distance. Therefore if there is a voltage problem at one end of the zone but reactive power reserves are present at the other end of the zone, VSAT will not identify that zone as a troubled zone because of the presence of reactive power reserves in a zone. Similarly if a zone is very small in size, exhaustion of the reactive power will not affect the zone as it will obtain the reactive power from the neighboring zones if the neighboring zones have abundant reactive power reserves. In this study both scenarios were identified. Zone 112 is a large zone with 187 AC buses and it has sufficient reactive reserves at the peak load case therefore it is not identified as weak zone in the reactive power reserve margin method but sensitivity analysis in time domain and modal analysis showed that there are some buses which are very prone to voltage instability. On the other hand zone 120 consists of only 20 AC buses and none of these buses were identified as weak buses in modal analysis and sensitivity studies although zone 120 has no reactive power reserves at the peak load case.

From the results obtained during this research, it is observed that the reactive power reserve of a zone of a large system is not a very good indicator of voltage instability. One suggestion would be to develop an algorithm such that the system can be divided into clusters of buses instead of the zones and each cluster should have sufficient reactive power sources for specific load patterns under a range of contingencies.

5.3 Future research directions

Identification of critical contingencies and zones has been made based on modal analysis and reactive reserves method. Consistency of the results can be checked with the application of other static voltage stability analysis techniques such as loading margin.

Time domain simulations can be carried out to confirm the critical contingencies identified in static analysis.

Bifurcation (saddle node and Hopf) studies [3] can be done to determine the system loading margin and action to increase the margin based on those criteria.

Preventive and corrective actions to mitigate voltage collapse resulting from the identified contingencies can be determined. Optimal location for reactive power sources to enhance voltage security of the system can also be determined.

References

[1] IEEE/CIGRE Joint task force on Stability Terms and Definitions, "Definitions and classifications of power system stability," *IEEE Trans. Power Systems*, vol. 19, no. 2, pp. 1387-1401, May 2004.

[2] P. Kundur, *Power system stability and control*, MC Graw Hill, New York, 1994.

[3] IEEE Power Engineering Society, "Voltage stability assessment: Concepts, practices and tools," Power System Stability Subcommittee Special Publication, Aug. 2002.

[4] G. K. Morison, B. Gao, P. Kundur, " Voltage stability analysis using static and dynamic approaches," *IEEE Trans. Power Systems*, vol. 8, no. 3, pp. 1159-1171, Aug. 1993.

[5] G. M Huang, N C Nair, "Detection of dynamic voltage collapse," IEEE/PES summer meeting, 2002.

[6] "Suggested techniques for voltage stability analysis," technical report 93TH0620-5PWR, IEEE/PES, 1993.

[7] "Indices predicting voltage collapse including dynamic phenomena," technical report TF 38-02-11, CIGRE, 1994.

[8] V. Ajjarapu, C. Christy, "The continuation power flow: A tool for steady state voltage stability analysis," *IEEE Trans. Power Systems*, vol. 7, no. 1, pp. 416-423, Feb. 1992.

[9] Powertech Labs Inc., Power Flow Program 5.0, Surrey, British Columbia, Canada.

[10] Arthur R. Bergen, Vijay Vittal, *Power systems analysis 2nd edition*, Prentice Hall, 2000.

[11] B. Gao, G.K. Morison, P. Kundur, "Voltage stability evaluation using modal analysis", IEEE Transactions on Power Systems, Vol. 7, No. 4. November 1992.

[12] S. Kolluri, A. Kumar, K. Tinnium, R. Daquila, "Innovative approach for solving dynamic voltage stability problem on the Entergy system," Power Engineering Society Summer Meeting, Vol. 2, pp. 988-993, July 25-25 2002.

[13] Sujit Mandal, Sharma Kolluri, "SVC application in Entergy system," Presented at the PES Substations Committee Meeting, April 5, 2004.

[14] Feng Dong, Badrul H. Chowdhury, Mariesa L. Crow, Levent Acar, "Improving voltage stability by reactive power reserve management," *IEEE Trans. Power Systems*, vol. 20, no. 1, pp. 338-345, Feb. 2005.

[15] Lixin Bao, Zhenyu Huang, Wilsun Xu, "Online voltage stability monitoring using VAr reserves," *IEEE Trans. Power Systems*, vol. 18, no. 4, pp. 1461-1469, Nov. 2003.

[16] L.C.P. Da Silva, V.F. da Costa, W. Xu, "Preliminary results on improving the modal analysis technique for voltage stability assessment," IEEE Power Engineering Society Summer Meeting, 2003.

[17] T. Van Cutsem, "A method to compute reactive power margins with respect to voltage collapse", *IEEE Trans. Power Systems*, vol. 6, no. 1, pp. 145-156, Feb. 1999.

[18] R. A. Schlueter, I. Hu, M.W. Chang, J.C. Lo, A. Costi, " Methods for determining proximity to voltage collapse," *IEEE Trans. Power Systems*, vol. 6, no. 1, pp. 285-292, Feb. 1991.

[19] G.C. Ejebe, H.P. Van Meteren, B.F. Wollenberg, "Fast contingency screening and evaluation for voltage security analysis," *IEEE Trans. Power Systems*, vol. 3, no. 4, pp. 1582-1590, Nov. 1988.

[20] C. L. Demarco, T.J. Overbye, "An energy based security measure for assessing vulnerability to voltage collapse," *IEEE Trans. Power Systems*, vol. 5, no. 2, pp. 419-427, May 1990.

[21] V. Ajjarapu, "Identification of steady state voltage stability in power systems," Int. J. of Electric Power and Energy Systems, vol. 11, pp. 43-46, 1991.

[22] S. Abe, Y. Fukunaga, A. Isono, B. Kondo, "Power system voltage stability," IEEE Transaction on Power Apparatus and Systems, Vol. PAS-101, no. 10, October 1982.

Appendix 1: Complete results of the modal analysis and reactive reserve margin studies conducted on the Entergy energy system.

The details of the modal analysis results are summarized for loading scenario I in Tables A.1 and A.2 and results details of loading scenario II are summarized in Tables A.3 through A.6. Critical modes of the both cases are discussed earlier in the report.

Table A.1 Mode 2 with eigenvalue = 0.12727 – Loading Scenario I

Bus No.	Bus Name	Area	Zone	Participation factor
99187	3MURRLA	EES	140	0.95603
99185	MURRU56	EES	140	0.95603
99183	MURRU12	EES	140	0.95603
99184	MURRU34	EES	140	0.95603
99186	MURRU78	EES	140	0.67412
97305	3BLKRVR	LAGN	999	0.67406
50408	JNESVIL3	LEPA	999	0.61801
99117	3PLANT	EES	140	0.58430
50409	VIDALIA3	LEPA	999	0.55625
99119	3SFERTAP	EES	140	0.54836
97326	3PMILL	LAGN	999	0.52104
99022	3NAT-IN	EES	152	0.48679
99024	3NAT-S	EES	152	0.47481
99021	3IP.CO.	EES	152	0.45541
99020	3J.MANV	EES	152	0.42770
99023	3NATCHZ	EES	152	0.41102
99018	NAT-GND	EES	152	0.40759
99016	3EPA-PNR	EES	152	0.40634
99026	3EPA-KIN	EES	152	0.40631
99019	3P.RDG*	EES	152	0.39843
995	3NA-SE*	EES	152	0.39720
99017	3NATSES	EES	152	0.39460
99118	3REDGUM	EES	140	0.35231
99044	3WSHTN*	EES	152	0.28094
99105	3METRPLS	EES	140	0.28035
99038	3WOODVL	EES	152	0.27248
99120	3WISNER	EES	140	0.25496
99037	3CTRVIL	EES	152	0.25445
99034	3CROSBY	EES	152	0.24420
97307	3GILBRT	LAGN	999	0.23755
99015	3FAYETE	EES	152	0.21258
99033	3GLOSTR	EES	152	0.19386
99043	3ROXIE	EES	152	0.18655

Table A.2 Mode 5 with eigenvalue = 0.17387 – Loading Scenario I

Bus No.	Bus Name	Area	Zone	Participation factor
98082	1PPG A7	EES	112	1.00000
98081	1PPA LD2	EES	112	0.75147
98080	1PPA LD1	EES	112	0.72663
98086	1ZIGZAG1	EES	112	0.61659
98087	1ZIGZAG2	EES	112	0.61659
98076	1PPA T3	EES	112	0.58623
98079	1PPGA1A3	EES	112	0.54954
98062	1PPG C3	EES	112	0.53554
98059	1CSYNCH	EES	112	0.53293
98061	1PPG C2	EES	112	0.53277
98060	1PPG C1	EES	112	0.53276
98088	1ZIGZAGG	EES	112	0.39019
98078	1PPA T1	EES	112	0.37484
98072	1PPG R1	EES	112	0.32827
98068	1VCMII 1	EES	112	0.31334
98067	1VCMII 2	EES	112	0.31258
98074	2PPG R2	EES	112	0.29377
98073	2PPG R3	EES	112	0.29050
98091	1RSCO R4	EES	112	0.20743
98089	1RSCO R6	EES	112	0.20435
98083	1PPA T1	EES	112	0.20369
98071	2RIVS SO	EES	112	0.20016
98075	2RVIS NO	EES	112	0.19998
98093	2CT6	EES	112	0.19785
98092	2CT5	EES	112	0.19750
98066	2VCMII 2	EES	112	0.19537
98065	2VCMII 1	EES	112	0.19501
98090	1RSCO R5	EES	112	0.18612
98052	2PPC SO	EES	112	0.16335
98051	2PPC NO	EES	112	0.16310
98053	2CEXPSP	EES	112	0.16298
98054	2CEXPCP	EES	112	0.16286
98058	1PPG C5	EES	112	0.15338
98057	1PPG C4	EE	112	0.15326

Table A.3 Mode 4 with eigenvalue = 0.18724 – Loading Scenario II

Bus No.	Bus Name	Area	Zone	Participation factor
97515	2CALVERT	EES	100	1.00000
97527	2SINHERN	EES	100	0.77733
97516	2HEARNE	EES	100	0.56474
97517	2TXHEARN	EES	100	0.54959
97525	2HUMBHRN	EES	100	0.51328
97523	2APLHERN	EES	105	0.49064
97807	6WEIRGAT	EES	105	0.43883
97806	6HORWEIR	EES	105	0.35808
97808	6HORTON	EES	105	0.35021
97511	2TESCO	EES	105	0.28331
97810	6TEMPL2	EES	105	0.24158
97809	6TEMPL1	EES	105	0.23923
97804	6TEMPLSW	EES	105	0.23846
97805	6PINELOW	EES	100	0.22534
97504	2BRYAN B	EES	105	0.15734
97640	2BLUWATR	EES	100	0.14259
97501	2CALDWEL	EES	105	0.13421
97761	2SNDYSHR	EES	100	0.13159
97505	2BRYAN A	EES	105	0.10940
97813	4ETOIL	EES	10	0.10402
97812	4BROADUS	EES	100	0.10122

Table A.4 Mode 5 with eigenvalue = 0.2010 – Loading Scenario II

Bus No.	Bus Name	Area	Zone	Participation factor
98082	1PPG A7	EES	112	1.000
98081	1PPA LD2	EES	112	0.83451
98080	1PPA LD1	EES	112	0.81637
98087	1ZIGZAG2	EES	112	0.72790
98086	1ZIGZAG1	EES	112	0.72787
98077	1PPA T2	EES	112	0.69300
98076	1PPA T3	EES	112	0.69296
98062	1PPG C3	EES	112	0.61241
98059	1CSYNCH	EES	112	0.61023
98063	1PPC C25	EES	112	0.61014
98064	1PPC C32	EES	112	0.61014
98061	1PPG C2	EES	112	0.60997
98060	1PPG C1	EES	112	0.60996
98079	1PPGA1A3	EES	112	0.60596
98088	1ZIGZAGG	EES	112	0.48252
98078	1PPA T1	EES	112	0.46365
98068	1VCMII 1	EES	112	0.42974
98067	1VCMII 2	EES	112	0.42899
98072	1PPG R1	EES	112	0.40843
98074	2PPG R2	EES	112	0.37076
98073	2PPG R3	EES	112	0.36850
98091	1RSCO R4	EES	112	0.29509
98089	1RSCO R6	EES	112	0.29005
98085	1PPA T2	EES	112	0.28869
98084	1PPA T3	EES	112	0.28861
98083	1PPA T1	EES	112	0.28857
98075	2RVIS NO	EES	112	0.28443
98071	2RIVS SO	EES	112	0.28390
98090	1RSCO R5	EES	112	0.28234
98092	2CT5	EES	112	0.28162
98093	2CT6	EES	112	0.28092

Table A.5 Mode 6 with eigenvalue = 0.2227 – Loading Scenario II

Bus No.	Bus Name	Area	Zone	Participation factor
97807	6WEIRGAT	EES	105	1.0000
97806	6HORWEIR	EES	105	0.79403
97808	6HORTON	EES	105	0.77374
97810	6TEMPL2	EES	105	0.49931
97809	6TEMPL1	EES	105	0.49345
97804	6TEMPLSW	EES	105	0.49168
97805	6PINELOW	EES	105	0.46013
97813	4ETOIL	EES	105	0.17497
97812	4BROADUS	EES	105	0.16939
97811	4PINELND	EES	105	0.15800
97640	2BLUWATR	EES	105	0.15480
97761	2SNDYSHR	EES	105	0.14132
97515	2CALVERT	EES	100	0.12058

Table A.6 Mode 7 with eigenvalue = 0.2381 – Loading Scenario II

Bus No.	Bus Name	Area	Zone	Participation factor
98042	2LKARTHR	EES	112	1.0000
98041	2KLONDKE	EES	112	0.94614
98169	2MORSE	EES	111	0.80710
98167	2GUEYDAN	EES	111	0.78284
98168	2L-270TP	EES	111	0.77308
98166	2CAMPBEL	EES	111	0.74748
98165	2L610TP	EES	111	0.28202
98164	4ETOIL	EES	111	0.04711

The following tables provide the details of the reactive power reserves analysis. Three cases with loads 10010 MW, 18000 MW and 30070 MW are discussed in chapter 4 while the results of the remaining cases are given below. Reactive reserves of the zones which are less than 20% in a base case are provided for each load case with the zones contingencies which violate the criteria.

Load = 11220 MW

Table B.1 Reactive power reserves in base case – 11220 MW

Zone	MVAr Output	Reserve
120	212.85	0.0 %
160	112.25	0.0 %
109	79.29	0.0 %

Load = 12000 MW

Table B.2 Reactive power reserves in base case – 12000 MW

Zone	MVAr Output	Reserve
120	208.52	0.0 %
108	52.53	0.0 %

Load = 13000 MW

Table B.3 Reactive power reserves in base case – 13000 MW

Zone	MVAr Output	Reserve
120	207.90	0.0 %
108	81.21	6.6 %

Table B.4 Single line outages – 13000 MW

Line	Zone	MVAr Output	Reserve
99520-99522 (Zone 160-160)	160	87.04	0.0 %

Table B.5 Double line outages – 13000 MW

Contingency	Zone	MVAr Output	Reserve
97554-97514 '1' (Zone 111-100) 97554-97514 '2'	108	85.97	0.0 %
97854 97837 '1' (Zone 111-100) 97854 97837 '2'	108	86.32	0.0 %
98097 98108 '1' (Zone 111-111) 98097 98108 '2'	108	86.01	0.0 %

Load = 14000 MW

Table B.6 Reactive power reserves in base case – 14000 MW

Zone	MVAr Output	Reserve
120	215.25	0.0%
160	114.24	0.0%
130	359.77	19.4%
123	68.89	0.0%
108	54.40	0.0%

Load = 15000 MW

Table B.7 Reactive power reserves in base case – 15000 MW

Zone	MVAr Output	Reserve
120	215.63	0.0%
160	113.45	0.0%
130	358.37	19.4%
109	78.29	0.0%
123	68.73	0.0%
108	54.46	0.0%

Load = 16000 MW

Table B.8 Reactive power reserves in base case – 16000 MW

Zone	MVAr Output	Reserve
120	214.88	0.0%
101	146.85	0.0%
160	112.61	0.0%
130	356.39	19.4%
109	77.86	0.0%
123	68.52	0.0%
108	54.40	0.0%

Load = 17000 MW

Table B.9 Reactive power reserves in base case – 17000 MW

Zone	MVAr Output	Reserve
120	213.22	0.0%
102	170.52	0.0%
101	144.45	0.0%
160	111.71	0.0%
130	353.48	19.5%
109	76.62	0.0%
123	68.24	0.0%
108	54.17	0.0%

TableB.10 Single line outages – 17000 MW

Line	Zone	MVAr Output	Reserve
53526-97513 (Zone 999-100)	112	200.55	4.0 %
97513-97554 (Zone 100-111)	112	200.85	4.0 %
97717-99162 (Zone 105-140)	112	203.33	4.0 %
97916-97917 (Zone 112-105)	112	202.09	3.9 %

Table B.11 Double line outages – 17000 MW

Contingency	Zone	MVAr Output	Reserve
97554-97514 '1' (Zone 111-100) 97554-97514 '2'	112	201.00	4.0 %

Load = 19000 MW

Table B.12 Reactive power reserves in base case – 19000 MW

Zone	MVAr Output	Reserve
105	486.58	9.2 %
120	210.77	0.0 %
102	168.57	0.0 %
101	144.10	0.0 %
106	95.67	0.0 %
130	345.45	19.5 %
109	75.09	0.0 %
108	53.13	0.0 %
160	104.02	14.4 %

Table B.13 Generators outages – 19000 MW

Bus	Zone	MVAr Output	Reserve
99489(Zone 162)	162	425.40	7.5 %

Table B.14 Single line outages – 19000 MW

Line	Zone	MVAr Output	Reserve
97717-97916 (Zone 105-105)	105	480.32	9.5 %
	112	281.28	0.0 %
99486-99489 (Zone 162-162)	105	485.88	9.2 %
	162	425.80	7.5 %

Table B.15 Double line outages – 19000 MW

Contingency	Zone	MVAr Output	Reserve
99148-99203 '1' (Zone 140-140) 99148-99203 '2'	112	282.12	0.6 %
99565-99566 '1' (Zone 160-160) 99565-99566 '2'	160	112.86	0.0 %

Load = 20000 MW

Table B.16 Reactive power reserves in base case – 20000 MW

Zone	MVAr Output	Reserve
120	209.84	0.0 %
105	597.31	16.4 %
102	167.73	0.0 %
101	143.64	0.0 %
106	96.10	0.0 %
109	76.64	0.0 %
130	344.58	19.5 %
160	103.08	14.6 %

Table B.17 Generators outages – 20000 MW

Bus	Zone	MVAr Output	Reserve
97572 (Zone 105)	112	281.28	2.5 %
97772 (Zone 108)	108	53.00	18.5 %

Table B.18 Single line outages – 20000 MW

Line	Zone	MVAr Output	Reserve
97717-97916 (Zone 105-105)	112	283.20	2.5 %
97717-99162 (Zone 105-140)	112	283.22	2.5 %
99197-99486 (Zone 140-162)	162	705.16	9.7 %
97572-97705 (Zone 105-105)	112	281.48	2.5 %
99486-99489 (Zone 162-162)	162	423.40	7.6 %

Load = 21000 MW

Table B.19 Reactive power reserves in base case – 21000 MW

Zone	MVAr Output	Reserve
105	611.16	12.2 %
120	208.87	0.0 %
102	165.56	0.0 %
101	141.38	0.0 %
109	75.44	0.0 %
130	343.69	19.6 %
160	102.93	14.6 %

Table B.20 Generators outages – 21000 MW

Bus	Zone	MVAr Output	Reserve
97451 (Zone 103)	112	338.72	3.1 %
97452 (Zone 103)	112	338.72	3.1 %
97572 (Zone 105)	112	333.79	0.8 %
97911 (Zone 112)	112	289.02	4.1 %
98061 (Zone 112)	112	298.65	8.0 %
98062 (Zone 112)	112	298.65	8.0 %

Table B.21 Single line outages – 21000 MW

Line	Zone	MVAr Output	Reserve
97717-97916 (Zone 105-105)	112	338.74	2.1 %
	108	82.81	4.8 %
97451-97461 (Zone 103-103)	112	338.33	3.2 %
97572-97705 (Zone 105-105)	112	333.38	0.9 %
97583-97772 (Zone 108-108)	108	57.88	8.3 %
97918-97911 (Zone 112-112)	112	288.95	4.2 %
97918-97912 (Zone 112-112)	112	288.84	4.2 %

Table B.22 Double line outages – 21000 MW

Contingency	Zone	MVAr Output	Reserve
98032-98031 '1' (Zone 112-112) 98032-98031 '2'	112	314.69	7.1 %
99148-99203 '1' (Zone 140-140) 99148-99203 '2'	111	338.12	2.9 %

Load = 22000 MW

Table B.23 Reactive power reserves in base case – 22000 MW

Zone	MVAr Output	Reserve
120	239.21	1.6 %
102	166.24	0.0 %
101	143.13	0.0 %
109	77.54	0.0 %
130	343.13	19.6 %
160	105.81	19.5 %

Table B.24 Generators outages – 22000 MW

Bus	Zone	MVAr Output	Reserve
97573 (Zone 105)	105	619.07	9.6 %
97829 (Zone 106)	106	93.11	0.0 %

Table B.25 Single line outages – 22000 MW

Line	Zone	MVAr Output	Reserve
97573-97705 (Zone 105-105)	105	619.13	9.6 %
99562-99563 (Zone 221-162)	120	238.96	1.7 %
	160	119.22	5.5 %
99565-99566 (Zone 160-160)	120	238.98	1.7 %
	160	120.94	3.4 %

Table B.26 Double line outages – 22000 MW

Contingency	Zone	MVAr Output	Reserve
99312-99341 '1' (Zone 161-161) 99312-99341 '2'	160	119.69	5.3 %
99565-99566 '1' (Zone 160-160) 99565-99566 '2'	160	119.85	0.0 %
99572-99571 '1' (Zone 162-162) 99572-99571 '2'	160	119.13	5.5 %
99572-99571 '1' (Zone 162-162) 99572-99571 '3'	160	119.13	5.5 %
99572-99571 '2' (Zone 162-162) 99572-99571 '3'	160	119.13	5.5 %

Load = 23000 MW

Table B.27 Reactive power reserves in base case – 23000 MW

Zone	MVAr Output	Reserve
20	240.16	0.8 %
102	164.06	0.0 %
101	140.99	0.0 %
160	119.43	5.6 %
109	76.48	0.0 %

Table B.28 Generators outages – 23000 MW

Bus	Zone	MVAr Output	Reserve
97573 (Zone 105)	105	634.50	12.7 %
	106	120.59	3.3 %
	108	85.40	1.5 %
97829 (Zone 106)	106	95.12	0.0 %

Table B.29 Single line outages – 23000 MW

Line	Zone	MVAr Output	Reserve
97573-97705 (Zone 105-105)	106	10.64	3.2 %
	160	119.45	5.6 %
	108	85.61	1.2 %
97757-97829 (Zone 106-106)	106	95.13	0.0 %

Table B.30 Double line outages – 23000 MW

Contingency	Zone	MVAr Output	Reserve
97702-97757 '1' (Zone 105-106) 97702-97757 '2'	106	117.80	9.7 %

Load = 24000 MW

Table B.31 Reactive power reserves in base case – 24000 MW

Zone	MVAr Output	Reserve
120	240.96	0.0 %
102	161.94	0.0 %
101	138.96	0.0 %
160	119.33	5.3 %
109	75.63	0.0 %

Table B.32 Generators outages – 24000 MW

Bus	Zone	MVAr Output	Reserve
97573 (Zone 105)	101	673.31	8.6 %
	108	84.63	0.0 %
97829 (Zone 106)	106	93.32	0.0 %

Table B.33 Single line outages – 24000 MW

Line	Zone	MVAr Output	Reserve
97916-98107 (Zone 112-111)	105	919.50	10.5 %
	112	500.72	6.7 %
97573-97705 (Zone 105-105)	1051	673.39	8.6 %
97757-97829 (Zone 106-106)	106	93.30	0.0 %

Table B.34 Double line outages – 24000 MW

Contingency	Zone	MVAr Output	Reserve
97554-97514 '1' (Zone 111-100)	105	938.45	4.5 %
97554-97514 '2'	112	498.04	8.9 %
	103	432.52	8.3 %
	106	116.94	0.0 %
97702-97757 '1' (Zone 105-106)	106	122.20	4.4 %
97702-97757 '2'			

Load = 25000 MW

Table B.35 Reactive power reserves in base case – 25000 MW

Zone	MVAr Output	Reserve
120	240.34	0.0 %
102	161.58	0.0 %
101	139.21	0.0 %
160	119.23	4.9 %
109	76.75	0.0 %
162	756.16	23.3 %
104	151.51	24.8 %

Table B.36 Generators outages – 25000 MW

Bus	Zone	MVAr Output	Reserve
97829 (Zone 106)	106	95.33	0.0 %

Table B.37 Single line outages – 25000 MW

Line	Zone	MVAr Output	Reserve
97757-97829 (Zone)	106	95.33	0.0 %

Table B.38 Double line outages – 25000 MW

Contingency	Zone	MVAr Output	Reserve
97702-97757 '1' (Zone 105-106) 97702-97757 '2'	106	120.81	7.2 %
99565-99566 '1' (Zone 160-160) 99565-99566 '2'	160	118.64	0.0 %

Load = 26000 MW

Table B.39 Reactive power reserves in base case – 26000 MW

Zone	MVAr Output	Reserve
162	794.67	17.1 %
120	238.42	0.0 %
102	159.85	0.0 %
101	137.85	0.0 %
160	115.54	0.0 %
109	76.37	0.0 %
130	339.98	19.7 %

Table B.40 Generators outages – 26000 MW

Bus	Zone	MVAr Output	Reserve
97772 (Zone 108)	108	59.26	6.0 %
97829 (Zone 106)	104	94.71	0.0 %

Table B.41 Single line outages – 26000 MW

Line	Zone	MVAr Output	Reserve
97842-97844 (Zone 109-109)	106	117.38	9.6 %
97583-97772 (Zone 108-108)	108	59.24	6.1 %

Table B.42 Double line outages – 26000 MW

Contingency	Zone	MVAr Output	Reserve
97554-97514 '1' (Zone 111-100) 97554-97514 '2'	103	432.11	8.3 %
97702-97757 '1' (Zone 105-106) 97702-97757 '2'	106	124.54	3.5 %

Load = 27000 MW

Table B.43 Reactive power reserves in base case – 27000 MW

Zone	MVAr Output	Reserve
120	237.11	0.0 %
102	159.93	0.0 %
101	136.33	0.0 %
160	115.09	0.0 %
109	75.98	0.0 %
130	339.16	19.7 %

Table B.44 Generators outages – 27000 MW

Bus	Zone	MVAr Output	Reserve
97772 (Zone 108)	108	62.39	0.7 %

Table B.45 Single line outages – 27000 MW

Line	Zone	MVAr Output	Reserve
97513-97554 (Zone 100-111)	105	1235.29	9.2 %
	103	421.31	7.7 %
	106	114.35	4.9 %
97583-97772 (Zone 108-108)	108	62.47	0.5 %

Table B.46 Double line outages – 27000 MW

Contingency	Zone	MVAr Output	Reserve
97554-97514 '1' (Zone 111-100)	105	1235.23	9.2 %
97554-97514 '2'	103	421.32	7.7 %
	106	114.35	4.9 %
97702-97757 '1' (Zone 105-106)	106	127.83	0.0 %
97702-97757 '2'			

Load = 28000 MW

Table B.47 Reactive power reserves in base case – 28000 MW

Zone	MVAr Output	Reserve
162	927.00	17.3 %
120	236.24	0.0 %
102	155.57	0.0 %
101	134.85	0.0 %
160	114.56	0.0 %
109	75.52	0.0 %
106	106.86	19.2 %

Table B.48 Generators outages – 28000 MW

Bus	Zone	MVAr Output	Reserve
97772 (Zone 108)	108	62.79	0.0 %

Table B.49 Single line outages – 28000 MW

Line	Zone	MVAr Output	Reserve
97573-97705 (Zone 105-105)	106	115.07	9.9 %
	108	80.01	9.0 %
97583-97772 (Zone 105-108)	108	62.79	0.0 %
97605-97617 (Zone 108-108)	108	79.99	9.8 %
99651-99648 (Zone 162-162)	162	867.33	6.9 %

Table B.50 Double line outages – 28000 MW

Contingency	Zone	MVAr Output	Reserve
97554-97514 '1' (Zone 111-100)	103	411.15	7.2 %
97554-97514 '2'	106	117.19	1.6 %
97702-97757 '1' (Zone 105-106)	106	126.88	0.0 %
97702-97757 '2'			

Load = 29000 MW

Table B.51 Reactive power reserves in base case – 29000 MW

Zone	MVAr Output	Reserve
120	234.88	0.0 %
162	966.43	20.0 %
102	153.50	0.0 %
101	133.34	0.0 %
160	123.20	0.0 %
109	75.31	0.0 %

Table B.52 Single line outages – 29000 MW

Line	Zone	MVAr Output	Reserve
97463-97467 (Zone 102-104)	103	431.65	8.4 %
97567-97714 (Zone 104-105)	103	433.07	8.4 %

Optimal Allocation of Static and Dynamic VAR Resources

Volume 2

Prepared by

V. Ajjarapu
Iowa State University

Information about this project

For information about this volume contact:

V. Ajjarapu
Iowa State University
Electrical and Computer Engineering Dept.
Ames, Iowa 50011
Phone: 515-294-7687
Fax: 515-294-4263
Email: vajjarap@iastate.edu

Power Systems Engineering Research Center

This is a project report from the Power Systems Engineering Research Center (PSERC). PSERC is a multi-university Center conducting research on challenges facing the electric power industry and educating the next generation of power engineers. More information about PSERC can be found at the Center's website: http://www.pserc.org.

For additional information, contact:

Power Systems Engineering Research Center
Arizona State University
577 Engineering Research Center
Box 878606
Tempe, AZ 85287-8606
Phone: 480-965-1643
FAX: 480-965-0745

Notice Concerning Copyright Material

PSERC members are given permission to copy without fee all or part of this publication for internal use if appropriate attribution is given to this document as the source material. This report is available for downloading from the PSERC website.

© 2008 Georgia Institute of Technology, Arizona State University, Iowa State University, and the Board of Regents of the University of Wisconsin System. All rights reserved.

TABLE OF CONTENTS

CHAPTER 1. INTRODUCTION 1

1.1 Voltage Stability 2
1.2 Report Organization 4

CHAPTER 2. CONTINGENCY ASSESSMENT FOR VOLTAGE DIP AND SHORT TERM VOLTAGE INSTABILITY ANALYSIS 6

2.1 Introduction 6
2.2 Contingency Assessment 12
2.2.1 Filtering Block 13
2.2.2 Ranking Block 17
2.3 Assessment and Control 22
2.4 Results 23
2.5 Conclusions 26

CHAPTER 3. OPTIMAL ALLOCATION OF DYNAMIC VAR USING MIXED INTEGER TRAJECTORY OPTIMIZATION 28

3.1 Introduction 28
3.2 Problem Formulation 31
3.2.1 Trajectory optimization for primal problem 34
3.2.2 Simulated Annealing for master problem 39
3.3 Results 40
3.3.1 2-Bus system 40
3.3.2 IEEE 39 Bus system 42
3.4 Conclusions 45

CHAPTER 4. CONTRIBUTIONS 46

4.1 Publications related to proposed research 46

LIST OF FIGURES

Figure 1.1 Voltage performance parameters for NREC/WECC planning standards..... 3
Figure 2.1 . Flow Chart of the Proposed Contingency Filtering, Ranking and Assessment Technique..... 12
Figure 2.2 Inner Layout of Filtering Block..... 15
Figure 2.3 Inner layout of Ranking Block 18
Figure 3.1 Simulated Annealing and Trajectory Optimization formulation for optimal allocation..... 34
Figure 3.2 Power system trajectory optimization concept..... 34
Figure 3.3 2-Bus power system diagram. 41
Figure 3.4 Trajectories after disturbance without control..... 42
Figure 3.5 Constrained optimal trajectories with reactive power compensation..... 42
Figure 3.6 Voltage trajectory after disturbance. 43
Figure 3.7 Voltage trajectory after control. 44

LIST OF TABLES

Table 2.1 Output of Filtering Block..... 25
Table 2.2 Output of Ranking Block (CSI)..... 25
Table 2.3 Ranking of buses based on DBVVI..... 26
Table 3.1 Different feasible solutions..... 44

CHAPTER 1. INTRODUCTION

Electric power industry has changed and evolved from vertically integrated structure to de-regulated electricity market. This new reform has changed the way utilities behave in the current power market. The generator owners want to make maximum use of their generating facility by running the generators to its limit. Transmission line owners want to maximize their revenues by using every MW of transmission line capacity. This has led to stressing of power system equipments and making power system more critical.

On one side where this privatization of power industry is going on with a rapid pace there is lack of incentive from market participants on making the power system robust. The present state of power system is not comforting as the old generation units are aging. The new generation units are sited based upon the availability of resource such as wind or natural gas, thus making them far away from load centers. Also, there is very less incentive towards transmission line expansion due to political and financial reasons. In addition to all these problems there are contingencies in the system such as line outage, transformer outage or generator outage which lead the system to stressed level to the extent of collapse. These all problems lead to instability of power system and are a threat to reliable and secure power delivery.

During contingency the system may experience severe voltage dip problem, low voltage problem, voltage instability or complete voltage collapse. During past few decades, power industries all over the world have witnessed voltage instability related system failures. In 1965 Northeast blackout in North America, eastern coast interconnection separated into several areas and 30 millions people were affected [1]. In the August 14, 2003 Northeast blackout in North America, power supply to 50 million people was interrupted and the financial losses were estimated between 4 billion and 6 billion U.S. dollars [2, 3]. In order to ensure the reliability and stability of power system proper control action is needed.

1.1 Voltage Stability

Like any other dynamical system it is advantageous to classify power system stability based upon physical phenomena. In the IEEE/CIGRE report [4], classification of power system stability is done based upon different criteria. Power system stability can be classified based upon:

- Physical nature of instability: rotor angle stability, frequency stability and voltage stability
- Size of disturbance: small-disturbance stability (load increase) and large-disturbance stability (contingency)
- Time of stability: short-term stability and long-term stability

All the 3 above mentioned stability problems can lead to system instability [5]. However, as mentioned above voltage instability has been a cause of several blackouts worldwide [4, 5]. In this work, the focus is on voltage stability related problem. The proposed definition of voltage stability in [5] is:

Voltage stability refers to the capability of a power system for maintenance of steady voltages at all buses in the system subjected to a disturbance under given initial operating conditions.

Contingencies are a major threat to power system stability. In order to ensure system reliability NERC (North American Electric Reliability Corporation)/WECC (Western Electricity Coordinating Council) [6] has a minimum post-disturbance performance specifications w.r.t. to voltage. During a contingency or disturbance, system may experience voltage dip/swell [7]. Excessive voltage deviation from normal permissible limit may cause voltage collapse [8]. Reference [9] summarizes NERC/WECC voltage dip criteria following a fault.

The WECC voltage dip criteria are specified as: (A) no contingency, (B) an event

resulting in the loss of a single element, (C) event(s) resulting in the loss of two or more (multiple) elements, and (D) an extreme event resulting in two or more (multiple) elements removed or cascading out of service conditions, as follows:

- NERC Category A: Not applicable.
- NERC Category B: Not to exceed 25% at load buses or 30% at non-load buses. Not exceed 20% for more than 20 cycles at load buses.
- NERC Category C: Not to exceed 30% at any bus. Not to exceed 20% for more than 40 cycles at load buses.
- NERC Category D: No specific voltage dip criteria.

Figure 1.1 shows the WECC voltage performance parameters with the transient voltage dip criteria clearly illustrated [6]. Again, appropriate power system controls can be utilized to mitigate the post-contingency transient voltage dip problem.

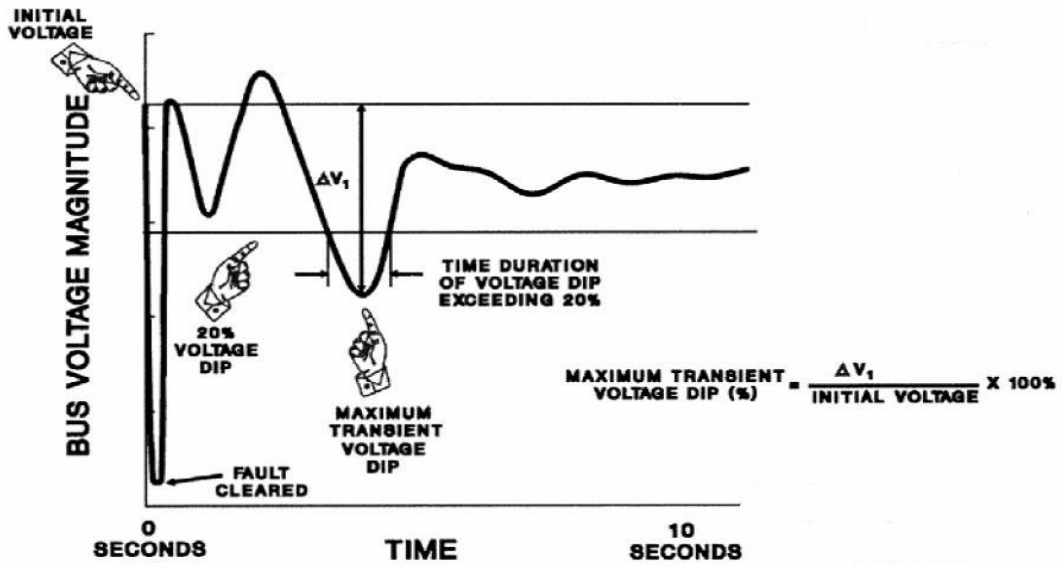


Figure 1.1 Voltage performance parameters for NREC/WECC planning standards.

The major challenge during a contingency is that system reliability and security is maintained without power interruption to consumers. Thus the challenge is to ensure that the system will remain robust even under such large disturbance. The system transition post-contingency to new operating state should not violate dynamic limits and the new operating point should be stable. Incase if this is not the case then we need proper control action to ensure that system limits are respected. There are two commonly used control devices, static such as Mechanically Switched Capacitor (MSC) and dynamic such as SVC and other FACTS devices. The static devices have a slow and discrete response whereas dynamic devices have fast and continuous response. In order to take care of transient voltage dip and short term voltage instability use of dynamic devices is inevitable.

1.2 Report Organization

The rest of the report is organized as follows:

Chapter 2 presents a methodology for assessing contingencies which cause power quality and short term voltage instability problem. Thus at first from a list of credible contingencies the contingencies which are not severe are filtered out. Then the severe ones are ranked in terms of their severity. Thus a general framework for filtering, ranking and assessing contingencies is given in this chapter.

Chapter 3 proposes a new methodology for finding an optimal location and amount of dynamic VAR source which can ensure system robustness against any severe contingency. Thus the present problem is of the form of Mixed Integer Dynamic Optimization (MIDO) which is a challenging problem to solve.

Chapter 4 summarizes some of the major contributions of the work and discusses future work that needs to be done.

CHAPTER 2. CONTINGENCY ASSESSMENT FOR VOLTAGE DIP AND SHORT TERM VOLTAGE INSTABILITY ANALYSIS

2.1 Introduction

Due to competitive electricity market and less incentives of transmission expansion in the recent years, power system operation has become highly stressed, unpredictable and vulnerable [10]. For a stressed system more contingencies are considered as severe contingencies and system becomes more vulnerable to frequent voltage instability problem to the extent of complete voltage collapse [11, 12]. Reference [4] gives IEEE definitions on voltage instability and collapse. Voltage instability is divided into long term and short term voltage instability respectively. Today's deregulated power market and operators encounter dynamic limitations prior to steady state limits. In fact, what may seem stable in long term (due to sufficient time for shunt capacitors and transformers to response) may not be stable in short term. Short term voltage instability problem is growing with increase in induction motor loads at industrial, residential and wind farms and at places where HVDC links weak areas [13, 14, 15], which sometimes may even lead to voltage collapse. This has necessitated a deeper analysis of short term voltage instability. The problem of power quality gets aggravated after large disturbance; such as line contingency; which may cause large voltage dip resulting in stalling of induction motors, mal-operation of protection devices especially zone 3 relay [16, 17]. In recent years; due to blackouts occurring throughout the globe [18] and increased power quality problem [19] has attracted more attention from planners/operators.

This work will attempt to address the issue of contingency assessment scheme for voltage dip and short term voltage instability problem. It is crucial to understand dynamic impact of contingency (single or multiple) on system voltage profile. The vital point in voltage instability study is to determine the risk level or severity of each voltage contingency. Ranking dangerous contingencies out of credible ones based on their impact on system voltage profile will help planners/operators in deciding the most effective preventive/corrective action before system moves towards instability. At this point, it's worth mentioning that the commonly used steady state techniques may not be applicable in contingency assessment for dynamic security assessment (DSA).

Most existing contingency selection algorithms are based on real power flow limits. The commonly used DC power flow is used to screen and rank voltage contingencies based upon line overloading due to contingency [20, 21]. As DC power flow could not address the issue of voltage w.r.t. reactive power so AC power flow was used to address that issue. As power system is dynamic in nature and frequently subjected to contingencies, making voltage behavior dynamic and complex to comprehend. So time-domain methods are used for dynamic analysis to accurately observe and analyze the behavior of system and voltage in particular w.r.t. time. Eigenvalue sensitivity analysis has been proposed in literature for voltage contingency ranking [22, 23], but they are subjected to error due to approximation by the first two terms of Taylor series. This sensitivity analysis is based on dominant eigenvalue, but in [24] it showed that severe voltage contingencies can change dominant eigenvalue and singular value position. Thus, monitoring dominant eigenvalue/singular value of base case in sensitivity analysis can result in ranking errors for severe voltage contingencies. Thus the problem of efficiently filtering and ranking contingencies for voltage problem in DSA framework still remains an area of improvement and research.

Incase of power quality, to compare the severity of voltage violation due to different contingencies, dynamic performance criteria established by NERC [9] is used for ranking. In this work, we focus on the problem of dynamic voltage contingency ranking w.r.t. both contingency severity index (CSI) and dynamic bus voltage vulnerability index (DBVVI). Defining appropriate classification methodology for filtering and severity measures (performance indices) for ranking are difficult in dynamic framework and still an area which is yet to be explored deeply. Time-domain methods can be used to classify contingencies into "stable" and "unstable" with respect to a given stability limit criteria. They can certainly compute stability limits; but at the expense of prohibitive computing times.

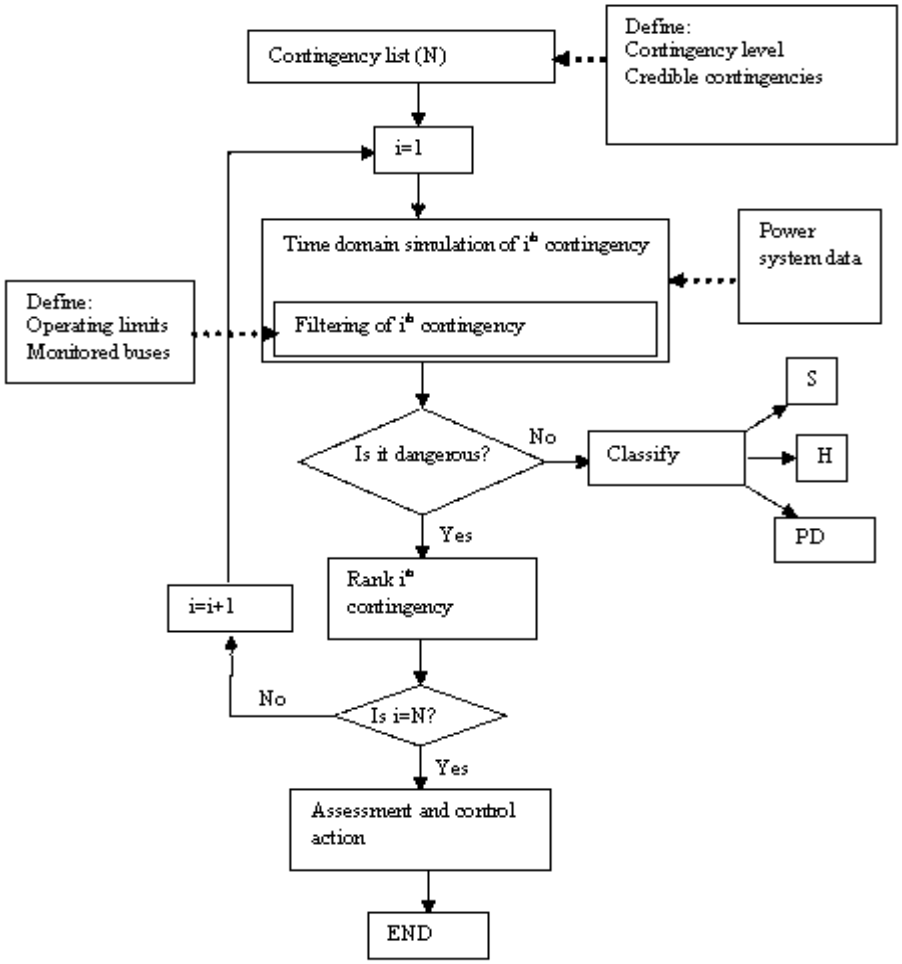
As power system is huge so there are a large number of credible contingencies which need to be analyzed. Thus, for dynamic contingency filtering and ranking there are two important aspects. First, to reduce computational time for contingency filtering. Different researchers have addressed this problem and have tried to reduce computational time by taking advantage of computer hardware such as parallel computing [25] and distributed computing [26]. Others have tried to reduce detailed system model to a simplified one; to save computational time, but at the sake of accuracy. Two, the methodology which is used for filtering and ranking of contingencies should be accurate and efficient i.e. zero misclassification and false alarm rate.

The filtering and ranking process is divided into two blocks: first block for filtering and second for ranking and analysis of contingencies. As will be discussed in the section II, this structure yields a unified approach for contingency filtering and ranking: i) same Decoupled time domain method [27] is used to filter, rank and then assess contingencies; ii) information obtained from first block is used in various ways; first, dangerous contingencies are fed into second block for ranking; second, contingencies which are not dangerous are further classified into sub-categories to give a better idea about system behavior to

planner/operator; iii) information obtained from second block is also used in various ways;

first, for ranking contingencies in order of their severity; second, ranking buses in order of

their vulnerability to contingency; last, analyzing them and deciding appropriate preventive/corrective control action. Another important aspect of this filtering and ranking process is the great flexibility in design of two blocks. Especially, the filtering block may consists of more than one sub-block, to classify a contingency into a more accurate category based upon the impact of that contingency on the system. Similarly, in ranking block more sub-blocks can be added based upon the extra information gained so as to accurately rank severity of a contingency. Thus ranking can be done more accurately by analyzing more than one



parameter. The basic framework of the proposed FRA approach is shown in Figure 2.1.

Figure 2.1 . Flow Chart of the Proposed Contingency Filtering, Ranking and Assessment Technique

2.2 Contingency Assessment

The number of credible contingencies may vary depending upon the level of analysis, number of elements (N) exposed to failure, and level of contingency. That is; zero level of contingency corresponds to N-0 (no element is subject to failure), first level of contingency corresponds to N-1, second level of contingency corresponds to N-2 and so forth. Thus, the

number of kth level contingencies can be given by NC_k for $k = 0, 1, 2,\ldots, N$. Then total number of all possible contingencies, *TNC*, can be given as:

$$TNC = \sum_{k=0}^{N} NC_k \tag{2.1}$$

where, NC_k can be given as:

$$NC_k = \frac{N!}{K!*(N-K)!} \tag{2.2}$$

For interconnected large scale power systems total number of credible contingencies may be large. So, normally N-1 and sometimes N-2 contingencies are also considered. In this work zero and first level of contingency are considered. So the total number of contingencies to be considered can be given as:

$$TNC = \sum_{k=0}^{1} NC_k = 1 + N \tag{2.3}$$

2.2.1 Filtering Block

After a line contingency there is a sudden dip in voltage. For severe line contingencies dip in voltage is large and it may violate NERC criteria, which is unacceptable from stability, reliability and power quality point of view. The NERC criterion [9] for N-1 line contingency is, "Not to exceed 25% at load buses or 30% at non-load buses of pre-disturbance voltage. Not to exceed 20% for more than 20 cycles at load buses of pre-disturbance voltage".

The filtering block uses detailed power system model for better accuracy. All the generators in the system are represented by two-axis model as in [28], the simplified IEEE type DC-1 exciter model is used [29], and governor model is same as in [30]. Thus each machine is represented by nine differential states. A practical power system has a generic load model which may be a combination of constant power, constant current, and constant impedance loads. Thus for all the loads in the system the real part is modeled as 30%

constant power, 50% constant current and 20% constant impedance and the reactive part is modeled as 30% constant power, 20% constant current and 50% constant impedance.

2.2.1.1 Filtering criteria

A good contingency filter should satisfy some key requirements:

i. Classification: A good classifier should be able to screen and classify contingencies on the basis of their severity. In the proposed filtering approach, contingencies are classified into satisfactory (S), harmless (H), potentially dangerous (PD) and dangerous (D) with respect to voltage dip or low voltage after first voltage dip. Further, dangerous contingencies are ranked according to their degree of severity and assessed. These terms are defined below and shown in Figure 2.2. A contingency is:

• Dangerous (D) if it drives the system to an unacceptable voltage level; which may result in poor power quality, stalling of motors, abnormal triggering of protection devices and even a complete system voltage collapse.

• Potentially Dangerous (PD) if it is “almost” dangerous, but may become dangerous under slightly different operating conditions (e.g. increase in load level, outage of another element).

ii. Accuracy: Contingencies which are not satisfactory must be assessed accurately. This is achieved by simulating them for maximum integration period (MIP).

iii. Reliability: The contingency filter should be extremely reliable; it should be able to capture all the dangerous contingencies. This is achieved by using detailed power system models and by selecting fairly large voltage limits.

iv. Efficacy: The contingency filter should have as low as possible rate of false alarms, i.e., contingency suspected to be dangerous while it is not.

v. Computational efficiency: The overall procedure of contingency filtering, ranking and assessment should be as fast as possible. This requirement becomes even more critical in case of real-time operation.

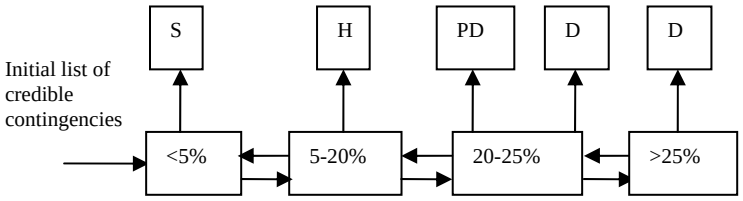


Figure 2.2 Inner Layout of Filtering Block

2.2.1.2 Design layout

The filtering block consists of 4 sub-blocks which are divided based upon the range of voltage deviation. These 4 sub-blocks can communicate with each other, so information from one sub-block can be transferred to another.

Sub-block 1: corresponds to situation when voltage deviation is less than 5% of pre-disturbance voltage.

Sub-block 2: corresponds to situation when voltage deviation is greater than 5% but less than 20% of pre-disturbance voltage.

Sub-block 3: corresponds to situation when voltage deviation is greater than 20% but less than 25% of pre-disturbance voltage.

Sub-block 4: corresponds to situation when voltage deviation is more than 25% of pre-disturbance voltage.

To classify a contingency the filtering block uses four different sub-blocks as described above. Contingencies belonging to sub-block 1-4 are further analyzed to determine whether they are stable or not. Below a brief description of each sub-block is given:

Sub-block 1:

1. If initial voltage deviation is less than 5% and voltage deviation is decreasing with time and has become constant for next ‘t’ seconds (here taken as 2sec), then discard that contingency and flag it as satisfactory (S).

2. If voltage deviation is decreasing with time and becomes less than 5% for next ‘t’ seconds (here taken as 2sec); then discard that contingency and flag it as S.

3. If voltage deviation is increasing with time and becomes more than 5%; then continue simulation and follow the rules of sub-block 2, 3 or 4.

Sub-block 2:

1. If initial voltage deviation is between 5%-20% and voltage deviation is decreasing with time and becomes less than 5%; then follow the rules of sub-block 1.

2. If voltage deviation remains within the limits of 5%-20% then flag it as harmless (H).

3. If voltage deviation is increasing and becomes more than 20% then continue simulation and follow the rules of sub-block 3 or 4.

Sub-block 3:

1. If initial voltage deviation is between 20%-25% and voltage deviation is decreasing with time and becomes less than 20%; then continue simulation and follow the rules of sub-block 1 or 2.

2. If voltage deviation becomes less than 20% for few cycles but returns back to 20%-25% limit, but for not more than 20 cycles then flag it as potentially dangerous (PD).

3. If voltage deviation is oscillatory and remains within the limits of 20%-25% for more than 20 cycles then flag it as dangerous (D) and send the contingency to block 2 for ranking and assessment.

4. If voltage deviation increases with time and becomes more than 25%; then follow the rules of sub-block 4.

Sub-block 4:

1. The contingency is sent to block 2 for ranking and assessment.

2.2.1.3 Advantages

1. A large number of contingencies are satisfactory and early termination of such contingencies can save lot of computational time making filtering process faster.

2. Classifying contingencies as S, H, PD, and D can given an idea about the system behavior. As H and PD are already simulated for MIP, thus it gives an additional benefit by sorting and storing contingency information as S, H and PD. This information becomes important when these contingencies are simulated for next operating state. Let's say a planner/operator wants to do contingency analysis for a higher load level then credible list of contingencies would be list of contingencies which belonged to category PD, then H and finally followed by S. Thus there is no need to simulate all the contingencies again, due to reduced set of credible contingencies.

2.2.2 Ranking Block

Contingency ranking is crucial as it reflects the bottleneck of power system in priority order, a property that is a key issue for both planners and operators. Thus, here both severe lines and vulnerable buses due to contingencies are ranked. Based on different aspects of voltage instability to accurately rank contingencies following things were taken into consideration:

1. No single performance index can reliably and fully capture the impact of contingency.

2. A combination of performance indices capturing different aspects of voltage instability can be used to reliably rank contingencies as shown in Figure 2.3. Such composite indices are suggested for voltage stability analysis in this work.

3. The performance indices should be general; to be used in any power system and their calculation should not be time intensive.

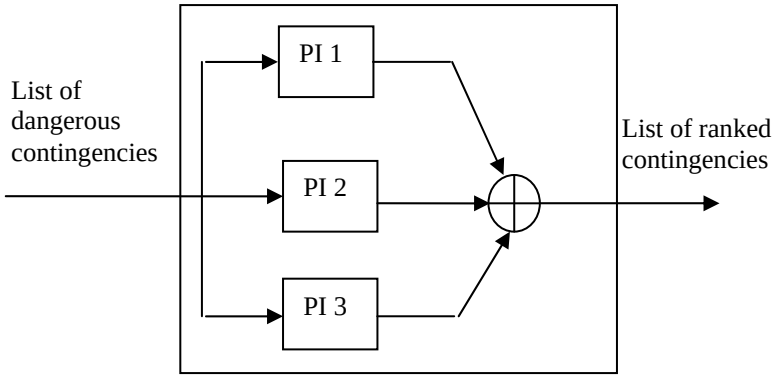


Figure 2.3 Inner layout of Ranking Block

Thus three different performance indices were developed and are discussed as follows. During a contingency power system may shift from normal to abnormal state. This abnormality is clearly reflected by voltage dip and predominantly low voltage at buses. Thus a performance index, PI_v, is used to measure and quantify voltage limit violation for contingency ranking. PI_v gives measure of voltage deviation by finding sum of voltage deviation at all buses where unacceptable voltage deviation occurs over time when voltage deviation is unacceptable. In this both low voltage as well as high voltage deviation (especially in case of generator buses) are considered and given as:

$$PI_v = \sum_{i=1}^{N}\sum_{s=0}^{T} \frac{w_{vi}}{2m}\left[\frac{V_{i\,s\ new} - V_i^0}{V_{i\max}}\right]^{2m} \tag{2.4}$$

where,

N = number of buses with unacceptable voltage deviation problem

T= total time of simulation

s = time instant for which bus voltage deviation is beyond specified limit

V_{isnew} = post-outage voltage at bus *i* at time instant *s*

V_i^0 = pre-contingency voltage at bus *i*

$V_{i\max}$ = maximum voltage deviation allowed

m = exponent of penalty function (taken as one in present study) for removing masking effect

w_{vi} = weight factor used to reflect sensitivity of load bus *i* w.r.t. voltage dip (taken as one in present study)

The time instant at which the system becomes unstable is also crucial and can be used for better ranking of contingencies. More severe a contingency is, faster the system will become unstable. Thus a performance index, PI_t, to measure this factor is also included in present contingency ranking. PI_t gives the measure of time of instability or time for which voltage deviation was unacceptable by finding the sum of time (beyond 20 cycles for N-1 contingency) for which the voltage deviation is beyond the specified limit (20% for N-1 contingency) at all the unacceptable voltage deviation buses.

$$PI_t = \sum_{i=1}^{N} \sum_{s=0}^{T} \frac{w_{ti}}{2m} \left[\frac{t_{is}}{t_{i\max}} \right]^{2m} \tag{2.5}$$

where,

t_{is} = time instant *s* after allowed time limit for which voltage deviation is unacceptable

$t_{i\max}$ = maximum time limit for which unacceptable voltage deviation is allowed

w_{ti} = weight factor used to reflect the sensitivity of load bus *i* w.r.t. low voltage for long time (taken as one in present study)

In case, a contingency causes voltage instability, then the time instant at which voltage instability occurs plays an important role in ranking of contingency. Thus, when there are more than one contingency causing voltage instability problem, then PI_t becomes dominant performance index and plays an important role in ranking of contingencies.

Sometimes, there maybe a situation whereby a severe contingency with a large voltage dip at one node is ranked equal to a less severe contingency with low voltage dip across many nodes. This problem is commonly known as masking problem. If the term *m* in equation (1) is increased from 1 to say 2, or 4, or some higher number; the final ranking may become even worse due to increased non-linearity of PI_v. To bridge gap between masking and misranking of contingencies, another performance index, $PI_{v\max}$, has been added to give

an extra emphasis to largest voltage deviation among all buses that have unacceptable voltage deviation caused by the contingency under consideration and can be given as:

$$PI_{v\max} = \max_i \left\{ w_{vi} \max_s \left\{ \left\| V_{i\,s\,new} - V_i^0 \right\| \right\}_{s=0}^{T} \right\}_{i=1}^{N} \tag{2.6}$$

w_{vi} and w_{ti} are weights w.r.t. voltage and time. Thus for load buses which are more sensitive to voltage dips can be given a higher value of w_{vi} and load buses which are more sensitive to low voltage for long time can be given a higher value of w_{ti}. Thus, line severity index of a contingency can be obtained by summing all the individual performance indices and can be given as:

$$CSI = PI_v + PI_t + PI_{v\max} \tag{2.7}$$

Normally in a contingency analysis the impact of a line contingency on system is observed, which is okay from operation/planning point of view. From planner's perspective, another crucial information is, "how different credible line contingencies will impact a particular bus voltage". Thus, here abnormal voltage behavior of a particular bus is observed due to different line contingencies. From this study, it can be know that how many line contingencies are making a particular bus vulnerable. Also, severity due to different line contingencies can be quantified by defining a performance index. Once, a performance index for all voltage violating buses is obtained, they can be ranked in order of their vulnerability. Thus "Dynamic Bus Voltage Vulnerability Index" (DBVVI) is defined, which can be helpful to a planner in deciding an initial set of candidate location for VAR placement. The bus with a higher DBVVI will get a higher priority in locating a VAR source at that bus.

It maybe possible that during stressed loading condition, even though there is no line contingency some buses have voltage limit violation. Thus, a weighted sum of performance index (PI) for base case and different contingency cases are computed at each bus and termed as "Dynamic Bus Voltage Vulnerability Index" (DBVVI). The performance index (PI),

defined in (2.10-2.12), has been taken as relative weightage for different contingencies, as it reflects relative severity of a particular line outage condition. This relative weighing of different line contingency becomes crucial if planner/operator has some kind of probabilistic information from historical data about the occurrence of that line outage. Thus a line with higher outage probability can be given a higher weightage. Thus DBVVI for a bus can be expressed as:

$$DBVVI_i = w_0 PI_{i,0} + PI_{i,l} \tag{2.8}$$

where, $PI_{i,0}$(base case) and $PI_{i,l}$(contingency case), $l \forall N_l$ are the normalized PI values corresponding to the lth most severe line outage contingency.

where, $PI_{i,l} = PI_{i,v} + PI_{i,t} + PI_{i,v\max}$, performance index of ith bus due to different line contingencies.

$PI_{i,0}$ gives the measure of voltage deviation at i^{th} bus, when voltage deviation is unacceptable at base case. In this both low and high voltage deviation are considered and given as:

$$PI_{i,0} = \frac{w_{vi}}{2m}\left[\frac{V_{is\,new} - V_i^0}{V_{i\max}}\right]^{2m}, \text{ here } V_{i\max} \text{ is 5\%} \tag{2.9}$$

$PI_{i,v}$ gives measure of voltage deviation at i^{th} bus, by finding sum of voltage deviation caused by line contingencies (which cause unacceptable voltage deviation) over the time when voltage deviation is unacceptable. In this both low and high voltage deviation are considered and given as:

$$PI_{i,v} = \sum_{l=1}^{N_l} w_l \sum_{s=0}^{T} \frac{w_{vi}}{2m}\left[\frac{V_{is\,new} - V_i^0}{V_{i\max}}\right]^{2m} \tag{2.10}$$

$PI_{i,t}$ gives the measure of time at i^{th} bus, by finding the sum of time for which voltage deviation is beyond the specified limit caused by all the line contingencies and given as:

$$PI_{i,t} = \sum_{l=1}^{N_l} w_l \sum_{s=0}^{T} \frac{w_{ti}}{2m} \left[\frac{t_{is}}{t_{i\max}} \right]^{2m} \tag{2.11}$$

Inorder, to avoid the problem of masking and misranking, another performance index has been added to give an extra emphasis to a line contingency which causes largest voltage deviation at i^{th} bus and is given as:

$$PI_{i,v\max} = \max_l \left\{ w_l \; w_{vi} \max_s \left\{ \left\| V_{is\,new} - V_i^0 \right\| \right\}_{s=0}^{T} \right\}_{l=1}^{N_l} \tag{2.12}$$

where, w_l = weight factor used to reflect probability of lth line outage (taken as one in present study).

2.3 Assessment and Control

The topic of control is beyond the objective of this work, however a basic idea as to how the information obtained from ranking block can be used for assessment and control is discussed. The potential benefit of using information provided by FRA is to come up with optimal or near-optimal preventive/corrective control to stabilize unstable contingencies. From ranking of contingencies (CSI), some preventive actions can be taken. For example, if a severe line is overloaded then generation shift technique can be applied to relieve overload in that line. From ranking of bus (DBVVI); candidate VAR location can be obtained which can be optimally analyzed for preventive/corrective action. Also, if a particular bus gets severely vulnerable due to a contingency then load shedding could be considered at that bus.

Sensitivity of voltage dip and duration of voltage dip or low voltage w.r.t. VAR source capacitive limit can be calculated using the above mentioned PIs. Sensitivity of voltage dip w.r.t. VAR source capacitive limit, S_v, can be given as, change in voltage dip for a given change in VAR source capacitive limit:

$$S_v = \frac{\partial PI_v}{\partial B_{VAR}} = \sum_{i=1}^{N} \sum_{s=0}^{T} \frac{w_{vi}}{2m} \left[\frac{\partial V_{i\,s\;new} \big/ \partial B_{VAR}}{V_{i\max}} \right]^{2m} \tag{2.13}$$

Sensitivity of voltage dip or low voltage time duration w.r.t. VAR source capacitive limit, S_t, can be given as, change in voltage dip or low voltage time duration for a given change in VAR source capacitive limit:

$$S_t = \frac{\partial PI_t}{\partial B_{VAR}} = \sum_{i=1}^{N}\sum_{s=0}^{T}\frac{w_{ti}}{2m}\left[\frac{\partial t_{is} \big/ \partial B_{VAR}}{t_{i\max}}\right]^{2m} \tag{2.14}$$

2.4 Results

The standard IEEE 39 bus New England system was considered for study. The New England system has 10 generators and all generators have detailed model represented by 9 differential states. 33, N-1 line contingencies, at 4 different operating states were considered for study, thus resulting in a total of 132 cases. In order to emulate realistic operational use, maximum integration period for simulation was fixed at 20s. Performance of proposed FRA approach is judged from different perspective as discussed below:

1) Reliability: All contingencies discarded by filtering block are indeed satisfactory (S), and all dangerous contingencies have been properly captured. Thus, False-dismissal rate (number of cases declared satisfactory by classifier while actually not satisfactory) was 0. False-alarm rate (number of cases declared unsatisfactory by classifier while actually satisfactory) was also 0.

2) Computational Efficiency: The full simulation for contingencies that fall in the category of H: 10 out of the 132 for the New England system are required and seem reasonable for guaranteeing full reliability.

3) Computing Performances: The saving in computing times required by FRA simulations are two fold. First, almost half of computational time is saved by using Decouple time-domain simulation. Second, as 86.4% of contingencies fall in the category of satisfactory (S)

thus by ‘early termination’ of simulation; 5 seconds, there is 64.8% of saving in computational time, which is really significant.

In contingency filtering block, most of the computational time is spent to explore existence of multi voltage dip or gradually increasing voltage deviation, especially the ones which fall in the category of H and PD. This computational time can be avoided if such behavior is not of concern (say, if the operator knows by experience and from historical data that they don’t exist). Thus a knowledge base sub block can be added to filtering sub-blocks to better and faster classify and discard the contingencies.

Table 2.1 shows the output of filtering block, in the table BC corresponds to Base Case and BC+5% means an increment in load by 5% by maintaining the same P/Q ratio. As can be seen from table most of the contingencies fall in the category of S. The 4 different load levels shown here can be considered as 4 different load levels in a day or in a year. For example BC+15% may correspond to summer peak load and BC+10% may correspond to winter peak load. Now say, if planner/operator has done contingency analysis at BC+15% load level and now wants to do contingency analysis for BC+10% in that case planner can easily reduce its set of credible contingencies from 33 to 8 as he doesn't needs to consider contingencies which were S at BC+15% load level as they will be satisfactory (S) at lower load level. Thus, this information becomes very useful to planner/operator in reducing the list of credible contingencies and also in managing contingency record in a useful manner. Another application of filtering block can be seen in case of line 21-22; which is stable at 4 different load levels; such information can be added to knowledge base to further reduce computation time.

Table 2.1 Output of Filtering Block.

Line	BC	BC+5%	BC+10%	BC+15%
2-3	S	S	S	H
2-25	S	S	S	D->VC
15-16	S	S	H	H
21-22	H	H	H	H
26-27	S	S	D->VC	D->VC
26-28	S	S	H	D->VC
26-29	S	S	H	D->VC
28-29	H	D->VC	D->VC	D->VC

*BC=Base Case, VC=Voltage Collapse

Table 2.2 Output of Ranking Block (CSI)

Line	BC	BC+5%	BC+10%	BC+15%
28-29	-	1	1	1
26-27	-	-	2	2
26-29	-	-	-	3
26-28	-	-	-	4
2-25	-	-	-	5

Table 2.3 Ranking of buses based on DBVVI.

Line	BC	BC+5%	BC+10%	BC+15%
28-29	-	29,28,26	29,28,26	29,28,26
26-27	-	-	29,28,26	29,28,26
26-29	-	-	-	29,28,26
26-28	-	-	-	28,29,26
2-25	-	-	-	28,29,26

Table 2.2 shows the output of ranking block and indicates the severity of line contingency as obtained from CSI. From this result planner/operator can know which line outage is most severe and gets aid in planning an appropriate preventive control action to ensure system reliability and quality incase that contingency does occur.

Table 2.3 ranks vulnerable buses in their decreasing order of vulnerability. In the table only 3 most vulnerable buses are shown due to space constraint. In case of BC+5% bus 29 is the most vulnerable bus followed by 28 and 26. This is very useful information as this information can be used in deciding control location and kind of control based upon the nature of load bus. A planner/operator may decide to shed load at that bus to ensure system stability. Also a planner may decide of installing a shunt capacitor at bus 29 as it the most vulnerable bus and it does gets effected by all contingencies which cause voltage instability problem.

2.5 Conclusions

This work has addressed an issue of power quality and short term voltage instability and has proposed a general approach to contingency filtering, ranking and assessment (FRA). The process is divided into two blocks; one for filtering out satisfactory contingencies and second block for ranking and assessment of dangerous contingencies. The methodology developed for early termination and filtering out of satisfactory (S) contingency helps in saving lot of computational time. Thus out of 132 contingencies that were screened for New England system, about 86.4% were readily discarded by filtering block thus giving a huge saving in computational time; while others were classified as harmless 7.6% and dangerous 6%.

In this work, Contingency Severity Index (CSI) is defined to measure the impact of contingency on power quality and system stability. Further, Dynamic Bus Voltage Vulnerability Index (DBVVI) is defined to measure the vulnerability of bus due to different contingencies. The DBVVI information was also used for control assessment by finding sensitivity of control location and amount to bus voltages.

Thus the proposed FRA approach is powerful due to efficient filtering, ranking, assessment and control tools. Most importantly; it is unified as it can handle any power

system modeling, uses same model throughout the analysis, any contingency scenario and any type of application.

CHAPTER 3. OPTIMAL ALLOCATION OF DYNAMIC VAR USING MIXED INTEGER TRAJECTORY OPTIMIZATION

3.1 Introduction

In recent years, full utilization of electrical equipments is done to maximize profit. This may result in overloading of some generators or transmission lines which may raise issues about system stability and reliability. The problem gets even more aggravated during contingencies. As electric power systems are frequently subjected to contingencies during operation. Some of these contingencies may create stability problem, while others may create power quality problem. In previous chapter, contingency analysis was introduced to identify severe contingencies and their amount of severity. Once severe contingencies are identified, the next step is to find control method to mitigate system failure due to such contingencies. In order to ensure voltage security and system robustness against contingencies a proper planning of system needs to be done. To achieve this contingency from different scenarios should be assessed to find out which contingencies out of credible ones are causing voltage acceptability problem. Optimization method incorporating system dynamics is proposed in this chapter to provide optimal control strategies to prevent system failure caused by severe contingencies.

Traditionally used steady state based optimal power flow which finds minimum amount of control needed to obtain required PV margin does not takes system dynamics into consideration. The issue is that what may seem stable in steady state analysis may not be stable in dynamic analysis. As power system is a dynamical system so it seems more realistic that dynamic system model should be used in the optimization framework to obtain accurate

control amount-time dependence. Often in blackout reports it is mentioned that the system could have been saved by applying this much amount of control at this time at this location. Thus the real challenge in the optimization part is to find the optimal location and the optimal amount of control at those locations.

In order to ensure system security during disturbance proper co-ordination of control at different locations is necessary. For example load shedding is one control option for saving the system from voltage instability but the decision, “where and how much to shed” is crucial. If load shedding is less then system may not be saved from voltage collapse, if load shedding is too much then it may result in huge financial loss to power industry and consumers.

To ensure normal operation of competitive electricity market a better understanding of power system dynamics and a proper identification of remedial actions is needed. Thus a control mechanism is needed to ensure post disturbance equilibrium. Also, post disturbance equilibrium should be achieved in a time frame such that the disturbance is not spread to other parts of the system. The post disturbance transition process should satisfy performance constraints. Like, low and high voltage due to transient behavior means poor power quality. Unwanted operation of protection relays (especially zone3 [31, 32]) due to bad power quality should be avoided as that can possibly lead to cascading events.

In this work, two important issues are addressed with respect to credible contingencies i.e. short term stability problem and power quality problem especially voltage dip. Fast acting reactive power control is needed to mitigate the above two problems. Thus there are two questions regarding the installation of dynamic VAR support in the system:

1. where to optimally locate the VAR support
2. what is the optimal amount of VAR support

As control resources have three aspects: amount, location, and time, the optimal control methodology developed in this work will coordinate these three elements to provide optimal control amount from appropriate control location at appropriate control time.

In [33, 34] optimal location of dynamic VAR sources is found for enhancing power system security and power quality. Most of these studies are done for steady state, but the problem of dynamic security is still not addressed.

The problem of dynamic security has two subproblems: a combinatorial optimization problem and a trajectory optimization problem. This gives rise to mixed integer trajectory optimization (MITO) problem, the solution of which is a formidable task. In this work the MITO is decomposed into a series of primal problems where the binary variables (control locations) are fixed, and a master problem which determines a new binary (control locations) configuration for the next primal problem. The master problem corresponds to combinatorial optimization and is solved using Simulated Annealing Algorithm and the primal problem corresponds to trajectory optimization.

The problem of finding optimal control location in dynamic framework is a complex optimization problem. The exact solution of optimal allocation can be obtained by complete enumeration of all feasible combinations of locations, which could be a very huge number especially for a large scale system. The optimal location problem is NP-complete problem.

The solution approaches for solving location problem can be divided into three categories:

1. Classical optimization methods: integer programming [35], cutting plane techniques, branch and bound and Lagrangian relaxation.

2. Heuristic methods: priority list

3. Artificial intelligence methods: neural networks, expert systems, genetic algorithms, tabu search and simulated annealing.

Classical optimization methods are direct means for solving such problems and can guarantee optimal solution. The problem with these methods is that they take lot of computational time and face the problem of dimensionality especially incase of large scale system. Heuristic methods are easy to implement but only suboptimal solution can be obtained due to incomplete search of solution space. Artificial intelligence methods are promising and still evolving. They guarantee optimal solution in limited computational time.

Simulated Annealing (SA) is one such powerful technique to solve combinatorial optimization problem. SA has been successfully applied for solving optimal location problem in different areas of power systems [33, 36, 37, 38]. In this work, SA is used for finding optimal location of VAR sources for solving dynamic security problem. Once the location is identified the next task is to find the optimal control amount at those locations which can ensure the stability and power quality of the system.

3.2 Problem Formulation

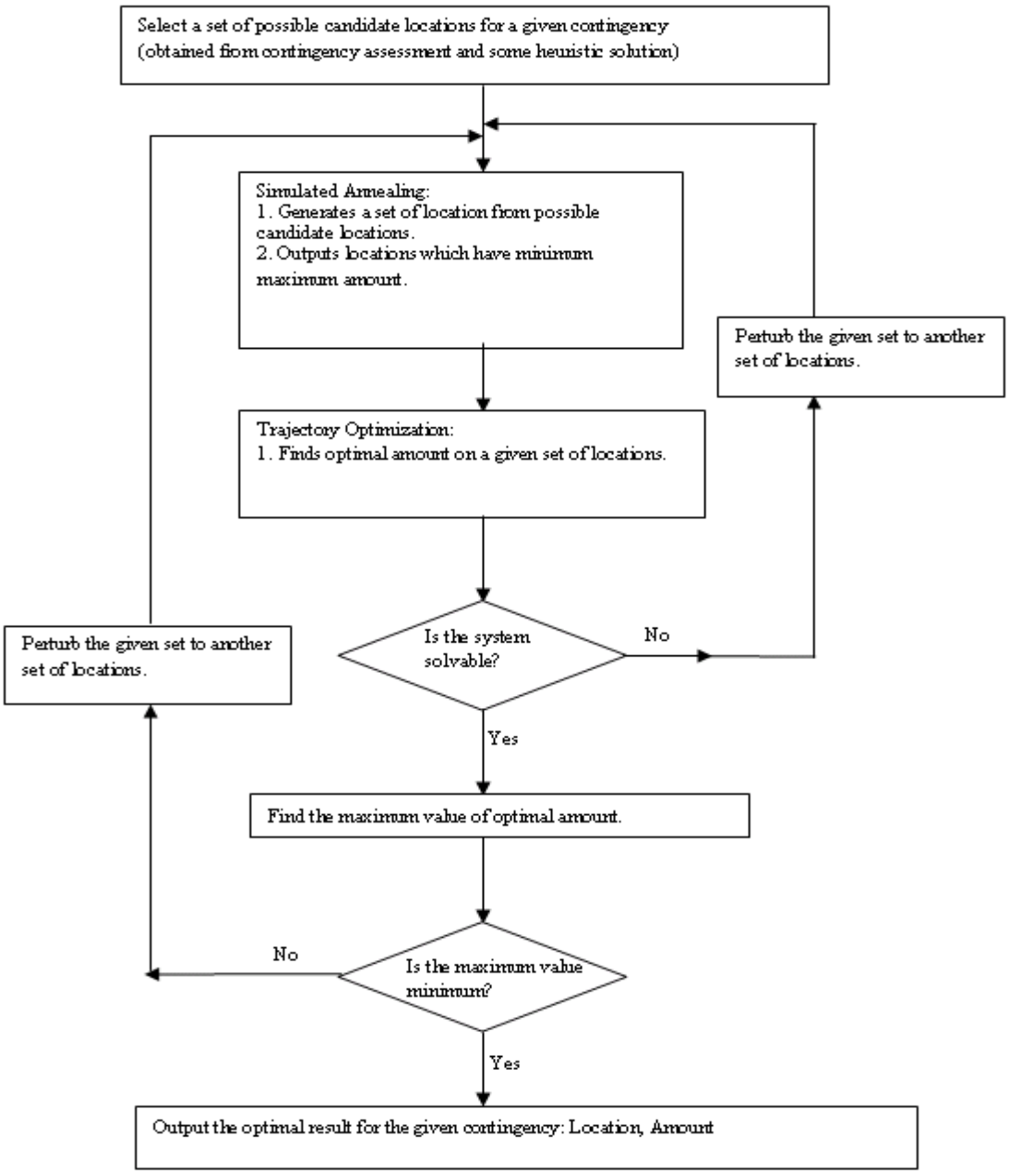
Power systems can be represented by a set of differential algebraic equations. In equation 3.1, *x, y* and *u* represent differential state variable corresponding to dynamical states of generator, algebraic variable, and control respectively.

$$\begin{aligned} \dot{x} &= f(x, y, u) \\ 0 &= g(x, y, u) \end{aligned} \tag{3.1}$$

The power systems also have the conditions at the initial time and the end time. For example, initial condition in power system dynamics may be the system states subject to disturbances, and end condition in power system dynamics may be the post disturbance equilibrium. The initial time and end time conditions are called boundary conditions. The general form of the boundary conditions is the mix of initial time and end time. The boundary conditions of the initial time for given initial condition and the end time conditions for post disturbance equilibrium can be represented as:

$$x(0) = x_0, y(0) = y_0, f(x_T, y_T) = 0, g(x_T, y_T) = 0 \tag{3.2}$$

As discussed earlier that SA is used for solving the master problem and trajectory optimization is used for solving the primal problem. In a general flowchart is given to show



how Simulated Annealing and Trajectory Optimization is used to for optimal allocation of VAR support.

Figure 3.1 Simulated Annealing and Trajectory Optimization formulation for optimal allocation.

3.2.1 Trajectory optimization for primal problem

The aim of trajectory optimization is to find optimal trajectory among all the possible trajectories with initial and end conditions. The concept of trajectory optimization is shown in Figure 3.2. In the figure, there exist different trajectories connecting power system initial state and final state under different control strategies. The objective of power system trajectory optimization problem is to find out the best control strategy and trajectory, for example green line in Figure 3.2 among all possible candidates.

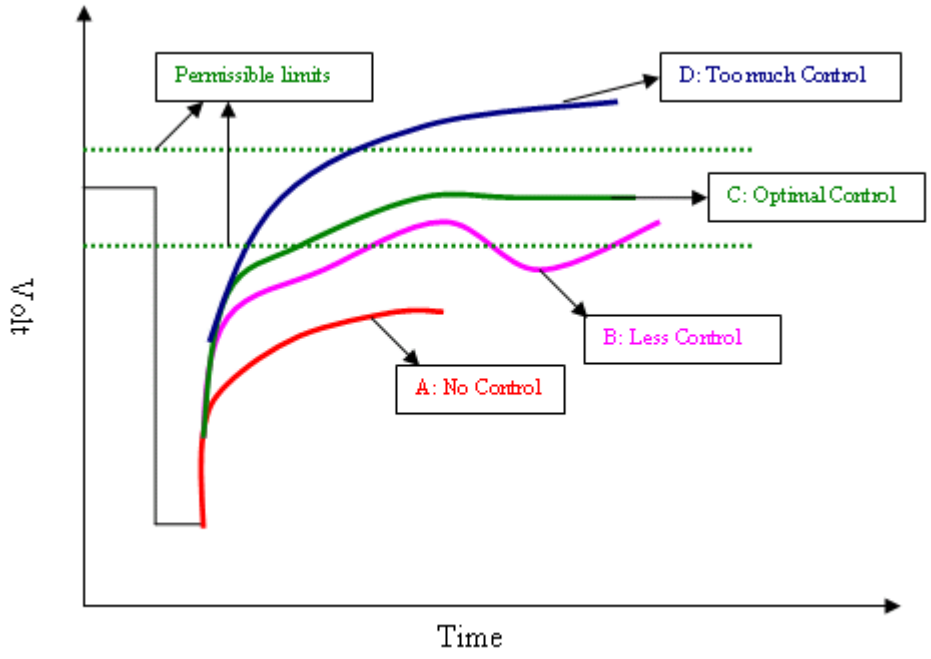


Figure 3.2 Power system trajectory optimization concept.

The cost function or objective function measuring the goodness of control is defined as $J = \int_0^T L(x,u)dt$. $L(x,u)$ can include control amount and deviation to desirable states depending on the function forms along the trajectory. Control amount can be represented as

$L = u^T Qu$ with Q as weighting matrix; deviation to desirable states can be represented as $L = (x - \bar{x})^T S(x - \bar{x})$ with $\bar{x}$ as desirable state and S as weighting matrix.

Besides the constraints of dynamical state law, there also exist constraints in control and state variables such as control function, upper and lower limits on control and state variables. These additional constraints can be represented as a set of equalities or inequalities in the problem formulation. Thus, the mathematical formulation of trajectory optimization [47] is given as:

$$\min \quad J = \int_0^T L(x, y, u)dt$$

s.t.

$$\begin{aligned} \dot{x} &= f(x, y, u) \\ 0 &= g(x, y, u) \\ 0 &\le d(x, y, u) \end{aligned} \tag{3.3}$$

where x represents the system state variables, corresponding to dynamical states of generators; y corresponds to the algebraic variables, usually associated to the transmission system and steady-state element models; vector u is used here to represent system parameters that are directly controllable, such as reactive power compensation, generator reference voltage, load level of non-disruptive load control etc. The necessary conditions for (3.3) without inequality constraints are given as Hamiltonian and defined as:

$$H(x, y, u, \lambda, \mu, \gamma) = \lambda^T f + L + \gamma^T g \tag{3.4}$$

The necessary conditions for (3.3) are given by Pontryagin's Minimum Principle:

$$\begin{cases} \dot{x} = H_\lambda^T = f(x, y, u) \\ 0 = g(x, y, u) \\ \dot{\lambda} = -H_x^T = -(\partial L / \partial x)^T - (\partial f / \partial x)^T \lambda - (\partial g / \partial x)^T \gamma \\ 0 = H_u^T = (\partial L / \partial u)^T + (\partial f / \partial u)^T \lambda + (\partial g / \partial u)^T \gamma \\ 0 = H_y^T = (\partial L / \partial y)^T + (\partial f / \partial y)^T \lambda + (\partial g / \partial y)^T \gamma \end{cases} \tag{3.5}$$

An extended penalty function [39] is defined for inequality constraints with penalty parameter ρ_k .

$$D_i = \begin{cases} 1/d_i & d_i \geq \sqrt{\rho_k} \\ (1/\sqrt{\rho_k})[3 - 3d_i/\sqrt{\rho_k} + (d_i/\sqrt{\rho_k})^2] & d_i \leq \sqrt{\rho_k} \end{cases} \tag{3.6}$$

The objective of original problem 3.3 can now be given by Hamiltonian:

$$H(x, y, u, \lambda, \gamma) = \lambda^T f + L + \rho_k \sum D_i(\rho_k, x, y, u) + \gamma^T g \tag{3.7}$$

The necessary conditions can be given as:

$$\begin{cases} \dot{x} = H_\lambda^T = f(x, y, u) \\ 0 = g(x, y, u) \\ \dot{\lambda} = -H_x^T = -(\partial L/\partial x)^T - (\partial f/\partial x)^T \lambda - (\partial g/\partial x)^T \gamma - \rho_k \sum \partial D_i/\partial x \\ 0 = H_u^T = (\partial L/\partial u)^T + (\partial f/\partial u)^T \lambda + (\partial g/\partial u)^T \gamma + \rho_k \sum \partial D_i/\partial u \\ 0 = H_y^T = (\partial L/\partial y)^T + (\partial f/\partial y)^T \lambda + (\partial g/\partial y)^T \gamma + \rho_k \sum \partial D_i/\partial y \end{cases} \tag{3.8}$$

The formulation of necessary conditions is a two point boundary value problem. Such problem can be solved by finite difference method or shooting method [40, 41]. In the next section, numerical algorithm of finite difference method is given.

3.2.1.1 Numerical algorithm for boundary value problem

The necessary condition of trajectory optimization is a Boundary Value Problem (BVP), more specifically, a Two-Point Boundary Value Problem (TPBVP) for Differential Algebraic Equation. The boundary value problem in (3.8) can be written in a general form as follows.

$$\begin{aligned} \dot{x} &= f(x, y) \\ 0 &= g(x, y) \end{aligned} \tag{3.9}$$

$$0 = b(x_0, y_0, x_T, y_T)$$

In the formulation of (3.9), the compact forms of system representation and variable representation are used. For example, the variable vector *x* include both the system differential states and the co-states or the multiplier in the trajectory optimization. The variable vector *y* represents both power flow variables, control variables and the co-states. The power flow variables may be bus voltage magnitude and bus voltage angle, and the control variables may be reactive power compensation, generator reference voltage, and load. The boundary conditions are also in the compact form consisting of both initial time and end time conditions for power system differential states and algebraic states.

The boundary value problem can be solved by finite difference methods or by shooting methods [42, 43]. The finite difference methods aim to find the numerical approximation over the entire time interval, and thus these methods are sometimes referred to as global methods. The shooting methods employ numerical solution of the initial value problem to find the solution of the boundary value problems. In the mathematical literature, both methods are applied to solve the boundary value problem, and there is no well established conclusion on which method is superior to the other. In this section, the finite difference methods are applied to solve the boundary value problem from the necessary condition of the trajectory optimization. A survey of some global methods to solve BVP-ODE is shown in [44].

The basic idea of the finite difference methods is to transform boundary value problem into a set of nonlinear equations in a mesh of the time interval. The differential quotients in the differential equations are replaced by the finite difference quotients. For a time interval defined in [0, T], a mesh or a sequence of steps is defined with *N* subintervals:

$$0 = t_0 < t_1 < \cdots < t_{N-1} < t_N = T$$

The corresponding differential and algebraic states at the mesh points are denoted as:

$$x_0 < x_1 < \cdots < x_{N-1} < x_N = x_T$$

$$y_0 < y_1 < \cdots < y_{N-1} < y_N = y_T$$

The differential operator $\dot{x} = f(x, y)$ can be numerically approximated by the finite difference $FD(x_0, \cdots, x_N, y_0, \cdots, y_N) = 0$. Then the boundary value problem can be replaced by the nonlinear equation set as:

$$0 = FD_i(x_0, \cdots, x_N, y_0, \cdots, y_N) \qquad 1 \le i \le N \qquad (0.1)$$

$$0 = g(x_i, y_i) \qquad 0 \le i \le N \qquad (0.2)$$

$$0 = b(x_0, y_0, x_N, y_N) \qquad (0.3)$$

By using finite difference methods, a compact form of the finite difference equations can be written as a set of nonlinear equation

$$\Phi(X, Y) = 0$$

where

$$X = [x_0^T, \cdots, x_N^T]^T \qquad Y = [y_0^T, \cdots, y_N^T]^T$$

The finite difference quotients may be defined by the trapezoidal method, that is, $FD_i(x_0, \cdots, x_N, y_0, \cdots, y_N) = x_i - x_{i-1} - h[f(x_i, y_i) + f(x_{i-1}, y_{i-1})]/2$ for $1 \le i \le N$. Thus the general form of nonlinear equations $\Phi(V, W)$ becomes:

$$\Phi_0(X, Y) = \begin{cases} b(x_0, y_0, x_N, y_N) \\ g(x_0, y_0) \end{cases}$$

$$\Phi_i(X, Y) = \begin{cases} x_i - x_{i-1} - h[f(x_i, y_i) + f(x_{i-1}, y_{i-1})]/2 \\ g(x_i, y_i) \end{cases} \qquad 1 \le i \le N$$

By solving the nonlinear equation set $\Phi(X, Y) = 0$, the solution of the two-point boundary value problem for differential algebraic equation can be obtained, which gives the optimal control strategy for power system dynamics.

3.2.2 Simulated Annealing for master problem

Simulated Annealing (SA) is inspired by the physical process of slowly cooling a metal [45].The temperature is decreased in steps and is maintained constant for sufficient time period so that the solid reaches thermal equilibrium. At equilibrium the solid can have many configurations. Thus new configuration is constructed by imposing a random change to the current configuration.

Thus SA is stochastic improvement method. It solves combinatorial optimization problem based on probabilistic local search technique. Instead, of always accepting a better solution, a worse solution may occasionally be accepted with an acceptance probability, the Metropolis criterion [46]. The probability of accepting worse solution decreases as the temperature decreases.

Metropolis, proposed a Monte Carlo method to simulate the process of reaching thermal equilibrium at a fixed temperature T. In this method, a randomly generated perturbation of the current configuration is applied so that a new configuration is obtained. Let E_c and E_n denote the energy level of the current and new configuration respectively. If $E_c > E_n$, then the new configuration is accepted as a current configuration. Otherwise, the acceptance probability of new solution is given by $\exp(E_c - E_n/T)$, where T is temperature. Due to probabilistic selection criteria, the process can always come out of local minimum and proceed to global minimum.

The system reaches thermal equilibrium after a large number of perturbations, when the probability distribution of new configuration approaches Boltzmann distribution. By slowly decreasing T lower energy levels are achievable. Thus a solution with minimum energy is achievable as T approaches zero. The steps involved in SA are as follows:

start

Set the initial temperature $T=T_0$, to be sufficiently high such that the probability of accepting any solution is close to 1.

Set an initial feasible solution q_o, set current solution $q_c = q_o$

Initialize the iteration count k=0

repeat

iter=0

Set the length of Markov chain L_m

repeat

Generate next solution q_n by perturbation

Calculate the optimal control amount (Energy) corresponding to q_n from Trajectory optimization program.

if $E_c > E_n$ **then** set $q_c = q_n$

if $\exp[(E_c - E_n)/T_k] >$ random[0,1) **then** set $q_c = q_n$

if optimal solution found **then**

Stop

iter=iter+1

until iter > L_m

Decrease the control temperature, $T_{k+1} = \alpha T_k$

k=k+1

until optimal solution is found

return best solution

end

3.3 Results

3.3.1 2-Bus system

In this section, trajectory optimization is applied to a simple 2-bus power system [15]. In the power system, a load bus is connected with a generator through a transmission line as shown in Figure 3.3 . The control resource is a reactive power compensation device B*c* with continuous output at the load bus.

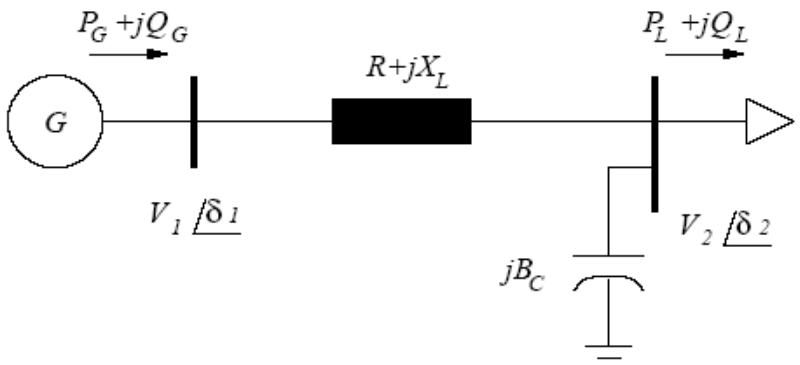


Figure 3.3 2-Bus power system diagram.

The disturbance of the system is the transmission line impedance change from 0.5 to 0.6. The system will experience collapse if no control is applied, and the collapse trajectory is shown in Figure 3.4.

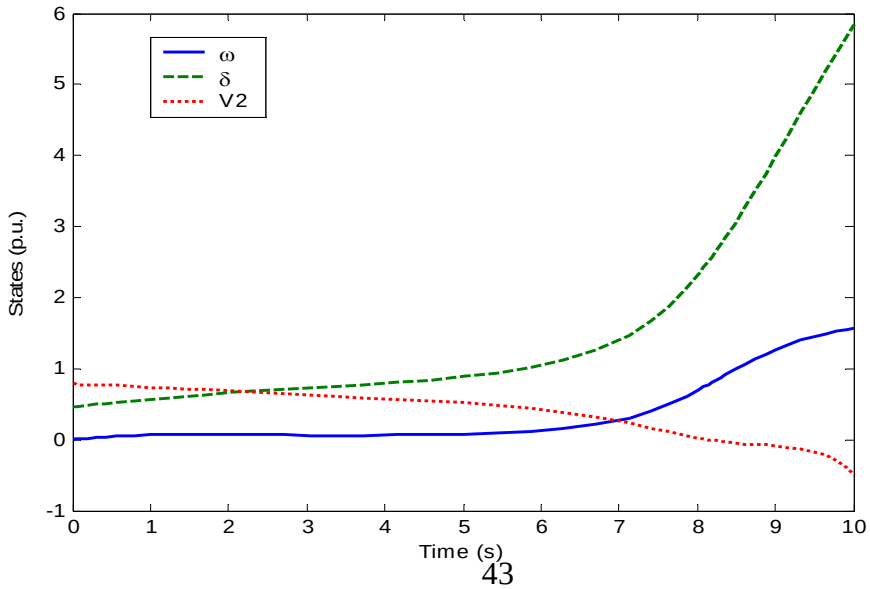


Figure 3.4 Trajectories after disturbance without control.

The system can reach post disturbance equilibrium if reactive power compensation is applied at load bus. The objective is chosen to minimize cost function $0.5\int_0^T B_C{}^2 dt$ where the end time is specified as 10 second, that is, the system will restore to a new operation points after 10 seconds. Load bus voltage is required to be greater than 0.75 during the transition period. The optimal control action of the reactive power compensation and the corresponding system trajectories are plotted in Figure 3.5.

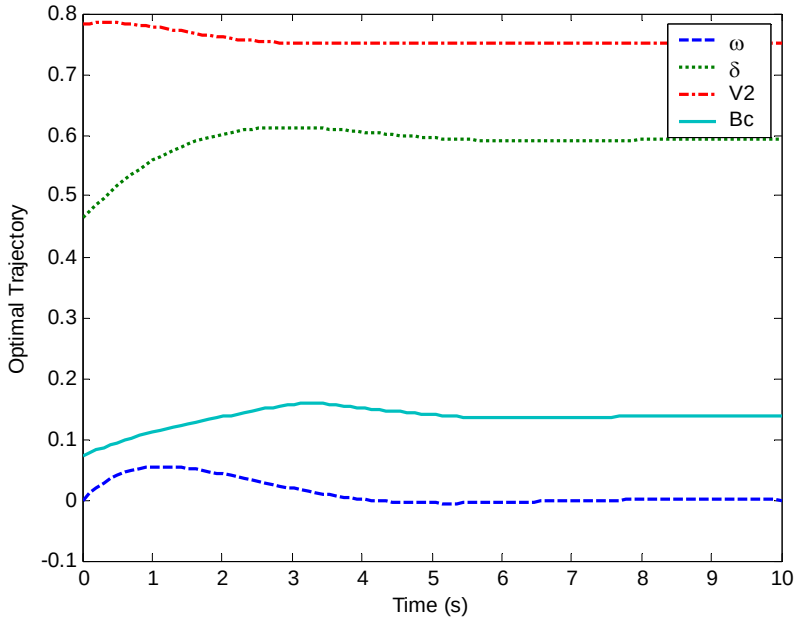


Figure 3.5 Constrained optimal trajectories with reactive power compensation.

3.3.2 IEEE 39 Bus system

The trajectory optimization method is applied to IEEE 39 bus New England system which has 39 buses and 10 generators. The disturbance is the loss of two transmission lines

line 2-3 and line 6-7. The system response after line loss is shown in Figure 3.6. This is a very interesting problem as it has voltage dip problem followed by low voltage problem which may trigger protection device, and finally voltage collapse.

An initial set of 10 possible candidate locations is selected [3, 6, 13, 16, 19, 23, 25, 26, 29, 39] from the given 39 bus system. It can be observed that even for this reduced set of 10 candidate locations there are 1023 different possible control locations. However this complete enumeration has been avoided by using SA. By using SA only 150 different combinations were used thus a huge saving in computational time. Another advantage of SA is that it can avoid entrapment in local minima and can give a solution closer to global optimum. The final optimal solution obtained from Simulated Annealing and Trajectory Optimization is dynamic VAR support at 3 buses i.e. at bus 6, 23, 29. This gives the minimum number of locations and their amount.

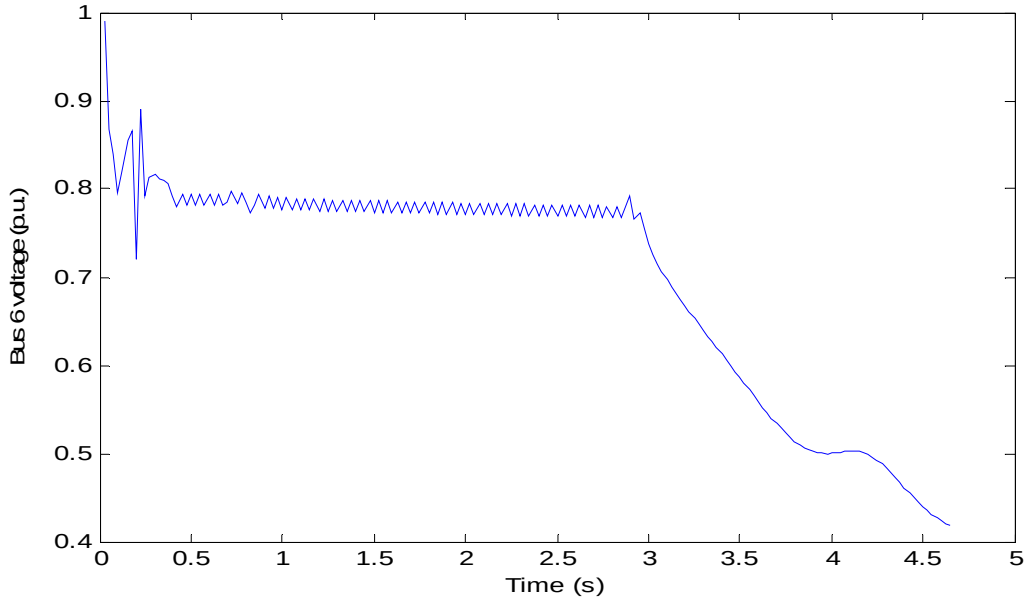


Figure 3.6 Voltage trajectory after disturbance.

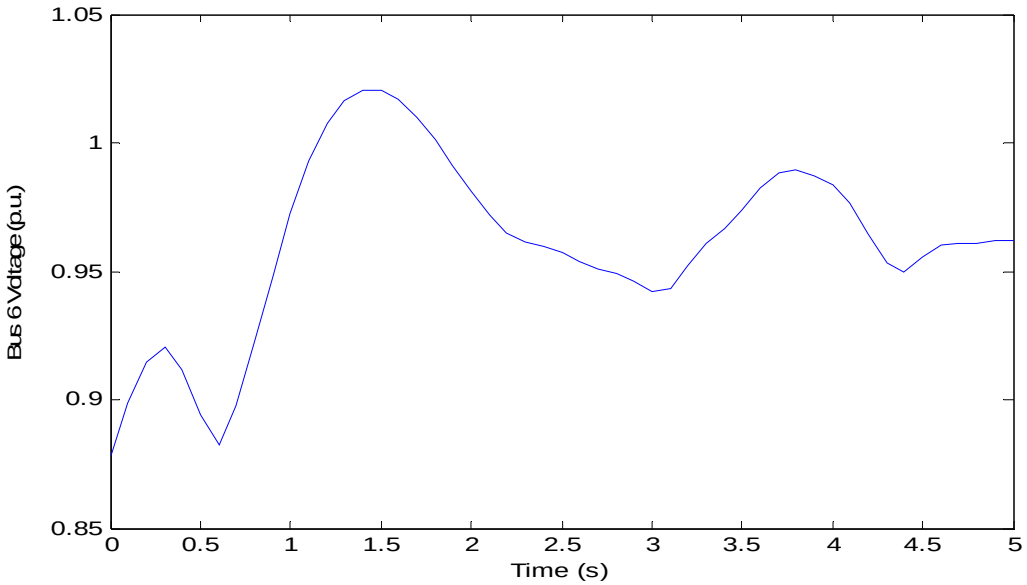


Figure 3.7 Voltage trajectory after control.

Figure 3.7 shows voltage trajectory after applying optimal control at locations 6, 23, 29. In Table 3.1 a small portion of the result is shown to compare different feasible solutions. It can be observed from the result that there exist different feasible and local optimal solutions.

Table 3.1 Different feasible solutions

Buses	Max. Q Output (p.u.)	Total Max. Q Output (p.u.)
6, 23, 29	0.89, 0.44, 0.38	1.71
6, 23, 26	0.89, 0.63, 0.58	2.10
6, 19, 29	0.86, 0.67, 0.71	2.24
6, 29, 39	1.43, 0.53, 0.44	2.39

3.4 Conclusions

In this work, mixed integer trajectory optimization methodology is being developed to solve dynamic VAR allocation problem. The problem is divided into two subproblems: master and primal problem. The master problem deals with binary variables and is solved by using simulated annealing. The primal problem corresponds to trajectory optimization part and is solved by using Hamiltonian method. The trajectory optimization problem is formulated as a DAE model to accurately examine system dynamics. In addition to that point equalities, inequalities and path inequality constraints are also considered. Thus the optimal VAR allocation obtained after solving the MITO problem ensures system robustness and reliability against credible contingencies. Also, w.r.t. to control the information obtained from MITO such as time varying response and maximum amount of control needed a proper dynamic VAR device selection can be made.

CHAPTER 4. CONTRIBUTIONS

The major contributions of this project are:

1) Developed a generalized methodology for contingency filtering and ranking with respect to voltage dip and instability problem.
2) Developed an early termination methodology for safe contingencies to make the filtering process fast. Also further classification of safe contingencies is proposed which can be used for better understanding of system dynamics.
3) Both contingency severity index and dynamic bus voltage vulnerability index have been defined to find severity of a contingency and vulnerability of a bus.
4) The information obtained from contingency assessment is used in optimization framework to find optimal VAR location and amount.
5) The optimal VAR allocation problem is formulated and solved using Mixed Integer Trajectory Optimization approach. The obtained optimal location and amount of VAR sources ensure system robustness against any credible contingency.

4.1 Publications related to proposed research

1. A. Tiwari, V. Ajjarapu, “Optimal allocation of dynamic VAR for enhancing stability and power quality” IEEE Trans. (To be submitted)

2. D. Yang, V. Ajjarapu, “Power system dynamic security analysis via trajectory optimization” IEEE Trans. (To be submitted)

3. D. Yang, V. Ajjarapu, “A decoupled time domain simulation method via invariant subspace partition for power system analysis” IEEE Trans. vol. 21, issue 1, Feb. 2006.

4. A. Tiwari, V. Ajjarapu, “Contingency Assessment for Voltage Dip and Short Term Voltage Stability Analysis" Bulk Power System Dynamics and Control, Aug. 19-24, 2007.

REFERENCES

[1] G. S. Vassell, "Northeast Blackout of 1965," *IEEE Power Engineering Review*, vol. 11, pp. 4-8, Jan. 1991.

[2] U.S.-Canada Power System Outage Task Force, "Final Report on the August 14, 2003, Blackout in the United States and Canada: Causes and Recommendations," U.S. Department of Energy, Washington, D.C. April 2004.

[3] P. Fairley, "The unruly power grid," *IEEE Spectrum*, vol. 41, pp. 22-27, August 2004.

[4] P. Kundur, J. Paserba, V. Ajjarapu, G. Andersson, A. Bose, C. Canizares, N. Hatziargyriou, D. Hill, A. Stankovic, C. Taylor, T. Van Cutsem, and V. Vittal, "Definition and classification of power system stability IEEE/CIGRE joint task force on stability terms and definitions," *IEEE Transactions on Power Systems*, vol. 19, pp. 1387-1401, 2004.

[5] X. Wang, and J. R. McDonald, Modern power system planning, New York: McGraw Hill, 1994.

[6] Western Electricity Coordinating Council. NERC/WECC planning standards. [Online]. Available: http://www.wecc.biz/documents/library/procedures/CriteriaMaster.pdf (Date accessed: Mar. 9, 2007).

[7] IEC 61000-4-30 "Electromagnetic Compatibility (EMC) – Part 4-30: Testing and Measurement Techniques – Power Quality Measurement Methods," Feb. 2003.

[8] A. Hammad and M. El-Sadek, “Prevention of transient voltage instabilities due to induction motor loads by static VAr compensators,” *IEEE Trans. Power Syst.*, Vol. 4, pp. 1182– 1190, Aug. 1989.

[9] D. J. Shoup, J. J. Paserba, C. W. Taylor, "A survey of current practices for transient voltage dip/sag criteria related to power system stability," in *Proc. of the IEEE Power Engineering Society Power Systems Conference and Exposition*, Oct. 2004, pp. 1140-1147.

[10] M. Ni, J. D. McCalley, V. Vittal, T. Tayyib, “Online risk-based security assessment,” IEEE Trans. Power Syst., vol. 18, no. 1, pp. 258–265, Feb. 2003.

[11] B. Venkatesh, G. Sadasivam, M. A. Khan, “Optimal reactive power planning against voltage collapse using the successive multiobjective fuzzy LP technique,” Proc. Inst. Elect. Eng., Gen., Trans., Distrib., vol. 146, no. 4, pp. 343–348, Jul. 1999.

[12] T. Jain, L. Srivastava, and S. N. Singh, “Fast voltage contingency screening using radial basis function neural network,” IEEE Trans. Power Syst., vol. 18, no. 4, pp. 1359–1366, Nov. 2003.

[13] C.D. Vournas, E.G. Potamianakis, “Induction Machine Short-term Voltage Stability and Protection Measures”, IEEE PSCE, pp: 993 – 998, Oct. 29-Nov. 1 2006.

[14] J.A. Diaz de Leon II, C.W. Taylor, “Understanding and solving short-term voltage stability problems”, IEEE PES, Vol. 2, pp: 745-752, June 2002.

[15] V. Stewart, E.H. Camm, “Modeling of stalled motor loads for power system short-term voltage stability analysis”, IEEE PES, Vol. 2, pp: 1887-1892, June 2005.

[16] B. Koeunyi, J.S. Thorp, “An importance sampling application: 179 bus WSCC system undervoltage based hidden failures and relay misoperations”, Thirty-First Hawaii International Conference on System Sciences, Vol.3, pp: 39-46, 1998.

[17] Geun-Joon Lee, M.M. Albu, G. T. Heydt, “A power quality index based on equipment sensitivity, cost, and network vulnerability” IEEE Trans. on Power Delivery, Vol. 19, Issue 3, July 2004 pp:1504-1510.

[18] C. W. Taylor, *Power System Voltage Stability*, EPRI/McGraw Hill, 1994.

[19] J.W. Shaffer, “Air conditioner response to transmission faults”, IEEE Trans. on Power Systems, Vol. 12, Issue 2, May 1997, pp:614 – 621.

[20] V. Brandwajn, “Efficient bounding method for linear contingency analysis,”IEEE Trans. Power Syst., vol. 3, no. 1, pp. 38–43, Feb. 1988.

[21] F. D. Galiana, “Bound estimates of the severity of line outages in power system contingency analysis and ranking,” IEEE Trans. Power App. Syst., vol. 103, no. 9, pp. 2612–2624, Sep. 1984.

[22] T. Smed, “Feasible eigenvalue sensitivity for large power systems,” IEEE Trans. Power Syst., vol. 8, no. 2, pp. 555–561, May 1993.

[23] H. K. Nam, Y. K. Kim, K. S. Shim, and K. Y. Lee, “A new Eigen-sensitivity theory of augmented matrix and its applications to power system stability analysis,” *IEEE Trans. Power Syst.*, vol. 15, no. 1, pp. 363–369, Feb. 2000.

[24] A. C. Zambroni, “Identifying a vanishing eigenvalue in voltage collapse analysis with consideration of limits,” Proc. Inst. Elect. Eng., Gen., Trans., Distrib., vol. 148, no. 2, pp. 263–267, Mar. 2001.

[25] D.J. Tylavsky, A. Bose, et al, "Parallel Processing in Power Systems Computation", IEEE Transactions on Power Systems, Vo1.7, no.2, pp. 629-638, May 1992.

[26] G. Aloisio, M.A. Bochicchio, M. La Scala, R. Sbrizzai, “A distributed computing approach for real-time transient stability analysis”, IEEE Transactions on Power Systems, Vo1.12, no.2, May 1997, pp. 981-987.

[27] D. Yang, V. Ajjarapu, “A decoupled time-domain simulation method via invariant subspace partition for power system analysis”, IEEE Trans. on power systems, Vol. 21, no. 1, Feb. 2006.

[28] P.W. Sauer, M.A. Pai, “Power system dynamics and stability” Englewood cliffs, NJ: Prentice-Hall, 1998.

[29] P. Kundur, “Power system stability and control” New York: McGraw-Hill, 1994.

[30] Z. Feng, V. Ajjarapu, B. Long, “Identification of voltage collapse through direct equilibrium tracing,” IEEE Trans. Power Syst., Vol. 15, no.1, pp.342-349, Feb. 2000.

[31] Henville C.F., “Power quality impacts on protective relays-and vice versa”, IEEE PES, vol. 1, Jul.2001, pp: 587-592.

[32] Bae K., Thorp J. S., “An importance sampling application: 179 bus WSCC system under voltage based hidden failures and relay misoperations”, System Sciences, HICSS Proc., vol. 3, Jan. 1998, pp: 39-46.

[33] Gerbex S., Cherkaoui R., Germond A.J., “Optimal location of FACTS devices to enhance power system security”, IEEE Proc., Power Tech. Conference, vol. 3, Jun. 2003.

[34] Mahdad B., Bouktir T., Srairi K., “Strategy of location and control of FACTS devices for enhancing power quality”, IEEE MELCON, May 2006, pp: 1068-1072.

[35] Chakrabarti B.B., Chattopadhyay D., Krumble C., “Voltage stability constrained VAr planning-a case study for New Zealand ”, IEEE power engineering LESCOPE, Jul. 2001, pp: 86-91.

[36] Hsiao Y.-T., Liu C.-C., Chiang H.-D., Chen Y.-L., “A new approach for optimal VAr sources planning in large scale electric power systems”, IEEE Trans. on Power Systems, vol. 8, no. 3 Aug. 1993.

[37] Chiang H.-D., Thorp J.S., Wang J.-C., Lu J., Aubert B., “Optimal controller placements in large-scale linear systems”, IEE Proc., Control Theory and Applications, vol. 139, no. 1, Jan. 1992, pp. 79–87.

[38] Nuqui R.F., Phadke A.G., “Phasor measurement unit placement techniques for complete and incomplete observability”, IEEE Trans. on Power Delivery, vol. 20, no. 4, Oct. 2005, pp. 2381–2388.

[39] Brian C. Fabien, "An extended penalty function approach to the numerical solution of constrained optimal control problems," *Optimal Control Applications & Methods*, vol. 17, pp. 341-355, 1996.

[40] Stephen Wiggins, *Introduction to applied nonlinear dynamical systems and chaos*, 2nd ed. New York: Springer, 2003.

[41] John Guckenheimer and Philip Holmes, *Nonlinear oscillations, dynamical systems and bifurcations of vector fields*. New York: Springer-Verlag, 1983.

[42] U. M. Ascher, Robert M. M. Mattheij, and R. D. Russell, *Numerical solution of boundary value problems for ordinary differential equations*. Englewood Cliffs, N.J.: Prentice Hall, 1988.

[43] Josef Stoer and Roland Bulirsch, *Introduction to numerical analysis*, 3rd ed. New York: Springer, 2002.

[44] J. R. Cash, "A survey of some global methods for solving two-point BVPs," *Applied Numerical Analysis and Computational Mathematics*, vol. 1, pp. 7-17, 2004.

[45] Aarts E., Korst J., “Simulated Annealing and Boltzmann machines”, A stochastic approach to combinatorial optimization and neural computing. John Wiley & sons Ltd., 1989.

[46] Laarhoven P. J. M., Aarts E., “Simulated Annealing: theory and applications”, Kluwer Academic Publisher, 1987.

[47] Yang D., “Power system dynamic security analysis via decoupled time domain simulation and trajectory optimization” PhD Thesis 2006.

Optimal Allocation of Static and Dynamic VAR Resources

Volume 3

Prepared by

Jim McCalley
Iowa State University

Information about this project

For information about this project contact:

James D. McCalley
Iowa State University
Electrical and Computer Engineering Dept.
Ames, Iowa 50011
Phone: 515-294-4844
Fax: 515-294-4263
Email: jdm@iastate.edu

Power Systems Engineering Research Center

This is a project report from the Power Systems Engineering Research Center (PSERC). PSERC is a multi-university Center conducting research on challenges facing the electric power industry and educating the next generation of power engineers. More information about PSERC can be found at the Center's website: http://www.pserc.org.

For additional information, contact:

Power Systems Engineering Research Center
Arizona State University
577 Engineering Research Center
Box 878606
Tempe, AZ 85287-8606
Phone: 480-965-1643
FAX: 480-965-0745

Notice Concerning Copyright Material

PSERC members are given permission to copy without fee all or part of this publication for internal use if appropriate attribution is given to this document as the source material. This report is available for downloading from the PSERC website.

**© 2008 Georgia Institute of Technology, Arizona State University, Iowa State University, and the Board of Regents of the University of Wisconsin System.
All rights reserved.**

Table of Contents

1.0 Introduction 1
1.1 Voltage Stability and Reactive Power Control 1
1.2 Reactive Power Control Planning 5
1.3 Report Organization 9
2.0 Linear Complexity Search Algorithm to Locate Reactive Control 11
2.1 Introduction 11
2.2 Voltage Stability Margin Sensitivity 11
2.3 Optimization Problem Formulation 13
2.4 Methodology 14
2.4.1 Overall Procedure 14
2.4.2 Backward Search Algorithm 16
2.4.3 Forward Search Algorithm 18
2.5 Case Study 19
2.5.1 Candidate Location Selection for Shunt Capacitors 20
2.5.2 Candidate Location Selection for Series Capacitors 24
2.6 Summary 26
3.0 Reactive Power Control Planning to Restore Equilibrium 27
3.1 Introduction 27
3.2 Contingency Analysis via Parameterization and Continuation 27
3.2.1 Parameterization of Branch Outage 27
3.2.2 Parameterization of HVDC Link Outage 28
3.2.3 Parameterization of Generator Outage 30
3.2.4 Continuation Method 30
3.3 Formulation for Reactive Power Control Planning 32
3.3.1 Flowchart for Reactive Power Control Planning 32
3.3.2 Voltage Stability Analysis 32
3.3.3 Selection of Candidate Control Locations 33
3.3.4 Formulation of Initial Mixed Integer Programming 33
3.3.5 Formulation of MIP with Updated Information 34
3.4 Application to New England System 35
3.5 Summary 38
4.0 Reactive Power Control Planning to Increase Voltage Stability Margin 39
4.1 Introduction 39
4.2 Algorithm of Reactive Power Control Planning 40
4.2.1 Selection of Candidate Control Locations 40
4.2.2 Formulation of Initial Mixed Integer Programming 41
4.2.3 Formulation of MIP with Updated Information 42
4.3 Numerical Results 43
4.4 Summary 45

5.0 Optimal Allocation of Static and Dynamic Var Resources 47
5.1 Introduction 47
5.2 Transient Voltage Sensitivities 48
5.2.1 Sensitivity of Voltage Dip Time Duration to SVC Capacitive Limit 49
5.2.2 Sensitivity of Maximum Transient Voltage Dip to SVC Capacitive Limit 49
5.2.3 Numerical Approximation 50
5.3 Algorithm of Optimal Allocation of Static and Dynamic VAR Resources 50
5.3.1 Contingency Analysis 51
5.3.2 Selection of Candidate VAR Locations 52
5.3.3 Formulation of Initial Mixed Integer Programming 52
5.3.4 Formulation of MIP with Updated Information 54
5.4 Numerical Results 55
5.5 Summary 60
6.0 Application to Large-Scale System 61
6.1 Introduction 61
6.2 Basecase and Stress Direction 61
6.3 Contingency Screening for MZ1 63
6.4 Reactive Resources To Restore Equilibrium 65
6.4.1 Candidate location selection 65
6.4.2 Cost information used 68
6.4.3 Required margin 69
6.4.4 Optimal allocation 69
6.5 Reactive Resources to Increase Voltage Stability Margin 71
6.5.1 First iteration optimization 71
6.5.2 Successive iteration optimization 72
6.6 Reactive Resources for Static and Dynamic Problems 75
6.6.1 Contingency Screening and Analysis 75
6.6.2 Candidate Locations for SVC 81
6.6.3 Sensitivities 82
6.6.4 Stage 1 Optimization 82
6.7 Summary 89
7.0 Conclusions and Future Work 90
7.1 Conclusions 90
7.2 Future Work 91
Appendix A: Hybrid System Model 92
Appendix B: Trajectory Sensitivities 93
References 94

List of Tables

Table 1.1 Capabilities of different reactive power control devices 5
Table 1.2 Cost comparison for reactive power control devices 5
Table 2.1 Base case loading and dispatch for the modified WECC system 20
Table 2.2 Voltage stability margin under contingencies for the WECC system 20
Table 2.3 Steps taken in the backward search algorithm for shunt capacitor planning 21
Table 2.4 Steps taken in forward search algorithm for shunt capacitor planning 23
Table 2.5 Steps taken in forward search algorithm for series capacitor planning 25
Table 3.1 Parameter values in the optimization formulation to restore equilibrium 36
Table 3.2 Critical point under two severe contingencies for the New England system 37
Table 3.3 Control allocations for shunt and series capacitors to restore equilibrium 37
Table 3.4 Critical point under planned controls 38
Table 4.1 Parameter values in the optimization formulation 44
Table 4.2 Voltage stability margin under three moderate contingencies 44
Table 4.3 Control allocations for shunt capacitors to increase voltage stability margin 45
Table 4.4 Control allocations for shunt, series capacitors to increase voltage stability margin 45
Table 4.5 Voltage stability margin under planned controls 45
Table 5.1 Parameter values adopted in optimization problem 56
Table 5.2 Contingencies violating reliability criteria 56
Table 5.3 Allocation of mechanically switched shunt capacitors 57
Table 5.4 Allocation of SVCs 57
Table 5.5 System performance under planned static and dynamic VARs 58
Table 6.1 Summary of the basecase 62
Table 6.2 Market Zones within the Study Area 62
Table 6.3 Performance measure for basecase conditions 63
Table 6.4 Critical Contingencies 64
Table 6.5 Candidate location set for N-G-T, where Gen at 97451 is outaged 66
Table 6.6 Candidate location set for N-G-T, where Gen at 97452 is outaged 66
Table 6.7 Maximum shunt compensation at various voltage levels 67
Table 6.8 Initial candidate control location set - stage1 MIP for planning problem # 1 68
Table 6.9 Cost formulation at various voltage levels 69
Table 6.10 Optimal allocation from first iteration for equilibrium restoration problem 70
Table 6.11 Optimal allocation from second iteration for equilibrium restoration problem 70
Table 6.12 Final optimal allocation solution for equilibrium restoration 71
Table 6.13 Optimal allocation from first iteration to increase margin 72
Table 6.14 Final solution for optimal allocation to increase margin 73
Table 6.15 Final solution for static vars considering subset of contingencies 74
Table 6.16 Final solution for static vars considering all contingencies 74
Table 6.17 Buses resulting in transient voltage dip violation for contingency 1 76
Table 6.18 Buses resulting in transient voltage dip violation for contingency 2 77
Table 6.19 Buses resulting in transient voltage dip violation for contingency 3 78

Table 6.20 Buses resulting in transient voltage dip violation for contingency 4 78
Table 6.21 Buses resulting in transient voltage dip violation for contingency 5 79
Table 6.22 Buses resulting in transient voltage dip violation for contingency 6 80
Table 6.23 Buses resulting in transient voltage dip violation for contingency 7 81
Table 6.24 Contingency ranking in terms of worst-case recovery times 81
Table 6.25 Candidate SVC locations 82
Table 6.26 Recovery time sensitivity ($\Delta\tau_i dip/\Delta B_j SVC$) for Contingency 1 82
Table 6.27 Result of first iteration stage 1 MIP optimization 83
Table 6.28 Voltage instability margin for stage 1 solution 84
Table 6.29 Result of second iteration stage 1 MIP optimization 87
Table 6.30 Final Solution 89

List of Figures

Figure 1-1 Classification of power system stability 2
Figure 1-2 Voltage stability margin under different conditions 3
Figure 1-3 Voltage performance parameters for NREC/WECC planning standards 4
Figure 1-4 Flowchart for reactive power control planning 9
Figure 2-1 Determination of expansion year 15
Figure 2-2 Flowchart for candidate control location selection 16
Figure 2-3 Graph for 4-switch problem 18
Figure 2-4 Modified WECC nine-bus system 19
Figure 2-5 Graph for the backward search algorithm for shunt capacitor planning 22
Figure 2-6 Graph for the forward search algorithm for shunt capacitor planning 23
Figure 2-7 Graph for the forward search algorithm for series capacitor planning 25
Figure 3-1 Parameterization of branch outage 28
Figure 3-2 Parameterization of HVDC link outage 29
Figure 3-3 Bifurcation curve obtained by the continuation method 31
Figure 3-4 Flowchart for the minimum reactive power control planning to restore equilibrium 32
Figure 3-5 New England 39-bus test system 36
Figure 4-1 Flowchart for reactive power control planning to increase voltage stability margin 40
Figure 5-1 Static VAR compensator model 48
Figure 5-2 Slow voltage recovery after a fault 49
Figure 5-3 Flowchart for the static and dynamic VAR allocation 51
Figure 5-4 Voltage response at bus 7 under contingency 2 58
Figure 5-5 SVC output at bus 6 under contingency 2 59
Figure 5-6 SVC output at bus 7 under contingency 2 59
Figure 6-1 Bus 97455 voltage profile under contingency 1 with SVC after stage 1 MIP 84
Figure 6-2 Voltage profiles of some buses under contingency 2 without SVC 85
Figure 6-3 Voltage profiles of some buses under contingency 2 with SVC from first iteration optimization 85
Figure 6-4 Voltages under contingency 3 before and after first iteration SVC placement 86
Figure 6-5 Bus voltages under contingency 1 without any SVCs 87
Figure 6-6 Bus voltages under contingency 1 for SVC solution of 2nd iteration optimization 88
Figure 6-7 Bus 97455 voltage profile under contingency 1 with SVC after implementing solution from second iteration stage 1 optimization 88

1.0 Introduction

Future reliability levels of the electric transmission system require proper long-term planning to strengthen and expand transmission capability so as to accommodate expected transmission usage growth from normal load growth and increased long-distance power transactions. There are three basic options for strengthening and expanding transmission: (1) build new transmission lines, (2) build new generation at strategic locations, and (3) introduce additional control capability. Although all of these will continue to exist as options in the future, it is clear that options (1) and (2) have and will continue to become less and less viable. One obvious impediment to construction of new transmission is the need to acquire new right-of-way. This is not only expensive but also politically difficult due to environmental concerns as well as the public's inherent resistance to siting high voltage facilities close to home or work. The recent emphasis on managing (particularly maintaining) existing assets is a response to this trend. In addition, the disaggregation of the traditional regulated, monopolistic utility company into a multiplicity of generation, transmission, distribution, and power marketing companies hinders strategic siting of generation for purposes of transmission enhancement since generation and transmission are owned and operated by separate organizations.

As a result, there is significantly increased potential for application of additional power system control in order to strengthen and expand transmission in the face of growing transmission usage. The incentives for doing so are clear: there is little or no right-of-way, and relative to building new transmission or generation facilities, capital investment is much less.

Although considerable work has been done in planning transmission in the sense of options (1)-(2), there has been little effort towards planning transmission control options in the sense of option (3), yet the ability to consider these devices in the planning process is a clear need to the industry [1, 2, 3, 4]. The capacity of electric transmission systems may be constrained by thermal limits, voltage magnitude limits, or stability limits. Reference [5] provides a summary of power system planning methods to relieve thermal overloads or voltage magnitude violations on transmission facilities. There is less work done in the field of power system control planning to enhance the transmission system constrained by stability problems.

The objective of this work is to design systematic control system planning algorithms to expand the capability of electric transmission systems with stability constraints. The proposed control planning algorithm will answer the following three questions:

- what type of control device is needed,
- where to implement the enhancement, and
- how much is the control device needed.

1.1 Voltage Stability and Reactive Power Control

In the IEEE/CIGRE report [6], power system stability can be classified into rotor angle stability, voltage stability, and frequency stability as shown in Figure 1-1:

- Rotor angle stability refers to the capability of synchronous machines in an interconnected power system to remain in synchronism subjected to a disturbance.

- Voltage stability refers to the capability of a power system for maintenance of steady voltages at all buses in the system subjected to a disturbance under given initial operating conditions.
- Frequency stability refers to the capability of a power system for maintenance of steady frequency following a severe system upset resulting in a significant imbalance between generation and load.

All these stability problems can lead to system failure [7]. However, voltage instability has been a cause of several recent major power outages worldwide [7], [8]. In this work, we focus on systems only having the voltage stability problem. The proposed control planning approach can be extended to consider other stability/security problems as well.

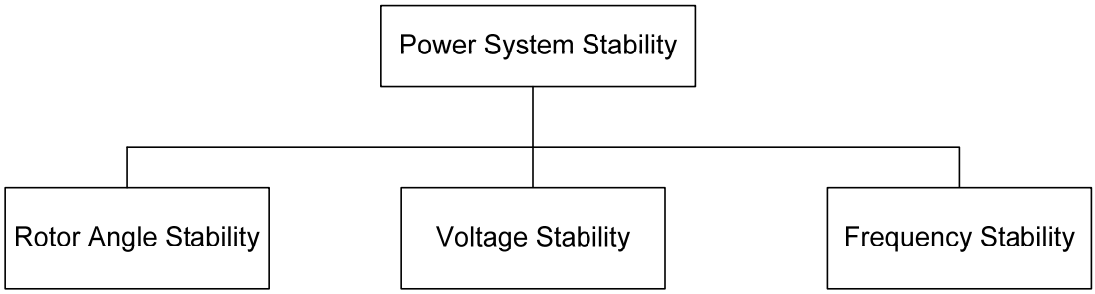


Figure 1-1 Classification of power system stability

Planning power systems is invariably performed under the assumption that the system is designed to withstand a certain set of contingencies. There is currently a disturbance-performance table within the NERC (North American Electric Reliability Corporation)/WECC (Western Electricity Coordinating Council) planning standards [9] which provides minimum post-disturbance performance specifications for credible events. The post-disturbance performance criteria regarding voltage stability include:

- Minimum post-contingency voltage stability margin,
- Transient voltage dip criteria (magnitude and duration).

The rest of this section will introduce voltage stability margin and transient voltage dip. Voltage stability margin is defined as the amount of additional load in a specific pattern of load increase that would cause voltage instability as shown in Figure 1-2. The potential for contingencies such as unexpected component (generator, transformer, transmission line) outages in an electric power system often reduces the voltage stability margin [10], [24]. Note that severe contingencies may cause the voltage stability margin to be negative (i.e. voltage instability).

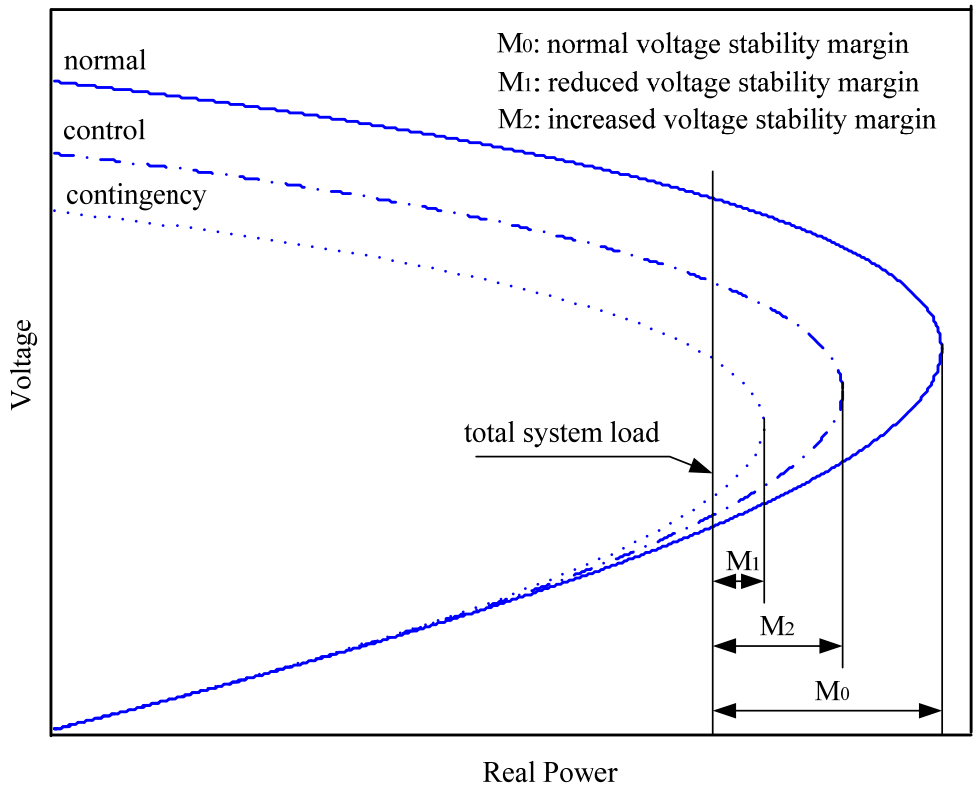


Figure 1-2 Voltage stability margin under different conditions

A power system may have the minimum post-contingency voltage stability margin requirement. For example, the NERC/WECC voltage stability criteria require that:

- The post-contingency voltage stability margin must be greater than 5% for N-1 contingencies;
- The post-contingency voltage stability margin must be greater than 2.5% for N-2 contingencies;
- The post-contingency voltage stability margin must be greater than 0% for N-3 contingencies.

Appropriate power system control devices can be used to increase the voltage stability margin. Figure 1-2 shows the voltage stability margin under different operating conditions and controls.

On the other hand, transient voltage dip is a temporary reduction of the voltage at a point in the electrical system below a threshold [11]. It is also called transient voltage sag. Excessive transient voltage dip may cause fast voltage collapse [4]. In this work, we focus on the transient voltage dip after a fault is cleared. Reference [12] provides information on transient voltage dip criteria following fault clearing related to power system stability. Information was included from utilities, reliability councils, relevant standards, and industry-related papers. The WECC criteria on transient voltage dip are summarized in the following and will be used to illustrate the proposed control planning approach.

The WECC transient voltage dip criteria are specified in a manner consistent with the NERC performance levels of (A) no contingency, (B) an event resulting in the loss of a

single element, (C) event(s) resulting in the loss of two or more (multiple) elements, and (D) an extreme event resulting in two or more (multiple) elements removed or cascading out of service conditions, as follows:

- NERC Category A: Not applicable.
- NERC Category B: Not to exceed 25% at load buses or 30% at non-load buses. Not exceed 20% for more than 20 cycles at load buses.
- NERC Category C: Not to exceed 30% at any bus. Not to exceed 20% for more than 40 cycles at load buses.
- NERC Category D: No specific voltage dip criteria.

Figure 1-3 shows the WECC voltage performance parameters with the transient voltage dip criteria clearly illustrated [9]. Again, appropriate power system controls can be utilized to mitigate the post-contingency transient voltage dip problem.

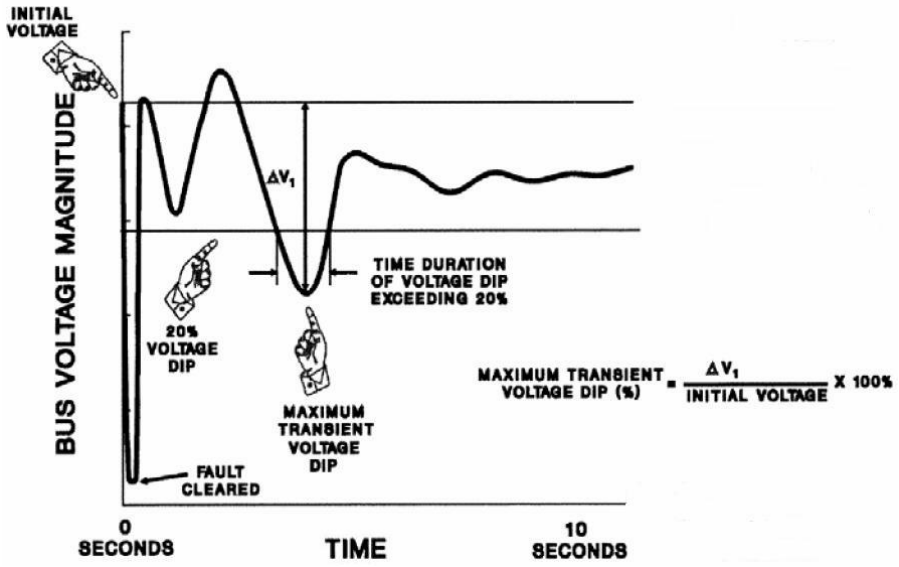


Figure 1-3 Voltage performance parameters for NREC/WECC planning standards

There are two types of control technologies that are today and most certainly will continue to be available to power system control engineers to counteract voltage stability problems. These include:

- Power-electronic based transmission control: static VAR compensators (SVC), thyristor controlled series capacitors (TCSC), Static Compensator (STATCOM) and others that comprise the family of control technology generally referred to as flexible AC transmission systems (FACTS) [13].
- System protection schemes (SPS): mechanically switched shunt/series capacitors (MSC) and others. MSCs have been used for post-contingency control [14, 15, 16, 17, 18, 19, 20, 21].

Of these, the first exerts continuous feedback control action; the second exerts discrete open-loop control action. Based on the response time, SVC and TCSC are often called dynamic VAR resources. MSC belongs to static VAR resources. Both static and dynamic VAR resources belong to reactive (power) control devices. SVC and TCSC are effective countermeasures to increase voltage stability margin and to counteract transient voltage dip

problems. However, much cheaper MSC is often sufficient for increasing voltage stability margin [22]. In the MSC family, mechanically switched shunt capacitors are usually cheaper than mechanically switched series capacitors while their effectiveness depends on characteristics of power systems.

On the other hand, SVC and TCSC can effectively mitigate transient voltage dip problems since they can provide almost instantaneous and continuously variable reactive power in response to grid voltage transients. It is hard for MSCs to counteract transient voltage dip problems because they can not be switched on and off rapidly and frequently and because the control amount is discrete. The various functions achievable by different reactive power control devices are summarized in Table 1.1.

Table 1.1 Capabilities of different reactive power control devices

	Static VAR		Dynamic VAR	
	Mechanically switched shunt cap.	Mechanically switched series cap.	SVC	TCSC
Increase voltage stability margin	Yes	Yes	Yes	Yes
Transient voltage dip	No	No	Yes	Yes

A cost comparison of static and dynamic VAR resources is presented in Table 1.2 [23], [24]. The final selection of a specific reactive power control devices should be based on a comprehensive technical and economic analysis.

Table 1.2 Cost comparison for reactive power control devices

	Static VAR		Dynamic VAR	
	Mechanically switched shunt capacitor (500 kV)	Mechanically switched series capacitor (500 kV)	SVC	TCSC
Variable cost ($ million/100 MVar)	0.41	0.75	5.0	5.0
Fixed cost ($ million)	1.3	2.8	1.5	1.5

1.2 Reactive Power Control Planning

The problem addressed in this work is similar to the traditional reactive power planning problem [25], [26], [27], [28]. Generally, the reactive power planning problem can be formulated as a mixed integer nonlinear programming problem to minimize the installation cost of reactive power devices plus the system real power loss or production cost under the normal operating condition subject to a set of power system equality and inequality constraints. In the work described in this report, however, we explicitly target the planning of

reactive power controls, i.e., reactive power devices intended to serve as control response for contingency conditions. Thus the system real power loss or production cost is not included in this work.

The reactive power control planning problem can be formulated as follows: minimize the installation cost of reactive power control devices subject to voltage stability margin and/or transient voltage dip requirements under a set of contingencies. It is complex to solve this problem because of its large solution space, large number of contingencies, difficulty in evaluating the performance of candidate solutions, and lack of efficient mathematical solution technique as described in what follows:

- Large solution space: The space of possible solutions is extremely large, since every bus and every transmission line offer possible control locations. If there are n candidate locations, the number of possible location combinations is 2^n. In addition, the control amount at each candidate location can vary from the minimum allowable value to the maximum allowable value.
- Large number of contingencies: There may exist a large number of N-1, N-2, or even N-3 contingencies having voltage stability problems. In the reactive power control planning, all of these contingencies need to be addressed.
- System performance evaluation: Voltage stability margin and transient voltage dip magnitude and duration are used to measure system performance. However, they can not be analytically expressed as functions of control variables. Measuring these indices under a certain disturbance followed by a specific control action requires numerical simulation.
- Lack of efficient mathematical solution technique: The reactive power control planning to increase voltage stability margin is essentially a MINLP problem. However, there is no general efficient mathematical programming technique for solving MINLP problems.

The existing literature about reactive power control planning can be classified into two groups. The first group deals with static VAR planning to increase voltage stability margin. The second group is about dynamic VAR planning to improve transient voltage performance or coordinated static and dynamic VAR planning.

There are a few references which address static VAR planning to increase voltage stability margin. Obadina et. al. in [29] developed a method to identify reactive power control that will enhance voltage stability margin. The reactive power control planning problem was formulated in two stages. The first stage involves solving a nonlinear optimization problem which minimizes the control amount at pre-specified locations. The second stage utilizes a mixed integer linear programming which maximizes the number of deleted locations and minimizes the control amount at the remaining locations. Xu, et. al. in [30] used the conventional power flow method to assess the voltage stability margin. The method scale up entire system load in variable steps until the voltage instability point is reached. The modal analysis of the power flow Jacobian matrix was used to determine the most effective reactive power control sites for voltage stability margin improvement. Mansour, et. al. in [31] presented a tool to determine optimal locations for shunt reactive power control devices. The tool first computes the critical modes in the vicinity of the point of voltage collapse. Then system participation factors are used to determine the most suitable sites of shunt reactive power control devices for transmission system reinforcement. Ajjarapu, et. al. in [32]

introduced a method of identifying the minimum amount of shunt reactive power support which indirectly maximizes the real power transfer before voltage collapse is encountered. The predictor-corrector optimization scheme was utilized to determine the maximum system loading point. The sensitivity of the voltage stability index derived from the continuation power flow (CPF) was used to select weak buses for locating shunt reactive power devices. A sequential quadratic programming algorithm was adopted to solve the optimization problem with the system security constraint. The objective function is minimizing the total reactive power injection at the selected weak buses. Overbye, et. al. in [33] presented a method to identify optimal control recommendations to mitigate severe contingencies under which the voltage stability margin is negative (i.e. there is no post-contingency equilibrium). The degree of instability was quantified using the distance in parameter space between the desired operating point and the closest solvable point. The sensitivities of this measure to system controls were used to determine the best way to mitigate the severe contingency. Chen, et. al. in [34] presented a weak bus oriented reactive power planning to counteract voltage collapse. The algorithm identifies weak buses based on the right singular vector of the power flow Jacobian matrix. Then the identified weak buses were selected as candidate shunt reactive power control locations. The smallest singular value was used as the voltage collapse proximity index. The optimization problem was formulated to maximize the minimum singular value. Simulated annealing was applied to search for the final optimal solution. Granville, et. al. in [35] described an application of an optimal power flow [36], solved by a direct interior point method, to restore post-contingency equilibrium. The set of control actions includes rescheduling of generator active power, adjustments on generator terminal voltage, tap changes on LTC transformers, and minimum load shedding. Chang, et. al. in [37] presented a hybrid algorithm based on the simulated annealing method, the Lagrange multiplier, and the fuzzy performance index method for the optimal reactive power control allocation. The proposed procedure has three identified objectives: maximum voltage stability margin, minimum system real power loss, and maximum voltage magnitudes at critical points. Vaahedi, et. al. in [38] evaluated the existing optimal VAR planning/OPF tools for the voltage stability constrained reactive power control planning. A minimum cost reactive power support scheme was designed to satisfy the minimum voltage stability margin requirement given a pre-specified set of candidate reactive power control locations. The problem formulation does not include the fixed VAR cost. The obtained results indicated that the OPF/VAR planning tools can be used to address the voltage stability constrained reactive power control planning. Additional advantages of these tools are: easier procedures and avoidance of engineering judgment in identifying the reactive power control amount at the candidate locations. Feng, et. al. in [39] identified reactive power controls to increase voltage stability margin under a single contingency using linear programming with the objective of minimizing the control cost. This formulation is suitable to the operational decision making problem. The fixed cost of new controls is not included in the formulation. Yorino, et. al. in [40] proposed a mixed integer nonlinear programming formulation for reactive power control planning which takes into account the expected cost for voltage collapse and corrective controls. The Generalized Benders Decomposition technique was applied to obtain the solution. The convergence of the solution can not be guaranteed because of the nonconvexity of the optimization problem. The proposed model does not include the minimum voltage stability margin requirement.

On the other hand, the available literature on the dynamic VAR planning or coordinated static and dynamic VAR planning is very limited. Donde et. al. [41] presented a method to calculate the minimum capacity requirement of an SVC which satisfies the post-fault transient voltage recovery requirement which is a specific case of the transient voltage dip requirement. Given the target transient voltage recovery time, the minimum SVC capacity was obtained by solving a boundary value problem using numerical shooting methods. The CIGRE report [42] presented a Q-V analysis based procedure for the use by system planners to determine the appropriate mixture of static and dynamic VAR resources at a certain bus. First, the intersection of the required minimum voltage and the post-fault Q-V curve considering the short-term exponential load characteristic determines the dynamic VAR requirement. Then, the intersection of the required minimum voltage and the post-fault Q-V curve with load modeled as constant power less the dynamic VAR requirement identified in the previous step is the needed amount of static VAR. An approach was presented in [3], [43], and [44] to identify static and dynamic reactive power compensation requirements for an electric power transmission system. First, optimal power flow techniques were used to determine the best locations for reactive power compensation. Then, Q-V analysis with the constant power load model was utilized to find the total amount of reactive compensation at identified locations. Finally, iterative time domain simulations were performed to determine a prudent mix of static and dynamic VAR resources. Kolluri et. al. presented a similar method in [45] to obtain the right mix of static and dynamic VAR resources in a utility company's load pocket. All of the coordinated methods mentioned above use a sequential procedure to allocate static and dynamic VAR resources.

This work develops a systematic approach for coordinated planning of static and dynamic VAR resources to satisfy the requirements of voltage stability margin and/or transient voltage dip under a set of contingencies and thus enhance transmission capability in voltage stability limited systems. We emphasize the coordinated planning of different types of VAR resources to achieve potential economic benefit. The proposed procedures for solving the reactive power control planning problem are based on the following assumptions:

- No new transmission equipment (lines and transformers) is installed, and that generation expansion occurs only at existing generation facilities. This assumption creates conditions that represent the extreme form of current industry trend of relying heavily on control to strengthen and expand transmission capability without building new transmission or strategically siting new generation.
- Existing continuous controllers: The power system has an existing set of continuous controllers that are represented in the model, including controls on existing generators.
- Candidate controllers: Candidate controllers include mechanically switched shunt/series capacitors or SVCs or coordinated use of any of these in combination.

The proposed reactive power control planning approach requires three basic steps: (i) development of generation/load growth futures, (ii) contingency analysis, (iii) planning of reactive power controls to satisfy the requirements of voltage stability margin and/or transient voltage dip. The overall flowchart of the proposed reactive power control planning algorithm is illustrated in Figure 1-4.

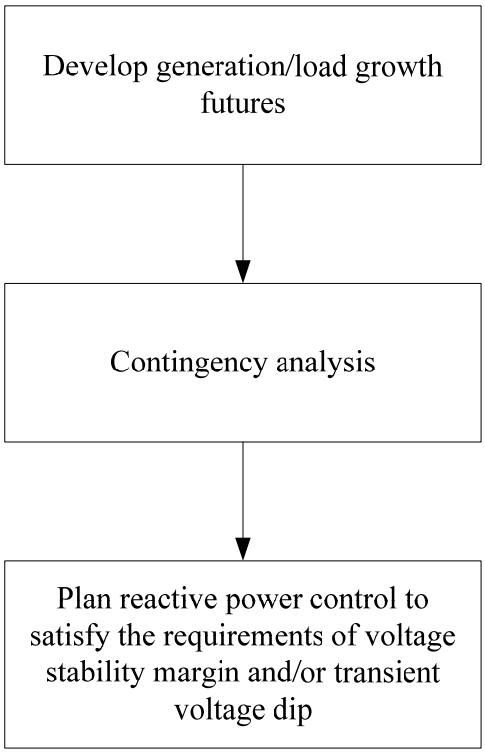


Figure 1-4 Flowchart for reactive power control planning

1.3 Report Organization

The rest of the report is organized as follows:

Chapter 2 presents a methodology to select candidate locations for reactive power controls while satisfying power system performance requirements. Optimal locations of new reactive power controls are obtained by the forward/backward search on a graph representing discrete configuration of controls. Further refinement of the control location and amount is ready to be done using the optimization methods presented in Chapters 3, 4 and 5. The proposed algorithm has complexity linear in the number of feasible reactive power control locations whereas the solution space is exponential.

Chapter 3 proposes a new successive mixed integer programming (MIP) based algorithm to plan the minimum amount of switched shunt and series capacitors to restore equilibria of a power system after severe contingencies. Through parameterization of the severe contingencies, the continuation method is applied to find the critical points. Then, the backward/forward search method and the bifurcation point sensitivities to reactive power controls are used to select candidate locations for switched shunt and series capacitors. Next, a mixed integer programming formulation is proposed to estimate locations and amounts of switched shunt and series capacitors. Finally, mixed integer programming problems with updated information are utilized to further refine the reactive power control locations and amounts.

Chapter 4 presents a successive MIP based method of reactive power control planning to increase voltage stability margin under a set of contingencies. The backward/forward search

algorithm and voltage stability margin sensitivities are used to select candidate locations for switched shunt and series capacitors. Optimal locations and amounts of new reactive power controls are obtained by solving a sequence of mixed integer programming problems.

Chapter 5 proposes a method to coordinate planning of static and dynamic VAR resources when simultaneously considering the performance requirements of voltage stability margin and transient voltage dip. Transient voltage dip sensitivities are derived to select candidate locations for dynamic VAR resources. The successive MIP is proposed to calculate the optimal mix of static and dynamic VAR resources.

Chapter 6 provides results for application of the approach to a large-scale power system.

Chapter 7 summarizes the specific contribution of the work and discusses the future work that needs to be done.

2.0 Linear Complexity Search Algorithm to Locate Reactive Control

2.1 Introduction

For reactive power control planning in large scale power systems, the pre-selection of the candidate locations to install new reactive power control devices is important. Usually, candidate control locations are chosen only based on the engineering judgment. There is no guarantee that the selected candidate control locations are effective and sufficient to provide required reactive power support for all concerned contingencies. On the other hand, the computational cost to solve the mixed integer linear/nonlinear programming problem for reactive power control planning may be high if the number of the candidate locations is large.

This chapter presents a method to select appropriate candidate locations for reactive power control devices using the backward/forward search. The proposed method is illustrated in selecting candidate reactive power control locations to increase post-contingency voltage stability margin. The same method will be used to select candidate reactive power control locations to restore post-contingency equilibria and to mitigate transient voltage dip in Chapters 4 and 5 respectively.

The chapter is organized as follows. Some fundamental concepts of voltage stability margin sensitivity are introduced in Section 2.2. Section 2.3 presents the problem formulation. Section 2.4 describes the proposed method of locating reactive power control devices. Numerical results are discussed in Section 2.5. Section 2.6 concludes.

2.2 Voltage Stability Margin Sensitivity

The goal of the chapter is to determine locations for reactive power control devices so as to enable improve voltage stability margin. Here, we formally define the notion of voltage stability margin sensitivity to parameters, for we use such sensitivities in determining the desired reactive power control locations. The potential for contingencies such as unexpected component (generator, transformer, transmission line) outages in an electric power system often reduces the voltage stability margin to be less than the required value. We are interested in finding effective and economically justified reactive power controls at appropriate locations to steer operating points far away from voltage collapse points by having a pre-specified margin under a set of concerned contingencies.

It is cost-effective to use mechanically switched shunt or series capacitors to increase the voltage stability margin although more expensive dynamic VAR resources such as SVC and TCSC can also be used. The voltage stability margin sensitivity is useful in comparing the effectiveness of the same type of controls at different locations [39]. In this chapter, the margin sensitivity [46], [47], [48], [49], [50] is used in candidate control location selection and contingency screening (see steps 2, 4, and 5 of the overall procedure in Section 2.4.1). In the following, an analytical expression of the margin sensitivity is given, which is what we use for its computation. The details of the margin sensitivity can be found in [46], [47], [49].

Suppose that the steady state of the power system satisfies a set of equations expressed in the vector form

$$F(x, p, \lambda) = 0 \tag{2.1}$$

where x is the vector of state variables, p is any parameter in the power system steady state equations such as the susceptance of shunt capacitors or the reactance of series capacitors, λ is the bifurcation parameter which is a scalar. At the voltage instability point, the value of the bifurcation parameter is equal to λ^*.

A specified system scenario can be parameterized by λ as

$$P_{li} = (1 + K_{lpi}\lambda)P_{li0} \tag{2.2}$$

$$Q_{li} = (1 + K_{lqi}\lambda)Q_{li0} \tag{2.3}$$

$$P_{gj} = (1 + K_{gj}\lambda)P_{gj0} \tag{2.4}$$

Here, P_{li0} and Q_{li0} are the initial loading conditions at the base case where λ is assumed to be zero. K_{lpi} and K_{lqi} are factors characterizing the load increase pattern. P_{gj0} is the real power generation at bus j at the base case. K_{gj} represents the generator load pick-up factor.

The voltage stability margin can be expressed as

$$M = \sum_{i=1}^{n} P_{li}^* - \sum_{i=1}^{n} P_{li0} = \lambda^* \sum_{i=1}^{n} K_{lpi} P_{li0} \tag{2.5}$$

The sensitivity of the voltage stability margin with respect to the control variable at location i, S_i, is

$$S_i = \frac{\partial M}{\partial p_i} = \frac{\partial \lambda^*}{\partial p_i} \sum_{i=1}^{n} K_{lpi} P_{li0} \tag{2.6}$$

If the voltage collapse is due to a saddle-node bifurcation, the bifurcation point sensitivity with respect to the control variable p_i evaluated at the saddle-node bifurcation point is

$$\frac{\partial \lambda^*}{\partial p_i} = -\frac{w^* F_{p_i}^*}{w^* F_\lambda^*} \tag{2.7a}$$

where w is the left eigenvector corresponding to the zero eigenvalue of the system Jacobian F_x, F_λ is the derivative of F with respect to the bifurcation parameter λ and F_{p_i} is the derivative of F with respect to the control variable parameter p_i.

If the voltage collapse is due to a limit-induced bifurcation [51], the bifurcation point sensitivity with respect to the control variable p_i evaluated at the critical limit point (as opposed to at the saddle-node bifurcation point) is

$$\frac{\partial \lambda^*}{\partial p_i} = -\frac{w^* \begin{pmatrix} F_{p_i}^* \\ E_{p_i}^* \end{pmatrix}}{w^* \begin{pmatrix} F_\lambda^* \\ E_\lambda^* \end{pmatrix}} \tag{2.7b}$$

where $E(x, \lambda, p) = 0$ is the limit equation representing the binding control limit (i.e. $Q_i - Q_i^{\max} = 0$ representing generator i reaches its reactive power limit), E_λ is the derivative of E with respect to the bifurcation parameter λ, and E_{pi} is the derivative of E with respect to the control variable p_i, w is the nonzero row vector orthogonal to the range of the Jacobian J_c of the equilibrium and limit equations where

$$J_c = \begin{pmatrix} F_x^* \\ E_x^* \end{pmatrix}.$$

2.3 Optimization Problem Formulation

The reactive power control planning problem to increase voltage stability margin can be formulated as follows:

min

$$J = \sum_{i \in \Omega} (C_{fi} + C_{vi} X_i) q_i \tag{2.8}$$

subject to

$$\overline{M}^{(k)}(X_i^{(k)}) \geq M_{\min}, \quad \forall k \tag{2.9}$$

$$0 \leq X_i^{(k)} \leq X_i, \quad \forall k \tag{2.10}$$

$$0 \leq X_i \leq q_i X_{i\max} \tag{2.11}$$

$$q_i = 0,1 \tag{2.12}$$

The decision variables are X_i, $X_i^{(k)}$ and q_i.

Here,

- C_f is fixed installation cost and C_v is variable cost of reactive power control devices,
- X_i is the size (capacity) of reactive power control devices at location i,
- q_i=1 if the location i is selected for reactive power control expansion, otherwise, q_i=0,
- the superscript k represents the contingency that leads the voltage stability margin to be less than the required value,
- Ω is the set of pre-selected feasible candidate locations to install reactive power control devices,
- $X_i^{(k)}$ is the size of reactive power control devices to be switched on at location i under contingency k,
- M_{min} is an arbitrarily specified voltage stability margin in percentage,
- $\overline{M}^{(k)}(X_i^{(k)})$ is the voltage stability margin under contingency k with control $X_i^{(k)}$, and
- $X_{i\max}$ is the maximal size of reactive power control devices at location i which may be determined by physical and/or environmental considerations.

This is a mixed integer nonlinear programming problem, with q being the collection of discrete decision variables and X being the collection of continuous decision variables. For k contingencies that have the voltage stability margin less than the required value and n pre-selected feasible candidate control locations, there are $n(k+2)$ decision variables. In order to reduce the computational cost, it is important to limit the number of candidate control locations to a relative small number for problems of the size associated with practical large-scale power systems. The candidate control locations could be selected by assessing the relative margin sensitivities [39], [40]. However, there is no guarantee that the pre-selected candidate control locations are appropriate. We propose an algorithm in Section 2.4 for selecting candidate control locations under the assumption that $X_i^{(k)}$ and X_i are fixed at their maximal allowable value, i.e. $X_i^{(k)} = X_i = X_{i\max}$; this reduces the problem to an integer programming problem where the decision variables are locations for reactive power control devices as follows:

min

$$J = \sum_{i \in \Omega} (C_{fi} + C_{vi} X_{i\max}) q_i \tag{2.13}$$

subject to

$$\overline{M}^{(k)}(q_i^{(k)} X_{i\max}) \geq M_{\min}, \quad \forall k \tag{2.14}$$

$$q_i^{(k)} \leq q_i, \quad \forall k \tag{2.15}$$

$$q_i^{(k)} = 0,1, \quad \forall k \tag{2.16}$$

$$q_i = 0,1 \tag{2.17}$$

where $q_i^{(k)} = 1$ if the location i is selected for reactive power control expansion under contingency k, otherwise, $q_i^{(k)} = 0$. Here, the decision variables are q_i and $q_i^{(k)}$.

2.4 Methodology

2.4.1 Overall Procedure

In order to select appropriate candidate reactive power control locations the following procedure is applied:

1) Develop generation and load growth future. In this step, the generation/load growth future is identified, where the future is characterized by a load growth percentage for each load bus and a generation allocation for each generation bus. For example, one future may assume uniformly increasing load at 5% per year and allocation of that load increase to existing generation (with associated increase in unit reactive capability) based on percentage of total installed capacity. Such generation/load growth future can be easily implemented in the continuation power flow (CPF) program [52], [53], [54] by parameterization as shown in (2.2), (2.3) and (2.4).

2) Assess voltage stability by fast contingency screening and the CPF technique. We can use the CPF program to calculate the voltage stability margin of the system under each prescribed contingency. However, the CPF algorithm is time-consuming. If many contingencies must be assessed, the calculation time is large. The margin sensitivity can be used to speed up the procedure of contingency analysis as mentioned in Section 2.2. First, the CPF program is used to calculate (i) the voltage stability margin at the base case, (ii) the margin sensitivity with respect to line admittances, and (iii) the margin sensitivity with respect to bus power injections. The margin sensitivities are calculated according to (2.6). For circuit outages, the resulting voltage stability margin is estimated as

$$M^{(k)} = M^{(0)} + S_l \Delta l \tag{2.18}$$

where $M^{(k)}$ is the voltage stability margin under contingency k, $M^{(0)}$ is the voltage stability margin at the base case, S_l is the margin sensitivity with respect to the admittance of line l, and Δl is the negative of the admittance vector for the outaged circuits.

For generator outages, the resulting voltage stability margin is estimated as

$$M^{(k)} = M^{(0)} + S_g \Delta pq \tag{2.19}$$

where S_g is the margin sensitivity with respect to the power injection of generator g, and Δpq is the negative of the output power of the outaged generators.

Then the contingencies are ranked from most severe to least severe according to the value of the estimated voltage stability margin. After the ordered contingency list is obtained, we evaluate each contingency starting from the most severe one using the accurate CPF program and stop testing after encountering a certain number of sequential contingencies that have the voltage stability margin greater than or equal to the required value, where the

number depends on the size of the contingency list. A similar idea has been used in online risk-based security assessment [55].

3) Determination of Expansion Year

Assuming positive load growth but without system enhancement, the voltage stability margin decreases with time as shown in Figure 2-1. The year when the voltage stability margin becomes less than the required value is the time to enhance the transmission system by adding the reactive power control.

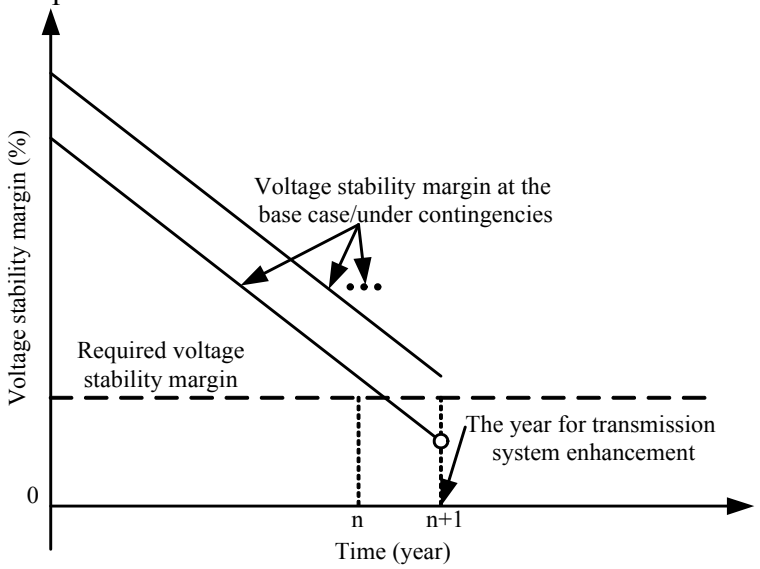


Figure 2-1 Determination of expansion year

4) Choose an initial set of switch locations using the bisection approach for each identified contingency possessing unsatisfactory voltage stability margin according to the following 3 steps:

a) Rank the feasible control locations according to the numerical value of margin sensitivity in descending order with location 1 having the largest margin sensitivity and location *n* having the smallest margin sensitivity.

b) Estimate the voltage stability margin with top half of the switches included as

$$M_{est}^{(k)} = \sum_{i=1}^{\lfloor n/2 \rfloor} X_{i\max}^{(k)} S_i^{(k)} + M^{(k)} \tag{2.20}$$

where $M_{est}^{(k)}$ is the estimated voltage stability margin and $\lfloor n/2 \rfloor$ is the largest integer less than or equal to *n/2*. If the estimated voltage stability margin is greater than the required value, then reduce the number of control locations by one half, otherwise increase the number of control locations by adding the remaining one half.

c) Continue in this manner until we identify the set of control locations that satisfies the voltage stability margin requirement.

5) Refine candidate control locations for each identified contingency possessing unsatisfactory voltage stability margin using the proposed backward/forward search algorithm. We will present the backward/forward search algorithm in Sections 2.4.2 and 2.4.3.

6) Obtain the final candidate control locations as the union of nodes for which voltage

stability margin is satisfied, as found in step 5) for every identified contingency.

The current backward/forward search over discrete modes has been done "one contingency at a time". This can be modified by considering all the contingencies simultaneously and it will result in a smaller set of candidate control locations. When we use the proposed optimization formulation to further refine control locations and compute control amounts, it is expected that the final solution will be less optimal than considering one contingency at each time. In addition, the present approach ensures there is at least one effective candidate location for every contingency having unacceptable margin. The alternative approach does not offer this assurance, and so it could result in one or more contingencies not having an effective control location in the optimization.

The overall procedure for selecting candidate control locations is shown in Figure 2-2.

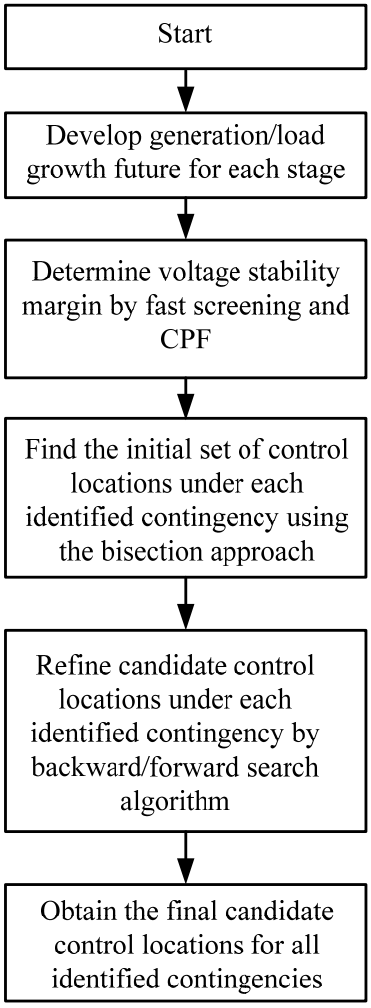


Figure 2-2 Flowchart for candidate control location selection

2.4.2 Backward Search Algorithm

In the proposed search algorithms, we assume that there is only one reactive power switch at each location. The backward/forward search algorithm begins at an initial node

representing control configuration and searches from that node in a prescribed direction, either backward or forward. The set of controls corresponding to the selected initial node can be chosen by the bisection approach. The two extreme cases are either searching backward from the node corresponding to all switches included (the strongest node) or forward from the node corresponding to all switches excluded (the weakest node).

Consider the graph where each node represents a configuration of discrete switches, and two nodes are connected if and only if they are different in one switch configuration. The graph has 2^n nodes where n is the number of feasible switches. We pictorially conceive of this graph as consisting of layered groups of nodes, where each successive layer (moving from left to right) has one more switch included (or "closed") than the layer before it, and the tth layer (where $t=0,\ldots,n$) consists of a number of nodes equal to $n!/t!(n-t)!$. Figure 2-3 illustrates the graph for the case of 4 switches.

The backward search algorithm has 4 steps.

1) Select the node corresponding to all switches in the initial set that are closed.

2) For the selected node, check if voltage stability margin requirement is satisfied for the concerned contingency on the list. If not, then stop, the solution corresponds to the previous node (if there is a previous node, otherwise use the forward search algorithm).

3) For the selected node, exclude (open) the switch that has the smallest margin sensitivity. We denote this as switch i^*:

$$i^* = \arg\left\{\min_{i\in\Omega_c} S_i^{(k)}\right\} \tag{2.21}$$

where Ω_c ={set of closed switches for the selected node}, $S_i^{(k)}$ is the margin sensitivity with respect to the susceptance of shunt capacitors or the reactance of series capacitors under contingency k, at location i.

4) Choose the neighboring node corresponding to the switch i^* being off. If there is more than one switch identified in step 3, i.e. $|i^*|>1$, then choose any one of the switches in i^* to exclude (open). Return to step 2.

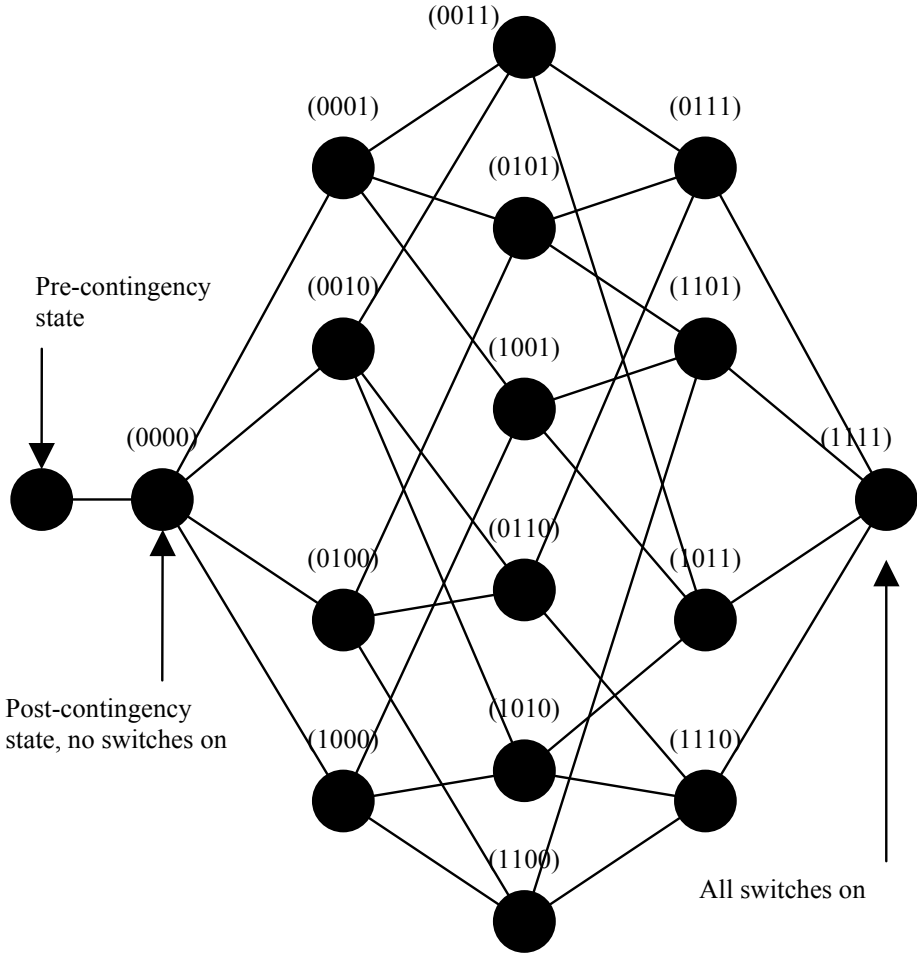


Figure 2-3 Graph for 4-switch problem

2.4.3 Forward Search Algorithm

The forward search algorithm has 4 steps.

1) Start from an initial node.
2) For the selected node, check if voltage stability margin requirement is satisfied for the concerned contingency on the list. If yes, then stop, the solution corresponds to the previous node (if there is a previous node, otherwise use the backward search algorithm).
3) For the selected node, include (close) the switch that has the largest margin sensitivity. We denote this as switch j^*:

$$j^* = \arg\{\max_{j\in\Omega} S_j^{(k)}\} \tag{2.22}$$

where Ω = {set of pre-selected feasible locations}.

4) Choose the neighboring node corresponding to the switch j^* being closed. If there is more than one switch identified in step 3, i.e. $|j^*|>1$, then choose any one of the switches in j^* to include (close). Return to step 2.

2.5 Case Study

The proposed method has been applied to a test system adapted from [56] as shown in Figure 2-4 to identify good candidate locations for shunt or series reactive power control devices. Table 2.1 shows the system loading and generation of the base case.

In the simulations, the following conditions are implemented unless stated otherwise:

- Constant power loads;
- Required voltage stability margin is assumed to be 15%;
- In computing voltage stability margin, the power factor of the load bus remains constant when the load increases, and load and generation increase are proportional to their base case value.

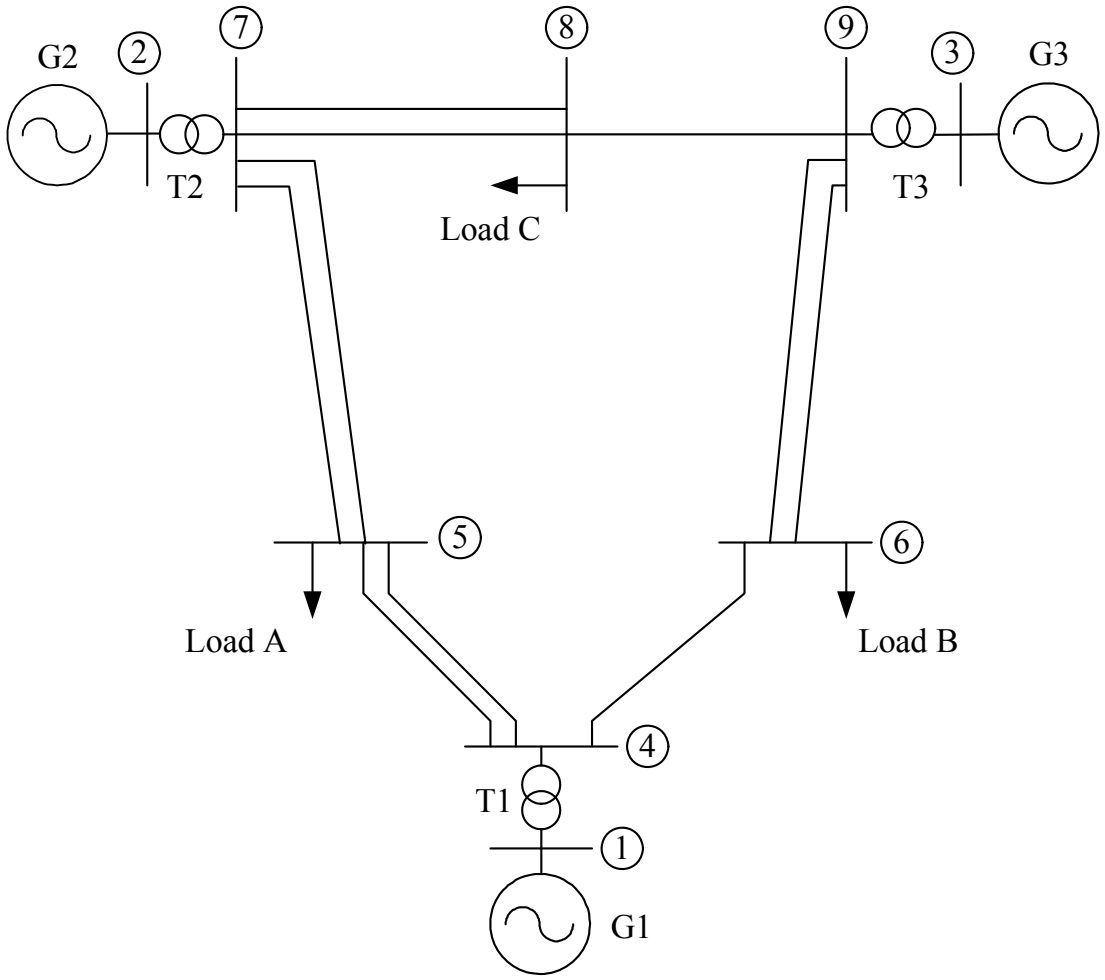


Figure 2-4 Modified WECC nine-bus system

Table 2.1 Base case loading and dispatch for the modified WECC system

	Load A	Load B	Load C	G1	G2	G3
MW	147.7	106.3	118.2	128.9	163.0	85.0
MVar	59.1	35.5	41.4	41.4	16.7	-1.9

A contingency analysis was performed on the system. For each bus, consider the simultaneous outage of 2 components (generators, lines, transformers) connected to the bus. There exist 2 contingencies that reduce the post-contingency voltage stability margin to be less than 15%, and they are shown in Table 2.2.

Table 2.2 Voltage stability margin under contingencies for the WECC system

Contingency	Voltage stability margin (%)
1. Outage of lines 5-4A and 5-4B	4.73
2. Outage of transformer T1 and line 4-6	4.67

2.5.1 Candidate Location Selection for Shunt Capacitors

We first select candidate locations for shunt capacitors under the outage of lines 5-4A and 5-4B. Table 2.3 summarizes the steps taken by the backward search algorithm in terms of switch sensitivities, where we have assumed the susceptance of shunt capacitors to be installed at feasible buses $X_i^{(k)} = X_i = X_{i\max} = 0.3\ p.u.$ We take the initial network configuration as six shunt capacitors at buses 4, 5, 6, 7, 8, and 9 are switched on. The voltage stability margin with all six shunt capacitors switched on is 17.60% which is greater than the required value of 15%. Therefore, the number of switches can be decreased to reduce the cost. At the first step of the backward search, we compute the margin sensitivity for all six controls as listed in the 4th column. From this column, we see that the row corresponding to the shunt capacitor at bus 4 has the minimal sensitivity. So in this step of backward search, this capacitor is excluded from the list of control locations indicated by the strikethrough. Continuing in this manner, in the next three steps of the backward search we exclude shunt capacitors at buses 6, 9, and 8 sequentially. However, as seen from the last column of Table 2.3, with only 2 controls at buses 5 and 7, the voltage stability margin is unacceptable at 13.98%. Therefore the final solution must also include the capacitor excluded in the last step, i.e., the shunt capacitor at bus 8. The location of these controls are intuitively pleasing given that, under the contingency, Load A, the largest load, must be fed radially by a long transmission line, a typical voltage stability problem.

Table 2.3 Steps taken in the backward search algorithm for shunt capacitor planning

No.		no cntrl.	6 cntrls.	5 cntrls. (reject #6)	4 cntrls. (reject#5)	3 cntrls. (reject#4)	2 cntrls. (reject#3)
1	Sens. of shunt cap. at bus 5	0.738	0.879	0.877	0.874	0.868	0.851
2	Sens. of shunt cap. at bus 7	0.334	0.384	0.384	0.382	0.379	0.370
3	Sens. of shunt cap. at bus 8	0.240	0.284	0.284	0.282	~~0.278~~	
4	Sens. of shunt cap. at bus 9	0.089	0.106	0.105	~~0.104~~		
5	Sens. of shunt cap. at bus 6	0.046	0.056	~~0.056~~			
6	Sens. of shunt cap. at bus 4	0.019	~~0.023~~				
	Loadability (MW)	389.8	437.7	437.0	435.4	432.4	424.3
	Voltage stability margin (%)	4.73	17.60	17.42	16.99	16.17	13.98

Figure 2-5 shows the corresponding search via the graph. In the figure, node O represents the origin configuration of discrete switches from where the backward search originates, and node R represents the restore configuration associated with a minimal set of discrete switches which satisfies the voltage stability margin requirement (this is the node where the search ends).

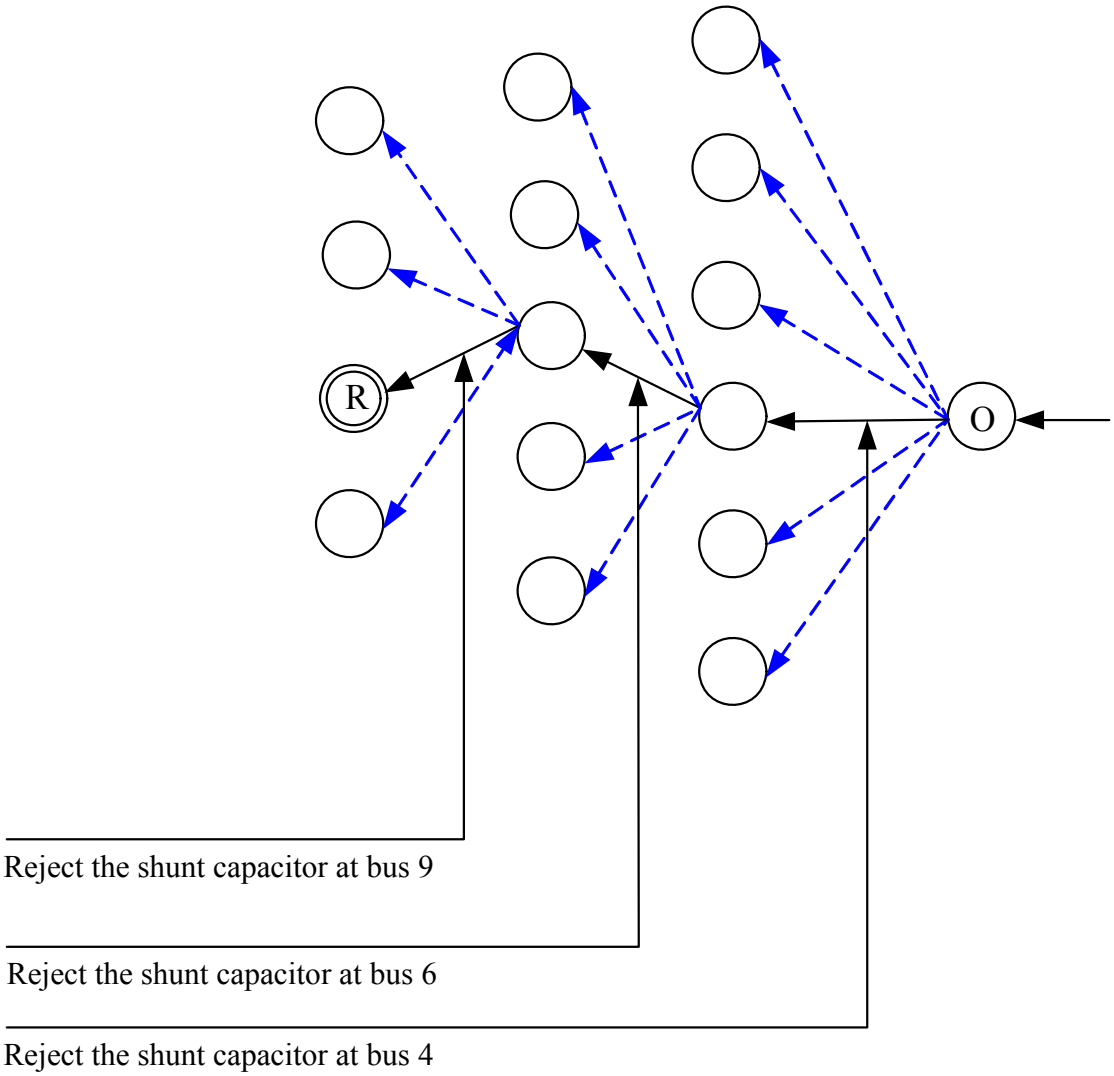


Figure 2-5 Graph for the backward search algorithm for shunt capacitor planning

Table 2.4 summarizes the steps taken by the forward search algorithm in terms of switch sensitivities, where we have again assumed $X_i^{(k)} = X_i = X_{i\max} = 0.3\ p.u.$ The initial network configuration is chosen as no shunt capacitor is switched on. Here, at each step, the switch with the maximal margin sensitivity is included (closed), as indicated in each column by the numerical value within the box. Figure 2-6 shows the corresponding search via the graph.

Table 2.4 Steps taken in forward search algorithm for shunt capacitor planning

No.		no cntrl	1 cntrl add # 1	2 cntrls add # 2	3 cntrls add # 3
1	Sensitivity of shunt cap. at bus 5	0.738			
2	Sensitivity of shunt cap. at bus 7	0.334	0.356		
3	Sensitivity of shunt cap. at bus 8	0.240	0.256	0.265	
4	Sensitivity of shunt cap. at bus 9	0.089	0.095	0.098	
5	Sensitivity of shunt cap. at bus 6	0.046	0.049	0.050	
6	Sensitivity of shunt cap. at bus 4	0.019	0.021	0.021	
	Loadability (MW)	389.8	413.3	424.2	432.4
	Voltage stability margin (%)	4.73	11.04	13.97	16.17

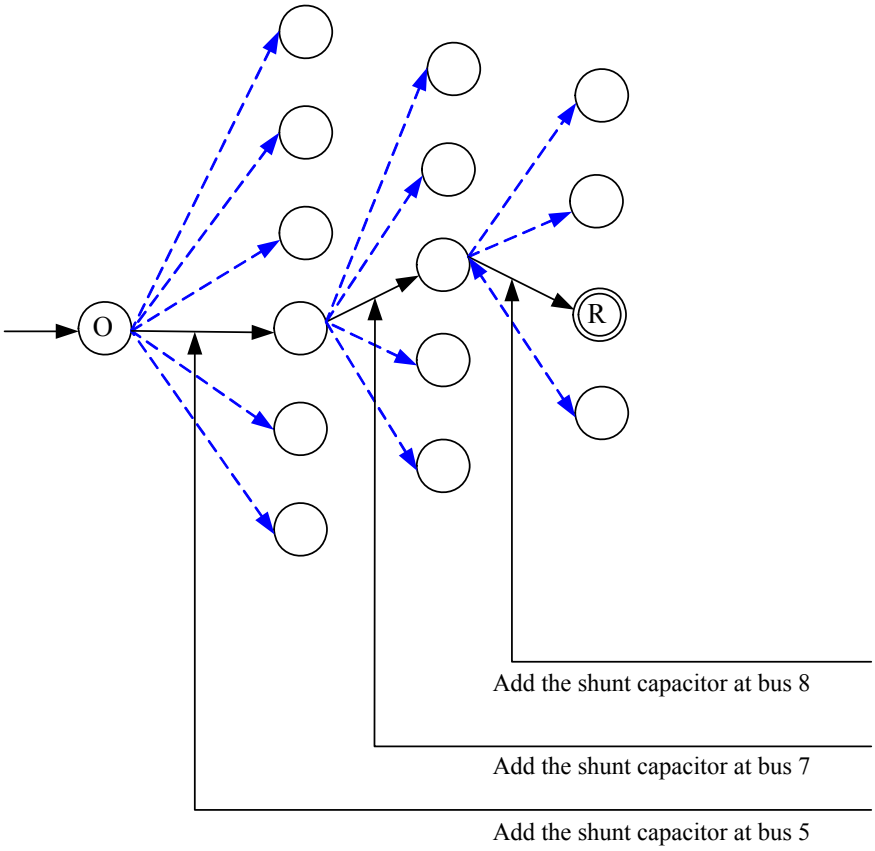


Figure 2-6 Graph for the forward search algorithm for shunt capacitor planning

The solution obtained from the forward search algorithm is the same as that obtained using the backward search algorithm: shunt capacitors at buses 5, 7 and 8. This is guaranteed

to occur if switch sensitivities do not change as the switching configuration is changed, i.e., if the system is linear. We know power systems are nonlinear, and the changing sensitivities across the columns for any given row of Tables 2.3 or 2.4 confirm this. However, we also observe from Tables 2.3 and 2.4 that the sensitivities do not change much, thus giving rise to the agreement between the algorithms. For large systems, however, we do not expect the two algorithms to identify the same solution. And of course, neither algorithm is guaranteed to identify the optimal solution. But both algorithms will generate good solutions. This will facilitate good reactive power planning design.

The optimization problem of (2.13)-(2.17) could be solved by a traditional integer programming method, e.g., the branch-and-bound algorithm. However, our algorithm has complexity linear in the number of switches n, whereas branch and bound has worst case complexity of order 2^n. The improvement in complexity comes at the expense of optimality: branch-and-bound finds an optimal solution, whereas our algorithm finds a solution that is set-wise minimal. There can exist more than one minimal set solution, and to compute an optimal solution, one will have to examine all of them which we avoid for the sake of complexity gain.

For the outage of transformer T1 and line 4-6, the solution obtained by the forward search algorithm is: shunt capacitors at buses 4 and 5. Therefore, the final candidate locations for shunt capacitors are buses 4, 5, 7, and 8 which guarantee that the voltage stability margin under all prescribed N-2 contingencies is greater than the required value.

2.5.2 Candidate Location Selection for Series Capacitors

Series capacitor compensation has two effects that are not of concern for shunt capacitor compensation. First, series capacitors can expose generator units to risk of sub-synchronous resonance (SSR), and such risk must be investigated. Second, series capacitors also have significant effect on real power flows. In our work, we intend that both shunt and series capacitors be used as contingency-actuated controls (and therefore temporary) rather than continuously operating compensators. As a result, the significance of how they affect real power flows may decrease. However, the SSR risk is still a significant concern. To address this issue, the planner must identify *a-priori* lines where series compensation would create SSR risk and eliminate those lines from the list of candidates.

Table 2.5 summarizes the steps taken by the forward search algorithm to plan series capacitors for the outage of lines 5-4A and 5-4B, where we have assumed the reactance of series capacitor to be installed in feasible lines $X_i^{(k)} = X_i = X_{i\max} = 0.06\ p.u.$ We take the initial network configuration as no series capacitor is switched on. At each step, the switch with the maximal margin sensitivity is included, as indicated in each column by the numerical value within the box. Figure 2-7 shows the corresponding search via the graph.

Table 2.5 shows that the solution utilizes 2 controls. These controls are series capacitors in lines 5-7A and 5-7B. Again, the location of these controls are intuitively pleasing.

For the outage of transformer T1 and line 4-6, the solution obtained by the forward algorithm is the same as the result for the outage of lines 5-4A and 5-4B: series capacitors in lines 5-7A and 5-7B. Therefore, the final candidate locations for series capacitors are lines 5-7A and 5-7B.

Table 2.5 Steps taken in forward search algorithm for series capacitor planning

No.		no cntrl	1 cntrl add # 1	2 cntrls add # 2
1	Sensitivity of series cap. in line 5-7A	4.861		
2	Sensitivity of series cap. in line 5-7B	4.861	4.575	
3	Sensitivity of series cap. in line 8-9	1.747	2.056	
4	Sensitivity of series cap. in line 4-6	0.288	0.332	
5	Sensitivity of series cap. in line 7-8A	0.046	0.045	
6	Sensitivity of series cap. in line 7-8B	0.046	0.045	
7	Sensitivity of series cap. in line 6-9A	0.008	0.007	
8	Sensitivity of series cap. in line 6-9B	0.008	0.007	
	Loadability (MW)	389.8	415.3	439.8
	Voltage stability margin (%)	4.73	11.58	18.16

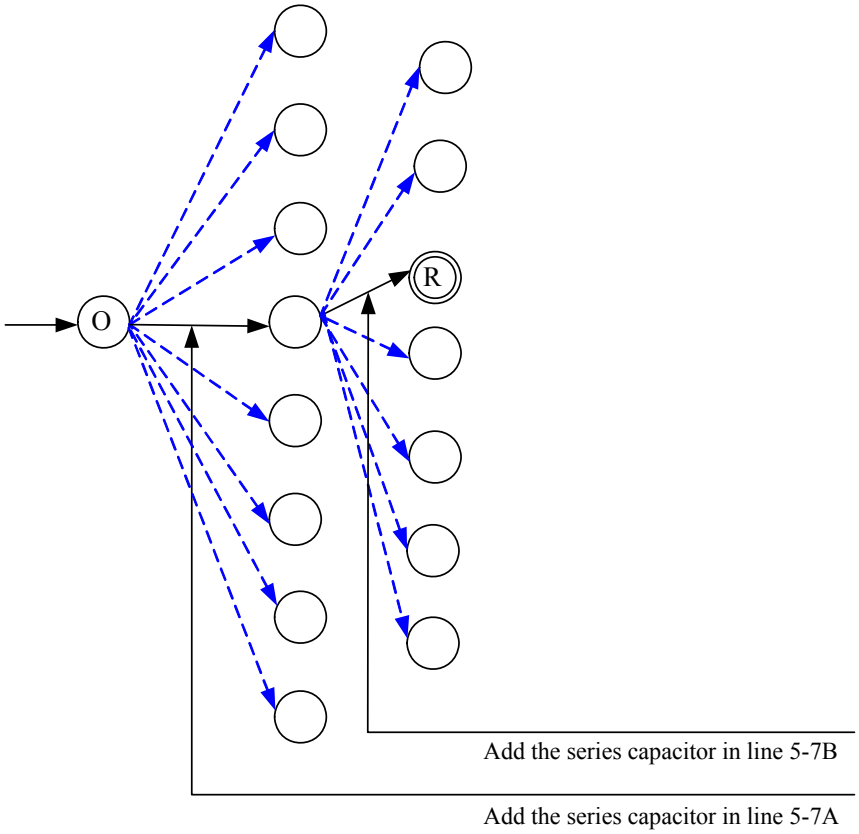


Figure 2-7 Graph for the forward search algorithm for series capacitor planning

2.6 Summary

This chapter presents a method of locating reactive power controls in electric transmission systems to satisfy performance requirements under contingencies. Further refinement of control locations and amounts is ready to be done using the optimization methods proposed in Chapters 3, 4 and 5. The proposed algorithm has complexity linear in the number of feasible reactive power control locations whereas the solution space is exponential. The effectiveness of the method is illustrated by using a modified WSCC 9-bus system. The results show that the method works satisfactorily to find good candidate locations for reactive power controls.

3.0 Reactive Power Control Planning to Restore Equilibrium

3.1 Introduction

Voltage instability is one of the major threats to power system operation [24]. Severe contingencies such as tripping of heavily loaded transmission lines or outage of large generating units can cause voltage instability when no new equilibrium of the power system exists (i.e. the voltage stability margin is negative) after contingencies. In face of the loss of equilibrium voltage instability, switched shunt and series capacitors are generally effective control candidates [10], [18], [24]. The problem, also referred to as power flow solvability restoration, was initially addressed through the so-called non-divergent power flow [33], [57]. An approach for determining the minimum load shedding to restore an equilibrium of a power system based on the total equilibrium tracing method [58] was proposed in [59]. In [40], a mixed integer nonlinear programming formulation was presented for the reactive power control planning problem. Load shedding was used to guarantee the existence of power flow solution after contingencies.

In this chapter, we present a new approach for planning the minimum amount of switched shunt and series capacitors to restore the voltage stability when no equilibria exist due to severe contingencies. Through parameterization of severe contingencies, the continuation method is applied to find the critical point. Then, the backward/forward search algorithm with linear complexity is used to select candidate locations for switched shunt and series capacitors. Next, a mixed integer programming formulation is proposed for estimating locations and amounts of switched shunt and series capacitors to withstand a planned set of contingencies. A sequence of MIP problems with updated information is utilized to further refine the control locations and amounts. Because our problem formulation is linear, it is scalable and at the same time provides good solutions as evidenced by the application to the New England 39-bus system.

3.2 Contingency Analysis via Parameterization and Continuation

A power system may lose equilibrium after severe contingencies. The techniques of contingency parameterization and continuation can be used for planning corrective reactive power controls to restore equilibrium. This section presents the technique of contingency analysis via parameterization and continuation. There are basically two types of contingencies that cause voltage instability. One is branch type of contingency such as the outage of transformers or transmission lines. The other is node type of contingency such as the outage of generators or shunt reactive power compensation devices. The contingency parameterization for both types of contingencies is as follows.

3.2.1 Parameterization of Branch Outage

The set of parameterized power flow equations at bus i for the outage of branch br connecting bus i to bus m is as follows:

$$\begin{cases} P_i^{inj} - V_i \sum_{j \in L(i), j \neq m} V_j (G_{ij} \cos\theta_{ij} + B_{ij} \sin\theta_{ij}) - V_i V_m (G_{im}^{new} \cos\theta_{im} + B_{im}^{new} \sin\theta_{im}) \\ - V_i^2 G_{ii}^{new} - P_{im}(V_i, V_m, \lambda) = 0 \\ Q_i^{inj} - V_i \sum_{j \in L(i), j \neq m} V_j (G_{ij} \sin\theta_{ij} - B_{ij} \cos\theta_{ij}) - V_i V_m (G_{im}^{new} \sin\theta_{im} - B_{im}^{new} \cos\theta_{im}) + V_i^2 B_{ii}^{new} \\ - Q_{im}(V_i, V_m, \lambda) = 0 \end{cases} \quad (3.1)$$

where $L(i) = \{j : Y_{ij} \neq 0,\ j \neq i\}$ is the set of buses that are directly connected to bus *i* through transmission lines, $G_{ij}+jB_{ij}$ is the (i, j) element of the bus admittance matrix, $G_{ii}+jB_{ii}$ is the i*th* diagonal element of the bus admittance matrix, θ_{ij} is the voltage angle difference between bus *i* and bus *j*, V_i and V_j are voltage magnitude of bus *i* and bus *j* respectively, $G_{ii}^{new} + jB_{ii}^{new}$ is the new *k*th diagonal element of the bus admittance matrix and $G_{im}^{new} + jB_{im}^{new}$ is the new (i, m) element of the bus admittance matrix after branch *br* has been removed from the system, P_i^{inj} and Q_i^{inj} are real power and reactive power injections at bus *i*. $P_{im}(V_i, V_m, \lambda)$ and $Q_{im}(V_i, V_m, \lambda)$ are defined as follows:

$$P_{im}(V_i, V_m, \lambda) = (1-\lambda)\{V_i V_m (G_{im}^{br} \cos\theta_{im} + B_{im}^{br} \sin\theta_{im}) + V_i^2 G_{ii}^{br}\} \quad (3.2)$$

$$Q_{im}(V_i, V_m, \lambda) = (1-\lambda)\{V_i V_m (G_{im}^{br} \sin\theta_{im} - B_{im}^{br} \cos\theta_{im}) - V_i^2 B_{ii}^{br}\} \quad (3.3)$$

When λ=0, (3.1) represents the original set of power flow equations before contingency. On the other hand, when λ=1, (3.1) is the new set of power flow equations with branch *br* removed. Figure 3-1 shows the parameterization of branch outage where Y_c is one-half of the total shunt admittance per phase to neutral of the branch and Y_{series} is the total series admittance per phase of the branch. Similar formulation was presented in [60] which uses the parameterization of branch outage to investigate the effects of varying branch parameters on power flow solutions.

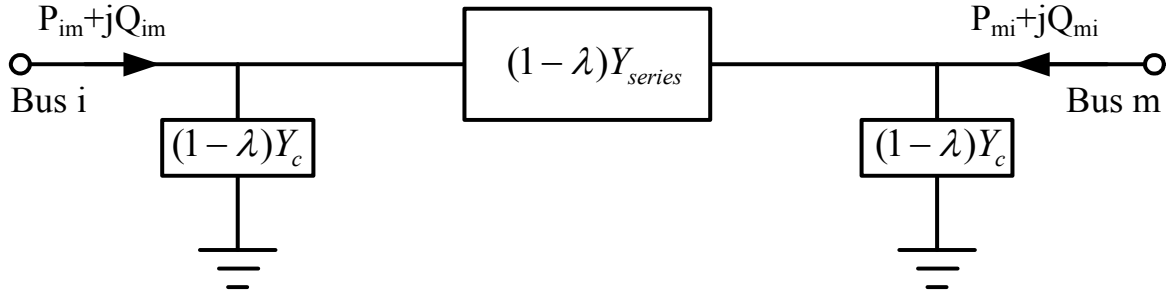


Figure 3-1 Parameterization of branch outage

3.2.2 <u>Parameterization of HVDC Link Outage</u>

A high voltage direct current (HVDC) link consists of a rectifier and an inverter as shown in Figure 3-2. The rectifier side of the HVDC link may be represented as a load consuming positive real and reactive power. On the other hand, the inverter side of the HVDC link may be represented as a generator providing positive real power and negative reactive power (i.e. absorbing positive reactive power) [61].

The set of parameterized power flow equations at the terminal bus r of the rectifier side of the HVDC link is as follows:

$$\begin{cases} -P_{rec}(1-\lambda) - V_r \sum_{j \in L(r)} V_j (G_{rj} \cos\theta_{rj} + B_{rj} \sin\theta_{rj}) - V_r^2 G_{rr} = 0 \\ -Q_{rec}(1-\lambda) - V_r \sum_{j \in L(r)} V_r (G_{rj} \sin\theta_{rj} - B_{rj} \cos\theta_{rj}) + V_r^2 B_{rr} = 0 \end{cases} \tag{3.4}$$

where P_{rec}, Q_{rec} are real and reactive power as seen from the AC network at the rectifier terminal bus under the normal operating condition respectively.

The set of parameterized power flow equations at the terminal bus i of the inverter side of the HVDC link is as follows:

$$\begin{cases} P_{inv}(1-\lambda) - V_i \sum_{j \in L(i)} V_j (G_{ij} \cos\theta_{ij} + B_{ij} \sin\theta_{ij}) - V_i^2 G_{ii} = 0 \\ -Q_{inv}(1-\lambda) - V_i \sum_{j \in L(i)} V_j (G_{ij} \sin\theta_{ij} - B_{ij} \cos\theta_{ij}) + V_i^2 B_{ii} = 0 \end{cases} \tag{3.5}$$

where P_{inv}, Q_{inv} are real and reactive power as seen from the AC network at the inverter terminal bus under the normal operating condition respectively.

When λ=0, (3.4) and (3.5) represent the set of power flow equations before contingency. On the other hand, when λ=1, (3.4) and (3.5) are the set of power flow equations after the HVDC link is shut down.

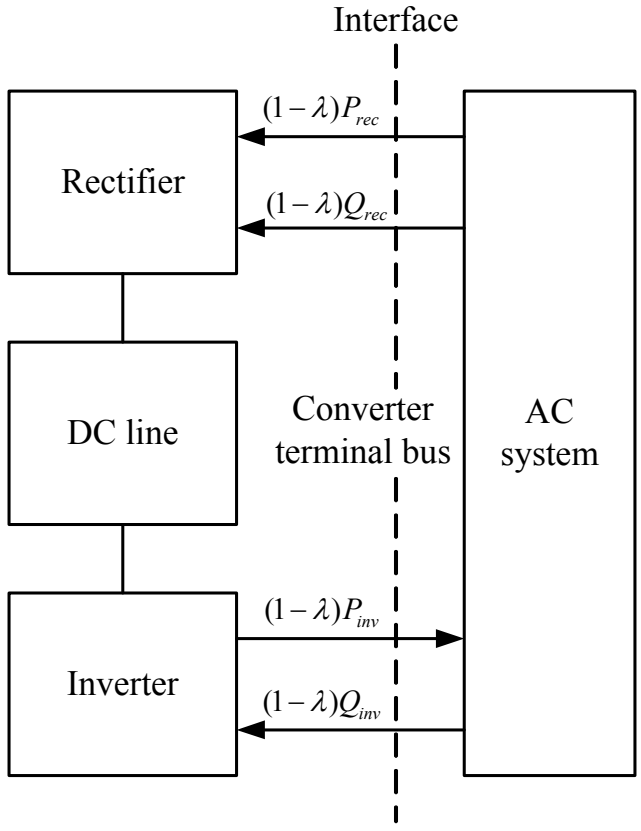


Figure 3-2 Parameterization of HVDC link outage

3.2.3 Parameterization of Generator Outage

The parameterized power flow equation at bus *i* for the outage of the generator at that bus is as follows:

$$\begin{cases} P_{gi}(1-\lambda) - P_{di} - V_i \sum_{j \in L(i)} V_j (G_{ij} \cos\theta_{ij} + B_{ij} \sin\theta_{ij}) - V_i^2 G_{ii} = 0 \\ Q_{gi}(1-\lambda) - Q_{di} - V_i \sum_{j \in L(i)} V_j (G_{ij} \sin\theta_{ij} - B_{ij} \cos\theta_{ij}) + V_i^2 B_{ii} = 0 \end{cases} \tag{3.6}$$

where P_{gi} and P_{di} are generator real power output and load real power respectively, Q_{gi} and Q_{di} are generator reactive power output and load reactive power respectively. For a generator of PV type, Q_{gi} is the reactive power output under the normal operating condition.

Assume the real power generation loss P_{gi} is reallocated among the available generators as follows:

$$\sum_{z \neq i} \Delta P_{gz} = P_{gi} \tag{3.7}$$

Where ΔP_{gz} is the specified real power increase of available generator *z* after the faulted generator *i* is removed from the system.

The parameterized power flow equation at generator bus *z* for the outage of the generator at bus *i* is as follows:

$$P_{gz} + \lambda \Delta P_{gz} - P_{dz} - V_z \sum_{j \in L(i)} V_j (G_{zj} \cos\theta_{zj} + B_{zj} \sin\theta_{zj}) - V_z^2 G_{zz} = 0 \tag{3.8}$$

When λ=0, (3.6) and (3.8) represent the power flow equations before contingency. On the other hand, when λ=1, (3.6) and (3.8) are the power flow equations after the generator at bus *i* is shut down.

3.2.4 Continuation Method

Generally, the parameterized set of equations representing steady state operation of a power system under a *N-k* contingency (where $k \geq 1$) can be represented as

$$F(x, p, \lambda) = 0 \tag{3.9}$$

where *x* is the vector of state variables, *p* is any controllable parameter such as the susceptance of switched shunt capacitors or the reactance of switched series capacitors, λ is the scalar uncontrollable bifurcation parameter which parameterizes the simultaneous outage of *k* components. Specifically, when λ=0, the set of parameterized steady state equations represents the one before contingency. On the other hand, when λ=0, the set of parameterized steady state equations is the one after all faulted *k* components are removed from the system.

The continuation method can be used to find the critical point associated with a contingency precisely and reliably. In addition, the sensitivity information obtained as a by-product of the continuation method is useful for reactive power control planning. Generally, the continuation method can be applied to solve the following problem [62].

Given a mapping *F*: $R^n \times R \times R \to R^n$, find solutions to $F(x, p, \lambda) = 0$ where $x \in R^n, p \in R, \lambda \in R$.

Power system engineers have applied the continuation method to continuation power flow on varying bus power injections [52], [53], [54] and on varying branch parameters [60]. [63] combines the continuation power flow on varying bus injections and branch parameters

to study the existence of power flow solution under severe contingencies. During the continuation process, λ is increased from 0 to 1 as shown in Figure 3-3. If there is a stable operating point after a contingency, the continuation method can find this point with $\lambda^* = 1$. If there is no power flow solution following a contingency, the continuation method will obtain a critical point with $\lambda^* < 1$.

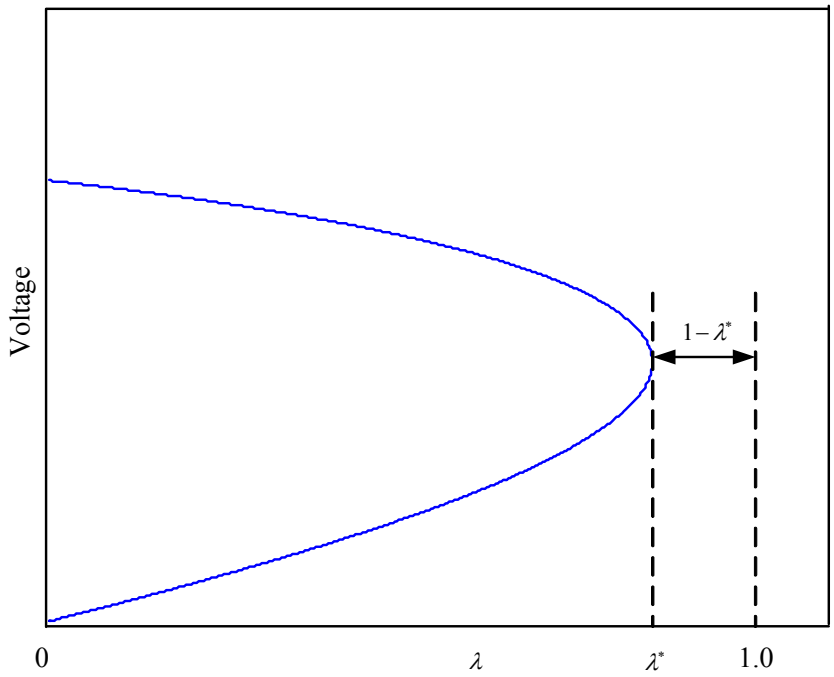


Figure 3-3 Bifurcation curve obtained by the continuation method

If the critical point is due to saddle-node bifurcation, the sensitivity of the critical point with respect to the control variable p is

$$\frac{\partial \lambda^*}{\partial p} = -\frac{w^* F_p^*}{w^* F_\lambda^*} \tag{3.10}$$

where F_λ^* is the derivative of F with respect to the bifurcation parameter λ evaluated at the critical point and F_p^* is the derivative of F with respect to the control variable p evaluated at the critical point. In the following section, the bifurcation parameter sensitivity is used to plan cost-effective reactive power controls against voltage collapse.

If the critical point is due to a limit-induced bifurcation, the sensitivity of the critical point to the control variable p_i is

$$\frac{\partial \lambda^*}{\partial p_i} = -\frac{w^* \begin{pmatrix} F_{p_i}^* \\ E_{p_i}^* \end{pmatrix}}{w^* \begin{pmatrix} F_\lambda^* \\ E_\lambda^* \end{pmatrix}} \tag{3.11}$$

where $E(x, \lambda, p) = 0$ is the limit equation representing the binding control limit, E_λ is the derivative of E with respect to the bifurcation parameter λ, and E_{pi} is the derivative of E with respect to the control variable p_i, w is the nonzero row vector orthogonal to the range of the Jacobian J_c of the equilibrium and limit equations where

$$J_c = \begin{pmatrix} F_x^* \\ E_x^* \end{pmatrix} \tag{3.12}$$

3.3 Formulation for Reactive Power Control Planning

3.3.1 Flowchart for Reactive Power Control Planning

A flowchart for planning minimum switched shunt and series capacitors to restore an equilibrium of a power system after severe contingencies is shown in Figure 3-4.

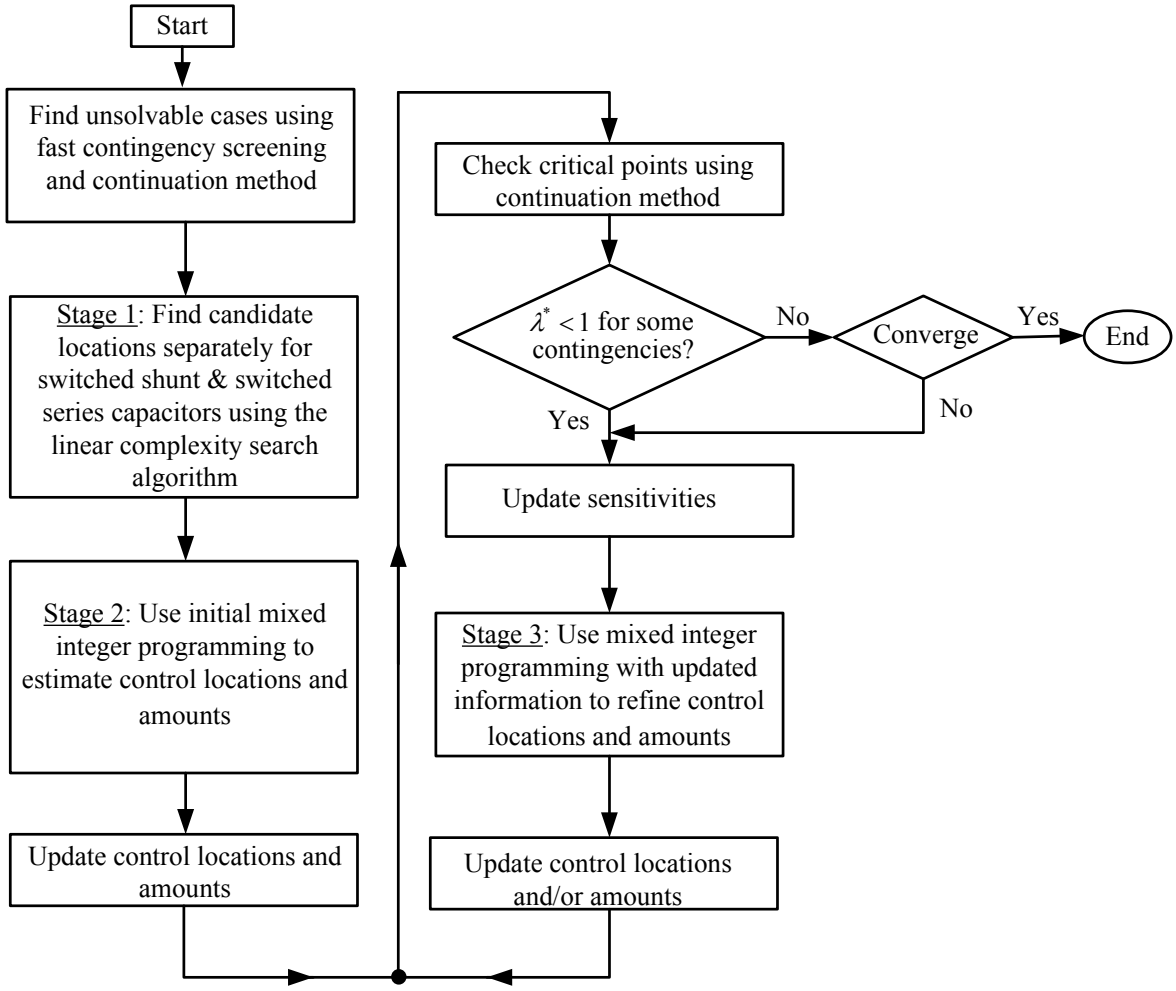


Figure 3-4 Flowchart for the minimum reactive power control planning to restore equilibrium

3.3.2 Voltage Stability Analysis

The procedure of voltage stability analysis is similar to the one presented in Section 2.4.1, Chapter 2. The contingencies are ranked from most severe to least severe according to the value of the estimated voltage stability margin using the procedure introduced in Section 2.4.1. After the ordered contingency list is obtained, we evaluate each contingency starting

from the most severe one using the accurate continuation method and stop testing after encountering a certain number of sequential contingencies having the critical value λ^* greater than or equal to one, where the number depends on the size of the contingency list.

3.3.3 Selection of Candidate Control Locations

An important step in the reactive power control planning problem is the selection of the candidate locations for switched shunt and series capacitors. The backward/forward search algorithm with linear complexity proposed in Chapter 2 can be used to find candidate locations separately for switched shunt and switched series capacitors under every contingency where we use the contingency parameterization instead of the conventional generation/load parameterization. It is assumed that the capacities of switched shunt and switched series capacitors are fixed at the maximum allowable value in this step.

3.3.4 Formulation of Initial Mixed Integer Programming

In the previous step, we find the candidate locations for switched shunt and series capacitors separately. There exists redundancy of control locations when we plan switched shunt and series capacitors together. We use a mixed integer programming (MIP) to estimate control locations and amounts. The MIP minimizes control installation cost while restoring equilibria (i.e. the bifurcation parameter at the critical point λ^* is greater than or equal to one):

minimize

$$J = \sum_{i\in\Omega_1}(C_{vi}B_i + C_{fi}q_i) + \sum_{j\in\Omega_2}(C_{vj}X_j + C_{fj}q_j) \tag{3.13}$$

subject to

$$\left(\sum_{i\in\Omega_1} S_i^{(k)}B_i^{(k)} + \sum_{j\in\Omega_2} S_j^{(k)}X_j^{(k)}\right) + \lambda^{*(k)} \geq 1, \quad \forall k \tag{3.14}$$

$$0 \leq B_i^{(k)} \leq B_i, \quad \forall k \tag{3.15}$$

$$0 \leq X_j^{(k)} \leq X_j, \quad \forall k \tag{3.16}$$

$$0 \leq B_i \leq B_{i\max}q_i \tag{3.17}$$

$$0 \leq X_j \leq X_{j\max}q_j \tag{3.18}$$

$$q_i, q_j = 0,1 \tag{3.19}$$

The decision variables are $B_i^{(k)}$, B_i, q_i, $X_j^{(k)}$, X_j, and q_j.

Here,

- C_f is fixed installation cost and C_v is variable cost of switched shunt or series capacitors,
- B_i is the size (susceptance) of the switched shunt capacitor at location i,
- X_j is the size (reactance) of the switched series capacitor at location j,
- q_i=1 if location i is selected for reactive power control expansion, otherwise, q_i=0 (the same to q_j),
- the superscript k represents the contingency under which there is no equilibrium,

- Ω_1 is the set of candidate locations to install switched shunt capacitors,
- Ω_2 is the set of candidate locations to install switched series capacitors,
- $B_i^{(k)}$ is the size of the shunt capacitor to be switched on at location i under contingency k,
- $X_j^{(k)}$ is the size of the series capacitor to be switched on at location j under contingency k,
- $S_i^{(k)}$ is the sensitivity of the bifurcation parameter with respect to the susceptance of the shunt capacitor at location i under contingency k,
- $S_j^{(k)}$ is the sensitivity of the bifurcation parameter with respect to the reactance of the series capacitor at location j under contingency k,
- $\lambda^{*(k)}$ is the bifurcation parameter evaluated at the critical point under contingency k and without controls,
- $B_{i\max}$ is the maximum size of the switched shunt capacitor at location i, and
- $X_{j\max}$ is the maximum size of the switched series capacitor at location j.

Note that the minimization of the objective function (3.13) and the constraints (3.17), (3.18) and (3.19) guarantee that (i) if the size of the switched shunt or series capacitors is zero, the location variable is zero, (ii) if the size of the switched shunt or series capacitors is nonzero, the location variable is nonzero, (iii) if the location variable is zero, the size of the switched shunt or series capacitors is zero, and (iv) if the location variable is non-zero, the size of the switched shunt or series capacitors is nonzero. Therefore the objective function in (3.13) is equivalent to

$$J' = \sum_{i\in\Omega_1}(C_{vi}B_i + C_{fi})q_i + \sum_{j\in\Omega_2}(C_{vj}X_j + C_{fj})q_j \tag{3.20}$$

However, the objective function in (3.13) is preferred because it is a mixed integer linear objective function instead of the mixed integer nonlinear objective function in (3.20).

For k contingencies that do not have post-fault equilibria and n pre-selected candidate control locations, there are $n(k+2)$ decision variables and $k+3n+2kn$ constraints. The number of candidate control locations can be limited to a relative small number even for problems of the size associated with practical power systems by using the backward/forward search algorithm. Therefore, computational cost for solving the above MIP is not high even for large power systems.

The output of the MIP is the control locations and amounts for all k contingencies and the combined control location and amount. For each concerned contingency, the identified controls are switched on, and λ^* is recalculated to check if an equilibrium is restored. However, because we use the linear sensitivity to estimate the effect of the variations of control variables on the value of the bifurcation parameter at the critical point, there may be contingencies that have λ^* less than one after the network configuration is updated according to the results of the MIP. Also, the obtained solution may not be optimal after one iteration of MIP. The control locations and/or amounts can be further refined by solving a second-stage mixed integer programming with updated information. In the successive MIP, we use updated sensitivity at each iteration.

3.3.5 Formulation of MIP with Updated Information

The successive MIP is formulated to minimize the total control installation cost subject

to the constraint of equilibrium restoration, as follows:

minimize

$$J = \sum_{i \in \Omega_1} (C_{vi} \overline{B}_i + C_{fi} \overline{q}_i) + \sum_{j \in \Omega_2} (C_{vj} \overline{X}_j + C_{fj} \overline{q}_j) \tag{3.21}$$

subject to

$$\left(\sum_{i \in \Omega_1} \overline{S}_i^{(k)} (\overline{B}_i^{(k)} - B_i^{(k)}) + \sum_{j \in \Omega_2} \overline{S}_j^{(k)} (\overline{X}_j^{(k)} - X_j^{(k)}) \right) + \overline{\lambda}^{*(k)} \geq 1 \ \forall k \tag{3.22}$$

$$0 \leq \overline{B}_i^{(k)} \leq \overline{B}_i, \quad \forall k \tag{3.23}$$

$$0 \leq \overline{X}_j^{(k)} \leq \overline{X}_j, \quad \forall k \tag{3.24}$$

$$0 \leq \overline{B}_i \leq B_{i\max} \overline{q}_i \tag{3.25}$$

$$0 \leq \overline{X}_j \leq X_{j\max} \overline{q}_j \tag{3.26}$$

$$\overline{q}_i, \overline{q}_j = 0,1 \tag{3.27}$$

The decision variables are $\overline{B}_i^{(k)}$, $\overline{B}_i$, $\overline{q}_i$, $\overline{X}_j^{(k)}$, $\overline{X}_j$ and $\overline{q}_j$.

Here,

- $\overline{B}_i$ is the new size of the switched shunt capacitor at location *i*,
- $\overline{X}_j$ is the new size of the switched series capacitor at location *j*,
- $\overline{q}_i$ and $\overline{q}_j$ are new binary control location variables,
- $\overline{S}_i^{(k)}$ is the updated sensitivity of the bifurcation parameter with respect to the susceptance of the switched shunt capacitor at location *i* under contingency *k*,
- $\overline{S}_j^{(k)}$ is the updated sensitivity of the bifurcation parameter with respect to the reactance of the switched series capacitor at location *j* under contingency *k*,
- $\overline{B}_i^{(k)}$ is the new size of the switched shunt capacitor at location *i* under contingency k,
- $\overline{X}_j^{(k)}$ is the new size of the switched series capacitor at location *j* under contingency k, and
- $\overline{\lambda}^{*(k)}$ is the updated bifurcation parameter evaluated at the critical point under contingency k.

The above successive MIP will end until all post-contingency equilibria are restored and there is no significant movement of the decision variables from the previous MIP solution as shown in Figure 3-4.

3.4 Application to New England System

The proposed method has been applied to the New England 39 bus system [64] shown in Figure 3-5.

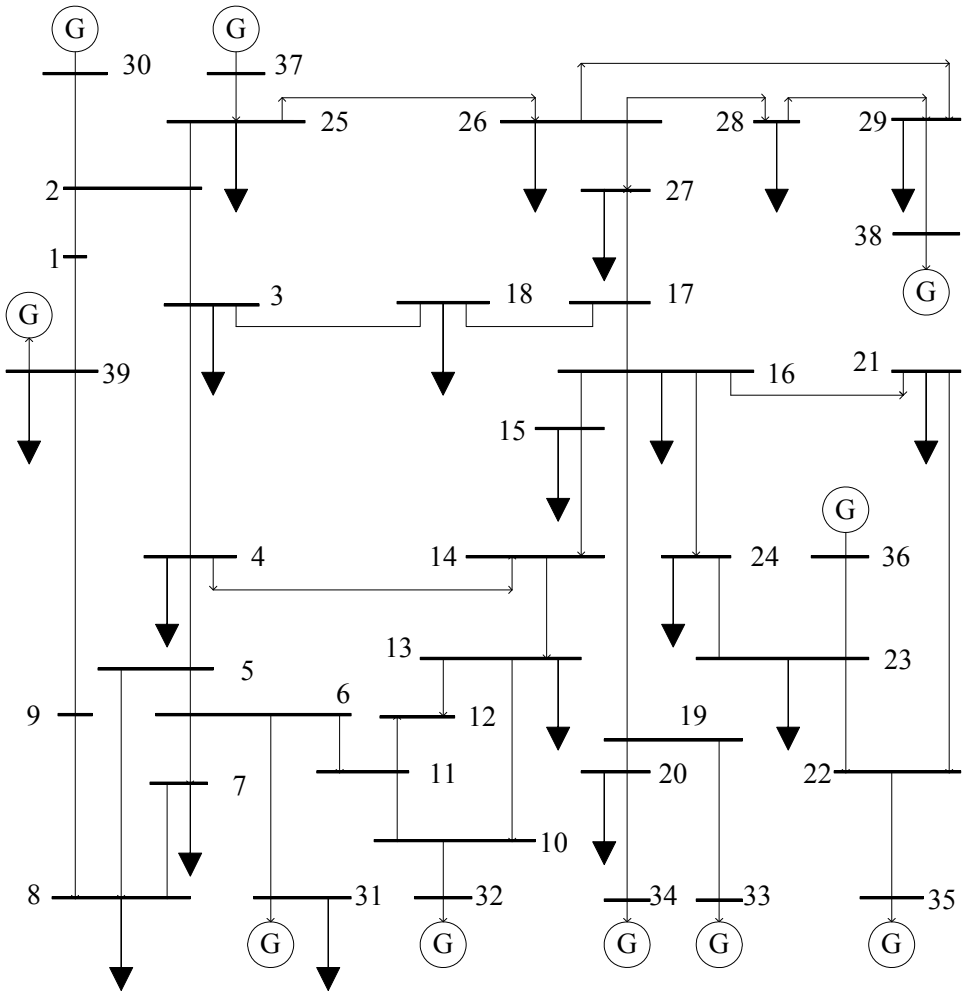


Figure 3-5 New England 39-bus test system

In the simulations, the following conditions are implemented unless stated otherwise:

- Constant power load model is used;
- For generator outage, the generation loss is picked up by available generators proportional to their base case value;
- The branch-and-bound method and the primal-dual interior-point method are used to solve the mixed integer programming problems [66].
- The parameter values adopted in the optimization problem are given in Table 3.1.

Table 3.1 Parameter values in the optimization formulation to restore equilibrium

	Shunt capacitor	Series capacitor
Maximum size (p.u.)	2.0	50% compensation

Considering all N-1 contingencies, the voltage stability of the system is analyzed by the fast contingency screening and the continuation method presented in section 3.3.2. There exist 2 contingencies that cause the system to be unsolvable as shown in Table 3.2.

Table 3.2 Critical point under two severe contingencies for the New England system

Contingency	λ^*
(1). Outage of the generator at bus 38	0.92
(2). Outage of the generator at bus 39	0.82

The candidate control locations are determined based on the backward/forward search algorithm presented in Section 2.4. The best five candidate buses to install switched shunt capacitors are buses 1, 9, 28, 29, 39. The best three candidate lines to install switched series capacitors are lines 1-2, 6-7, 25-26. For these candidate locations, the reactive power control planning algorithm presented in Section 3.3 was carried out.

The optimal control allocations are shown in Table 3.3 indicating that a switched series capacitor of 0.0205 p.u. on line 1-2, a switched series capacitor of 0.0150 p.u. on line 25-26 and a switched shunt capacitor of 0.5094 p.u. at bus 39. The total cost for the control allocation is \$7.1355 million. If only switched shunt capacitors were chosen as candidate reactive power controls, the total cost for the control allocation is \$9.3569 million which is 31.1% higher than that of coordinated planning of switched shunt and series capacitors. This result shows that benefit could be obtained by coordinated planning of different types of discrete reactive power controls. Table 3.4 gives the verified results of the reactive power control planning with the continuation method. Clearly, the value of the bifurcation parameter at the critical point λ^* under the concerned contingencies is increased to the required value of 1.0 p.u. with the planned controls. The iteration number in the second column represents the number of times of performing the MIP to obtain the optimal solution.

Table 3.3 Control allocations for shunt and series capacitors to restore equilibrium

Candidate locations for shunt and series capacitors	Maximal size limit (p.u.)	Overall optimal control allocation (p.u.)	Solution to cont. (1) (p.u.)	Solution to cont. (2) (p.u.)
Bus 39	2.0	0.5094	0	0.5094
Line 1-2	0.0205	0.0205	0.0205	0.0205
Line 25-26	0.0162	0.0150	0.0150	0

Table 3.4 Critical point under planned controls

Candidate control	Iteration number for MIP	λ^* for cont. (1)	λ^* for cont. (2)
Shunt and series capacitors	3	1.00	1.00

The computation in the proposed reactive control planning method is done only to (a) calculate the critical points and sensitivities and (b) solve the optimization. It is only in calculating the critical points and sensitivities that we must deal with the full size of the power system. Computation associated with optimization is mainly affected by the number of candidate controls. The CPU time for solving the coordinated planning of switched shunt and series capacitors is 1.43 seconds on a standard 2.2 GHz machine.

3.5 Summary

This chapter presents an optimization based method of planning reactive power controls in electric transmission systems to restore equilibria under severe contingencies. The planned reactive power controls are capable to serve a planned set of contingencies. Optimal locations and amounts of new switch controls are obtained by solving a sequence of mixed integer programming problems. The proposed approach can handle a large-scale power system because it significantly reduces the computational cost by fully utilizing the information of the sensitivity of the bifurcation parameter at the critical point. The effectiveness of the method is illustrated by applying to the New England 39 bus system. The results show that the method works satisfactorily to plan switched shunt and series capacitors to restore post-contingency equilibria. After the equilibria are restored, the post-contingency voltage stability margin of the system can be increased to a required value by solving an optimization problem proposed in the next chapter.

4.0 Reactive Power Control Planning to Increase Voltage Stability Margin

4.1 Introduction

In the last chapter, we propose an algorithm to restore equilibria of a power system under severe contingencies by adding the minimum amount of switched shunt/series capacitors. After the equilibrium is restored under each severe contingency, the voltage stability margin is just equal to zero. At this point, a small disturbance can result in a negative voltage stability margin and cause voltage collapse. On the other hand, the potential for moderate contingencies often leads to small voltage stability margins. We need to add more reactive power control devices to increase the voltage stability margin to be greater than a pre-specified value.

In this chapter, a method is presented for the reactive power control planning to increase post-contingency voltage stability margin. Mechanically switched shunt and series capacitors are used as the reactive power control means. Instead of considering only the most severe contingency or considering several contingencies sequentially [65] the proposed planning method considers multiple contingencies simultaneously. The backward/forward search algorithm with linear complexity is used to select candidate control locations. An initial mixed integer linear programming (MILP) formulation using voltage stability margin sensitivities is proposed to estimate reactive power control locations and amounts from the candidates. The objective function of the MILP is to minimize the total installation cost including fixed cost and variable cost of new controls while satisfying the voltage stability margin requirement under contingencies. A sequence of MILP with updated margin sensitivities is proposed to refine control amounts and/or locations from the initial MILP result until the voltage stability margin requirement is satisfied and there is no significant movement of the decision variables from the previous MIP solution. The CPF program is utilized to check the true voltage stability margin after each MILP. This iterative process is required to account for system nonlinearities. The branch-and-bound and primal-dual interior-point methods [66] are used to solve the optimization problem. Because the optimization formulation is linear, it is fast, yet it provides good solutions for large-scale power systems compared with nonlinear optimization formulations.

The following assumptions are made in this chapter:

- The system planner has identified a-priori lines where series compensation would create sub-synchronous resonance (SSR) risk and has eliminated those lines from the list of candidates.
- Voltage magnitude control is addressed as a refinement following identification of the reactive power resources necessary to satisfy the voltage stability margin requirements.

The chapter is organized as follows. Section 4.2 describes the proposed method of the reactive power control planning. Numerical results are discussed in Section 4.3. Section 4.4 concludes.

4.2 Algorithm of Reactive Power Control Planning

The proposed reactive power control planning approach requires three stages: (1) select candidate control locations, (2) use MIP to estimate control locations and amounts from stage 1 locations, and (3) use MIP with updated information to refine control amounts and/or locations from stage 2 locations and amounts. The overall procedure for the reactive power control planning is shown in Figure 4-1 which integrates the above mentioned steps.

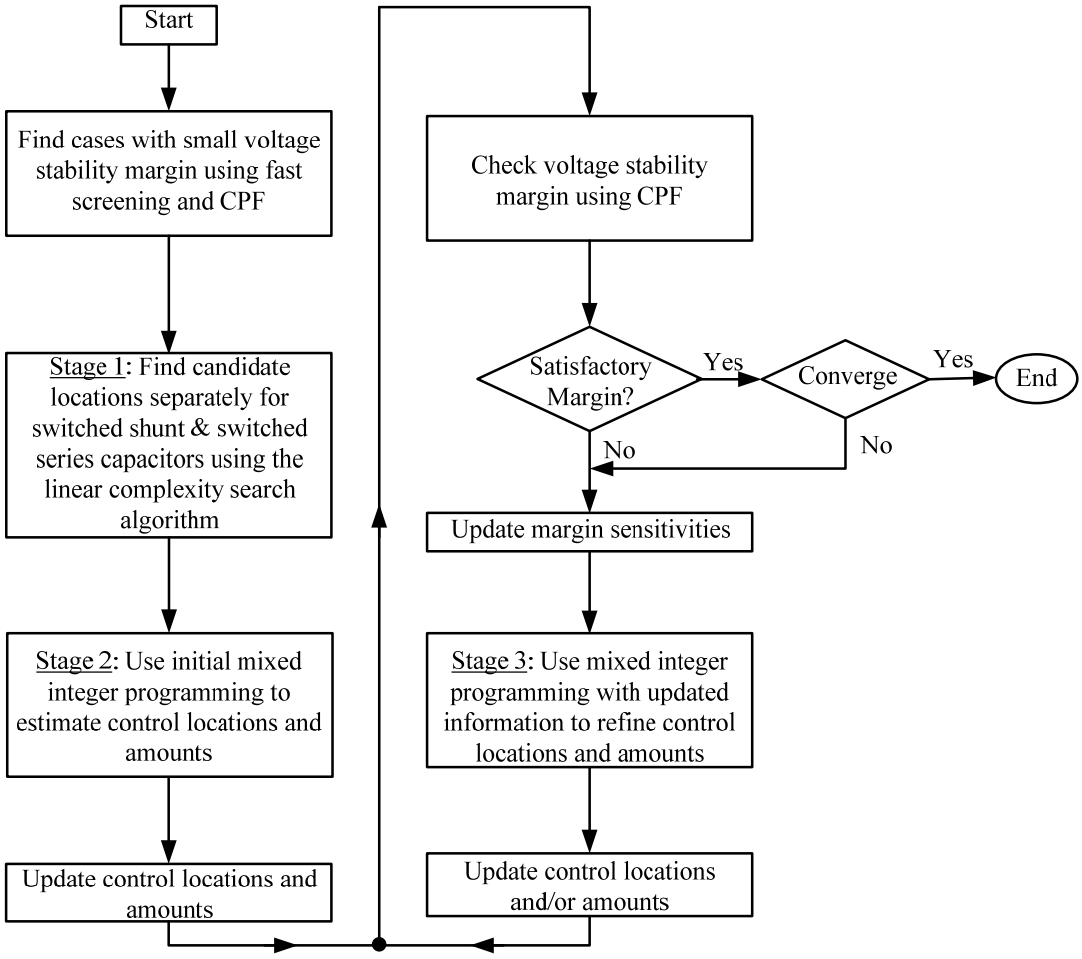


Figure 4-1 Flowchart for reactive power control planning to increase voltage stability margin

4.2.1 Selection of Candidate Control Locations

The backward/forward search algorithm with linear complexity presented in Chapter 2 is used to find candidate locations separately for switched shunt and switched series capacitors under every contingency.

4.2.2 Formulation of Initial Mixed Integer Programming

In stage 1, we find the candidate locations for switched shunt and series capacitors separately. In this stage, we use a mixed integer programming (MIP) to estimate control locations and amounts from candidate control locations. The MIP minimizes the total control installation cost while increasing the voltage stability margin to a required percentage x for each concerned contingency.

minimize

$$J = \sum_{i \in \Omega_1} (C_{vi} B_i + C_{fi} q_i) + \sum_{j \in \Omega_2} (C_{vj} X_j + C_{fj} q_j) \tag{4.1}$$

subject to

$$\sum_{i \in \Omega_1} S_i^{(k)} B_i^{(k)} + \sum_{j \in \Omega_2} S_j^{(k)} X_j^{(k)} + M^{(k)} \geq x P_{l0}, \quad \forall k \tag{4.2}$$

$$0 \leq B_i^{(k)} \leq B_i, \quad \forall k \tag{4.3}$$

$$0 \leq X_j^{(k)} \leq X_j, \quad \forall k \tag{4.4}$$

$$0 \leq B_i \leq B_{i\max} q_i \tag{4.5}$$

$$0 \leq X_j \leq X_{j\max} q_j \tag{4.6}$$

$$q_i, q_j = 0,1 \tag{4.7}$$

The decision variables are $B_i^{(k)}$, B_i, q_i, $X_j^{(k)}$, X_j, and q_j.

Here,

- C_{fi} is fixed installation cost and C_{vi} is variable cost of mechanically switched shunt capacitors,
- C_{fj} is fixed installation cost and C_{vj} is variable cost of mechanically switched series capacitors,
- B_i is the size (susceptance) of the switched shunt capacitor at location i,
- X_j is the size (reactance) of the switched series capacitor at location j,
- q_i=1 if location i is selected for reactive power control expansion, otherwise, q_i=0 (the same to q_j),
- the superscript k represents the contingency under which there is insufficient voltage stability margin,
- Ω_1 is the set of candidate locations to install switched shunt capacitors,
- Ω_2 is the set of candidate locations to install switched series capacitors,
- $B_i^{(k)}$ is the size of the shunt capacitor to be switched on at location i under contingency k,
- $X_j^{(k)}$ is the size of the series capacitor to be switched on at location j under contingency k,
- $S_i^{(k)}$ is the sensitivity of the voltage stability margin with respect to the susceptance of the shunt capacitor at location i under contingency k,
- $S_j^{(k)}$ is the sensitivity of the voltage stability margin with respect to the reactance of the series capacitor at location j under contingency k,
- x is an arbitrarily specified voltage stability margin in percentage,
- P_{l0} is the forecasted system load,

- $M^{(k)}$ is the voltage stability margin under contingency k and without controls,
- $B_{i\max}$ is the maximum size of the switched shunt capacitor at location i, and
- $X_{j\max}$ is the maximum size of the switched series capacitor at location j.

Note that, we identify the minimum set of switched shunt and series capacitors to restore equilibrium points under severe contingencies using the successive MIP in Chapter 3. We may then increase the voltage stability margin for these contingencies to the required value along with other contingencies having insufficient voltage stability margin. In order to minimize the total installation cost of switched shunt and series capacitors, the previously identified switched shunt and series capacitors can be utilized to increase the voltage stability margin for other contingencies. For example, if B_i amount of switched shunt capacitor is identified at location i and $B_i^{(k)}$ amount ($B_i^{(k)}$ can be zero under other contingencies) of switched shunt capacitor at location i needs to be switched on under contingency k to restore the equilibrium point, there will be no cost for using B_i-$B_i^{(k)}$ and no fixed cost for using $B_{i\max}$-B_i to increase the voltage stability margin. Consequently, the fixed as well as variable cost for B_i-$B_i^{(k)}$ is set to be zero and the fixed cost for $B_{i\max}$-B_i is set to be zero in the above MIP problem.

For k contingencies that have the voltage stability margin less than the required value and n selected candidate control locations, there are $n(k+2)$ decision variables and $k+3n+2kn$ constraints. For the same reason as in Section 3.3.4, the computational cost for solving the above mixed integer programming formulation is not high even for large-scale power systems. The branch-and-bound and primal-dual interior-point methods are used to solve this mixed integer programming problem.

The output of the mixed integer programming problem is the control locations and amounts for all k contingencies and the combined control location and amount. Then the network configuration is updated by switching in the controls under each contingency. After that, the voltage stability margin is recalculated using CPF to check if sufficient margin is achieved for each concerned contingency. This step is necessary because the voltage stability margin nonlinearly depends on control variables, and our mixed integer programming algorithm uses linear margin sensitivities to estimate the effect of variations of control variables on the voltage stability margin. As a result, there may be contingencies that have insufficient voltage stability margin after updating the network configuration according to results of the initial mixed integer programming problem. Also, the obtained solution may not be optimal after one iteration of MIP. The control locations and/or amounts are further refined by recomputing margin sensitivities (with updated network configuration) under each concerned contingency, and solving a second-stage successive MIP with updated information, as described in the next subsection.

4.2.3 Formulation of MIP with Updated Information

The successive MIP is formulated to minimize the total control installation cost subject to the constraint of the voltage stability margin requirement, as follows:

minimize

$$J = \sum_{i\in\Omega_1}(C_{vi}\overline{B}_i + C_{fi}\overline{q}_i) + \sum_{j\in\Omega_2}(C_{vj}\overline{X}_j + C_{fj}\overline{q}_j) \tag{4.8}$$

subject to

$$\left(\sum_{i\in\Omega_1}\overline{S}_i^{(k)}(\overline{B}_i^{(k)}-B_i^{(k)})+\sum_{j\in\Omega_2}\overline{S}_j^{(k)}(\overline{X}_j^{(k)}-X_j^{(k)})\right)+\overline{M}^{(k)}\geq xP_{l0},\quad \forall k \tag{4.9}$$

$$0\leq\overline{B}_i^{(k)}\leq\overline{B}_i,\quad \forall k \tag{4.10}$$

$$0\leq\overline{X}_j^{(k)}\leq\overline{X}_j,\quad \forall k \tag{4.11}$$

$$0\leq\overline{B}_i\leq B_{i\max}\overline{q}_i \tag{4.12}$$

$$0\leq\overline{X}_j\leq X_{j\max}\overline{q}_j \tag{4.13}$$

$$\overline{q}_i,\overline{q}_j=0,1 \tag{4.14}$$

The decision variables are $\overline{B}_i^{(k)}$, $\overline{B}_i$, $\overline{q}_i$, $\overline{X}_j^{(k)}$, $\overline{X}_j$ and $\overline{q}_j$.

Here,

- $\overline{B}_i$ is the new size of the switched shunt capacitor at location *i*,
- $\overline{X}_j$ is the new size of the switched series capacitor at location *j*,
- $\overline{q}_i$ and $\overline{q}_j$ are new binary control location variables,
- $\overline{S}_i^{(k)}$ is the updated sensitivity of the voltage stability margin with respect to the susceptance of the shunt capacitor at location *i* under contingency *k*,
- $\overline{S}_j^{(k)}$ is the updated sensitivity of the voltage stability margin with respect to the reactance of the series capacitor at location *j* under contingency *k*,
- $\overline{B}_i^{(k)}$ is the new size of the switched shunt capacitor at location *i* under contingency k,
- $\overline{X}_j^{(k)}$ is the new size of the switched series capacitor at location *j* under contingency k, and
- $\overline{M}^{(k)}$ is the updated voltage stability margin under contingency *k*.

The above successive MIP will end until all concerned contingencies have satisfactory voltage stability margin and there is no significant movement of the decision variables from the previous MIP solution.

4.3 Numerical Results

The proposed method has been applied to the New England 39-bus system. In the simulations, the following conditions are implemented unless stated otherwise:

- Loads are modeled as constant power;
- In computing voltage stability margin, the power factor of the load bus remains constant when the load increases, and load and generation increase are proportional to their base case value;
- The system MVA base is 100;
- Required voltage stability margin is assumed to be 10%;
- The parameter values adopted in the optimization problem are given in Table 4.1.

Table 4.1 Parameter values in the optimization formulation

	Shunt capacitor	Series capacitor
Maximum size (p.u.)	1.5	70% compensation

Considering all N-1 contingencies, using the fast contingency screening and CPF methods, there exist 3 contingencies that result in a post-contingency voltage stability margin less than 10% as shown in Table 4.2.

Table 4.2 Voltage stability margin under three moderate contingencies

Contingency	Voltage Stability Margin (%)
(1). Outage of the generator at bus 31	2.69
(2). Outage of the generator at bus 32	2.46
(3). Outage of the generator at bus 35	2.42

The candidate control locations are determined based on the linear search algorithm presented in Chapter 2. The best seven candidate buses to install switched shunt capacitors are buses 5, 6, 7, 10, 11, 12, and 13. The best eight candidate lines to install switched series capacitors are lines 2-3, 3-4, 4-5, 6-7, 8-9, 13-14, 15-16, and 16-19. For these candidate locations, the optimization based reactive power control planning algorithm presented in Sections III.E and III.F was carried out.

In order to demonstrate the efficacy of the proposed method, two cases are considered as follows. In case 1, only switched shunt capacitors are chosen as candidate controls while both switched shunt and switched series capacitors are chosen as candidate controls in case 2. Table 4.3 shows the results for case 1 where the optimal allocations for switched shunt capacitors are 0.747 p.u., 1.500 p.u., 0.866 p.u., 1.500 p.u. and 1.500 p.u. at buses 5, 6, 10, 11, and 12 respectively. The total cost is $ 9.006 million for the control allocations in case 1. On the other hand, the optimal control allocations for case 2 are shown in Table 4.4 indicating a switched series capacitor of 0.011 p.u. on line 2-3, a switched series capacitor of 0.025 p.u. on line 8-9 and a switched shunt capacitor of 0.973 p.u. at bus 12. For case 2, the total cost for control allocations is $ 7.326 million which is 18.7% less than that of case 1. This result shows that benefit can be obtained by coordinated planning of different types of discrete reactive power controls. Table 4.5 gives the verified results of the reactive power control planning with the continuation power flow program. Clearly, the voltage stability margins of the concerned contingencies are all increased to be greater than the required value of 10% under the planned controls. The iteration number in the second column represents the number of times of performing the MIP to get the optimal solution. The CPU time for

solving the coordinated planning of switched shunt and series capacitors is 1.81 seconds on a standard 2.2 GHz machine for problems having 15 candidate control locations.

Table 4.3 Control allocations for shunt capacitors to increase voltage stability margin

Locations for shunt cap.	Maximum size Limit (p.u.)	Overall optimal control allocation (p.u.)	Solution to cont. (1) (p.u.)	Solution to cont. (2) (p.u.)	Solution to cont. (3) (p.u.)
Bus 5	1.500	0.747	0.747	0.747	0.747
Bus 6	1.500	1.500	1.384	1.500	1.500
Bus 10	1.500	0.866	0.866	0.866	0.866
Bus 11	1.500	1.500	1.500	1.500	1.500
Bus 12	1.500	1.500	1.500	1.500	1.500

Table 4.4 Control allocations for shunt, series capacitors to increase voltage stability margin

Locations for shunt and series cap.	Maximum size limit (p.u.)	Overall optimal control allocation (p.u.)	Solution to cont. (1) (p.u.)	Solution to cont. (2) (p.u.)	Solution to cont. (3) (p.u.)
Bus 12	1.500	0.973	0.258	0.361	0.973
Line 2-3	0.011	0.011	0.011	0.011	0.011
Line 8-9	0.025	0.025	0.025	0.025	0.025

Table 4.5 Voltage stability margin under planned controls

Candidate controls	Iteration number for MIP	Voltage stability margin for cont. (1)	Voltage stability margin for cont. (2)	Voltage stability margin for cont. (3)
Shunt capacitors	6	10.01%	10.01%	10.01%
Shunt and series capacitors	3	10.01%	10.01%	10.02%

4.4 Summary

This chapter presents an optimization based method of planning reactive power controls in electric transmission systems to satisfy the voltage stability margin requirement under a set of contingencies. The backward/forward search algorithm with linear complexity is used to select candidate locations for switched shunt and series capacitors. Optimal locations and amounts of new switch controls are obtained by solving a sequence of mixed integer

programming problems. The effectiveness of the method is illustrated using the New England 39 bus system. The results show that the method works satisfactorily to plan reactive power controls.

5.0 Optimal Allocation of Static and Dynamic Var Resources

5.1 Introduction

Sufficient controllable reactive power resources are essential for reliable operation of electric power systems. Inadequate reactive power support has led to voltage collapses and has been a cause of several recent major power outages worldwide. While the August 2003 blackout in the United States and Canada was not due to a voltage collapse, the final report of the U.S.-Canada Power System Outage Task force said that "insufficient reactive power was an issue in the blackout" [67].

Generally, reactive power supply can be divided into two categories: static and dynamic VAR resources. Dynamic VAR resources such as Static VAR Compensators (SVCs) have a fast response time while static VAR resources such as Mechanically Switched Capacitors (MSCs) have a relatively slow response time [10]. In addition, dynamic VAR devices can continuously control reactive power output but static VAR devices can not. On the other hand, the cost of static VAR resources is much lower than that of dynamic VAR resources [24]. Differences in effectiveness and costs of different devices dictate that reactive power generally is provided by a mix of static and dynamic VAR resources. Mechanically switched capacitors are cost-effective to increase post-contingency voltage stability margin. More expensive SVCs are usually used to deal with transient voltage dip and short-term voltage stability problems [4, 61, 68, 69, 70, 71] because the capability for rapid on-off switching of mechanically switched capacitors is significantly limited [72]. In this chapter, we focus on mechanically switched shunt capacitors as static VAR resources and SVCs as dynamic VAR resources because they have been widely used in the electric power industry as reactive power support. However, the proposed algorithm is applicable to plan other VAR resources as well.

There are three basic problems to be addressed for planning static and dynamic VAR resources:

1) how much reactive capacity to build;
2) where to build;
3) what should be split between static and dynamic VAR resources.

There is a limited amount of publications about coordinated planning of static and dynamic VAR resources. The methods in [42] [43] [44] [45] use a sequential procedure to allocate static and dynamic VAR resources. In this chapter, an optimization based method is presented to simultaneously determine the optimal allocation of static and dynamic VAR resources to satisfy the requirements of voltage stability margin and transient voltage dip. The remaining parts of this chapter are organized as follows. Section 5.2 presents transient voltage dip sensitivities. Section 5.3 describes the proposed mixed integer programming based method to optimally allocate static and dynamic VAR resources. Section 5.4 provides numerical results to illustrate the effectiveness of the approach. Section 5.5 concludes.

5.2 Transient Voltage Sensitivities

An SVC is an effective means to mitigate transient voltage dip by providing dynamic reactive power support. The ability of an SVC to mitigate transient voltage dip depends on the SVC's capacitive limit (size) B_{svc}, as shown in Figure 5-1. Dynamic reactive power support increases with B_{svc}, but so does the SVC cost. We desire to identify the most effective locations and to determine the minimum capacitive limits of SVCs such that the transient voltage dip criteria are satisfied. To do this, we deploy a sequence of linear search/optimizations which require voltage dip magnitude and duration sensitivities to the SVC capacitive limit. These sensitivities are derived in this section.

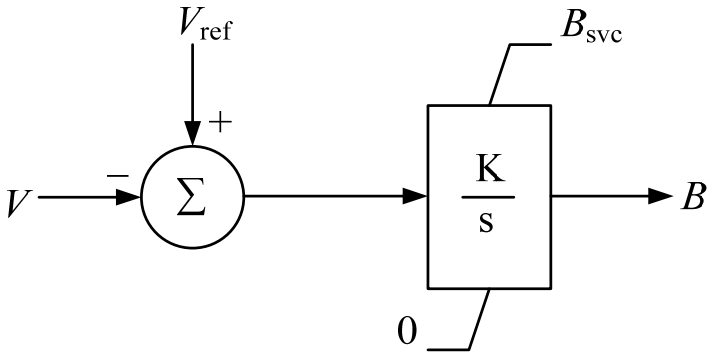


Figure 5-1 Static VAR compensator model

As shown in Figure 5-1, there is a non-windup limit on the SVC output, constraining the SVC susceptance output B. When the SVC output reaches the capacitive limit, the SVC becomes non-controllable and is equivalent to a shunt capacitor. Therefore, the power system model when the SVC output reaches the limit is different from that when the SVC output is within the limit. There are also hard limits on other power system controllers such as generator excitation systems [73]. Thus, the response of a power system is hybrid when studying large disturbances. It exhibits periods of smooth behavior, interspersed with discrete events. Smooth behavior is driven by devices such as generators and loads that are described by differential-algebraic equations. Discrete events are arising, for example, from enforcement of controller hard limits. Systems that exhibit intrinsic interactions between continuous dynamics and discrete events are generally called hybrid systems [74].

In order to derive the sensitivities of the voltage dip time duration and the maximum transient voltage dip to the SVC capacitive limit, the hybrid system nature of a power system need to be considered. The hybrid system model proposed in [73] and [75] is adopted here to derive the sensitivities. An overview of the hybrid system model is provided in Appendix A. The sensitivities of the voltage dip time duration and the maximum transient voltage dip to the SVC capacitive limit are derived based on the trajectory sensitivities of hybrid systems presented in [75]. The trajectory sensitivities provide a way of quantifying the variation of a trajectory resulting from (small) changes to parameters and/or initial conditions [76]. An overview of the trajectory sensitivities is proved in Appendix B.

5.2.1 *Sensitivity of Voltage Dip Time Duration to SVC Capacitive Limit*

The sensitivity of the voltage dip time duration to the SVC capacitive limit is the change of the voltage dip time duration for a given change in the SVC capacitive limit which can be treated as a parameter and be included in x_0 which is a vector including parameters and initial conditions of state variables in Appendix B.

Let $\tau^{(1)}$ be the time at which the transient voltage dip begins after a fault is cleared and $\tau^{(2)}$ the time at which the transient voltage dip ends as shown in Figure 1-3 Then the time duration of the transient voltage dip τ_{dip} is given by

$$\tau_{\text{dip}} = \tau^{(2)} - \tau^{(1)} \tag{5.1}$$

Thus, the sensitivity of the voltage dip time duration to the capacitive limit of an SVC, S_τ, is

$$S_\tau \equiv \frac{\partial \tau_{dip}}{\partial B_{\text{svc}}} = \frac{\partial(\tau^{(2)} - \tau^{(1)})}{\partial B_{\text{svc}}} = \frac{\partial \tau^{(2)}}{\partial B_{\text{svc}}} - \frac{\partial \tau^{(1)}}{\partial B_{\text{svc}}} = \tau^{(2)}_{B_{\text{svc}}} - \tau^{(1)}_{B_{\text{svc}}} \tag{5.2}$$

where $\tau^{(1)}_{B_{\text{svc}}}$ and $\tau^{(2)}_{B_{\text{svc}}}$ are calculated in (B.9) of Appendix B. Note that the hypersurface $s(x,y)$ in (B.9) is defined by $0.8V_i(0) - V_i(t)$ when calculating $\tau^{(1)}_{B_{\text{svc}}}$, and is defined by $V_i(t) - 0.8V_i(0)$ when calculating $\tau^{(2)}_{B_{\text{svc}}}$ where V_i is the voltage at load bus i.

Bus voltage recovery may be slow after a fault is cleared as shown in Figure 5-2. In this case, $\tau^{(1)}$ is equal to the time at which the fault is cleared. Therefore, $\tau^{(1)}_{B_{\text{svc}}} = 0$ and $S_\tau = \tau^{(2)}_{B_{\text{svc}}}$.

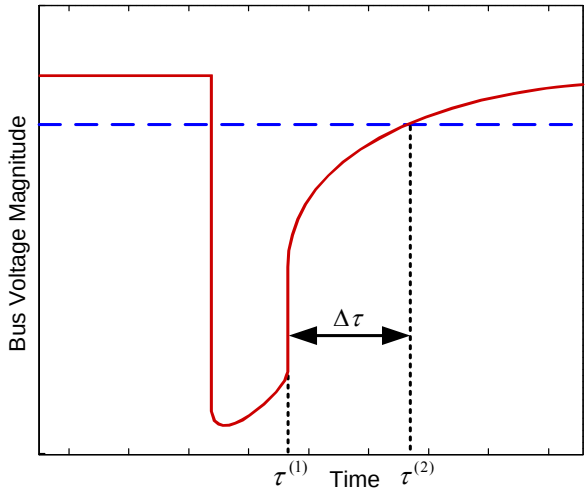


Figure 5-2 Slow voltage recovery after a fault

5.2.2 *Sensitivity of Maximum Transient Voltage Dip to SVC Capacitive Limit*

The maximum transient voltage dip V_{dip} after the fault is cleared is defined as

$$V_{\text{dip}} = \frac{V_0 - V_{\min}}{V_0} \times 100\% \tag{5.3}$$

where V_0 is the pre-fault voltage and $V_{\min}$ is the minimum voltage magnitude during the

transient voltage dip.

The sensitivity of the maximum transient voltage dip to the SVC capacitive limit, S_V, is the change of the maximum transient voltage dip for a given change in the SVC capacitive limit

$$S_V \equiv \frac{\partial V_{dip}}{\partial B_{\text{svc}}} = -(\frac{\partial V_{\min}}{\partial B_{\text{svc}}})/V_0 = -(\frac{\partial V}{\partial B_{\text{svc}}}\Big|_{t=t_{\max\_\text{dip}}})/V_0 \tag{5.4}$$

where $\partial V/\partial B_{\text{svc}}$ is the voltage trajectory sensitivity to the SVC capacitive limit which is calculated by solving (B.3) and (B.4) in Appendix B, and $t_{\max\_\text{dip}}$ is the time when the maximum transient voltage dip (minimum voltage magnitude) occurs after the fault is cleared. Note that the sensitivity given in (5.4) is approximate, as it neglects the dependence of $t_{\max\_\text{dip}}$ on B_{svc}. Generally, $t_{\max\_\text{dip}}$ changes very little with B_{svc} though, so the approximation is quite accurate.

5.2.3 Numerical Approximation

From computation point of view, the trajectory sensitivities and the transient voltage dip sensitivities require the integration of a set of differential algebraic equations as shown in Appendix B. For large systems, these equations have high dimension. The computational cost of obtaining the sensitivities is minimal when an implicit numerical integration technique such as trapezoidal integration is used to generate the trajectory [75], [77], [78]. An alternative to calculate the sensitivities is using numerical approximation

$$S_\tau = \frac{\partial \tau_{\text{dip}}}{\partial B_{\text{svc}}} \approx \frac{\Delta \tau_{\text{dip}}}{\Delta B_{\text{svc}}} = \frac{\tau_{\text{dip}}(B_{\text{svc}} + \Delta B_{\text{svc}}) - \tau_{\text{dip}}(B_{\text{svc}})}{\Delta B_{\text{svc}}} \tag{5.5}$$

and

$$S_V = \frac{\partial V_{\text{dip}}}{\partial B_{\text{svc}}} \approx \frac{\Delta V_{\text{dip}}}{\Delta B_{\text{svc}}} = \frac{V_{\text{dip}}(B_{\text{svc}} + \Delta B_{\text{svc}}) - V_{\text{dip}}(B_{\text{svc}})}{\Delta B_{\text{svc}}} \tag{5.6}$$

The procedure requires repeated runs of simulation of the system model for the SVC capacitive limits B_{svc} and $B_{\text{svc}}+\Delta B_{\text{svc}}$. The senstivities are then given by the change of the voltage dip time duration or the maximum transient voltage dip divided by the SVC capacitive limit change ΔB_{svc}. The involved computational cost of this procedure may be greater than direct calculation of the sensitivities if many sensitivities are desired. However, it is easier to implement for a practical large power system. In this work, time domain simulations and voltage dip sensitivities were obtained using Siemens PTI's PSS/E™ version 30.1 software.

5.3 Algorithm of Optimal Allocation of Static and Dynamic VAR Resources

A flowchart for planning static and dynamic VAR resources is shown in Figure 5-3. Each block in the flowchart will be explained in detail in the following subsections. After the contingency analysis, the proposed algorithm of allocation of static and dynamic VAR resources has three stages.

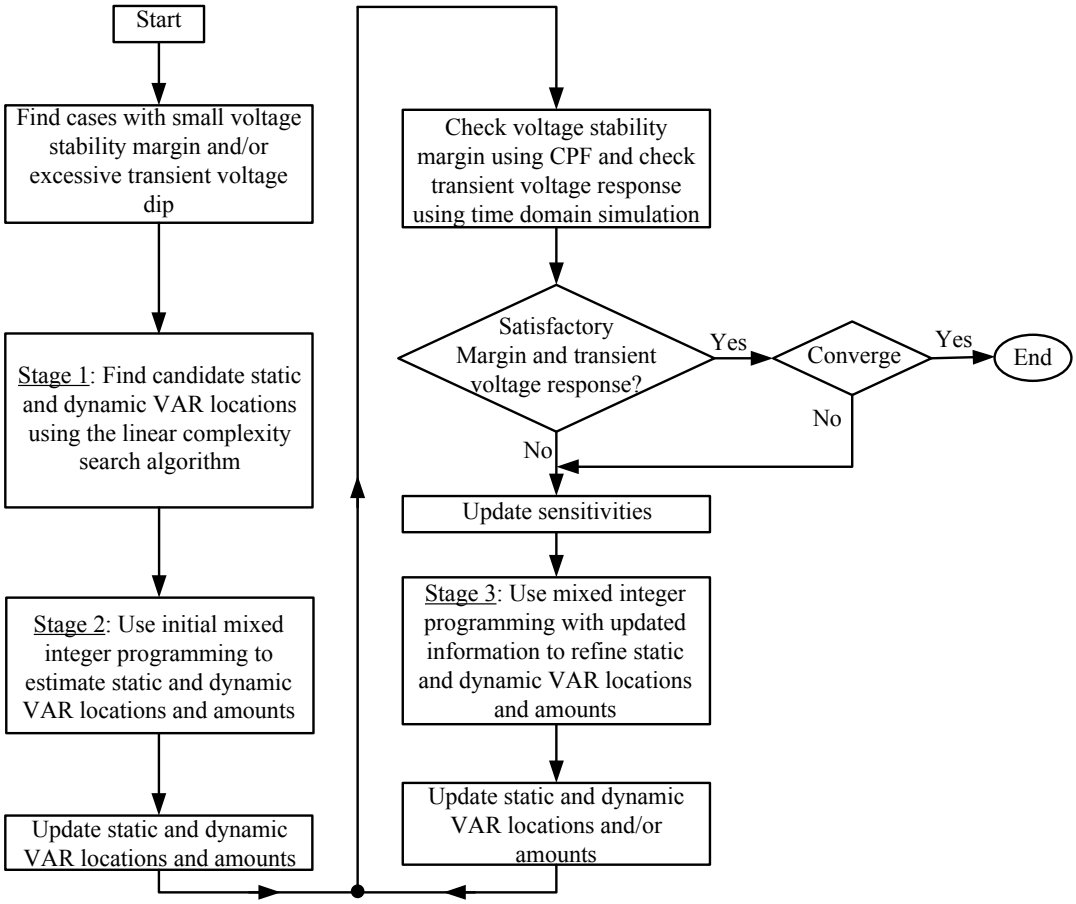


Figure 5-3 Flowchart for the static and dynamic VAR allocation

5.3.1 Contingency Analysis

In this step, the contingencies which cause insufficient voltage stability margin and/or excessive transient voltage dip problems are identified. In finding the contingencies having insufficient voltage stability margin, the fast contingency screening technique proposed in [55] is used. First, the post fault voltage stability margin is estimated based on voltage stability margin sensitivities. Then, the contingencies are ranked from most severe to least severe according to the value of the estimated voltage stability margin. After the ordered contingency list is obtained, each contingency is evaluated starting from the most severe one using the continuation power flow. Evaluation terminates after encountering a certain number of sequential contingencies having the voltage stability margin greater than or equal to the required value, where the number depends on the size of the contingency list.

In finding the contingencies having excessive transient voltage dip problems, the time domain simulation is used. A program was developed to automate identification of contingencies and buses which violate the transient voltage dip criteria based on the output of the time domain simulation.

5.3.2 Selection of Candidate VAR Locations

An important step in the VAR planning problem is the selection of candidate locations. Candidate locations may be chosen based on experience and/or the relative value of linear sensitivities of new reactive power compensation devices. In this case, however, there is no guarantee that the selected candidate locations for reactive compensation are sufficient to satisfy the requirements of voltage stability margin and transient voltage dip. On the other hand, the computational cost to solve the Stage 2 mixed integer programming problem is high if all buses in a large power system are selected as candidates. To identify a sufficient but not excessive number of locations, the backward/forward search algorithm with linear complexity proposed in Chapter 2 can be used to find candidate locations for switched shunt capacitors and SVCs to increase voltage stability margin, and to find candidate locations for SVCs to deal with transient voltage dip problems. It is assumed that the capacities of switched shunt capacitors and SVCs are fixed at the maximum allowable value in this step.

5.3.3 Formulation of Initial Mixed Integer Programming

In stage 1, we find the candidate locations for mechanically switched shunt capacitors and SVCs. A mixed integer program (MIP) is used in stage 2 to exclude candidate locations not needed, and to estimate the mix of mechanically switched shunt capacitors and SVCs at needed locations. The MIP minimizes the total installation cost of mechanically switched shunt capacitors and SVCs while satisfying the requirements of voltage stability margin and transient voltage dip.

minimize

$$J = \sum_{i\in\Omega}[C_{vi\_\text{shunt}}B_{i\_\text{shunt}} + C_{fi\_\text{shunt}}q_{i\_\text{shunt}} + C_{vi\_\text{svc}}B_{i\_\text{svc}} + C_{fi\_\text{svc}}q_{i\_\text{svc}}] \tag{5.7}$$

subject to

$$\sum_{i\in\Omega} S_{M,i}^{(k)}[B_{i\_\text{shunt}}^{(k)} + B_{i\_\text{svc}}^{(k)}] + M^{(k)} \geq M_{\text{r}},\ \forall k \tag{5.8}$$

$$\sum_{i\in\Omega_{\text{svc}}} S_{\tau,n,i}^{(k)}B_{i\_\text{svc}}^{(k)} + \tau_{\text{dip},n}^{(k)} \leq \tau_{\text{dip},n,\text{r}},\ \forall n,k \tag{5.9}$$

$$\sum_{i\in\Omega_{\text{svc}}} S_{V,n,i}^{(k)}B_{i\_\text{svc}}^{(k)} + V_{\text{dip},n}^{(k)} \leq V_{\text{dip},n,\text{r}},\ \forall n,k \tag{5.10}$$

$$0 \leq B_{i\_\text{shunt}}^{(k)} \leq B_{i\_\text{shunt}},\ \forall k \tag{5.11}$$

$$0 \leq B_{i\_\text{svc}}^{(k)} \leq B_{i\_\text{svc}},\ \forall k \tag{5.12}$$

$$0 \leq B_{i\_\text{shunt}} \leq B_{i\,\text{max\_shunt}}q_{i\_\text{shunt}} \tag{5.13}$$

$$0 \leq B_{i\_\text{svc}} \leq B_{i\,\text{max\_svc}}q_{i\_\text{svc}} \tag{5.14}$$

$$q_{i\_\text{shunt}}, q_{i\_\text{svc}} = 0,1 \tag{5.15}$$

The decision variables are $B_{i\_\text{shunt}}^{(\text{k})}$, B_{i_shunt}, q_{i_shunt}, $B_{i\_\text{svc}}^{(\text{k})}$, B_{i_svc}, and q_{i_svc}.

Variable definition follows:

- C_{f_shunt} is fixed installation cost and C_{v_shunt} is variable cost of shunt capacitors,
- C_{f_svc} is fixed installation cost and C_{v_svc} is variable cost of SVCs,
- B_{i_shunt}: size of the shunt capacitor at location i,

- B_{i_svc}: size of the SVC at location i,
- q_{i_shunt}=1 if the location i is selected for installing shunt capacitors, otherwise, q_{i_shunt}=0,
- q_{i_svc}=1 if the location i is selected for installing SVCs, otherwise, q_{i_svc}=0,
- the superscript k represents the contingency causing insufficient voltage stability margin and/or excessive transient voltage dip problems,
- Ω_{shunt}: set of candidate locations to install shunt capacitors,
- Ω_{svc}: set of candidate locations to install SVCs,
- Ω : union of Ω_{shunt} and Ω_{svc},
- $B_{i\_shunt}^{(k)}$: size of the shunt capacitor to be switched on at location i under contingency k,
- $B_{i\_svc}^{(k)}$: size of the SVC at location i under contingency k,
- $S_{M,i}^{(k)}$: sensitivity of the voltage stability margin with respect to the shunt susceptance at location i under contingency k,
- $S_{\tau,n,i}^{(k)}$: sensitivity of the voltage dip time duration at bus n with respect to the size of the SVC at location i under contingency k,
- $S_{V,n,i}^{(k)}$: sensitivity of the maximum transient voltage dip at bus n with respect to the size of the SVC at location i under contingency k,
- $M^{(k)}$: voltage stability margin under contingency k and without controls,
- M_r: required voltage stability margin,
- $\tau_{\mathrm{dip},n}{}^{(k)}$: time duration of voltage dip at bus n under contingency k and without controls,
- $\tau_{\mathrm{dip},n,\mathrm{r}}$: maximum allowable time duration of voltage dip at bus n,
- $V_{\mathrm{dip},n}{}^{(k)}$: maximum transient voltage dip at bus n under contingency k and without controls,
- $V_{\mathrm{dip},n,\mathrm{r}}$: maximum allowable transient voltage dip at bus n,
- $B_{i\max\_shunt}$: maximum size of the shunt capacitor at location i, and
- $B_{i\max\_svc}$: maximum size of the SVC at location i.

The inequality constraint in (5.8) requires that the voltage stability margin under each concerned contingency is greater than the required value. Note that SVCs can also be used to increase the voltage stability margin. The inequality constraint in (5.9) requires that the time duration of transient voltage dip for each concerned bus under each concerned contingency is less than the maximum allowable value. The inequality constraint in (5.10) requires that the maximum transient voltage dip for each concerned bus under each concerned contingency is less than the maximum allowable value.

The optimization formulation in (5.7)-(5.15) does not directly involve complex steady state and dynamic power system models. Instead, it uses the corresponding sensitivity information. In addition, the backward/forward search algorithm provides that the number of candidate locations for reactive compensation can be limited to be relatively small even for problems of the size associated with practical power systems. Therefore, the computational cost for solving the above mixed integer programming formulation is not high even for large-scale power systems. The branch-and-bound method is used to solve this mixed integer programming problem.

The output of the mixed integer programming problem is the reactive compensation locations and amounts for all concerned contingencies and the combined reactive compensation location and amount. Then the network configuration is updated by including the identified reactive power support under each contingency. After that, the voltage stability margin is recalculated using CPF to check if sufficient margin is achieved for each concerned contingency. Also, time domain simulations are carried out to check whether the requirement of the transient voltage dip performance is met. This step is necessary because the power system model is inherently nonlinear, and the mixed integer programming algorithm uses linear sensitivities to estimate the effect of variations of reactive support levels on the voltage stability margin and transient voltage dip. As a result, there may be contingencies that have insufficient voltage stability margin or excessive transient voltage dip after updating the network configuration according to results of the initial mixed integer programming problem. Also, the obtained solution may not be optimal after one iteration of MIP. The reactive compensation locations and/or amounts can be further refined by recomputing sensitivities (with updated network configuration) under each concerned contingency, and solving a second-stage mixed integer programming problem, as described in the next subsection.

5.3.4 Formulation of MIP with Updated Information

The successive MIP problem is formulated to minimize the total installation cost of mechanically switched shunt capacitors and SVCs subject to the constraints of the requirements of voltage stability margin and transient voltage dip, as follows:

minimize

$$J = \sum_{i\in\Omega}[C_{vi\_\text{shunt}}\overline{B}_{i\_\text{shunt}} + C_{fi\_\text{shunt}}\overline{q}_{i\_\text{shunt}} + C_{vi\_\text{svc}}\overline{B}_{i\_\text{svc}} + C_{fi\_\text{svc}}\overline{q}_{i\_\text{svc}}] \tag{5.16}$$

subject to

$$\sum_{i\in\Omega}\overline{S}_{M,i}^{(k)}[(\overline{B}_{i\_\text{shunt}}^{(k)} - B_{i\_\text{shunt}}^{(k)}) + (\overline{B}_{i\_\text{svc}}^{(k)} - B_{i\_\text{svc}}^{(k)})] + \overline{M}^{(k)} \geq M_{\text{r}},\ \forall k \tag{5.17}$$

$$\sum_{i\in\Omega_{svc}}\overline{S}_{\tau,n,i}^{(k)}(\overline{B}_{i\_\text{svc}}^{(k)} - B_{i\_\text{svc}}^{(k)}) + \overline{\tau}_{\text{dip},n}^{(k)} \leq \tau_{\text{dip},n,\text{r}},\ \forall n,k \tag{5.18}$$

$$\sum_{i\in\Omega_{svc}}\overline{S}_{V,n,i}^{(k)}(\overline{B}_{i\_\text{svc}}^{(k)} - B_{i\_\text{svc}}^{(k)}) + \overline{V}_{\text{dip},n}^{(k)} \leq V_{\text{dip},n,\text{r}},\ \forall n,k \tag{5.19}$$

$$0 \leq \overline{B}_{i\_\text{shunt}}^{(k)} \leq \overline{B}_{i\_\text{shunt}},\ \forall k \tag{5.20}$$

$$0 \leq \overline{B}_{i\_\text{svc}}^{(k)} \leq \overline{B}_{i\_\text{svc}},\ \forall k \tag{5.21}$$

$$0 \leq \overline{B}_{i\_\text{shunt}} \leq B_{i\,\text{max\_shunt}}\overline{q}_{i\_\text{shunt}} \tag{5.22}$$

$$0 \leq \overline{B}_{i\_\text{svc}} \leq B_{i\,\text{max\_svc}}\overline{q}_{i\_\text{svc}} \tag{5.23}$$

$$\overline{q}_{i\_\text{shunt}}, \overline{q}_{i\_\text{svc}} = 0,1 \tag{5.24}$$

The decision variables are $\overline{B}_{i\_\text{shunt}}^{(k)}$, $\overline{B}_{i\_\text{shunt}}$, $\overline{q}_{i\_\text{shunt}}$, $\overline{B}_{i\_\text{svc}}^{(k)}$, $\overline{B}_{i\_\text{svc}}$ and $\overline{q}_{i\_\text{svc}}$.

Variable definition follows:

- $\overline{B}_{i\_\text{shunt}}$: new size of the shunt capacitor at location *i*,

- $\overline{B}_{i\_\text{svc}}$: new size of the SVC at location *i*,
- $\overline{q}_{i\_\text{shunt}}$ and $\overline{q}_{i\_\text{svc}}$ are new binary location variables for shunt capacitors and SVCs,
- $\overline{S}_{M,i}^{(k)}$: updated sensitivity of the voltage stability margin with respect to the shunt susceptance at location *i* under contingency *k*,
- $\overline{S}_{\tau,n,i}^{(k)}$: updated sensitivity of the voltage dip time duration at bus *n* with respect to the size of the SVC at location *i* under contingency *k*,
- $\overline{S}_{V,n,i}^{(k)}$: updated sensitivity of the maximum transient voltage dip at bus *n* with respect to the size of the SVC at location *i* under contingency *k*,
- $\overline{B}_{i\_\text{shunt}}^{(k)}$: new size of the shunt capacitor at location *i* under contingency *k*,
- $\overline{B}_{i\_\text{svc}}^{(k)}$: new size of the SVC at location *i* under contingency *k*,
- $\overline{M}^{(k)}$: updated voltage stability margin under contingency *k*,
- $\overline{\tau}_{\text{dip},n}^{(k)}$: updated time duration of voltage dip at bus *n* under contingency *k*, and
- $\overline{V}_{\text{dip},n}^{(k)}$: updated maximum transient voltage dip at bus *n* under contingency *k*.

The inequalities in (5.17)-(5.19) are the constraints of voltage stability margin, time duration of voltage dip and the maximum transient voltage dip respectively. They incorporate updated sensitivities, voltage stability margin and transient voltage dip behavior under each concerned contingency. The above successive MIP will end until all concerned contingencies have satisfactory voltage stability margin and transient voltage response and there is no significant movement of the decision variables from the previous MIP solution.

5.4 Numerical Results

The proposed method has been applied to the New England 39 bus system, In the simulations, the following conditions are implemented unless stated otherwise:

- The required voltage stability margin is assumed to be 10%;
- The WECC reliability criteria is adopted for transient voltage dip problems;
- In computing voltage stability margin and margin sensitivities, 1) loads are modeled as constant power, 2) reactive power output limits of generators are modeled, 3) the power factor of the load remains constant when the load increases, and load and generation increase are proportional to their base case value;
- In performing time domain simulations and calculating the transient voltage dip sensitivities, loads are modeled as 30% constant impedance, 30% constant current and 40% constant power;
- The parameter values adopted in the optimization problem are given in Table 5.1.

Table 5.1 Parameter values adopted in optimization problem

	Shunt capacitor	SVC
Variable cost ($ million/100 Mvar)	0.41	5
Fixed cost ($ million)	1.3	1.5
Maximum size (p.u.)	1.0	1.0

Two contingencies violating reliability criteria are considered to illustrate the proposed algorithm of optimal allocating static and dynamic VAR resources. The first contingency is outage of the generator at bus 31. The second contingency is a three-phase-to-ground short-circuit fault on the transmission line 5-6, followed by clearance of the fault by removal of the transmission line. The details of the two contingencies are listed in Table 5.2. The first contingency violates the voltage stability margin criteria while the second contingency violates the transient voltage dip criteria at the load bus 7.

Table 5.2 Contingencies violating reliability criteria

Contingency	Voltage stability margin (%)	Time duration of voltage dip exceeding 20% (cycles)	Maximum transient voltage dip (%)
(1). Outage of the generator at bus 31	2.69	No violation	No violation
(2). Short circuit and outage of the line 5-6 (voltage at load bus 7)	No violation	29.10	26.83

The candidate control locations are determined based on the linear search algorithm presented in Section 5.3.2. Six candidate buses are chosen to install switched shunt capacitors and SVCs. They are buses 6, 7, 8, 10, 11 and 12. For these candidate locations, the optimization based reactive power planning algorithm presented in Sections 5.3.3 and 5.3.4 was carried out. Table 5.3 shows the allocation of mechanically switched shunt capacitors as 1.0 p.u., 0.178 p.u., 1.0 p.u., 1.0 p.u., 1.0 p.u. at buses 6, 7, 10, 11, 12 respectively. These capacitors will be switched on under contingency 1 to increase the voltage stability margin. Table **5.4** shows the allocation of SVCs as 0.6 p.u., 1.0 p.u. at buses 6 and 7 respectively. The identified SVCs can eliminate the transient voltage dip problem under contingency 2. The SVCs along with the switched shunt capacitors can increase the voltage stability margin to 10% under contingency 1.

Table 5.5 shows that the requirements of voltage stability margin and transient voltage dip are satisfied with the planned static and dynamic VAR resources under the concerned two contingencies. Figure 5-4 shows the voltage responses at bus 7 under contingency 2 with and without SVCs. Figure 5-5 shows the SVC output at bus 6 under contingency 2. Figure 5-6 shows the SVC output at bus 7 under contingency 2. The outputs of both SVCs reach the capacitive limits during the transient voltage dip.

Table 5.3 Allocation of mechanically switched shunt capacitors

Locations for shunt cap.	Maximum size limit (p.u.)	Overall optimal control allocation (p.u.)	Solution to cont. (1) (p.u.)	Solution to cont. (2) (p.u.)
Bus 6	1.0	1	1	N/A
Bus 7	1.0	0.178	0.178	N/A
Bus 8	1.0	0	0	N/A
Bus 10	1.0	1	1	N/A
Bus 11	1.0	1	1	N/A
Bus 12	1.0	1	1	N/A

Table 5.4 Allocation of SVCs

Locations for SVC	Maximum size limit (p.u.)	Overall optimal control allocation (p.u.)	Solution to cont. (1) (p.u.)	Solution to cont. (2) (p.u.)
Bus 6	1.0	0.6	0.6	0.6
Bus 7	1.0	1.0	1.0	1.0
Bus 8	1.0	0	0	0
Bus 10	1.0	0	0	0
Bus 11	1.0	0	0	0
Bus 12	1.0	0	0	0

Table 5.5 System performance under planned static and dynamic VARs

Contingency	Voltage stability margin (%)	Time duration of voltage dip exceeding 20% (cycles)	Maximum transient voltage dip (%)
(1). Outage of the generator at bus 31	10.02%	No violation	No violation
(2). Short circuit and outage of the line 5-6 (voltage at load bus 7)	No violation	20	23.74

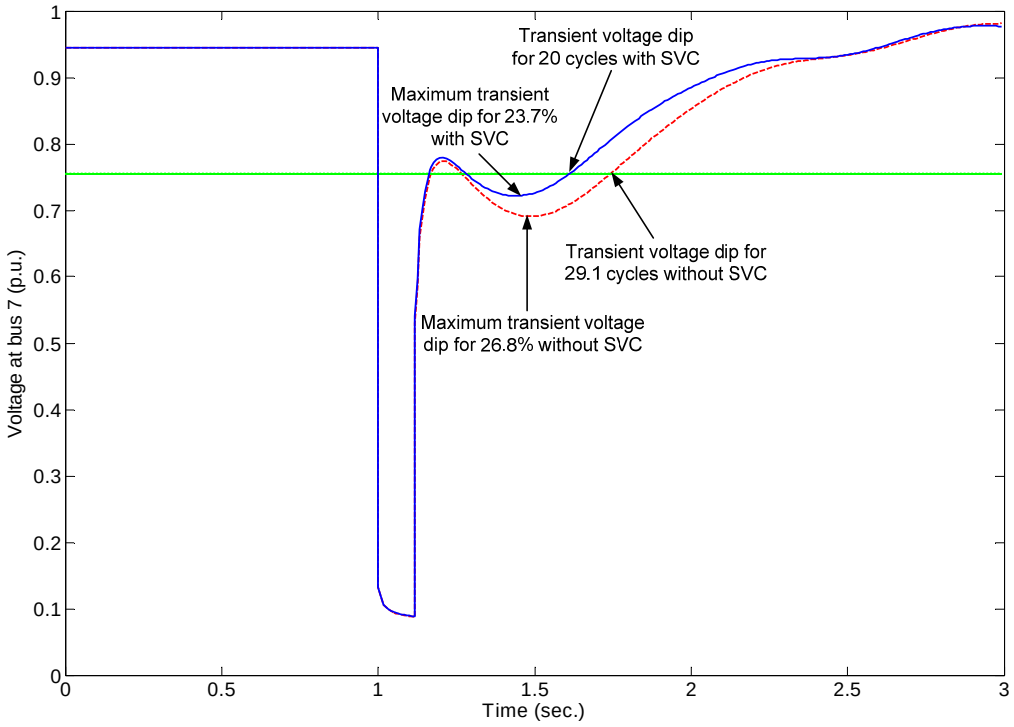


Figure 5-4 Voltage response at bus 7 under contingency 2

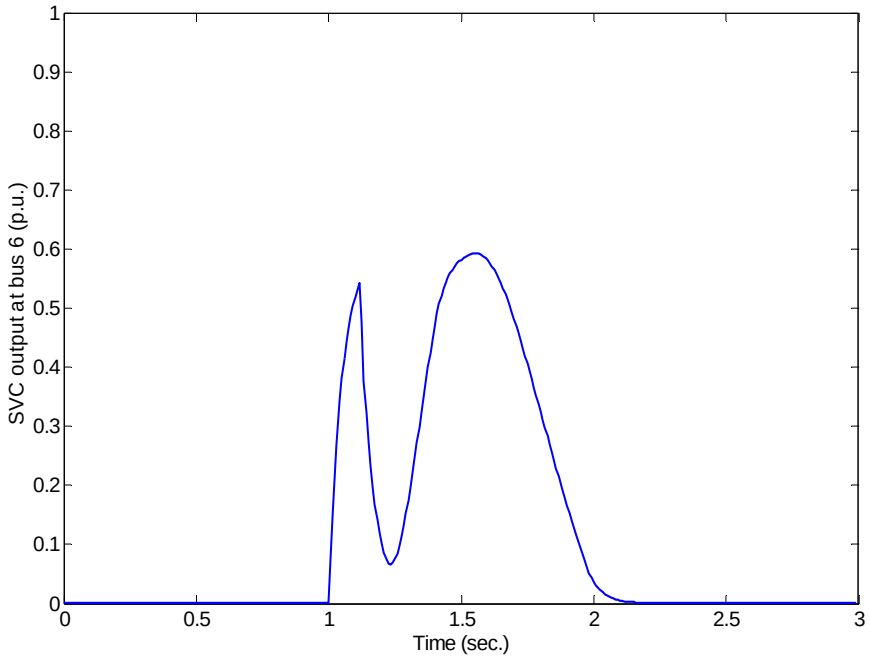


Figure 5-5 SVC output at bus 6 under contingency 2

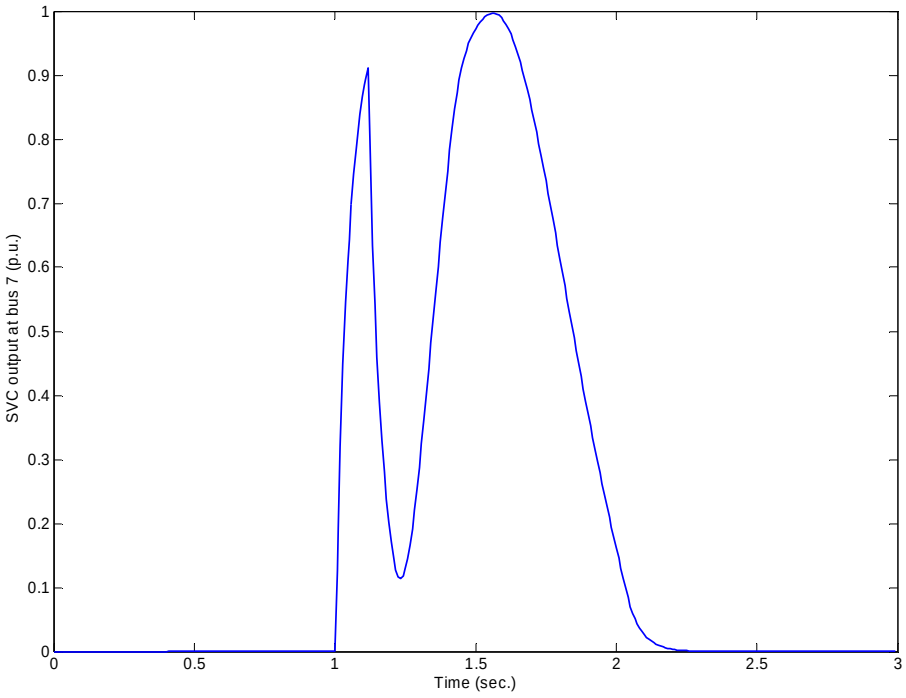


Figure 5-6 SVC output at bus 7 under contingency 2

5.5 Summary

This chapter presents an optimization based method of coordinated planning of static and dynamic VAR resources in electric transmission systems to satisfy the requirements of voltage stability margin and transient voltage dip under contingencies. The backward/forward search algorithm with linear complexity is used to select candidate locations for VAR resources. Optimal locations and amounts of new VAR resources are obtained by solving a sequence of mixed integer programming problems. The effectiveness of the method is illustrated using the New England 39 bus system. The results show that the method works satisfactorily to plan static and dynamic VAR resources under a set of contingencies.

6.0 Application to Large-Scale System

6.1 Introduction

This chapter illustrates the results of the reactive power planning method described in previous chapters using a large-scale model. The result of the method is a cost effective solution to plan optimal mix of static and dynamic reactive power sources.

All the required data for the study, i.e., power flow base case data, and the dynamic files including the models for generator and load systems, and the various parameter settings for the dynamic simulation, were obtained from a utility. This study targeted a subsystem of the utility's control area, henceforth referred to as the "study area."

The dynamic data includes dynamic models for generators, exciter and governor systems. An appropriate load model is used for detailed voltage stability analysis in the control area, where load at every bus is portioned as 50% motor load and 50% ZIP load with the motor loads further split into three different kinds, i.e., large, small, and trip motors (1/3 each). The ZIP model for the remaining 50% load is modeled as 50% constant impedance and 50% constant current for P load and 100% constant impedance for Q load. CPF based PV analysis and time domain simulation are the tools used to study the steady state and dynamic system performances respectively. The sensitivity information of the system performance with respect to the reactive control device is important in order to optimally allocate the reactive resources. Matlab programming and PTI PSS/E power flow and dynamics packages are the software tools used for this work.

The contingencies considered for the study are the more probable ones, i.e., N-1 and N-G-T. The objective is to identify a minimum cost mix of static and dynamic Var resources that results in satisfactory voltage stability and transient voltage dip performance for all considered contingencies. The voltage stability criteria used was that steady state voltage stability margin must be no less than 5% of total load, and transient voltage dip must not exceed 20% of the initial voltage for more than 20 cycles.

This chapter is organized as follows. Section 6.2 summarizes the basecase power flow model and the particular stress direction used in the illustration. Section 6.3 reports the results of a contingency selection process used in the study. Sections 6.4 and 6.5 illustrate the planning procedure implemented assuming that only voltage stability is of concern. Section 6.6 extends these results for the case when both voltage stability and transient voltage dip are of concern.

6.2 Basecase and Stress Direction

A summary of the base case used for the study is provided in Table 6.1. Information specific to the study area is provided in a separate column. It was assumed that this basecase represented the topology and loading conditions for which a reactive power plan is desired.

Table 6.1 Summary of the basecase

#	Total	Study Area	External to Study Area
Buses	16173	2069	14104
Generators	2711	239	2472
Transformers	7261	463	6798
Pgen (MW)	603798.9	37946.7	565852.2
P (load) (MW)			
[Const. P,	591927.2	30065.2	561862
Const. I,	100.3	0	100.3
Const. Z]	116.4	0	116.4
Q (load) (MVar)			
[Const. Q,	208138.8	9067.6	199071.2
Const. I,	26.4	0	26.4
Const. Z]	125	0	125

As described in Chapters 2-4, continuation power flow (CPF) is used to analyze the steady state performance characteristics of the system. CPF requires an assumption of a stress direction depicting a future power loading or transfer pattern in the system. To this end, the area of interest is divided into 88 different zones, which are grouped into 6 Market zones as shown in the Table 6.2 below.

Table 6.2 Market Zones within the Study Area

Market Zones	Zones
MZ1	100 - 104; 200 - 204; 501 - 504; 600 - 603; 701
MZ2	105 - 109; 111-112; 205 - 209; 211 - 212; 306; 312; 505 - 508; 511 - 512;
MZ3	110 ; 140 - 152; 161; 210; 240 - 252; 310; 410; 451; 510; 540 - 552; 561; 650 - 651; 750; 850; 938
MZ4	120 - 122; 220 - 222; 322; 422; 521; 720 - 721; 820 - 821
MZ5	123 - 130; 223 - 230
MZ6	160; 162 - 163; 261 - 262; 462; 560; 562 - 563; 939

These 6 market zones represent 6 different stress directions typically studied by planning engineers, with the stress direction Sink characterized by the set of loads inside the zones, and the stress direction Source characterized by generators outside of these zones, but within the study area. The CPF scales the Sink loads upwards with corresponding increase to the Source generators to find the collapse point (nose of the PV curve). Increased load is allocated to the source generators in proportion to each generator's rating while enforcing generator reactive power limits.

Voltage instability analysis using CPF-based contingency screening was performed on the basecase and for all credible contingencies under these six different stress directions. The list of credible contingencies included all possible N-1 and N-G-T contingencies in the study area. The number of such contingencies was 2268 N-1 contingencies (2100 branch contingencies and 168 generator contingencies) and all possible combinations (2100*168=352,800) for N-G-T contingencies.

Results indicated only the stress direction corresponding to the MZ1 region was found to have post contingency steady state voltage stability related problems. As a result, we studied only MZ1 to determine reactive resources and the corresponding static vs. dynamic mix, so as to limit the work while appropriately illustrating the approach. Table 6.3 below provides the voltage instability performance measure for the basecase conditions.

Table 6.3 Performance measure for basecase conditions

Base case load in the MZ1 sink (MW)	Critical point (MW)	Stability margin (%)
2073	2393	15.43657

6.3 Contingency Screening for MZ1

As stated in Section 6.2, contingency screening indicated voltage instability problems occur only in MZ1. This section describes the contingency screening performed in order to identify those contingencies that drive the need for additional reactive resources in MZ1.

The 5% voltage stability margin requirement described in Section 6.1 means for MZ1 (with 2073 MW load) that 103 MW should be the minimum load margin, for both N-1 and N-G-T contingencies. Contingencies that violate this criterion are used in the ensuing reactive power planning analysis.

Modeling of N-1 generator contingencies and N-G-T contingencies requires special considerations, as follows:

- N-1 Generator contingencies: Remaining generators within the study area pick up the loss of generation in proportion to their MVA rating. The system slack bus compensates only for losses.
- N-G-T contingencies: The generator outage is simulated first consistent with the comment made in the previous bullet. Then, based on the assumption that the interevent time is long enough (e.g., at least 15 minutes), system adjustments (switched shunts, taps, and area interchange) are made, and the second contingency is then simulated.

Modeling of N-1 branch outages requires no special consideration.

The result from contingency screening process shows a total of 82 contingencies that either violated voltage instability margin criteria or led to voltage instability (negative stability margin). The 82 contingencies included 2 N-1 contingencies corresponding to the two critical generator outages at buses 97451 (G1LEWIS) and 97452 (G2LEWIS). The remaining 80 contingencies were N-G-T contingencies, with a set of 40 line contingencies repeating themselves under the two critical generators being outaged separately.

Full CPF analysis was performed on the 82 contingencies identified in the screening process, using both our Matlab code, with results verified using PSS/E. This resulted in elimination of 26 of the contingencies due to the fact that CPF indicated post-disturbance performance for these 26 satisfied all criteria. The remaining 56 contingencies therefore comprised the set that would drive subsequent reactive power planning. These 56 contingencies are summarized in Table 6.4.

All of the selected 56 contingencies were N-G-T (none of the N-1 contingencies had any post-contingency margin violation problem). These 56 N-G-T contingencies either resulted in voltage instability (rows 1-7), or they violated loading margin criteria (rows 8-28), as indicated in the right-hand columns of Table 6.4.

Table 6.4 Critical Contingencies

S.No	Transmission Line		Bus Name		Zone	Base KV		Stability / Index (Margin in %)	
	From	To	From	To	From	To	KV	LEWIS Gen#1 -97451	LEWIS Gen # 2 -97452
1	97463	97467	4OAKRIDG	4PORTER	102	104	138	Voltage Instable	Voltage Instable
2	97478	97721	6JACINTO	CHJC_SER	104	105	230	Voltage Instable	Voltage Instable
3	97567	97714	6PORTER	6CHINA	104	105	230	Voltage Instable	Voltage Instable
4	97691	97717	8CYPRESS	8HARTBRG	105	105	500	Voltage Instable	Voltage Instable
5	97714	97716	6CHINA	6SABINE	105	105	230	Voltage Instable	Voltage Instable
6	97714	97721	6CHINA	CHJC_SER	105	105	230	Voltage Instable	Voltage Instable
7	53526	97513	CROCKET7	7GRIMES	999	100	345	Voltage Instable	Voltage Instable
8	97461	97464	4LEWIS	4PANORAM	103	100	138	1.495417	1.784853
9	97514	97526	4GRIMES	4MAG AND	100	100	138	2.411963	2.556681
10	97513	97546	7GRIMES	7FRONTR	100	100	345	2.556681	2.701399
11	97689	97714	6AMELIA	6CHINA	106	105	230	2.990835	3.135552
12	97690	97697	4CYPRESS	4HONEY	105	105	138	2.990835	3.135552
13	97455	97463	4METRO2	4OAKRIDG	102	102	138	3.28027	3.424988
14	97510	97526	4SOTA 1	4MAG AND	100	100	138	3.28027	3.424988
15	97493	97758	4MENARD	4BRAGG	101	105	138	3.617945	3.617945
16	97532	97627	4HICKORY	4EASTGAT	104	105	138	3.617945	3.762663
17	97697	97758	4HONEY	4BRAGG	105	105	138	3.617945	3.907381
18	97508	97510	4NAVSOTA	4SOTA 1	100	100	138	3.907381	3.907381
19	97532	97533	4HICKORY	4NEWCANY	104	104	138	3.907381	3.907381
20	97627	97723	4EASTGAT	6L533TP8	105	105	138	3.907381	4.052098
21	97632	97723	4ADAYTON	6L533TP8	105	105	138	3.907381	4.052098
22	97717	97916	8HARTBRG	8NELSON	105	112	500	3.907381	4.052098
23	97490	97493	4GULFLIV	4MENARD	101	101	138	3.95562	4.052098
24	97692	97706	4CHEEK	4SO.BMT.	106	105	138	4.196816	4.341534
25	97518	97685	4CAMDEN	4DEER 1	101	105	138	4.245055	4.486252
26	97487	97514	4MT.ZION	4GRIMES	101	100	138	4.486252	4.63097
27	97490	97494	4GULFLIV	4POCO 1	101	101	138	4.486252	4.63097
28	97633	97692	4BDAYTON	4CHEEK	105	106	138	4.63097	4.823927

6.4 Reactive Resources To Restore Equilibrium

The first step in the planning process is to identify reactive resources necessary to ensure all contingencies result in an equilibrium, i.e., have positive loading margin. The approach taken in this step is consistent with that described in Chapter 3. It is possible to find operational solutions for restoring post-contingency equilibrium, e.g., using load shedding. Our planning approach restores equilibrium by identifying an amount and location of reactive resources *just* sufficient to restore equilibrium.

Since these contingencies are N-G-T, a base case with a generator removed is solved, the branch to be outaged is then parameterized as described in Section 3.3 of chapter 3. The parameterized system equations are then used to simulate the branch contingency and identify the necessary reactive resources for that contingency. This process can require several iterations, as the use of linear sensitivities at the bifurcation point does not guarantee an optimal solution on the first attempt. The parameterization is done for every branch contingency under the N-G base case, and the bifurcation parameter and its sensitivities are obtained for each case.

The mixed integer programming (MIP) optimization problem used to identify the investment solution to the equilibrium restoration problem requires candidate locations, margin sensitivity information at those locations, reactive resource cost information for each voltage level, and amount of additional margin for each contingency. We describe procedures for obtaining the candidate locations (in Subsection 6.4.1), the cost information (in Subsection 6.4.2), and the required margin (in Subsection 6.4.3).

6.4.1 Candidate location selection

The obtained bifurcation parameter sensitivities with respect to shunt capacitance ($d\lambda/dB$) under each contingency are used to select the candidate location set for planning reactive control. In this work, the bifurcation parameter sensitivity is converted into loading margin sensitivity; i.e., dM/dB, where M is the loading margin. The candidate locations under each contingency are obtained by ranking all the study area buses in descending order of the dM/dB under each contingency. Table 6.5 below indicates the top 20 candidate locations in descending order of dM/dB for the top seven most severe contingencies that resulted in voltage instability (and therefore require equilibrium restoration), when generator at 97451 is outaged. Bus numbers that are in bold font are 138 KV buses. The bus numbers in regular fonts are 69 KV buses.

Table 6.6 below shows the top 20 candidate locations in descending order of dM/dB for the top seven most severe contingencies (as listed in Table 6.4) that resulted in voltage instability (and therefore require equilibrium restoration), when generator at 97452 is outaged. Bus numbers that are in bold font are 138 KV buses. The bus numbers in regular fonts are 69 KV buses.

Table 6.5 Candidate location set for N-G-T, where Gen at 97451 is outaged

	Contingency Number						
Rank	# 1	# 2	# 3	# 4	# 5	# 6	# 7
1	**97463**	97511	97504	97504	97511	97511	97516
2	**97457**	97504	97511	97511	97525	97504	97517
3	**97455**	97525	97523	97503	97516	97501	97523
4	**97468**	97523	97525	97500	97502	97500	97511
5	**97544**	97516	97517	97524	97517	97503	97525
6	97504	97517	97516	97523	97523	97524	**97457**
7	97511	97502	97524	97525	97504	97523	**97455**
8	97500	97524	97500	97517	97524	97525	97503
9	97501	97500	97503	97516	97527	97517	97504
10	97524	97501	97502	97505	97500	97516	97500
11	97523	97503	97501	97502	**97506**	97502	**97464**
12	97502	97505	97505	**97506**	97501	97505	97524
13	97525	97527	**97506**	97501	97505	**97506**	97501
14	97517	**97506**	97527	97527	97503	97527	97505
15	97516	**97507**	**97507**	**97507**	97515	**97507**	97527
16	97505	97515	**97455**	**97455**	**97507**	**97457**	97502
17	**97506**	**97457**	**97463**	**97468**	**97457**	97452	**97506**
18	97527	**97455**	**97468**	**97463**	**97455**	**97464**	**97507**
19	**97507**	**97508**	97562	**97457**	**97522**	**97455**	97515
20	**97464**	**97457**	**97457**	97569	**97509**	**97468**	**97514**

Table 6.6 Candidate location set for N-G-T, where Gen at 97452 is outaged

	Contingency Number						
Rank	# 1	# 2	# 3	# 4	# 5	# 6	# 7
1	**97463**	97511	97504	97504	97511	97511	97511
2	**97457**	97525	97511	97511	97525	97525	97516
3	**97455**	97516	97500	97503	97516	97504	97517
4	**97468**	97517	97524	97500	97504	97516	97523
5	97504	97523	97503	97524	97517	97517	97525
6	**97544**	97504	97523	97523	97523	97523	**97457**
7	97511	97501	97525	97525	97524	97502	**97455**
8	97501	97502	97517	97517	97502	97524	97504
9	97525	97524	97516	97516	97500	**97506**	97503
10	97523	97500	97502	97505	97503	97527	97500
11	97516	97503	97505	97502	97505	97500	97524
12	97517	97527	**97506**	**97506**	97527	97501	97505
13	97502	97505	**97463**	97527	**97506**	97505	97501
14	97524	**97506**	97501	97501	97501	97503	**97464**
15	97500	97515	**97455**	**97507**	97515	**97507**	**97506**
16	97503	**97507**	97527	**97455**	**97507**	97515	97527
17	97505	**97509**	**97468**	**97468**	**97457**	**97457**	97502
18	**97506**	**97455**	**97457**	**97463**	**97455**	**97522**	97515
19	97527	**97508**	**97544**	**97457**	**97468**	**97508**	**97468**
20	**97507**	**97457**	**97465**	**97544**	**97463**	**97510**	**97507**

It is observed that buses at 69 kV transmission level are generally more effective to increasing load margin than buses at 138 kV. But care should be taken not to

over-compensate these buses as they might lead to excessive voltage magnitudes. To address this issue, an iterative approach was introduced where the optimization solution is found, which is the investment solution, and then each operational solution (as indexed by parameter k in the formulations of Chapters 4 and 5) corresponding to each contingency k is implemented for each post-contingency solution. For any bus having post-contingency voltage exceeding 1.06 pu, a maximum shunt MVAR constraint is developed, and the optimization is re-run with that constraint included. This procedure begins with a default set of MVAR constraints on each bus according to voltage level, as indicated in Table 6.7 below.

Table 6.7 Maximum shunt compensation at various voltage levels

Bus Base Voltage (KV)	Maximum Shunt capacitance amount (MVar)
69	30
100	75
115	120
138	150
230	200
345	300
500	300

While the maximum shunt capacitance amount at 138 KV buses is 150 Mvar, some of the buses which are connected to the very sensitive low voltage 69 KV buses are constrained to have a maximum shunt capacitance amount of 75 Mvar under these set of contingencies, as it was found that more Mvar on those buses result in unacceptable post-contingency overvoltages. Buses 97506 (4BRYAN), 97507 (4COLSTTA), 97522 (4TABULAR) are examples of such buses that were constrained to 75 Mvar.

In order to ensure that all good reactive resource locations are included, we selected the top 50 candidate control locations for each contingency from the ranked list of sensitivities. (Tables 6.5 and 6.6 show such a list, but in order to conserve space, Tables 6.5 and 6.6 provide only the top 20 locations for each contingency). The final set of candidate locations was obtained as a union of all the locations for all critical contingencies considered for the equilibrium restoration problem. The union of all the candidate locations provided an initial set of 64 candidate location buses (many locations were in the ranked lists of more than one contingency), as shown in Table 6.8.

It is possible to use the linear complexity search algorithm of Chapter 2 to reduce the number of candidate locations. However, we have found mixed integer programming (MIP) optimization software we are using (CPLEX) to be so efficient that reduction in the number of locations is unnecessary. It is estimated that reasonable MIP running time can be obtained for up to 500 locations, well in excess of what a standard planning problem might require.

Table 6.8 Initial candidate control location set - stage1 MIP for planning problem # 1

S No	Bus #	Bus Name	Base KV		S No	Bus #	Bus Name	Base KV
1	97453	4DOBBIN	138		33	97507	4COLSTTA	138
2	97454	4WALDEN	138		34	97508	4NAVSOTA	138
3	97455	4METRO2	138		35	97509	4SPEEDWY	138
4	97457	4LONGMIR	138		36	97510	4SOTA 1	138
5	97458	4CONAIR	138		37	97511	2TESCO	69
6	97459	4CONROE	138		38	97512	4PEE DEE	138
7	97460	4CRYSTAL	138		39	97513	7GRIMES	345
8	97461	4LEWIS	138		40	97514	4GRIMES	138
9	97462	5L523T58	138		41	97515	2CALVERT	69
10	97463	4OAKRIDG	138		42	97516	2HEARNE	69
11	97464	4PANORAM	138		43	97517	2TXHEARN	69
12	97465	4PLANTAT	138		44	97519	4GEORGIA	138
13	97466	4SHEAWIL	138		45	97522	4TUBULAR	138
14	97467	4PORTER	138		46	97523	2APLHERN	69
15	97468	4GOSLIN	138		47	97524	2IN.AT$T	69
16	97469	4APRILTX	138		48	97525	2HUMBHRN	69
17	97470	4LFOREST	138		49	97526	4MAG AND	138
18	97471	4CANEYCK	138		50	97527	2SINHERN	69
19	97480	L558T485	138		51	97533	4NEWCANY	138
20	97481	4CEDAR	138		52	97538	8LNG 413	138
21	97482	4CINCINT	138		53	97539	4WDHAVN	138
22	97483	4GOREE	138		54	97540	4EVGRN	138
23	97484	4HUNTSVL	138		55	97544	4ALDEN	138
24	97486	4WYNTEX	138		56	97545	4LACON	138
25	97487	4MT.ZION	138		57	97546	7FRONTR	345
26	97488	4TEMCO	138		58	97551	4CEDHILL	138
27	97500	2INDEPEN	69		59	97554	GRMXF	345
28	97502	2ANAVSOT	69		60	97555	4BISHOP	138
29	97503	2SOMERVL	69		61	97566	4TAMINA	138
30	97504	2BRYAN B	69		62	97567	6PORTER	230
31	97505	2BRYAN A	69		63	97570	4DRYCRK	138
32	97506	4BRYAN	138		64	97721	CHJC_SER	230

6.4.2 Cost information used

As discussed in the previous chapters a cost model similar to what has been mentioned in [24] has been used, where the investment cost of shunt capacitor is modeled as two components: fixed installation cost and variable operating cost. Table 6.9 indicates that while the operating cost in $/MVar is constant for all the voltage levels; the fixed cost varies at different voltage levels with the installation cost at highest voltage level the highest.

Table 6.9 Cost formulation at various voltage levels

Cost Information[1]		
Bus Base Voltage level (KV)	Fixed Cost (Million $)	Variable Cost (Million $/MVar)
69	0.025	0.41
100	0.05	0.41
115	0.07	0.41
138	0.1	0.41
230	0.28	0.41
345	0.62	0.41
500	1.3	0.41

6.4.3 Required margin

In the case of severe contingencies that lead to voltage instability, the performance index is load margin. The bifurcation parameter λ must reach 1 or in other words, the load margin must be 0 in order to simulate the line contingency. So planning is done until that criterion is satisfied, so that sufficient reactive resource is obtained that can withstand such a severe contingency and not result in voltage instability.

The amount of margin necessary under each contingency needed is input to the optimization model so that sufficient amount of capacitor can be switched in to restore solvability. The expression for computing the amount of load margin ΔLM needed under a particular contingency is:

$$\Delta LM = w_i^p * P^*_i + w_i^q * Q^*_i + w_j^p * P^*_j + w_j^q * Q^*_j \qquad \textbf{6.1}$$

where P^* and Q^* are the real and reactive power injections at the parameterized branch at the pre-contingency[2] operating point, i and j indicate the buses connected by the parameterized branch that has to be finally removed, and w_i^p is the scaled left eigenvector component corresponding to the real power at bus i, *and* w_i^q is the scaled left eigenvector component corresponding to the reactive power at bus i.

6.4.4 Optimal allocation

After obtaining all the necessary inputs such as critical contingencies, the bifurcation sensitivities, amount of increase in load margin, cost information etc, the final step in the planning is to solve the MIP optimization with the objective of minimizing the total reactive resource allocation cost while satisfying the required constraint of having enough load margin for each contingency, which is 0 in our case indicating power system solvability. The optimization problem is solved iteratively, as a result of the fact that we utilize linear sensitivities to characterize nonlinear relationships. The result from the first iteration is provided in Table 6.10.

[1] Cost information at 230 KV and 500 KV levels are given in [24], extrapolated to get the cost information at the other voltage levels.

[2] For an N-G-T contingency, the operating point for which this calculation is done is the one corresponding to after the generator outage but before the branch outage.

Table 6.10 Optimal allocation from first iteration for equilibrium restoration problem

Bus No	Name	Base KV	Amount if (p.u) of B (or p.u. Q injection)						
			Generator outage at bus 97451						
			# 1	# 2	# 3	# 4	# 5	# 6	# 7
97457	4LONGMIR	138	1	1	0.65	0.775	0.6	1	1.5
97455	4METRO2	138	0	0	0	0	0	0	0.88
			Generator outage at bus 97452						
			# 1	# 2	# 3	# 4	# 5	# 6	# 7
97457	4LONGMIR	138	0.95	1	0.65	0.775	0.627	1	1.5
97455	4METRO2	138	0	0	0	0	0	0	0.7

The solution provided in Table 6.10 was validated according to the following procedure. For each N-G-T contingency, the generation outage was simulated, with automatic readjustments (switched shunts, taps, and tie line control) enabled. All such adjustments were then frozen, and the branch outage was simulated with automatic readjustments disabled, but with the Table 6.10 planning solution modeled for the particular branch contingency.

Following this validation procedure, it was observed that all contingencies do solve for the solution provided in Table 6.10, except the contingency 7 (345 KV tie line from area 151 EES to 520 CESW) under both generator outages. To address this unsolved contingency, a second optimization iteration was performed using updated sensitivities and cost information. In performing this iteration, we desire to determine how much *additional* reactive compensation is needed at each bus, relative to the solution identified in the first iteration. Therefore, the fixed costs are made 0 for buses receiving reactive compensation in the previous iteration, since it is assumed that the fixed cost of installation is already incurred for these locations. Buses 97457 and 97455 are such buses. Furthermore, for these buses receiving reactive compensation in the previous iteration, the maximum compensation amount needs to be adjusted to ensure the compensation will not exceed the actual maximum amount.

The bifurcation parameter sensitivities for the capacitor re-enforced system are obtained for the branch contingency under each generator outage that needs further compensation. Then the initial set of candidate locations are again found, and the optimal reactive power solution is computed. The result from the second optimization iteration is updated to the first optimization to get the updated amount of compensation that is provided in Table 6.11.

Table 6.11 Optimal allocation from second iteration for equilibrium restoration problem

Bus	Base KV	Amount of per unit susceptance, B (or p.u. Q injection)	
		Contingency # 7 (Gen at 97451)	Contingency # 7 (Gen at 97452)
97455 4METRO2	138	1.15	1.10

So the final result for the equilibrium restoration problem, to restore power system solvability for contingencies resulting in voltage instability (contingencies 1-6 in Table 6.4) is provided in Table 6.12. The total investment cost for this solution is 1.2865 **M $**.

Table 6.12 Final optimal allocation solution for equilibrium restoration

Bus	Base KV	Amount if (p.u) of B (or p.u. Q injection)
97457 4LONGMIR	138	1.5
97455 4METRO2	138	1.15

6.5 Reactive Resources to Increase Voltage Stability Margin

After the reactive power planning has been done to restore the equilibrium under those contingencies that result in voltage instability, the loading margin under those contingencies is just above 0, in violation of the margin criteria (in this case, 5%). Along with these contingencies, there are also other contingencies that did not require equilibrium restoration but are in violation of the margin criteria. So the problem addressed in this section involves finding a minimum cost solution to plan reactive control to increase the voltage stability margin to at least 5% under a given set of contingencies, none of which satisfy the margin requirement. The approach taken in this step is consistent with that described in Chapter 4.

6.5.1 First iteration optimization

As in the second iteration of the equilibrium restoration problem described in Subsection 6.4.4, it is necessary to modify input data for buses receiving reactive compensation in previous steps, i.e., fixed costs should be 0, and the maximum compensation amount needs to be adjusted to ensure the compensation will not exceed the actual maximum amount. This was done for buses 97457 4LONGMIR and 97455 4METRO2. Once the initial set of candidate locations is found, the margin sensitivities at every candidate location and the voltage stability margin under every contingency are provided as input to the MIP optimizer to identify the optimal reactive compensation necessary to satisfy the margin criteria for all identified contingencies.

It is determined from a first optimization run, and confirmed by simulation, that for all contingencies which did not result in voltage instability (i.e., those contingencies that are stable but violated margin criteria, which are rows 8-28 in Table 6.4), the solution to the equilibrium restoration problem provides enough additional reactive support to ensure all of these contingencies satisfy the margin criteria. That is, the optimal solution of the equilibrium restoration problem, placing capacitors at locations 97457 4LONGMIR and 97455 4METRO2, increases margin for these less severe contingencies above 5%. So no further reactive resources are needed for these contingencies.

However, the contingencies that were voltage unstable (rows 1-7 of Table 6.4), now having equilibrium *just* restored and therefore margin *just* exceeding 0, require additional margin to satisfy the 5% (103 MW) criteria.

The candidate locations used in the optimization were the same as the candidate locations

used in the equilibrium restoration optimization. The main difference here, however, was the required margin for each contingency was set to satisfy the 5% requirement. Results of this first iteration optimization which is updated to the earlier amount at every location are provided in Table 6.13.

Table 6.13 Optimal allocation from first iteration to increase margin

Bus No	Name	Base KV	Amount if (p.u) of B (or p.u. Q injection)						
			Generator outage at bus 97451 & 97452						
			# 1	# 2	# 3	# 4	# 5	# 6	# 7
97457	4LONGMIR	138	1.5	1.5	1.2	0.775	1.5	1.5	1.5
97455	4METRO2	138	0	0.55	0.7	0	0.45	0.7	1.5
97464	4PANORAM	138	0.45	0	0	0.65	0	0	0.7

To validate the solution of Table 6.13, all contingencies that addressed (rows 1-7 of Table 6.4) were tested via simulation after updating the system with the respective amount of compensation under any contingency identified by MIP. It was determined that none of them satisfied the minimum margin criterion. We therefore performed a second iteration (succesiive MIP) to increase margin for these contingencies.

6.5.2 Successive iteration optimization

The second iteration optimization to increase margin uses margin sensitivities from the system reinforced by the reactive resources identified in the first iteration optimization. Candidate locations were again the same as the candidate locations used in the equilibrium restoration process. The amount obtained from the second iteration was good enough for contingencies 1-6 that the mininum criteria were satisfied, except for contingency 7 under both the generator outages. Then another successive MIP was performed to plan further for this particular contingency. This procedure was carried out till the minimum steady state stability criteria were satisfied under all the contingencies. Table 6.14 provides the final solution after updating the solution obtained from all the successive optimizations. This solution is the final solution of the steady state planning problem to ensure the system satisfies margin criteria for all contingencies. The total investment cost is 2.665 M $.

Table 6.14 Final solution for optimal allocation to increase margin

S.No	Transmission Line		Bus Name		KV		Capacitor Allocation (Mvar)			
	From	To	From	To			97457	97455	97464	97544
							4LONGMIR	4METRO2	4PANORAM	4ALDEN
1	97463	97467	4OAKRIDG	4PORTER	138		1.5	0	1.5	0.25
2	97478	97721	6JACINTO	CHJC_SER	230		1.5	1.5	0.75	0
3	97567	97714	6PORTER	6CHINA	230		1.2	1.5	0	0.85
4	97691	97717	8CYPRESS	8HARTBRG	500		1.0	1.2	1.25	0
5	97714	97716	6CHINA	6SABINE	230		1.5	1.5	0.5	0
6	97714	97721	6CHINA	CHJC_SER	230		1.5	1.5	0.9	0
7	53526	97513	CROCKET7	7GRIMES	345		1.5	1.5	1.5	1
8	97461	97464	4LEWIS	4PANORAM	138		0.3	0	0	0
9	97514	97526	4GRIMES	4MAG AND	138		0.65	0	0	0
10	97513	97546	7GRIMES	7FRONTR	345		0.85	0	0	0
11	97689	97714	6AMELIA	6CHINA	230		0.68	0	0	0
12	97690	97697	4CYPRESS	4HONEY	138		0.65	0	0	0
13	97455	97463	4METRO2	4OAKRIDG	138		0.57	0	0	0
14	97510	97526	4SOTA 1	4MAG AND	138		0.55	0	0	0
15	97493	97758	4MENARD	4BRAGG	138		0.52	0	0	0
16	97532	97627	4HICKORY	4EASTGAT	138		0.45	0	0	0
17	97697	97758	4HONEY	4BRAGG	138		0.52	0	0	0
18	97508	97510	4NAVSOTA	4SOTA 1	138		0.5	0	0	0
19	97532	97533	4HICKORY	4NEWCANY	138		0.4	0	0	0
20	97627	97723	4EASTGAT	6L533TP8	138		0.5	0	0	0
21	97632	97723	4ADAYTON	6L533TP8	138		0.5	0	0	0
22	97717	97916	8HARTBRG	8NELSON	500		0.5	0	0	0
23	97490	97493	4GULFLIV	4MENARD	138		0.5	0	0	0
24	97692	97706	4CHEEK	4SO.BMT.	138		0.47	0	0	0
25	97518	97685	4CAMDEN	4DEER 1	138		0.35	0	0	0
26	97487	97514	4MT.ZION	4GRIMES	138		0.4	0	0	0
27	97490	97494	4GULFLIV	4POCO 1	138		0.4	0	0	0
28	97633	97692	4BDAYTON	4CHEEK	138		0.4	0	0	0

This section presents results for optimal allocation of MSCs to solve voltage instability issues in the study area. The method described in the previous chapters was implemented on this power system for contingencies that lead to voltage instability or have post-contingency voltage stability margin less than the minimum criteria. The method selected 4 buses in the subsystem to solve the voltage instability problems in that area. All N-1 and N-G-T contingencies, under 6 different stress directions were considered.

The final optimal solution depends to a great deal on the list of contingencies considered. If only contingencies 5, 6 and 8-28 are considered (these are contingencies that violate stability margin but exclude contingencies that result in voltage instability), then the final solution includes three 69 KV buses and two 138 KV buses with the total cost being 1.3 M$, as shown in Table 6.15.

Table 6.15 Final solution for static vars considering subset of contingencies

Bus No	Bus Name	Base KV	Amount of p.u. Q injection
97501	2CALDWEL	69	0.25
97504	2BRYAN B	69	0.25
97511	2TESCO[3]	69	0.25
97506	4BRYAN	138	1
97507	4COLSTTA	138	0.732

In validating the solution of Table 6.15, we observe that although this solution has acceptable loading margins, it results in post-contingency voltage magnitudes of 1.15 at the three 69 kV buses where we have located reactive compensation, clearly unacceptable. To adjust for this, one would need to tighten the maximum reactive compensation allowable at these buses and resolve the MIP. We do not make this adjustment here because Table 6.15 is illustrative only, i.e., it was obtained for only a subset of contingencies.

Table 6.16 below shows the final solution when all contingencies were considered. The solution satisfies reliability criteria for the set of line contingencies under both sets of generator outages, i.e., all 56 N-G-T cases listed in the contingency list of Table 6.4. The voltage stability margin for all considered contingencies is now at least 5%, and the total investment cost is 2.665 M $. It is interesting to note that the post-contingency high voltage problem observed for the solution of Table 6.15 does not occur for the solution of Table 6.16. This is due to the fact that the solution of Table 6.16 contains no 69 kV buses (which have greater voltage magnitude sensitivity to reactive injection than the 138 kV buses). The reason the solution of Table 6.16 contains no 69 kV buses is that the contingencies for which it is developed require a significantly high amount of reactive resource. The discrete nature of the MIP favors 138 kV buses in this case because, despite the lower cost per unit Q for 69 kV buses, it would require too many of them to satisfy the loading margin (since 69 kV buses have tighter maximum Q constraints than do 138 kV buses in order to avoid high voltage problems), incurring the high fixed cost for each additional 69 kV bus. This is a reasonable and satisfying feature of the MIP.

Table 6.16 Final solution for static vars considering all contingencies

Bus No.	Bus Name	Base KV	Amount of p.u. Q injection
97457	4LONGMIR	138	1.5
97455	4METRO2	138	1.5
97464	4PANORAM	138	1.5
97544	4ALDEN	138	1.0

The results show the effectiveness of the method to find optimal allocation of static

[3] Sometimes it is observed that there are a number of candidate locations that have same cost and similar margin sensitivities forming a cluster of locations where any location is equally effective. In such cases the planner can consider other factors like geographic location, limitation on maximum size that can be installed at those locations, etc., before making the final decision. In this case capacitor re-enforcement at buses 97502, 97522, 97525, 97511 are almost equally effective.

compensation against post contingency steady state voltage instability problems. In the next section, we present results to develop a coordinated control plan against steady state as well dynamic voltage stability problems to optimally allocate a mix of static and dynamic Var sources.

6.6 Reactive Resources for Static and Dynamic Problems

The dynamic data includes dynamic models for generators, exciter and governor systems. An appropriate load model is used for detailed voltage stability analysis in the control area, where load at every bus is portioned as 50% motor load and 50% ZIP load with the motor loads further split into three different kinds, i.e., large, small, and trip motors (1/3 each). The ZIP model for the remaining 50% load is modeled as 50% constant impedance and 50% constant current for P load and 100% constant impedance for Q load. Time domain simulation is used to study the system dynamic performance. The sensitivity information of the system performance (dip magnitude and duration) with respect to the reactive control device (SVC) is important in order to optimally allocate the reactive resources. PTI PSS/E dynamics package is the software tool used for this work.

6.6.1 Contingency Screening and Analysis

The contingency set for our study was chosen as the contingencies that lead to steady state post contingency voltage instability. These contingencies (top 7 contingencies in Table 6.4) were the ones which resulted in relatively low bus voltages even after installing the static reactive resources of Section 6.6.

These contingencies were all N-G-T. These contingencies were simulated by removing a generator, resolving the power flow case, and then running time domain simulation for the circuit outage. Time domain simulations were run by applying a 3-phase fault at t=0 at one end of the transmission circuit and then clearing the fault and the circuit at 6 cycles (t = 0.1s). The simulation was run for about 3 sec to detect any of the following transient voltage problems:

1. Slow voltage recovery problem: voltage recovery time (time taken to reach 80% of initial voltage after fault has been cleared) > 20 cycles , i.e., 0.333s.
2. Transient voltage dip magnitude problem: after the voltage recovery has taken place, i.e., dip magnitude > 25% of initial voltage.
3. Transient voltage dip time duration problem: voltage dip of > 20% of initial voltage with a dip duration of > 20 cycles.

A slow voltage recovery problem can lead to tripping of induction motors. So it is very important to prevent the voltage recovery problem. The nature of this problem demands a fast acting Var source. Hence static var compensators (SVCs) must be employed. Yet, as described in Sections 6.5 and 6.6, there may also be static voltage problems to which SVCs can contribute. Hence an optimal combination of SVCs and static capacitors is desired, to address both post contingency voltage instability and transient voltage dip problems. Chapter 5 demonstrates the procedure developed on the IEEE New England 39 bus system. This same approach is now applied to a larger system.

When time domain simulation was done to analyze all 7 severe contingencies, it was

found that none of them resulted in transient voltage dip magnitude and duration problem (transient after voltage recovery). But all the contingencies lead to a slow voltage recovery due to the presence of induction motor loads. This slow voltage recovery resulted in the tripping of induction motor at the respective buses. The following summarizes results of each contingency. In each case, the contingency is identified, the buses having low voltage dips below 20% of initial voltage and recovery time exceeding 20 cycles are identified, and the recovery time is given.

Contingency 1

Generator at 97451 or 97452 is outaged and the transmission line between buses 97463-97467 is tripped due to fault. Table 6.17 lists those buses resulting in transient voltage dip violation.

Table 6.17 Buses resulting in transient voltage dip violation for contingency 1

Bus Number	Bus Name	Recovery time	Cycles
97463	4OAKRIDG	0.841	50.46
97455	4METRO2	0.771	46.26
97468	4GOSLIN	0.694	41.64
97544	4ALDEN	0.614	36.84

Contingency 2

Generator at 97451 or 97452 is outaged and the transmission line between buses 97478-97721 is tripped due to fault. Table 6.18 lists those buses resulting in transient voltage dip violation.

Table 6.18 Buses resulting in transient voltage dip violation for contingency 2

Bus Number	Bus Name	Recovery time	cycles	Bus Number	Bus Name	Recovery time	cycles
97468	4GOSLIN	0.495	29.7	97482	4CINCINT	0.386	23.16
97544	4ALDEN	0.492	29.52	97484	4HUNTSVL	0.386	23.16
97455	4METRO2	0.491	29.46	97527	2SINHERN	0.385	23.1
97463	4OAKRIDG	0.467	28.02	97530	4WALKER	0.385	23.1
97460	4CRYSTAL	0.439	26.34	97481	4CEDAR	0.384	23.04
97521	4JEFCON	0.439	26.34	97485	L558TP91	0.384	23.04
97520	4FWPIPE	0.438	26.28	97555	4BISHOP	0.382	22.92
97456	4SECURTY	0.436	26.16	97536	4RIVTRIN	0.381	22.86
97458	4CONAIR	0.436	26.16	97486	4WYNTEX	0.379	22.74
97462	5L523T58	0.436	26.16	97503	2SOMERVL	0.378	22.68
97459	4CONROE	0.435	26.1	97454	4WALDEN	0.377	22.62
97542	4JAYHAWK	0.428	25.68	97512	4PEE DEE	0.377	22.62
97466	4SHEAWIL	0.424	25.44	97480	L558T485	0.376	22.56
97457	4LONGMIR	0.421	25.26	97500	2INDEPEN	0.373	22.38
97475	4CLVELND	0.421	25.26	97516	2HEARNE	0.373	22.38
97464	4PANORAM	0.42	25.2	97517	2TXHEARN	0.372	22.32
97461	4LEWIS	0.418	25.08	97524	2IN.AT$T	0.37	22.2
97465	4PLANTAT	0.418	25.08	97525	2HUMBHRN	0.37	22.2
97545	4LACON	0.418	25.08	97528	4GULFTRN	0.369	22.14
97471	4CANEYCK	0.416	24.96	97535	4CARLILE	0.369	22.14
97543	4PECHCK#	0.414	24.84	97501	2CALDWEL	0.368	22.08
97476	4JACINTO	0.413	24.78	97523	2APLHERN	0.367	22.02
97538	8LNG 413	0.413	24.78	97566	4TAMINA	0.367	22.02
97539	4WDHAVN	0.41	24.6	97467	4PORTER	0.366	21.96
97479	4SHEPERD	0.407	24.42	97552	4ONLASKA	0.363	21.78
97488	4TEMCO	0.407	24.42	97502	2ANAVSOT	0.36	21.6
97540	4EVGRN*	0.407	24.42	97474	4HIGHTWR	0.355	21.3
97453	4DOBBIN	0.406	24.36	97522	4TUBULAR	0.355	21.3
97519	4GEORGIA	0.403	24.18	97537	4STALEY	0.354	21.24
97478	6JACINTO	0.402	24.12	97492	4BLANCHD	0.352	21.12
97551	4CEDHILL	0.402	24.12	97509	4SPEEDWY	0.352	21.12
97483	4GOREE	0.397	23.82	97511	2TESCO	0.352	21.12
97515	2CALVERT	0.396	23.76	97508	4NAVSOTA	0.351	21.06
97534	4SPLENDR	0.396	23.76	97487	4MT.ZION	0.344	20.64
97470	4LFOREST	0.394	23.64	97491	4LIVSTON	0.344	20.64
97531	4APOLLO	0.391	23.46	97477	4TARKING	0.343	20.58
97495	4RICH 1	0.39	23.4	97504	2BRYAN B	0.34	20.4
97469	4APRILTX	0.386	23.16	97553	4BLDSPRG	0.34	20.4

Contingency 3

Generator at 97451 or 97452 is outaged and the transmission line between buses 97567-97714 is tripped due to fault. Table 6.19 lists those buses resulting in transient voltage dip violation.

Table 6.19 Buses resulting in transient voltage dip violation for contingency 3

Bus Number	Bus Name	Recovery time	cycles
97455	4METRO2	0.36	21.6
97468	4GOSLIN	0.36	21.6
97544	4ALDEN	0.353	21.18
97463	4OAKRIDG	0.344	20.64

Contingency 4

Generator at 97451 or 97452 is outaged and the transmission line between buses 97691-97717 is tripped due to fault. Table 6.20 lists those buses resulting in transient voltage dip violation.

Table 6.20 Buses resulting in transient voltage dip violation for contingency 4

Bus Number	Bus Name	Recovery time	cycles
97468	4GOSLIN	0.394	23.64
97455	4METRO2	0.392	23.52
97544	4ALDEN	0.392	23.52
97463	4OAKRIDG	0.377	22.62
97515	2CALVERT	0.376	22.56
97459	4CONROE	0.357	21.42
97527	2SINHERN	0.357	21.42
97462	5L523T58	0.355	21.3
97458	4CONAIR	0.354	21.24
97465	4PLANTAT	0.347	20.82
97539	4WDHAVN	0.343	20.58
97516	2HEARNE	0.337	20.22
97551	4CEDHILL	0.337	20.22
97482	4CINCINT	0.336	20.16
97457	4LONGMIR	0.335	20.1
97517	2TXHEARN	0.335	20.1
97530	4WALKER	0.335	20.1
97481	4CEDAR	0.334	20.04

Contingency 5

Generator at 97451 or 97452 is outaged and the transmission line between buses 97714-97716 is tripped due to fault. Table 6.21 lists those buses resulting in transient voltage dip violation.

Table 6.21 Buses resulting in transient voltage dip violation for contingency 5

Bus Number	Bus Name	Recovery time	cycles	Bus Number	Bus Name	Recovery time	cycles
97468	4GOSLIN	0.781	46.86	97532	4HICKORY	0.415	24.9
97455	4METRO2	0.78	46.8	97503	2SOMERVL	0.412	24.72
97544	4ALDEN	0.764	45.84	97516	2HEARNE	0.412	24.72
97463	4OAKRIDG	0.743	44.58	97517	2TXHEARN	0.41	24.6
97459	4CONROE	0.605	36.3	97484	4HUNTSVL	0.409	24.54
97462	5L523T58	0.582	34.92	97525	2HUMBHRN	0.408	24.48
97465	4PLANTAT	0.57	34.2	97481	4CEDAR	0.406	24.36
97458	4CONAIR	0.563	33.78	97500	2INDEPEN	0.406	24.36
97551	4CEDHILL	0.543	32.58	97542	4JAYHAWK	0.406	24.36
97539	4WDHAVN	0.517	31.02	97482	4CINCINT	0.405	24.3
97566	4TAMINA	0.502	30.12	97485	L558TP91	0.405	24.3
97467	4PORTER	0.501	30.06	97530	4WALKER	0.405	24.3
97533	4NEWCANY	0.485	29.1	97555	4BISHOP	0.405	24.3
97461	4LEWIS	0.484	29.04	97523	2APLHERN	0.404	24.24
97470	4LFOREST	0.484	29.04	97524	2IN.AT$T	0.402	24.12
97545	4LACON	0.484	29.04	97512	4PEE DEE	0.401	24.06
97464	4PANORAM	0.481	28.86	97486	4WYNTEX	0.4	24
97457	4LONGMIR	0.48	28.8	97501	2CALDWEL	0.4	24
97466	4SHEAWIL	0.479	28.74	97536	4RIVTRIN	0.4	24
97520	4FWPIPE	0.47	28.2	97480	L558T485	0.397	23.82
97469	4APRILTX	0.469	28.14	97502	2ANAVSOT	0.39	23.4
97538	8LNG 413	0.469	28.14	97511	2TESCO	0.385	23.1
97460	4CRYSTAL	0.468	28.08	97522	4TUBULAR	0.384	23.04
97521	4JEFCON	0.468	28.08	97508	4NAVSOTA	0.38	22.8
97471	4CANEYCK	0.464	27.84	97509	4SPEEDWY	0.38	22.8
97454	4WALDEN	0.456	27.36	97528	4GULFTRN	0.378	22.68
97488	4TEMCO	0.455	27.3	97535	4CARLILE	0.378	22.68
97540	4EVGRN*	0.455	27.3	97475	4CLVELND	0.371	22.26
97456	4SECURTY	0.447	26.82	97537	4STALEY	0.371	22.26
97519	4GEORGIA	0.446	26.76	97552	4ONLASKA	0.369	22.14
97453	4DOBBIN	0.443	26.58	97504	2BRYAN B	0.368	22.08
97567	6PORTER	0.443	26.58	97479	4SHEPERD	0.362	21.72
97515	2CALVERT	0.442	26.52	97487	4MT.ZION	0.358	21.48
97531	4APOLLO	0.439	26.34	97495	4RICH 1	0.353	21.18
97483	4GOREE	0.435	26.1	97505	2BRYAN A	0.351	21.06
97543	4PECHCK#	0.432	25.92	97492	4BLANCHD	0.35	21
97527	2SINHERN	0.427	25.62	97510	4SOTA 1	0.35	21
97534	4SPLENDR	0.424	25.44	97477	4TARKING	0.335	20.1

Contingency 6

Generator at 97451 or 97452 is outaged and the transmission line between buses 97714-97721 is tripped due to fault. Table 6.22 lists those buses resulting in transient voltage dip violation.

Table 6.22 Buses resulting in transient voltage dip violation for contingency 6

Bus Number	Bus Name	Recovery time	cycles	Bus Number	Bus Name	Recovery time	cycles
97468	4GOSLIN	0.942	56.52	97474	4HIGHTWR	0.48	28.8
97455	4METRO2	0.938	56.28	97477	4TARKING	0.48	28.8
97544	4ALDEN	0.93	55.8	97484	4HUNTSVL	0.476	28.56
97463	4OAKRIDG	0.894	53.64	97485	L558TP91	0.474	28.44
97459	4CONROE	0.818	49.08	97482	4CINCINT	0.473	28.38
97462	5L523T58	0.81	48.6	97530	4WALKER	0.473	28.38
97458	4CONAIR	0.801	48.06	97503	2SOMERVL	0.472	28.32
97465	4PLANTAT	0.793	47.58	97516	2HEARNE	0.472	28.32
97460	4CRYSTAL	0.774	46.44	97481	4CEDAR	0.471	28.26
97521	4JEFCON	0.774	46.44	97517	2TXHEARN	0.47	28.2
97456	4SECURTY	0.772	46.32	97536	4RIVTRIN	0.47	28.2
97520	4FWPIPE	0.769	46.14	97525	2HUMBHRN	0.468	28.08
97551	4CEDHILL	0.767	46.02	97555	4BISHOP	0.468	28.08
97542	4JAYHAWK	0.76	45.6	97500	2INDEPEN	0.466	27.96
97475	4CLVELND	0.749	44.94	97486	4WYNTEX	0.464	27.84
97539	4WDHAVN	0.731	43.86	97512	4PEE DEE	0.464	27.84
97476	4JACINTO	0.723	43.38	97523	2APLHERN	0.464	27.84
97534	4SPLENDR	0.715	42.9	97480	L558T485	0.463	27.78
97466	4SHEAWIL	0.71	42.6	97524	2IN.AT$T	0.462	27.72
97531	4APOLLO	0.708	42.48	97528	4GULFTRN	0.46	27.6
97543	4PECHCK#	0.672	40.32	97535	4CARLILE	0.46	27.6
97566	4TAMINA	0.664	39.84	97501	2CALDWEL	0.459	27.54
97467	4PORTER	0.652	39.12	97552	4ONLASKA	0.455	27.3
97471	4CANEYCK	0.649	38.94	97502	2ANAVSOT	0.451	27.06
97461	4LEWIS	0.637	38.22	97567	6PORTER	0.448	26.88
97545	4LACON	0.636	38.16	97522	4TUBULAR	0.447	26.82
97478	6JACINTO	0.614	36.84	97511	2TESCO	0.444	26.64
97464	4PANORAM	0.604	36.24	97509	4SPEEDWY	0.443	26.58
97457	4LONGMIR	0.593	35.58	97492	4BLANCHD	0.442	26.52
97470	4LFOREST	0.572	34.32	97508	4NAVSOTA	0.442	26.52
97538	8LNG 413	0.57	34.2	97491	4LIVSTON	0.435	26.1
97479	4SHEPERD	0.568	34.08	97537	4STALEY	0.43	25.8
97469	4APRILTX	0.542	32.52	97553	4BLDSPRG	0.426	25.56
97488	4TEMCO	0.539	32.34	97504	2BRYAN B	0.425	25.5
97540	4EVGRN*	0.539	32.34	97487	4MT.ZION	0.419	25.14
97519	4GEORGIA	0.526	31.56	97489	4ISRAEL	0.414	24.84
97454	4WALDEN	0.522	31.32	97494	4POCO 1	0.413	24.78
97533	4NEWCANY	0.519	31.14	97510	4SOTA 1	0.407	24.42
97453	4DOBBIN	0.518	31.08	97505	2BRYAN A	0.405	24.3
97495	4RICH 1	0.517	31.02	97532	4HICKORY	0.404	24.24
97483	4GOREE	0.513	30.78	97506	4BRYAN	0.374	22.44
97515	2CALVERT	0.506	30.36	97529	4MAGROVE	0.337	20.22
97527	2SINHERN	0.489	29.34	97526	4MAG AND	0.335	20.1

Contingency 7

Generator at 97451 or 97452 is outaged and the transmission line between buses 53526-97513 is tripped due to fault. Table 6.23 lists those buses resulting in transient voltage dip violation.

Table 6.23 Buses resulting in transient voltage dip violation for contingency 7

Bus Number	Bus Name	Recovery time	cycles
97515	2CALVERT	0.366	21.96
97527	2SINHERN	0.343	20.58

Table 6.24 ranks the 7 contingencies based on their severity, where severity is quantified in terms of worst-case recovery times. It can be expected that the most severe contingencies will drive the amount of dynamic vars needed.

Table 6.24 Contingency ranking in terms of worst-case recovery times

Contingency No	Bus Numbers		Bus Names		kV	Rank
	From	To	From	To		
1	97463	97467	4OAKRIDG	4PORTER	138	2
2	97478	97721	6JACINTO	CHJC_SER	230	4
3	97567	97714	6PORTER	6CHINA	230	6
4	97691	97717	8CYPRESS	8HARTBRG	500	7
5	97714	97716	6CHINA	6SABINE	230	3
6	97714	97721	6CHINA	CHJC_SER	230	1
7	53526	97513	CROCKET7	7GRIMES	345	5

6.6.2 Candidate Locations for SVC

As indicated by the tables above, there are quite a number of buses having transient voltage dip violations. Many of these buses have induction motor load connected to them that trip under these conditions. The following criteria were used to identify candidate locations for SVCs to mitigate this problem:

1. Buses for which one or more contingencies result in
    a. the bus being among the top 5 worst voltage dips and
    b. the bus has induction motor load that trips
2. Buses must have high voltage stability margin sensitivity so that they can also increase the stability margin when installed; this criterion provides that most of the buses that were part of the steady state solution to increase the post contingency steady state voltage stability margin are candidate SVC locations.

Application of the above criteria resulted in a list of candidate locations as given in Table 6.25.

Table 6.25 Candidate SVC locations

Candidate Bus	Name	Zone	KV
97455	4METRO2	102	138
97468	4GOSLIN	102	138
97544	4ALDEN	102	138
97457	4LONGMIR	103	138
97464	4PANORAM	100	138
97459	4CONROE	103	138
97463	4OAKRIDG	102	138

6.6.3 Sensitivities

To compute the optimal mix of static and dynamic vars, we must obtain the sensitivity of recovery time to the SVC capacity. The sensitivity calculation is described in Section 5.2.1. For every candidate location considered at least two time domain simulation solutions are obtained, one with SVC having capacity of B1 Mvar and another with SVC having capacity of B2 Mvar. Then the difference in voltage dip recovery time is obtained, and the sensitivity is calculated per equation (5.2).

The first time domain simulation was run with an SVC capacity of 300 Mvar. It was observed that the top 5 buses in the list of candidate location in Table 6.25 had a better effect on voltage recovery under most of the contingencies than the last two. So the last two were dropped from the list to reduce computation. Then another set of time domain simulations was run with SVC capacity limit being 150 Mvar for the first 5 candidate locations. Sensitivities were then computed for every bus voltage dip change under every contingency. The table below shows the sensitivity of SVC placement at buses 97455, 97468 and 97544 on the bus voltage characteristics of buses 97463, 97455, 97468, 97544 (most severe voltage dip buses) for contingency 1. Similarly sensitivities can be calculated for all the affected bus voltages with respect to SVC placement under every contingency.

Table 6.26 Recovery time sensitivity ($\Delta\tau_i dip/\Delta B_j SVC$) for Contingency 1

SVC placement bus (j)	Bus (i) for which recovery time is measured			
	97463	97455	97468	97544
97455	0.1947853	0.180272	0.149442	0.129305
97468	0.1847081	0.177179	0.149262	0.131107
97544	0.1738613	0.158503	0.142828	0.129502

6.6.4 Stage 1 Optimization

The obtained sensitivities along with the performance measures in terms of dip duration violation are used in the MIP optimization to find the optimal allocation of dynamic Vars. To find the optimal mix of static and dynamic Var sources to mitigate both steady state and

dynamic voltage stability issues, we also input voltage instability margin sensitivities with respect to MSCs and SVCs at every bus along with the list of contingencies that require margin stability increase. The result of the stage 1 MIP optimization is given in Table 6.27.

Table 6.27 Result of first iteration stage 1 MIP optimization

Contingency						SVC (pu MVAR)	
No.	Bus Number		Bus Name		kV	At 97455 4METRO2	At 97568 4GOSLIN
	From	To	From	To			
1	97463	97467	4OAKRIDG	4PORTER	138	3	0.85
2	97478	97721	6JACINTO	CHJC_SER	230	3	0.8
3	97567	97714	6PORTER	6CHINA	230	3	0.7
4	97691	97717	8CYPRESS	8HARTBRG	500	1.7	0
5	97714	97716	6CHINA	6SABINE	230	3	1.5
6	97714	97721	6CHINA	CHJC_SER	230	3	1.53
7	53526	97513	CROCKET7	7GRIMES	345	3	0.95

Although the stage 1 MIP optimization is formulated to admit both capacitors and SVCs in finding a minimum cost solution which satisfies both voltage instability requirements and transient voltage dip requirements, we obtain here a solution which does not select shunt capacitor at all, i.e., the solution provided by the MIP optimization selects only SVC. Investigation indicates the reason for this is that the transient voltage dip problems are so severe that the amount of SVC required to solve them is also sufficient to mitigate the voltage stability problems.

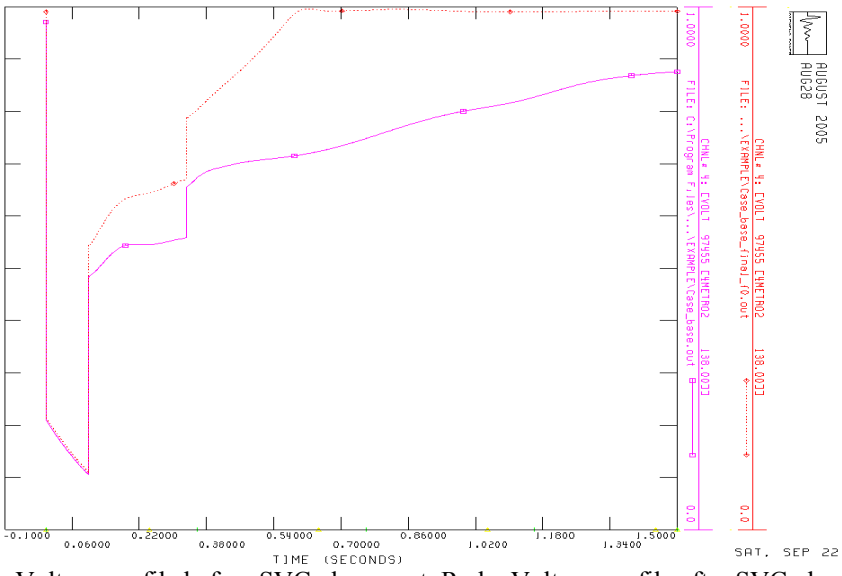
Stage 1 optimization is designed to identify a solution for post contingency voltage instability (finding equalibria) and transient voltage dip violations. Once a stage 1 solution is identified, then another MIP optimization stage, stage 2, is performed to increase voltage stability margin beyond 5% as necessary. Before doing that, however, we performed simulations to validate the obtained solution.

It was found that the SVCs placed at the two buses do solve the steady state voltage instability, and in fact increase the post contingency stability margin well beyond 5% margin requirement. Post contingency voltage stability margin after placing the two SVCs is provided in Table 6.28.

Table 6.28 Voltage instability margin for stage 1 solution

Contingency						Stability Margin (%)
No	Bus Numbers		Bus Names		kV	
	From	To	From	To		
1	97463	97467	4OAKRIDG	4PORTER	138	9.64
2	97478	97721	6JACINTO	CHJC_SER	230	9.16
3	97567	97714	6PORTER	6CHINA	230	9.4
4	97691	97717	8CYPRESS	8HARTBRG	500	8.68
5	97714	97716	6CHINA	6SABINE	230	9.4
6	97714	97721	6CHINA	CHJC_SER	230	8.92
7	53526	97513	CROCKET7	7GRIMES	345	5.1

When time domain simulations were done to validate, it was found that contingencies 1, 2, 5, 6, and 7 still had buses that violated the minimum recovery time requirement, resulting in tripping of some motors. To illustrate effect of the first iteration stage 1 solution, **Figure 6-1** compares the voltage at bus 97455 with and without the SVC solution from the first iteration stage 1 optimization. Although the SVCs improve the voltage, recovery time still exceeds 20 cycles. For additional comparison, **Figure 6-2** shows the five most severe bus voltage plots for contingency 2 without SVCs, and **Figure 6-3** shows plots for these same buses for contingency 2, but with the SVCs from the first iteration stage 1 optimization. We observe significant improvement in **Figure 6-3** relative to **Figure 6-2**, but voltage dip recovery time still exceeds 20 cycles. To further illustrate, **Figure 6-4** compares, for contingency 3, bus voltage plots with and without SVCs, and it also provides SVC outputs. The SVCs placed at buses 97455 and 97468 produced an output of 290 Mvar and 75 Mvar respectively. Plots for the other contingencies are similar and so are not provided.



Legend: Pink – Voltage profile before SVC placement; Red – Voltage profile after SVC placement

Figure 6-1 Bus 97455 voltage profile under contingency 1 with SVC after stage 1 MIP

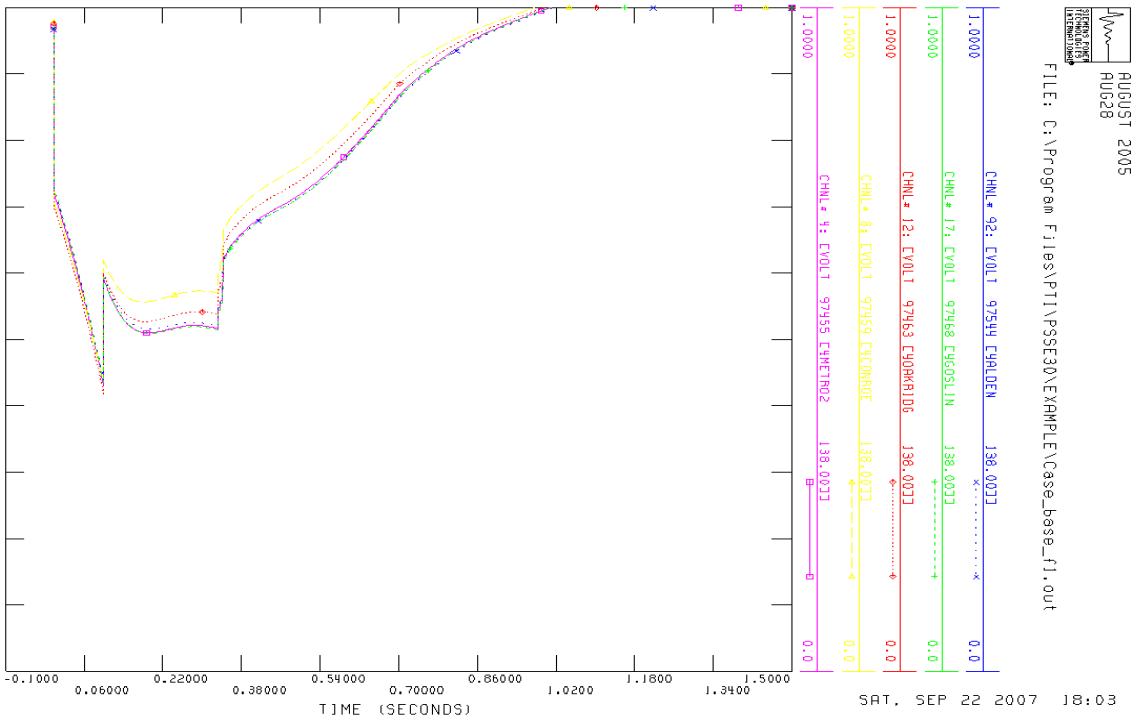


Figure 6-2 Voltage profiles of some buses under contingency 2 without SVC

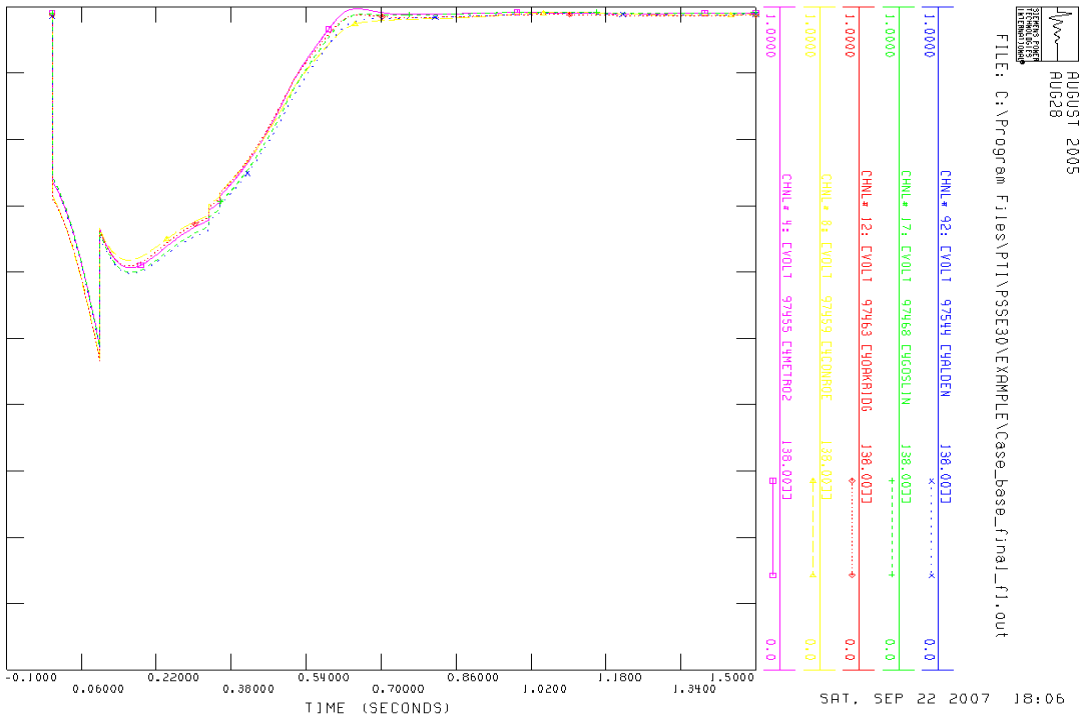
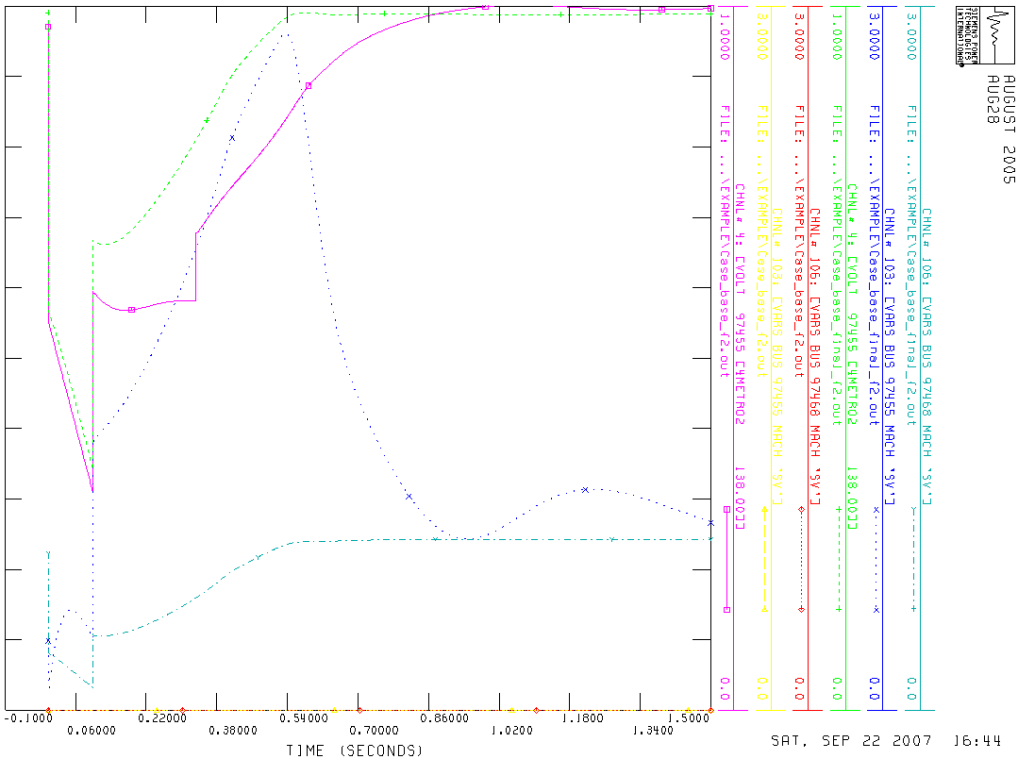


Figure 6-3 Voltage profiles of some buses under contingency 2 with SVC from first iteration optimization



Legend: Pink – voltage before control; Green – Voltage after SVC placement; Dark blue – SVC output at bus 97455; Light blue – SVC output at Bus 97468.

Figure 6-4 Voltages under contingency 3 before and after first iteration SVC placement

As indicated in **Figure 6-1**and **Figure 6-3**, voltage dip recovery time for some buses is insufficient, even after implementing the SVC solution from the first iteration stage 1 optimization. So a second iteration of stage 1 optimization is required. In the second iteration of the stage 1 optimization, we fixed bus 97455 SVC at its maximum capacity of 3 pu since the first iteration solution (Table 6.27) indicates this is required. We direct the second iteration stage 1 optimization to optimize between SVC placement at the next two most desirable buses, which are buses 97468 and 97544. Thus, we provide voltage dip sensitivities only for these two buses (there was not much difference between the old and new sensitivities). The result of the second iteration stage 1 MIP optimization is given in Table 6.29. After validation, it was found that none of the contingencies had any voltage dip problems with the two SVCs placed at buses 97455 and 97468[4]. Given that the first iteration stage 1 optimization resulted in sufficient voltage stability margin, and we have added var resources in the second iteration stage 1 optimization, there is no need to check voltage stability margin for this solution or to perform a stage 2 optimization. And so the solution of Table 6.29 represents the final solution.

[4] It is to be noted that the Bus 97544 also has good sensitivities that are almost close to Bus 97468's. Buses 97459, 97463, 97457, 97464 do form another group of buses that have a very good influence on bus voltages to solve the voltage dip problems. So any other technical or non-technical constraint could well make the planner interested in these buses that are capable of solving the transient dip problems at an equal or only slightly higher cost.

Table 6.29 Result of second iteration stage 1 MIP optimization

Contingency						SVC (pu MVAR) located at bus 97568, 4GOSLIN (amount includes MIP 1 solution)
No	Bus Numbers		Bus Names		kV	
	From	To	From	To		
1	97463	97467	4OAKRIDG	4PORTER	138	2.65
2	97478	97721	6JACINTO	CHJC_SER	230	2.7
3	97567	97714	6PORTER	6CHINA	230	Not considered for MIP 2
4	97691	97717	8CYPRESS	8HARTBRG	500	Not considered for MIP 2
5	97714	97716	6CHINA	6SABINE	230	2.7
6	97714	97721	6CHINA	CHJC_SER	230	2.85
7	53526	97513	CROCKET7	7GRIMES	345	2.1

To illustrate the effect of the second iteration stage 1 optimization, Figure 6-5 and Figure 6-6 compares bus voltages at buses 97455, 97459, 97463, 97468, and 97544 under contingency 1 for the case of no SVC and the case of the SVC solution from the second iteration stage 1 optimization, showing significant improvement. Voltage recovery time for the buses in Figure 6-6 are within 20 cycles.

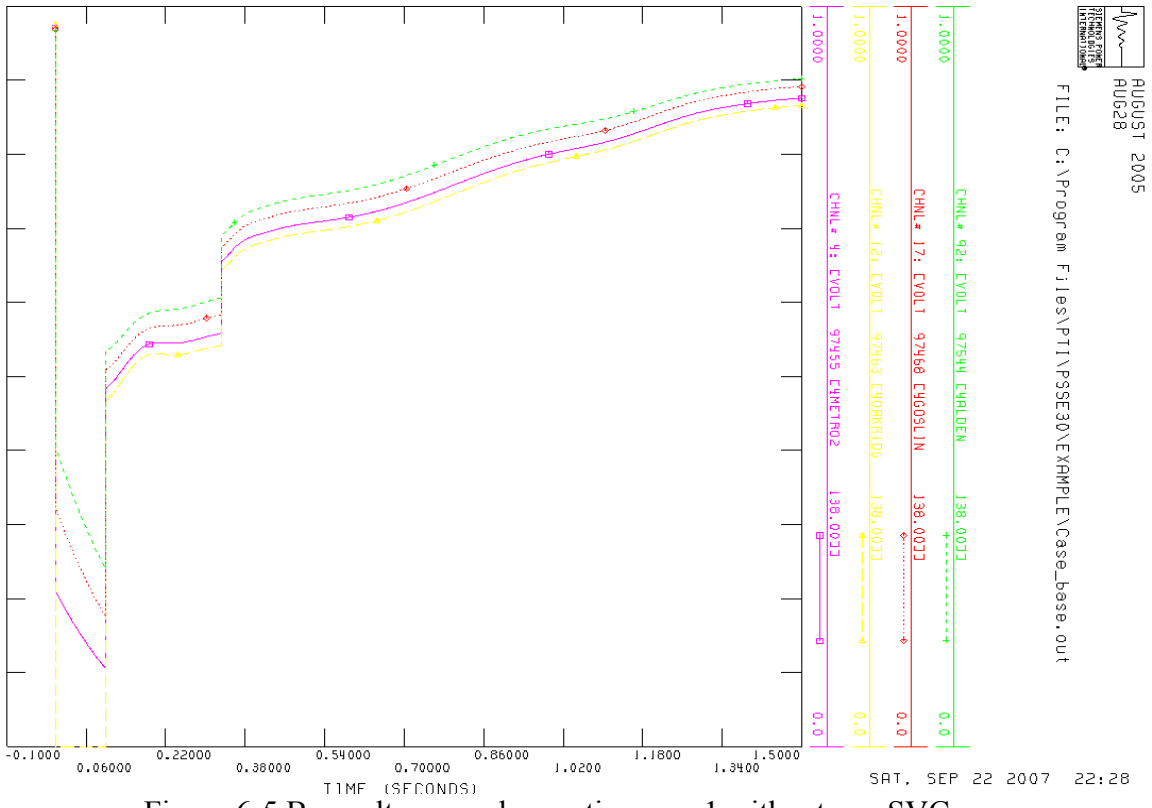


Figure 6-5 Bus voltages under contingency 1 without any SVCs

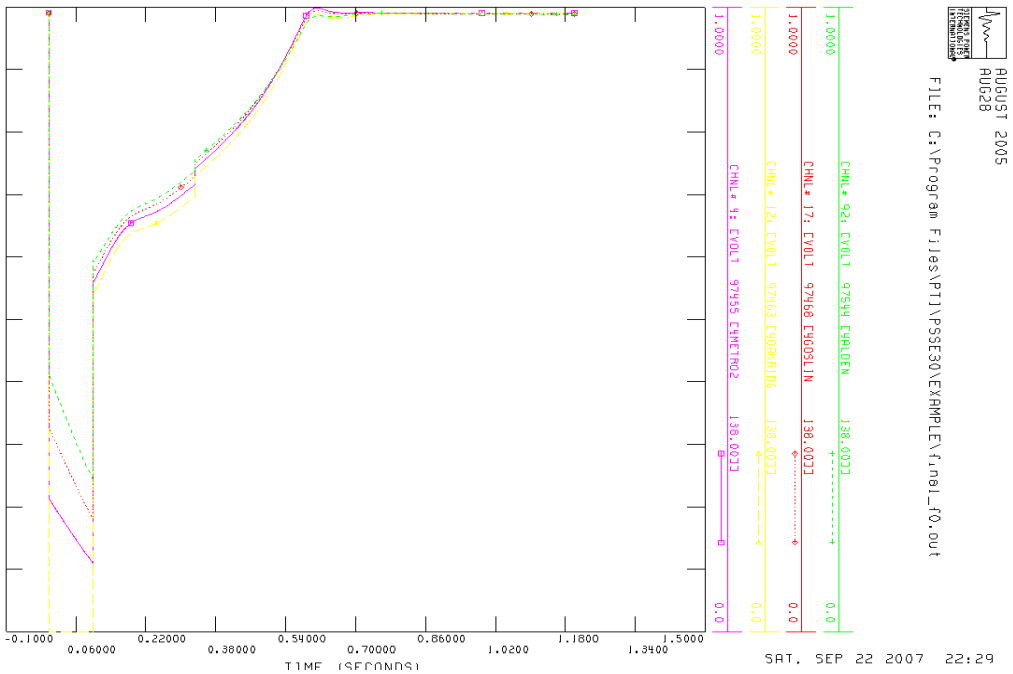
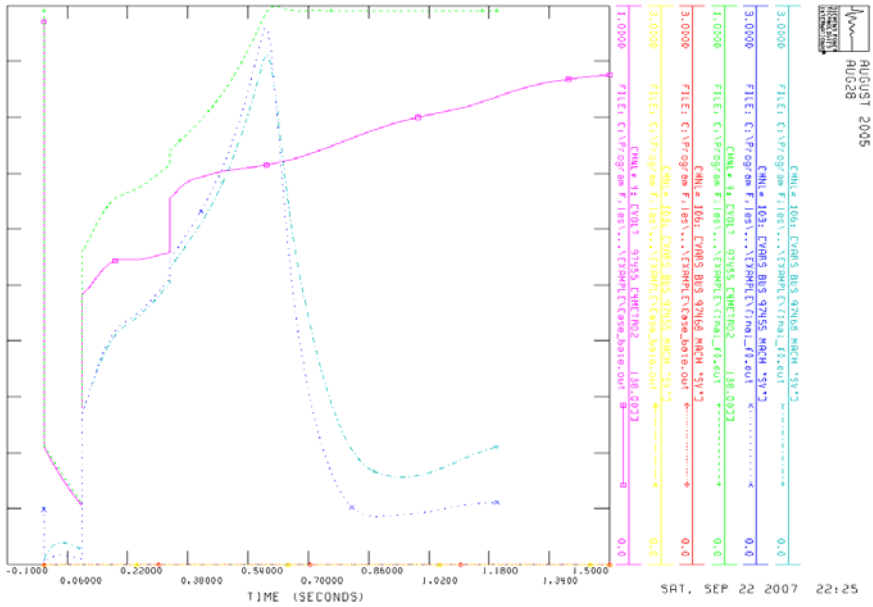


Figure 6-6 Bus voltages under contingency 1 for SVC solution of 2nd iteration optimization

Figure 6-7 shows the improved voltage profile at Bus 97455 under contingency 1 after implementing the SVC solution from the second iteration stage 1 optimization. Figure 6-7 also shows the output of the two SVCs. The SVC peak output at bus 97455 is about 290 Mvar, and that of bus 97468 is about 270 Mvar.



Legend: Pink – Voltage profile before SVC placement; Green – Voltage profile after SVC placement; Dark Blue – SVC output at Bus 97455; Light Blue – SVC output at Bus 97468

Figure 6-7 Bus 97455 voltage profile under contingency 1 with SVC after implementing solution from second iteration stage 1 optimization

6.7 Summary

The first part of this chapter performed a study to determine least cost reactive resources to satisfy constraints imposed only by voltage instability for a subsystem of a large interconnection. Critical contingencies inside the subsystem that cause voltage instability were considered. In this work, only static var solutions were considered. The final result was given in Table 6.16, repeated below for convenience, and cost 2.665 M $ under the cost assumptions used for this study.

Bus No.	Bus Name	Base KV	Amount of p.u. Q injection
97457	4LONGMIR	138	1.5
97455	4METRO2	138	1.5
97464	4PANORAM	138	1.5
97544	4ALDEN	138	1.0

The second part of this chapter performed a *coordinated* planning for static and dynamic Var sources was done for the same subsystem, to plan against voltage instability problems as well as transient voltage dip issues. Critical contingencies inside the subsystem that cause voltage instability and/or that cause transient voltage dip problems were considered. The transient dip problems were so severe that the solution required a lot of SVC, which meant there was no role for capacitors. Several transient voltage profile plots under different contingencies were shown to present the effectiveness of the solution. The final solution was attained through a successive MIP planning algorithm. A second iteration of the stage 1 MIP optimization was needed as some of the contingencies still had voltage dip problems following the first iteration stage 1 solution implementation. Table 6.30 below shows the final solution for the coordinated planning problem. No capacitors[5] are required. The total cost is 32.25 M $ under the cost assumptions used for this study.

Table 6.30 Final Solution

Bus	Base KV	Amount if (p.u) of B (or p.u. Q injection)
97455 4METRO2	138	3.0
97468 4GOSLIN	138	2.85

[5] There can be cases, when the required SVC to mitigate the transient dip problems might be less, and they might still not solve the steady state voltage stability margin violation problems. So in that case Capacitors can be an effective addition to the solution.

7.0 Conclusions and Future Work

7.1 Conclusions

This project developed systematic algorithms to plan reactive power controls for transmission enhancement. The research has been motivated by recent major power outages worldwide caused by voltage instability and the industry need of effective algorithms of reactive power control planning to counteract voltage instability and thus enhance the electric transmission system. The main contributions of this research are the development of algorithms to select candidate control locations to satisfy system performance requirements, the derivation of transient voltage dip sensitivities for dynamic VAR planning, and the development of reactive power control planning algorithms to restore post-contingency equilibria, to increase post-contingency voltage stability margin, and to mitigate post-contingency transient voltage dip. All the proposed algorithms have been implemented with MATLAB and tested on the New England 39-bus system and a large-scale utility system. The simulation results indicate that they can be used to effectively plan reactive power controls for electric transmission system enhancement.

The specific contributions of this research are summarized as follows:

1. Development of a backward/forward search algorithm to select candidate locations of reactive power controls while satisfying power system performance requirements. In the past, candidate control locations are usually chosen based on the engineering judgment. There is no guarantee that the selected locations are effective and sufficient to provide required reactive power support for all concerned contingencies. The proposed algorithm, however, can identify effective and sufficient candidate locations for reactive power control planning. It reduces the computational cost to solve the MIP/MINLP based reactive power control planning problem by limiting the number of candidate locations. It has complexity linear in the number of feasible reactive power control locations whereas the solution space is exponential. Simulation results show that the backward/forward search algorithm can effectively find candidate reactive power control locations.
2. Development of a mixed integer programming based algorithm of reactive power control planning to restore equilibria under a set of severe contingencies. In the past, optimal power flow techniques could be used to restore post-contingency equilibrium for each contingency. It is hard to solve the conventional OPF problems considering multiple contingencies at the same time since they need to incorporate the power system models for all the concerned contingencies. However, it is very easy for the proposed algorithm to handle multiple contingencies. It is only in calculating the critical points and associated sensitivities that we must deal with the full size of the power system. Simulation results indicate that this algorithm is effective and fast to find good reactive power controls for the restoration of post-contingency equilibria.
3. Development of a mixed integer programming based algorithm of reactive power control planning to increase voltage stability margin under a set of contingencies. Again, the proposed algorithm is very effective in dealing with voltage stability requirements under multiple contingencies compared with conventional methods.

Because the optimization formulation is linear, it is fast, yet it provides good solutions for large-scale power systems compared with MINLP. Simulation results show that this algorithm is effective to plan reactive power controls for the increase of the post-contingency voltage stability margin.

4. Development of a systematic algorithm of coordinated planning of static and dynamic VAR resources while satisfying the performance requirements of voltage stability margin and transient voltage dip. It is the first time to use the optimization based method for the determination of the optimal balance between static and dynamic VAR resources. This work is also the first to propose the use of transient voltage dip sensitivities for dynamic VAR planning. Simulation results indicate that the proposed algorithm is effective to determine the optimal mix of static and dynamic VAR resources. The total installation cost of reactive power control devices can be reduced by using the proposed simultaneous optimization formulation.

7.2 Future Work

In the future work, the following issues should be addressed:

1. *Automation of sensitivity calculation*: Some of the procedures to obtain the static and dynamic sensitivities could be more highly automated. This would result in a more efficient process of implementing the optimization process.
2. *Consideration of other stability/security constraints*: This research has focused on the reactive power control planning to increase the voltage stability margin and to mitigate the transient voltage dip. Other stability/security constraints such as transient stability and post-contingency bus voltage magnitude requirements may also be included in the optimization formulation of the reactive power control planning.
3. *Economic benefit analysis and cost allocation*: The planned reactive power control devices (switched shunt capacitors and static var compensators) are intended to serve as control response for contingencies. Further research on quantifying the economic benefit of these devices and efficiently allocating the investment cost is important.

Appendix A: Hybrid System Model

Without any discrete event, a power system can be described by a set of differential algebraic equations

$$\dot{x} = f(x, y) \tag{A.1}$$

$$0 = g(x, y) \tag{A.2}$$

with the vectors

$$x = \begin{bmatrix} \underline{x} \\ p \end{bmatrix}, \quad f = \begin{bmatrix} f \\ 0 \end{bmatrix} \tag{A.3}$$

where $\underline{x} \in R^n$ are true dynamic states, $p \in R^l$ are parameters, $y \in R^m$ are algebraic states. Incorporating parameters into dynamic states allows a compact development of trajectory sensitivities in Appendix B.

Switching events, such as network topology changing, will alter the algebraic equations in (A.2) as

$$0 = \begin{cases} g^-(x, y) & s(x, y) < 0 \\ g^+(x, y) & s(x, y) > 0 \end{cases} \tag{A.4}$$

where $g^-(x,y)$ and $g^+(x,y)$ are sets of algebraic equations before and after the triggering event respectively, $s(x,y)$ is the triggering function. After the triggering event, algebraic variables y may have a step change in order to satisfy the new algebraic constraints.

Other event, such as transformer tap changing, can be modeled by a reset equation

$$x^+ = h(x^-, y^-) \qquad s(x, y) = 0 \tag{A.5}$$

with the vector

$$h = \begin{bmatrix} \underline{h} \\ p \end{bmatrix} \tag{A.6}$$

where $\underline{h}$ is the reset function of the dynamic states $\underline{x}$. Reset events (A.5) cause a discrete change in elements of $\underline{x}$.

The flows of x and y are defined as

$$x(t) = \phi_x(x_0, t) \tag{A.7}$$

$$y(t) = \phi_y(x_0, t) \tag{A.8}$$

with initial conditions,

$$\phi_x(x_0, t_0) = x_0 \tag{A.9}$$

$$g(x_0, \phi_y(x_0, t_0)) = 0 \tag{A.10}$$

More details of the above model can be found in [73] and [75].

Appendix B: Trajectory Sensitivities

Changes of the flows ϕ_x and ϕ_y causing by deviations of the initial conditions and/or parameters are obtained by a Taylor series expansion of (A.7) and (A.8) and neglecting higher order terms

$$\Delta x(t) = \frac{\partial x(t)}{\partial x_0}\Delta x_0 \equiv \Phi_x(x_0,t)\Delta x_0 \tag{B.1}$$

$$\Delta y(t) = \frac{\partial y(t)}{\partial x_0}\Delta x_0 \equiv \Phi_y(x_0,t)\Delta x_0 \tag{B.2}$$

where Φ_x and Φ_y are the trajectory sensitivities [76].

The variational equations describing the evolution of trajectory sensitivities away from discrete events are obtained by differentiating (A.1) and (A.2) with respect to x_0

$$\dot{\Phi}_x = f_x(t)\Phi_x + f_y(t)\Phi_y \tag{B.3}$$

$$0 = g_x(t)\Phi_x + g_y(t)\Phi_y \tag{B.4}$$

Initial conditions for Φ_x and Φ_y are obtained from (A.9) and (B.4) as

$$\Phi_x(x_0,t_0) = I \tag{B.5}$$

$$0 = g_x(t_0) + g_y(t_0)\Phi_y(x_0,t_0) \tag{B.6}$$

The trajectory sensitivities are often discontinuous at a discrete event. The step changes in Φ_x and Φ_y are described by the jump conditions which also provide the initial conditions for the post-event evolution of trajectory sensitivities. Assume the trajectory crosses the hypersurface $s(x,y)=0$ at the point $(x(\tau),y(\tau))$. This point is called the junction point and τ is the junction time. The jump conditions for the sensitivities Φ_x are given by

$$\Phi_x(x_0,\tau^+) = h_x^*\Phi_x(x_0,\tau^-) - (f^+ - h_x^* f^-)\tau_{x0} \tag{B.7}$$

where

$$h_x^* = (h_x - h_y(g_y^-)^{-1}g_x^-)\,|_{\tau^-} \tag{B.8}$$

$$\tau_{x_0} = \frac{d\tau}{dx_0}(\tau^-) = -\frac{(s_x - s_y(g_y^-)^{-1}g_x^-)\,|_{\tau^-}\ \Phi_x(x_0,\tau^-)}{(s_x - s_y(g_y^-)^{-1}g_x^-)\,|_{\tau^-}\ f^-} \tag{B.9}$$

$$f^- \equiv f(x(\tau^-), y^-(\tau^-)) \tag{B.10}$$

$$f^+ \equiv f(x(\tau^+), y^+(\tau^+)) \tag{B.11}$$

Equation (B.9) describes the sensitivity of the junction time τ to the initial conditions and parameters. The sensitivities Φ_y are given by

$$\Phi_y(x_0,\tau^+) = -(g_y^+(\tau^+))^{-1}g_x^+(\tau^+)\Phi_x(x_0,\tau^+) \tag{B.12}$$

More details about derivation and numerical solution approaches for trajectory sensitivities can be found in [73] and [75].

References

[1] L. Dale, “Reactive compensation using static VAR compensators-a planning case study using security constrained techniques,” in *Proc. International Conference on AC and DC Power Transmission*, Sept. 1991, pp. 50 – 54.

[2] R. Koessler, J. Mountford, L. Lima, and J. Rosende, “The Brazilian interconnected system: a study on transfer limits, reactive compensation and voltage collapse,” in *Proc. of the IEEE Power Engineering Society Winter Meeting*, Jan. 2001, pp. 1147 – 1153.

[3] P. Pourbeik, R. Koessler, and B. Ray, “Tools and techniques for analyzing voltage stability related reliability challenges,” in *Proc. of the IEEE Power Engineering Society Transmission and Distribution Conference and Exposition*, Sept. 2003, pp. 417 – 421.

[4] A. Hammad and M. El-Sadek, “Prevention of transient voltage instabilities due to induction motor loads by static VAr compensators,” *IEEE Trans. Power Syst.*, Vol. 4, pp. 1182 – 1190, Aug. 1989.

[5] X. Wang and J. R. McDonald, *Modern Power System Planning*. New York: McGraw Hill, 1994.

[6] IEEE/CIGRE joint task force on stability terms and definitions, “Definition and classification of power system stability”, *IEEE Trans. Power Syst*., vol. 19, pp. 1387-1401, Aug. 2004.

[7] U.G. Knight, *Power System in Emergencies from Contingency Planning to Crisis Management*. Chichester: John Wiley & Sons Ltd, 2001.

[8] NERC (North American Electric Reliability Corporation) Disturbance Analysis Working Group. Disturbances, load reductions, and unusual occurrences 1984-2002. [Online]. Available: http://www.nerc.com/~dawg/database.html (Date accessed: Mar. 9, 2007).

[9] Western Electricity Coordinating Council. NERC/WECC planning standards. [Online]. Available: http://www.wecc.biz/documents/library/procedures/CriteriaMaster.pdf (Date accessed: Mar. 9, 2007).

[10] T. Van Cutsem and C. Vournas, *Voltage Stability of Electric Power Systems*. Boston: Kluwer Academic Publishers, 1998.

[11] IEC 61000-4-30 "Electromagnetic Compatibility (EMC) – Part 4-30: Testing and Measurement Techniques – Power Quality Measurement Methods," Feb. 2003.

[12] D. J. Shoup, J. J. Paserba, C. W. Taylor, "A survey of current practices for transient voltage dip/sag criteria related to power system stability," in *Proc. of the IEEE Power Engineering Society Power Systems Conference and Exposition*, Oct. 2004, pp. 1140-1147.

[13] N. G. Hingorani and L. Gyugyi, *Understanding FACTS: Concepts and Technology of Flexible AC Transmission Systems*. New York: IEEE Press, 2000.

[14] “System protection schemes in power networks,” CIGRE Publication, CIGRE Task Force 38-02-19, 2001.

[15] E. W. Kimbark, “Improvement of system stability by switched series capacitors,” *IEEE Trans. Power Apparatus and Systems*, vol. PAS-85, pp. 180–188, Feb. 1966.

[16] W. Mittelstadt, C. W. Taylor, M. Klinger, J. Luini, J. D. McCalley, and J. Mechenbier, “Voltage instability modeling and solutions as applied to the Pacific Intertie,” in *CIGRE Proc.*, chapter 38-230, 1990.

[17] P. M. Anderson and R. G. Farmer, *Series Compensation of Power Systems*. Encinitas: PBLSH! Inc., 1996.

[18] C. W. Taylor and A. L. Van Leuven, “CAPS: improving power system stability using the time-overvoltage capability of large shunt capacitor banks,” *IEEE Trans. Power Delivery*, vol. 11, pp. 783–789, Apr. 1996.
[19] WECC. Emergency reporting and restoration procedures. [Online]. Available: http://www.wecc.biz/documents/library/RCS/RC001_Emerg_Reporting%204-21-04_WO%20diagrams.pdf (Date accessed: Mar. 9, 2007).
[20] C. W. Taylor, D. C. Erickson, K. E. Martin, R. E. Wilson, and V. Venkatasubramanian, “WACS - wide-area stability and voltage control systems: R&D and online demonstration,” *Proc. IEEE*, vol. 93, pp. 892–906, May 2005.
[21] G. E. Lee and D. L. Goldsworthy, "BPA’s pacific ac intertie series capacitors: experience, equipment & protection," *IEEE Trans. Power Delivery*, vol. 11, pp. 253-259, Jan. 1996.
[22] T. Van Cutsem, “Voltage instability: phenomena, countermeasures, and analysis methods,” *Proc. IEEE*, vol. 88, pp. 208–227, Feb. 2000.
[23] IEEE Power Engineering Society, *FACTS Applications*, Publication 96TP 116-0, IEEE Press, New York, 1996
[24] C. W. Taylor, *Power System Voltage Stability*. EPRI Power System Engineering Series. New York: McGraw Hill, 1994.
[25] K. H. Abdul-Rahman and S. M. Shahidehpour, “Application of fuzzy sets to optimal reactive power planning with security constraints,” *IEEE Trans. Power Syst*., vol. 9, pp. 589-597, May 1994.
[26] J. A. Momoh, S. X. Guo, E. C. Ogbuobiri, and R. Adapa, “The quadratic interior point method solving power system optimization problems,” *IEEE Trans. Power Syst*., vol. 9, pp. 1327-1336, Aug. 1994.
[27] K. Y. Lee, X. Bai, and Y. M. Park, “Optimization method for reactive power planning by using a modified simple genetic algorithm,” *IEEE Trans. Power Syst*., vol. 10, pp. 1843-1850, Nov. 1995.
[28] W. D. Rosehart, C. A. Canizares, and V. H. Quintana, “Effect of detailed power system models in traditional and voltage-stability-constrained optimal power flow problems,” *IEEE Trans. Power Syst*., vol. 18, pp.27-35, Feb. 2003.
[29] O. O. Obadina and G. J. Berg, “Var planning for power system security,” *IEEE Trans. Power Syst*., vol. 4, pp. 677-686, May 1989.
[30] W. Xu, Y. Mansour and P. G. Harrington, “Planning methodologies for voltage stability limited power systems,” *Electrical Power and Energy Systems*, vol. 15, pp. 221-228, Aug. 1993.
[31] Y. Mansour, W. Xu, F. Alvarado, and C. Rinzin “SVC placement using critical modes of voltage instability”, *IEEE Trans. Power Syst.*, vol. 9, pp. 757-763, May 1994.
[32] V. Ajjarapu, P. L. Lau, and S. Battula, “An optimal reactive power planning strategy against voltage collapse”, *IEEE Trans. Power Syst.*, vol. 9, pp. 906-917, May 1994.
[33] T. J. Overbye, “Computation of a practical method to restore power flow solvability”, *IEEE Trans. Power Syst.*, vol. 10, pp. 280-287, Feb. 1995.
[34] Y. L. Chen, “Weak bus oriented reactive power planning for system security,” *IEE Proc. – Gener. Transm. Distrib.*, vol. 143, pp. 541-545, Nov. 1996.
[35] S. Granville, J. C. O. Mello, and A. C. G. Melo, “Application of interior point methods to power flow unsolvability,” *IEEE Trans. Power Syst*., vol. 11, pp. 1096-1103, May 1996.

[36] A. J. Wood and B. F. Wollenberg, *Power Generation Operation and Control*, 2nd ed. New York: John Wiley & Sons, Inc., 1996.
[37] C. S. Chang and J. S. Huang, "Optimal multiobjective SVC planning for voltage stability enhancement," *IEE Proc. – Gener. Transm. Distrib.*, vol. 145, pp. 203-209, Mar. 1998.
[38] E. Vaahedi, Y. Mansour, D. Sun, J. Tamby, and W. Li , "Large scale voltage stability constrained optimal VAR planning and voltage stability applications using existing OPF/optimal VAR planning tools," *IEEE Trans. Power Syst*., vol. 14, pp. 65-74, Feb. 1999.
[39] Z. Feng and V. Ajjarapu, "A comprehensive approach for preventive and corrective control to mitigate voltage collapse", *IEEE Trans. Power Syst*., Vol. 15, pp. 791-797, May 2000.
[40] N. Yorino, E. E. El-Araby, H. Sasaki and S. Harada, "A new formulation for FACTS allocation for security enhancement against voltage collapse", *IEEE Trans. Power Syst*., Vol 18, pp. 3-10, Feb., 2003.
[41] V. Donde and I. A. Hiskens, "Dynamic performance assessment: grazing and related phenomena," *IEEE Trans. Power Syst*., vol. 20, pp. 1967-1975, Nov. 2005.
[42] "Planning against voltage collapse," Electra, vol. 111, pp. 55-75, 1987.
[43] P. Pourbeik, R. J. Koessler, and B. Ray, "Addressing voltage stability related reliability challenges of San Francisco by area with a comprehensive reactive analysis," in *Proc. of the IEEE Power Engineering Society General Meeting*, Jul. 2003, pp. 2634-2639.
[44] P. Pourbeik, R. J. Koessler, W. Quaintance and W. Wong, "Performing comprehensive voltage stability studies for the determination of optimal location, size and type of reactive compensation," in *Proc. of the IEEE Power Engineering Society General Meeting*, Jun. 2006.
[45] V. S. Kolluri and S. Mandal, "Determining reactive power requirements in the southern part of the Entergy system for improving voltage security – a case study," *in Proc. of the IEEE Power Engineering Society General Meeting*, Jun. 2006.
[46] I. Dobson and L. Lu, "Computing an optimal direction in control space to avoid saddle node bifurcation and voltage collapse in electrical power systems," *IEEE Trans. Automatic Control*, vol. 37, pp. 1616-1620, Oct. 1992.
[47] S. Greene, I. Dobson, and F. L. Alvarado, "Sensitivity of the loading margin to voltage collapse with respect to arbitrary parameters," *IEEE Trans. Power Syst*., vol. 11, pp. 845-850, May 1996.
[48]S. Greene, I. Dobson, and F. L. Alvarado, "Contingency ranking for voltage collapse via sensitivities from a single nose curve," *IEEE Trans. Power Syst*., vol. 14, pp. 232-240, Feb. 1999.
[49] B. Long and V. Ajjarapu, "The sparse formulation of ISPS and its application to voltage stability margin sensitivity and estimation," *IEEE Trans. Power Syst*., vol. 14, pp. 944-951, Aug. 1999.
[50] S. Greene, I. Dobson, and F. L. Alvarado, "Sensitivity of transfer capability margins with a fast formula," *IEEE Trans. Power Syst*., vol. 17, pp. 34-40, Feb. 2002.
[51] I. Dobson and L. Lu, "Voltage collapse precipitated by the immediate change in stability when generator reactive power limits are encountered," *IEEE Trans. Circuits Syst*., vol. 39, pp. 762-766, Sept. 1992.
[52] V. Ajjarapu and C. Christy, "The continuation power flow: a tool for steady state voltage

stability analysis," *IEEE Trans. Power Syst*., vol. 7, pp. 416-423, Feb. 1992.
[53] C. A. Canizares and F. L. Alvarado, "Point of collapse and continuation methods for large AC/DC systems," *IEEE Trans. Power Syst*., vol. 8, pp. 1-8, Feb. 1993.
[54] H. D. Chiang, A. J. Flueck, K. S. Shah, and N. Balu, "CPFLOW: a practical tool for tracing power system steady-state stationary behavior due to load and generation vacations," *IEEE Trans. Power Syst*., vol. 10, pp. 623-634, May 1995.
[55] M. Ni, J. D. McCalley, V. Vittal, S. Greene, C. Ten, V. S. Ganugula, and T. Tayyib, "Software implementation of online risk-based security assessment," *IEEE Trans. Power Syst*., vol. 18, pp. 1165-1172, Aug. 2003.
[56] P. M. Anderson and A. A. Fouad, *Power System Control and Stability*, 2nd ed. Piscataway, N.J.: IEEE Press; Wiley-Interscience, 2003.
[57] T. J. Overbye. "A power flow measure for unsolvable cases." *IEEE Trans. Power Syst.*, vol. 9, pp. 1359-1365, Aug. 1994.
[58] Z. Feng, V. Ajjarapu, and B. Long. "Identification of voltage collapse through direct equilibrium tracing." *IEEE Trans. Power Syst.*, vol. 15, pp. 342-349, Feb. 1998.
[59] Z. Feng, V. Ajjarapu, and D. J. Maratukulam. "A practical minimum load shedding strategy to mitigate voltage collapse." *IEEE Trans. Power Syst.*, vol. 13, pp. 1285-1291, Nov. 1998.
[60] A. J. Flueck and J. R. Dondeti, "A new continuation power flow tool for investigating the nonlinear effects of transmission branch parameter variations," *IEEE Trans. Power Syst.*, vol. 15, pp.223-227, Feb. 2000.
[61] P. Kundur, *Power System Stability and Control*. EPRI Power System Engineering Series. McGraw Hill, 1994.
[62] S. L. Richter and R. A. DeCarlo, "Continuation methods: theory and application," *IEEE Trans. Circuits Syst*., vol. 30, pp. 347–352, Jun. 1983.
[63] J. Zhao, H. D. Chiang, and H. Li, "A new contingency parameterization CPF model and sensitivity method for voltage stability control," in *Proc. of the IEEE Power Engineering Society General Meeting*, pp. 376-382, Jun. 2005.
[64] M. A. Pai, *Energy Function Analysis for Power System Stability*. Boston: Kluwer Academic Publishers, 1989.
[65] E. Vaahedi, Y. Mansour, C. Fuchs, S. Granville, M. L. Latore and H. Hamadanizadeh, "Dynamic security constrained optimal power flow/Var planning," *IEEE Trans. Power Syst*., vol. 16, pp. 38-43, Feb. 2001.
[66] G. L. Nemhauser and L. A. Wolsey, *Integer and Combinatorial Optimization*. New York : Wiley, 1988.
[67] U.S.-Canada Power System Outage Task Force. Final report on the August 14, 2003 blackout in the United States and Canada: Causes and recommendations. [Online]. Available: https://reports.energy.gov/BlackoutFinal-Web.pdf (Date accessed: Mar. 9, 2007).
[68] "Criteria and countermeasures for voltage collapse," Electra, vol. 162, pp. 159-167, 1995.
[69] S. Kolluri, A. Kumar, K. Tinnium and R. Daquila, "Innovative Approach for solving dynamic voltage stability problem on the Entergy system," in *Proc. of the IEEE Power Engineering Society Summer Meeting*, pp. 988-993, Jul. 2002.
[70] V. S. Kolluri, S. Mandal, Douglas Mader, M. Claus and H. Spachtholz, "Application of

static var compensator in Entergy system to address voltage stability issues – planning and design considerations," in *Proc. of the IEEE Power Engineering Society Transmission and Distribution Conf*., pp. 1407-1411, May 2006.
[71] P. Pourbeik, A. Bostrom, and B. Ray, "Modeling and application studies for a modern static var system installation," *IEEE Trans. Power Delivery*, vol. 21, pp. 368-377, Jan. 2006.
[72] J. A. Diaz de Leon II and C. W. Taylor, "Understanding and solving short-term voltage stability problems," *in Proc. of the IEEE Power Engineering Society Summer Meeting*, pp. 745-752, Jul. 2002.
[73] I. A. Hiskens, "Power system modeling for inverse problems," *IEEE Trans. Circuits and Systems* I, vol. 51, pp. 539-551, Mar. 2004.
[74] A. van der Schaft and H. Schumacher, *An Introduction to Hybrid Dynamical Systems*. London, U.K.: Springer-Verlag, 2000.
[75] I. A. Hiskens and M. A. Pai, "Trajectory sensitivity analysis of hybrid systems," *IEEE Trans. Circuits and Systems* I, vol. 47, pp. 204-220, Feb. 2000.
[76] P. M. Frank, *Introduction to System Sensitivity Theory*. New York: Academic Press, 1978.
[77] W. F. Feehery, J. E. Tolsma, and P. I. Barton, "Efficient sensitivity analysis of large-scale differential-algebraic systems," *Applied Numerical Mathematics*, vol. 25, pp. 41-54, Oct. 1997.
[78] S. Li, L. Petzold, and W. Zhu, "Sensitivity analysis of differential-algebraic equations: A comparison of methods on a special problem," *Applied Numerical Mathematics*, vol. 32, pp. 161-174, Feb. 2000.

Optimal Allocation of Static and Dynamic VAR Resources

Volume 4

Prepared by

A.P. Sakis Meliopoulos
Dr. Salman Mohagheghi
George Stefopoulos
Hua Fan
Georgia Institute of Technology

Information about this project

For information about this volume contact:

A. P. Meliopoulos, Project Leader
Georgia Power Distinguished Professor
Department of Electrical & Computer Engineering
Georgia Institute of Technology
Van Leer Electrical Engineering Building
777 Atlantic Drive NW
Atlanta, GA 30332-0250
Phone: 404-894-2926
Fax: 404-894-4641
sakis.meliopoulos@ee.gatech.edu

Power Systems Engineering Research Center

This is a project report from the Power Systems Engineering Research Center (PSERC). PSERC is a multi-university Center conducting research on challenges facing the electric power industry and educating the next generation of power engineers. More information about PSERC can be found at the Center's website: http://www.pserc.org.

For additional information, contact:

Power Systems Engineering Research Center
Arizona State University
577 Engineering Research Center
Box 878606
Tempe, AZ 85287-8606
Phone: 480-965-1643
FAX: 480-965-0745

Notice Concerning Copyright Material

PSERC members are given permission to copy without fee all or part of this publication for internal use if appropriate attribution is given to this document as the source material. This report is available for downloading from the PSERC website.

© 2008 Georgia Institute of Technology, Arizona State University, Iowa State University, and the Board of Regents of the University of Wisconsin System. All rights reserved.

Table of Contents

Table of Contents ____ *i*

List of Figures ____ *v*

List of Tables ____ *xii*

1. Introduction ____ *1*

Project Description ____ **1**

2. Overall Approach Description ____ *5*

Introduction ____ **5**

Problem Statement ____ **6**

Methodology for Voltage Recovery Study ____ **7**

3. Electric Load Model ____ *9*

Introduction ____ **9**

Static Load Modeling ____ **9**

Three phase constant impedance load ____ 10
Single phase constant impedance load ____ 12
Three phase constant power load ____ 14
Single phase constant power load ____ 19

Dynamic Load Modeling ____ **21**

Quadratized Induction Motor Model ____ 23

4. Synchronous Generating Unit Model ____ *35*

Single-Axis Generator Model ____ **35**

Steady-State Model ____ 35
Dynamic Model ____ 39
User Interface and Model Parameters ____ 40

Two-Axis Generator Model ____ **42**

Electrical System ____ 43
Mechanical System ____ 47
Steady-State Model ____ 54
Dynamic Model ____ 56
User Interface and Model Parameters ____ 60

Contant Torque/Power Prime Mover Model ____ **63**

Steady-State Model ____ 63
Dynamic Model ____ 64
User Interface and Model Parameters ____ 64

Generic Prime Mover Model ____ **65**

Steady-State Model ____ 65
Dynamic Model ____ 69

User Interface and Model Parameters 73

Constant Voltage/Current Excitation System Model 75
Steady-State Model 75
Dynamic Model 77
User Interface and Model Parameters 80

Generic Excitation System Model 81
Steady-State Model 81
Dynamic Model 83
User Interface and Model Parameters 92

5. Electric Network Model 94

Transmission Line Model 94

Multiphase Cable Model 103

Transformer Model 104

Three Phase Breaker/Switch Model 114

Single Phase Connector/Switch Model 115

Breaker Model with Time Varying Status 115

Ground Impedance Model 118

Substation Model 119

Network Model 122

6. Design Criteria 123

7. Optimal Placing of Voltage Control Devices 125

Introduction 125

Contingencies 125

Dynamic VAR Source Modeling 125
Steady State Model 127
Dynamic Model 129

Static VAR Source Modeling 131
Steady State Model 131
Dynamic Model 132
User Interface 132

Optimization Problem 133

Solution Method 135

Contingency Selection 140
PI Methods for contingency ranking 141
Higher Order State-Linearization PI-Based Contingency Ranking 145

Static Sensitivity Analysis for Candidate Location Selection Using the Costate Method 148
Objective Function First Order Sensitivity Analysis for Candidate Location Selection 149
Higher Order State-Sensitivity Analysis for Candidate Location Selection 151

Trajectory Sensitivity Computation for Candidate Location Selection Using Quadratic Integration 152

8. Example Results ***161***

Power System Modeling and Simulation of Voltage Recovery 161
Introduction 161
Motor Model Estimation 162
Steady State Analysis 169
Quasi Steady State Analysis 175

Optimization of VAr sources 183

9. Future Research Directions ***189***

References ***190***

Appendix A: Quadratized Three-Phase Power System Modeling and Analysis ***197***

Introduction 197

Quadratic Three Phase Modeling: Steady State Analysis 200

Quadratic Three Phase Modeling: Dynamic Analysis 202

Solution Method 205

Appendix B: Quadratic Integration Method ***208***

Introduction 208

Description of Quadratic Integration Method 209

Numerical properties 210

Appendix C: Review of VAR Sources and Models ***213***

Introduction 213

Literature Survey 213
Thyristor-Controlled Reactor (TCR) 213
Thyristor-Switched Capacitor (TSC) 213
Fixed-Capacitor-Thyristor-Controlled Reactor Type VAr Compensator (FC-TCR) 214
Thyristor-Switched Capacitor-Thyristor-Controlled Reactor Type VAr Compensator (TSC-TCR) 215
Unidirectional Power Switched Var Compensator 216
Hybrid Converter TCR Var Compensator 216
Three Phase Synchronous Solid-State Var Compensator (SSVC) 217
Multilevel Voltage Source Inverter (VSI) Var Compensator 218
Synchronous Machine 219

Type DC – Direct Current Commutator Excitation Systems 222
Type AC – Alternator Supplied Rectifier Excitation Systems 225
Type ST – Static Excitation Systems 230
Converters 233

Harmonics 234
Thyristor-Controlled Reactor (TCR) 235
Thyristor-Switched Capacitor (TSC) 235
Fixed Capacitor-Thyristor Controlled Reactor (FC-TCR) 235
Thyristor Controlled Reactor-Thyristor Switched Capacitor (TCR-TSC) 235
Unidirectionally Switched 235
Hybrid Thyristor Controlled Reactor 235
Three Phase Synchronous Solid State SVC 235
Multilevel Voltage Source Inverter (VSI) 236
Synchronous Machine 236

Steady-State Operation 236
Thyristor-Controlled Reactor (TCR) 237
Thyristor-Switched Capacitor (TSC) 237
Fixed Capacitor-Thyristor Controlled Reactor (FC-TCR) 237
Thyristor Controlled Reactor-Thyristor Switched Capacitor (TCR-TSC) 237
Unidirectional Switched 237
Hybrid Thyristor Controlled Reactor 237
Three Phase Synchronous Solid State SVC 237
Multilevel Voltage Source Inverter (VSI) 238
Synchronous Machine 238

Project Publications 239

List of Figures

Figure 1.1. Illustration of Voltage Recovery After a Disturbance. 1
Figure 1.2. System Snapshot of Voltage Collapse at the Center of Transient Power Swings. 2
Figure 2.1. Possible Behavior of Voltage Recovery During and After a Disturbance. 7
Figure 3.1. Three phase constant impedance load model parameters. 10
Figure 3.2. Single Phase Constant Impedance Load Model Parameters. 13
Figure 3.3. Three Phase Constant Power Load Model Parameters. 14
Figure 3.4. Four-Bus Test System for Illustration of Non-Conforming Load Model. 18
Figure 3.5. Single Phase Constant Power Load Model Parameters. 20
Figure 3.6. Voltage Profile of the 24-bus RTS After a Line Contingency, with Constant Power Load Representation. 23
Figure 3.7. Voltage Profile of the 24-bus RTS After a Line Contingency, with Induction Motors Assuming 2% Transient Slowdown. 23
Figure 3.8. Induction Motor Sequence Networks. 24
Figure 3.9. Induction Motor Input Data Form. 25
Figure 3.10. Qualitative Representation of Slip-Dependent Rotor Resistance. 26
Figure 3.11. Qualitative Representation of Slip-Dependent Rotor Reactance. 27
Figure 3.12. NEMA Designs for AC Induction Motors: Designs B and C Cannot Be Accurately Represented using the Classical Equivalent Circuit. 27
Figure 3.13. Block Diagram of Motor Parameter Estimation Procedure. 31
Figure 3.14. Induction Motor Model Parameters Estimation User Interface. 34
Figure 4.1. Equivalent Circuit of Single Axis Synchronous Generator Model. 36
Figure 4.2. Single Axis Synchronous Generator Model Parameters. 41
Figure 4.3. Single Axis Synchronous Generator Additional Model Parameters. 41
Figure 4.4. Electrical Model of a Synchronous Machine as a Set of Mutually Coupled Windings. 42
Figure 4.5. Mechanical model of asynchronous machine as a rotating mass. 43
Figure 4.6. Stator Self-Inductance as a Function of θ. 45
Figure 4.7. Mutual Inductance Between Stator Windings. 46
Figure 4.8. Generating Unit User Interface. 61
Figure 4.9. Synchronous Machine User Interface. 62
Figure 4.10. Synchronous Machine Physical Parameter Interface. 63

Figure 4.11. Constant Torque Input Prime Mover Model Interface. 64
Figure 4.12. Constant Power Input Prime Mover Model Interface. 65
Figure 4.13. Generic Prime Mover Model Interface. Unit not on AGC, Power-Controlled. 74
Figure 4.14. Generic Prime Mover Model Interface. Unit not on AGC, Speed-Controlled. 74
Figure 4.15. Generic Prime Mover Model Interface. Unit on AGC Mode. 75
Figure 4.16. Voltage Source with Internal Resistance. 76
Figure 4.17. Current Source Circuit. 77
Figure 4.18. Voltage Source with Internal Resistance. 78
Figure 4.19. Voltage Source with Internal Inductance. 79
Figure 4.20. Voltage Source with Internal Impedance. 79
Figure 4.21. Current Source Circuit. 80
Figure 4.22. Constant Voltage Source Excitation System. 80
Figure 4.23. Constant Current Source Excitation System. 81
Figure 4.24. DC armature circuit with internal resistance. 82
Figure 4.25. DC Armature Circuit with Internal Resistance 83
Figure 4.26. DC Armature Circuit with Internal Inductance. 86
Figure 4.27. DC Armature Circuit with Internal Impedance. 89
Figure 4.28. User Interface of Generic Exciter Model. 93
Figure 5.1. Transmission Line Model Input Data. 95
Figure 5.2. Conductor Library Interface. 96
Figure 5.3. Tower Library Interface. 96
Figure 5.4. Series Admittance Matrix of Transmission Line Model. 97
Figure 5.5. Shunt Admittance Matrix of Transmission Line Model. 97
Figure 5.6. Transmission Line Model Sequence Parameters. 98
Figure 5.7. Transmission Line Model Sequence Networks. 99
Figure 5.8. Multi-section, Three Phase Overhead Transmission Line Model (A Two Section Example Is Illustrated). 100
Figure 5.9. Mutually Coupled Multiphase Line Model Interface. 101
Figure 5.10. Sequence Network Based Transmission Line Model (model data). 102
Figure 5.11. Sequence Network Based Transmission Line Model (sequence networks). 102
Figure 5.12. Multiphase Cable Model Interface. 103

Figure 5.13. Cable Library Interface. 104
Figure 5.14. Three Phase, Two Winding Transformer Model Interface and Data. 105
Figure 5.15. Three Phase, Three Winding Transformer Interface and Input Data. 105
Figure 5.16. Three Phase, Three Winding Transformer Physical Circuit Model. 106
Figure 5.17. Three Phase Autotransformer Model with Tertiary. 107
Figure 5.18. Three Phase Autotransformer Model without Tertiary. 107
Figure 5.19. Three Phase Autotransformer with Tertiary Physical Circuit Model. 108
Figure 5.20. Three Phase Autotransformer without Tertiary Physical Circuit Model.... 109
Figure 5.21. Single Phase, Two Winding Transformer Model Interface. 110
Figure 5.22. Single Phase, Two Winding Transformer with Secondary Center Tap Model Interface. 110
Figure 5.23. Single Phase, Three Winding Transformer Model Interface and Data. 111
Figure 5.24. Single Phase, Three Winding Transformer Physical Model Equivalent Circuit. 111
Figure 5.25. Single Phase Autotransformer with Tertiary Model Interface and Data. ... 112
Figure 5.26. Single Phase Autotransformer without Tertiary Model Interface and Data. 113
Figure 5.27. Single Phase Autotransformer with Tertiary Physical Model Equivalent Circuit. 113
Figure 5.28. Single Phase Autotransformer without Tertiary Physical Model Equivalent Circuit. 114
Figure 5.29. Three Phase Breaker/Switch Model Interface. 114
Figure 5.30. Single Phase Connector/Switch Model Interface. 115
Figure 5.31. Three Phase Circuit Breaker with Opening Capability. 115
Figure 5.32. Three Phase Circuit Breaker with Opening and Reclosing Capability. 116
Figure 5.33. Single Phase Circuit Breaker with Opening and Reclosing Capability. 116
Figure 5.34. Three Phase Motor Breaker with Opening and Reclosing Capability. 117
Figure 5.35. Single Phase Motor Breaker with Opening and Reclosing Capability. 118
Figure 5.36. Ground Impedance Model. 119
Figure 5.37. Substation Interface Model. 120
Figure 5.38. Geographic Coordinate Interface of Substation Model. 120
Figure 5.39. Substation Model Data. 121
Figure 5.40. Example Substation Configuration. The Arrow Symbol is the Interface to the Network. 121

Figure 5.41. One Line Diagram of a Small Electric Power System. 122
Figure 6.1. Illustration of Design Criteria for Voltage Recovery. 123
Figure 7.1. Illustration of TCR-FC SVC Configuration. 126
Figure 7.2. Schematic of SVS PI Control Scheme. 127
Figure 7.3. User Interface of Three-Phase Capacitor or Inductor Bank Model. 132
Figure 7.4. Block Diagram of the Successive Dynamic Programming Procedure 134
Figure 7.5. Flow Diagram of Proposed Successive Dynamic Programming Approach. 139
Figure 7.6. Circuit Outage Control Variable u_c. 141
Figure 7.7. Generating Unit Outage Control Variable u_c. 142
Figure 7.8. Representation of Common Mode Outages with Control Variable u_c. 142
Figure 7.9. Plots of Circuit-Loading Index vs. the Contingency Control Variable u_c. ... 147
Figure 7.10. Plots of Voltage Index vs. the Contingency Control Variable u_c. 148
Figure 7.11. Illustration of voltage recovery and defined performance objective function. 159
Figure 8.1. One-Line Diagram of Three Phase Model of Test System. 161
Figure 8.2. One-Line Diagram of Generating Substation Configuration. 162
Figure 8.3. One Line Diagram of Distribution Substation Configuration. 162
Figure 8.4. Nominal Slip-Torque Characteristic of Design A Induction Motor. 163
Figure 8.5. Nominal Slip-Torque Characteristic of Design B Induction Motor. 163
Figure 8.6. Nominal Slip-Torque Characteristic of Design C Induction Motor. 164
Figure 8.7. Nominal Slip-Torque Characteristic of Design D Induction Motor. 164
Figure 8.8. Error Between Actual and Estimated Slip-Torque Characteristic, for Design A Motor. 166
Figure 8.9. Error Between Actual and Estimated Slip-Torque Characteristic, for Design B Motor. 167
Figure 8.10. Error Between Actual and Estimated Slip-Torque Characteristic, for Design C Motor. 167
Figure 8.11. Error Between Actual and Estimated Slip-Torque Characteristic, for Design D Motor. 168
Figure 8.12. Convergence of iterative estimation process for design C motor. 169
Figure 8.13. Steady state analysis results for NEMA class A motor. 170
Figure 8.14. Steady State Analysis Results for NEMA Class B Motor. 170
Figure 8.15. Steady State Analysis Results for NEMA Class C Motor. 171

Figure 8.16. Steady State Analysis Results for NEMA Class D Motor. 171
Figure 8.17. Voltage and Current Values at the Terminals of a Distribution Line. Notice the Significant Imbalance Among the Phases. 172
Figure 8.18. Active and Reactive Power Production of Second Generating Unit. 173
Figure 8.19. Phasor Diagram of Voltages and Currents of the Substation Transformer at BUS03. Note again the system imbalance. 173
Figure 8.20. Voltage Profile Along a System Transmission Line. 174
Figure 8.21. Surface Plot of System Voltage Profile (positive sequence). Green color indicates normal voltage, yellow deviations up to ±5% and red deviations above ±5%. 174
Figure 8.22. Surface Plot of System Voltage Profile (positive sequence), after application of capacitive support. 175
Figure 8.23. Motor Speeds After Line to Line Fault, cleared by Line Removal. 176
Figure 8.24. Voltage Recovery of Phase A at the Induction Motor Terminal Buses. 176
Figure 8.25. Voltage Recovery of Phase C at Induction Motor 4 Terminal Bus. 177
Figure 8.26. Voltage Recovery of Phase C at Induction Motor 2 Terminal Bus. 177
Figure 8.27. Induction Motor Reactive Power Absorption during Fault and Post-Fault Period. 178
Figure 8.28. Motor Speeds After Three Phase Fault, cleared by Line Removal. 178
Figure 8.29. Voltage Recovery of Phase A at the Induction Motor Terminal Buses. 179
Figure 8.30. Voltage Recovery of Phase A at Induction Motor 4 Terminal Bus. 179
Figure 8.31. Voltage Recovery of Phase C at Induction Motor 2 Terminal Bus. 180
Figure 8.32. Induction Motor Reactive Power Absorption during Fault and Post-Fault Period. 180
Figure 8.33. Induction Motor Reactive Power Absorption during Fault and Post-Fault Period, for Motor 4. 181
Figure 8.34. Motor Speeds After Three Phase Fault, cleared by Line Removal, with Motor Tripping and Reconnection. 182
Figure 8.35. Voltage Recovery of Phase A at the Induction Motor Terminal Buses Following a Line to Line fault, with Motor Tripping and Reconnection. . 182
Figure 8.36. Induction Motor Reactive Power Absorption during Fault and Post-Fault Period, Following a Line to Line fault, with Motor Tripping and Reconnection. 183
Figure 8.37. Three Phase Model of the IEEE 24-Bus RTS. 184
Figure 8.38. First Iterate of Successive Dynamic Programming. 188

Figure A.1. Actual three phase voltages and currents in MARCY 345 kV substation, at NYPA. 198
Figure A.2. Typical transmission line construction. 199
Figure A.3. Line Asymmetry Indices (Line of Figure 9.2). 200
Figure A.4. General power system bus. 201
Figure B.9.5. Illustration of the Quadratic Integration Method - Basic Assumption. 209
Figure C.1. Thyristor-Controlled Reactor. 213
Figure C.2. Thyristor-Switched Capacitor. 214
Figure C.3. Fixed-Capacitor Thyristor-Controlled Reactor. 215
Figure C.4. Thyristor Controlled Reactor-Thyristor Switched Capacitor. 215
Figure C.5. Unidiretionally power switched compensator. 216
Figure C.6. Hybrid Thyristor Controlled Reactor. 217
Figure C.7. Solid-State VAR Compensator. 218
Figure C.8. Multilevel Voltage Source Inverter. 219
Figure C.9. Synchronous Machine 220
Figure C.10. Schematic of Self-Excited Rotating-Rectifier. 220
Figure C.11. Phasor Diagram of a Synchronous Machine in Steady-State. 221
Figure C.12. Typical Capability Curve of a Synchronous Machine. 221
Figure C.13. Functional Diagram of Synchronous Machine Excitation System. 222
Figure C.14. Type DC1A DC Commutator Exciter. 223
Figure C.15. Type DC2A DC Commutator Exciter With Bus-Fed Regulator. 224
Figure C.16. Type DC3A DC Commutator Exciter With Noncontinuously Acting Regulators. 225
Figure C.17. Type AC1A Alternator-Rectifier Excitation System With Noncontrolled 226
Figure C.18. Type AC2A High Initial Response Alternator-Rectifier Excitation System 227
Figure C.19. Type AC3A Alternator-Rectifier Exciter With Alternator Field Current Limiter. 228
Figure C.20. Type AC4A Alternator Supplied Controlled-Rectifier Exciter. 229
Figure C.21. Type AC5A Simplified Rotating Rectifier Excitation System Representation. 229
Figure C.22. Type AC6A Alternator-Rectifier Excitation System With Noncontrolled 230
Figure C.23. Type ST1A Potential-Source Controlled-Rectifier Exciter. 231
Figure C.24. Type ST2A Compound-Source Rectifier Exciter. 232

Figure C.25. Type ST3A Potential or Compound-Source Controlled-Rectifier Exciter With 233
Figure C.26. Topology of a Six-Pulse Converter. 234

List of Tables

Table 8-1 Estimation Results For Design A Motor 165
Table 8-2 Estimation Results For Design B Motor 165
Table 8-3 Estimation Results For Design B Motor 165
Table 8-4 Estimation Results For Design D Motor 166
Table 8-5 Performance index change and ranking results for the voltage index for the IEEE 24-bus reliability test system. 186

1. Introduction

Project Description

The August 2003 blackout has brought into focus the importance of the VAR/voltage control problem. Two major issues were identified: (a) during stability swings near voltage collapse is experienced near the center of oscillations, (b) voltage recovery is delayed by the dynamics of the electric loads (such as induction motors, etc.) when not enough fast responding VAR sources exist (dynamic VAR sources). These issues are not new. Electric power systems have experienced slow voltage recovery following a disturbance, such as indicated in Figure 1.1. Although a plethora of publications exist that describe voltage phenomena, a comprehensive methodology and satisfactory analysis and design tools that addresses the issue of static/dynamic VAR source mix is not readily available. It is also known that slow voltage recovery phenomena have secondary effects such as operation of protective relays, electric load disruption, motor stalling, etc. It is important to note that utilities around the nation are aware of the potential VAR/voltage recovery control problems from off-line studies and are preparing for averting the potential problems utilizing their own criteria. Indeed the usual way of addressing this problem is by extensive simulations of system response and deciding on the amount of dynamic VAR sources on the basis of the simulation results – a laborious procedure that may not be encompassing all possibilities.

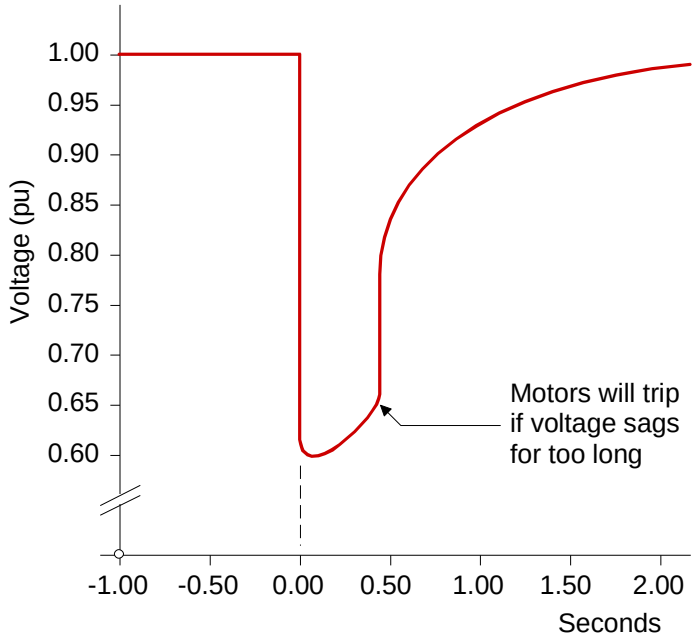


Figure 1.1. Illustration of Voltage Recovery After a Disturbance.

Another phenomenon associated with voltage issues is the topic of voltage collapse. This phenomenon relates to a relatively fast sequence of events after voltage instability that lead to a voltage decay to unacceptably low values. It is in general a non-recoverable situation. Voltage collapse may occur during transient swings, near the center of

oscillations. Figure 1.2 illustrates a snapshot of a transient swing in a small system and the resulting low voltage at the center of the swing between the two oscillating units.

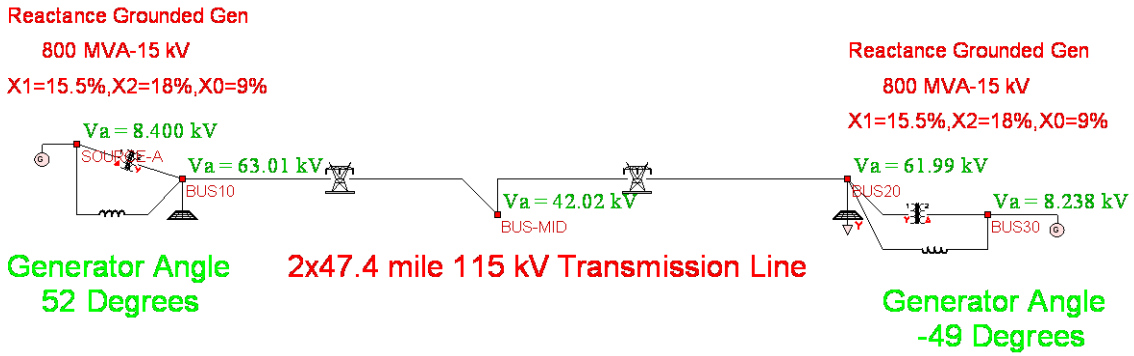


Figure 1.2. System Snapshot of Voltage Collapse at the Center of Transient Power Swings.

More specifically, Figure 1.2 shows a time snapshot of the system. The two generating units operate and nearly the same voltage magnitude, which is very close to the nominal voltage level, but at almost opposite phase. This phase difference results in significant power oscillations along the lines connecting the two units, and in a collapse of the voltage at the center of the connecting line to a level of less than 70% of the nominal value.

Tools for controlling VAR/voltage recovery are not as realistic as need to be and are not robust as it is necessary. Most off-line studies are based on traditional power flow analysis that does not take into account the dynamics of the load while dynamic off-line studies that take into consideration the dynamics of the loads are relatively few and depend on assumed data for the dynamics of the electric load. Real time tools are almost exclusively based on traditional power flow models and they are not capable of capturing the voltage recovery phenomena identified in this proposal. This practice leads to a disconnect between real time models/tools and reality because the dynamics of the loads are not modeled – the majority of which are electric motors. The electric load characteristics play an important role in determining the voltage response/VAR requirements of the system following a severe distress. Indeed electric loads that are predominantly induction motors delay the voltage recovery of the system once the disturbance has been removed. The voltage recovery can be improved with dynamic VAR sources, i.e. VAR sources that have a fast response time, such as Static VAR Compensators.

The objectives of this project are (a) to develop realistic models that accurately model the dynamics of the system and realistically capture voltage recovery phenomena [1] and (b) to develop criteria for the selection of the optimal mix and placement of static and dynamic VAR resources in large power systems using the tools from part (a). The criteria include but are not be limited to speed of voltage recovery, avoidance of unnecessary relay operations, avoidance of motor stalling and avoidance of voltage collapse [2]. The criteria are incorporated into a unified optimization model for minimizing the deployment of static and dynamic VAR resources while meting the criteria. More specifically, the overall approach in this project and an outline of the report is described next.

First a literature review and criteria for acceptable voltage recovery and in general voltage phenomena in power systems was performed. Appropriate models were reviewed to determine their suitability for properly capturing the phenomena that affect voltage recovery. Criteria and models formed the building blocks for the selection of the optimal mix and placement of static and dynamic VAR resources in large power systems. The criteria include but are not limited to (a) speed of voltage recovery, (b) avoidance of unnecessary relay operations, (c) avoidance of motor stalling and (d) avoidance of voltage collapse. The criteria are incorporated into an integrated optimization model for minimizing the deployment of static and dynamic VAR resources while meeting the criteria. Dynamic programming techniques are used for the optimization problem which are capable of incorporating above criteria. The unique advantage of the developed approach is the ability of the new power system analysis tools to explicitly model the dynamics of the load, while they provide performance comparable to usual power flow models. These tools include (a) the single and three phase quadratized power flow [3], [4], (b) the continuation based dynamic simulation [5], [6] and (c) dynamic sensitivity based methods [7], [8].

An important task was the development of a suitable simulation method. For this purpose, the models and tools developed by the research team were integrated. The overall integrated methodology is capable of (a) modeling the dynamics of the electric load (i.e. each load may be consisting of a certain percentage of induction motors – various motor designs may be represented, certain percentage of synchronous motors, certain percentage of lighting load, certain percentage of regulated load, etc.) and (b) capturing the effects of system oscillations on voltage and reactive power absorption. For the purposes of this project a parameterized dynamic electric load model was utilized from physical considerations, such as percentage of motor load, lighting, computers, etc. Note that the simulation methodology combines the advantages of the quadratized power flow and the continuation based time domain simulation. The proposed electric load model permits to routinely perform load scenario simulations. In addition, trajectory sensitivity information [7], [8] quantifies the significant model parameters, such as percentage of load types on the voltage recovery speed. The proposed integrated methodology accurately simulates the voltage behavior of the system during disturbances. Specifically, it precisely predicts voltage dips, voltage recovery rates as well as it determines the most sensitive parameters that affect voltage recovery phenomena. It is also important to stress that the integrated simulation method is capable of determining the cause of slow voltage recovery for example load dynamics, system oscillations or combination of the two.

The major achievements of this project are (a) the characterization of criteria for determining the optimal mix and placement of static and dynamic VAR sources. The criteria ensure better voltage recovery following a disturbance, avoidance of relay operations, load disruption and electric motor stalling. (b) development of a research tool for optimal selection of size and placement of static and dynamic VAR resources. From an operations perspective, the same tool may be used to determine the adequacy of available resources in real time. The development tool is flexible and capable of incorporating complex criteria such as maximum permissible voltage dip duration, etc..

The report is organized as follows.

First, in section 2, the overall methodology is described.

Section 3 describes the modeling of the electric load dynamics. The model considers the dynamics of the load and especially those from induction motors since they represent the majority of the electric load. Examples of various motor designs are provided as well as their impact on voltage recovery.

Section 4 deals with a very important device and source of dynamic VARs, the synchronous generator. It is important to note that the synchronous generator pays a very important role in fast transient voltage recovery and its proper modeling results in realistic voltage recovery models. The section presents the model of the synchronous generator that has been incorporated into the overall methodology.

Section 5 presents the modeling of the network. A breaker-oriented three-phase network model is utilized.

Section 6 presents design criteria for fast transient voltage recovery. The criteria have been developed by considering modern protective relaying practices and requirements for non load disruptions.

Section 7 presents the overall optimization approach for selecting the optimal mix of static and dynamic VAR resources to meet the design criteria. The optimization method is flexible and powerful based on successive dynamic programming.

Section 8 presents example results utilizing the IEEE Reliability test system. This system was designed to exhibit voltage problems and therefore it is appropriate to use it for testing the methodology.

Finally, Section 9 provides thoughts for further research activities in this area.

Appendix A describes the quadratic simulation method.

Appendix B presents the quadratic integration method.

Appendix C present a review of static and dynamic VAR resources and models used in this report.

2. Overall Approach Description

Introduction

This part of the report discusses voltage recovery phenomena following typical faults in a power system considering the existence of dynamic loads, consisting mainly of induction motors. It is well-known that voltage recovery after a disturbance is affected or delayed by load dynamics (such as the dynamics of induction motors, etc.), especially when not enough fast reacting reactive resources (dynamic VAR sources) exist [13]-[21]. This phenomenon has caused serious problems on specific systems and it is typically studied either using static load flow techniques or with full scale transient simulations. In addition, in case of generating unit transient oscillations after the successful clearance of a fault, voltages may dip or collapse near the center of oscillation. During periods of low voltage motors decelerate and when the disturbance is removed, the voltage recovery is affected by the dynamics of the load. The end result may be sluggish voltage recovery and in extreme cases prolonged voltage dips and subsequent motor tripping before voltage recovery. Therefore, both of these phenomena may trigger secondary effects such as motor tripping and other relay operations.

Most off-line studies are mainly based on traditional load flow analysis that does not take into account the dynamics of the load. The proper way to analyze these phenomena is to use dynamic simulation techniques that take into consideration the load dynamics. These approaches are relatively few and depend on assumed data for the dynamic behavior of the electric load.

Real-time tools are almost exclusively based on traditional load flow models and they are not capable of capturing the dynamic nature of voltage recovery phenomena. This practice leads to discrepancies between the analytical models and the real behavior of the system.

The issue of load modeling and the effects of dynamic loads on voltage phenomena have been studied to a significant extent in literature [13]-[30]. In [13] the issues of voltage dips in 3-phase systems after symmetric or asymmetric faults and the accurate modeling of voltage recovery are addressed. In [14] and [15] the voltage recovery phenomena and the effect of induction motor loads are studied from a practical point of view, based on actual events from utility experience. References [16] and [17] study the voltage recovery of wind turbines after short-circuits. The issue of mitigating the delayed voltage recovery using fast VAR resources is addressed in [18]-[20]. The impact of induction motor loads on voltage phenomena has also been studied on a more general research basis. Reference [21] addresses the topic of voltage oscillatory instability caused by induction motors, in particular in isolated power systems, while [22] refers to the impact of induction motor loads in the system loadability margins and in the damping of inter-area oscillations. Finally, references [23]-[32] are indicative of current research approaches and issues in induction motor load modeling in power systems.

This work focuses on modeling and simulation of voltage recovery phenomena taking into consideration the key dynamic characteristics of the load. The approach is based on an advanced load flow modeling for the electric network, which is assumed to operate at quasi-steady state, coupled with quasi-dynamic models of generating units and loads. The quasi-dynamic models explicitly represent the electromechanical oscillations of generators and dynamic loads (mainly motors) while neglect the electrical transients. This allows a more realistic representation of load dynamics. While the methodology is capable of handling various classes of electric loads, we focus our attention on induction motor loads, which represents the majority of electric loads. Emphasis is also given in utilizing a unified model for representing induction motors of different designs.

The induction motor nonlinearities depend on the slip and cause singularities as the slip approaches zero. To avoid numerical problems, the proposed solution method is based on quadratization of the induction motor model [31]-[34]. This model is interfaced with the quadratized power flow model to provide a robust solution method for a system with induction motors. In addition, this model is a more realistic representation of a power system with moderate increase of the complexity of the power flow equations [32]-[38]. The system modeling is based on full three-phase models of all the elements, allowing therefore consideration of system asymmetries and unbalanced operating conditions. Furthermore the methodology makes use of an advanced numerical integration scheme with improved numerical stability properties, which provides a means of overcoming possible numerical problems [39]-[43].

Problem Statement

The problem of transient voltage sags during disturbances and voltage recovery after the disturbance has been removed is quite well known. The importance of the problem has been well identified and has been detected as a contributing factor to many recent blackouts. Its significance is increasing especially in modern restructured power systems that may frequently operate close to their limits under heavy loading conditions. Furthermore, the increased number of voltage-sensitive loads and the requirements for improved power system reliability and power quality are imposing more strict criteria for the voltage recovery after severe disturbances. It is well known that slow voltage recovery phenomena have secondary effects such as operation of protective relays, electric load disruption, motor stalling, etc. Many sensitive loads may have stricter settings of protective equipment and therefore will trip faster in the presence of slow voltage recovery resulting in loss of load with severe economic consequences. A typical situation of voltage recovery following a disturbance is illustrated in Figure 2.1. Note there is a fault during which the voltage collapses to a certain value. When the fault clears, the voltage recovers quickly to another level and then slowly will build up to the normal voltage. The last period of slow recovery is mostly affected by the load dynamics and especially induction motor behavior.

The objective of the project is to present a method that can be used to study voltage recovery events after a disturbance and propose ways and methods to mitigate delayed voltage recovery problems. More specifically the problem is stated as follows: Assume a power system with dynamic loads, like, for example, induction motors. A fault occurs at

some place in the system and it is cleared by the protection devices after some period of time. The objective it to study the voltage recovery after the disturbance has been cleared at the buses where dynamic or other sensitive loads are connected and also determine how these loads affect the recovery process. Moreover, if the recovery rate is not satisfactory, based on specific criteria, then ways are proposed to mitigate the problem and improve the system voltage profile.

In the present paper a hybrid approach is used to the study of voltage recovery that is based on static network modeling integrated with a dynamic model of the load and generators. More specifically, the power network is assumed to be operating in sinusoidal quasi-steady state but the slow electromechanical dynamics of generating units and loads are explicitly included in the model. This approach provides a more realistic tool compared to traditional static power flow, avoiding however the full scale transient simulation which requires detailed system and load dynamic models.

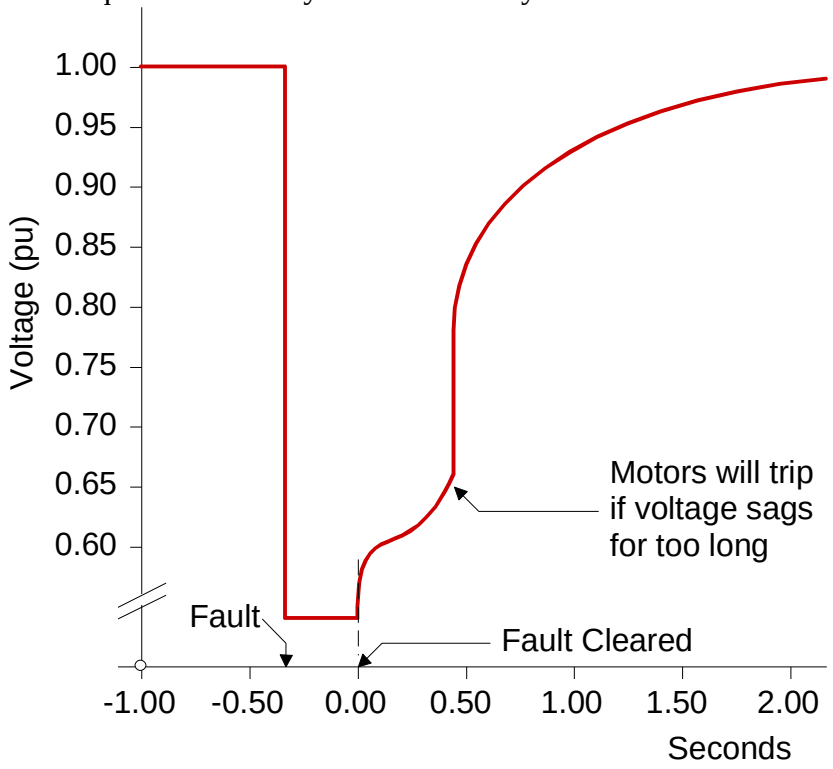


Figure 2.1. Possible Behavior of Voltage Recovery During and After a Disturbance.

Methodology for Voltage Recovery Study

The proposed approach for voltage recovery with dynamic load representation is based on simulating the dynamical equation describing the motor or generator rotor dynamics and solving along with the network load flow equations and the additional internal device equations. We refer to this procedure as quasi steady state, or quasi-static analysis.

Therefore, following a disturbance, the electrical torque produced by the motor will change, due to the terminal voltage variation, causing a deviation in the torque balance between motor torque and load torque. The rotor speed will transiently change. Since

there is an imbalance between the load torque and the motor torque, the rotor speed of the machines will change in accordance to the equation of motion.

More specifically a typical scenario consists of the following phases:

1) Pre-fault phase: The system is operating at steady state condition. The solution is obtained by load-flow analysis using the motor at torque equilibrium mode.

2) During-fault phase: When a fault (or a disturbance in general) takes place the motor enters a transient operating condition. Typically, the motor is supplied by a considerably reduced voltage resulting in a decrease in the motor electro-mechanical torque. Subsequently the motor decelerates since the mechanical load will be higher than the electro-magnetic torque. Depending on the voltage level and on the mechanical load characteristics (the load may be constant torque or it may depend on the speed) the motor will decelerate and most likely will stall unless the fault is cleared and the voltage is restored in time. The deceleration of the induction motor is computed as described earlier. Specifically at each time step the electromechanical torque and the mechanical load torque are computed and the deceleration of the motor over the time step is computed. Then the process is repeated at the new operating point. The analysis procedure is applied throughout the fault duration. The final operating condition at the end of the fault period provides the initial conditions for the post-fault period.

3) Post-fault phase: The same simulation approach is also applied to the post-contingency system. The procedure provides the voltage recovery transient at each bus without using full-scale transient simulation during the longer post-fault period. As mentioned before, the final operating condition at the end of the fault period is the initial conditions of the post fault system.

3. Electric Load Model

Introduction

It has become abundantly clear that load dynamics have played a crucial role in recent power system disturbances. Yet, most study models ignore load dynamics. This section presents work towards implementation of static and dynamic load models for improving the overall models that predict voltage dynamics in electric power systems. We first review the electric load models used in traditional power flow analysis and contingency simulation methods [44] and then describe the implemented load models, both static and dynamic.

Emphasis has been given on load modeling and accurate and realistic simulation of voltage recovery phenomena, especially in the area of dynamic characteristics of industrial loads and in particular, three phase induction motors. A full three-phase, physically-based induction motor model has been developed and implemented. The model accounts for both steady-state and dynamic behavior of the load, under both balanced or unbalanced conditions. System asymmetries are also incorporated into the power system modeling by virtue of the physically-based modeling approach. A slip-dependent rotor impedance model has been used, to allows a unified approach in representing motors of anyone of the various NEMA standardized motor designs (A, B, C and D). The significant differences in the electrical characteristics among these designs make the ability to represent all the different motor types highly desirable. Furthermore, an estimation procedure has been developed and is being implemented and incorporated in the model for computing the motor model parameters from readily available data, such as the slip-torque characteristic and the slip-current characteristic. Since the three-phase modeling approach can account for system imbalances, an extension of the above described work will be to also include similar steady-state and dynamic models of single-phase induction motors, which comprise a significant portion of residential loads. Finally, some work is being underway for the representation of motor protection schemes that can simulate motor tripping under low voltage conditions.

Static Load Modeling

Most load models used in traditional power flow, contingency analysis and static security assessment are static models. Such models can provide accurate representation of specific load types; however, they may fail to capture specific phenomena exhibit by load, in particular when they involve specific dependence on voltage or frequency, or dynamic behavior. The following static load models have been considered as part of this project, for both steady state and quasi steady state analysis:

1. Three phase constant impedance load
2. Single phase constant impedance load
3. Three phase constant power load
4. Single phase constant power load

These models are briefly described next. The difference between this implementation and other approaches found in literature is that here, full three phase models are considered.

Three phase constant impedance load

This section describes a three-phase constant impedance load model for 3-phase network analysis. Models for both steady state and quasi-dynamic analysis are developed, however since the model is static, the equations are the same for both types of analysis. The purpose of this model is to represent balanced, 3-phase loads, of constant impedance per phase. The loads can be internally connected either as wye or as delta. The model input data include the nominal operating voltage level of the load, the active and reactive power absorbed by the load under nominal voltage and the connection type. The load can be reactive, capacitive or purely resistive. The model computes and uses the value of the nominal impedance for the specific load, as derived from the user data. The input data form is illustrated in Figure 3.1, below.

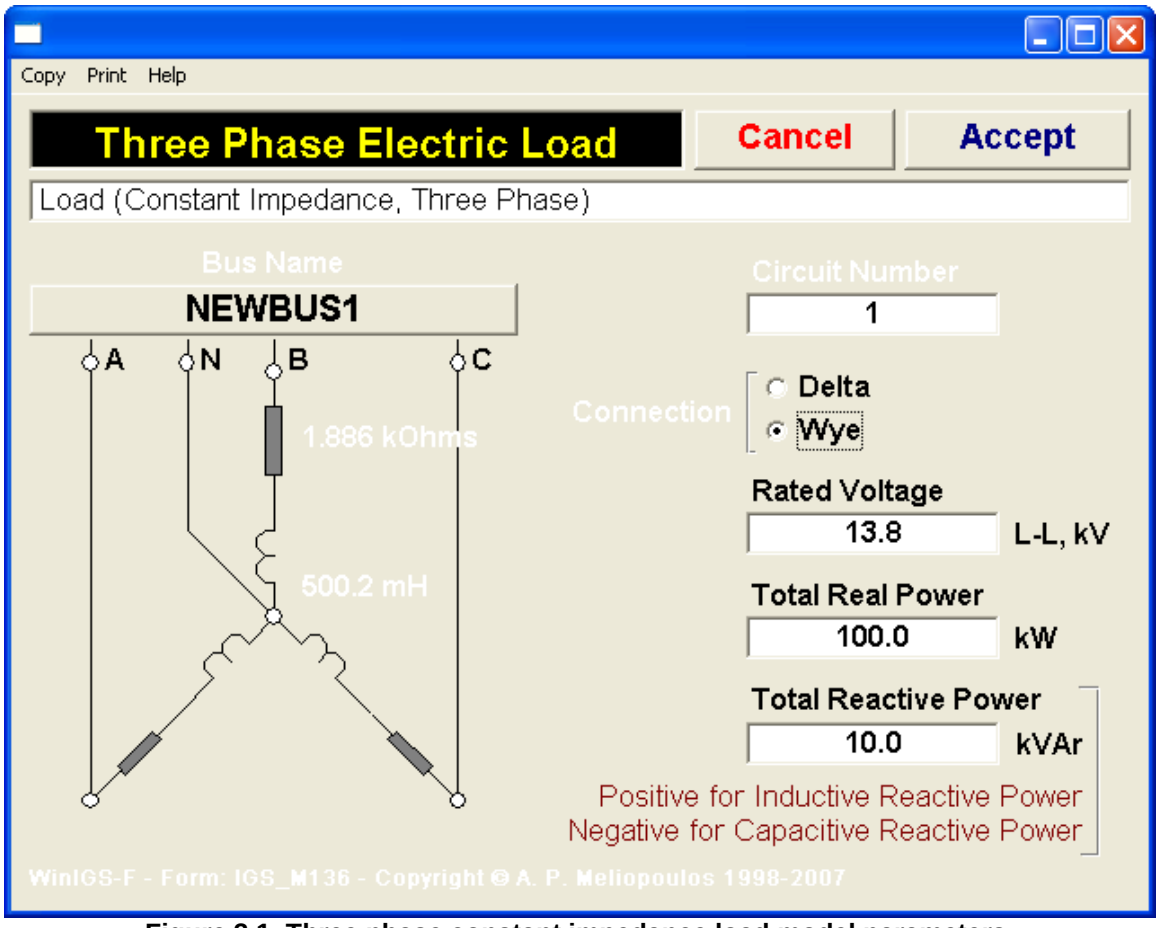


Figure 3.1. Three phase constant impedance load model parameters.

The compact model is based on the fact that the current absorbed by each phase of the load is the product of the complex admittance $\tilde{Y}_L$ times the phasor of the voltage difference at the two ends of the load.

For a wye connected load the equations are:

$$\begin{aligned}
\tilde{\tilde{I}}_A &= \tilde{\tilde{Y}}_L \cdot \left(\tilde{\tilde{V}}_A - \tilde{\tilde{V}}_N\right) \\
\tilde{\tilde{I}}_B &= \tilde{\tilde{Y}}_L \cdot \left(\tilde{\tilde{V}}_B - \tilde{\tilde{V}}_N\right) \\
\tilde{\tilde{I}}_C &= \tilde{\tilde{Y}}_L \cdot \left(\tilde{\tilde{V}}_C - \tilde{\tilde{V}}_N\right) \\
\tilde{\tilde{I}}_N &= -\tilde{\tilde{Y}}_L \cdot \left(\tilde{\tilde{V}}_A + \tilde{\tilde{V}}_B + \tilde{\tilde{V}}_C - 3\tilde{\tilde{V}}_N\right)
\end{aligned} \tag{3.1}$$

where $\tilde{\tilde{V}}_A$, $\tilde{\tilde{V}}_B$, $\tilde{\tilde{V}}_C$, $\tilde{\tilde{V}}_N$ are the voltages at the load terminals, and $\tilde{\tilde{I}}_A$, $\tilde{\tilde{I}}_B$, $\tilde{\tilde{I}}_C$, $\tilde{\tilde{I}}_N$ the phase and neutral currents the load absorbs from the network. The value of $\tilde{\tilde{Y}}_L = g_L + jb_L$ is computed as:

$$\tilde{\tilde{Y}}_L = \frac{\tilde{\tilde{S}}^*}{3V_L^2} = \frac{P - jQ}{3V_L^2} \tag{3.2}$$

Separating real and imaginary parts the model in standard real number form is obtained:

$$\begin{aligned}
I_{Ar} &= g_L V_{Ar} - g_L V_{Nr} - b_L V_{Ai} + b_L V_{Ni} \\
I_{Ai} &= g_L V_{Ai} - g_L V_{Ni} + b_L V_{Ar} - b_L V_{Nr} \\
I_{Br} &= g_L V_{Br} - g_L V_{Nr} - b_L V_{Bi} + b_L V_{Ni} \\
I_{Bi} &= g_L V_{Bi} - g_L V_{Ni} + b_L V_{Br} - b_L V_{Nr} \\
I_{Cr} &= g_L V_{Cr} - g_L V_{Nr} - b_L V_{Ci} + b_L V_{Ni} \\
I_{Ci} &= g_L V_{Ci} - g_L V_{Ni} + b_L V_{Cr} - b_L V_{Nr} \\
I_{Nr} &= -g_L V_{Ar} + g_L V_{Nr} + b_L V_{Ai} - b_L V_{Ni} - g_L V_{Br} + g_L V_{Nr} + b_L V_{Bi} - b_L V_{Ni} - g_L V_{Cr} + g_L V_{Nr} + b_L V_{Ci} - b_L V_{Ni} \\
I_{Ni} &= -g_L V_{Ai} + g_L V_{Ni} - b_L V_{Ar} + b_L V_{Nr} - g_L V_{Bi} + g_L V_{Ni} - b_L V_{Br} + b_L V_{Nr} - g_L V_{Ci} + g_L V_{Ni} - b_L V_{Cr} + b_L V_{Nr}
\end{aligned}$$

For a delta connected load the equations are:

$$\begin{aligned}
\tilde{\tilde{I}}_A &= \frac{\tilde{\tilde{Y}}_L}{3} \cdot \left(2\tilde{\tilde{V}}_A - \tilde{\tilde{V}}_B - \tilde{\tilde{V}}_C\right) \\
\tilde{\tilde{I}}_B &= \frac{\tilde{\tilde{Y}}_L}{3} \cdot \left(2\tilde{\tilde{V}}_B - \tilde{\tilde{V}}_A - \tilde{\tilde{V}}_C\right) \\
\tilde{\tilde{I}}_C &= \frac{\tilde{\tilde{Y}}_L}{3} \cdot \left(2\tilde{\tilde{V}}_C - \tilde{\tilde{V}}_A - \tilde{\tilde{V}}_B\right)
\end{aligned} \tag{3.3}$$

where $\tilde{\tilde{V}}_A$, $\tilde{\tilde{V}}_B$, $\tilde{\tilde{V}}_C$ are the voltages at the load terminals, and $\tilde{\tilde{I}}_A$, $\tilde{\tilde{I}}_B$, $\tilde{\tilde{I}}_C$ the phase currents the load absorbs from the network. The value of $\tilde{\tilde{Y}}_L = g_L + jb_L$ is computed as:

$$\tilde{Y}_L = \frac{\tilde{S}^*}{3V_L^2} = \frac{P - jQ}{3V_L^2} \tag{3.4}$$

Separating real and imaginary parts the model in standard real number form is obtained:

$$\begin{aligned}
I_{Ar} &= \frac{1}{3}\left(2g_L V_{Ar} - g_L V_{Br} - g_L V_{Cr} - 2b_L V_{Ai} + b_L V_{Bi} + b_L V_{Ci}\right) \\
I_{Ai} &= \frac{1}{3}\left(2g_L V_{Ai} - g_L V_{Bi} - g_L V_{Ci} + 2b_L V_{Ar} - b_L V_{Br} - b_L V_{Cr}\right) \\
I_{Br} &= \frac{1}{3}\left(2g_L V_{Br} - g_L V_{Ar} - g_L V_{Cr} - 2b_L V_{Bi} + b_L V_{Ai} + b_L V_{Ci}\right) \\
I_{Bi} &= \frac{1}{3}\left(2g_L V_{Bi} - g_L V_{Ai} - g_L V_{Ci} + 2b_L V_{Br} - b_L V_{Ar} - b_L V_{Cr}\right) \\
I_{Cr} &= \frac{1}{3}\left(2g_L V_{Cr} - g_L V_{Ar} - g_L V_{Br} - 2b_L V_{Ci} + b_L V_{Ai} + b_L V_{Bi}\right) \\
I_{Ci} &= \frac{1}{3}\left(2g_L V_{Ci} - g_L V_{Ai} - g_L V_{Bi} + 2b_L V_{Cr} - b_L V_{Ar} - b_L V_{Br}\right)
\end{aligned} \tag{3.5}$$

Single phase constant impedance load

This section describes a single-phase constant impedance load model for 3-phase network analysis. Models for both steady state and quasi-dynamic analysis are developed, however since the model is static, the equations are the same for both types of analysis. The purpose of this model is to represent unbalanced, non 3-phase loads that are connected to specific phases in the system, and therefore introduce imbalances in the system operation. The model can connect between a phase and the neutral, or between two phases. The model input data include the nominal operating voltage level of the load, and the active and reactive power absorbed by the load under nominal voltage. The load can be reactive, capacitive or purely resistive. The model computes and uses the value of the nominal impedance for the specific load, as derived from the user data. The input data form is illustrated in Figure 3.2, below.

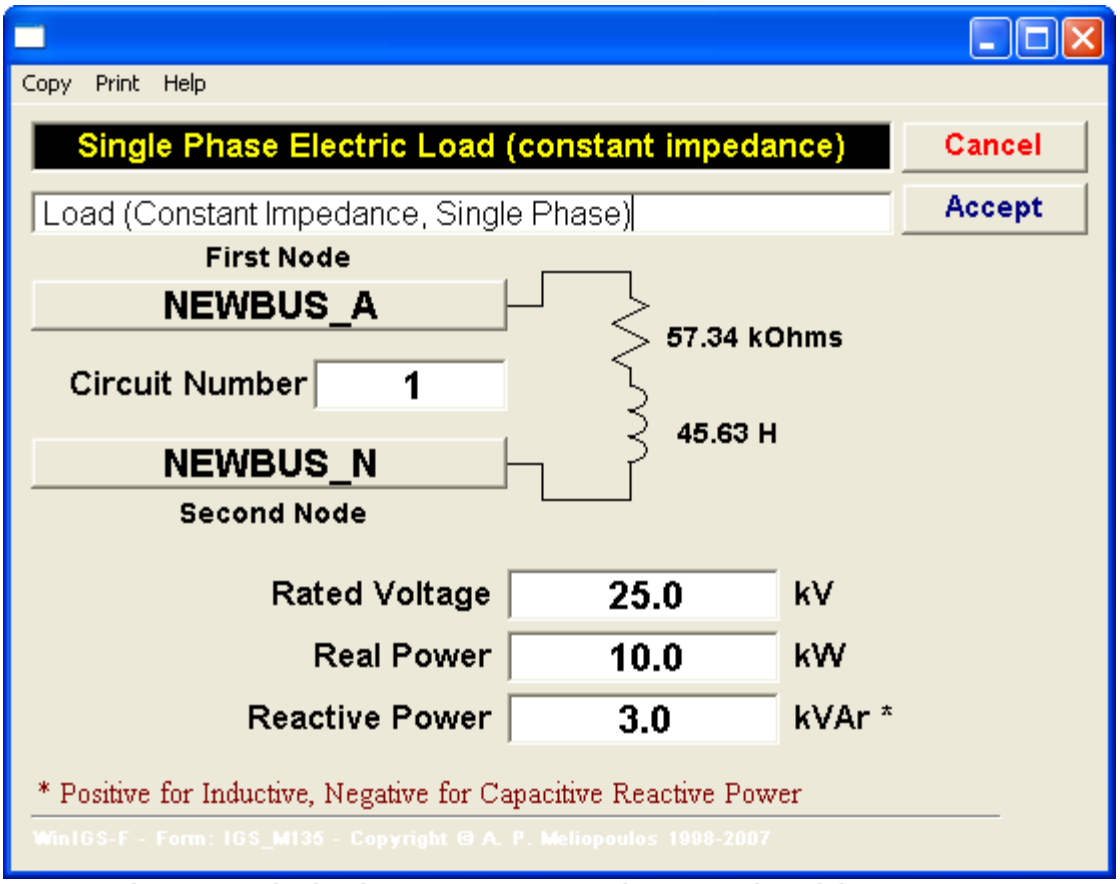


Figure 3.2. Single Phase Constant Impedance Load Model Parameters.

The compact model is based on the fact that the current absorbed by the load is the product of the complex admittance $\tilde{Y}_L$ times the phasor of the voltage difference at the two ends of the load:

$$\tilde{I}_L = \tilde{Y}_L \cdot \tilde{V}_L = \tilde{Y}_L \cdot \left(\tilde{V}_1 - \tilde{V}_2\right) \tag{3.6}$$

where $\tilde{V}_L$ is the voltage across the load terminals and $\tilde{I}_L$ the current the load absorbs from the network. The value of $\tilde{Y}_L = g_L + jb_L$ is computed as:

$$\tilde{Y}_L = \frac{\tilde{S}^*}{V_L^2} = \frac{P - jQ}{V_L^2} \tag{3.7}$$

In standard notation the model has the form:

$$\begin{aligned} \tilde{I}_1 &= \tilde{Y}_L \cdot \left(\tilde{V}_1 - \tilde{V}_2\right) \\ \tilde{I}_2 &= -\tilde{I}_1 \end{aligned} \tag{3.8}$$

Separating real and imaginary parts the model in standard real number form is obtained:

$$
\begin{aligned}
I_{1r} &= g_L V_{1r} - g_L V_{2r} - b_L V_{1i} + b_L V_{2i} \\
I_{1i} &= g_L V_{1i} - g_L V_{2i} + b_L V_{1r} - b_L V_{2r} \\
I_{2r} &= -g_L V_{1r} + g_L V_{2r} + b_L V_{1i} - b_L V_{2i} \\
I_{2i} &= -g_L V_{1i} + g_L V_{2i} - b_L V_{1r} + b_L V_{2r}
\end{aligned}
\qquad (3.9)
$$

Three phase constant power load

This section describes a three-phase constant power load model for 3-phase network analysis. Models for both steady state and quasi-dynamic analysis are developed, however since the model is static, the equations are the same for both types of analysis. The purpose of this model is to represent balanced, 3-phase loads that absorb constant power from the network. The loads can be internally connected either as wye or as delta. The model input data include the nominal operating voltage level of the load, the active and reactive power absorbed by the load and the connection type. The load can be reactive, capacitive or purely resistive. The model can also compute the value of the nominal per phase impedance for the specific load, as derived from the user data. Furthermore, a non-conforming model is included in this load model, to more realistically capture load variations, like for example daily load variations, or load growth. The non-conforming load model is presented at the end of this section. The input data form is illustrated in Figure 3.3, below.

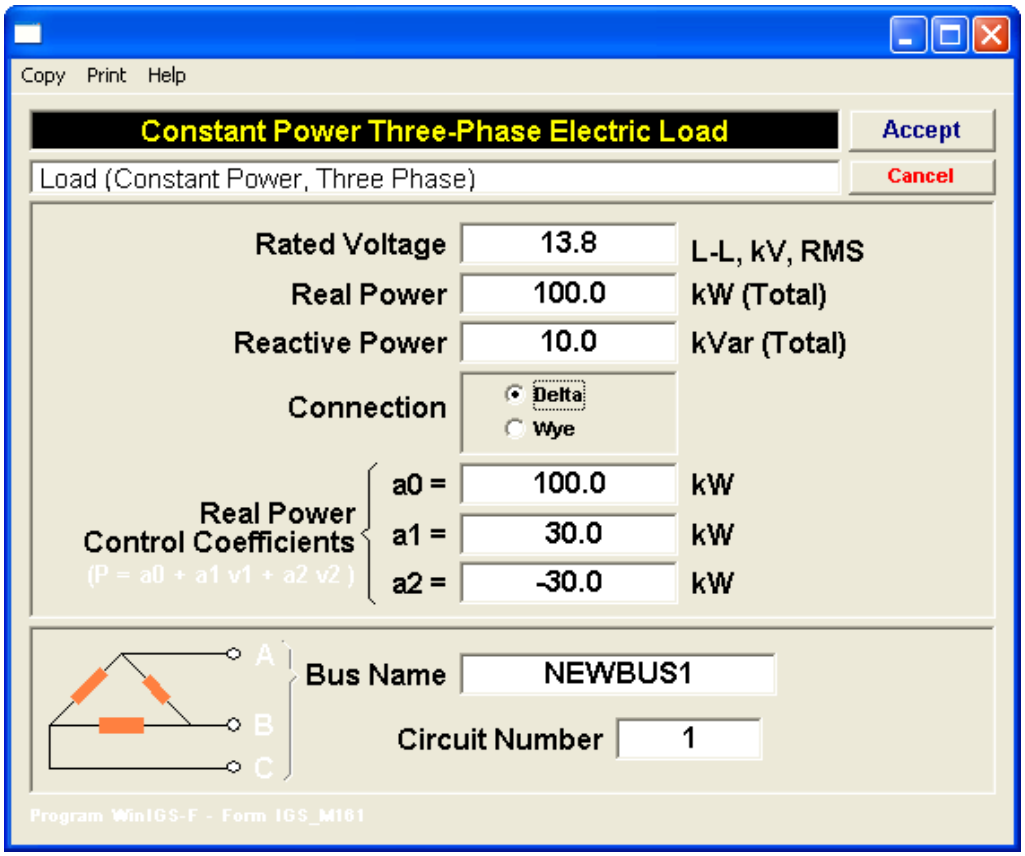


Figure 3.3. Three Phase Constant Power Load Model Parameters.

For a wye connected load the model is:

The total complex power of the load is $S_{dk} = P_{dk} + jQ_{dk}$. It is assumed that the load is constant, i.e. independent of the voltage magnitude at the bus.

Define the nominal admittance of the load to be:

$$Y_{dn,k} = \frac{1}{3V_{ph}^2}\left(P_{dk} - jQ_{dk}\right) = g + jb$$

Then the compact model is:

$$\begin{bmatrix} \tilde{I}_A \\ \tilde{I}_B \\ \tilde{I}_C \\ \tilde{I}_N \end{bmatrix} = \begin{bmatrix} g+jb & 0 & 0 & -g-jb \\ 0 & g+jb & 0 & -g-jb \\ 0 & 0 & g+jb & -g-jb \\ -g-jb & -g-jb & -g-jb & 3g+j3b \end{bmatrix} \begin{bmatrix} \tilde{V}_A \\ \tilde{V}_B \\ \tilde{V}_C \\ \tilde{V}_N \end{bmatrix} + u \begin{bmatrix} g+jb & 0 & 0 & -g-jb \\ 0 & g+jb & 0 & -g-jb \\ 0 & 0 & g+jb & -g-jb \\ -g-jb & -g-jb & -g-jb & 3g+j3b \end{bmatrix} \begin{bmatrix} \tilde{V}_A \\ \tilde{V}_B \\ \tilde{V}_C \\ \tilde{V}_N \end{bmatrix}$$

$$P + jQ = (1+u)(g - jb)\left\{\left|\tilde{V}_A - \tilde{V}_N\right|^2 + \left|\tilde{V}_B - \tilde{V}_N\right|^2 + \left|\tilde{V}_C - \tilde{V}_N\right|^2\right\}$$

In order to quadratize the constant power load model, we introduce three new state variables, u_2, u_3, u_4, i.e.

$$\begin{bmatrix} \tilde{I}_A \\ \tilde{I}_B \\ \tilde{I}_C \\ \tilde{I}_N \end{bmatrix} = \begin{bmatrix} g+jb & 0 & 0 & -g-jb \\ 0 & g+jb & 0 & -g-jb \\ 0 & 0 & g+jb & -g-jb \\ -g-jb & -g-jb & -g-jb & 3g+j3b \end{bmatrix} \begin{bmatrix} \tilde{V}_A \\ \tilde{V}_B \\ \tilde{V}_C \\ \tilde{V}_N \end{bmatrix}$$

$$+ u \begin{bmatrix} g+jb & 0 & 0 & -g-jb \\ 0 & g+jb & 0 & -g-jb \\ 0 & 0 & g+jb & -g-jb \\ -g-jb & -g-jb & -g-jb & 3g+j3b \end{bmatrix} \begin{bmatrix} \tilde{V}_A \\ \tilde{V}_B \\ \tilde{V}_C \\ \tilde{V}_N \end{bmatrix}$$

$$0 = g\{u_2 + u_3 + u_4\} + g\{u_1u_2 + u_1u_3 + u_1u_4\} - P \qquad (3.10)$$

$$0 = u_2 - (V_{Ar} - V_{Nr})^2 - (V_{Ai} - V_{Ni})^2$$

$$0 = u_3 - (V_{Br} - V_{Nr})^2 - (V_{Bi} - V_{Ni})^2$$

$$0 = u_4 - (V_{Cr} - V_{Nr})^2 - (V_{Ci} - V_{Ni})^2$$

Above equations represent the quadratized model of the constant power three-phase electric load.

For a delta connected load the model is:

Define the nominal admittance of the load to be:

$$Y_{dn,k} = \frac{1}{3V_{ph}^2}\left(P_{dk} - jQ_{dk}\right) = g + jb$$

Then the compact model is:

$$\begin{bmatrix}\tilde{I}_A\\ \tilde{I}_B\\ \tilde{I}_C\end{bmatrix}=\begin{bmatrix}2g+j2b & -g-jb & -g-jb\\ -g-jb & 2g+j2b & -g-jb\\ -g-jb & -g-jb & 2g+j2b\end{bmatrix}\begin{bmatrix}\tilde{V}_A\\ \tilde{V}_B\\ \tilde{V}_C\end{bmatrix}+u\begin{bmatrix}2g+j2b & -g-jb & -g-jb\\ -g-jb & 2g+j2b & -g-jb\\ -g-jb & -g-jb & 2g+j2b\end{bmatrix}\begin{bmatrix}\tilde{V}_A\\ \tilde{V}_B\\ \tilde{V}_C\end{bmatrix}$$

$$P+jQ=(1+u)(g-jb)\left\{\left|\tilde{V}_A-\tilde{V}_B\right|^2+\left|\tilde{V}_B-\tilde{V}_C\right|^2+\left|\tilde{V}_C-\tilde{V}_A\right|^2\right\}$$

In order to quadratize the constant power load model, we introduce three new state variables, u_2, u_3, u_4, i.e.

$$\begin{bmatrix}\tilde{I}_A\\ \tilde{I}_B\\ \tilde{I}_C\end{bmatrix}=\begin{bmatrix}2g+j2b & -g-jb & -g-jb\\ -g-jb & 2g+j2b & -g-jb\\ -g-jb & -g-jb & 2g+j2b\end{bmatrix}\begin{bmatrix}\tilde{V}_A\\ \tilde{V}_B\\ \tilde{V}_C\end{bmatrix}+u\begin{bmatrix}2g+j2b & -g-jb & -g-jb\\ -g-jb & 2g+j2b & -g-jb\\ -g-jb & -g-jb & 2g+j2b\end{bmatrix}\begin{bmatrix}\tilde{V}_A\\ \tilde{V}_B\\ \tilde{V}_C\end{bmatrix}$$

$$0=g\{u_2+u_3+u_4\}+g\{u_1u_2+u_1u_3+u_1u_4\}-P \qquad (3.11)$$
$$0=u_2-(V_{Ar}-V_{Br})^2-(V_{Ai}-V_{Bi})^2$$
$$0=u_3-(V_{Br}-V_{Cr})^2-(V_{Bi}-V_{Ci})^2$$
$$0=u_4-(V_{Cr}-V_{Ar})^2-(V_{Ci}-V_{Ai})^2$$

Above equations represent the quadratized model of the constant power three-phase electric load.

Non-Conforming Load Model[45]

The typical constant power load model is a conforming electric load model, i.e. a specific bus load is a percent of the total system load. Statistically, this means that the bus loads are correlated one hundred percent. This practice fails to represent the fact that the actual loads are not fully correlated. For a more realistic representation of the electric load, it is necessary to represent the bus electric load as a non-conforming load. For this purpose a non-conforming electric load model is proposed in terms of n independent variables. In the implementation used in this work, n = 2. The load at any system bus k can be expressed as

$$P_{dk}=P_{dk}^0+\sum_{i=1}^{n}p_{dk}^i\cdot v_i \qquad (3.12)$$

where

P_{dk} : active power demand (load) at bus k,

P_{dk}^0 : nominal load value at bus k,

v_i : ith variable from the set of independent, zero-mean load control variables,

p_{dk}^i : participation coefficient of the ith control variable v_i.

The presented non-conforming load model assumes correlation between the various bus loads, which is in fact a realistic assumption. However, the bus loads not are not fully correlated, as it would be the case in a conventional conforming load model. This depicts a more realistic situation. If $v_i = 0$ for $i = 2,...n$ then the above model becomes a simple conforming load. The load variations at every bus have the exact same statistics, imposed by the single random variable v_i. If $n \geq 2$ then the above model becomes a non-conforming load model.

The characterization of the random variables can be obtained with load forecasting methods, using Auto-Regressive Moving Average (ARIMA) models. Such models have been extensively used to represent the electric load. This is, however, beyond the scope of this work, so here it is assumed that the model of the independent variables is given.

An additional assumption made in the load model is that the load at each bus k maintains a constant power factor; therefore the reactive power consumption at bus k is proportional to the active power consumption, which a constant of proportionality a_k depending on the power factor:

$$Q_{dk} = a_k \cdot P_{dk} \qquad (3.13)$$

where

Q_{dk} : reactive power consumption (load) at bus k.

The non-conforming electric load concept is illustrated in Figure 3.4 with a simple example system.

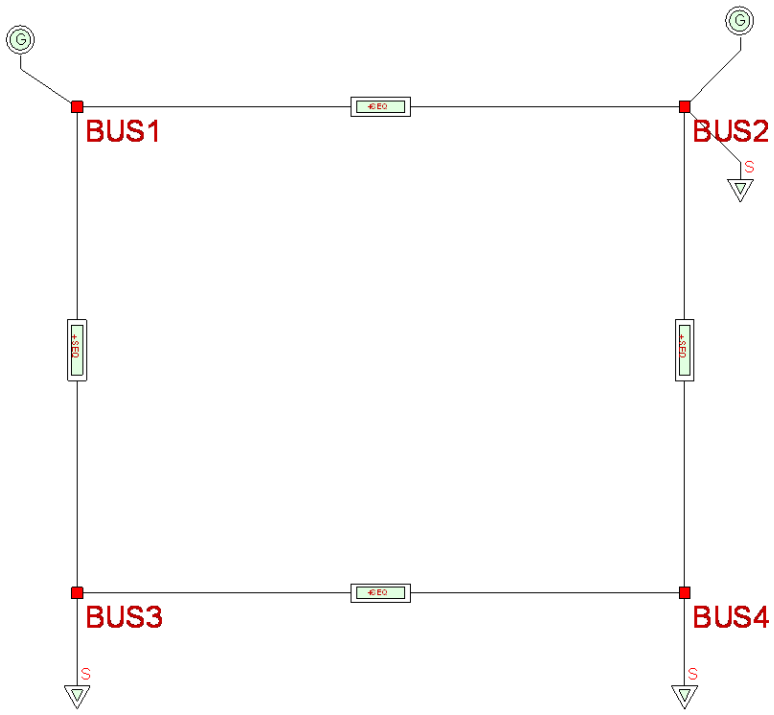


Figure 3.4. Four-Bus Test System for Illustration of Non-Conforming Load Model.

For a conforming load model case the following constant power load values are assumed:

$$P_2 = 60 + 2\mathbf{v_1}$$
$$P_3 = 50 + 2\mathbf{v_1}$$
$$P_4 = 50 + \mathbf{v_1}$$

where $\mathbf{v_1}$ is the load control variable, assumed here to be a zero mean random variable and specifically, $\mathbf{v_1} \sim N(0,0.1)$. The correlation between the three loads, defined as

$$Cor(P_i, P_j) = \frac{Cov(P_i, P_j)}{\sigma_{P_i}\sigma_{P_j}}$$

can be computed to be:

$$Cor[P_2, P_3] = 1.0$$
$$Cor[P_2, P_4] = 1.0$$
$$Cor[P_3, P_4] = 1.0$$

This means that the loads are fully correlated.

For a non-conforming load model case the following constant power load values are assumed:

$$P_2 = 60 + 2\mathbf{v_1} + \mathbf{v_2}$$
$$P_3 = 50 + 2\mathbf{v_1} + 5\mathbf{v_2}$$
$$P_4 = 50 + \mathbf{v_1}$$

where $\mathbf{v_1}$ and $\mathbf{v_2}$ are the two load control variable, assumed here to be a zero mean random variables and in particular, $\mathbf{v_1} \sim N(0,0.1)$ and $\mathbf{v_2} \sim N(0,0.2)$. The correlation between the three loads, defined again as

$$Cor(P_i, P_j) = \frac{Cov(P_i, P_j)}{\sigma_{P_i}\sigma_{P_j}}$$

can be computed to be:

$$Cor[P_2, P_3] = 0.7778$$
$$Cor[P_2, P_4] = 0.8165$$
$$Cor[P_3, P_4] = 0.2722$$

based on the fact that

$$E[P_2] = 60,\ \sigma^2_{P_2} = 0.6$$
$$E[P_3] = 50,\ \sigma^2_{P_3} = 5.4$$
$$E[P_4] = 50,\ \sigma^2_{P_4} = 0.1$$

This means that in this case the loads are only partially correlated, which is a more realistic assumption.

Single phase constant power load

This section describes a single-phase constant power load model for 3-phase network analysis. Models for both steady state and quasi-dynamic analysis are developed, however since the model is static, the equations are the same for both types of analysis. The purpose of this model is to represent unbalanced, non 3-phase loads that are connected to specific phases in the system, and therefore introduce imbalances in the system operation. The model can connect between a phase and the neutral, or between two phases. The model input data include the nominal operating voltage level of the load, and the active and reactive power absorbed. The load can be reactive, capacitive or purely resistive. The model can also compute and provide the value of the nominal impedance for the specific load, as derived from the user data. The input data form is illustrated in Figure 3.5, below.

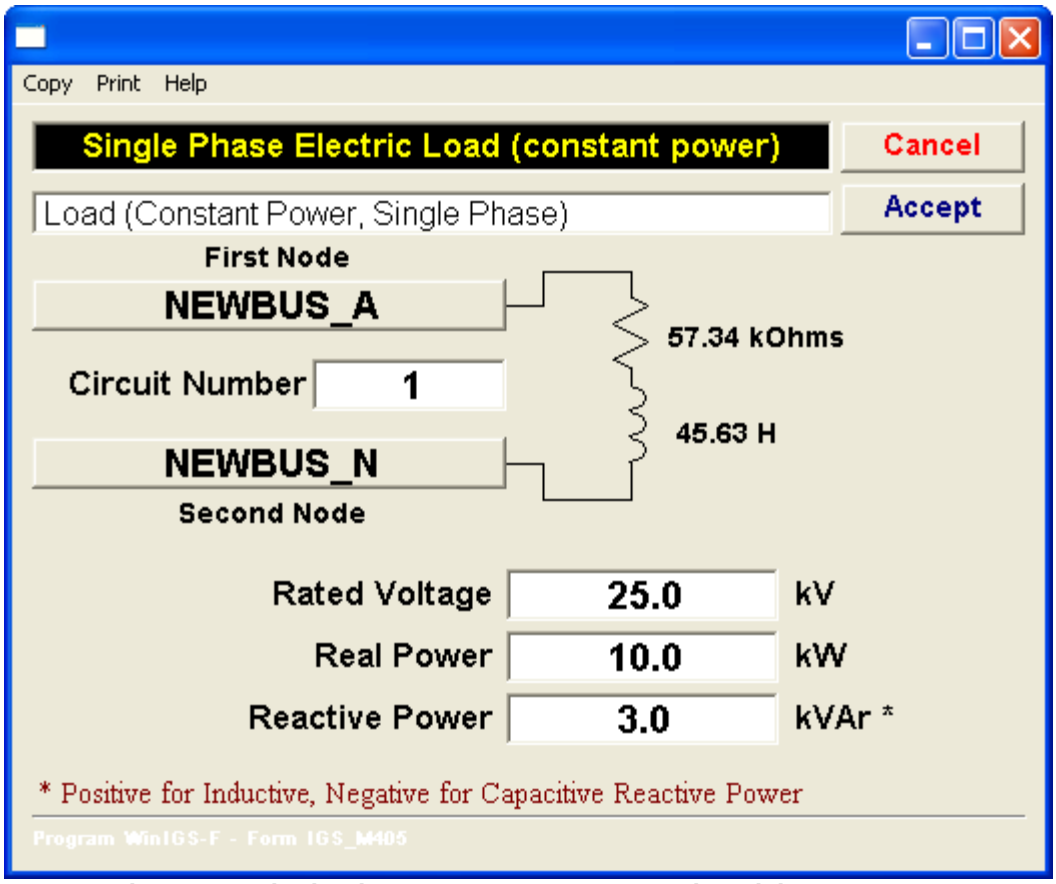


Figure 3.5. Single Phase Constant Power Load Model Parameters.

The compact model is based on the fact that the complex power absorbed by the load is the product of the voltage phasor times the conjugate of the current phasor:

$$\begin{aligned} \tilde{S} &= P + jQ = \tilde{V}_L \cdot \tilde{I}_L^* = (\tilde{V}_1 - \tilde{V}_2) \cdot \tilde{I}_1^* \\ P &= \mathrm{Re}\{\tilde{S}\} \\ Q &= \mathrm{Im}\{\tilde{S}\} \end{aligned} \qquad (3.14)$$

where $\tilde{V}_L$ is the voltage across the load terminals and $\tilde{I}_L$ the current the load absorbs from the network.
In standard notation the model has the form:

$$\begin{aligned} \tilde{I}_1 &= \tilde{I}_L \\ \tilde{I}_2 &= -\tilde{I}_L \\ 0 &= \mathrm{Re}\{\tilde{V}_1 \tilde{I}_L^*\} - P \\ 0 &= \mathrm{Im}\{\tilde{V}_1 \tilde{I}_L^*\} - Q \end{aligned} \qquad (3.15)$$

Separating real and imaginary parts the model in standard real number form is obtained.

$$
\begin{aligned}
I_{1r} &= I_{Lr} \\
I_{1i} &= I_{Li} \\
I_{2r} &= -I_{Lr} \\
I_{2i} &= -I_{Li} \\
0 &= V_{1r} I_{Lr} + V_{1i} I_{Li} - V_{2r} I_{Lr} - V_{2i} I_{Li} - P \\
0 &= -V_{1r} I_{Li} + V_{1i} I_{Lr} + V_{2r} I_{Li} - V_{2i} I_{Lr} - Q
\end{aligned}
\qquad (3.16)
$$

Dynamic Load Modeling

This section addresses the issue of induction motor modeling and model estimation for power system analysis studies. Load modeling in power systems is of great importance, for both steady-state and dynamic analysis, and has been addressed extensively in literature [13]-[31], [44]. Induction motors constitute the most significant part of industrial load and their performance has a considerable impact on the behavior of a power system [44]. Nevertheless, power system analysis studies usually refrain from explicitly representing induction motor loads, and thus taking their behavior into consideration, especially at the level of transmission systems; constant power or constant impedance load models, or voltage and frequency dependent models are commonly used in such cases providing adequately accurate results in many situation. However, such models fail to capture all the phenomena, especially under highly stressed conditions that deviate significantly from normal operation. Furthermore, this type of modeling is static, suitable only for steady-state analysis and cannot be used for dynamic load modeling.

The work presented in this section describes an induction motor model that can be readily incorporated into the network equations of a power system. Thus the model can be immediately used for steady-state (load flow) analysis for both transmission and distribution systems. The model optionally includes rotor parameters that are speed-dependent and vary depending on the operating point. This allows a unified representation of all motor types and designs including double cage models or deep bar rotor models. Augmentation of the model with appropriate dynamic equations allows its use in quasi-steady state analysis, as well, with practically very little model modification, which enables capturing dynamic events in the system.

One of the main problems with induction motor representation is the unavailability of parameter values to construct accurate models. This is one of the reasons motors are not usually explicitly represented in system studies. The issue of induction motor parameter estimation has been addressed by several researchers [46]–[61]. In many of these cases high accuracy is demanded in the parameter determination, when the problem is viewed from the electric machinery point of view [46]–[53]. However, when load modeling is concerned for power system analysis applications (like load flow analysis, stability analysis, dynamic simulation or power system protection coordination) the level of accuracy needed is considerably less, of the order of 10-15% [54]. Field measurements after specific tests can be used for accurate motor model estimation, however such test

are usually difficult or impossible to perform in actual, operational industrial motors [55]–[56]. Furthermore, performing such tests makes little sense when accuracy requirements are low.

Therefore, several approaches have been presented for induction model identification based on data that can become easily available [54]–[59]. Almost all the approaches formulate the estimation problem as a nonlinear least squares minimization problem that estimates all the unknown parameters simultaneously. This problem is being solved either by traditional mathematical numerical techniques (Newton type) [58]–[61] or by computational intelligence-based techniques (e.g genetic algorithms) [54]–[57]. Numerical techniques are very efficient; however, they are reported not to be very robust and prone to provide suboptimal solutions or no solution at all, depending on the stiffness of the problem and on the initialization of the iterative solution algorithm [54]–[57]. Furthermore, they require good knowledge of the analytical models used [54]–[57]. Due to these drawbacks, computational intelligence techniques have been also applied that require less information on the underlying mathematical model and are more robust, at the expense of large amount of computational time [54]–[57].

This part of the report will also discuss the implementation of an induction motor parameter estimation algorithm that is based on numerical solution techniques [32]-[33]. The algorithm is implemented based on the state of the art nonlinear least squares numerical solution techniques. The proposed algorithm is applied to the described induction motor models and estimates the model rotor parameters using the slip-torque motor characteristic. For the estimation of all the motor equivalent circuit parameters the slip-torque characteristic alone is not enough and the slip-current characteristic or the slip-power factor characteristic can be additionally used, to provide extra information. Such characteristics can be most of the times obtained by the manufacturers. Here the characteristics are assumed to be known as a number of discrete points.

Typically induction motors are represented in power system studies as constant power loads. Although this is a valid representation for steady-state operation under certain conditions, induction motors do not always operate under constant power, especially when large deviations of voltage occur. In reality induction motors in steady-state operate at a point where the electro-mechanical torque of the motor equals the mechanical torque of the electric load. As the voltage at the terminals of the induction motor changes, the operating point will change. Here, we present an induction motor model that can more accurately describe the motor behavior. The model is in quadratic form, that is, it consists of equations that are at most quadratic [31]-[38], and can be readily integrated into the power flow model. In addition, the model can be used to determine the operation of the system at a specific instant of time assuming that the speed of the induction motor is fixed (for example, after a disturbance). The significance of this modeling capability is described with an example illustrated in Figure 3.6 and Figure 3.7. The IEEE 24-bus reliability test system (RTS) is used. Figure 3.6 shows the voltage profile after a line contingency, assuming constant power load representation. Green indicates voltage magnitudes within 5% of the nominal voltage; yellow indicates a voltages deviation of more than 5%, but less than 10% of the nominal voltage; and red indicates a voltage

deviation of more than 10%. Figure 3.7 illustrates the same condition assuming that half of the electric load at each bus has been replaced with induction motor loads. The difference between the two figures (i.e. Figure 3.6 and Figure 3.7) is that the induction motors in Figure 3.7 operate at different slip (or speed) as dictated by the solution – at the solution the electro-magnetic torque equals the mechanical torque of the load. The reactive power absorption of the induction motors is different at different slip values and therefore they affect the voltage profile of the system. This behavior cannot be captured by a simple, static, constant power load model.

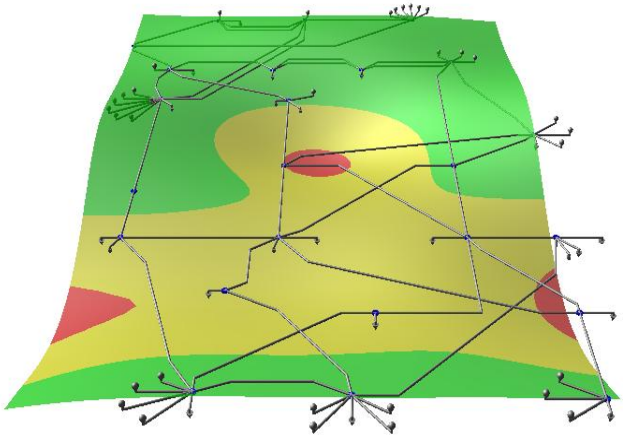


Figure 3.6. Voltage Profile of the 24-bus RTS After a Line Contingency, with Constant Power Load Representation.

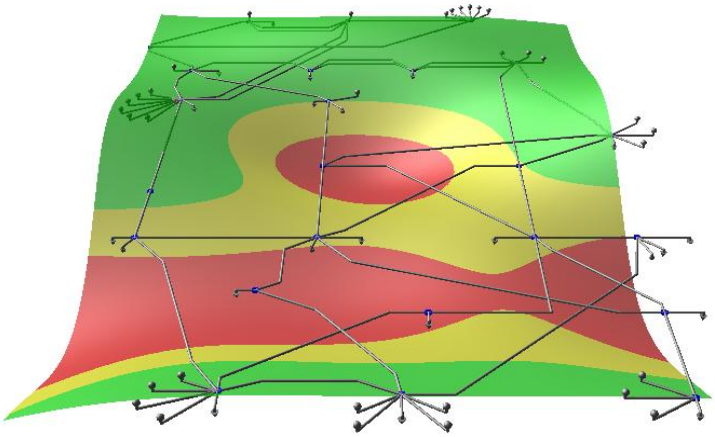


Figure 3.7. Voltage Profile of the 24-bus RTS After a Line Contingency, with Induction Motors Assuming 2% Transient Slowdown.

Quadratized Induction Motor Model

A quadratic, three-phase induction machine model has been developed [32]-[33], [36]-[38], as an extension of a similar single-phase equivalent model [31], [34], [35]. The model is based on the typical steady state sequence circuits of the induction motor, shown in Figure 3.8. Note that induction motors have in general little or no asymmetry, so their representation with sequence networks is valid and accurate. The model input data include typical motor nominal (nameplate) data, plus electrical parameters, and mechanical load data. The user interface of the model is presented in Figure 3.9 and

shows the model implementation details. The model supports two mechanical loading modes: (a) torque equilibrium, and (b) constant slip. In the torque equilibrium mode, the mechanical torque can be either constant, or depend linearly or quadratically on the mechanical speed.

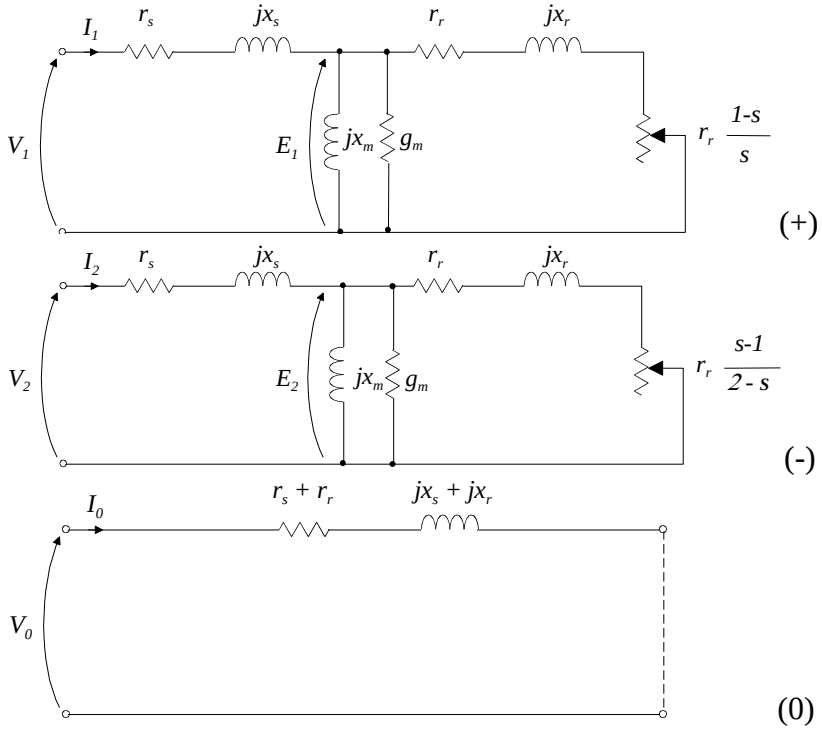


Figure 3.8. Induction Motor Sequence Networks.

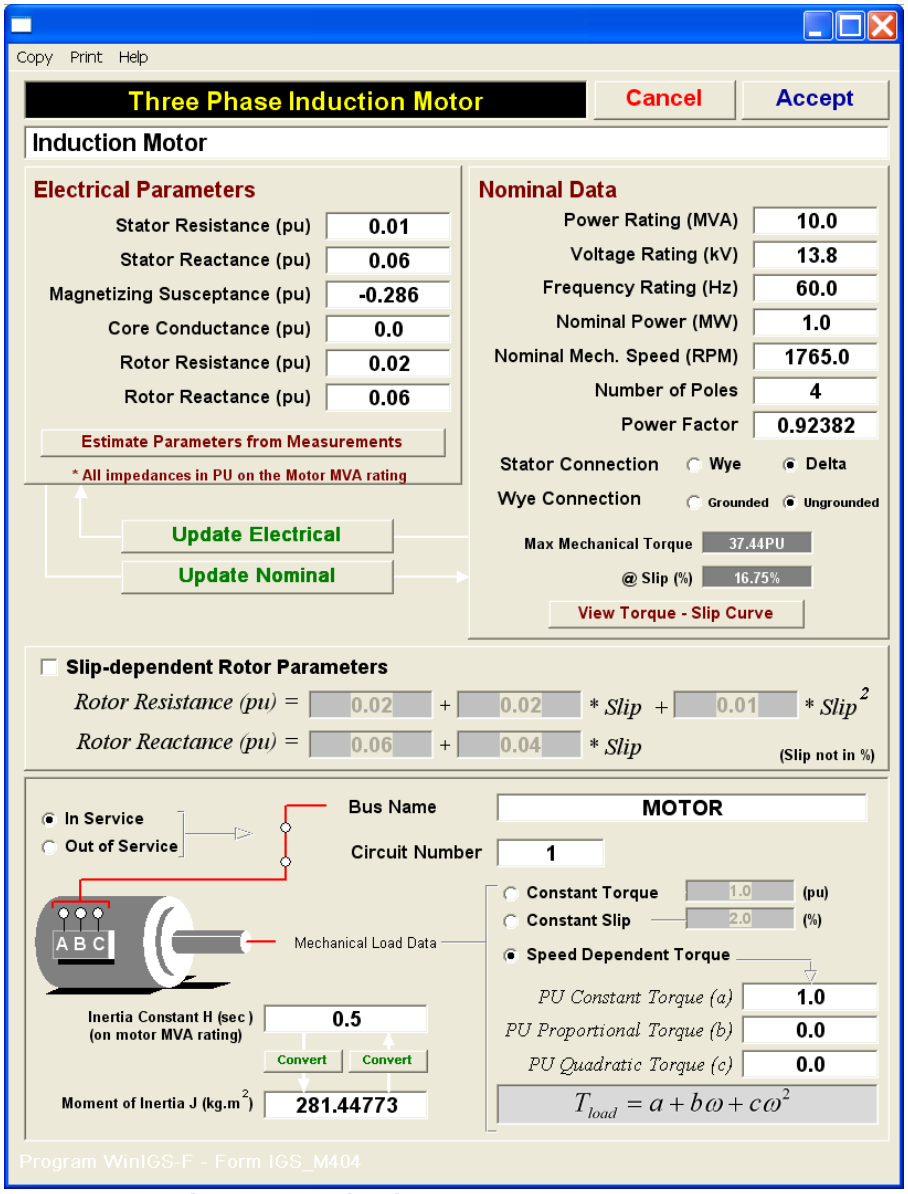


Figure 3.9. Induction Motor Input Data Form.

Slip-dependent Rotor Parameter Model

The model described above is based on the standard equivalent circuit of an induction machine. This model is in general capable of representing a wide variety of motors; however, there are several motor types that cannot be adequately represented, like for example motors with double cage or deep bar rotors. For the representation of such motors a slightly modified equivalent circuit has been used [54], [56], [57]–[59]. Here, a generalized model is proposed that assumes that the rotor parameters are not constant, but depend on the slip the motor is operating at. A quadratic dependence is assumed for the rotor resistance and a linear dependence for the rotor reactance. Therefore, the rotor parameters are:

$$r_r(s) = \alpha + \beta \cdot s + \gamma \cdot s^2$$
$$x_r(s) = \delta + \varepsilon \cdot s \qquad (3.17)$$

where s is the operating slip. These equations are included in the motor model. Note that in the constant slip operating mode the model is not significantly affected, since the slip is know and thus the rotor impedance is simply computed for this slip value. In the constant torque mode, however, the rotor parameters become part of the state vector after the inclusion of equations (3.17). The variation of the rotor parameters is graphically shown in Figure 3.10 and Figure 3.11. The values of the resistance reduce as the speed increases, while the reactance may have some very small variation with speed. In fact the reactance value changes slightly and remains mainly constant, as it is also linearly related to the stator reactance which we assume constant. A similar change could also be assumed for the stator reactance, to make the model more precise.

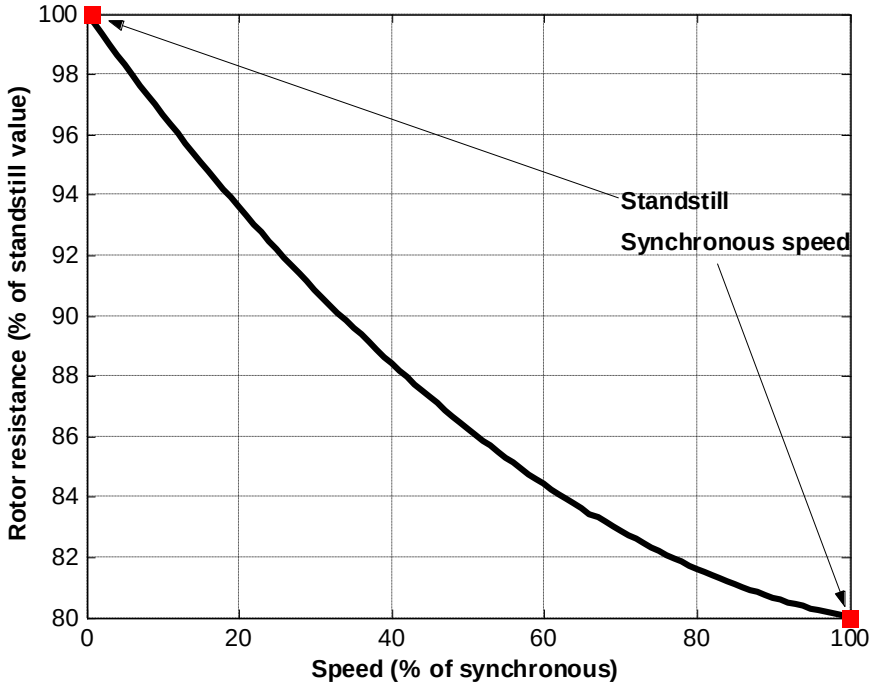


Figure 3.10. Qualitative Representation of Slip-Dependent Rotor Resistance.

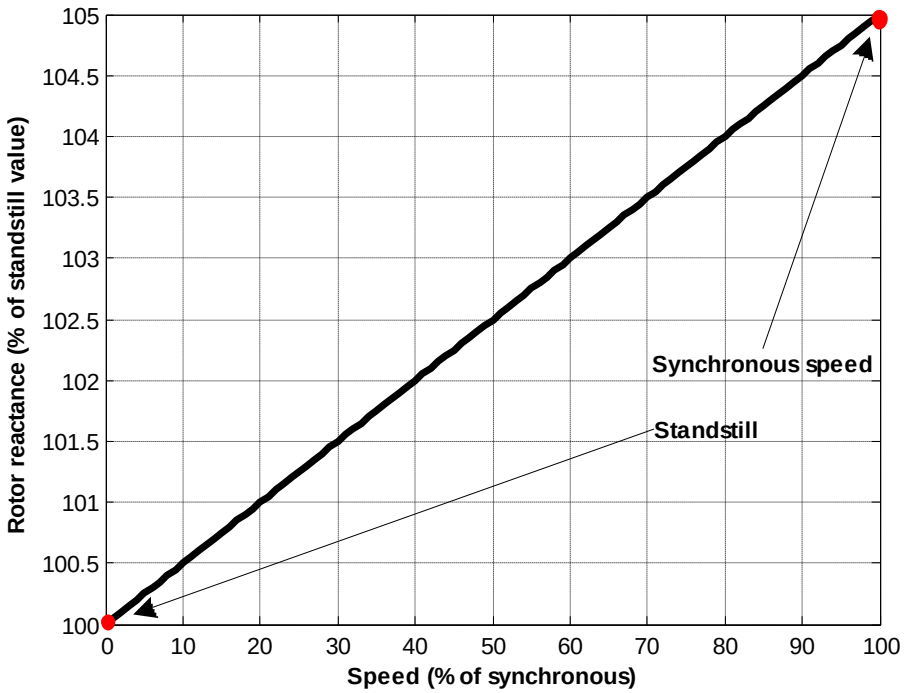


Figure 3.11. Qualitative Representation of Slip-Dependent Rotor Reactance.

A model with slip dependent rotor parameters can adequately represent, in a unified way, motors of every type and every NEMA design (A, B, C or D), including motors with double cage, or deep bar rotors. Figure 3.12 shows the slip-torque characteristics of four main NEMA motor designs. Designs A and D can be accurately represented using constant parameter models; for designs B and C the slip-depended model is used for more realistic representation.

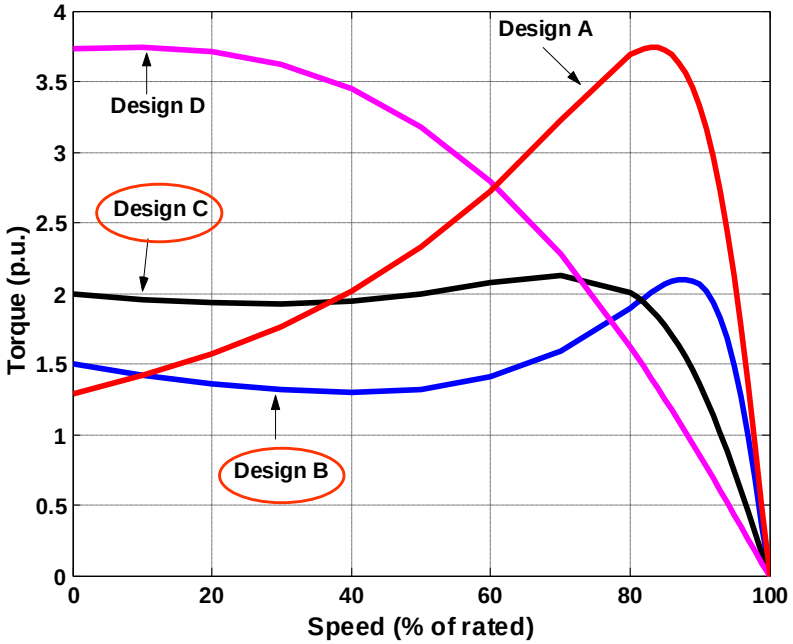


Figure 3.12. NEMA Designs for AC Induction Motors: Designs B and C Cannot Be Accurately Represented using the Classical Equivalent Circuit.

Circuit analysis yields the following equations:

$$
\begin{aligned}
&\tilde{I}_{abc} = T^{-1}\tilde{I}_{120} \\
&0 = \tilde{V}_{abc} - T^{-1}\tilde{V}_{120} \\
&0 = \tilde{I}_1 + (g_s + jb_s)(\tilde{E}_1 - \tilde{V}_1) \\
&0 = \tilde{I}_2 + (g_s + jb_s)(\tilde{E}_2 - \tilde{V}_2) \\
&0 = \tilde{I}_0 - (g_0 + jb_0)\tilde{V}_0 \\
&0 = (g_m + jb_m)\tilde{E}_1 + \tilde{E}_1 \frac{s}{r_r + jx_r s} - (g_s + jb_s)(\tilde{V}_1 - \tilde{E}_1) \\
&0 = (g_m + jb_m)\tilde{E}_2 + \tilde{E}_2 \frac{2-s}{r_r + jx_r(2-s)} - (g_s + jb_s)(\tilde{V}_2 - \tilde{E}_2)
\end{aligned}
\qquad (3.18)
$$

where:

$$T^{-1} = \begin{bmatrix} 1 & 1 & 1 \\ e^{j240^0} & e^{j120^0} & 1 \\ e^{j120^0} & e^{j240^0} & 1 \end{bmatrix}, \text{ with } e^{j\theta} = \cos\theta + j\sin\theta,$$

$$g_s + jb_s = \frac{1}{r_s + jx_s},$$

$$g_m + jb_m = \frac{1}{r_m + jx_m},$$

$$g_0 + jb_0 = \frac{1}{r_s + r_r + jx_s + jx_r} \qquad \text{for grounded Y, and 0 otherwise.}$$

An additional equation links the electrical state variables to the mechanical torque. This equation is derived by equating the mechanical power (torque times mechanical frequency) to the power consumed by the variable resistors in the positive and negative circuits of Figure 3.8.

$$0 = \left|\frac{\tilde{E}_1}{r_r + jx_r s}\right|^2 sr_r - \left|\frac{\tilde{E}_2}{r_r + jx_r(2-s)}\right|^2 (2-s)r_r - T_{em}\omega_s \qquad (3.19)$$

where:

s_n : induction machine slip,
T_{em} : electromechanical motor torque (=mechanical load torque in steady state),
ω_s : synchronous mechanical speed.

Two operating mode, for steady state operation are defined from the above equations:

(a) Constant Slip Model (Linear):

$$
\begin{aligned}
&\tilde{I}_{abc} = T^{-1}\tilde{I}_{120} \\
&0 = \tilde{V}_{abc} - T^{-1}\tilde{V}_{120} \\
&0 = \tilde{I}_1 + (g_s + jb_s)(\tilde{E}_1 - \tilde{V}_1) \\
&0 = \tilde{I}_2 + (g_s + jb_s)(\tilde{E}_2 - \tilde{V}_2) \\
&0 = \tilde{I}_0 - (g_0 + jb_0)\tilde{V}_0 \\
&0 = (g_m + jb_m)\tilde{E}_1 + \tilde{E}_1 \frac{s}{r_r + jx_r s} - (g_s + jb_s)(\tilde{V}_1 - \tilde{E}_1) \\
&0 = (g_m + jb_m)\tilde{E}_2 + \tilde{E}_2 \frac{2-s}{r_r + jx_r(2-s)} - (g_s + jb_s)(\tilde{V}_2 - \tilde{E}_2)
\end{aligned}
\qquad (3.20)
$$

In the constant slip mode the motor operates at constant speed. The value of the slip is known from the operating speed and therefore the model is linear. If a neutral exists at the stator side (wye connection) the neutral voltage, $\tilde{V}_n$, is added as state, along with the equation $\tilde{I}_n = \tilde{I}_A + \tilde{I}_B + \tilde{I}_C = 3\tilde{I}_0$.

(b) Torque Equilibrium Model (Nonlinear-Quadratic):

$$
\begin{aligned}
&\tilde{I}_{abc} = T^{-1}\tilde{I}_{120} \\
&0 = \tilde{V}_{abc} - T^{-1}\tilde{V}_{120} \\
&0 = \tilde{I}_1 + (g_s + jb_s)(\tilde{E}_1 - \tilde{V}_1) \\
&0 = \tilde{I}_2 + (g_s + jb_s)(\tilde{E}_2 - \tilde{V}_2) \\
&0 = \tilde{I}_0 - (g_0 + jb_0)\tilde{V}_0 \\
&0 = -T_{em}\omega_s + U_1 s r_r - U_2(2-s)r_r \\
&0 = -(g_s + jb_s)\tilde{V}_1 + (g_s + g_m + j(b_s + b_m))\tilde{E}_1 + \tilde{W}_1 s \\
&0 = -(g_s + jb_s)\tilde{V}_2 + (g_s + g_m + j(b_s + b_m))\tilde{E}_2 + \tilde{W}_2(2-s) \\
&0 = r_r\tilde{Y}_1 + jx_r s\tilde{Y}_1 - 1 \\
&0 = r_r\tilde{Y}_2 + jx_r(2-s)\tilde{Y}_2 - 1 \\
&0 = \tilde{W}_1 - \tilde{Y}_1\tilde{E}_1 \\
&0 = \tilde{W}_2 - \tilde{Y}_2\tilde{E}_2 \\
&0 = \tilde{W}_1\tilde{W}_1^{*} - U_1 \\
&0 = \tilde{W}_2\tilde{W}_2^{*} - U_2
\end{aligned}
\qquad (3.21)
$$

If the mechanical torque is not constant, but depends on the speed (slip), equation (3.22) is also added creating a more general model.

$$0 = T_m - a - b\omega_s - c\omega_s{}^2 + (b\omega_s + 2\omega_s{}^2)s - \omega_s{}^2 s^2 \qquad (3.22)$$

In the torque equilibrium model the motor electromechanical torque T_{em} is equal to the mechanical load torque, T_m. The slip is not a known constant and thus it becomes part of the state vector. Note that this model is nonlinear. Note also that the state vector and the equations are given in compact complex format. They are to be expanded in real and imaginary parts to get the actual real form of the model. Note also that the last equation is real. As in the previous mode, if a neutral exists at the stator side (wye-connection) the neutral voltage, $\tilde{V}_n$, is added as state, along with the equation $\tilde{I}_n = \tilde{I}_A + \tilde{I}_B + \tilde{I}_C = 3\tilde{I}_0$.

Dynamic Motor Representation

In order to capture the essential dynamic behavior of induction motor loads the model described in the previous section is augmented by the dynamical equation (3.23) describing the rotor motion:

$$J \cdot \frac{d\omega_m}{dt} = T_{em} - T_m, \qquad (3.23)$$

where

J : rotor-load moment of inertia,

ω_m : rotor mechanical speed,

T_{em} : electrical motor torque,

T_m : mechanical load torque,

and equation (3.24) relating the speed and slip:

$$0 = \omega_n - s_n\omega_s - \omega_s. \qquad (3.24)$$

This simplified transient model can capture the effects of the motor in the voltage profile of the power system. The electrical transients in the motor are neglected, as they do not have significant effect in the network solution, especially for the time scales of interest, which are very long compared to the time scales of the electrical transients. Phasor representation is therefore used for the electrical quantities. The elimination of stator electrical transients makes it possible to interface the motor with the network that is assumed to operate in quasi steady state conditions.

Motor Parameter Estimation

Problem Formulation

The estimation methodology makes use of data that, in general, can become available from the motor manufacturer, or are easily measured, like the slip-torque characteristic, or the slip-current or slip-power factor characteristics. A parameter estimation procedure becomes even more important, when a slip-dependent parameter model is used. In this case, the model coefficients of equations (3.17) are difficult of impossible to be evaluated without the use of an estimation procedure.

When the rotor circuit parameters are to be estimated, assuming that the stator and core parameters are known, the slip-torque characteristic of the motor provides adequate information. However, when all the equivalent circuit parameters are to be estimated (6 in total if constant rotor parameters are assumed and 9 if slip-dependent rotor parameters are used), the slip-torque characteristic itself is not enough and some additional information is necessary. Such information can be provided using, for example, the slip-current characteristic of the motor along with the slip-torque curve. In this paper the estimation problem will be formulated in its general form, assuming that all the equivalent circuit parameters are to be estimated.

The parameters estimation problem can be formulated as a least squares optimization problem, the objective being the minimization of the deviation between the measured torque and current curves and the model generated curves, as illustrated in Figure 3.13. These curves are known as a set of discrete measurement points.

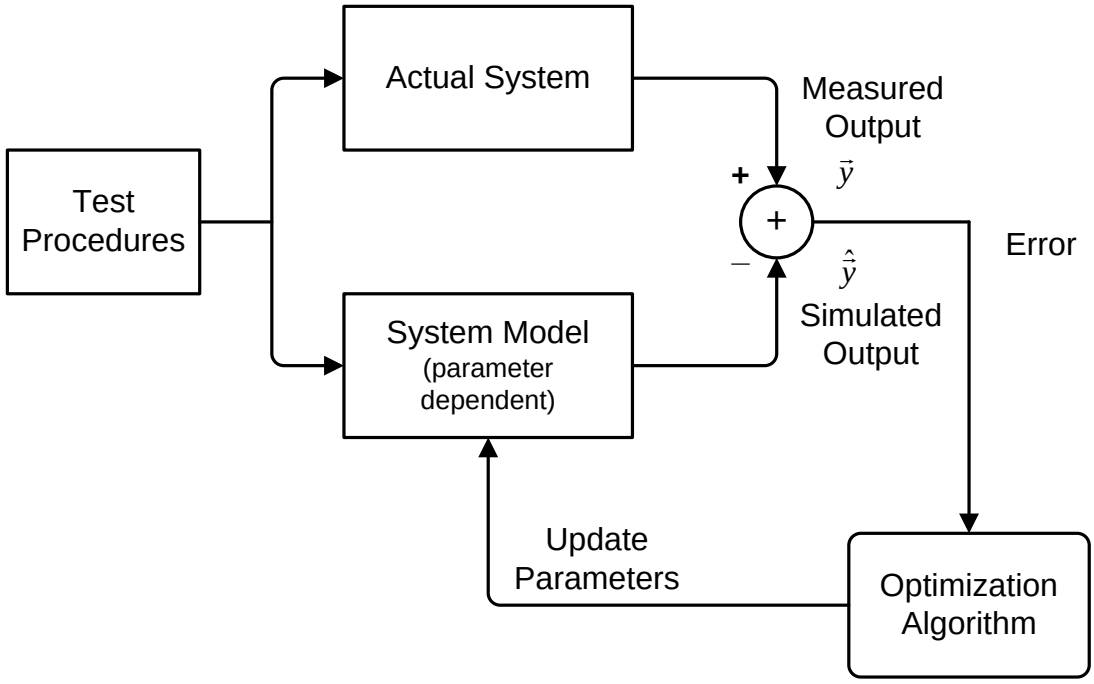


Figure 3.13. Block Diagram of Motor Parameter Estimation Procedure.

The mathematical problem formulation is as follows:

$$\min J = \sum_{i=1}^{m} w_i r_i^2 = r^T W r \tag{3.25}$$

subject to:

$$\begin{aligned}
&\tilde{I} = (g_s + jb_s)\tilde{V} - (g_s + jb_s)\tilde{E} \\
&T_{em} = Usr_r / \omega_s \\
&0 = U - \tilde{W}_n \tilde{W}_n^{\,*} \\
&0 = \tilde{W}_n - \tilde{Y}_n \tilde{E}_n \\
&0 = -(g_1 + jb_1)\tilde{V}_k + (g_1 + j(b_1 + b_m))\tilde{E}_n + \tilde{W}_n s_n \\
&0 = r_2 \tilde{Y}_n + jx_2 s_n \tilde{Y}_n - 1
\end{aligned} \tag{3.26}$$

where

$$r_i = \begin{cases} T_{em,i}(p) - T_{measured,i}, \text{ if } i \text{ is a torque measurement.,} \\ I_i(p) - I_{measured,i}, \text{ if } i \text{ is a current measurement,} \end{cases}$$

w_i : weight of measurement i,

m : total number of measurements,

p : parameter vector.

Equations (3.10) are the single-phase equivalent quadratised equations of the induction motor model. They are derived assuming that the motor is operating under balanced conditions, and thus only the positive sequence network is active. These equations are used in the estimation procedure because the motor curves and thus the measurement data are obtained under nominal operating conditions. Therefore the estimation is performed under nominal conditions.

Solution Methodology

The above optimization problem is a nonlinear least squares minimization problem. The solution of such a problem can be only approximated (no analytical solution exists) using some numerical solution method. The most commonly used approach is the Gauss-Newton method, which is a Newton-type iterative process for the solution of over-determined systems of equations [62]. Application of this method to a least squares optimization problem as the one described above yields the following iterative algorithm:

$$p^{n+1} = p^n - \left(H(p^n)^T \cdot W \cdot H(p^n)\right)^{-1} \cdot H(p^n)^T \cdot W \cdot r(p^n) \tag{3.27}$$

where:

p : parameter vector to be estimated,

r : residual vector with elements as described earlier,

W : weight matrix with elements as described above,

n : iteration index,

H : Jacobian matrix of measurement equations with respect to parameters, i.e. in general, assuming that torque and current measurements are used:

$$H(p^n) = \left[\partial T_{em} / \partial p^T \quad \partial I / \partial p^T\right]^T \Big|_{p=p^n}.$$

The Jacobian matrix can be easily computed based on the model equations (3.26) using the chain rule of differentiation.

As it has been observed in literature [54]–[57], [62] Newton-type numerical methods are very efficient and can provide accurate results provided that a good initial guess of the solution is available. Otherwise, the algorithm may converge to an incorrect solution, or may even diverge, providing no solution at all. To mitigate such problems, to some extent, two global convergence strategies are implemented and are optionally used along with the Gauss-Newton solution procedure. Such strategies guarantee the convergence of the algorithm to a solution irrespectively of the initial guess. Therefore, the implemented algorithm is not prone to divergence. The solution is not guaranteed to be the global optimum, but inclusion of such strategies increases the robustness of the estimation algorithm and the probability of providing the correct solution, even with a less accurate initial estimate.

Two global convergence strategies have been implemented: the line search algorithm and the trust region algorithm. For the trust region algorithm the Levenberg-Marquardt method with locally constrained optimal step has been used [62]. They are employed if the simple Gauss-Newton procedure (without global convergence) fails to provide a solution or a reasonable solution.

The basic idea of the line search method is that the search in the solution space should always proceed at steps that result is a continuous decrease of the objective function (for minimization problems). That is, the objective function should not be allowed to increase at a new estimate, compared to the previous one. The search always follows the Newton direction, as computed by the standard Newton method, but the full Newton step is not taken in it does not result in a decrease in the objective function. Instead a smaller step is taken along the Newton line, until the step size is such that the new estimate results in a lower value of the objective function. This way, the possibility of taking a large Newton step at an early stage of the algorithm that would overshoot the solution and take the search far away from the neighborhood of the solution is eliminated. This is one of the main reasons that may cause divergence of the Newton method and therefore the line search algorithms provides very good results most of the times.

Contrary to the line search algorithm the trust region approach does not limit the search only along the Newton direction. A local quadratic model of the system is constructed at each iteration, and the search direction is defined based on this model. The size of the step is defined based on a computed trust region radius, which is a estimation of the radius of validity of the quadratic model. The locally constrained optimal step approach is used [62]. More details on the specifics of the estimation algorithm and its implementation are outside the scope of this particular paper. Some mathematical background on the underling theory can be found in [62].

The data interface of the parameters estimation procedure is presented in Figure 3.14.

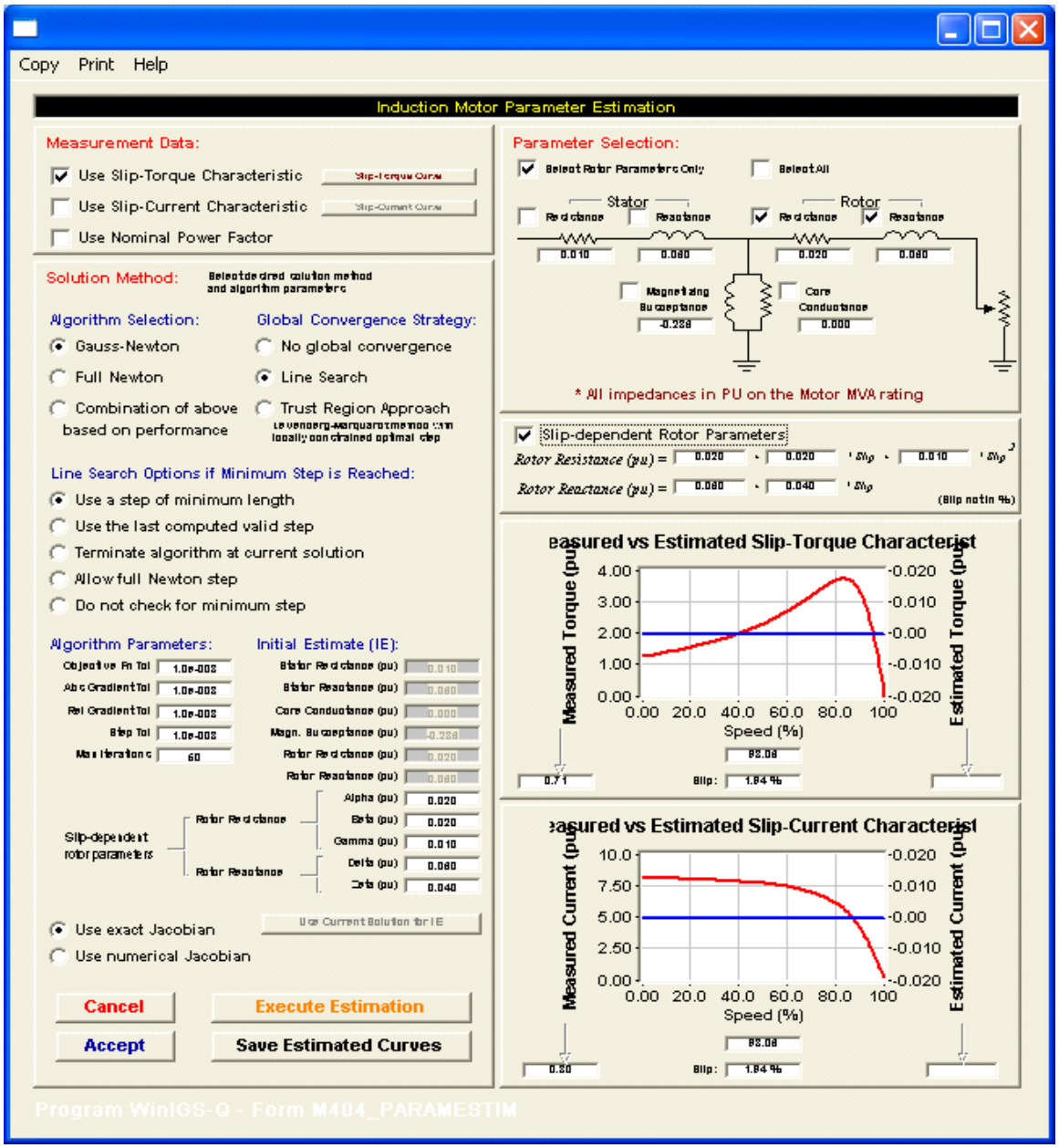


Figure 3.14. Induction Motor Model Parameters Estimation User Interface.

4. Synchronous Generating Unit Model

The dynamics of the generating units, including their control subsystems are of great importance in the study of voltage recovery. Furthermore, the synchronous generator is the main VAR source in power systems, and thus the main control device of voltage phenomena. Therefore, this section is dedicated to describing the model of the generating unit, along with its excitation system and prime mover [44], [63].

Since the synchronous generator is the main device for controlling reactive power, emphasis has been given on the modeling of synchronous generators for both steady-state and dynamic analysis. Three-phase, physically-based, single and two-axis models have been implemented for steady-state analysis. These models are being augmented to include the dynamic characteristics of the synchronous generator. Furthermore, exciter and turbine-governor models are also incorporated. Realistic modeling of the exciter system, as well as the generator and excitation system limit is important for voltage support studies, since they can be used to construct the actual unit capability curves, which may change based on the configuration and operating data of the electric grid where the unit is connected.

Single-Axis Generator Model

Steady-State Model

This section presents the compact steady state model of a single axis synchronous generator. The model includes three control options:

- PQ mode
- PV mode
- Slack bus mode

The generator model includes the following features:

- Real and Reactive Power Limits
- Voltage Control at user specified node
- Reactive Power Allocation Factor
- Quadratic Operating Cost model
- Failure/Repair Rate Model
- Impedance

The device equivalent circuit is as follows:

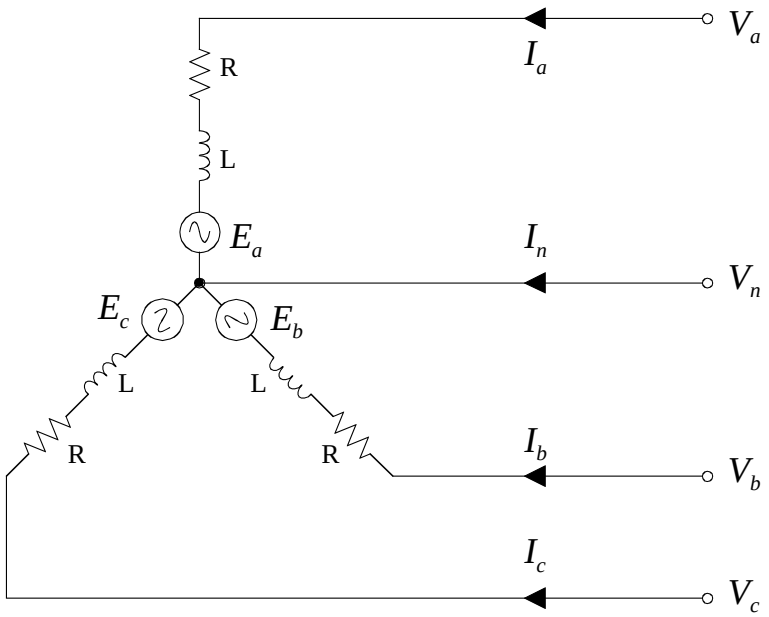


Figure 4.1. Equivalent Circuit of Single Axis Synchronous Generator Model.

The internal sources provide a set of balanced three phase voltages, described with the state variables $E,\ \delta$. The model equations for each control mode are described next. The state vector is: $x = \left[V_{ar} \quad V_{ai} \quad V_{br} \quad V_{bi} \quad V_{cr} \quad V_{ci} \quad V_{nr} \quad V_{ni} \quad E_r \quad E_i\right]$.

PQ Control Mode – Compact Form

The PQ control mode forces the real and reactive power output of the generator to the user specified values P and Q. The model equations are as follows:

$$\begin{aligned}
\tilde{I}_a &= (g + jb)(\tilde{V}_a - \tilde{V}_n - \tilde{E}_a) \\
\tilde{I}_b &= (g + jb)(\tilde{V}_b - \tilde{V}_n - \tilde{E}_b) \\
\tilde{I}_c &= (g + jb)(\tilde{V}_c - \tilde{V}_n - \tilde{E}_c) \\
\tilde{I}_n &= (g + jb)(-\tilde{V}_a - \tilde{V}_b - \tilde{V}_c + 3\tilde{V}_n) \\
\mathrm{Re}\left\{\tilde{V}_a \tilde{I}_a^* + \tilde{V}_b \tilde{I}_b^* + \tilde{V}_c \tilde{I}_c^*\right\} &= -P_{specified} \\
\mathrm{Im}\left\{\tilde{V}_a \tilde{I}_a^* + \tilde{V}_b \tilde{I}_b^* + \tilde{V}_c \tilde{I}_c^*\right\} &= -Q_{specified}
\end{aligned} \tag{4.1}$$

where:

$$g = -\frac{R}{R^2 + \omega^2 L^2}$$

$$b = -\frac{\omega L}{R^2 + \omega^2 L^2}$$

and:

$$\tilde{E}_a = Ee^{j\delta}$$

$$\tilde{\tilde{E}}_b = Ee^{j(\delta - \frac{2\pi}{3})}$$

$$\tilde{\tilde{E}}_c = Ee^{j(\delta - \frac{4\pi}{3})}$$

The above equations, cast in compact matrix form, are as follows:

$$\begin{bmatrix} I_a \\ I_b \\ I_c \\ I_n \end{bmatrix} = \begin{bmatrix} y & 0 & 0 & -y & -y \\ 0 & y & 0 & -y & -ye^{-j2\pi/3} \\ 0 & 0 & y & -y & -ye^{-j4\pi/3} \\ -y & -y & -y & 3y & 0 \end{bmatrix} \cdot \begin{bmatrix} V_a \\ V_b \\ V_c \\ V_n \\ E \end{bmatrix} \qquad (4.2)$$

$$0 = \mathrm{Re}\left\{\tilde{\tilde{V}}_a \tilde{\tilde{I}}_a^* + \tilde{\tilde{V}}_b \tilde{\tilde{I}}_b^* + \tilde{\tilde{V}}_c \tilde{\tilde{I}}_c^*\right\} + P_{specified}$$

$$0 = \mathrm{Im}\left\{\tilde{\tilde{V}}_a \tilde{\tilde{I}}_a^* + \tilde{\tilde{V}}_b \tilde{\tilde{I}}_b^* + \tilde{\tilde{V}}_c \tilde{\tilde{I}}_c^*\right\} + Q_{specified}$$

PV Control Mode – Compact Form

The PV control mode forces the real power output to the user specified value of P, and the line to line voltage (phases A, B) to the user specified value . The model equations are as follows:

$$\tilde{\tilde{I}}_a = (g + jb)(\tilde{\tilde{V}}_a - \tilde{\tilde{V}}_n - \tilde{\tilde{E}}_a)$$

$$\tilde{\tilde{I}}_b = (g + jb)(\tilde{\tilde{V}}_b - \tilde{\tilde{V}}_n - \tilde{\tilde{E}}_b)$$

$$\tilde{\tilde{I}}_c = (g + jb)(\tilde{\tilde{V}}_c - \tilde{\tilde{V}}_n - \tilde{\tilde{E}}_c) \qquad (4.3)$$

$$\tilde{\tilde{I}}_n = (g + jb)(-\tilde{\tilde{V}}_a - \tilde{\tilde{V}}_b - \tilde{\tilde{V}}_c + 3\tilde{\tilde{V}}_n)$$

$$\mathrm{Re}\left\{\tilde{\tilde{V}}_a \tilde{\tilde{I}}_a^* + \tilde{\tilde{V}}_b \tilde{\tilde{I}}_b^* + \tilde{\tilde{V}}_c \tilde{\tilde{I}}_c^*\right\} = -P_{specified}$$

$$\left|\tilde{\tilde{V}}_a - \tilde{\tilde{V}}_b\right| = V_{specified}$$

where:

$$g = -\frac{R}{R^2 + \omega^2 L^2}$$

$$b = -\frac{\omega L}{R^2 + \omega^2 L^2}$$

and:

$$\tilde{\tilde{E}}_a = Ee^{j\delta}$$

$$\tilde{\tilde{E}}_b = Ee^{j(\delta - \frac{2\pi}{3})}$$

$$\tilde{\tilde{E}}_c = Ee^{j(\delta - \frac{4\pi}{3})}$$

The above equations, cast in compact matrix form, are as follows:

$$\begin{bmatrix} I_a \\ I_b \\ I_c \\ I_n \end{bmatrix} = \begin{bmatrix} y & 0 & 0 & -y & -y \\ 0 & y & 0 & -y & -ye^{-j2\pi/3} \\ 0 & 0 & y & -y & -ye^{-j4\pi/3} \\ -y & -y & -y & 3y & 0 \end{bmatrix} \cdot \begin{bmatrix} V_a \\ V_b \\ V_c \\ V_n \\ E \end{bmatrix} \tag{4.4}$$

$$0 = \mathrm{Re}\left\{\tilde{V}_a \tilde{I}_a^* + \tilde{V}_b \tilde{I}_b^* + \tilde{V}_c \tilde{I}_c^*\right\} + P_{specified}$$

$$\left|\tilde{V}_a - \tilde{V}_b\right| = V_{specified}$$

Slack Bus Control Mode – Compact Form

The slack bus control mode forces the internal source phase angle to zero, and the line to line voltage (phases A, B) to the user specified value. The model equations are as follows:

$$\begin{aligned} \tilde{I}_a &= (g + jb)(\tilde{V}_a - \tilde{V}_n - \tilde{E}_a) \\ \tilde{I}_b &= (g + jb)(\tilde{V}_b - \tilde{V}_n - \tilde{E}_b) \\ \tilde{I}_c &= (g + jb)(\tilde{V}_c - \tilde{V}_n - \tilde{E}_c) \\ \tilde{I}_n &= (g + jb)(-\tilde{V}_a - \tilde{V}_b - \tilde{V}_c + 3\tilde{V}_n) \\ \delta &= 0.0 \\ \left|\tilde{V}_a - \tilde{V}_b\right| &= V_{specified} \end{aligned} \tag{4.5}$$

where:

$$g = -\frac{R}{R^2 + \omega^2 L^2}$$

$$b = -\frac{\omega L}{R^2 + \omega^2 L^2}$$

and:

$$\tilde{E}_a = Ee^{j\delta}$$

$$\tilde{E}_b = Ee^{j(\delta - \frac{2\pi}{3})}$$

$$\tilde{E}_c = Ee^{j(\delta - \frac{4\pi}{3})}$$

The above equations, cast in compact matrix form, are as follows:

$$\begin{bmatrix} I_a \\ I_b \\ I_c \\ I_n \end{bmatrix} = \begin{bmatrix} y & 0 & 0 & -y & -y \\ 0 & y & 0 & -y & -ye^{-j2\pi/3} \\ 0 & 0 & y & -y & -ye^{-j4\pi/3} \\ -y & -y & -y & 3y & 0 \end{bmatrix} \cdot \begin{bmatrix} V_a \\ V_b \\ V_c \\ V_n \\ E \end{bmatrix} \tag{4.6}$$

$$\delta = 0.0$$

$$\left| \tilde{V}_a - \tilde{V}_b \right| = V_{specified}$$

The $P_{specified}$ and $V_{specified}$ values can be either constants, as defined by the user, or be provided by the steady state model of a prime mover and exciter system respectively.

Dynamic Model

The dynamic model is based on a quasi steady state model that assumes that the generator is operating under sinusoidal steady state conditions as far as the electrical system is concerned. Only the rotor mechanical system dynamics are assumed, therefore the steady state equations described in the previous section also hold, with the augmentation of the system with the swing equation of the rotor rotational movement. This equation defines the mechanical rotational speed $\omega(t)$ as well as the internal voltage angle $\delta(t)$ which is now a time varying quantity. The internal voltage magnitude $E(t)$ is specified by the excitation system, or may have constant value. Therefore the model compact equations are as follows:

$$\tilde{I}_a = (g + jb)(\tilde{V}_a - \tilde{V}_n - \tilde{E}_a)$$

$$\tilde{I}_b = (g + jb)(\tilde{V}_b - \tilde{V}_n - \tilde{E}_b)$$

$$\tilde{I}_c = (g + jb)(\tilde{V}_c - \tilde{V}_n - \tilde{E}_c)$$

$$\tilde{I}_n = (g + jb)(-\tilde{V}_a - \tilde{V}_b - \tilde{V}_c + 3\tilde{V}_n)$$

$$\frac{d\delta(t)}{dt} = \omega(t) - \omega_s$$

$$J\frac{d\omega(t)}{dt} = T_m(t) - T_e(t) - D\left(\omega(t) - \omega_s\right) \tag{4.7}$$

$$0 = P_e(t) + \mathrm{Re}\left\{\tilde{E}_a\tilde{I}_a^* + \tilde{E}_b\tilde{I}_b^* + \tilde{E}_c\tilde{I}_c^*\right\}$$

$$0 = T_e(t)\omega(t) - P_e(t)$$

$$0 = E(t) - KE_f(t)$$

where:

$$g = -\frac{R}{R^2 + \omega^2 L^2},$$

$b = -\dfrac{\omega L}{R^2 + \omega^2 L^2}$,

J is the moment of inertia of the generator,

D is a damping coefficient,

ω_s is the synchronous speed, and

K is a constant of proportionality.

Furthermore,

$\tilde{E} = E(t)e^{j\delta(t)} = E(t)\cos\delta(t) + jE(t)\sin\delta(t)$

$\tilde{E}_a = Ee^{j\delta}$

$\tilde{E}_b = Ee^{j(\delta - \frac{2\pi}{3})}$

$\tilde{E}_c = Ee^{j(\delta - \frac{4\pi}{3})}$

The state vector is:

$x = \left[V_{ar} \quad V_{ai} \quad V_{br} \quad V_{bi} \quad V_{cr} \quad V_{ci} \quad V_{nr} \quad V_{ni} \quad \delta(t) \quad \omega(t) \quad P_e(t) \quad T_e(t) \quad E(t)\right]$.

User Interface and Model Parameters

The user interface of the model is presented in Figure 4.2 and Figure 4.3. The user specifies the operation mode, as well as the sequence network parameters of the generator. Limits and nominal voltage and power values are also specified. The program internally computes the equivalent circuit parameters that are used in the analysis. The per unit inertia constant is also specified and used for the quasi steady state model. Additional parameters include reliability and cost data.

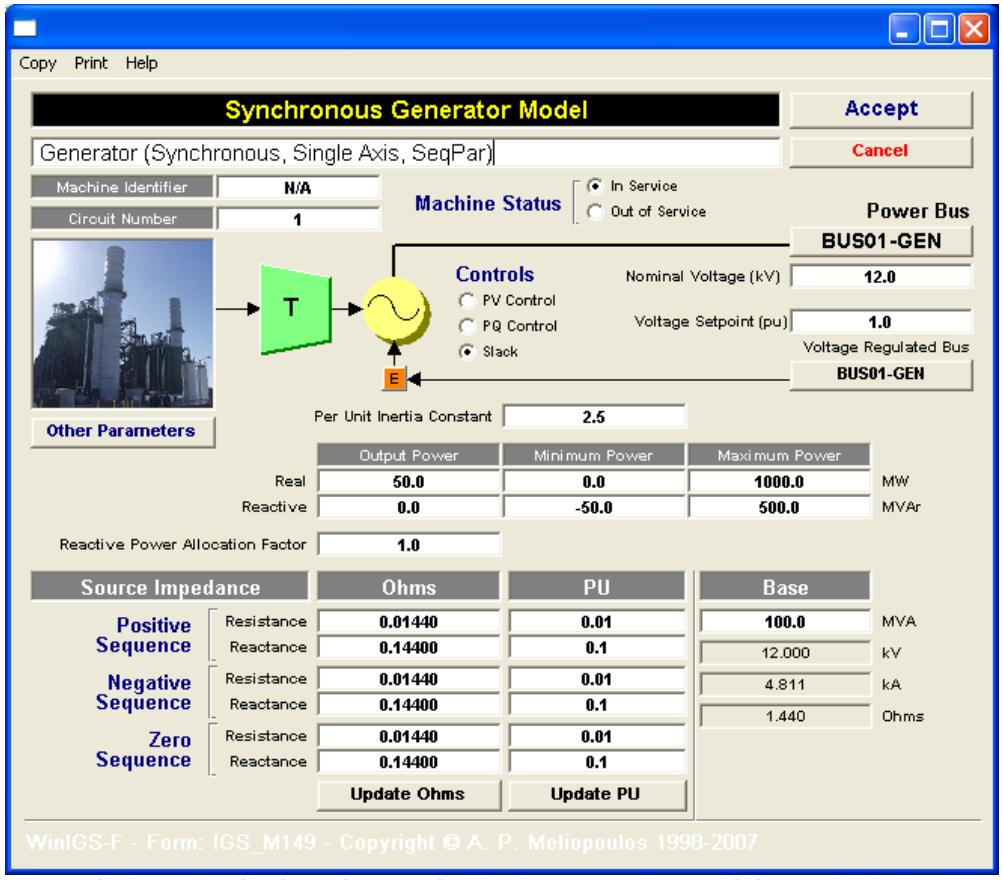


Figure 4.2. Single Axis Synchronous Generator Model Parameters.

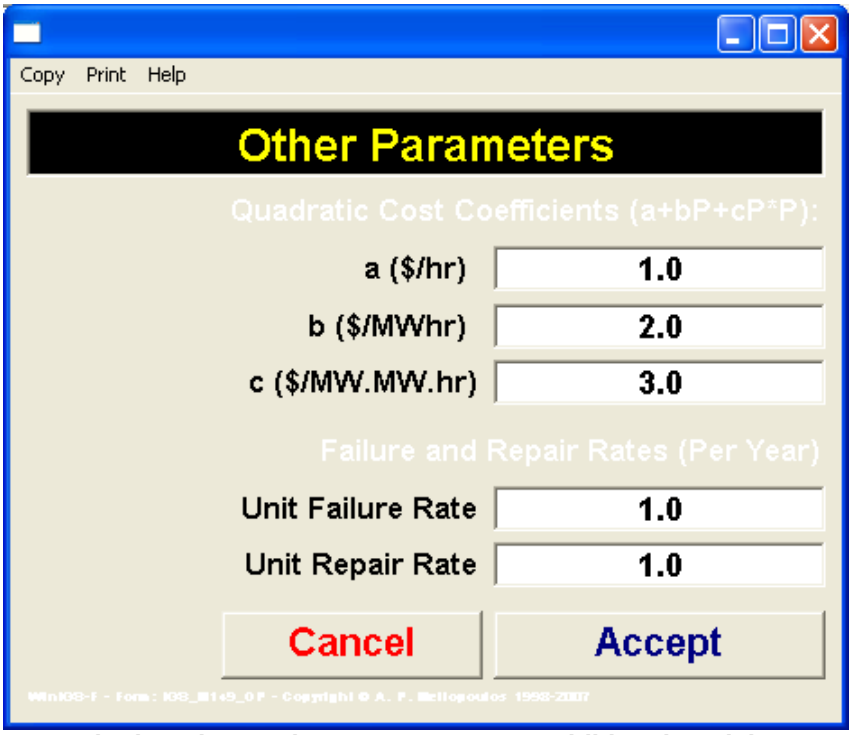


Figure 4.3. Single Axis Synchronous Generator Additional Model Parameters.

Two-Axis Generator Model

A full time-domain transient model of a synchronous generator with damper windings is presented, first [64]. Then the steady state and quasi steady state model is derived from these equations. The current model is based on a linear flux current relation; however, it can be easily extended to include nonlinear effects and harmonics.

Figure 4.4 illustrates the electrical subsystem model of a synchronous machine with two damper windings as a set of mutually coupled circuits.

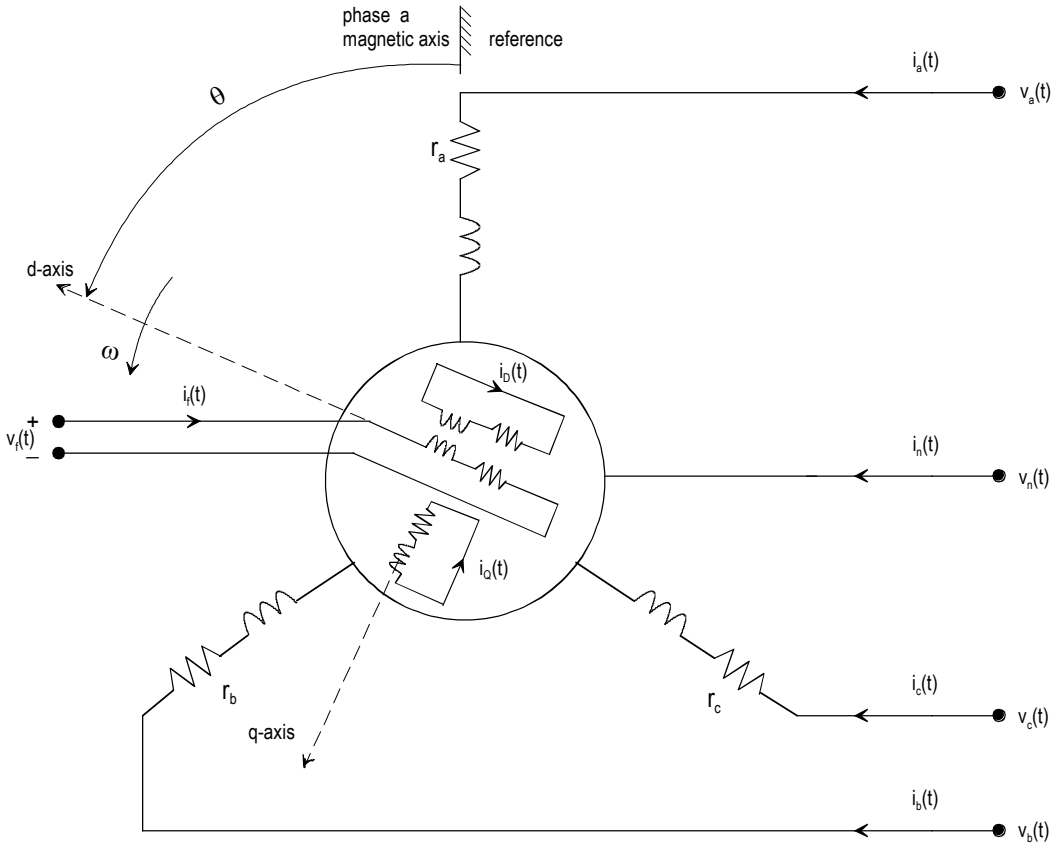


Figure 4.4. Electrical Model of a Synchronous Machine as a Set of Mutually Coupled Windings.

Figure 4.5 illustrates the model of the mechanical subsystem of the synchronous machine, which is a rotating mass subject to a mechanical torque as well as an electromagnetic torque.

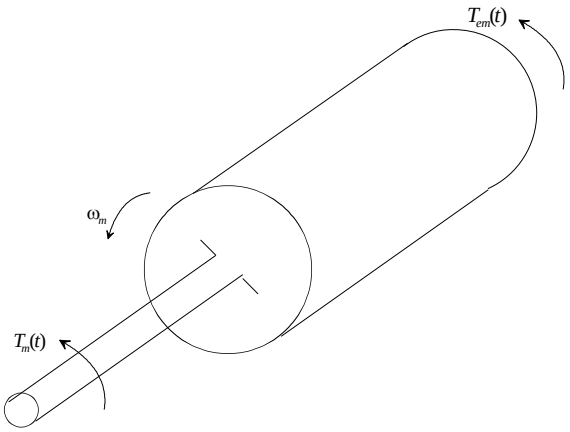


Figure 4.5. Mechanical model of asynchronous machine as a rotating mass.

Electrical System

The dynamic equations of the electrical system of a synchronous machine are derived in this section. The synchronous machine can be viewed as a set of mutually coupled inductors, which interact among themselves to generate electromagnetic torque. Straightforward circuit analysis leads to the derivation of an appropriate mathematical model.

In Figure 4.4, the stator and rotor windings of the synchronous machine are: three phase stator windings, ***a***, ***b***, and ***c***, a field winding, ***f***, and two damper windings ***D***, ***Q*** acting along the ***d***- and ***q***- axes respectively, with ***d***-axis pointing to the positive magnetic axis of the field winding. It is assumed that the phase windings are wye-connected. Note that all inductors are mounted on the same magnetic circuit and thus they are all magnetically coupled. The position of the rotating rotor is denoted with the angle $\theta_m(t)$, which is the position of its positive direct axis with respect to the static phase **a** magnetic axis. We postulate that the position $\theta_m(t)$ is the following function (without loss of generality):

$$\theta_m(t)=\omega_{sm}t+\delta_m(t)+\frac{\pi}{p} \qquad (4.8)$$

where ω_{sm} is the mechanical synchronous speed; p is the number of poles.

We perform the following manipulation. Multiplying equation (4.8) by $\frac{p}{2}$ results in:

$$\frac{p}{2}\theta_m(t)=\frac{p}{2}\omega_{sm}t+\frac{p}{2}\delta_m(t)+\frac{\pi}{2}$$

Define:

$$\theta(t)=\frac{p}{2}\theta_m(t),\ \omega_s=\frac{p}{2}\omega_{sm},\ \delta(t)=\frac{p}{2}\delta_m(t).$$

Then, we have:

$$\theta(t)=\omega_s t+\delta(t)+\frac{\pi}{2} \qquad (4.8a)$$

The quantities $\theta(t)$, ω_s $\delta(t)$ are now referring to electrical quantities, and are the electrical angle, the electrical synchronous angular velocity and the power angle respectively.

Application of Kirchhoff's voltage law and Faraday's Law to the circuit of Figure 1 yields

$$v_{abc}(t) = R_{abc} i_{abc}(t) + \frac{d}{dt}\lambda_{abc}(t) + \Gamma v_n(t) \tag{4.9}$$

$$0 = i_a(t) + i_b(t) + i_c(t) + i_n(t) \tag{4.10}$$

$$v_{fDQ}(t) = R_{fDQ} i_{fDQ}(t) + \frac{d}{dt}\lambda_{fDQ}(t) + \mathrm{E} v_{fn}(t) \tag{4.11}$$

where

$$v_{abc}(t) = \begin{bmatrix} v_a(t) & v_b(t) & v_c(t) \end{bmatrix}^T$$

$$v_{fDQ}(t) = \begin{bmatrix} v_f(t) & v_D(t) & v_Q(t) \end{bmatrix}^T = \begin{bmatrix} v_f(t) & 0 & 0 \end{bmatrix}^T$$

$$i_{abc}(t) = \begin{bmatrix} i_a(t) & i_b(t) & i_c(t) \end{bmatrix}^T$$

$$i_{fDQ}(t) = \begin{bmatrix} i_f(t) & i_D(t) & i_Q(t) \end{bmatrix}^T$$

$$\lambda_{abc}(t) = \begin{bmatrix} \lambda_a(t) & \lambda_b(t) & \lambda_c(t) \end{bmatrix}^T$$

$$\lambda_{fDQ}(t) = \begin{bmatrix} \lambda_f(t) & \lambda_D(t) & \lambda_Q(t) \end{bmatrix}^T$$

$$R_{abc} = diag\begin{pmatrix} r_a & r_b & r_c \end{pmatrix} = diag\begin{pmatrix} r & r & r \end{pmatrix}$$

$$R_{fDQ} = diag\begin{pmatrix} r_f & r_D & r_Q \end{pmatrix}$$

$$\Gamma = \begin{bmatrix} 1 & 1 & 1 \end{bmatrix}^T$$

$$\mathrm{E} = \begin{bmatrix} 1 & 0 & 0 \end{bmatrix}^T$$

$\lambda_{abc}(t)$ is the vector consisting of magnetic flux linkages of phase ***a***, ***b***, and ***c***. $\lambda_{fDQ}(t)$ is the vector consisting of magnetic flux linkages of the field winding ***f***, the ***D***-damper winding, and the ***Q***-damper winding.

In Equations (4.9) and (4.11), the magnetic flux linkages are complex functions of the rotor position and the electric currents flowing in the various windings of the machine. Assuming a linear flux-current relationship, the magnetic flux linkages of the phase *a*, *b*, and *c* windings are:

$$\lambda_a(t) = L_{aa} i_a(t) + L_{ab} i_b(t) + L_{ac} i_c(t) + L_{af} i_f(t) + L_{aD} i_D(t) + L_{aQ} i_Q(t)$$

$$\lambda_b(t) = L_{ba} i_a(t) + L_{bb} i_b(t) + L_{bc} i_c(t) + L_{bf} i_f(t) + L_{bD} i_D(t) + L_{bQ} i_Q(t)$$

$$\lambda_c(t) = L_{ca} i_a(t) + L_{cb} i_b(t) + L_{cc} i_c(t) + L_{cf} i_f(t) + L_{cD} i_D(t) + L_{cQ} i_Q(t)$$

$$\lambda_f(t) = L_{fa} i_a(t) + L_{fb} i_b(t) + L_{fc} i_c(t) + L_{ff} i_f(t) + L_{fD} i_D(t) + L_{fQ} i_Q(t)$$

$$\lambda_D(t) = L_{Da} i_a(t) + L_{Db} i_b(t) + L_{Dc} i_c(t) + L_{Df} i_f(t) + L_{DD} i_D(t) + L_{DQ} i_Q(t)$$

$$\lambda_Q(t) = L_{Qa} i_a(t) + L_{Qb} i_b(t) + L_{Qc} i_c(t) + L_{Qf} i_f(t) + L_{QD} i_D + L_{QQ} i_Q(t)$$

The notation in above equations is obvious. L_{ii} is the self-inductance of winding *i*, while L_{ij} $(i \neq j)$ is the mutual inductance between windings *i* and *j*. Many of the inductances in

above equations are dependent on the position of the rotor, which is time varying. Thus these inductances are time dependent. We can apply the same procedure to the rotor windings, which results in the following matrix notation:

$$\begin{bmatrix} \lambda_{abc}(t) \\ \lambda_{fDQ}(t) \end{bmatrix} = \begin{bmatrix} L_{ss}(\theta(t)) & L_{sr}(\theta(t)) \\ L_{rs}(\theta(t)) & L_{rr} \end{bmatrix} \begin{bmatrix} i_{abc}(t) \\ i_{fDQ}(t) \end{bmatrix} \tag{4.12}$$

where

$$L_{ss}(\theta(t)) = \begin{bmatrix} L_{aa}(\theta(t)) & L_{ab}(\theta(t)) & L_{ac}(\theta(t)) \\ L_{ab}(\theta(t)) & L_{bb}(\theta(t)) & L_{bc}(\theta(t)) \\ L_{ac}(\theta(t)) & L_{bc}(\theta(t)) & L_{cc}(\theta(t)) \end{bmatrix}$$

$$L_{sr}(\theta(t)) = \begin{bmatrix} L_{af}(\theta(t)) & L_{aD}(\theta(t)) & L_{aQ}(\theta(t)) \\ L_{bf}(\theta(t)) & L_{bD}(\theta(t)) & L_{bQ}(\theta(t)) \\ L_{cf}(\theta(t)) & L_{cD}(\theta(t)) & L_{cQ}(\theta(t)) \end{bmatrix}$$

$$L_{rs}(\theta(t)) = L_{sr}^{T}(\theta(t))$$

$$L_{rr} = \begin{bmatrix} L_{ff} & L_{fD} & L_{fQ} \\ L_{fD} & L_{DD} & L_{DQ} \\ L_{fQ} & L_{DQ} & L_{QQ} \end{bmatrix}$$

Detailed description of the above inductances is as follows:

Stator Self-Inductances

Stator self-inductances, L_{aa}, L_{bb}, and L_{cc}, in general depend on rotor position. An approximate expression of this dependence is:

$$L_{aa}(t) = L_s + L_m \cos(2\theta(t))$$

$$L_{bb}(t) = L_s + L_m \cos\left(2\theta(t) - 2\pi/3\right)$$

$$L_{cc}(t) = L_s + L_m \cos\left(2\theta(t) + 2\pi/3\right)$$

where L_s is the self-inductance due to space-fundamental air-gap flux and the armature leakage flux; the additional component that varies with 2θ is due to the rotor saliency. A typical variation of L_{ii} is shown in Figure 4.6.

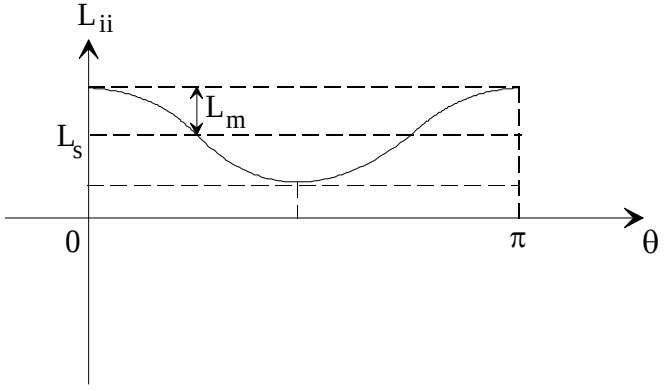


Figure 4.6. Stator Self-Inductance as a Function of θ.

Rotor Self-Inductances

Rotor self-inductances, L_{ff}, L_{DD}, and L_{QQ}, are approximately constants and can be symbolized with

$$L_{ff} = L_f \qquad L_{DD} = L_D \qquad L_{QQ} = L_Q$$

Stator Mutual Inductances

Stator mutual inductances, L_{ab}, L_{bc}, and L_{ca}, are negative. They are functions of the rotor position $\theta(t)$. Approximate expressions for these functions are:

$$L_{ab}(t) = L_{ba}(t) = -M_S - L_m \cos 2\left(\theta(t) + \pi/6\right) = -M_S - L_m \cos\left(2\theta(t) + \pi/3\right)$$
$$L_{bc}(t) = L_{cb}(t) = -M_S - L_m \cos 2\left(\theta(t) - \pi/2\right) = -M_S - L_m \cos\left(2\theta(t) - \pi\right)$$
$$L_{ca}(t) = L_{ac}(t) = -M_S - L_m \cos 2\left(\theta(t) - 7\pi/6\right) = -M_S - L_m \cos\left(2\theta(t) - \pi/3\right)$$

A typical variation of L_{ij} is shown in Figure 4.7.

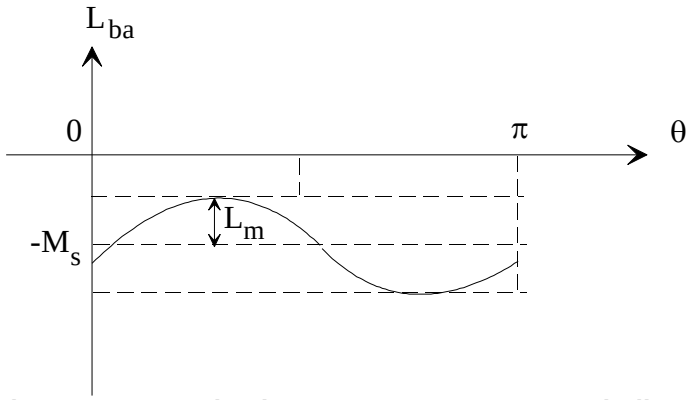


Figure 4.7. Mutual Inductance Between Stator Windings.

Rotor Mutual Inductances

Rotor mutual inductances, L_{fD}, L_{DQ}, and L_{Qf}, are constants and independent of $\theta(t)$, because the rotor windings are stationary with one another.

$$L_{fD} = L_{Df} = M_R \qquad L_{DQ} = L_{QD} = 0 \;\; L_{Qf} = L_{fQ} = 0$$

Mutual Inductances between Stator and rotor

Mutual inductances between stator's windings and rotor's, L_{af}, L_{bf}, and L_{cf}, are dependent upon the rotor position $\theta(t)$ as follows:

$$L_{af}(t) = L_{fa}(t) = M_F \cos\theta(t)$$

$$L_{bf}(t) = L_{fb}(t) = M_F \cos\left(\theta(t) - 2\pi/3\right)$$
$$L_{cf}(t) = L_{fc}(t) = M_F \cos\left(\theta(t) - 4\pi/3\right) = M_F \cos\left(\theta(t) + 2\pi/3\right)$$

Similarly

$$L_{aD}(t) = L_{Da}(t) = M_D \cos\theta(t)$$
$$L_{bD}(t) = L_{Db}(t) = M_D \cos\left(\theta(t) - 2\pi/3\right)$$
$$L_{cD}(t) = L_{Dc}(t) = M_D \cos\left(\theta(t) - 4\pi/3\right) = M_D \cos\left(\theta(t) + 2\pi/3\right)$$

The damper winding ***Q*** is orthogonal to the ***D*** winding. According to our definition of rotor d-axis and q-axis, we have:

$$L_{aQ}(t) = L_{Qa}(t) = M_Q \cos\left(\theta(t) - \pi/2\right) = M_Q \sin\theta(t)$$
$$L_{bQ}(t) = L_{Qb}(t) = M_Q \cos\left(\theta(t) - \pi/2 - 2\pi/3\right) = M_Q \sin\left(\theta(t) - 2\pi/3\right)$$
$$L_{cQ}(t) = L_{Qc}(t) = M_Q \cos(\theta(t) - \pi/2 - 4\pi/3) = M_Q \sin(\theta(t) - 4\pi/3) = M_Q \sin(\theta(t) + 2\pi/3)$$

Actually the inductances are perturbed from sinusoidal variation with harmonics. Generally speaking, these harmonics are kept low with the use of distributed coils, double layers and fractional pitch. The inclusion and effect of harmonics can be included in the above formulation. In the current model, however, these phenomena are omitted.

We can see that the inductance matrix in equation (4.12) is time dependent and nonlinear because many inductances are trigonometric functions of $\theta(t)$.

In summary the model of the electrical subsystem of the synchronous machine is

$$v_{abc}(t) = R_{abc} i_{abc}(t) + \frac{d}{dt}\lambda_{abc}(t) + \Gamma v_n(t) \tag{4.9}$$
$$0 = i_a(t) + i_b(t) + i_c(t) + i_n(t) \tag{4.10}$$
$$v_{fDQ}(t) = R_{fDQ} i_{fDQ}(t) + \frac{d}{dt}\lambda_{fDQ}(t) \tag{4.11}$$
$$\begin{bmatrix} \lambda_{abc}(t) \\ \lambda_{fDQ}(t) \end{bmatrix} = \begin{bmatrix} L_{ss}(\theta(t)) & L_{sr}(\theta(t)) \\ L_{rs}(\theta(t)) & L_{rr} \end{bmatrix} \begin{bmatrix} i_{abc}(t) \\ i_{fDQ}(t) \end{bmatrix} \tag{4.12}$$

Mechanical System

The dynamics of the synchronous machine rotor is determined by the motion equations:

$$J\frac{d\omega_m(t)}{dt} = T_m(t) + T_e(t) + T_{fw}(t) \tag{4.13}$$

$$\frac{d\theta_m(t)}{dt} = \omega_m(t) \tag{4.14}$$

where
J is the rotor moment of inertia;
$T_m(t)$ is the mechanical torque applied on the rotor shaft by a prime mover system;
$T_e(t)$ is the electromagnetic torque developed by the generator;
$T_{fw}(t)$ is the friction and windage torque;
$\theta_m(t)$ is the mechanical rotor position;
$\omega_m(t)$ is the mechanical rotor speed.

Based on the power balance in the synchronous machine, the electromagnetic torque, $T_e(t) = \frac{P_{cf}(t) - P_{em}(t)}{\omega_m(t)} = \frac{\partial w_{fld}(t)}{\partial \theta_m}$, is determined by the amount of power converted from electrical power into mechanical power, $P_{em}(t)$ and the amount of power in the coupling field between stator and rotor, $P_{cf}(t) = \frac{dw_{fld}(t)}{dt}$, and can be computed by differentiating the field energy function $w_{fld}(t)$ w.r.t. the rotor mechanical position $\theta_m(t)$, using the principal of virtual work displacement, using the fact that $\omega_m(t) = \frac{d\theta_m}{dt}$. The total power converted from mechanical into electrical is:

$$P_{em}(t) = \left(\frac{d\lambda_{abc}(t)}{dt}\right)^T i_{abc}(t) + \left(\frac{d\lambda_{fDQ}(t)}{dt}\right)^T i_{fDQ}(t)$$

or

$$P_{em}(t) = e_{abc}(t)^T i_{abc}(t) + e_{fDQ}(t)^T i_{fDQ}(t) \qquad (4.15)$$

Since this procedure is quite tedious if we work in actual phase quantities, another, more simple and practical, way of computing the electromagnetic torque is to go backwards from the torque expression in the d-q-o reference frame, after applying the d-q-o transformation. This procedure provides the following relationship for the electromagnetic torque:

$$T_e(t) = -\frac{1}{\sqrt{3}} \cdot \left(i_a(t)\lambda_b(t) - i_a(t)\lambda_c(t) + i_b(t)\lambda_c(t) - i_b(t)\lambda_a(t) + i_c(t)\lambda_a(t) - i_c(t)\lambda_b(t)\right) \qquad (4.16)$$

The friction and windage torque can be modeled as a quadratic function of the rotational speed of the rotor. Therefore:

$$T_{wf}(t) = -\left(D_{fw} \cdot \omega_m(t) + D'_{fw} \cdot \omega_m(t)^2\right) \qquad (4.17)$$

In summary the model of the mechanical subsystem of the synchronous machine is:

$$J\frac{d\omega_m(t)}{dt} = T_m(t) + T_e(t) + T_{fw}(t) \qquad (4.13)$$

$$\frac{d\theta_m(t)}{dt} = \omega_m(t) \tag{4.14}$$

$$T_e(t) = -\frac{1}{\sqrt{3}} \cdot \left(i_a(t)\lambda_b(t) - i_a(t)\lambda_c(t) + i_b(t)\lambda_c(t) - i_b(t)\lambda_a(t) + i_c(t)\lambda_a(t) - i_c(t)\lambda_b(t)\right) \tag{4.16}$$

$$T_{wf}(t) = -\left(D_{fw} \cdot \omega_m(t) + D'_{fw} \cdot \omega_m(t)^2\right) \tag{4.17}$$

$$\theta_m(t) = \omega_{sm} t + \delta_m(t) + \frac{\pi}{p} \tag{4.8}$$

Multiplying equations (4.13), (4.14) and (4.8) by $p/2$ and substituting we get the equivalent equations including the electrical quantities $\omega(t)$, $\theta(t)$, $\delta(t)$, instead of the mechanical $\omega_m(t)$, $\theta_m(t)$, $\delta_m(t)$.

$$\frac{2J}{p}\frac{d\omega(t)}{dt} = T_m(t) + T_e(t) \tag{4.18}$$

$$\frac{d\theta(t)}{dt} = \omega(t) \tag{4.19}$$

$$T_e(t) = -\frac{1}{\sqrt{3}} \cdot \left(i_a(t)\lambda_b(t) - i_a(t)\lambda_c(t) + i_b(t)\lambda_c(t) - i_b(t)\lambda_a(t) + i_c(t)\lambda_a(t) - i_c(t)\lambda_b(t)\right) \tag{4.20}$$

$$T_{wf}(t) = -\left(D_{fw} \cdot \omega_m(t) + D'_{fw} \cdot \omega_m(t)^2\right) \tag{4.21}$$

$$\theta(t) = \omega_s t + \delta(t) + \frac{\pi}{2} \tag{4.22}$$

We have derived electrical and mechanical equations for the synchronous machine. They are quite complex because some model equations are nonlinear and time varying.

Compact Model

Combining the equations described in the previous two sections we get the compact model of the synchronous generator. The equations are renumbered to make the model description mode legible.

$$v_{abc}(t) = R_{abc} i_{abc}(t) + \frac{d}{dt}\lambda_{abc}(t) + \Gamma v_n(t) \tag{cm.1}$$

$$i_n(t) = -i_a(t) - i_b(t) - i_c(t) \tag{cm.2}$$

$$0 = r_f i_f(t) + \frac{d\lambda_f(t)}{dt} - v_f(t) + v_{fn}(t) \tag{cm.3}$$

$$i_{fn}(t) = -i_f(t) \tag{cm.4}$$

$$T_m(t) = J\frac{d\omega_m(t)}{dt} - T_e(t) - T_{wf}(t) \tag{cm.5}$$

$$0 = \frac{d\theta_m(t)}{dt} - \omega_m(t) \tag{cm.6}$$

$$0 = \theta(t) - \frac{p}{2}\theta_m(t) \tag{cm.7}$$

$$0 = \omega(t) - \frac{p}{2}\omega_m(t) \quad \text{(cm.8)}$$

$$0 = -\theta(t) + \omega_s t + \delta(t) + \frac{\pi}{2} \quad \text{(cm.9)}$$

$$0 = R_{DQ} i_{DQ}(t) + \frac{d\lambda_{DQ}(t)}{dt} \quad \text{(cm.10)}$$

$$0 = \lambda_{abc}(t) - L_{ss}(\theta(t)) i_{abc}(t) - L_{sr}(\theta(t)) i_{fDQ}(t) \quad \text{(cm.11)}$$

$$0 = \lambda_{fDQ}(t) - L_{rs}(\theta(t)) i_{abc}(t) - L_{rr} i_{fDQ}(t) \quad \text{(cm.12)}$$

$$0 = T_e(t) + \frac{1}{\sqrt{3}} \cdot i_{abc}(t) \cdot \begin{bmatrix} 0 & 1 & -1 \\ -1 & 0 & 1 \\ 1 & -1 & 0 \end{bmatrix} \cdot \lambda_{abc}(t) \quad \text{(cm.13)}$$

$$0 = T_{wf}(t) + \left(D_{fw} \cdot \omega_m(t) + D'_{fw} \cdot \omega_m(t)^2 \right) \quad \text{(cm.14)}$$

where:

$R_{DQ} = diag\begin{pmatrix} r_D & r_Q \end{pmatrix}.$

$\lambda_{DQ}(t) = \begin{bmatrix} \lambda_D(t) & \lambda_Q(t) \end{bmatrix}^T$

Quadratic Model

Based on the analysis of the previous section and the presented compact model the following expanded quadratized model can be obtained. Additional state variables are introduced to expand the model and make it easier to formulate and to cast it in quadratic form.

The model equations are:

External equations:

$$\begin{aligned} i_a &= i_a(t) \\ i_b &= i_b(t) \\ i_c &= i_c(t) \\ i_n &= -i_a(t) - i_b(t) - i_c(t) \\ i_f &= i_f(t) \\ i_{fn} &= -i_f(t) \\ T_m &= T_m(t) \end{aligned} \quad \text{(4.23)}$$

State: $v(t) = \begin{bmatrix} v_a(t) & v_b(t) & v_c(t) & v_n(t) & v_f(t) & v_{fn}(t) & T_m(t) \end{bmatrix}^T$

Internal equations:

Differential Equations:

$$\frac{d\lambda_a(t)}{dt} = e_a(t)$$
$$\frac{d\lambda_b(t)}{dt} = e_b(t)$$
$$\frac{d\lambda_c(t)}{dt} = e_c(t)$$
$$\frac{d\lambda_f(t)}{dt} = e_f(t)$$
$$\frac{d\lambda_D(t)}{dt} = e_D(t) \qquad (4.24)$$
$$\frac{d\lambda_Q(t)}{dt} = e_Q(t)$$
$$\frac{d\theta_m(t)}{dt} = \omega_m(t)$$
$$\frac{d\omega_m(t)}{dt} = \frac{1}{J}T_{acc}(t)$$
$$\frac{dc(t)}{dt} = y_1(t)$$
$$\frac{ds(t)}{dt} = y_2(t)$$

State: $x(t) = \left[\lambda_a(t) \quad \lambda_b(t) \quad \lambda_c(t) \quad \lambda_f(t) \quad \lambda_D(t) \quad \lambda_Q(t) \quad \theta_m(t) \quad \omega_m(t) \quad c(t) \quad s(t)\right]^T$

Linear equations:

$$0 = T_{acc}(t) - T_e(t) - T_m(t) - T_{fw}(t)$$
$$0 = \theta(t) - \frac{p}{2}\theta_m(t)$$
$$0 = \omega(t) - \frac{p}{2}\omega_m(t)$$
$$0 = \delta(t) - \theta(t) + \omega_s t + \frac{\pi}{2} \qquad (4.25)$$
$$0 = e_a(t) + r_a i_a(t) - v_a(t) + v_n(t)$$
$$0 = e_b(t) + r_b i_b(t) - v_b(t) + v_n(t)$$
$$0 = e_c(t) + r_c i_c(t) - v_c(t) + v_n(t)$$
$$0 = e_f(t) + r_f i_f(t) - v_f(t) + v_{fn}(t)$$
$$0 = e_D(t) + r_D i_D(t)$$
$$0 = e_Q(t) + r_Q i_Q(t)$$

State: $y(t) = \left[T_{acc}(t) \quad \theta(t) \quad \omega(t) \quad \delta(t) \quad e_a(t) \quad e_b(t) \quad e_c(t) \quad e_f(t) \quad e_D(t) \quad e_Q(t)\right]^T$

Nonlinear Equations:

$$0 = T_e(t) + \frac{1}{\sqrt{3}}\left(i_a(t)\lambda_b(t) - i_a(t)\lambda_c(t) + i_b(t)\lambda_c(t) - i_b(t)\lambda_a(t) + i_c(t)\lambda_a(t) - i_c(t)\lambda_b(t)\right)$$

$$0 = T_{wf}(t) + D_{wf}\omega_m(t) + D'_{wf}\omega_m(t)^2$$

$$0 = y_1(t) + s(t)\cdot\omega(t)$$

$$0 = y_2(t) - c(t)\cdot\omega(t)$$

$$0 = \lambda_a(t) - L_{aa}(t)i_a(t) - L_{ab}(t)i_b(t) - L_{ac}(t)i_c(t) - L_{af}(t)i_f(t) - L_{aD}(t)i_D(t) - L_{aQ}(t)i_Q(t)$$

$$0 = \lambda_b(t) - L_{ba}(t)i_a(t) - L_{bb}(t)i_b(t) - L_{bc}(t)i_c(t) - L_{bf}(t)i_f(t) - L_{bD}(t)i_D(t) - L_{bQ}(t)i_Q(t)$$

$$0 = \lambda_c(t) - L_{ca}(t)i_a(t) - L_{cb}(t)i_b(t) - L_{cc}(t)i_c(t) - L_{cf}(t)i_f(t) - L_{cD}(t)i_D(t) - L_{cQ}(t)i_Q(t)$$

$$0 = \lambda_f(t) - L_{fa}(t)i_a(t) - L_{fb}(t)i_b(t) - L_{fc}(t)i_c(t) - L_f i_f(t) - M_R i_D(t) - L_{fQ}i_Q(t)$$

$$0 = \lambda_D(t) - L_{Da}(t)i_a(t) - L_{Db}(t)i_b(t) - L_{Dc}(t)i_c(t) - M_R i_f(t) - L_D i_D(t) - L_{DQ}i_Q(t)$$

$$0 = \lambda_Q(t) - L_{Qa}(t)i_a(t) - L_{Qb}(t)i_b(t) - L_{Qc}(t)i_c(t) - L_{Qf}i_f(t) - L_{QD}i_D(t) - L_Q i_Q(t)$$

$$0 = L_{aa}(t) - L_s - L_m c(t)^2 + L_m s(t)^2$$

$$0 = L_{bb}(t) - L_s - L_m\cos(\frac{2\pi}{3})c(t)^2 + L_m\cos(\frac{2\pi}{3})s(t)^2 + 2L_m\sin(\frac{2\pi}{3})c(t)s(t)$$

$$0 = L_{cc}(t) - L_s - L_m\cos(\frac{2\pi}{3})c(t)^2 + L_m\cos(\frac{2\pi}{3})s(t)^2 - 2L_m\sin(\frac{2\pi}{3})c(t)s(t)$$

$$0 = L_{ab}(t) + M_s + L_m\cos(\frac{\pi}{3})c(t)^2 - L_m\cos(\frac{\pi}{3})s(t)^2 - 2L_m\sin(\frac{\pi}{3})c(t)s(t)$$

$$0 = L_{ac}(t) + M_s + L_m\cos(\frac{7\pi}{3})c(t)^2 - L_m\cos(\frac{7\pi}{3})s(t)^2 + 2L_m\sin(\frac{7\pi}{3})c(t)s(t)$$

$$0 = L_{bc}(t) + M_s + L_m\cos(\pi)c(t)^2 - L_m\cos(\pi)s(t)^2 + 2L_m\sin(\pi)c(t)s(t)$$

$$0 = L_{af}(t) - M_F c(t) \qquad (4.26)$$

$$0 = L_{bf}(t) - M_F\cos(\frac{2\pi}{3})c(t) - M_F\sin(\frac{2\pi}{3})s(t)$$

$$0 = L_{cf}(t) - M_F\cos(\frac{4\pi}{3})c(t) - M_F\sin(\frac{4\pi}{3})s(t)$$

$$0 = L_{aD}(t) - M_D c(t)$$

$$0 = L_{bD}(t) - M_D\cos(\frac{2\pi}{3})c(t) - M_D\sin(\frac{2\pi}{3})s(t)$$

$$0 = L_{cD}(t) - M_D\cos(\frac{4\pi}{3})c(t) - M_D\sin(\frac{4\pi}{3})s(t)$$

$$0 = L_{aQ}(t) - M_Q s(t)$$

$$0 = L_{bQ}(t) - M_Q\cos(\frac{2\pi}{3})s(t) + M_Q\sin(\frac{2\pi}{3})c(t)$$

$$0 = L_{cQ}(t) - M_Q \cos(\frac{4\pi}{3})s(t) + M_Q \sin(\frac{4\pi}{3})c(t)$$

State:

$$z(t) = \begin{bmatrix} T_e(t) & T_{fw}(t) & y_1(t) & y_2(t) & i_a(t) & i_b(t) & i_c(t) & i_f(t) & i_D(t) & i_Q(t) & L_{aa}(t) & L_{bb}(t) & L_{cc}(t) \\ L_{ab}(t) & L_{ac}(t) & L_{bc}(t) & L_{af}(t) & L_{bf}(t) & L_{cf}(t) & L_{aD}(t) & L_{bD}(t) & L_{cD}(t) & L_{aQ}(t) & L_{bQ}(t) & L_{cQ}(t) \end{bmatrix}^T$$

Implicit Equations (linear – will be eliminated – do not introduce additional states):

$$0 = L_{ba}(t) - L_{ab}(t)$$
$$0 = L_{cb}(t) - L_{bc}(t)$$
$$0 = L_{ca}(t) - L_{ac}(t)$$
$$0 = L_{fa}(t) - L_{af}(t)$$
$$0 = L_{fb}(t) - L_{bf}(t)$$
$$0 = L_{fc}(t) - L_{cf}(t)$$
$$0 = L_{Da}(t) - L_{aD}(t) \qquad (4.27)$$
$$0 = L_{Db}(t) - L_{bD}(t)$$
$$0 = L_{Dc}(t) - L_{cD}(t)$$
$$0 = L_{Qa}(t) - L_{aQ}(t)$$
$$0 = L_{Qb}(t) - L_{bQ}(t)$$
$$0 = L_{Qc}(t) - L_{cQ}(t)$$

Note that $L_{fQ} = L_{Qf} = 0$ and $L_{DQ} = L_{QD} = 0$ since the Q and D windings are perpendicular.

In compact matrix notation the model is:

$$\begin{aligned} i(t) &= A_1 v(t) + A_4 z(t) \\ 0 &= \frac{dx(t)}{dt} + B_2 x(t) + B_3 y(t) + B_4 z(t) \\ 0 &= C_1 v(t) + C_2 x(t) + C_3 y(t) + C_4 z(t) \\ 0 &= q(v(t), x(t), y(t), z(t)) \end{aligned} \qquad (4.28)$$

The model is a 52-order model consisting of 52 states: 7 external states and 45 internal. Of the internal states 10 are dynamic and 35 algebraic. The model consists of 7 external equations, 10 linear differential and 35 algebraic equations. Of the algebraic equations 10 are linear, 25 nonlinear (there are 12 more linear equations that are implicit and will be eliminated from the final model). The number of equations is equal to the number of states, thus the model is consistent. The total state vector is defined as:

$$X(t) = \begin{bmatrix} v^T & x^T & y^T & z^T \end{bmatrix}^T$$

where

$$v(t) = \begin{bmatrix} v_a & v_b & v_c & v_n & v_f & v_{fn} & T_m \end{bmatrix}^T$$

$$x(t) = \begin{bmatrix} \lambda_a & \lambda_b & \lambda_c & \lambda_f & \lambda_D & \lambda_Q & \theta_m & \omega_m & c & s \end{bmatrix}^T$$

$$y(t) = \begin{bmatrix} T_{acc} & \theta & \omega & \delta & e_a & e_b & e_c & e_f & e_D & e_Q \end{bmatrix}^T$$

$$z(t) = \begin{bmatrix} T_e & T_{fw} & y_1 & y_2 & i_a & i_b & i_c & i_f & i_D & i_Q & L_{aa} & L_{bb} & L_{cc} \\ L_{ab} & L_{ac} & L_{bc} & L_{af} & L_{bf} & L_{cf} & L_{aD} & L_{bD} & L_{cD} & L_{aQ} & L_{bQ} & L_{cQ} \end{bmatrix}^T$$

The through variables are:

$$I = \begin{bmatrix} i_a & i_b & i_c & i_n & i_f & i_{fn} & T_m & 0 & \ldots & 0 \end{bmatrix}^T$$

Steady-State Model

The steady state equations are derived from the above set of model equations assuming that the machine is operating under sinusoidal steady state conditions. Therefore, the differential equations are replaced by their equivalent steady state equations either by setting the derivative to zero or by assuming sinusoidal conditions and therefore phasor representation, depending on the equation. Furthermore, some equations and states are not meaningful at steady state and thus are eliminated from the model. The sinusoidally time varying inductances are also converted to constant phasor quantities, based on the relations presented in the previous section.

Compact Model

In compact form the equations become:

$$\tilde{V}_{abc} = R_{abc}\tilde{I}_{abc} + j\omega\tilde{\Lambda}_{abc} + \Gamma\tilde{V}_n = R_{abc}\tilde{I}_{abc} + \tilde{E}_{abc} + \Gamma\tilde{V}_n \quad \text{(cm.15)}$$

$$\tilde{I}_n = -\tilde{I}_a - \tilde{I}_b - \tilde{I}_c \quad \text{(cm.16)}$$

$$0 = r_f I_f - V_f + V_{fn} \quad \text{(cm.17)}$$

$$I_{fn} = -I_f \quad \text{(cm.18)}$$

$$T_m = -T_e - T_{wf} \quad \text{(cm.19)}$$

$$0 = \omega_m - \omega_s \quad \text{(cm.20)}$$

$$0 = \omega - \frac{p}{2}\omega_m \quad \text{(cm.21)}$$

$$0 = R_{DQ} I_{DQ} \quad \text{(cm.22)}$$

$$0 = \tilde{\Lambda}_{abc} - \tilde{L}_{ss}\tilde{I}_{abc} - \tilde{L}_{sr} I_{fDQ} \quad \text{(cm.23)}$$

$$0 = \Lambda_{fDQ}(t) - \tilde{L}_{rs}\tilde{I}_{abc} - L_{rr} I_{fDQ} \quad \text{(cm.24)}$$

$$0 = T_e - \frac{\mathrm{Re}\{\tilde{E}_{abc}\tilde{I}_{abc}^H\}}{\omega_m} \quad \text{(cm.25)}$$

$$0 = T_{wf}(t) + \left(D_{fw} \cdot \omega_m + D'_{fw} \cdot \omega_m{}^2\right) \quad \text{(cm.26)}$$

where:

$$R_{DQ} = diag\begin{pmatrix} r_D & r_Q \end{pmatrix}.$$

$$\Lambda_{DQ}(t) = \begin{bmatrix} \Lambda_D & \Lambda_Q \end{bmatrix}^T$$

Quadratic Model

The expanded and quadraitized model becomes:

External equations:

$$
\begin{aligned}
I_a &= \tilde{\tilde{I}}_a \\
I_b &= \tilde{\tilde{I}}_b \\
I_c &= \tilde{\tilde{I}}_c \\
I_n &= -\tilde{\tilde{I}}_a - \tilde{\tilde{I}}_b - \tilde{\tilde{I}}_c \\
I_f &= I_f \\
I_{fn} &= -I_f \\
T_m &= -T_e - T_{fw}
\end{aligned}
\tag{4.29}
$$

Internal equations:

$$
\begin{aligned}
0 &= \tilde{\tilde{E}}_a - j\omega\tilde{\tilde{\Lambda}}_a \\
0 &= \tilde{\tilde{E}}_b - j\omega\tilde{\tilde{\Lambda}}_b \\
0 &= \tilde{\tilde{E}}_c - j\omega\tilde{\tilde{\Lambda}}_c \\
0 &= E_f \\
0 &= E_D \\
0 &= E_Q \\
0 &= \omega_m - \omega_s \\
0 &= \omega - \frac{p}{2}\omega_m \\
0 &= \tilde{\tilde{E}}_a + r_a\tilde{\tilde{I}}_a - \tilde{\tilde{V}}_a + \tilde{\tilde{V}}_n \\
0 &= \tilde{\tilde{E}}_b + r_b\tilde{\tilde{I}}_b - \tilde{\tilde{V}}_b + \tilde{\tilde{V}}_n \\
0 &= \tilde{\tilde{E}}_c + r_c\tilde{\tilde{I}}_c - \tilde{\tilde{V}}_c + \tilde{\tilde{V}}_n \\
0 &= E_f + r_f I_f - V_f + V_{fn} \\
0 &= E_D + r_D I_D \\
0 &= E_Q + r_Q I_Q \\
0 &= T_e - \frac{\mathrm{Re}\left\{\tilde{\tilde{E}}_a\tilde{\tilde{I}}_a^* + \tilde{\tilde{E}}_b\tilde{\tilde{I}}_b^* + \tilde{\tilde{E}}_c\tilde{\tilde{I}}_c^*\right\}}{\omega_m} \\
0 &= T_{wf} + D_{wf}\omega_m + D'_{wf}\omega_m{}^2 \\
0 &= \tilde{\Lambda}_a - \tilde{\tilde{L}}_{aa}\tilde{\tilde{I}}_a - \tilde{\tilde{L}}_{ab}\tilde{\tilde{I}}_b - \tilde{\tilde{L}}_{ac}\tilde{\tilde{I}}_c - \tilde{\tilde{L}}_{af}I_f - \tilde{\tilde{L}}_{aD}I_D - \tilde{\tilde{L}}_{aQ}I_Q \\
0 &= \tilde{\Lambda}_b - \tilde{\tilde{L}}_{ba}\tilde{\tilde{I}}_a - \tilde{\tilde{L}}_{bb}\tilde{\tilde{I}}_b - \tilde{\tilde{L}}_{bc}\tilde{\tilde{I}}_c - \tilde{\tilde{L}}_{bf}I_f - \tilde{\tilde{L}}_{bD}I_D - \tilde{\tilde{L}}_{bQ}I_Q
\end{aligned}
\tag{4.30}
$$

$$0 = \tilde{\Lambda}_c - \tilde{L}_{ca}\tilde{I}_a - \tilde{L}_{cb}\tilde{I}_b - \tilde{L}_{cc}\tilde{I}_c - \tilde{L}_{cf}I_f - \tilde{L}_{cD}I_D - \tilde{L}_{cQ}I_Q$$
$$0 = \Lambda_f - \tilde{L}_{fa}\tilde{I}_a - \tilde{L}_{fb}\tilde{I}_b - \tilde{L}_{fc}\tilde{I}_c - L_f I_f - M_R I_D - L_{fQ}I_Q$$
$$0 = \Lambda_D - \tilde{L}_{Da}\tilde{I}_a - \tilde{L}_{Db}\tilde{I}_b - \tilde{L}_{Dc}\tilde{I}_c - M_R I_f - L_D I_D - L_{DQ}I_Q$$
$$0 = \Lambda_Q - \tilde{L}_{Qa}\tilde{I}_a - \tilde{L}_{Qb}\tilde{I}_b - \tilde{L}_{Qc}\tilde{I}_c - L_{Qf}I_f - L_{QD}I_D - L_Q I_Q$$

Note that $L_{fQ} = L_{Qf} = 0$ and $L_{DQ} = L_{QD} = 0$ since the Q and D windings are perpendicular. Note also that in steady state the voltage and current in the damper windings is zero.

Dynamic Model

Similarly to the steady state case, the quasi steady state equations are derived from the set of model equations assuming that the machine is operating under sinusoidal quasi steady state conditions. Therefore, some differential equations are replaced by their equivalent steady state equations by assuming sinusoidal conditions and therefore phasor representation. Only some of the time domain equations are retained to represent the essential slow machine dynamics for the analysis. Also note that the time dependence is only shown explicitly for fully time domain quantities, not for phasor quantities. However, it is implied that the phasors are time varying phasors. Furthermore, the angle θ is of no interest for this type of analysis, since it changes considerably faster than the time scales of interest. Thus, it is eliminated from the set of equations. The angle δ however plays a more important role, now.

Compact Model

The compact quasi steady state model is of the form:

$$\tilde{V}_{abc} = R_{abc}\tilde{I}_{abc} + j\omega\tilde{\Lambda}_{abc} + \Gamma\tilde{V}_n = R_{abc}\tilde{I}_{abc} + \tilde{E}_{abc} + \Gamma\tilde{V}_n \quad \text{(cm.27)}$$

$$\tilde{I}_n = -\tilde{I}_a - \tilde{I}_b - \tilde{I}_c \quad \text{(cm.28)}$$

$$0 = r_f i_f(t) + \frac{d\lambda_f(t)}{dt} - v_f(t) + v_{fn}(t)$$
$$i_{fn}(t) = -i_f(t)$$

if field dynamics are considered (cm.29) (cm.30)

$$0 = r_f I_f - V_f + V_{fn}$$
$$I_{fn} = -I_f$$

if field dynamics are neglected

$$T_m(t) = J\frac{d\omega_m(t)}{dt} - T_e(t) - T_{wf}(t) \quad \text{(cm.31)}$$

$$0 = \frac{d\delta(t)}{dt} - \omega(t) + \omega_{s,elec} \quad \text{(cm.32)}$$

$$0 = \omega(t) - \frac{p}{2}\omega_m(t) \quad \text{(cm.33)}$$

$$0 = R_{DQ}i_{DQ}(t) + \frac{d\lambda_{DQ}(t)}{dt}$$

if damper windings are considered (cm.34)

$0 = R_{DQ} I_{DQ}$ if damper windings are neglected

$0 = \tilde{\Lambda}_{abc} - \tilde{L}_{ss} \tilde{I}_{abc} - \tilde{L}_{sr} I_{fDQ}$ (cm.35)

$0 = \Lambda_{fDQ} - \tilde{L}_{rs} \tilde{I}_{abc} - L_{rr} I_{fDQ}$ (cm.36)

$0 = T_e(t) - \frac{\mathrm{Re}\{\tilde{E}_{abc} \tilde{I}^{H}_{abc}\}}{\omega_m(t)}$ (cm.37)

(cm.41)

$0 = T_{wf}(t) + \left(D_{fw} \cdot \omega_m(t) + D'_{fw} \cdot \omega_m(t)^2\right)$ (cm.38)

where:

$R_{DQ} = diag\left(r_D \quad r_Q\right).$

$\lambda_{DQ}(t) = \left[\lambda_D(t) \quad \lambda_Q(t)\right]^T$

<u>*Quadratic Model*</u>

The model equations are:

External equations:

$I_a = \tilde{I}_a$

$I_b = \tilde{I}_b$

$I_c = \tilde{I}_c$

$\tilde{I}_n = -\tilde{I}_a - \tilde{I}_b - \tilde{I}_c$ (4.31)

$I_f = i_f(t)$ if field dynamics are considered

$I_{fn} = -i_f(t)$ if field dynamics are considered

$I_f = I_f$ if field dynamics are neglected

$I_{fn} = -I_f$ if field dynamics are neglected

$T_m = T_m(t)$

State: $v(t) = \left[\tilde{V}_a \quad \tilde{V}_b \quad \tilde{V}_c \quad \tilde{V}_n(t) \quad v_f(t) \quad v_{fn}(t) \quad T_m(t)\right]^T$ if field dynamics are considered.

State: $v(t) = \left[\tilde{V}_a \quad \tilde{V}_b \quad \tilde{V}_c \quad \tilde{V}_n(t) \quad V_f \quad V_{fn} \quad T_m(t)\right]^T$ if field dynamics are neglected.

Internal equations:

Differential Equations:

$\frac{d\lambda_f(t)}{dt} = e_f(t)$ if field dynamics are considered

$0 = E_f$ if filed dynamics are neglected

$\frac{d\lambda_D(t)}{dt} = e_D(t)$ if dampers are considered

$$\frac{d\lambda_Q(t)}{dt} = e_Q(t) \qquad \text{if dampers are considered} \qquad (4.32)$$

$$0 = E_D \qquad \text{if dampers are neglected}$$

$$0 = E_Q \qquad \text{if dampers are neglected}$$

$$\frac{d\delta(t)}{dt} = \omega(t) - \omega_{s,elec}$$

$$\frac{d\omega_m(t)}{dt} = \frac{1}{J} T_{acc}(t)$$

$$\frac{dc(t)}{dt} = y_1(t)$$

$$\frac{ds(t)}{dt} = y_2(t)$$

State: $x(t) = \left[\lambda_f(t) \quad \lambda_D(t) \quad \lambda_Q(t) \quad \delta(t) \quad \omega_m(t) \quad c(t) \quad s(t)\right]^T$ if field dynamics and dampers are considered.

State: $x(t) = \left[\Lambda_f \quad \lambda_D(t) \quad \lambda_Q(t) \quad \delta(t) \quad \omega_m(t) \quad c(t) \quad s(t)\right]^T$ if field dynamics are neglected and dampers are considered.

State: $x(t) = \left[\lambda_f(t) \quad \Lambda_D \quad \Lambda_Q \quad \delta(t) \quad \omega_m(t) \quad c(t) \quad s(t)\right]^T$ if field dynamics are considered and dampers are negelcted.

State: $x(t) = \left[\Lambda_f \quad \Lambda_D \quad \Lambda_Q \quad \delta(t) \quad \omega_m(t) \quad c(t) \quad s(t)\right]^T$ if both field dynamics and dampers are negelcted.

Linear equations – part 1:

$$0 = T_{acc}(t) - T_e(t) - T_m(t) - T_{fw}(t)$$

$$0 = \omega(t) - \frac{p}{2}\omega_m(t)$$

$$0 = \tilde{E}_a - j\omega\tilde{\Lambda}_a$$

$$0 = \tilde{E}_b - j\omega\tilde{\Lambda}_b$$

$$0 = \tilde{E}_c - j\omega\tilde{\Lambda}_c \qquad (4.33)$$

$$0 = \tilde{E}_a + r_a\tilde{I}_a - \tilde{V}_a + \tilde{V}_n$$

$$0 = \tilde{E}_b + r_b\tilde{I}_b - \tilde{V}_b + \tilde{V}_n$$

$$0 = \tilde{E}_c + r_c\tilde{I}_c - \tilde{V}_c + \tilde{V}_n$$

$$0 = e_f(t) + r_f i_f(t) - v_f(t) + v_{fn}(t) \text{ if field dynamics are considered}$$

$$0 = E_f + r_f I_f - V_f + V_{fn} \text{ if field dynamics are neglected}$$

$$0 = e_D(t) + r_D i_D(t) \text{ if D-damper is considered}$$

$$0 = E_D + r_D I_D \text{ if D-damper is neglected}$$

$$0 = e_Q(t) + r_Q i_Q(t) \text{ if Q-damper is considered}$$

$$0 = E_Q + r_Q I_Q \text{ if Q-damper is neglected}$$

State:

$$y^1(t) = \left[T_{acc}(t) \quad \theta(t) \quad \omega(t) \quad \delta(t) \quad \tilde{\tilde{\Lambda}}_a \quad \tilde{\tilde{\Lambda}}_b \quad \tilde{\tilde{\Lambda}}_c \quad \tilde{\tilde{E}}_a \quad \tilde{\tilde{E}}_b \quad \tilde{\tilde{E}}_c \quad e_f(t) \quad e_D(t) \quad e_Q(t)\right]^T$$

if field dynamics and dampers are considered

$$y^1(t) = \left[T_{acc}(t) \quad \theta(t) \quad \omega(t) \quad \delta(t) \quad \tilde{\tilde{\Lambda}}_a \quad \tilde{\tilde{\Lambda}}_b \quad \tilde{\tilde{\Lambda}}_c \quad \tilde{\tilde{E}}_a \quad \tilde{\tilde{E}}_b \quad \tilde{\tilde{E}}_c \quad e_f(t) \quad E_D \quad E_Q\right]^T$$

if field dynamics are considered and dampers are neglected

$$y^1(t) = \left[T_{acc}(t) \quad \theta(t) \quad \omega(t) \quad \delta(t) \quad \tilde{\tilde{\Lambda}}_a \quad \tilde{\tilde{\Lambda}}_b \quad \tilde{\tilde{\Lambda}}_c \quad \tilde{\tilde{E}}_a \quad \tilde{\tilde{E}}_b \quad \tilde{\tilde{E}}_c \quad E_f(t) \quad e_D(t) \quad e_Q(t)\right]^T$$

if field dynamics are neglected and dampers are considered

$$y^1(t) = \left[T_{acc}(t) \quad \theta(t) \quad \omega(t) \quad \delta(t) \quad \tilde{\tilde{\Lambda}}_a \quad \tilde{\tilde{\Lambda}}_b \quad \tilde{\tilde{\Lambda}}_c \quad \tilde{\tilde{E}}_a \quad \tilde{\tilde{E}}_b \quad \tilde{\tilde{E}}_c \quad E_f \quad E_D \quad E_Q\right]^T$$

if field dynamics and dampers are neglected

Linear equations – part 2:

If dampers and field dynamics are neglected:

$$\begin{aligned}
0 &= \tilde{\tilde{\Lambda}}_a - \tilde{\tilde{L}}_{aa}\tilde{\tilde{I}}_a - \tilde{\tilde{L}}_{ab}\tilde{\tilde{I}}_b - \tilde{\tilde{L}}_{ac}\tilde{\tilde{I}}_c - \tilde{\tilde{L}}_{af}I_f - \tilde{\tilde{L}}_{aD}I_D - \tilde{\tilde{L}}_{aQ}I_Q \\
0 &= \tilde{\tilde{\Lambda}}_b - \tilde{\tilde{L}}_{ba}\tilde{\tilde{I}}_a - \tilde{\tilde{L}}_{bb}\tilde{\tilde{I}}_b - \tilde{\tilde{L}}_{bc}\tilde{\tilde{I}}_c - \tilde{\tilde{L}}_{bf}I_f - \tilde{\tilde{L}}_{bD}I_D - \tilde{\tilde{L}}_{bQ}I_Q \\
0 &= \tilde{\tilde{\Lambda}}_c - \tilde{\tilde{L}}_{ca}\tilde{\tilde{I}}_a - \tilde{\tilde{L}}_{cb}\tilde{\tilde{I}}_b - \tilde{\tilde{L}}_{cc}\tilde{\tilde{I}}_c - \tilde{\tilde{L}}_{cf}I_f - \tilde{\tilde{L}}_{cD}I_D - \tilde{\tilde{L}}_{cQ}I_Q \\
0 &= \Lambda_f - \tilde{\tilde{L}}_{fa}\tilde{\tilde{I}}_a - \tilde{\tilde{L}}_{fb}\tilde{\tilde{I}}_b - \tilde{\tilde{L}}_{fc}\tilde{\tilde{I}}_c - L_f I_f - M_R I_D - L_{fQ}I_Q \\
0 &= \Lambda_D - \tilde{\tilde{L}}_{Da}\tilde{\tilde{I}}_a - \tilde{\tilde{L}}_{Db}\tilde{\tilde{I}}_b - \tilde{\tilde{L}}_{Dc}\tilde{\tilde{I}}_c - M_R I_f - L_D I_D - L_{DQ}I_Q \\
0 &= \Lambda_Q - \tilde{\tilde{L}}_{Qa}\tilde{\tilde{I}}_a - \tilde{\tilde{L}}_{Qb}\tilde{\tilde{I}}_b - \tilde{\tilde{L}}_{Qc}\tilde{\tilde{I}}_c - L_{Qf}I_f - L_{QD}I_D - L_Q I_Q
\end{aligned} \tag{4.34}$$

If dampers and field dynamics are included:

$$\begin{aligned}
0 &= \tilde{\tilde{\Lambda}}_a - \tilde{\tilde{L}}_{aa}\tilde{\tilde{I}}_a - \tilde{\tilde{L}}_{ab}\tilde{\tilde{I}}_b - \tilde{\tilde{L}}_{ac}\tilde{\tilde{I}}_c - \tilde{\tilde{L}}_{af}i_f(t) - \tilde{\tilde{L}}_{aD}i_D(t) - \tilde{\tilde{L}}_{aQ}i_Q(t) \\
0 &= \tilde{\tilde{\Lambda}}_b - \tilde{\tilde{L}}_{ba}\tilde{\tilde{I}}_a - \tilde{\tilde{L}}_{bb}\tilde{\tilde{I}}_b - \tilde{\tilde{L}}_{bc}\tilde{\tilde{I}}_c - \tilde{\tilde{L}}_{bf}i_f(t) - \tilde{\tilde{L}}_{bD}I_D - \tilde{\tilde{L}}_{bQ}I_Q \\
0 &= \tilde{\tilde{\Lambda}}_c - \tilde{\tilde{L}}_{ca}\tilde{\tilde{I}}_a - \tilde{\tilde{L}}_{cb}\tilde{\tilde{I}}_b - \tilde{\tilde{L}}_{cc}\tilde{\tilde{I}}_c - \tilde{\tilde{L}}_{cf}i_f(t) - \tilde{\tilde{L}}_{cD}I_D - \tilde{\tilde{L}}_{cQ}I_Q \\
0 &= \lambda_f(t) - \tilde{\tilde{L}}_{fa}\tilde{\tilde{I}}_a - \tilde{\tilde{L}}_{fb}\tilde{\tilde{I}}_b - \tilde{\tilde{L}}_{fc}\tilde{\tilde{I}}_c - L_f i_f(t) - M_R i_D(t) - L_{fQ}i_Q(t) \\
0 &= \lambda_D(t) - \tilde{\tilde{L}}_{Da}\tilde{\tilde{I}}_a - \tilde{\tilde{L}}_{Db}\tilde{\tilde{I}}_b - \tilde{\tilde{L}}_{Dc}\tilde{\tilde{I}}_c - M_R i_f(t) - L_D i_D(t) - L_{DQ}i_Q(t) \\
0 &= \lambda_Q(t) - \tilde{\tilde{L}}_{Qa}\tilde{\tilde{I}}_a - \tilde{\tilde{L}}_{Qb}\tilde{\tilde{I}}_b - \tilde{\tilde{L}}_{Qc}\tilde{\tilde{I}}_c - L_{Qf}i_f(t) - L_{QD}i_D(t) - L_Q i_Q(t)
\end{aligned} \tag{4.35}$$

State:

$y^2(t) = \left[\tilde{\tilde{I}}_a \quad \tilde{\tilde{I}}_b \quad \tilde{\tilde{I}}_c \quad i_f(t) \quad i_D(t) \quad i_Q(t)\right]^T$ if field dynamics and dampers are considered

$y^2(t) = \left[\tilde{\tilde{I}}_a \quad \tilde{\tilde{I}}_b \quad \tilde{\tilde{I}}_c \quad i_f(t) \quad I_D \quad I_Q\right]^T$ if field dynamics are considered and dampers are neglected

$y^2(t) = \left[\tilde{\tilde{I}}_a \quad \tilde{\tilde{I}}_b \quad \tilde{\tilde{I}}_c \quad I_F \quad i_D(t) \quad i_Q(t)\right]^T$ if field dynamics are neglected and dampers are considered

$y^2(t) = \left[\tilde{\tilde{I}}_a \quad \tilde{\tilde{I}}_b \quad \tilde{\tilde{I}}_c \quad I_f \quad I_D \quad I_Q\right]^T$ if field dynamics and dampers are neglected

Nonlinear Equations:

$$0 = T_e(t) - \frac{\mathrm{Re}\{\tilde{E}_{abc}\tilde{I}_{abc}^{H}\} + e_{fDQ}i_{fDQ}}{\omega_m(t)} \quad \text{or} \quad 0 = T_e(t) - \frac{\mathrm{Re}\{\tilde{E}_{abc}\tilde{I}_{abc}^{H}\} + E_{fDQ}I_{fDQ}}{\omega_m(t)}$$ if field and damper dynamics are neglected.

$$0 = T_{wf}(t) + D_{wf}\omega_m(t) + D'_{wf}\omega_m(t)^2$$
$$0 = y_1(t) + s(t)\cdot\left(\omega(t) - \omega_{s,elec}\right) \qquad (4.36)$$
$$0 = y_2(t) - c(t)\cdot\left(\omega(t) - \omega_{s,elec}\right)$$

State:

$$z(t) = \left[T_e(t) \quad T_{wf}(t) \quad y_1(t) \quad y_2(t)\right]^T$$

Note that $L_{fQ} = L_{Qf} = 0$ and $L_{DQ} = L_{QD} = 0$ since the Q and D windings are perpendicular.

$$X(t) = \left[v^T \quad x^T \quad y^T \quad z^T\right]^T$$

where

$$v(t) = \left[\tilde{V}_a \quad \tilde{V}_b \quad \tilde{V}_c \quad \tilde{V}_n \quad v_f \quad v_{fn} \quad T_m\right]^T$$
$$x(t) = \left[\lambda_f(t) \quad \lambda_D(t) \quad \lambda_Q(t) \quad \delta(t) \quad \omega_m(t) \quad c(t) \quad s(t)\right]^T$$
$$y^1(t) = \left[T_{acc}(t) \quad \theta(t) \quad \omega(t) \quad \delta(t) \quad \tilde{\Lambda}_a \quad \tilde{\Lambda}_b \quad \tilde{\Lambda}_c \quad \tilde{E}_a \quad \tilde{E}_b \quad \tilde{E}_c \quad e_f(t) \quad e_D(t) \quad e_Q(t)\right]^T$$
$$y^2(t) = \left[\tilde{I}_a \quad \tilde{I}_b \quad \tilde{I}_c \quad i_f(t) \quad i_D(t) \quad i_Q(t)\right]^T$$
$$y(t) = \begin{bmatrix} y^1(t) \\ y^2(t) \end{bmatrix}$$
$$z(t) = \left[T_e(t) \quad T_{wf}(t) \quad y_1(t) \quad y_2(t)\right]^T$$

The through variables are:

$$I = \left[\tilde{I}_a \quad \tilde{I}_b \quad \tilde{I}_c \quad \tilde{I}_n \quad \tilde{I}_f \quad \tilde{I}_{fn} \quad T_m \quad 0 \quad \ldots \quad 0\right]^T$$

User Interface and Model Parameters

User defines the synchronous machine parameters in p.u. and in the standard d-q-0 frame, as they are usually available. In the implementation the program itself computes the physical parameters as required by the model, by converting the user defined parameters. The user interface of the generating unit is shown in Figure 4.8.The user interface of the synchronous generator is presented in Figure 4.9. and the physical parameters that are used in the mathematical model are presented in the form in Figure 4.10.

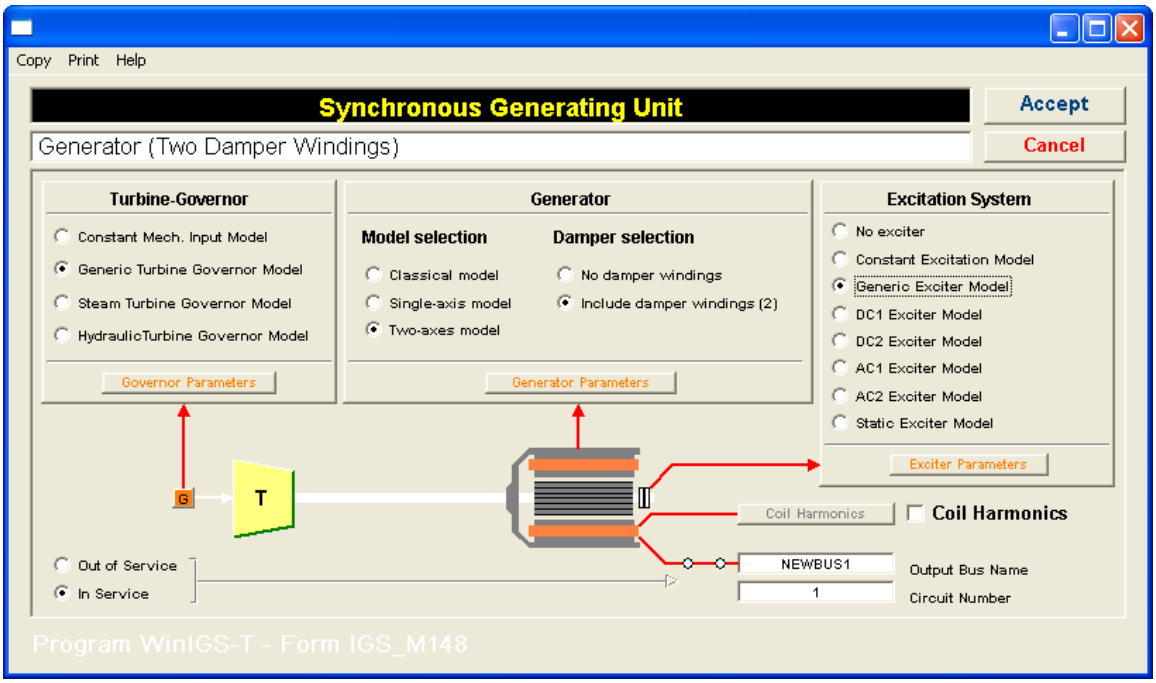


Figure 4.8. Generating Unit User Interface.

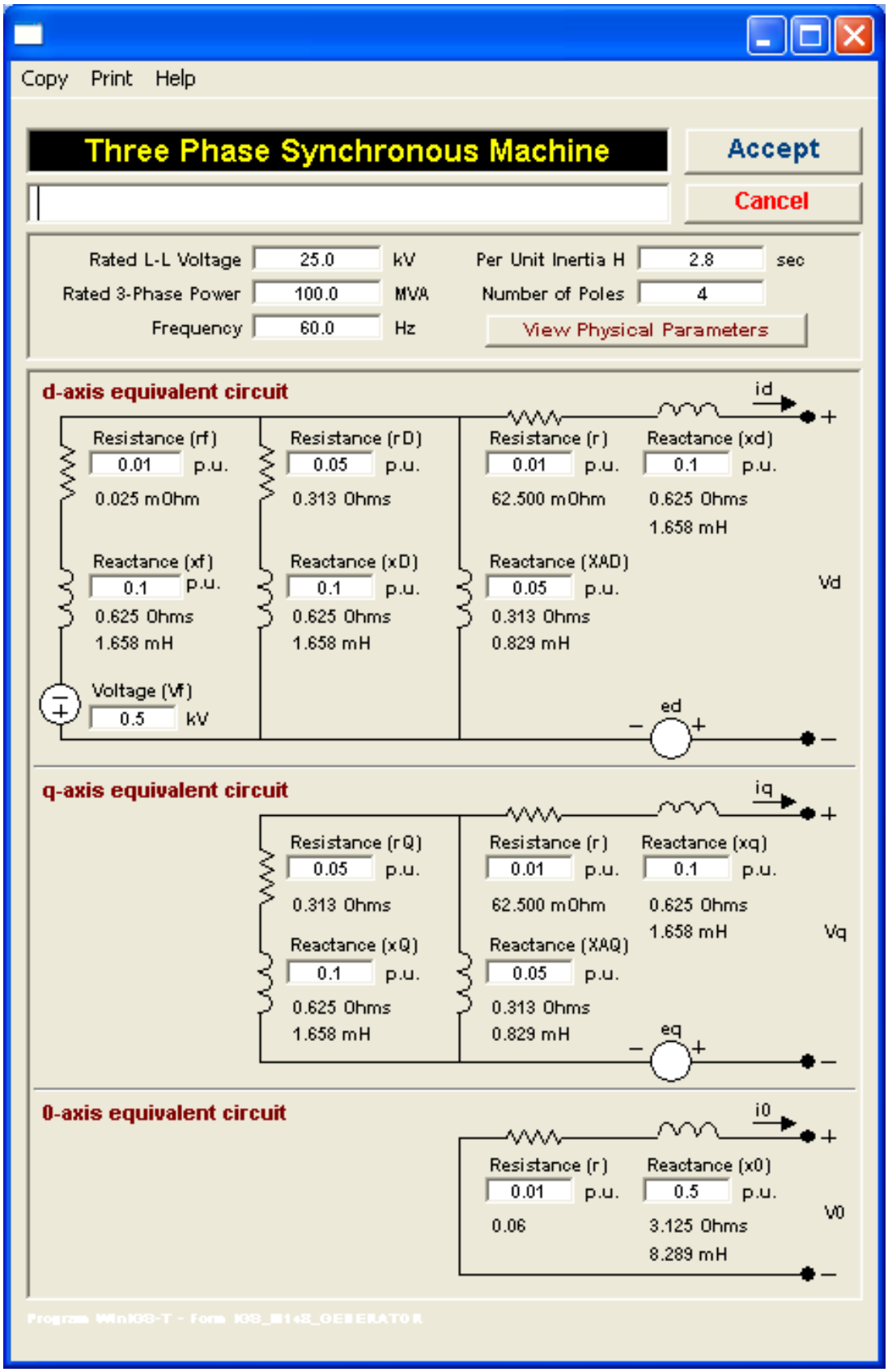


Figure 4.9. Synchronous Machine User Interface.

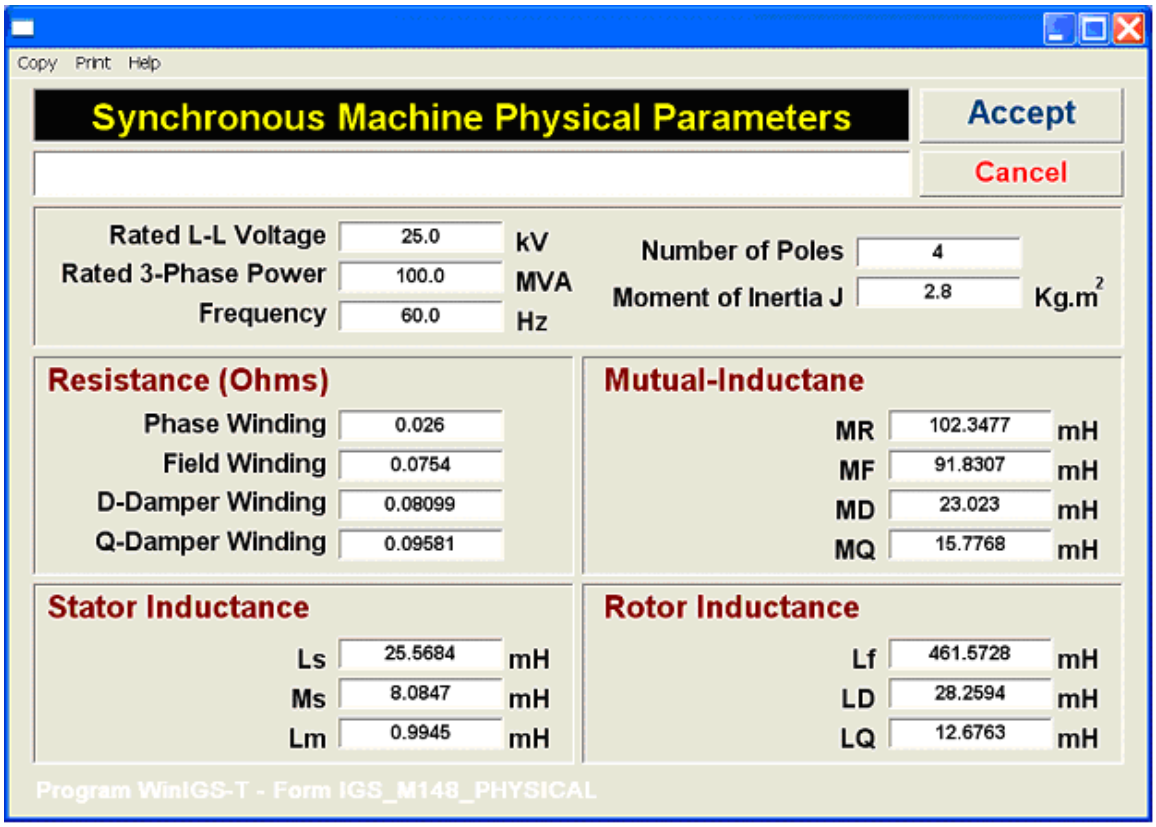


Figure 4.10. Synchronous Machine Physical Parameter Interface.

Contant Torque/Power Prime Mover Model

Steady-State Model

Constant Torque Mode

The compact model assumes a constant value for the mechanical torque T_m and is of the form:

$T_m = -T_m$. The minus sign is because of the convention that the positive direction is into the device. Note the difference between the variable T_m on the left hand side and the value on the right hand side.

Constant Power Mode

The compact model assumes a constant value for the mechanical power produced by the unit, P_m and is of the form:

$P_m = -P_m$. The minus sign is because of the convention that the positive direction is into the device. Note the difference between the variable P_m on the left hand side and the value on the right hand side. The produced torque value is computed as $T_m = \frac{P_m}{\omega_m}$, where

ω_m is the operating speed of the generating unit, typically the synchronous mechanical speed ω_{sm} for steady state analysis.

Dynamic Model

Since this model does not exhibit any sort of dynamic behavior the model for quasi steady state analysis is the same as the steady state model.

Constant Torque Mode

The compact model assumes a constant value for the mechanical torque $T_m(t)$ and is of the form:
$T_m(t) = -T_m$. The minus sign is because of the convention that the positive direction is into the device.

Constant Power Mode

The compact model assumes a constant value for the mechanical power produced by the unit, $P_m(t)$ and is of the form:
$P_m(t) = -P_m$. The minus sign is because of the convention that the positive direction is into the device. The produced torque value is computed as $T_m(t) = \frac{P_m(t)}{\omega_m(t)} = -\frac{P_m}{\omega_m(t)}$, where ω_m is the operating mechanical speed of the generating unit.

User Interface and Model Parameters

The model user interface for both constant torque and constant current modes are presented in Figure 4.11 and Figure 4.12 respectively.

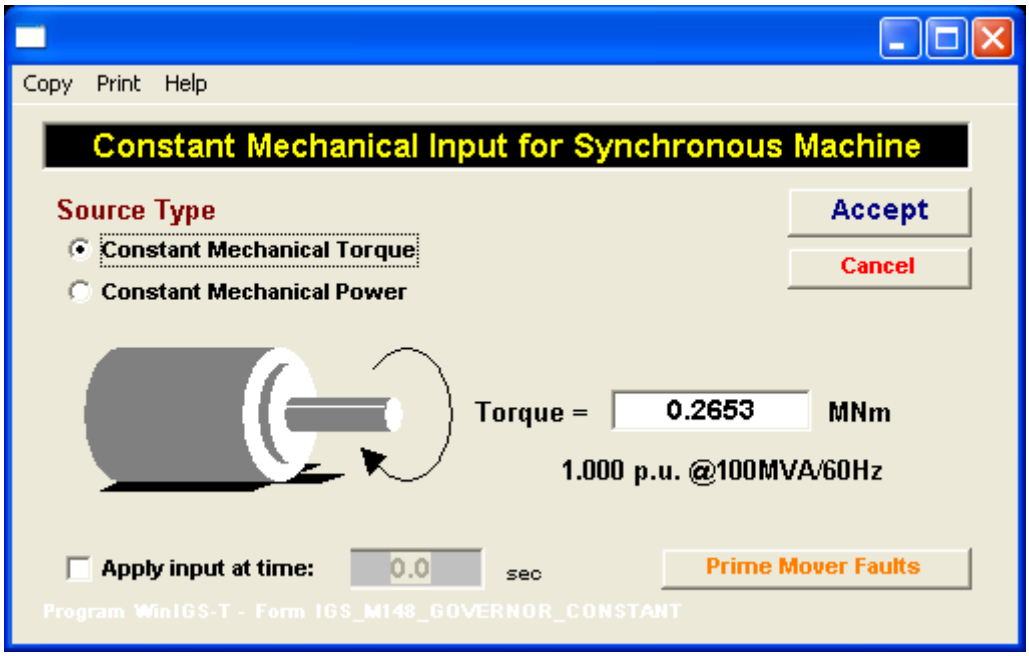


Figure 4.11. Constant Torque Input Prime Mover Model Interface.

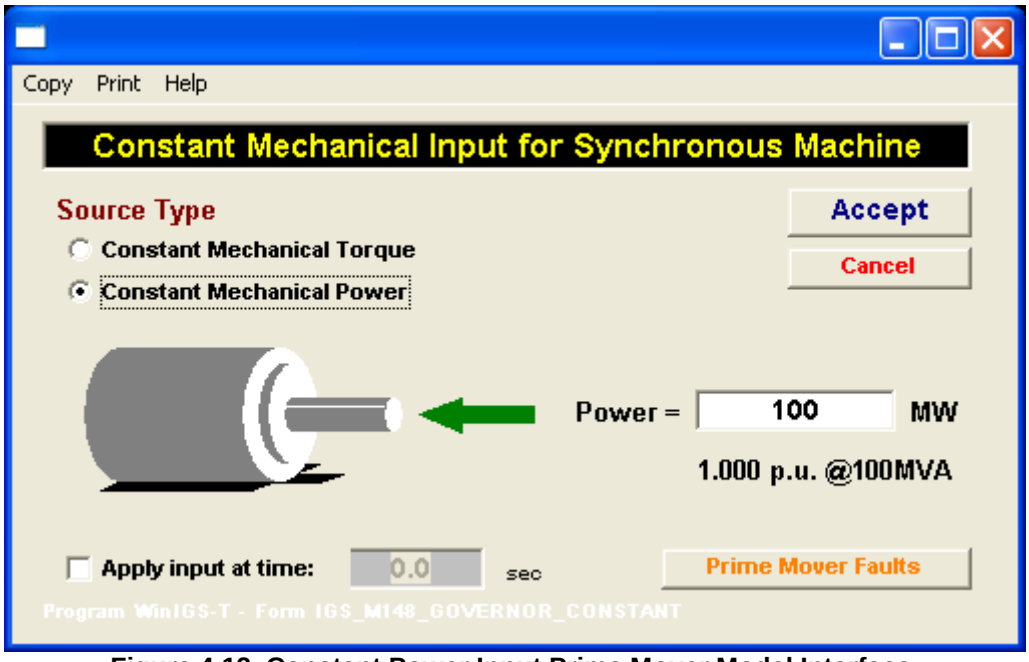


Figure 4.12. Constant Power Input Prime Mover Model Interface.

Generic Prime Mover Model

Steady-State Model

The static model used for steady state analysis is presented first. No changes take place in the system, and therefore all the derivatives of the full dynamic model (described in the next sections) are set to zero. The differential equations are therefore converted into algebraic equations and thus the model consists of a set of algebraic equations, linear or quadratic. The mechanical speed is a constant, usually assumed equal to the synchronous mechanical speed. These equations are also used for the initialization of the time domain models, based on a frequency domain system solution.

The compact model of a generic turbine-governor system is a second order system. Nonlinearities are introduced in the system by the conversion of mechanical power to mechanical torque and by adding a non-windup limiter that limits the output of the governor. Three operating modes are defined: (a) the unit is not on AGC (automatic generation control) and controls the produced output power, (b) the unit is not on AGC (automatic generation control) and controls its speed and (c) the unit is on AGC. In the first case a feedback is taken from the electrical power produced by the unit; this is compared to a power production setpoint and the error is the input of the governor system. In the second case, where the unit is controlling its speed, the speed setpoint is provided as reference and it is compared to a speed feedback. The error is fed to the governor system after being amplified by the droop of the unit. In the third case, where the unit is on AGC, apart from the speed setpoint an additional control signal is provided from the AGC system and goes though and integral control defining the unit power setpoint, so that the frequency error is zero. Based on the above description six modes of operation are defined: 1. Unit is not on AGC, power controlled, limits are not considered;

2. unit is not on AGC, power controlled, limits are considered; 3. unit is not on AGC, speed controlled, limits are not considered; 4. unit is not on AGC, speed controlled, limits are considered; 5. unit is on AGC, limits are not considered; 6. unit is on AGC, limits are considered.

1. Unit is not on AGC, power-controlled, limits are not considered

The compact model is of the form:

$$0 = 2P_{set} - P_m - P_T$$
$$0 = P_T - P_m \qquad (4.37)$$
$$T_m = \frac{P_m}{\omega_m}$$

2. Unit is not on AGC, power-controlled, limits are considered

The compact model is of the form:
For non-windup limits

If $P^{\min} \le P_T \le P^{\max}$

$$0 = 2P_{set} - P_m - P_T$$
$$0 = P_T - P_m$$
$$T_m = \frac{P_m}{\omega_m}$$

else if $P_T < P^{\min}$

$$P_T = P^{\min}$$
$$0 = 2P_{set} - P_m - P_T \qquad (4.38)$$
$$0 = P_T - P_m$$
$$T_m = \frac{P_m}{\omega_m}$$

else if $P_T > P^{\max}$

$$P_T = P^{\max}$$
$$0 = 2P_{set} - P_m - P_T$$
$$0 = P_T - P_m$$
$$T_m = \frac{P_m}{\omega_m}$$

For windup limits

$$0 = 2P_{set} - P_m - P_T$$
$$0 = P_T^* - P_m$$
$$T_m = \frac{P_m}{\omega_m}$$

If $P^{\min} \le P_T \le P^{\max}$

$$0 = P_T^* - P_T$$

else if $P_T < P^{\min}$ (4.39)

$$P_T^* = P^{\min}$$

else if $P_T > P^{\max}$

$$P_T^* = P^{\max}$$

3. Unit is not on AGC, speed-controlled, limits are not considered

The compact model is of the form:

$$0 = P_{set} - \frac{1}{R} \cdot (\omega_m - \omega_{set})$$

$$0 = P_T - P_m \quad (4.40)$$

$$T_m = \frac{P_m}{\omega_m}$$

4. Unit is not on AGC, speed-controlled, limits are considered

The compact model is of the form:
For non-windup limits
If $P^{\min} \le P_T \le P^{\max}$

$$0 = P_{set} - \frac{1}{R} \cdot (\omega_m - \omega_{set})$$

$$0 = P_T - P_m$$

$$T_m = \frac{P_m}{\omega_m}$$

else if $P_T < P^{\min}$

$$P_T = P^{\min}$$

$$0 = P_{set} - \frac{1}{R} \cdot (\omega_m - \omega_{set}) \quad (4.41)$$

$$0 = P_T - P_m$$

$$T_m = \frac{P_m}{\omega_m}$$

else if $P_T > P^{\max}$

$$P_T = P^{\max}$$

$$0 = P_{set} - \frac{1}{R} \cdot (\omega_m - \omega_{set})$$

$$0 = P_T - P_m$$

$$T_m = \frac{P_m}{\omega_m}$$

For windup limits
If $P^{\min} \le P_T \le P^{\max}$

$$0 = P_{set} - \frac{1}{R} \cdot (\omega_m - \omega_{set})$$
$$0 = P_T^* - P_m$$
$$T_m = \frac{P_m}{\omega_m}$$

else if $P_T < P^{\min}$

$$P_T^* = P^{\min}$$
$$0 = P_{set} - \frac{1}{R} \cdot (\omega_m - \omega_{set}) \qquad (4.42)$$
$$0 = P_T^* - P_m$$
$$T_m = \frac{P_m}{\omega_m}$$

else if $P_T > P^{\max}$

$$P_T^* = P^{\max}$$
$$0 = P_{set} - \frac{1}{R} \cdot (\omega_m - \omega_{set})$$
$$0 = P_T^* - P_m$$
$$T_m = \frac{P_m}{\omega_m}$$

5. Unit is on AGC, limits are not considered

The compact model is of the form:

$$0 = P_{set} - \frac{1}{R} \cdot (\omega_m - \omega_{set})$$
$$0 = P_T - P_m \qquad (4.43)$$
$$0 = -K(B(\omega_m - \omega_s) + P_{AGC})$$
$$T_m = \frac{P_m}{\omega_m}$$

6. Unit is on AGC, limits are considered

The compact model is of the form:
For non-windup limits
If $P^{\min} \le P_T \le P^{\max}$

$$0 = P_{set} - \frac{1}{R} \cdot (\omega_m - \omega_{set})$$
$$0 = P_T - P_m$$
$$0 = -K(B(\omega_m - \omega_s) + P_{AGC})$$
$$T_m = \frac{P_m}{\omega_m}$$

else if $P_T < P^{\min}$

$$P_T = P^{\min}$$

$$0 = P_{set} - \frac{1}{R} \cdot (\omega_m - \omega_{set}) \qquad (4.44)$$

$$0 = P_T - P_m$$

$$0 = -K(B(\omega_m - \omega_s) + P_{AGC})$$

$$T_m = \frac{P_m}{\omega_m}$$

else if $P_T > P^{\max}$

$$P_T = P^{\max}$$

$$0 = P_{set} - \frac{1}{R} \cdot (\omega_m - \omega_{set})$$

$$0 = P_T - P_m$$

$$0 = -K(B(\omega_m - \omega_s) + P_{AGC})$$

$$T_m = \frac{P_m}{\omega_m}$$

For windup limits

$$0 = P_{set} - \frac{1}{R} \cdot (\omega_m - \omega_{set})$$

$$0 = P_T^* - P_m$$

$$0 = -K(B(\omega_m - \omega_s) + P_{AGC})$$

$$T_m = \frac{P_m}{\omega_m}$$

If $P^{\min} \le P_T \le P^{\max}$ (4.45)

$$0 = P_T^* - P_T$$

else if $P_T < P^{\min}$

$$P_T^* = P^{\min}$$

else if $P_T > P^{\max}$

$$P_T^* = P^{\max}$$

Dynamic Model

The compact model of a generic turbine-governor system is a second order dynamical system. The governor is represented as a single time-delay unit and the turbine as a second time delay until. Nonlinearities are introduced in the system by the conversion of mechanical power to mechanical torque and by adding a non-windup limiter that limits the output of the governor. Three operating modes are defined: (a) the unit is not on AGC (automatic generation control) and controls the produced output power, (b) the unit is not on AGC (automatic generation control) and controls its speed and (c) the unit is on AGC. In the first case a feedback is taken from the electrical power produced by the unit; this is

compared to a power production setpoint and the error is the input of the governor system. In the second case, where the unit is controlling its speed, the speed setpoint is provided as reference and it is compared to a speed feedback. The error is fed to the governor system after being amplified by the droop of the unit. In the third case, where the unit is on AGC, apart from the speed setpoint an additional control signal is provided from the AGC system and goes though and integral control defining the unit power setpoint, so that the frequency error is zero. Based on the above description six modes of operation are defined: 1. Unit is not on AGC, power controlled, limits are not considered; 2. unit is not on AGC, power controlled, limits are considered; 3. unit is not on AGC, speed controlled, limits are not considered; 4. unit is not on AGC, speed controlled, limits are considered; 5. unit is on AGC, limits are not considered; 6. unit is on AGC, limits are considered.

1. Unit is not on AGC, power-controlled, limits are not considered

The compact model is of the form:

$$T_G \frac{dP_T(t)}{dt} = 2P_{set} - P_m(t) - P_T(t)$$
$$T_t \frac{dP_m(t)}{dt} = P_T(t) - P_m(t) \qquad (4.46)$$
$$T_m(t) = \frac{P_m(t)}{\omega_m(t)}$$

2. Unit is not on AGC, power-controlled, limits are considered

The compact model is of the form:
For non-windup limits

If $P^{\min} \le P_T(t) \le P^{\max}$

$$T_G \frac{dP_T(t)}{dt} = 2P_{set} - P_m(t) - P_T(t)$$

else if $P_T(t) < P^{\min}$ and $\frac{dP_T(t)}{dt} < 0$

$$P_T(t) = P^{\min}$$
$$\frac{dP_T(t)}{dt} = 0 \Leftrightarrow 2P_{set} - P_m(t) - P_T(t) = 0 \qquad (4.47)$$

else if $P_T(t) > P^{\max}$ and $\frac{dP_T(t)}{dt} > 0$

$$P_T(t) = P^{\max}$$
$$\frac{dP_T(t)}{dt} = 0 \Leftrightarrow 2P_{set} - P_m(t) - P_T(t) = 0$$

$$T_t \frac{dP_m(t)}{dt} = P_T(t) - P_m(t)$$
$$T_m(t) = \frac{P_m(t)}{\omega_m(t)}$$

For windup limits

$$T_G \frac{dP_T(t)}{dt} = 2P_{set} - P_m(t) - P_T(t)$$

$$T_t \frac{dP_m(t)}{dt} = P_T^*(t) - P_m(t)$$

$$T_m(t) = \frac{P_m(t)}{\omega_m(t)} \tag{4.48}$$

If $P^{\min} \le P_T(t) \le P^{\max}$

$$0 = P_T^*(t) - P_T(t)$$

else if $P_T(t) < P^{\min}$

$$P_T^*(t) = P^{\min}$$

else if $P_T(t) > P^{\max}$

$$P_T^*(t) = P^{\max}$$

3. Unit is not on AGC, speed-controlled, limits are not considered

The compact model is of the form:

$$T_G \frac{dP_T(t)}{dt} = P_{set} - \frac{1}{R} \cdot \left(\omega_m(t) - \omega_{set}\right)$$

$$T_t \frac{dP_m(t)}{dt} = P_T(t) - P_m(t) \tag{4.49}$$

$$T_m(t) = \frac{P_m(t)}{\omega_m(t)}$$

4. Unit is not on AGC, speed-controlled, limits are considered

The compact model is of the form:

For non-windup limits

If $P^{\min} \le P_T(t) \le P^{\max}$

$$T_G \frac{dP_T(t)}{dt} = P_{set} - \frac{1}{R} \cdot \left(\omega_m(t) - \omega_{set}\right)$$

else if $P_T(t) < P^{\min}$ and $\frac{dP_T(t)}{dt} < 0$

$$P_T(t) = P^{\min}$$

$$\frac{dP_T(t)}{dt} = 0 \Leftrightarrow P_{set} - \frac{1}{R} \cdot \left(\omega_m(t) - \omega_{set}\right) = 0 \tag{4.50}$$

else if $P_T(t) > P^{\max}$ and $\frac{dP_T(t)}{dt} > 0$

$$P_T(t) = P^{\max}$$

$$\frac{dP_T(t)}{dt} = 0 \Leftrightarrow P_{set} - \frac{1}{R} \cdot \left(\omega_m(t) - \omega_{set}\right) = 0$$

$$T_t \frac{dP_m(t)}{dt} = P_T(t) - P_m(t)$$

$$T_m(t) = \frac{P_m(t)}{\omega_m(t)}$$

For windup limits

$$T_G \frac{dP_T(t)}{dt} = P_{set} - \frac{1}{R} \cdot \left(\omega_m(t) - \omega_{set}\right)$$

$$T_t \frac{dP_m(t)}{dt} = P_T^*(t) - P_m(t)$$

$$T_m(t) = \frac{P_m(t)}{\omega_m(t)} \qquad (4.51)$$

If $P^{\min} \le P_T(t) \le P^{\max}$

$$0 = P_T^*(t) - P_T(t)$$

else if $P_T(t) < P^{\min}$

$$P_T^*(t) = P^{\min}$$

else if $P_T(t) > P^{\max}$

$$P_T^*(t) = P^{\max}$$

5. Unit is on AGC, limits are not considered

The compact model is of the form:

$$T_G \frac{dP_T(t)}{dt} = P_{set}(t) - \frac{1}{R} \cdot \left(\omega_m(t) - \omega_{set}\right)$$

$$T_t \frac{dP_m(t)}{dt} = P_T(t) - P_m(t) \qquad (4.52)$$

$$\frac{dP_{set}(t)}{dt} = -K\left(B\left(\omega_m(t) - \omega_s\right) + P_{AGC}\right)$$

$$T_m(t) = \frac{P_m(t)}{\omega_m(t)}$$

6. Unit is on AGC, limits are considered

The compact model is of the form:

For non-windup limits

If $P^{\min} \le P_T(t) \le P^{\max}$

$$T_G \frac{dP_T(t)}{dt} = P_{set}(t) - \frac{1}{R} \cdot \left(\omega_m(t) - \omega_{set}\right)$$

else if $P_T(t) < P^{\min}$ and $\frac{dP_T(t)}{dt} < 0$

$$P_T(t) = P^{\min}$$

$$\frac{dP_T(t)}{dt} = 0 \Leftrightarrow P_{set}(t) - \frac{1}{R} \cdot \left(\omega_m(t) - \omega_{set}\right) = 0$$

else if $P_T(t) > P^{\max}$ and $\frac{dP_T(t)}{dt} > 0$ (4.53)

$$P_T(t) = P^{\max}$$

$$\frac{dP_T(t)}{dt} = 0 \Leftrightarrow P_{set}(t) - \frac{1}{R} \cdot \left(\omega_m(t) - \omega_{set}\right) = 0$$

$$T_t \frac{dP_m(t)}{dt} = P_T(t) - P_m(t)$$

$$\frac{dP_{set}(t)}{dt} = -K\left(B\left(\omega_m(t) - \omega_s\right) + P_{AGC}\right)$$

$$T_m(t) = \frac{P_m(t)}{\omega_m(t)}$$

For windup limits

$$T_G \frac{dP_T(t)}{dt} = P_{set}(t) - \frac{1}{R} \cdot \left(\omega_m(t) - \omega_{set}\right)$$

$$T_t \frac{dP_m(t)}{dt} = P_T^*(t) - P_m(t)$$

$$\frac{dP_{set}(t)}{dt} = -K\left(B\left(\omega_m(t) - \omega_s\right) + P_{AGC}\right) \quad (4.54)$$

$$T_m(t) = \frac{P_m(t)}{\omega_m(t)}$$

If $P^{\min} \le P_T(t) \le P^{\max}$

$$0 = P_T^*(t) - P_T(t)$$

else if $P_T(t) < P^{\min}$

$$P_T^*(t) = P^{\min}$$

else if $P_T(t) > P^{\max}$

$$P_T^*(t) = P^{\max}$$

User Interface and Model Parameters

The model user interface for the three main operating modes are presented in Figure 4.13 through Figure 4.15.

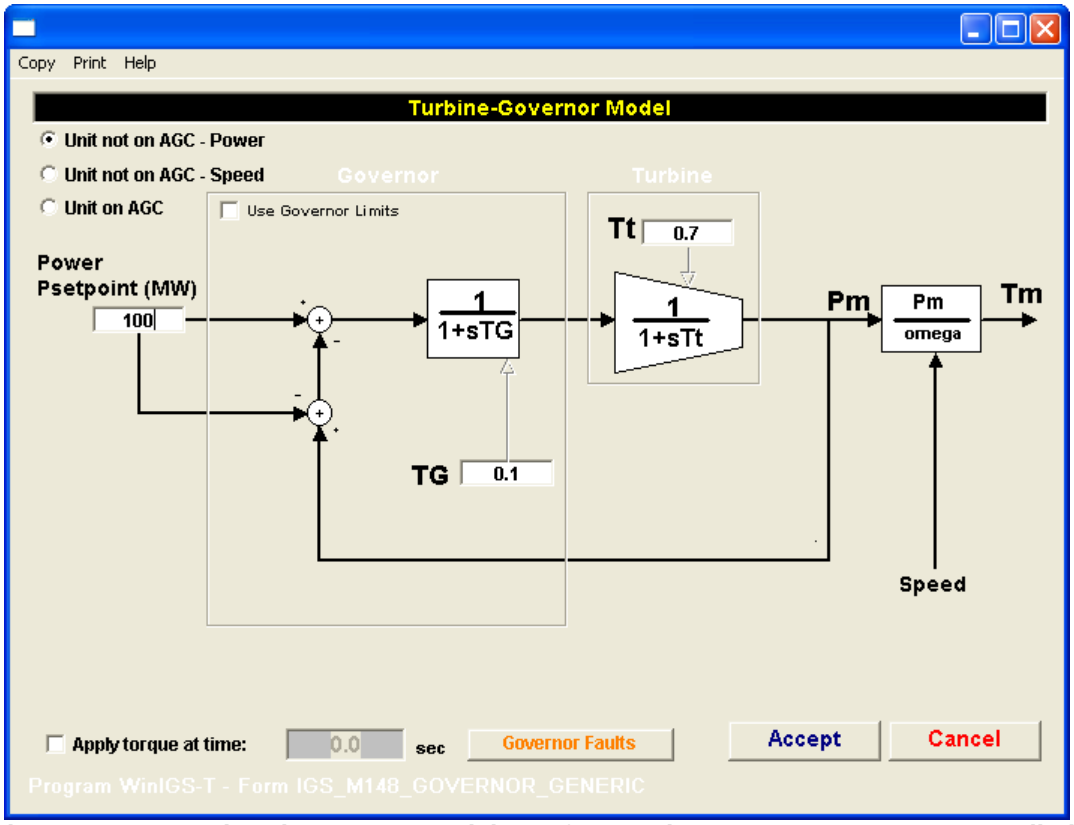


Figure 4.13. Generic Prime Mover Model Interface. Unit not on AGC, Power-Controlled.

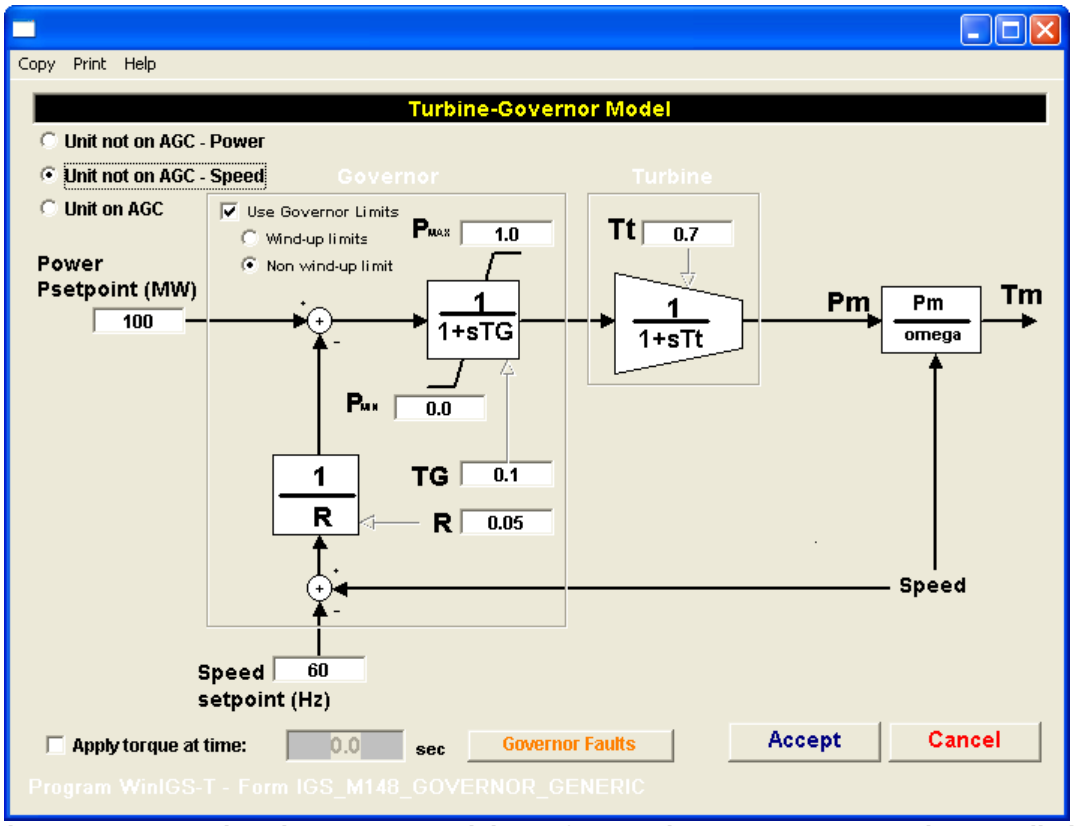


Figure 4.14. Generic Prime Mover Model Interface. Unit not on AGC, Speed-Controlled.

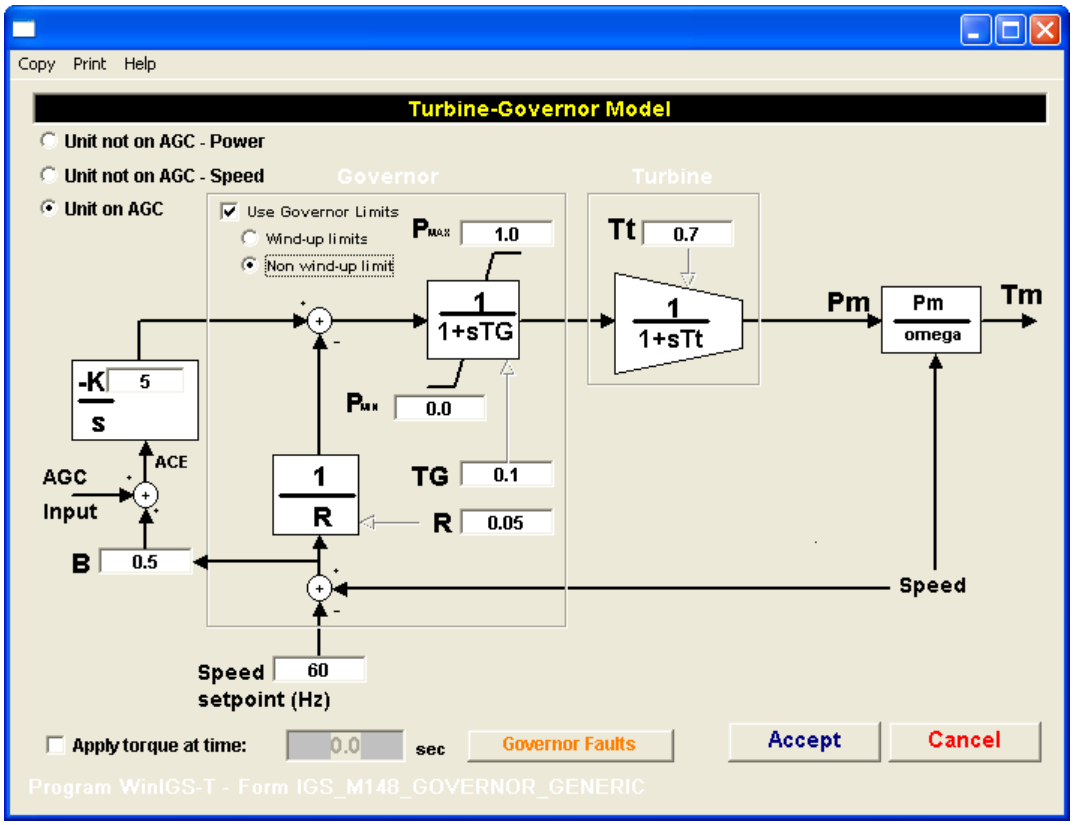


Figure 4.15. Generic Prime Mover Model Interface. Unit on AGC Mode.

Constant Voltage/Current Excitation System Model

In this model the dynamic effects of the excitation and voltage regulation system are ignored. In steady-state and quasi-static analysis it is assumed that the generator terminal voltage is maintained constant, by a voltage regulating system that acts practically instantaneously. For more detailed transient analysis it is assumed that a constant DC voltage source is connected to the field terminal that can act as an ideal voltage source, a voltage source with internal resistance or as an ideal current source. However, since the transients of such a source are very fast compared to the time scales of interest for quasi steady state analysis they will be normally neglected if such a model is used.

Steady-State Model

Three operating modes are specified:

(a) The model provides a constant DC field voltage to the generator field terminal. The field voltage does not change during transient operation of the generator, but is kept constant. It is equivalent to connecting an ideal constant DC source to the generator field.

(b) The model operates as a constant DC voltage source behind an internal impedance (resistance). It is equivalent to connecting a DC voltage source with an internal impedance to the field terminal of the generator. The internal EMF of the DC source

is constant, but the field voltage is not constant, as there is a voltage drop across the internal source impedance that is proportional to the field current.

(c) The model provides a constant DC field current value to the generator field winding. The field current is kept constant during the transient operation of the generator. It is equivalent to connecting an ideal current source to the generator field winding. This mode may cause numerical problems in the time domain simulation, because of the step changes in the field winding current, due to the series connection of a current source with an inductor. Therefore, its implementation might not be practical.

Three modes of operation are defined:
(a) Constant field voltage mode,
(b) DC voltage source mode, and
(c) Current source mode.

(a) Constant field voltage mode

The frequency domain model in this mode, in steady-state, is equivalent to having the generating unit operating under PV control. This means that the exciter and voltage regulation system are maintaining a constant voltage level at the output bus of the unit. No additional model for the excitation system is needed.

(b) DC voltage source mode

Alternatively the excitation can be modeled as a constant DC voltage source behind an internal impedance, which is simply a resistance in steady state, since this is a DC circuit. It is equivalent to connecting a DC voltage source with an internal impedance to the field terminal of the generator. The internal EMF of the DC source is constant, but the field voltage depends on the voltage drop across the internal source impedance that is proportional to the field current.

The voltage source with internal resistance is illustrated in Figure 4.18.

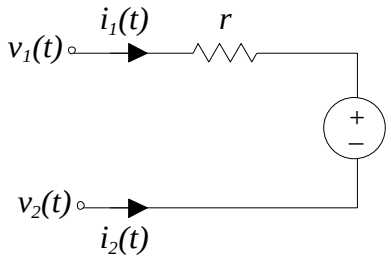


Figure 4.16. Voltage Source with Internal Resistance.

The compact model is:

$$I_1 = g\left(V_1 - V_2 - V_{DC}\right) \qquad (4.55)$$
$$I_2 = -I_1$$

where $g = \frac{1}{r}$ is the conductance of the resistor and V_{DC} denotes the voltage value of the source.

(c) Current Source

The current source diagram is illustrated in Figure 4.19.

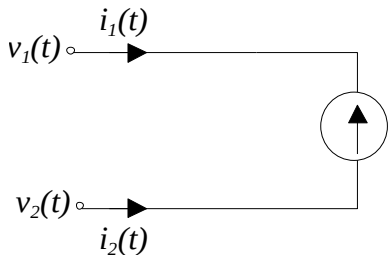


Figure 4.17. Current Source Circuit.

The compact model is:

$$I_1 = -I_{DC} \tag{4.56}$$

$$I_2 = -I_1$$

I_{DC} denotes the value of the current source.

Dynamic Model

Three operating modes are specified for the time domain model as well:

(a) The model provides a constant DC field voltage to the generator field terminal. The field voltage does not change during transient operation of the generator, but is kept constant. It is equivalent to connecting an ideal constant DC source to the generator field.

(b) The model operates as a constant DC voltage source behind an internal impedance. It is equivalent to connecting a DC voltage source with an internal impedance to the field terminal of the generator. The internal EMF of the DC source is constant, but the field voltage is not constant, as there is a voltage drop across the internal source impedance that is proportional to the field current.

(c) The model provides a constant DC field current value to the generator field winding. The field current is kept constant during the transient operation of the generator. It is equivalent to connecting an ideal current source to the generator field winding. This mode may cause numerical problems in the time domain simulation, because of the step changes in the field winding current, due to the series connection of a current source with an inductor. Therefore, its implementation might not be practical.

Three modes of operation are defined:

(a) Constant field voltage mode,
(b) DC voltage source mode, and
(c) Current source mode.

(a) Constant field voltage mode

The constant field voltage mode assumes that the field voltage is specified and remains constant. The two equations for this model are:

$$v_f(t) = V_{specified}$$
$$v_{fn}(t) = 0 \qquad (4.57)$$

Note, that special care needs to be taken in this case, in case a loss of excitation fault is to be applied. In that case, the only possible and meaningful fault that can be considered is a full loss of excitation, in which case the applied voltage becomes zero. This is equivalent to replacing the above two equations by:

$$v_f(t) = 0$$
$$v_{fn}(t) = 0 \qquad (4.58)$$

(b) DC voltage source mode

The DC voltage source mode assumes that a constant, non-ideal DC source, with an internal impedance is connected to the field terminal, supplying the field voltage. The compact equations for this model are:

1. Pure resistive internal impedance model

The voltage source with internal resistance is illustrated in Figure 4.18.

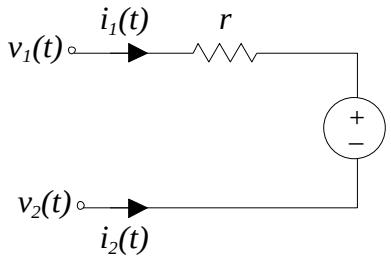


Figure 4.18. Voltage Source with Internal Resistance.

The compact model is:

$$i_1(t) = g\left(v_1(t) - v_2(t) - V_{DC}\right) \qquad (4.59)$$
$$i_2(t) = -i_1(t)$$

where $g = \frac{1}{r}$ is the conductance of the resistor and V_{DC} denotes the voltage value of the source.

2. Pure Inductive Internal Impedance Model

The voltage source with internal resistance is illustrated in Figure 4.19.

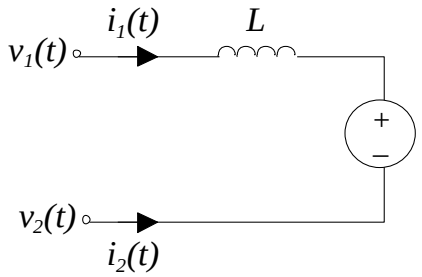


Figure 4.19. Voltage Source with Internal Inductance.

The compact model is:

$$0 = v_1(t) - v_2(t) - L\frac{di_1(t)}{dt} - V_{DC} \tag{4.60}$$
$$i_2(t) = -i_1(t)$$

V_{DC} denotes the voltage value of the source.

3. Resistive-Inductive Internal Impedance Model
The voltage source with internal resistance is illustrated in Figure 4.20.

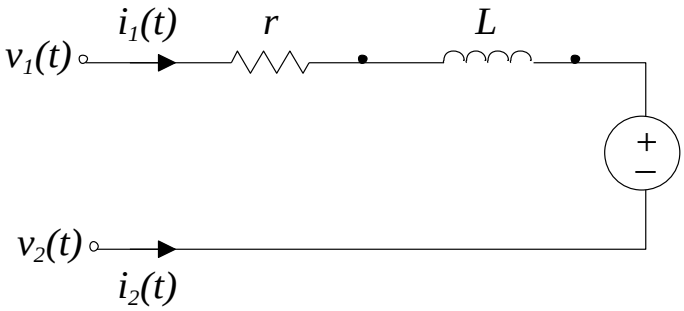


Figure 4.20. Voltage Source with Internal Impedance.

The compact model is:

$$i_1(t) = g\big(v_1(t) - v_2(t)\big) - gL\frac{di_1(t)}{dt} - gV_{DC} \tag{4.61}$$
$$i_2(t) = -i_1(t)$$

V_{DC} denotes the voltage value of the source.

(c) Current Source

The current source diagram is illustrated in Figure 4.21.

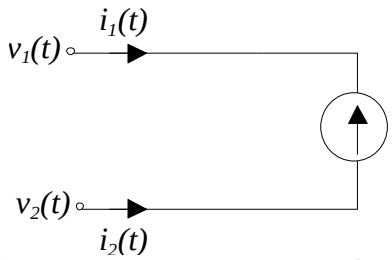


Figure 4.21. Current Source Circuit.

The compact model is:

$$i_1(t) = -I_{DC} \qquad (4.62)$$
$$i_2(t) = -i_1(t)$$

I_{DC} denotes the value of the current source.

User Interface and Model Parameters

The model user interface is presented in Figure 4.22 and Figure 4.23.

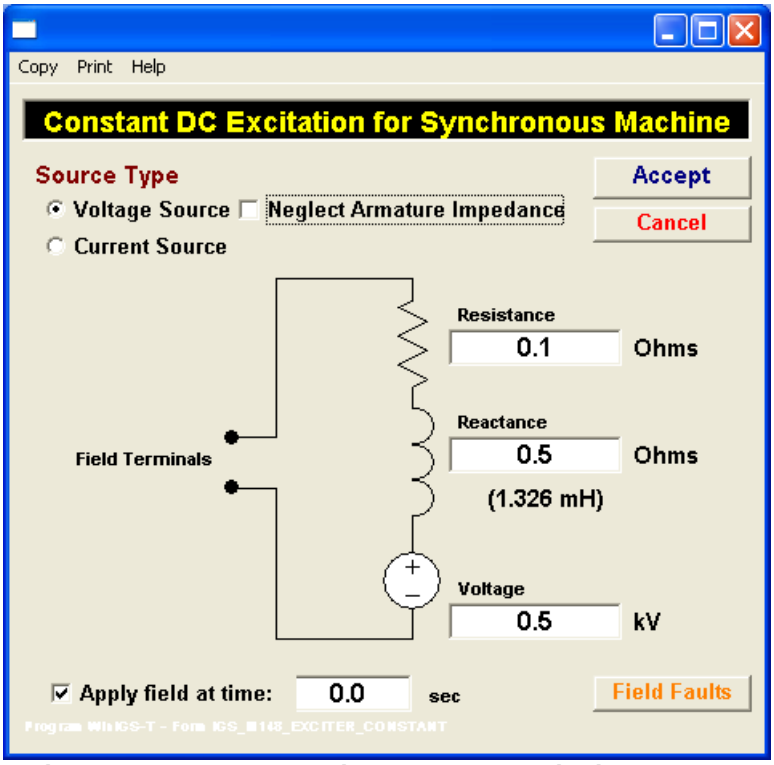


Figure 4.22. Constant Voltage Source Excitation System.

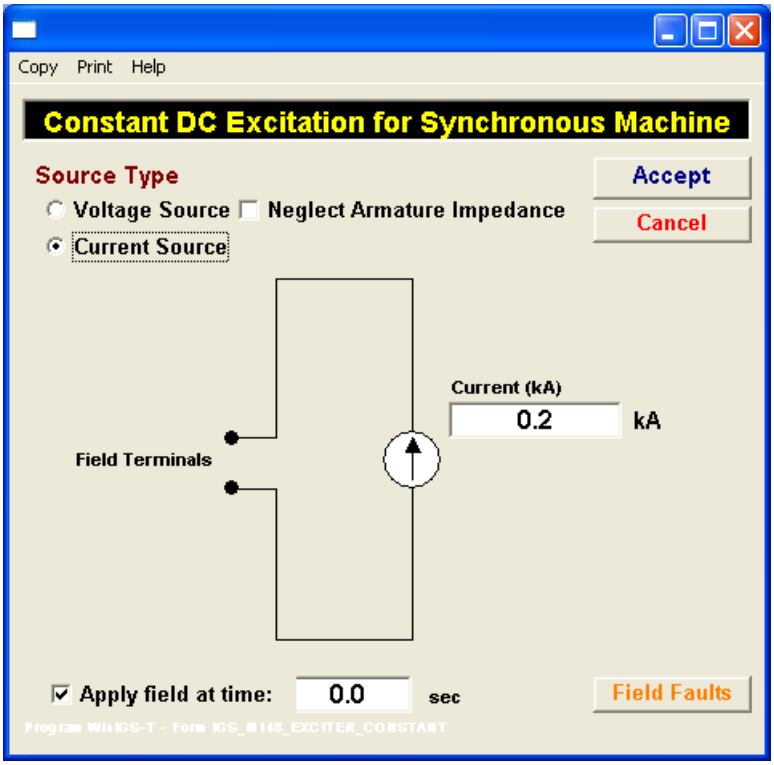


Figure 4.23. Constant Current Source Excitation System.

Generic Excitation System Model

This model of the excitation system assumes that a DC generator is acting as the excitation system of the unit. The model is similar to the DC exciter model, but it is a little bit simpler and more generic. The exciter is again modeled as a DC source with internal impedance connected to the field terminal, as in section 3.1. However, now the DC source is not constant. It is assumed to be a DC motor and its armature is connected to the filed of the generator. The source impedance is simply the armature impedance of the DC machine.

Steady-State Model

The steady state model is derived from the time domain model by assuming steady state conditions, therefore by setting the derivative values to zero. More details on the equations are presented in the time domain section where the complete model is presented.

A simple schematic of the armature circuit with internal resistance is illustrated in Figure 3.2.1.

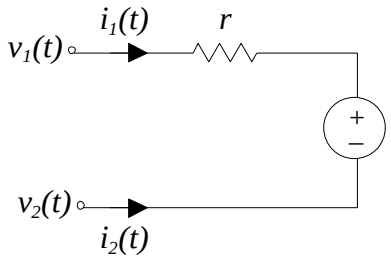


Figure 4.24. DC armature circuit with internal resistance.

The model, if no limits are imposed is:

$$
\begin{aligned}
&I_1 = g\left(V_1 - V_2 - V_{DC}\right)\\
&I_2 = -I_1\\
&0 = -\left(K_E + S_E(V_{DC})\right)\cdot V_{DC} + V_R\\
&0 = -V_R + K_A R_f - \frac{K_A K_F}{T_F} V_{DC} + K_A\left(V_{ref.} - V_t + V_s\right)\\
&0 = -R_f + \frac{K_F}{T_F} V_{DC}
\end{aligned}
\qquad (4.63)
$$

where $g = \frac{1}{r}$ is the conductance of the resistor. The function $S_E(V_{DC})$ models the saturation of the exciter. Its form has not been decided yet, so saturation is neglected. If no exciter saturation is modeled then $S_E(V_{DC}) = 0$.

If limits are imposed to the voltage regulator output the model becomes:

If $V_R^{\min} < V_R(t) < V_R^{\max}$

$$
\begin{aligned}
&I_1 = g\left(V_1 - V_2 - V_{DC}\right)\\
&I_2 = -I_1\\
&0 = -\left(K_E + S_E(V_{DC})\right)\cdot V_{DC} + V_R\\
&0 = -V_R + K_A R_f - \frac{K_A K_F}{T_F} V_{DC} + K_A\left(V_{ref.} - V_t + V_s\right)\\
&0 = -R_f + \frac{K_F}{T_F} V_{DC}
\end{aligned}
$$

else if $V_R(t) \le V_R^{\min}$ (4.64)

$$
\begin{aligned}
&I_1 = g\left(V_1 - V_2 - V_{DC}\right)\\
&I_2 = -I_1\\
&0 = -\left(K_E + S_E(V_{DC})\right)\cdot V_{DC} + V_R\\
&0 = -V_R + K_A R_f - \frac{K_A K_F}{T_F} V_{DC} + K_A\left(V_{ref.} - V_t + V_s\right)
\end{aligned}
$$

$$0 = -R_f + \frac{K_F}{T_F} V_{DC}$$

$$V_R = V_R^{\min}$$

else if $V_R(t) \geq V_R^{\max}$

$$I_1 = g\left(V_1 - V_2 - V_{DC}\right)$$

$$I_2 = -I_1$$

$$0 = -\left(K_E + S_E(V_{DC})\right) \cdot V_{DC} + V_R$$

$$0 = -V_R + K_A R_f - \frac{K_A K_F}{T_F} V_{DC} + K_A\left(V_{ref.} - V_t + V_s\right)$$

$$0 = -R_f + \frac{K_F}{T_F} V_{DC}$$

$$V_R = V_R^{\max}$$

Dynamic Model

Three cases are defined based on the armature impedance of the DC exciter. The following sets of DAEs describe the model of the excitation system in each case in compact form.

1. Pure resistive internal impedance model

A simple schematic of the armature circuit with internal resistance is illustrated in Figure 4.25.

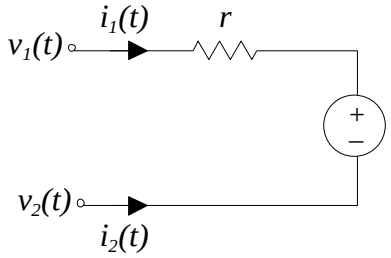


Figure 4.25. DC Armature Circuit with Internal Resistance

The compact model, if no limits are imposed is:

$$i_1(t) = g\left(v_1(t) - v_2(t) - V_{DC}(t)\right)$$

$$i_2(t) = -i_1(t)$$

$$T_E \frac{dV_{DC}(t)}{dt} = -\left(K_E + S_E(V_{DC}(t))\right) \cdot V_{DC}(t) + V_R(t) \qquad (4.65)$$

$$T_A \frac{dV_R(t)}{dt} = -V_R(t) + K_A R_f(t) - \frac{K_A K_F}{T_F} V_{DC}(t) + K_A\left(V_{ref.} - V_t(t) + V_s(t)\right)$$

$$T_F \frac{dR_f(t)}{dt} = -R_f(t) + \frac{K_F}{T_F} V_{DC}(t)$$

where $g = \frac{1}{r}$ is the conductance of the resistor. The function $S_E(V_{DC})$ models the saturation of the exciter. Its form has not been decided yet. If no exciter saturation is modeled then $S_E(V_{DC}) = 0$. The first differential equation represents the dynamics of the DC machine. The armature dynamics are neglected. The second differential equation models the voltage regulator. $V_{ref.}$ is a model input, while $V_t(t)$ is a feedback of the unit terminal voltage that is to be regulated. It can be uncompensated or compensated, to accommodate parallel operation of two units connected at the same bus, using load compensation. The last differential equation models the dynamic behavior of the stabilizing transformer or the system.

If non-windup limits are imposed to the voltage regulator output the compact model becomes:

If $V_R^{\min} < V_R(t) < V_R^{\max}$

$$i_1(t) = g\left(v_1(t) - v_2(t) - V_{DC}(t)\right)$$

$$i_2(t) = -i_1(t)$$

$$T_E \frac{dV_{DC}(t)}{dt} = -\left(K_E + S_E(V_{DC}(t))\right) \cdot V_{DC}(t) + V_R(t)$$

$$T_A \frac{dV_R(t)}{dt} = -V_R(t) + K_A R_f(t) - \frac{K_A K_F}{T_F} V_{DC}(t) + K_A\left(V_{ref.} - V_t(t) + V_s(t)\right)$$

$$T_F \frac{dR_f(t)}{dt} = -R_f(t) + \frac{K_F}{T_F} V_{DC}(t)$$

else if $V_R(t) \le V_R^{\min}$ and $\frac{dV_R(t)}{dt} < 0$

$$i_1(t) = g\left(v_1(t) - v_2(t) - V_{DC}(t)\right)$$

$$i_2(t) = -i_1(t)$$

$$T_E \frac{dV_{DC}(t)}{dt} = -\left(K_E + S_E(V_{DC}(t))\right) \cdot V_{DC}(t) + V_R(t)$$

$$V_R(t) = V_R^{\min}$$

$$\frac{dV_R(t)}{dt} = 0 \Leftrightarrow 0 = -V_R(t) + K_A R_f(t) - \frac{K_A K_F}{T_F} V_{DC}(t) + K_A\left(V_{ref.} - V_t(t) + V_s(t)\right)$$

$$T_F \frac{dR_f(t)}{dt} = -R_f(t) + \frac{K_F}{T_F} V_{DC}(t) \qquad (4.66)$$

else if $V_R(t) \ge V_R^{\max}$ and $\frac{dV_R(t)}{dt} > 0$

$$i_1(t) = g\left(v_1(t) - v_2(t) - V_{DC}(t)\right)$$

$$i_2(t) = -i_1(t)$$

$$T_E \frac{dV_{DC}(t)}{dt} = -\left(K_E + S_E(V_{DC}(t))\right) \cdot V_{DC}(t) + V_R(t)$$

$$V_R(t) = V_R^{\max}$$

$$\frac{dV_R(t)}{dt} = 0 \Leftrightarrow 0 = -V_R(t) + K_A R_f(t) - \frac{K_A K_F}{T_F} V_{DC}(t) + K_A\left(V_{ref.} - V_t(t) + V_s(t)\right)$$

$$T_F \frac{dR_f(t)}{dt} = -R_f(t) + \frac{K_F}{T_F} V_{DC}(t)$$

else if $V_R(t) \le V_R^{\min}$ and $\frac{dV_R(t)}{dt} \ge 0$

$$i_1(t) = g\left(v_1(t) - v_2(t) - V_{DC}(t)\right) \qquad (4.66)$$

$$i_2(t) = -i_1(t)$$

$$T_E \frac{dV_{DC}(t)}{dt} = -\left(K_E + S_E(V_{DC}(t))\right) \cdot V_{DC}(t) + V_R(t)$$

$$T_A \frac{dV_R(t)}{dt} = -V_R(t) + K_A R_f(t) - \frac{K_A K_F}{T_F} V_{DC}(t) + K_A\left(V_{ref.} - V_t(t) + V_s(t)\right)$$

$$T_F \frac{dR_f(t)}{dt} = -R_f(t) + \frac{K_F}{T_F} V_{DC}(t)$$

$$V_R(t) = V_R^{\min}$$

else if $V_R(t) \ge V_R^{\max}$ and $\frac{dV_R(t)}{dt} \le 0$

$$i_1(t) = g\left(v_1(t) - v_2(t) - V_{DC}(t)\right)$$

$$i_2(t) = -i_1(t)$$

$$T_E \frac{dV_{DC}(t)}{dt} = -\left(K_E + S_E(V_{DC}(t))\right) \cdot V_{DC}(t) + V_R(t)$$

$$T_A \frac{dV_R(t)}{dt} = -V_R(t) + K_A R_f(t) - \frac{K_A K_F}{T_F} V_{DC}(t) + K_A\left(V_{ref.} - V_t(t) + V_s(t)\right)$$

$$T_F \frac{dR_f(t)}{dt} = -R_f(t) + \frac{K_F}{T_F} V_{DC}(t)$$

$$V_R(t) = V_R^{\max}$$

If windup limits are imposed to the voltage regulator output the compact model becomes:

If $V_R^{\min} < V_R(t) < V_R^{\max}$

$$i_1(t) = g\left(v_1(t) - v_2(t) - V_{DC}(t)\right)$$

$$i_2(t) = -i_1(t)$$

$$T_E \frac{dV_{DC}(t)}{dt} = -\left(K_E + S_E(V_{DC}(t))\right) \cdot V_{DC}(t) + V_R(t)$$

$$T_A \frac{dV_R(t)}{dt} = -V_R(t) + K_A R_f(t) - \frac{K_A K_F}{T_F} V_{DC}(t) + K_A\left(V_{ref.} - V_t(t) + V_s(t)\right) \qquad (4.67)$$

$$T_F \frac{dR_f(t)}{dt} = -R_f(t) + \frac{K_F}{T_F} V_{DC}(t)$$

else if $V_R(t) \le V_R^{\min}$

$$i_1(t) = g\left(v_1(t) - v_2(t) - V_{DC}(t)\right)$$
$$i_2(t) = -i_1(t)$$
$$T_E \frac{dV_{DC}(t)}{dt} = -\left(K_E + S_E(V_{DC}(t))\right) \cdot V_{DC}(t) + V_R^*(t)$$
$$V_R^*(t) = V_R^{\min}$$
$$T_A \frac{dV_R(t)}{dt} = -V_R(t) + K_A R_f(t) - \frac{K_A K_F}{T_F} V_{DC}(t) + K_A\left(V_{ref.} - V_t(t) + V_s(t)\right)$$
$$T_F \frac{dR_f(t)}{dt} = -R_f(t) + \frac{K_F}{T_F} V_{DC}(t)$$
else if $V_R(t) \geq V_R^{\max}$ (4.67)
$$i_1(t) = g\left(v_1(t) - v_2(t) - V_{DC}(t)\right)$$
$$i_2(t) = -i_1(t)$$
$$T_E \frac{dV_{DC}(t)}{dt} = -\left(K_E + S_E(V_{DC}(t))\right) \cdot V_{DC}(t) + V_R^*(t)$$
$$V_R^*(t) = V_R^{\max}$$
$$T_A \frac{dV_R(t)}{dt} = -V_R(t) + K_A R_f(t) - \frac{K_A K_F}{T_F} V_{DC}(t) + K_A\left(V_{ref.} - V_t(t) + V_s(t)\right)$$
$$T_F \frac{dR_f(t)}{dt} = -R_f(t) + \frac{K_F}{T_F} V_{DC}(t)$$

2. Pure inductive internal impedance model

The voltage source with internal resistance is illustrated in Figure 4.26.

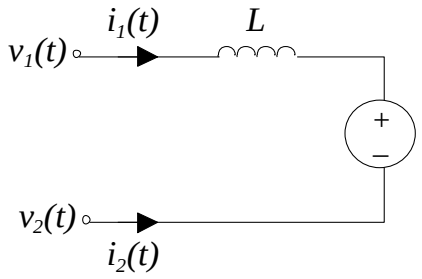


Figure 4.26. DC Armature Circuit with Internal Inductance.

The compact model, if no limits are imposed is:

$$0 = v_1(t) - v_2(t) - L\frac{di_1(t)}{dt} - V_{DC}(t)$$
$$i_2(t) = -i_1(t)$$
$$T_E \frac{dV_{DC}(t)}{dt} = -\left(K_E + S_E(V_{DC}(t))\right) \cdot V_{DC}(t) + V_R(t) \quad (4.68)$$

$$T_A \frac{dV_R(t)}{dt} = -V_R(t) + K_A R_f(t) - \frac{K_A K_F}{T_F} V_{DC}(t) + K_A \left(V_{ref.} - V_t(t) + V_s(t) \right)$$

$$T_F \frac{dR_f(t)}{dt} = -R_f(t) + \frac{K_F}{T_F} V_{DC}(t)$$

The explanation of symbols and equations is the same as in the previous paragraph.
If non-windup limits are imposed to the voltage regulator output the compact model becomes:

If $V_R^{\min} < V_R(t) < V_R^{\max}$

$$0 = v_1(t) - v_2(t) - L \frac{di_1(t)}{dt} - V_{DC}(t)$$

$$i_2(t) = -i_1(t)$$

$$T_E \frac{dV_{DC}(t)}{dt} = -\left(K_E + S_E(V_{DC}(t)) \right) \cdot V_{DC}(t) + V_R(t)$$

$$T_A \frac{dV_R(t)}{dt} = -V_R(t) + K_A R_f(t) - \frac{K_A K_F}{T_F} V_{DC}(t) + K_A \left(V_{ref.} - V_t(t) + V_s(t) \right)$$

$$T_F \frac{dR_f(t)}{dt} = -R_f(t) + \frac{K_F}{T_F} V_{DC}(t)$$

else if $V_R(t) \le V_R^{\min}$ and $\frac{dV_R(t)}{dt} < 0$

$$0 = v_1(t) - v_2(t) - L \frac{di_1(t)}{dt} - V_{DC}(t)$$

$$i_2(t) = -i_1(t)$$

$$T_E \frac{dV_{DC}(t)}{dt} = -\left(K_E + S_E(V_{DC}(t)) \right) \cdot V_{DC}(t) + V_R(t)$$

$$V_R(t) = V_R^{\min}$$

$$\frac{dV_R(t)}{dt} = 0 \Leftrightarrow 0 = -V_R(t) + K_A R_f(t) - \frac{K_A K_F}{T_F} V_{DC}(t) + K_A \left(V_{ref.} - V_t(t) + V_s(t) \right)$$

$$T_F \frac{dR_f(t)}{dt} = -R_f(t) + \frac{K_F}{T_F} V_{DC}(t)$$

else if $V_R(t) \ge V_R^{\max}$ and $\frac{dV_R(t)}{dt} > 0$ (4.69)

$$0 = v_1(t) - v_2(t) - L \frac{di_1(t)}{dt} - V_{DC}(t)$$

$$i_2(t) = -i_1(t)$$

$$T_E \frac{dV_{DC}(t)}{dt} = -\left(K_E + S_E(V_{DC}(t)) \right) \cdot V_{DC}(t) + V_R(t)$$

$$V_R(t) = V_R^{\max}$$

$$\frac{dV_R(t)}{dt} = 0 \Leftrightarrow 0 = -V_R(t) + K_A R_f(t) - \frac{K_A K_F}{T_F} V_{DC}(t) + K_A \left(V_{ref.} - V_t(t) + V_s(t) \right)$$

$$T_F \frac{dR_f(t)}{dt} = -R_f(t) + \frac{K_F}{T_F} V_{DC}(t)$$

else if $V_R(t) \le V_R^{\min}$ and $\frac{dV_R(t)}{dt} \ge 0$

$$0 = v_1(t) - v_2(t) - L\frac{di_1(t)}{dt} - V_{DC}(t)$$

$$i_2(t) = -i_1(t)$$

$$T_E \frac{dV_{DC}(t)}{dt} = -\left(K_E + S_E(V_{DC}(t))\right) \cdot V_{DC}(t) + V_R(t)$$

$$T_A \frac{dV_R(t)}{dt} = -V_R(t) + K_A R_f(t) - \frac{K_A K_F}{T_F} V_{DC}(t) + K_A\left(V_{ref.} - V_t(t) + V_s(t)\right)$$

$$T_F \frac{dR_f(t)}{dt} = -R_f(t) + \frac{K_F}{T_F} V_{DC}(t)$$

$$V_R(t) = V_R^{\min}$$

else if $V_R(t) \ge V_R^{\max}$ and $\frac{dV_R(t)}{dt} \le 0$ (4.69)

$$0 = v_1(t) - v_2(t) - L\frac{di_1(t)}{dt} - V_{DC}(t)$$

$$i_2(t) = -i_1(t)$$

$$T_E \frac{dV_{DC}(t)}{dt} = -\left(K_E + S_E(V_{DC}(t))\right) \cdot V_{DC}(t) + V_R(t)$$

$$T_A \frac{dV_R(t)}{dt} = -V_R(t) + K_A R_f(t) - \frac{K_A K_F}{T_F} V_{DC}(t) + K_A\left(V_{ref.} - V_t(t) + V_s(t)\right)$$

$$T_F \frac{dR_f(t)}{dt} = -R_f(t) + \frac{K_F}{T_F} V_{DC}(t)$$

$$V_R(t) = V_R^{\max}$$

If windup limits are imposed to the voltage regulator output the compact model becomes:

If $V_R^{\min} < V_R(t) < V_R^{\max}$

$$0 = v_1(t) - v_2(t) - L\frac{di_1(t)}{dt} - V_{DC}(t)$$

$$i_2(t) = -i_1(t)$$

$$T_E \frac{dV_{DC}(t)}{dt} = -\left(K_E + S_E(V_{DC}(t))\right) \cdot V_{DC}(t) + V_R(t)$$

$$T_A \frac{dV_R(t)}{dt} = -V_R(t) + K_A R_f(t) - \frac{K_A K_F}{T_F} V_{DC}(t) + K_A\left(V_{ref.} - V_t(t) + V_s(t)\right)$$

$$T_F \frac{dR_f(t)}{dt} = -R_f(t) + \frac{K_F}{T_F} V_{DC}(t)$$

else if $V_R(t) \le V_R^{\min}$ (4.70)

$$0 = v_1(t) - v_2(t) - L\frac{di_1(t)}{dt} - V_{DC}(t)$$

$$i_2(t) = -i_1(t)$$

$$T_E \frac{dV_{DC}(t)}{dt} = -\left(K_E + S_E(V_{DC}(t))\right)\cdot V_{DC}(t) + V_R^*(t)$$

$$T_A \frac{dV_R(t)}{dt} = -V_R(t) + K_A R_f(t) - \frac{K_A K_F}{T_F} V_{DC}(t) + K_A\left(V_{ref.} - V_t(t) + V_s(t)\right)$$

$$T_F \frac{dR_f(t)}{dt} = -R_f(t) + \frac{K_F}{T_F} V_{DC}(t)$$

$$V_R^*(t) = V_R^{\min}$$

else if $V_R(t) \geq V_R^{\max}$

$$0 = v_1(t) - v_2(t) - L\frac{di_1(t)}{dt} - V_{DC}(t)$$

$$i_2(t) = -i_1(t)$$

$$T_E \frac{dV_{DC}(t)}{dt} = -\left(K_E + S_E(V_{DC}(t))\right)\cdot V_{DC}(t) + V_R^*(t)$$

$$T_A \frac{dV_R(t)}{dt} = -V_R(t) + K_A R_f(t) - \frac{K_A K_F}{T_F} V_{DC}(t) + K_A\left(V_{ref.} - V_t(t) + V_s(t)\right)$$

$$T_F \frac{dR_f(t)}{dt} = -R_f(t) + \frac{K_F}{T_F} V_{DC}(t)$$

$$V_R^*(t) = V_R^{\max}$$

3. Resistive-inductive internal impedance model

The voltage source with internal resistance is illustrated in Figure 4.27.

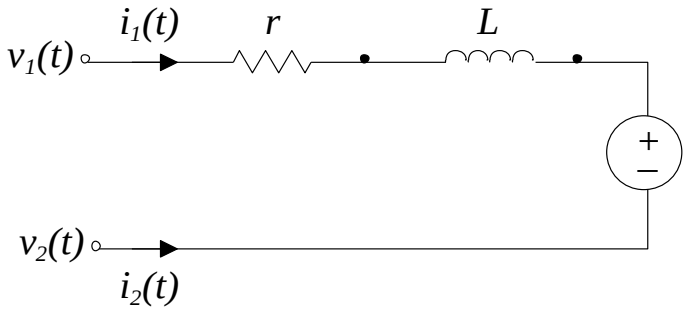


Figure 4.27. DC Armature Circuit with Internal Impedance.

The compact model, if no limits are imposed is:

$$i_1(t) = g\left(v_1(t) - v_2(t)\right) - gL\frac{di_1(t)}{dt} - gV_{DC}$$

$$i_2(t) = -i_1(t)$$

$$T_E \frac{dV_{DC}(t)}{dt} = -\left(K_E + S_E(V_{DC}(t))\right)\cdot V_{DC}(t) + V_R(t) \qquad (4.71)$$

$$T_A \frac{dV_R(t)}{dt} = -V_R(t) + K_A R_f(t) - \frac{K_A K_F}{T_F} V_{DC}(t) + K_A\left(V_{ref.} - V_t(t) + V_s(t)\right)$$

$$T_F \frac{dR_f(t)}{dt} = -R_f(t) + \frac{K_F}{T_F} V_{DC}(t)$$

The explanation of symbols and equations is the same as in the previous paragraph.
If non-windup limits are imposed to the voltage regulator output the compact model becomes:

If $V_R^{\min} < V_R(t) < V_R^{\max}$

$$i_1(t) = g\left(v_1(t) - v_2(t)\right) - gL\frac{di_1(t)}{dt} - gV_{DC}$$

$$i_2(t) = -i_1(t)$$

$$T_E \frac{dV_{DC}(t)}{dt} = -\left(K_E + S_E(V_{DC}(t))\right)\cdot V_{DC}(t) + V_R(t)$$

$$T_A \frac{dV_R(t)}{dt} = -V_R(t) + K_A R_f(t) - \frac{K_A K_F}{T_F} V_{DC}(t) + K_A\left(V_{ref.} - V_t(t) + V_s(t)\right)$$

$$T_F \frac{dR_f(t)}{dt} = -R_f(t) + \frac{K_F}{T_F} V_{DC}(t)$$

else if $V_R(t) \le V_R^{\min}$ and $\frac{dV_R(t)}{dt} < 0$ (4.72)

$$i_1(t) = g\left(v_1(t) - v_2(t)\right) - gL\frac{di_1(t)}{dt} - gV_{DC}$$

$$i_2(t) = -i_1(t)$$

$$T_E \frac{dV_{DC}(t)}{dt} = -\left(K_E + S_E(V_{DC}(t))\right)\cdot V_{DC}(t) + V_R(t)$$

$$V_R(t) = V_R^{\min}$$

$$\frac{dV_R(t)}{dt} = 0 \Leftrightarrow 0 = -V_R(t) + K_A R_f(t) - \frac{K_A K_F}{T_F} V_{DC}(t) + K_A\left(V_{ref.} - V_t(t) + V_s(t)\right)$$

$$T_F \frac{dR_f(t)}{dt} = -R_f(t) + \frac{K_F}{T_F} V_{DC}(t)$$

else if $V_R(t) \ge V_R^{\max}$ and $\frac{dV_R(t)}{dt} > 0$

$$i_1(t) = g\left(v_1(t) - v_2(t)\right) - gL\frac{di_1(t)}{dt} - gV_{DC}$$

$$i_2(t) = -i_1(t)$$

$$T_E \frac{dV_{DC}(t)}{dt} = -\left(K_E + S_E(V_{DC}(t))\right)\cdot V_{DC}(t) + V_R(t)$$

$$V_R(t) = V_R^{\max}$$

$$\frac{dV_R(t)}{dt} = 0 \Leftrightarrow 0 = -V_R(t) + K_A R_f(t) - \frac{K_A K_F}{T_F} V_{DC}(t) + K_A\left(V_{ref.} - V_t(t) + V_s(t)\right)$$

$$T_F \frac{dR_f(t)}{dt} = -R_f(t) + \frac{K_F}{T_F} V_{DC}(t)$$

else if $V_R(t) \le V_R^{\min}$ and $\frac{dV_R(t)}{dt} \ge 0$

$$i_1(t) = g\left(v_1(t) - v_2(t)\right) - gL\frac{di_1(t)}{dt} - gV_{DC} \qquad (4.72)$$

$$i_2(t) = -i_1(t)$$

$$T_E \frac{dV_{DC}(t)}{dt} = -\left(K_E + S_E(V_{DC}(t))\right) \cdot V_{DC}(t) + V_R(t)$$

$$T_A \frac{dV_R(t)}{dt} = -V_R(t) + K_A R_f(t) - \frac{K_A K_F}{T_F} V_{DC}(t) + K_A\left(V_{ref.} - V_t(t) + V_s(t)\right)$$

$$T_F \frac{dR_f(t)}{dt} = -R_f(t) + \frac{K_F}{T_F} V_{DC}(t)$$

$$V_R(t) = V_R^{\min}$$

else if $V_R(t) \ge V_R^{\max}$ and $\frac{dV_R(t)}{dt} \le 0$

$$i_1(t) = g\left(v_1(t) - v_2(t)\right) - gL\frac{di_1(t)}{dt} - gV_{DC}$$

$$i_2(t) = -i_1(t)$$

$$T_E \frac{dV_{DC}(t)}{dt} = -\left(K_E + S_E(V_{DC}(t))\right) \cdot V_{DC}(t) + V_R(t)$$

$$T_A \frac{dV_R(t)}{dt} = -V_R(t) + K_A R_f(t) - \frac{K_A K_F}{T_F} V_{DC}(t) + K_A\left(V_{ref.} - V_t(t) + V_s(t)\right)$$

$$T_F \frac{dR_f(t)}{dt} = -R_f(t) + \frac{K_F}{T_F} V_{DC}(t)$$

$$V_R(t) = V_R^{\max}$$

If windup limits are imposed to the voltage regulator output the compact model becomes:

If $V_R^{\min} < V_R(t) < V_R^{\max}$

$$i_1(t) = g\left(v_1(t) - v_2(t)\right) - gL\frac{di_1(t)}{dt} - gV_{DC}$$

$$i_2(t) = -i_1(t)$$

$$T_E \frac{dV_{DC}(t)}{dt} = -\left(K_E + S_E(V_{DC}(t))\right) \cdot V_{DC}(t) + V_R(t)$$

$$T_A \frac{dV_R(t)}{dt} = -V_R(t) + K_A R_f(t) - \frac{K_A K_F}{T_F} V_{DC}(t) + K_A\left(V_{ref.} - V_t(t) + V_s(t)\right)$$

$$T_F \frac{dR_f(t)}{dt} = -R_f(t) + \frac{K_F}{T_F} V_{DC}(t)$$

else if $V_R(t) \le V_R^{\min}$ (4.73)

$$i_1(t) = g\left(v_1(t) - v_2(t)\right) - gL\frac{di_1(t)}{dt} - gV_{DC}$$

$$i_2(t) = -i_1(t)$$

$$T_E \frac{dV_{DC}(t)}{dt} = -\left(K_E + S_E(V_{DC}(t))\right) \cdot V_{DC}(t) + V_R^*(t)$$

$$T_A \frac{dV_R(t)}{dt} = -V_R(t) + K_A R_f(t) - \frac{K_A K_F}{T_F} V_{DC}(t) + K_A\left(V_{ref.} - V_t(t) + V_s(t)\right)$$

$$T_F \frac{dR_f(t)}{dt} = -R_f(t) + \frac{K_F}{T_F} V_{DC}(t)$$

$$V_R^*(t) = V_R^{\min}$$

else if $V_R(t) \ge V_R^{\max}$

$$i_1(t) = g\left(v_1(t) - v_2(t)\right) - gL\frac{di_1(t)}{dt} - gV_{DC}$$

$$i_2(t) = -i_1(t)$$

$$T_E \frac{dV_{DC}(t)}{dt} = -\left(K_E + S_E(V_{DC}(t))\right) \cdot V_{DC}(t) + V_R^*(t)$$ (4.73)

$$T_A \frac{dV_R(t)}{dt} = -V_R(t) + K_A R_f(t) - \frac{K_A K_F}{T_F} V_{DC}(t) + K_A\left(V_{ref.} - V_t(t) + V_s(t)\right)$$

$$T_F \frac{dR_f(t)}{dt} = -R_f(t) + \frac{K_F}{T_F} V_{DC}(t)$$

$$V_R^*(t) = V_R^{\max}$$

User Interface and Model Parameters

The user interface and parameters of the generic exciter model are presented in Figure 4.28.

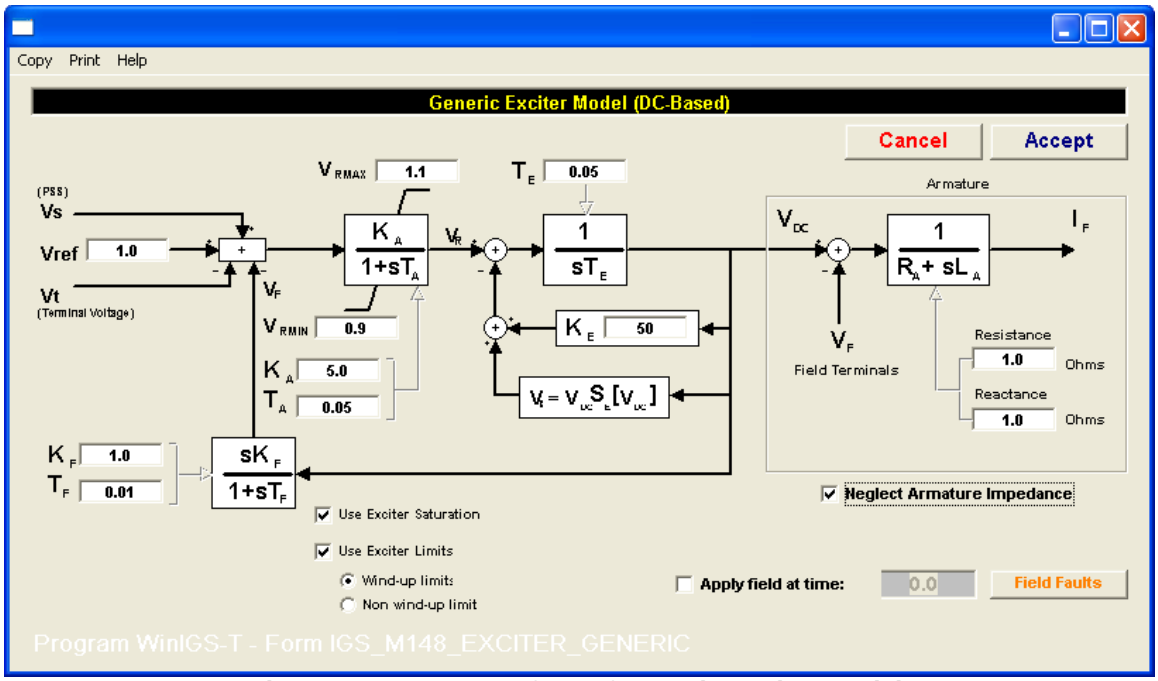


Figure 4.28. User Interface of Generic Exciter Model.

5. Electric Network Model

A three-phase, four-wire, physically based, breaker oriented model is utilized to represent the electric power network. Transmission lines are modeled in detail as three phase systems, based on their physical parameters. Substations are also modeled in detail including their internal configuration, with explicit representation of breakers, switches and transformers. For both steady state and quasi steady state analysis the network is assumed to be operating under sinusoidal steady state conditions. Therefore, phasor representation is used in all cases, and the models are the same. The difference between the two types of analysis is that the phasors in the quasi steady state analysis are time varying phasors. Since many of these models have been developed in the past, and were simply used in this project, the description of each one will be relatively brief. Implementation details and details on the mathematical model are in generally omitted for simplicity and for the shake of conciseness of the report.

Transmission Line Model

The mathematical transmission line model is based on the creation of the generalized pi equivalent of the line. The model is linear. In general, for a four-wire line this model is of the form:

$$\begin{bmatrix} \tilde{I}_{A1} \\ \tilde{I}_{B1} \\ \tilde{I}_{C1} \\ \tilde{I}_{N1} \\ \tilde{I}_{A2} \\ \tilde{I}_{B2} \\ \tilde{I}_{C2} \\ \tilde{I}_{N2} \end{bmatrix} = \begin{bmatrix} \tilde{Y}_{A1A1} & \tilde{Y}_{A1B1} & \tilde{Y}_{A1C1} & \tilde{Y}_{A1N1} & \tilde{Y}_{A1A2} & \tilde{Y}_{A1B2} & \tilde{Y}_{A1C2} & \tilde{Y}_{A1N2} \\ \tilde{Y}_{B1A1} & \tilde{Y}_{B1B1} & \tilde{Y}_{B1C1} & \tilde{Y}_{B1N1} & \tilde{Y}_{B1A2} & \tilde{Y}_{B1B2} & \tilde{Y}_{B1C2} & \tilde{Y}_{B1N2} \\ \tilde{Y}_{C1A1} & \tilde{Y}_{C1B1} & \tilde{Y}_{C1C1} & \tilde{Y}_{C1N1} & \tilde{Y}_{C1A2} & \tilde{Y}_{C1B2} & \tilde{Y}_{C1C2} & \tilde{Y}_{C1N2} \\ \tilde{Y}_{N1A1} & \tilde{Y}_{n1B1} & \tilde{Y}_{N1C1} & \tilde{Y}_{N1N1} & \tilde{Y}_{N1A2} & \tilde{Y}_{N1B2} & \tilde{Y}_{N1C2} & \tilde{Y}_{N1N2} \\ \tilde{Y}_{A2A1} & \tilde{Y}_{A2B1} & \tilde{Y}_{A2C1} & \tilde{Y}_{A2N1} & \tilde{Y}_{A2A2} & \tilde{Y}_{A2B2} & \tilde{Y}_{A2C2} & \tilde{Y}_{A2N2} \\ \tilde{Y}_{B2A1} & \tilde{Y}_{B2B1} & \tilde{Y}_{B2C1} & \tilde{Y}_{B2N1} & \tilde{Y}_{B2A2} & \tilde{Y}_{B2B2} & \tilde{Y}_{B2C2} & \tilde{Y}_{B2N2} \\ \tilde{Y}_{C2A1} & \tilde{Y}_{C2B1} & \tilde{Y}_{C2C1} & \tilde{Y}_{C2N1} & \tilde{Y}_{C2A2} & \tilde{Y}_{C2B2} & \tilde{Y}_{C2C2} & \tilde{Y}_{C2N2} \\ \tilde{Y}_{N2A1} & \tilde{Y}_{N2B1} & \tilde{Y}_{N2C1} & \tilde{Y}_{N2N1} & \tilde{Y}_{N2A2} & \tilde{Y}_{N2B2} & \tilde{Y}_{N2C2} & \tilde{Y}_{N2N2} \end{bmatrix} \cdot \begin{bmatrix} \tilde{V}_{A1} \\ \tilde{V}_{B1} \\ \tilde{V}_{C1} \\ \tilde{V}_{N1} \\ \tilde{V}_{A2} \\ \tilde{V}_{B2} \\ \tilde{V}_{C2} \\ \tilde{V}_{N2} \end{bmatrix} \quad (5.1)$$

The entries of the admittance matrix $\tilde{Y}$ as defined above are computed based on the physical parameters of the line provided by the user. The indices A, B, C, N indicate phases and neutral, while the indices 1 and 2 indicate the two ends of the line. The line model input data are presented in Figure 5.1. The length of the line can be specified by the user, or can be computed from GIS data, if the GPS coordinates of the substations at the ends of the line are known.

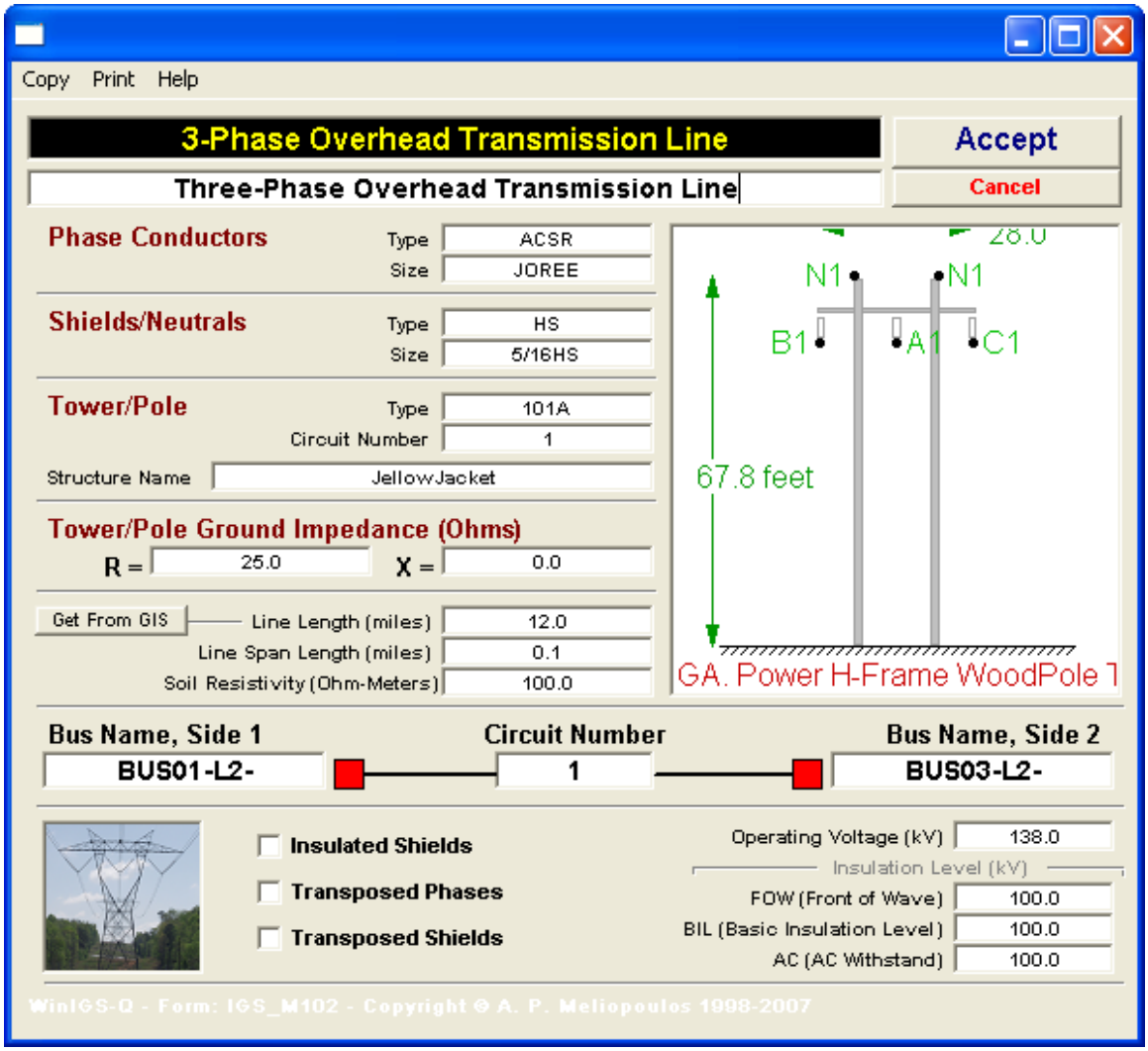


Figure 5.1. Transmission Line Model Input Data.

The type and size of the conductors are specified from an editable conductor library that contains existing industrial types along with their data. New cable types can also be created by the user of the software. The interface of these libraries is illustrates in Figure 5.2 and Figure 5.3.

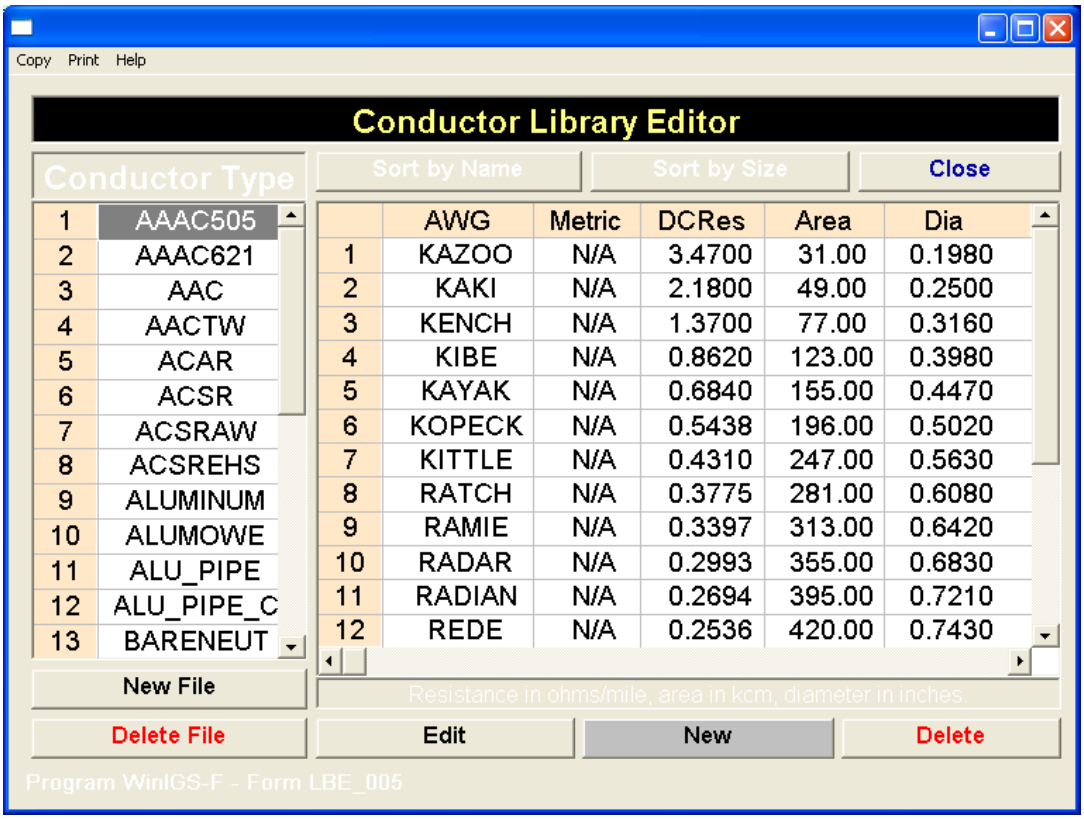


Figure 5.2. Conductor Library Interface.

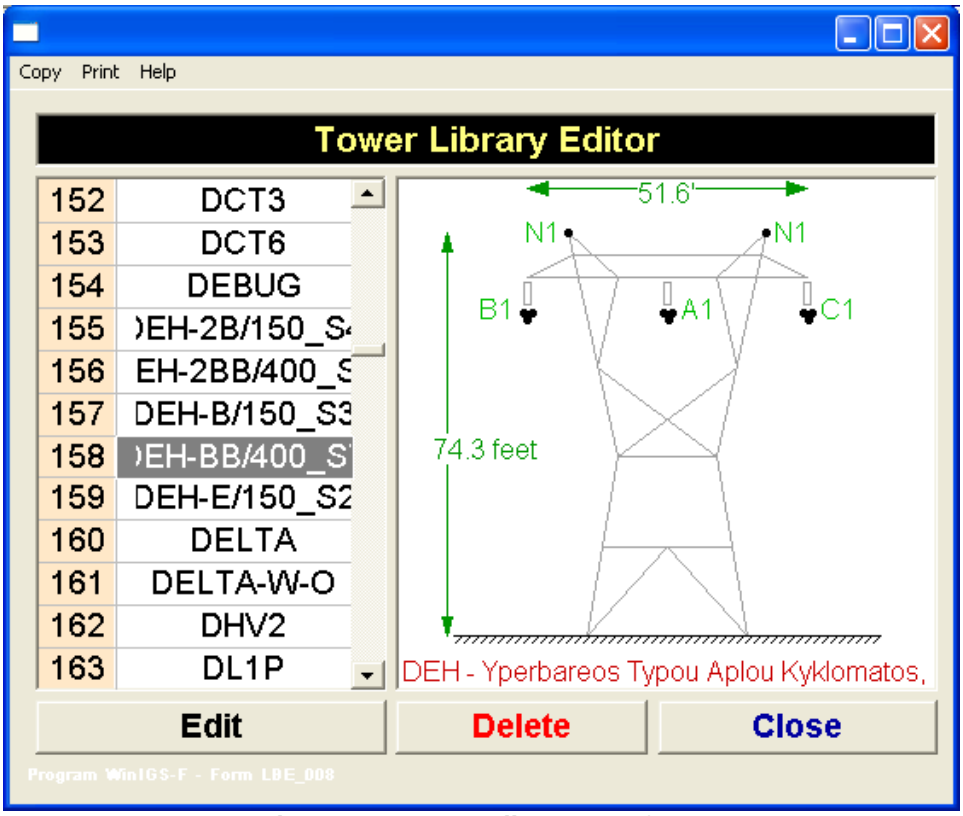
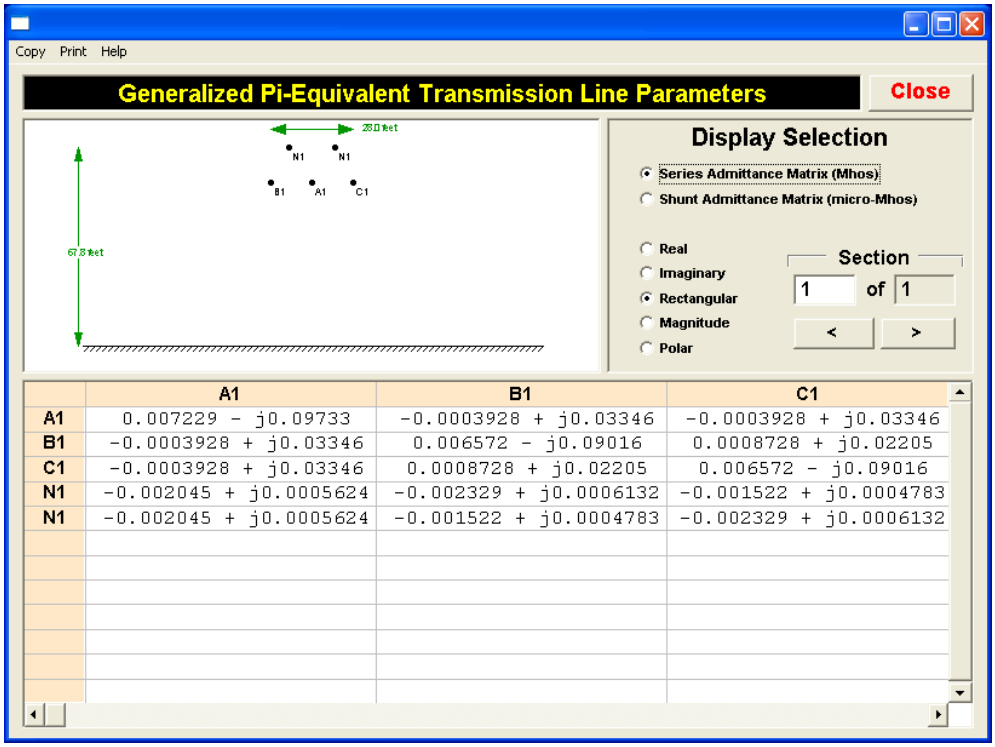


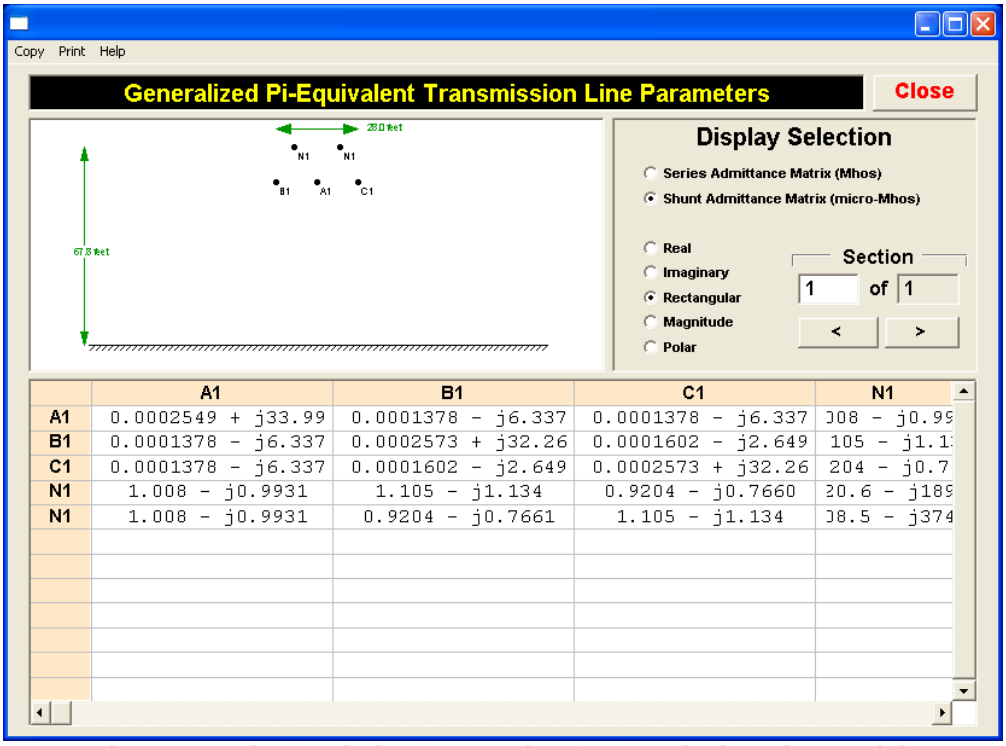
Figure 5.3. Tower Library Interface.

The series and shunt part of the generalized admittance matrix of the line configuration of Figure 5.1 are automatically computed and used by the program, as illustrated in Figure 5.4 and Figure 5.5.



	A1	B1	C1
A1	0.007229 - j0.09733	-0.0003928 + j0.03346	-0.0003928 + j0.03346
B1	-0.0003928 + j0.03346	0.006572 - j0.09016	0.0008728 + j0.02205
C1	-0.0003928 + j0.03346	0.0008728 + j0.02205	0.006572 - j0.09016
N1	-0.002045 + j0.0005624	-0.002329 + j0.0006132	-0.001522 + j0.0004783
N1	-0.002045 + j0.0005624	-0.001522 + j0.0004783	-0.002329 + j0.0006132

Figure 5.4. Series Admittance Matrix of Transmission Line Model.



	A1	B1	C1	N1
A1	0.0002549 + j33.99	0.0001378 - j6.337	0.0001378 - j6.337	308 - j0.99
B1	0.0001378 - j6.337	0.0002573 + j32.26	0.0001602 - j2.649	105 - j1.1
C1	0.0001378 - j6.337	0.0001602 - j2.649	0.0002573 + j32.26	204 - j0.7
N1	1.008 - j0.9931	1.105 - j1.134	0.9204 - j0.7660	20.6 - j189
N1	1.008 - j0.9931	0.9204 - j0.7661	1.105 - j1.134	38.5 - j374

Figure 5.5. Shunt Admittance Matrix of Transmission Line Model.

For completeness and for reference the sequence parameters of the line are also computed, as well as the sequence networks. However, these are not used in the actual computations.

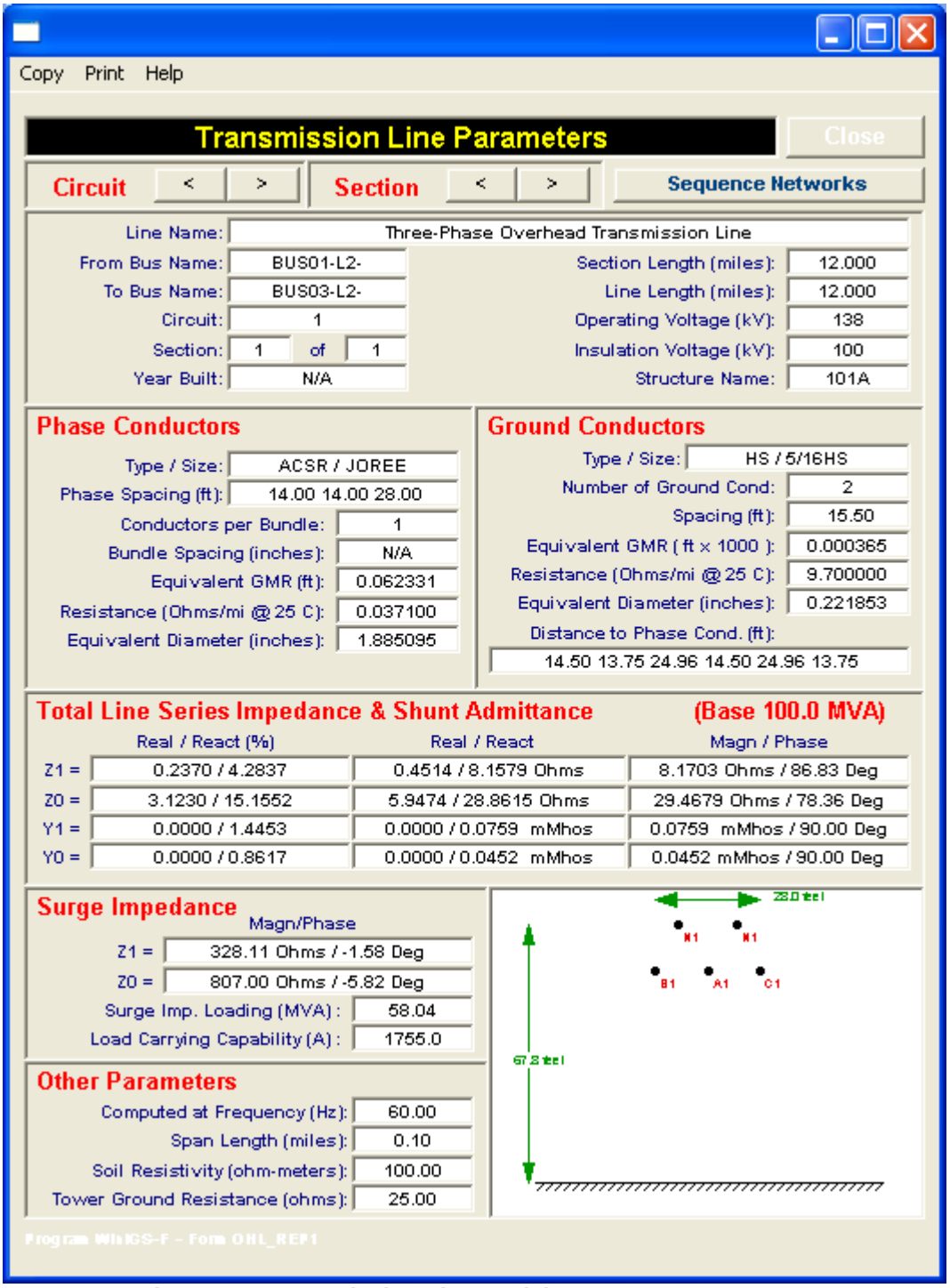


Figure 5.6. Transmission Line Model Sequence Parameters.

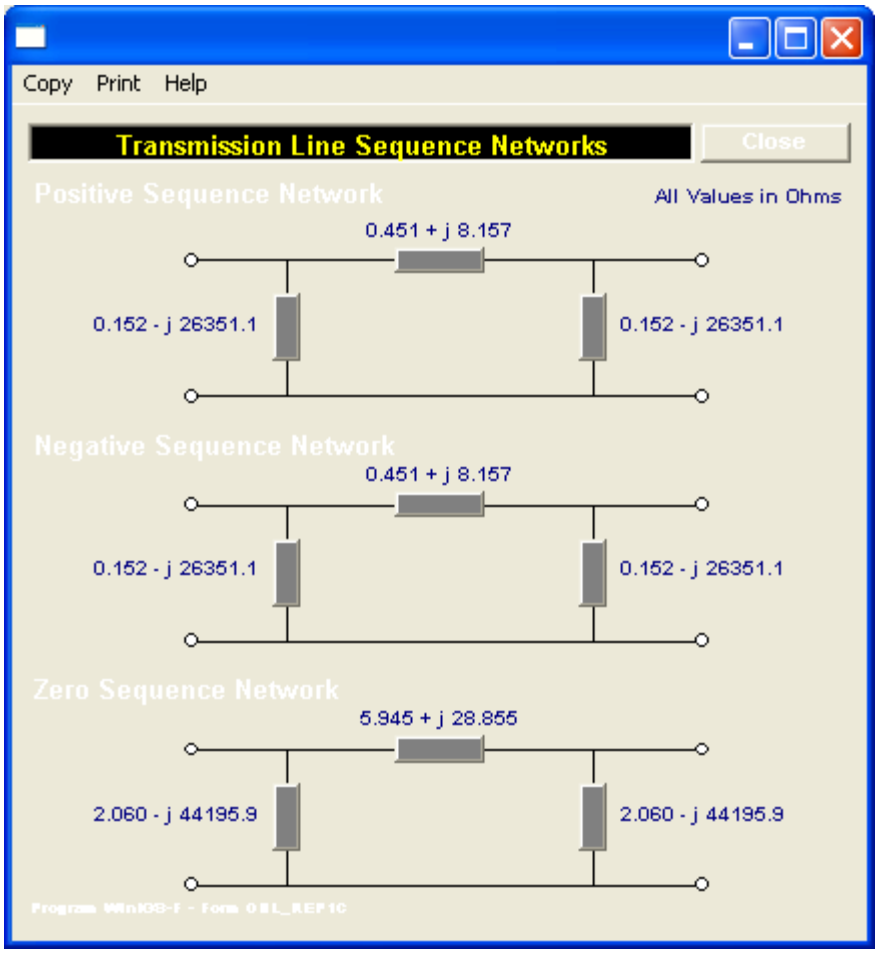


Figure 5.7. Transmission Line Model Sequence Networks.

In order to model transmission lines with multiple sections a multi-section transmission line model has been also developed, based on the series connection of the line models described above. The data of the model for each section are the same as described above. The interface of the multi-section transmission line model is shown in Figure 5.8.

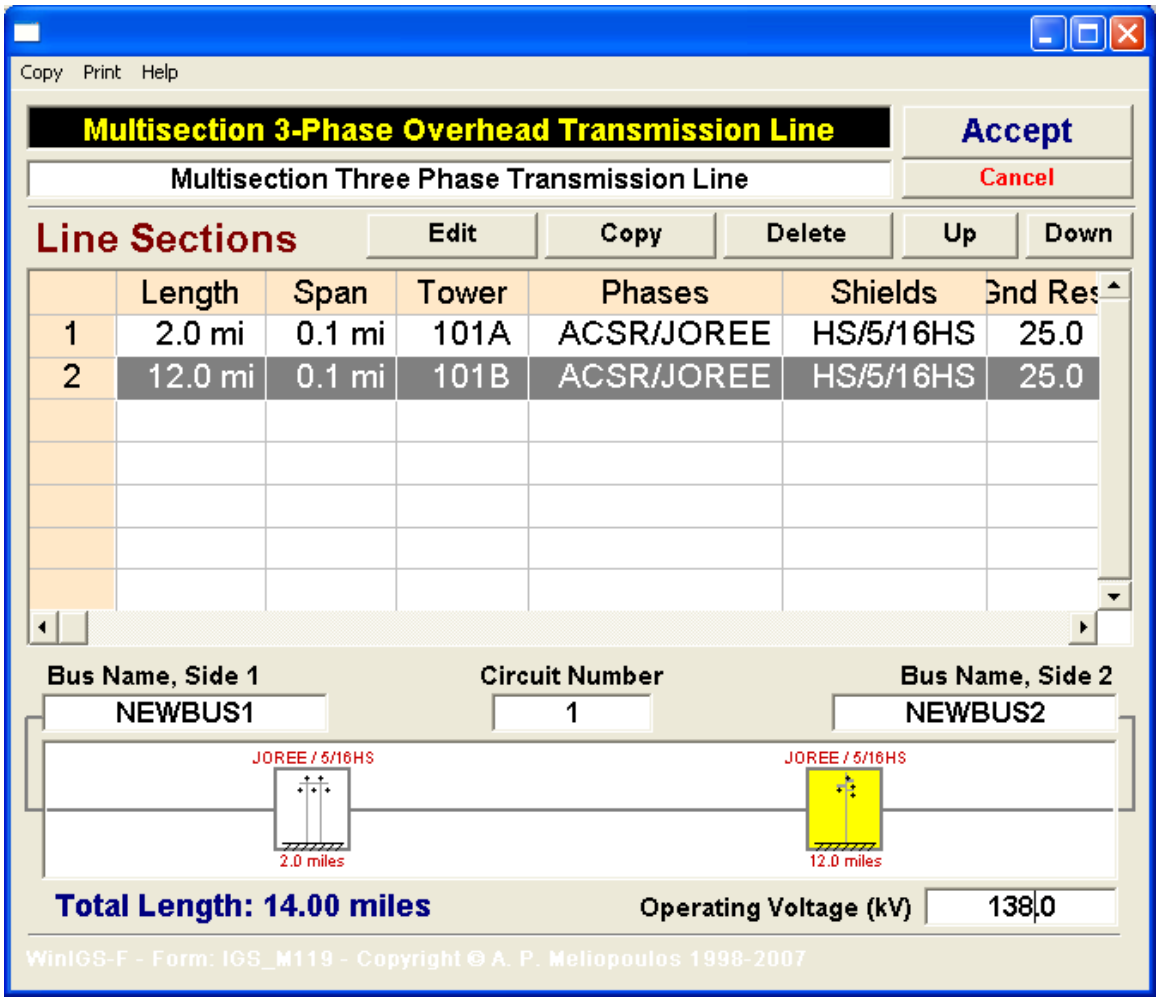


Figure 5.8. Multi-Section, Three Phase Overhead Transmission Line Model (A Two Section Example is Illustrated).

In order to model parallel transmission lines that are on the same tower structure or very close to each other, and therefore mutually coupled a mutually coupled transmission line model has been also developed, extending the line models described above. The data of the model for each section are the same as described above and the model is linked to the same tower and conductor libraries. The interface of the mutually coupled transmission lines model is shown in Figure 5.9. The mutual impedance between the conductors of one line and the conductors of the other are computed and taken into consideration when the admittance matrix of the model is computed.

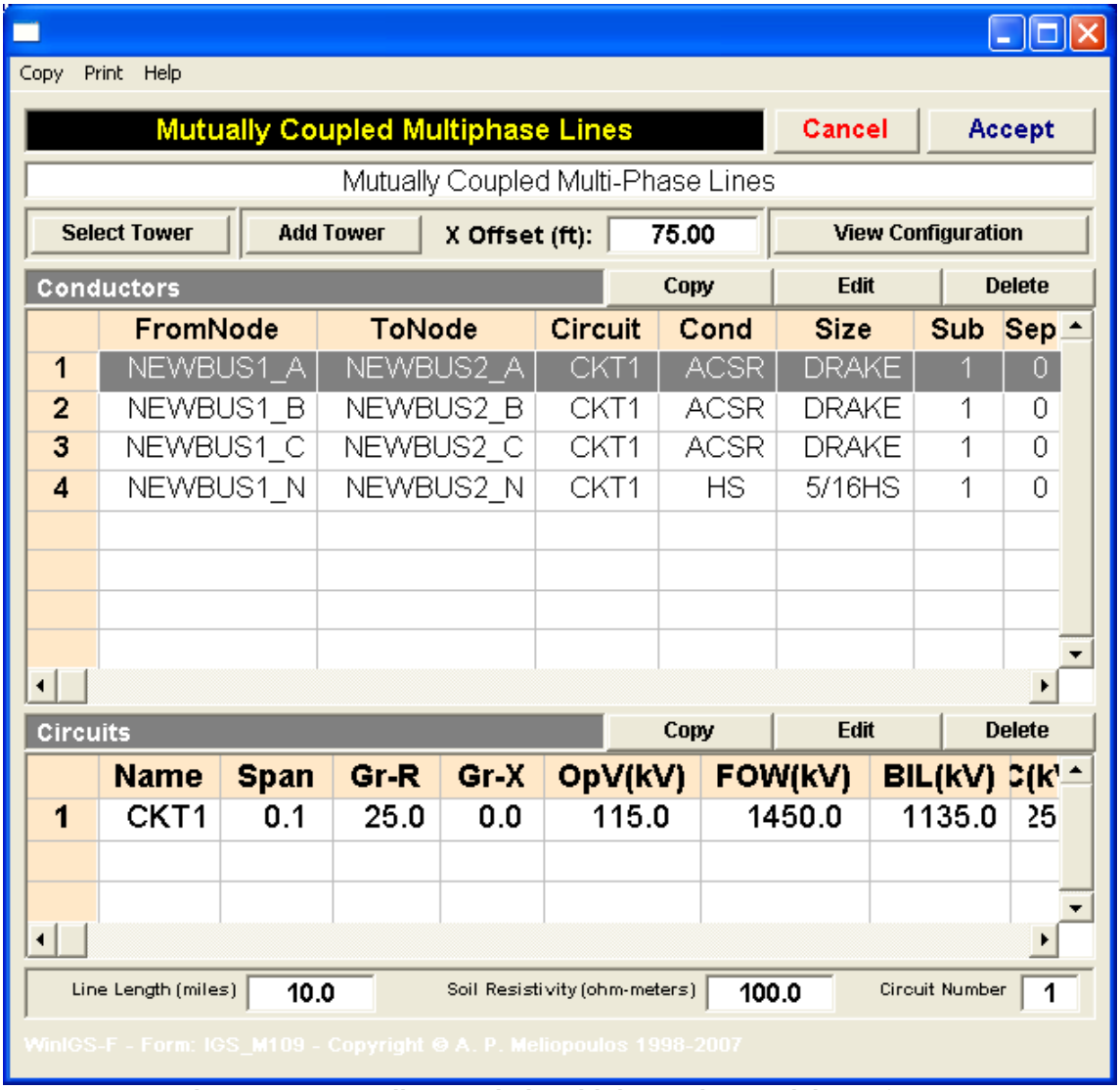


Figure 5.9. Mutually Coupled Multiphase Line Model Interface.

As an alternative a transmission line model based on positive, negative and zero sequence equivalent circuits has been also developed. The model is illustrated in Figure 5.10 and Figure 5.11.

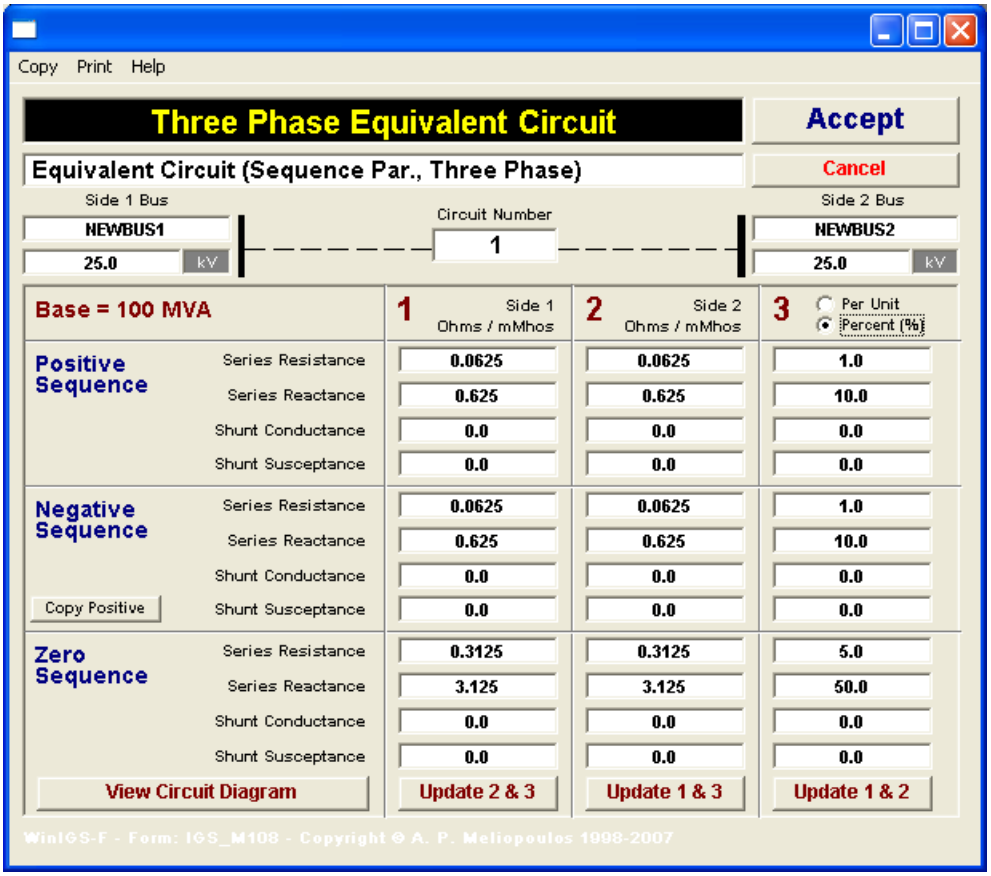


Figure 5.10. Sequence Network Based Transmission Line Model (model data).

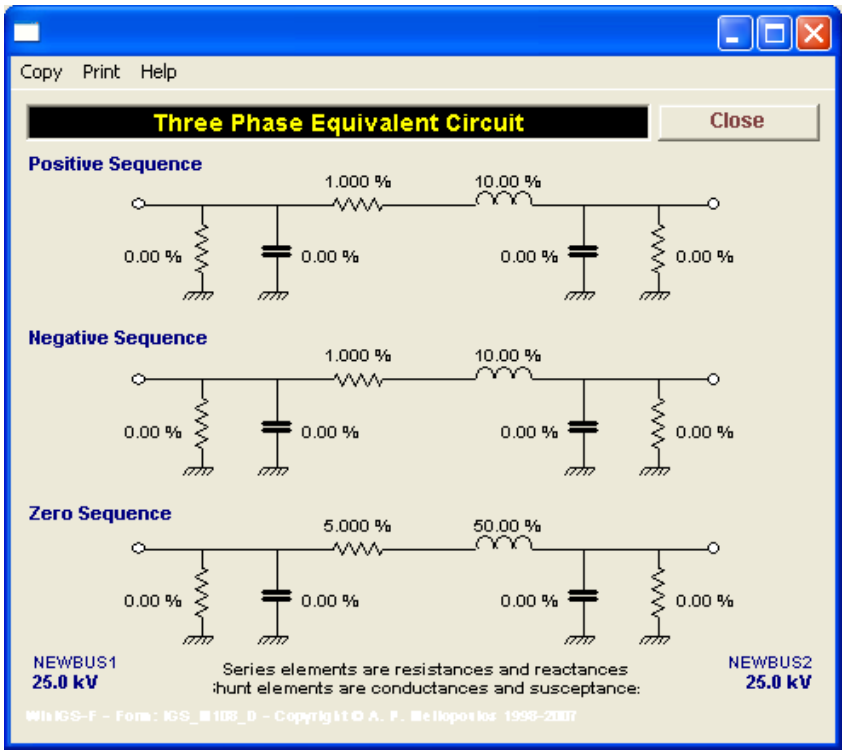


Figure 5.11. Sequence Network Based Transmission Line Model (sequence networks).

Multiphase Cable Model

The mathematical model of a multiphase cable is based on the creation of the generalized pi equivalent of the cable. The model is linear. Similarly to the overhead transmission line model, in general, for a four-wire line this model is of the form:

$$\begin{bmatrix} \tilde{I}_{A1} \\ \tilde{I}_{B1} \\ \tilde{I}_{C1} \\ \tilde{I}_{N1} \\ \tilde{I}_{A2} \\ \tilde{I}_{B2} \\ \tilde{I}_{C2} \\ \tilde{I}_{N2} \end{bmatrix} = \begin{bmatrix} \tilde{Y}_{A1A1} & \tilde{Y}_{A1B1} & \tilde{Y}_{A1C1} & \tilde{Y}_{A1N1} & \tilde{Y}_{A1A2} & \tilde{Y}_{A1B2} & \tilde{Y}_{A1C2} & \tilde{Y}_{A1N2} \\ \tilde{Y}_{B1A1} & \tilde{Y}_{B1B1} & \tilde{Y}_{B1C1} & \tilde{Y}_{B1N1} & \tilde{Y}_{B1A2} & \tilde{Y}_{B1B2} & \tilde{Y}_{B1C2} & \tilde{Y}_{B1N2} \\ \tilde{Y}_{C1A1} & \tilde{Y}_{C1B1} & \tilde{Y}_{C1C1} & \tilde{Y}_{C1N1} & \tilde{Y}_{C1A2} & \tilde{Y}_{C1B2} & \tilde{Y}_{C1C2} & \tilde{Y}_{C1N2} \\ \tilde{Y}_{N1A1} & \tilde{Y}_{n1B1} & \tilde{Y}_{N1C1} & \tilde{Y}_{N1N1} & \tilde{Y}_{N1A2} & \tilde{Y}_{N1B2} & \tilde{Y}_{N1C2} & \tilde{Y}_{N1N2} \\ \tilde{Y}_{A2A1} & \tilde{Y}_{A2B1} & \tilde{Y}_{A2C1} & \tilde{Y}_{A2N1} & \tilde{Y}_{A2A2} & \tilde{Y}_{A2B2} & \tilde{Y}_{A2C2} & \tilde{Y}_{A2N2} \\ \tilde{Y}_{B2A1} & \tilde{Y}_{B2B1} & \tilde{Y}_{B2C1} & \tilde{Y}_{B2N1} & \tilde{Y}_{B2A2} & \tilde{Y}_{B2B2} & \tilde{Y}_{B2C2} & \tilde{Y}_{B2N2} \\ \tilde{Y}_{C2A1} & \tilde{Y}_{C2B1} & \tilde{Y}_{C2C1} & \tilde{Y}_{C2N1} & \tilde{Y}_{C2A2} & \tilde{Y}_{C2B2} & \tilde{Y}_{C2C2} & \tilde{Y}_{C2N2} \\ \tilde{Y}_{N2A1} & \tilde{Y}_{N2B1} & \tilde{Y}_{N2C1} & \tilde{Y}_{N2N1} & \tilde{Y}_{N2A2} & \tilde{Y}_{N2B2} & \tilde{Y}_{N2C2} & \tilde{Y}_{N2N2} \end{bmatrix} . \begin{bmatrix} \tilde{V}_{A1} \\ \tilde{V}_{B1} \\ \tilde{V}_{C1} \\ \tilde{V}_{N1} \\ \tilde{V}_{A2} \\ \tilde{V}_{B2} \\ \tilde{V}_{C2} \\ \tilde{V}_{N2} \end{bmatrix} \quad (5.2)$$

The entries of the admittance matrix $\tilde{Y}$ as defined above are computed based on the physical parameters of the cable provided by the user, including cable type, configuration, length, soil resistivity and depth. The cable model input data are presented in Figure 5.12.

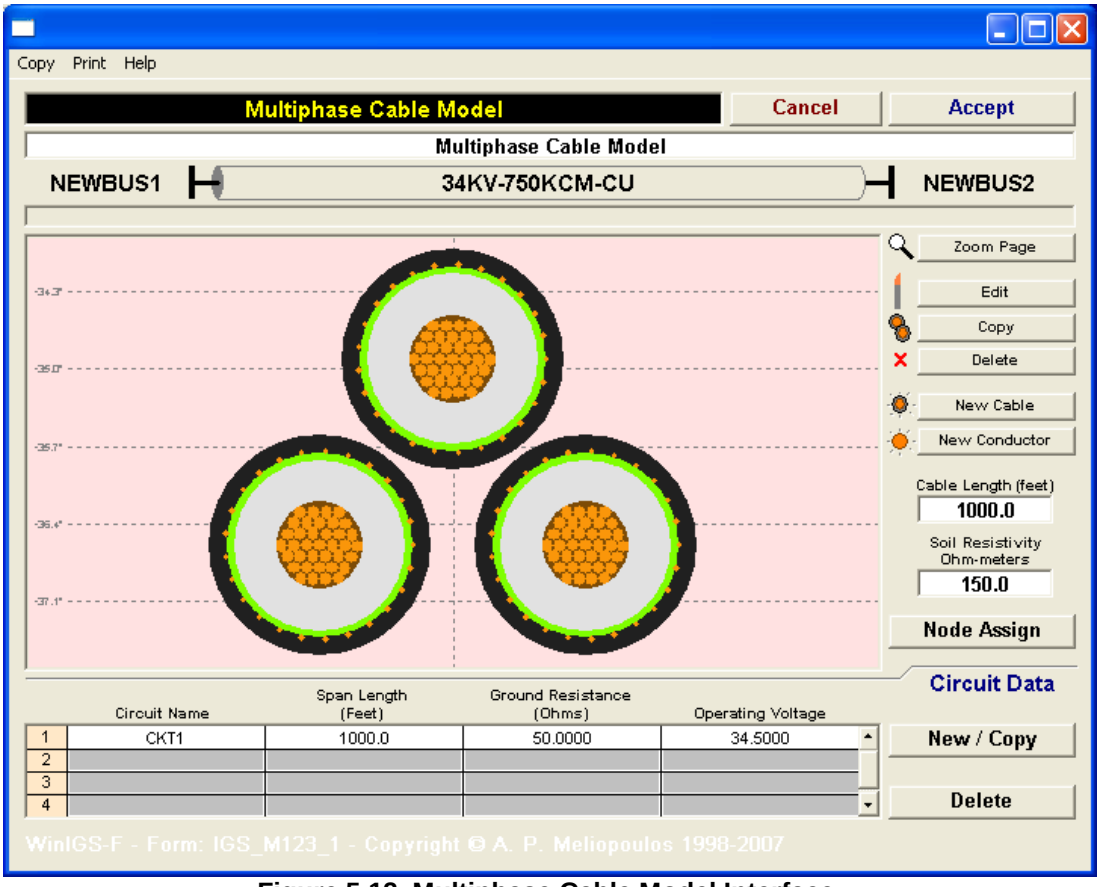


Figure 5.12. Multiphase Cable Model Interface.

Similarly to the conductor and tower library of in the overhead transmission line model, an editable cable library allows the selection of any existing industrial cable type as well as the creation of custom cable types and configurations. The cable library interface is illustrated in Figure 5.13.

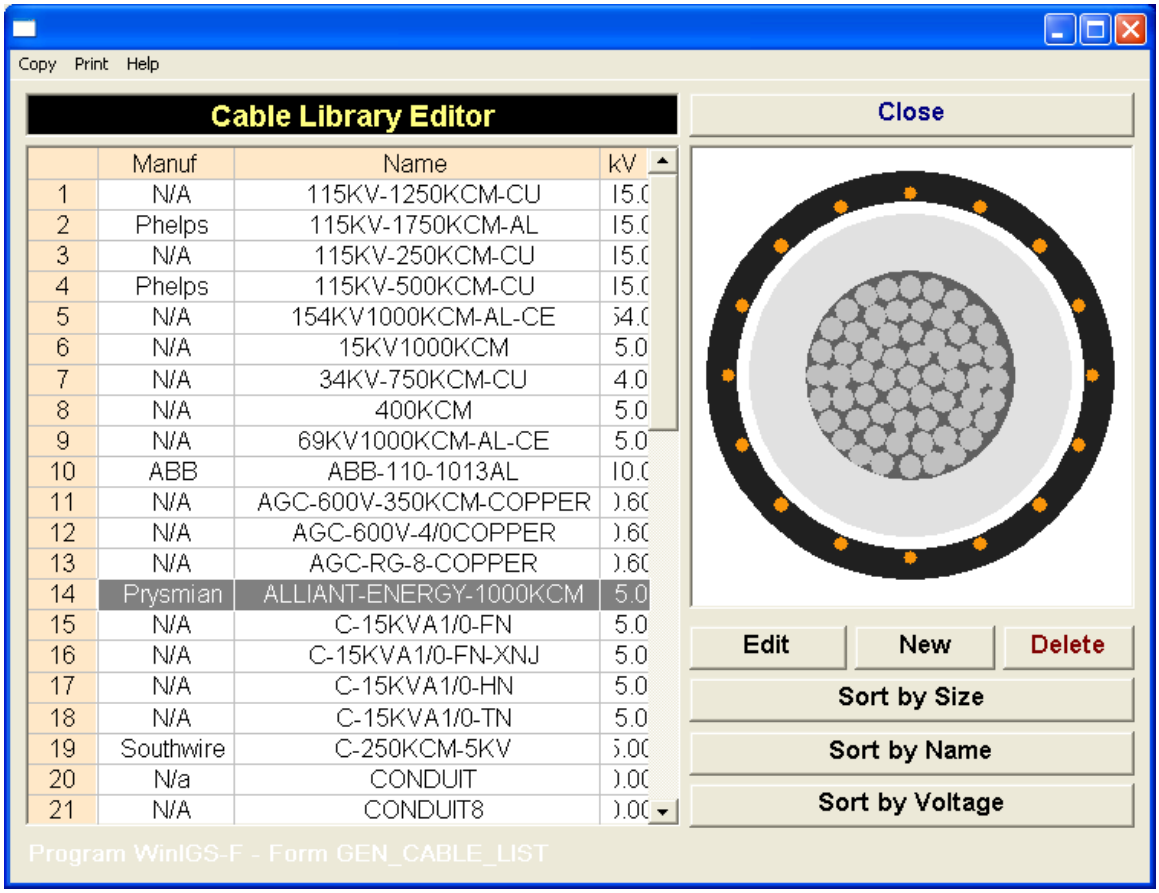


Figure 5.13. Cable Library Interface.

Transformer Model

The main transformer type used in this project is the standard *three-phase, two winding transformer*. The model and the associated data are illustrated in Figure 5.14.

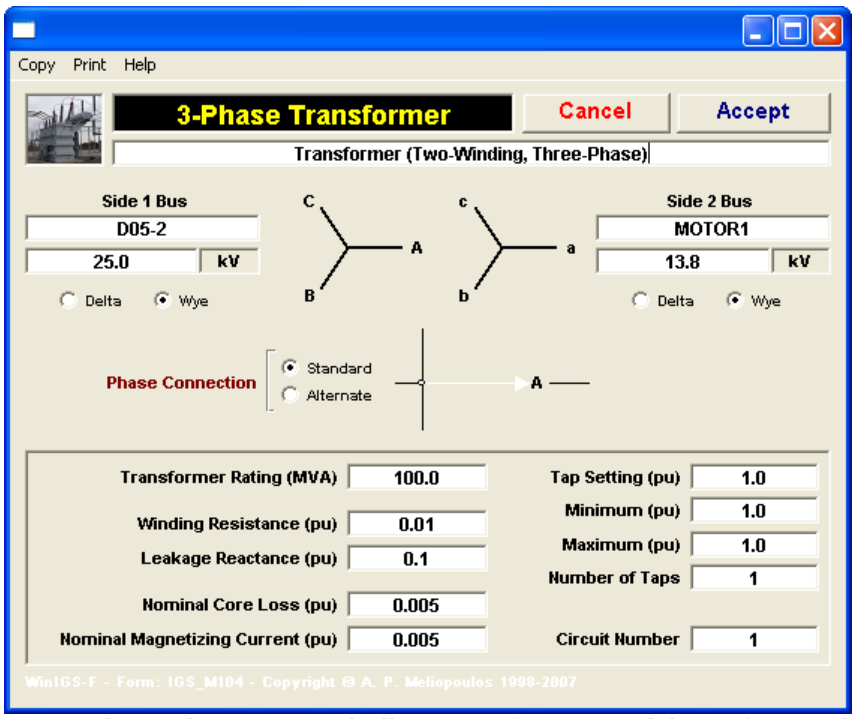


Figure 5.14. Three Phase, Two Winding Transformer Model Interface and Data.

A *three phase, three winding transformer* model is shown in Figure 5.15. The equivalent circuit model of the device is illustrated in Figure 5.16.

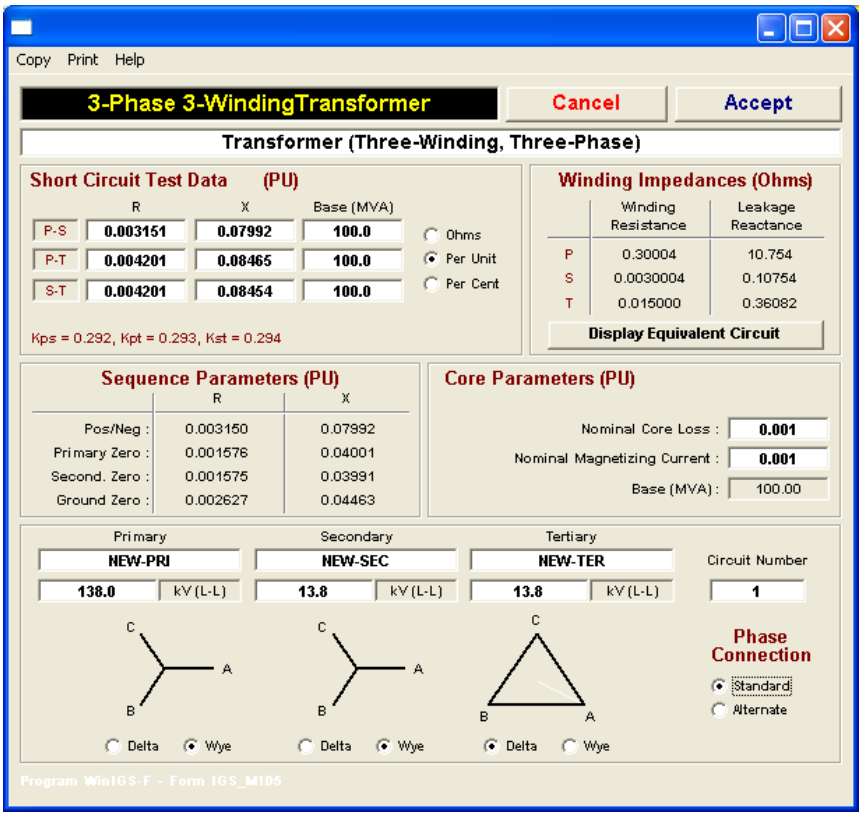


Figure 5.15. Three Phase, Three Winding Transformer Interface and Input Data.

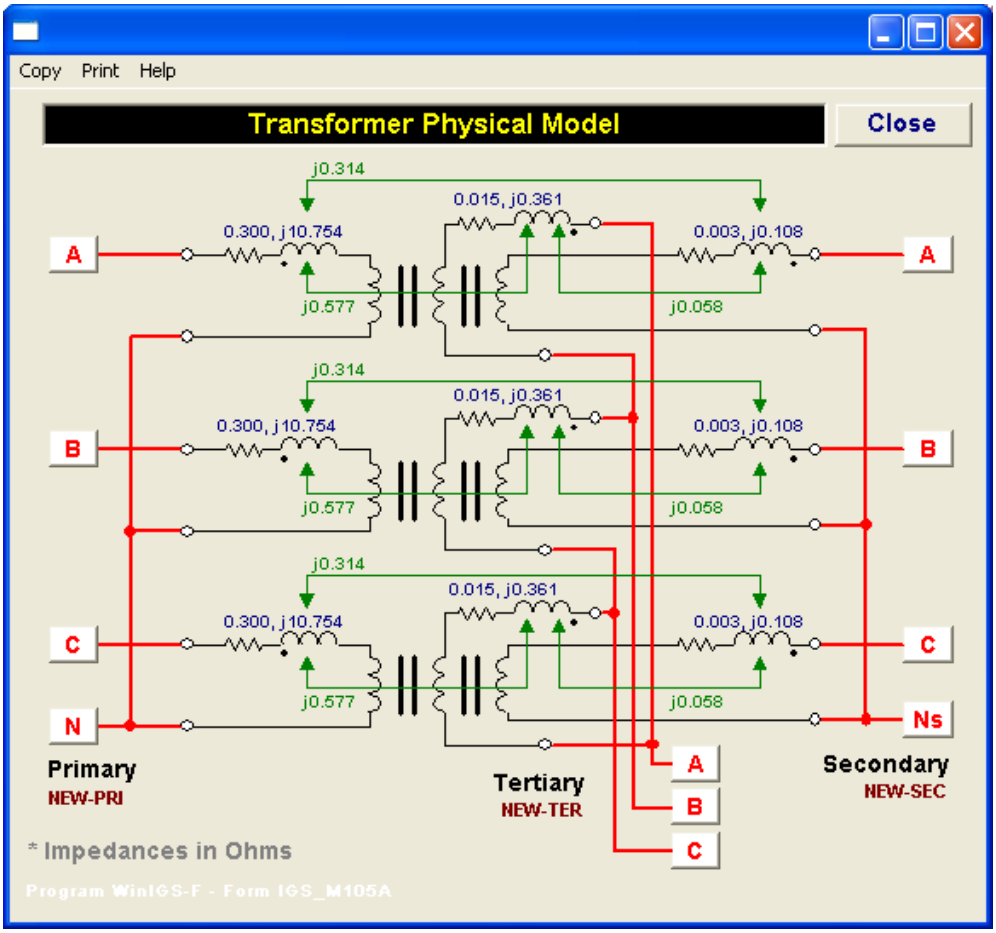


Figure 5.16. Three Phase, Three Winding Transformer Physical Circuit Model.

A *three phase, autotransformer model*, with and without tertiary is shown in Figure 5.17 and Figure 5.18. The equivalent circuit of each of the devices is illustrated in Figure 5.19 and Figure 5.20.

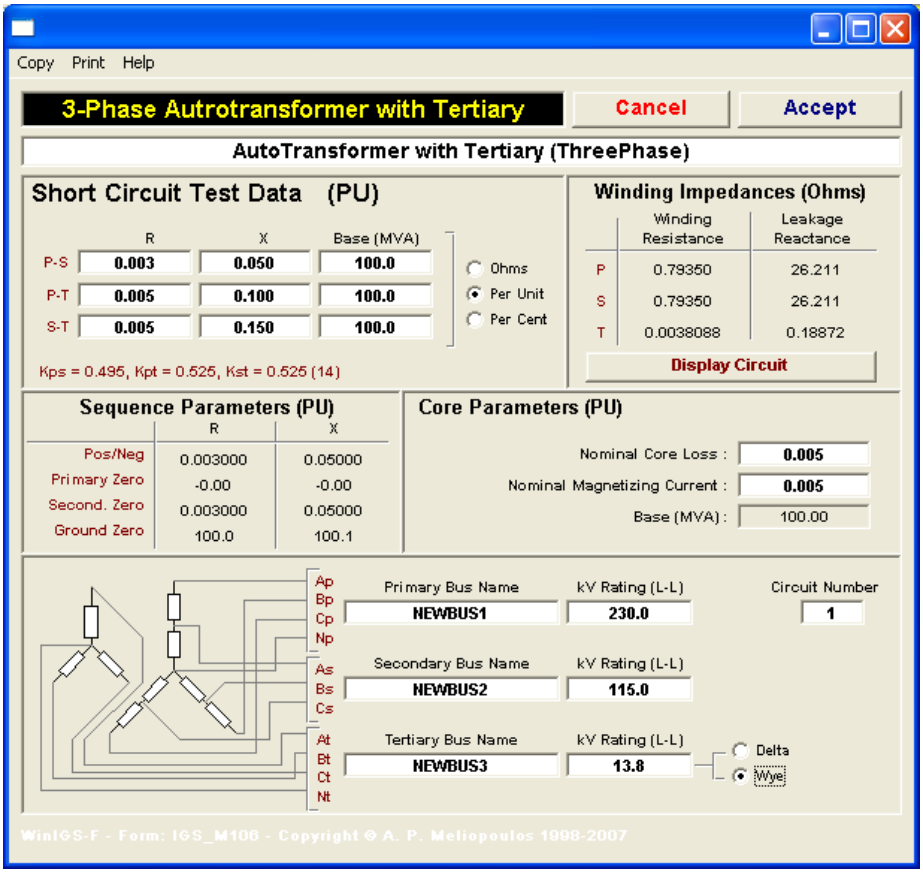


Figure 5.17. Three Phase Autotransformer Model with Tertiary.

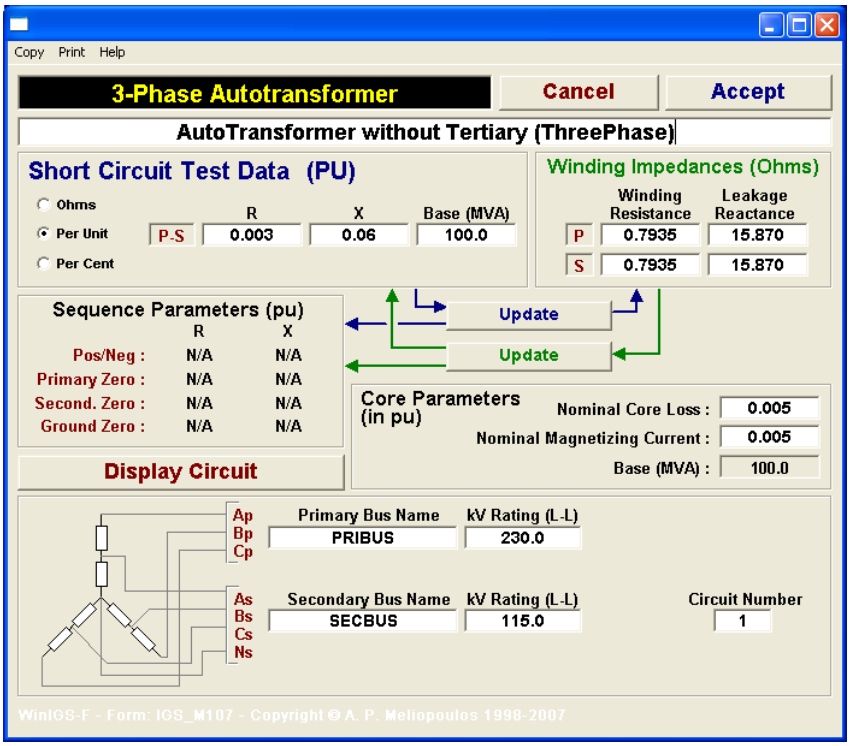


Figure 5.18. Three Phase Autotransformer Model without Tertiary.

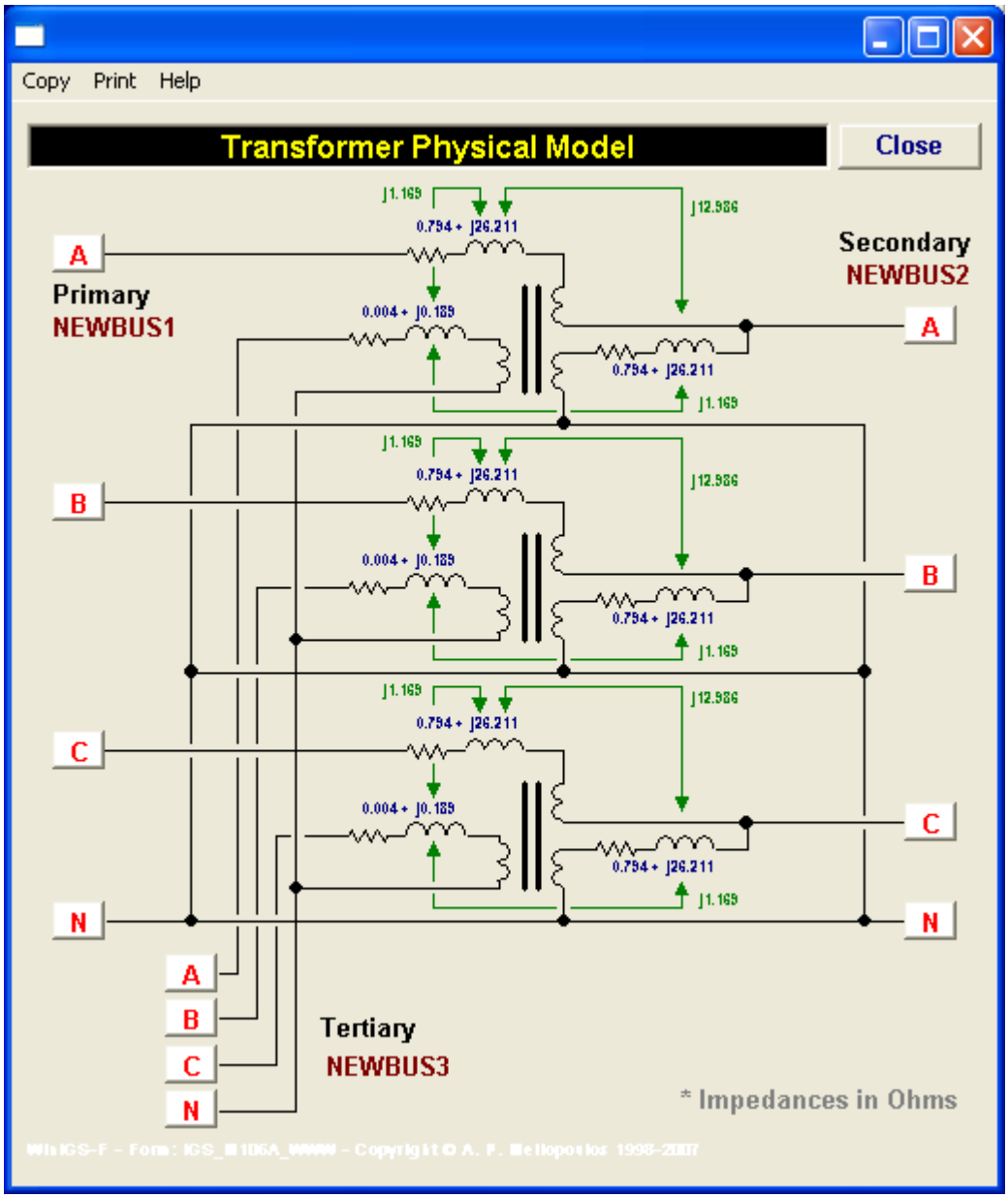


Figure 5.19. Three Phase Autotransformer with Tertiary Physical Circuit Model.

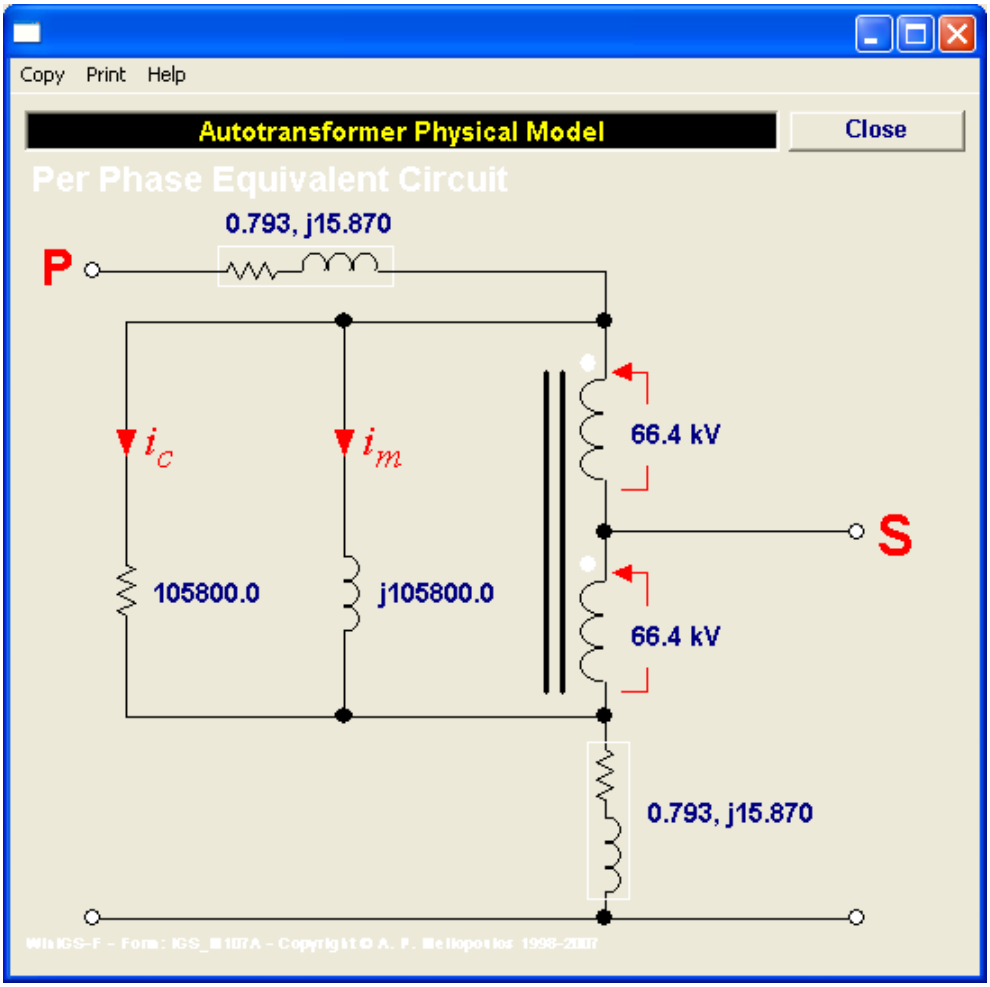


Figure 5.20. Three Phase Autotransformer without Tertiary Physical Circuit Model.

The above descried devices are also implemented in single phase models. This can be extremely useful when parts of distribution networks are to be modeled, since single phase devices are common in distribution feeders.

The model of a *single phase two winding transformer* is illustrated in Figure 5.21.

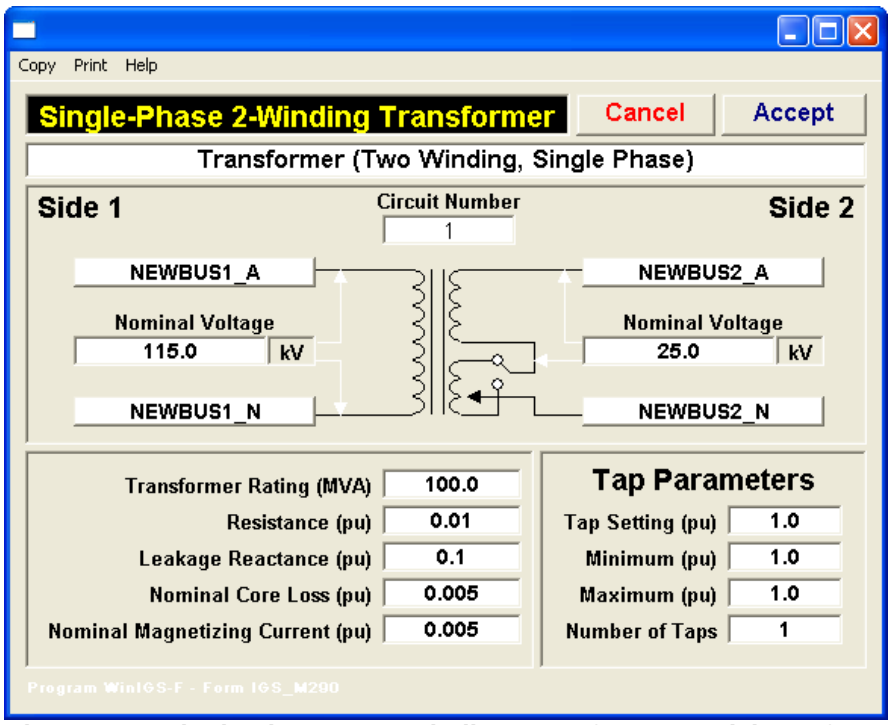


Figure 5.21. Single Phase, Two Winding Transformer Model Interface.

The model of a *single phase, two winding transformer* with secondary center tap is illustrated in Figure 5.22.

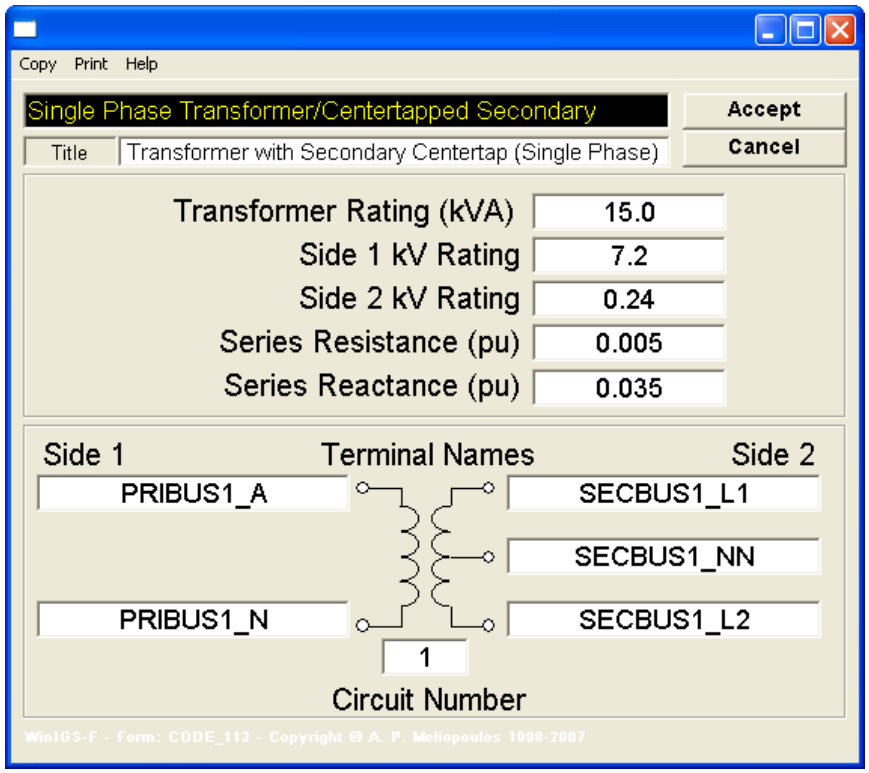


Figure 5.22. Single Phase, Two Winding Transformer with Secondary Center Tap Model Interface.

The model of a *single phase, three winding transformer* is illustrated in Figure 5.23. The physical model equivalent circuit is illustrated in Figure 5.24.

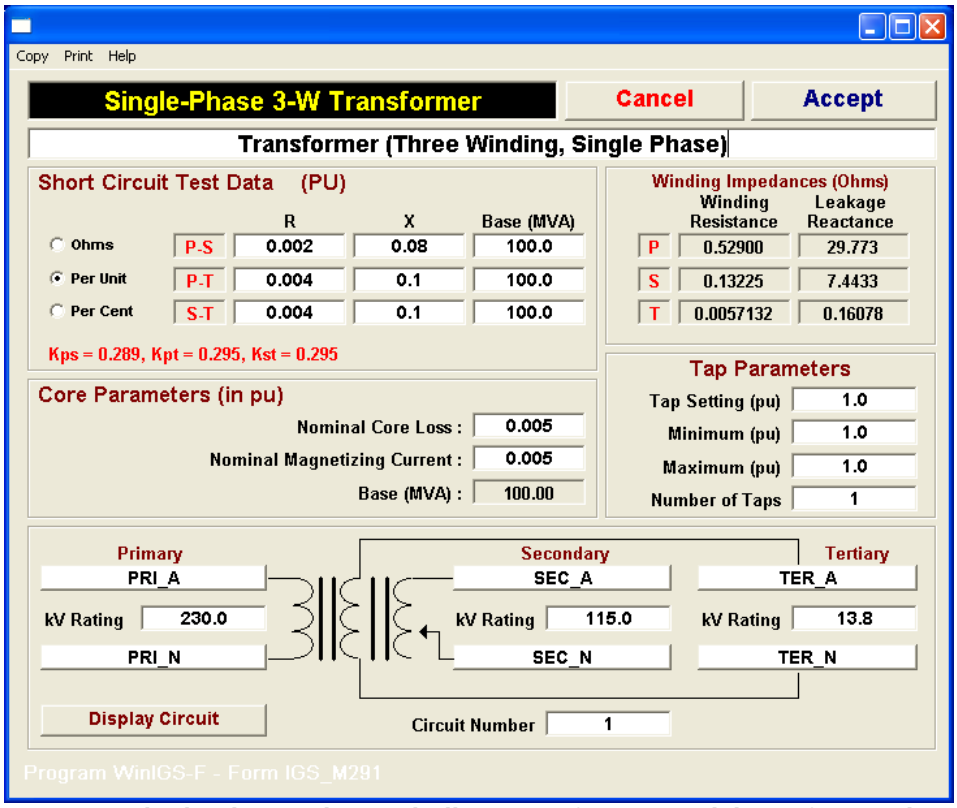


Figure 5.23. Single Phase, Three Winding Transformer Model Interface and Data.

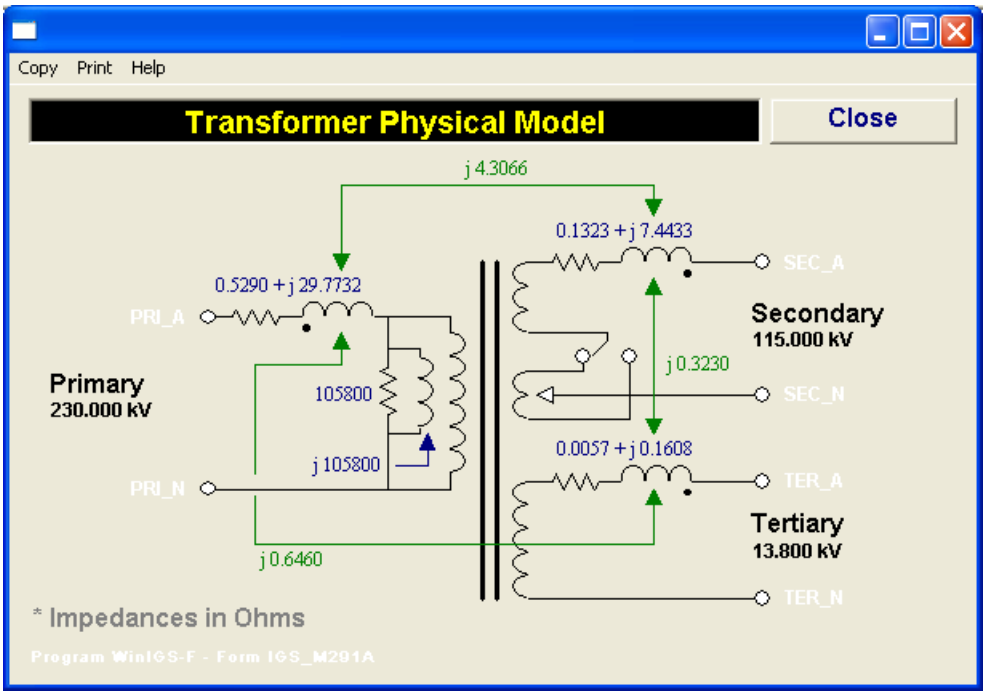


Figure 5.24. Single Phase, Three Winding Transformer Physical Model Equivalent Circuit.

The model of a *single phase, autotransformer with and without tertiary* is illustrated in Figure 5.25 and Figure 5.26. The physical model equivalent circuits are illustrated in Figure 5.27 and Figure 5.28.

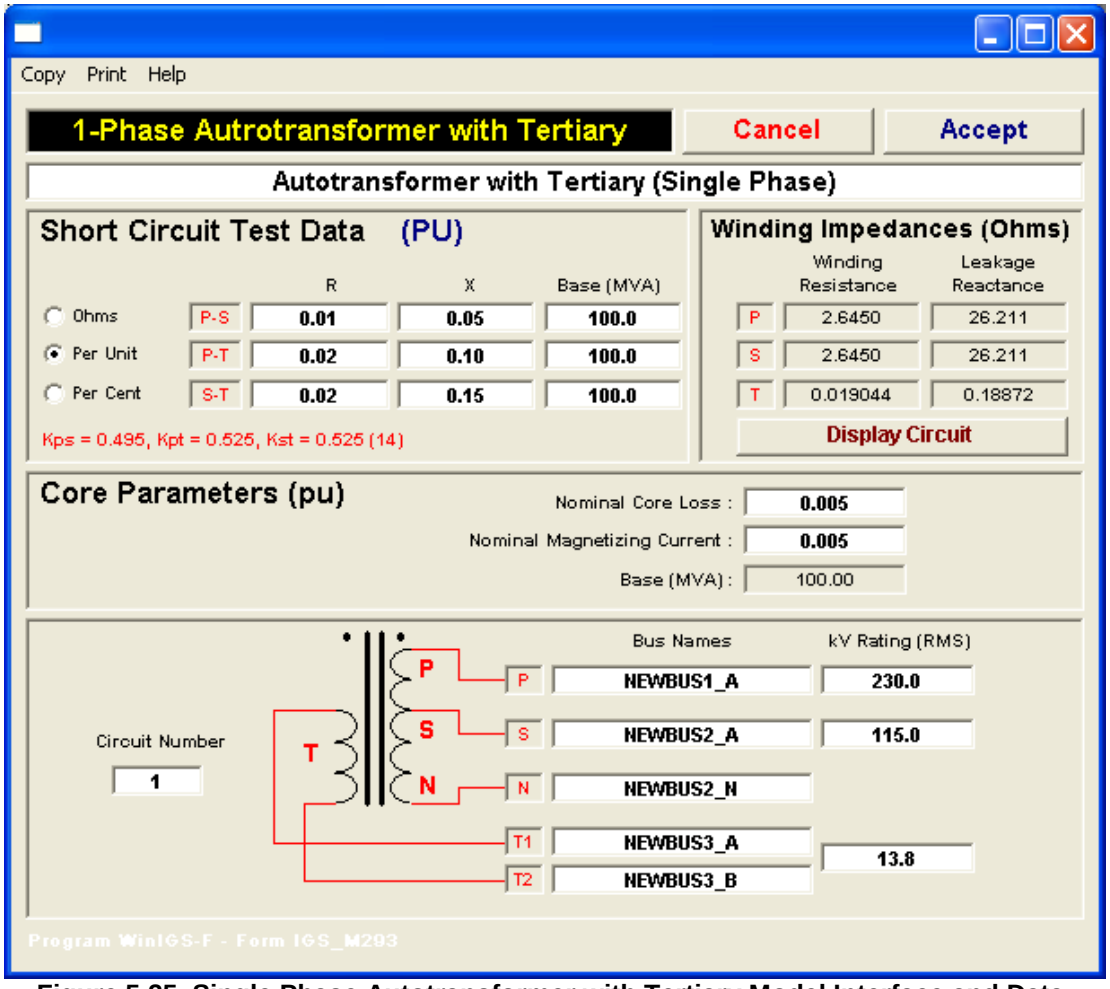


Figure 5.25. Single Phase Autotransformer with Tertiary Model Interface and Data.

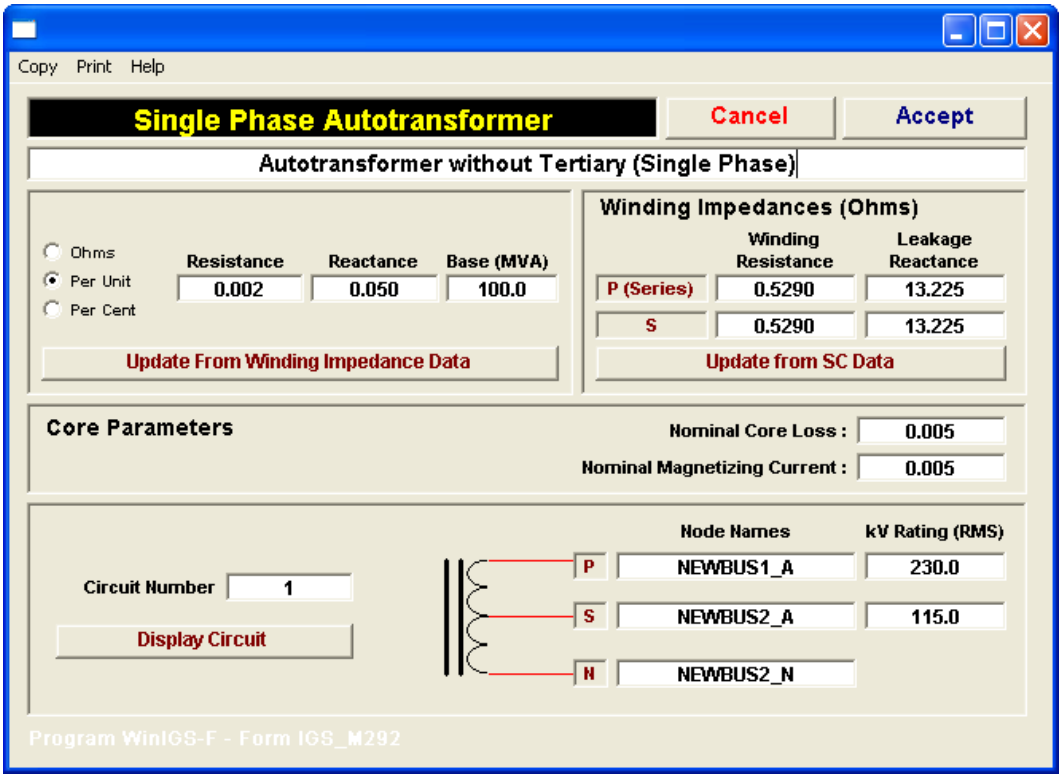


Figure 5.26. Single Phase Autotransformer without Tertiary Model Interface and Data.

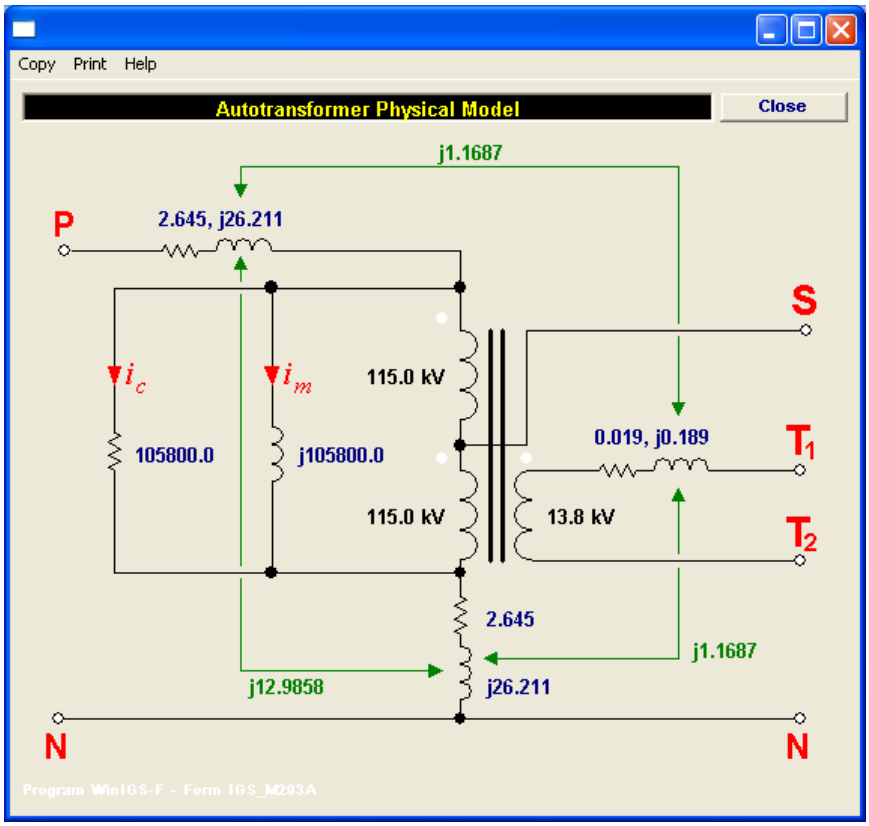


Figure 5.27. Single Phase Autotransformer with Tertiary Physical Model Equivalent Circuit.

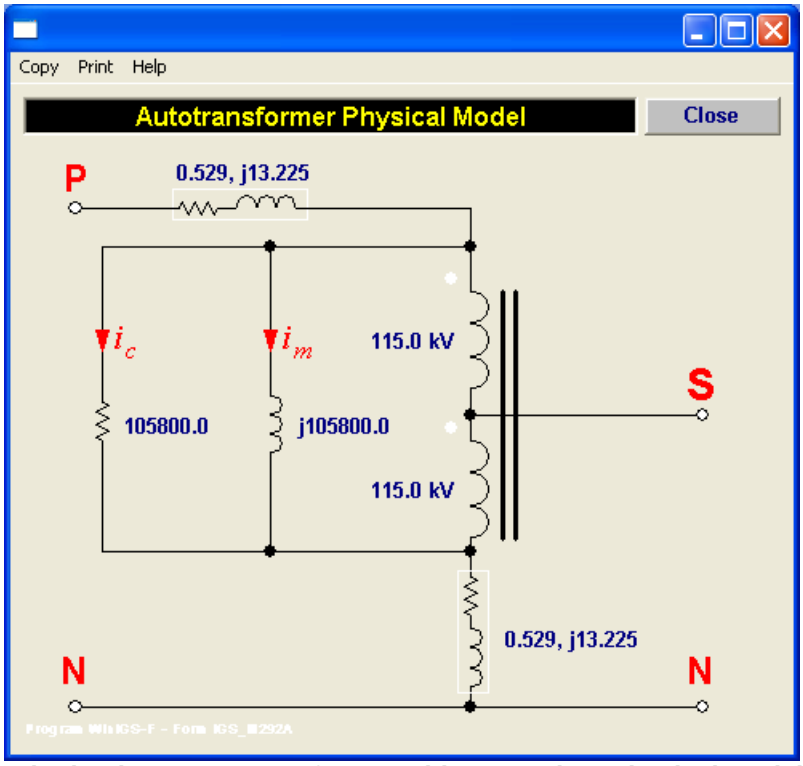


Figure 5.28. Single Phase Autotransformer without Tertiary Physical Model Equivalent Circuit.

Three Phase Breaker/Switch Model

A three phase circuit breaker/switch model has been developed to allow modeling of the actual internal substation configuration. The model interface is presented in Figure 5.29.

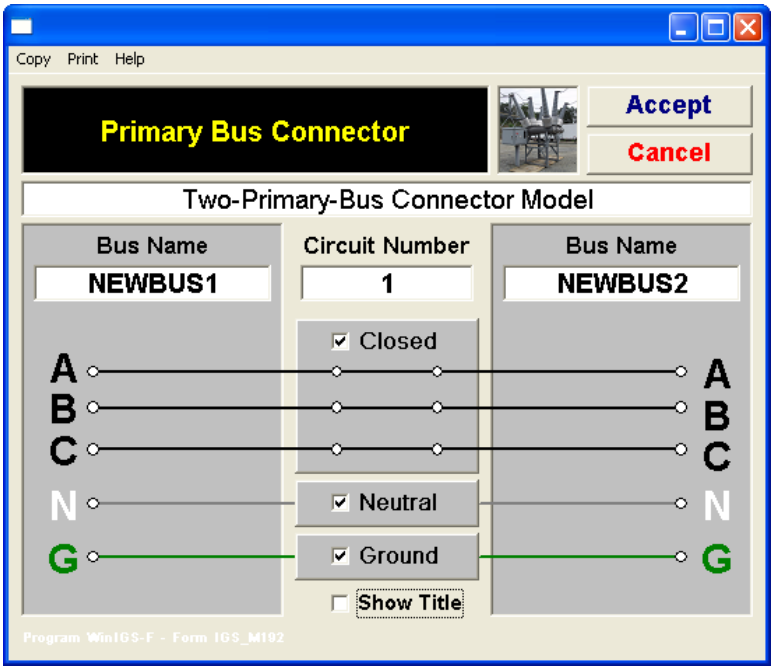


Figure 5.29. Three Phase Breaker/Switch Model Interface.

Single Phase Connector/Switch Model

A single phase circuit connector model has been developed to allow modeling of connections between single phase system nodes, like for example connections between neutral conductors. The model interface is presented in Figure 5.30.

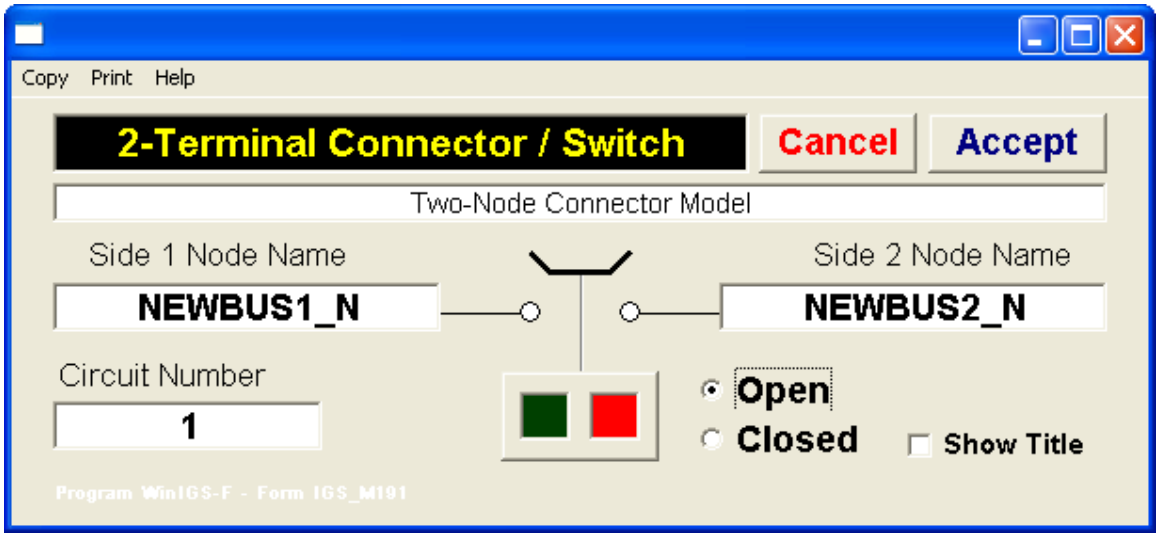


Figure 5.30. Single Phase Connector/Switch Model Interface.

Breaker Model with Time Varying Status

Five breaker models with time varying statues are implemented for quasi steady state (QSN) analysis. The breakers can operate at specific, predefined time instances, or if specific voltage conditions are met. Such models are simplified version of modeling relay operation, for disconnecting transmission lines and loads during fault conditions, therefore simulating predefined scenarios. More sophisticated relay models are currently under implementation, but are outside the scope of this particular project. Both three and single phase models of the above devices have been developed. The model interfaces are presented in Figure 5.29 through Figure 5.35.

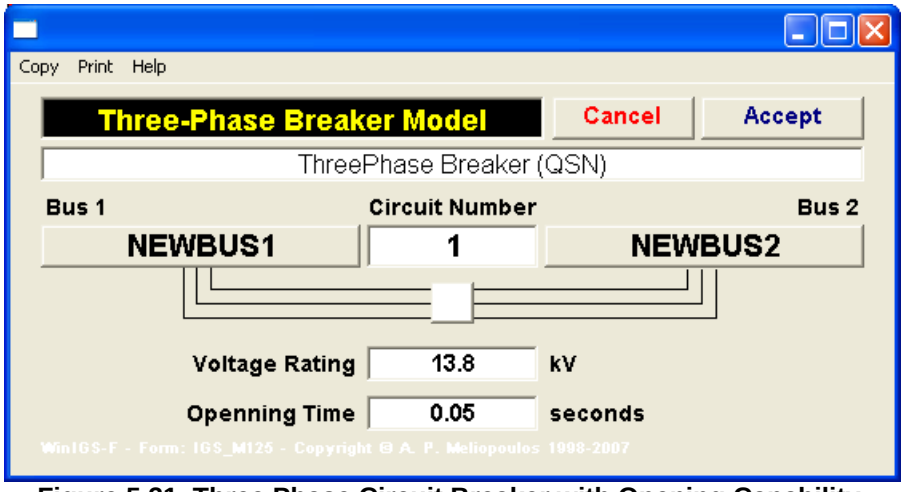


Figure 5.31. Three Phase Circuit Breaker with Opening Capability.

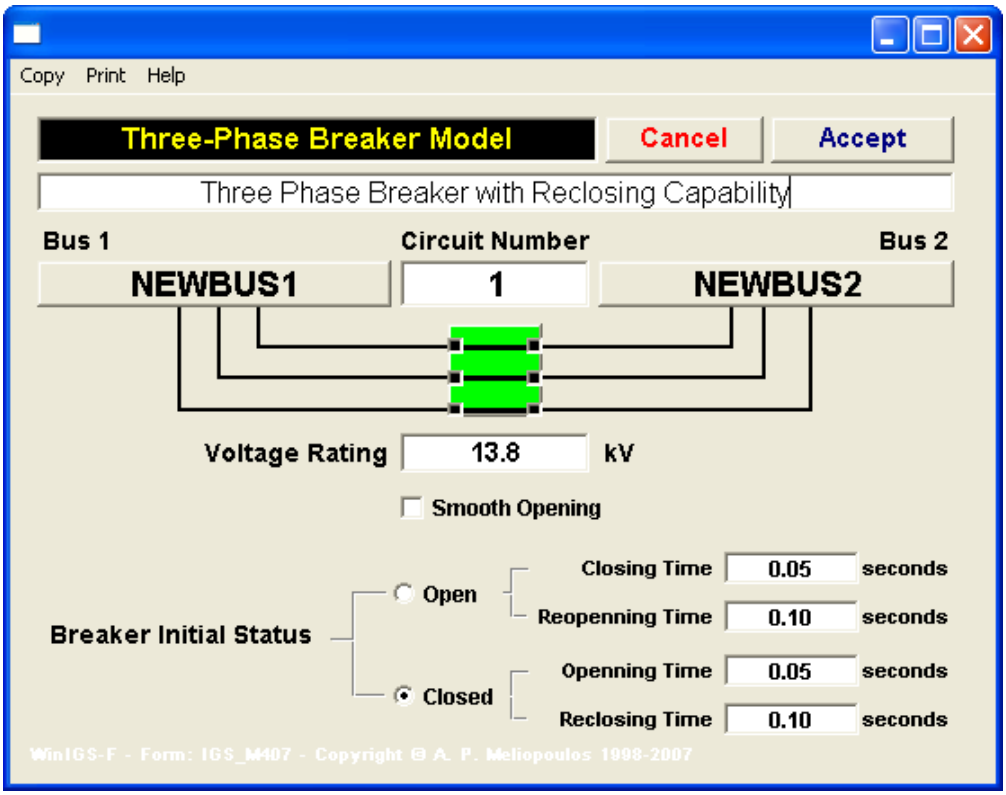


Figure 5.32. Three Phase Circuit Breaker with Opening and Reclosing Capability.

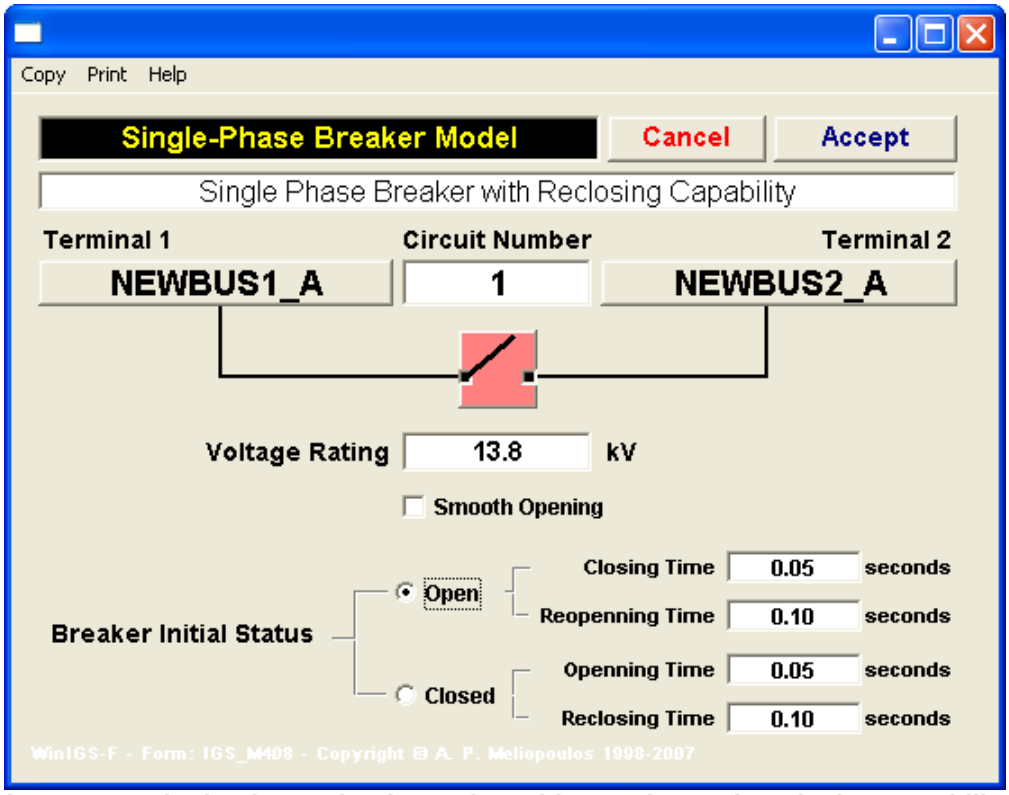


Figure 5.33. Single Phase Circuit Breaker with Opening and Reclosing Capability.

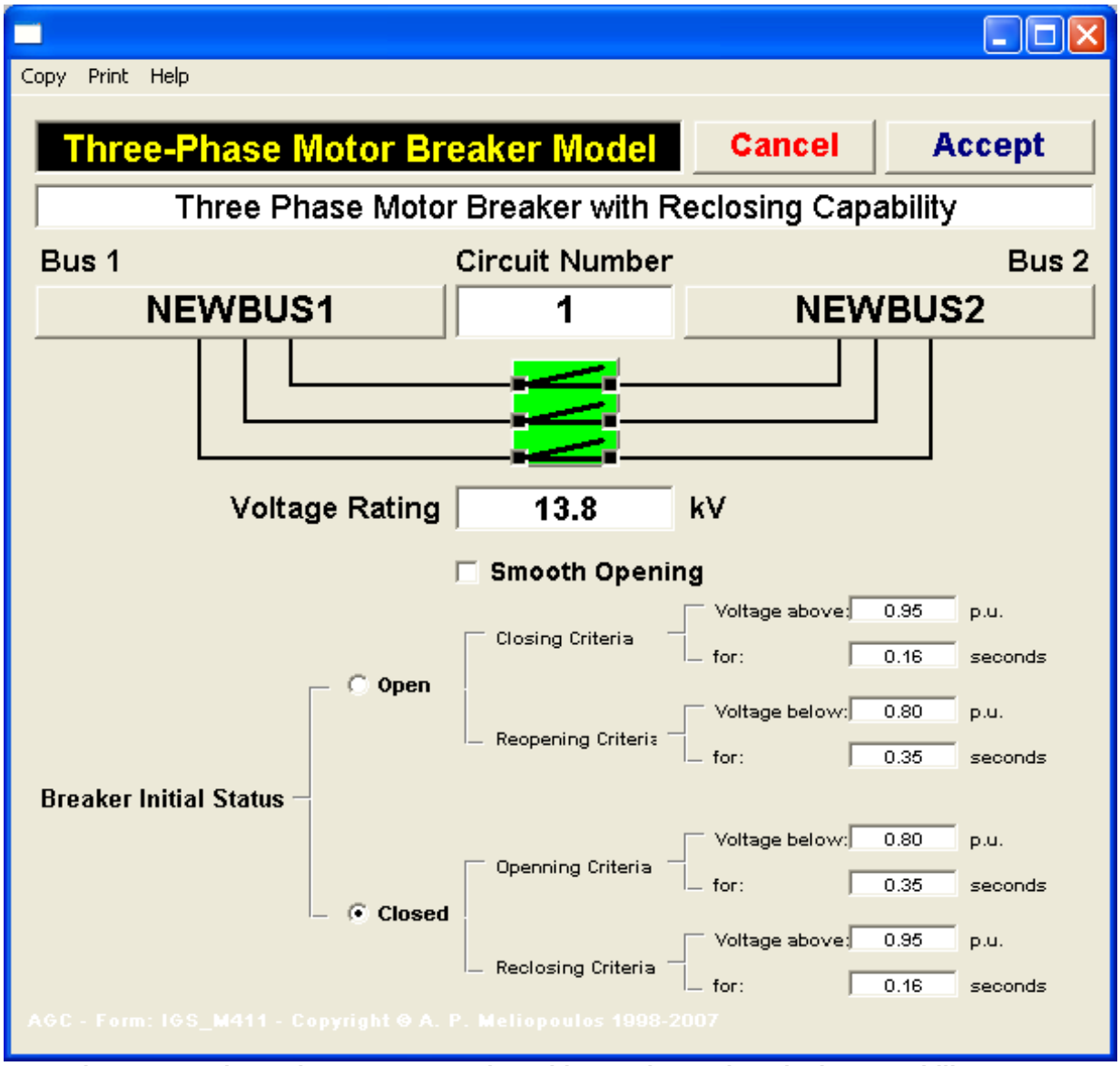


Figure 5.34. Three Phase Motor Breaker with Opening and Reclosing Capability.

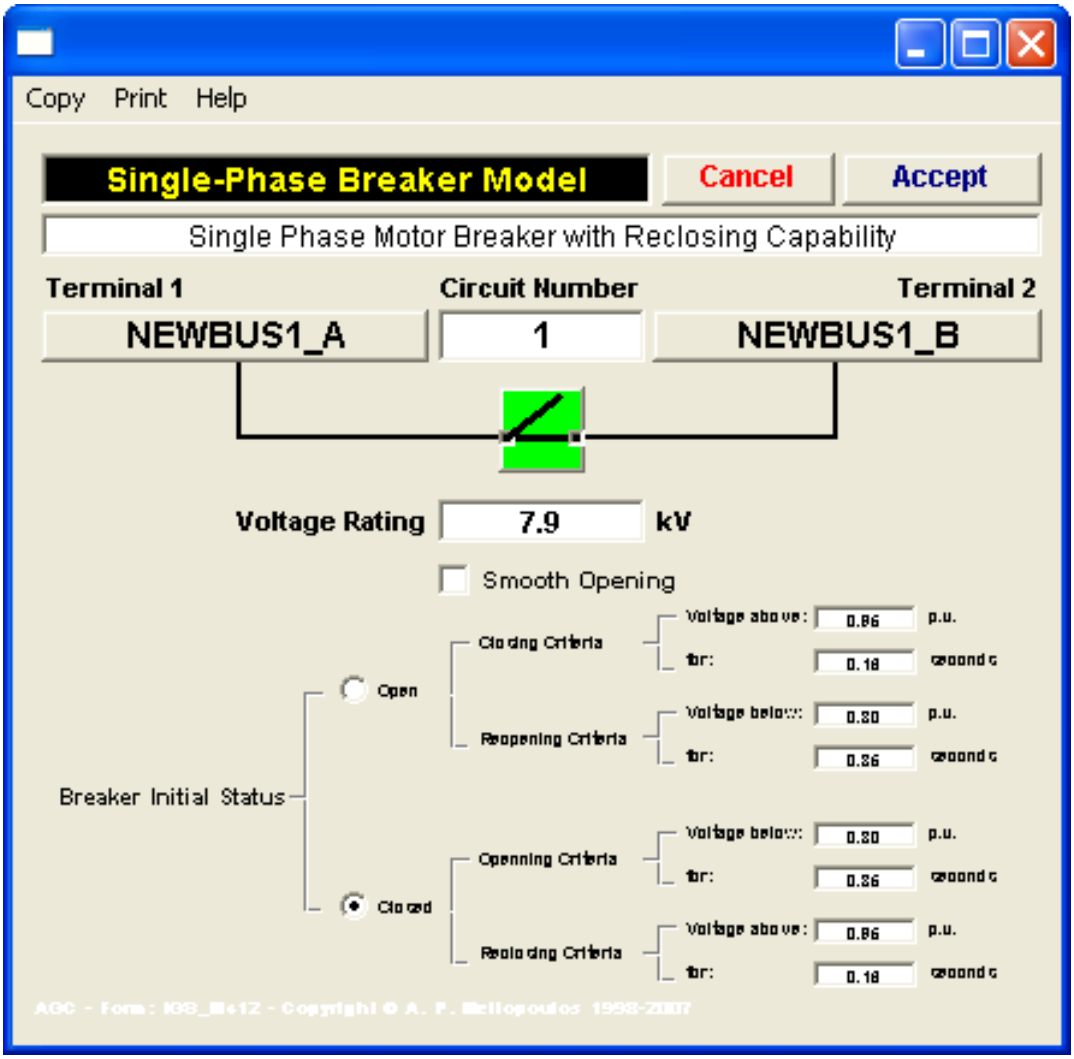


Figure 5.35. Single Phase Motor Breaker with Opening and Reclosing Capability.

Ground Impedance Model

A ground impedance model is used to ground the system neutrals (fourth wire) at selected locations. This device is modeled as an equivalent impedance connecting a system node to the remote earth node. This is a linear model of the form:

$$\begin{bmatrix} \tilde{I}_1 \\ \tilde{I}_2 \end{bmatrix} = \tilde{Y} \cdot \begin{bmatrix} \tilde{V}_1 \\ \tilde{V}_{RE} \end{bmatrix} \qquad (5.3)$$

where the subscript RE indicates the remote earth node, which is the reference node, thus the voltage of with is assumed to the zero.

The model is illustrated in Figure 5.36.

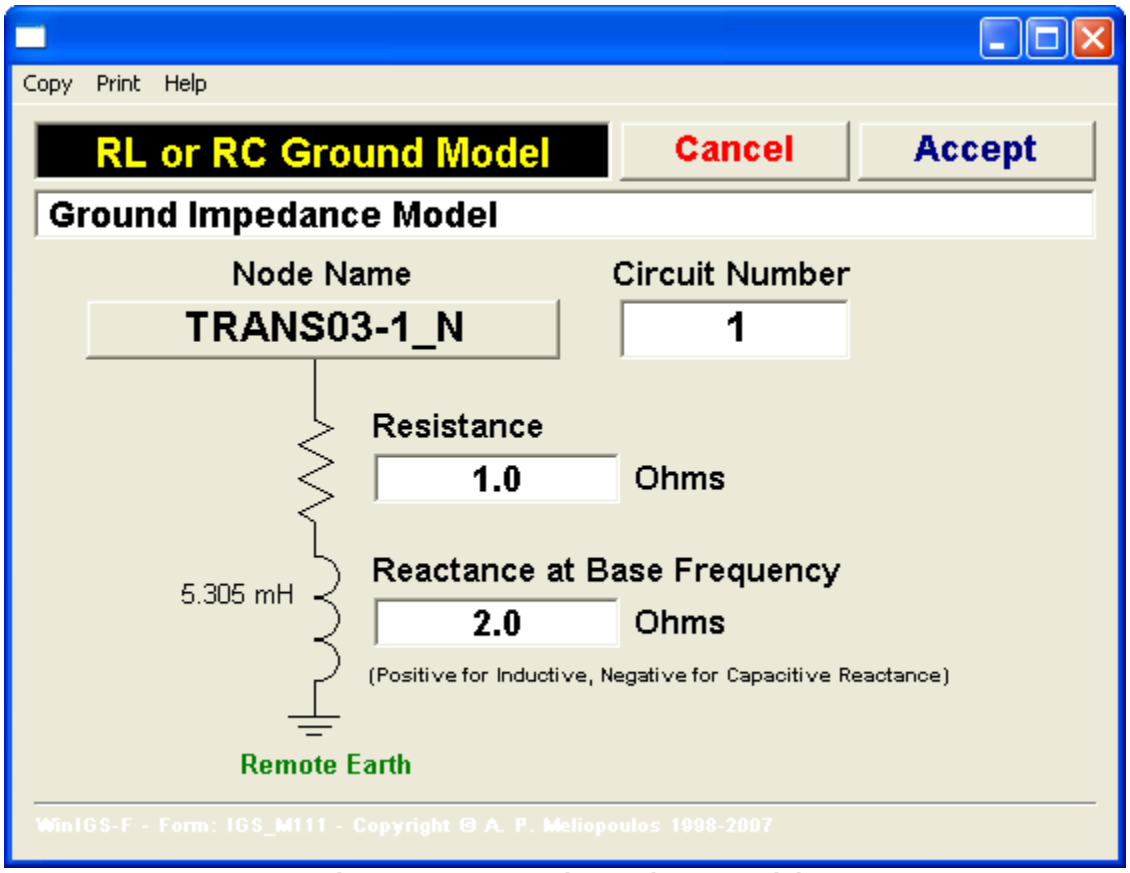


Figure 5.36. Ground Impedance Model.

Substation Model

Each system substation is modeled in detailed configuration using the breaker and switch models described earlier in the section. Since this may result in additional complication of the system one line diagram even in small systems a substation model is created that generates additional editor layers of the one line diagram, keeping therefore the whole system layer relatively simple. All of the internal substation devices can be viewed and accessed by going to the substation layer. An interface device connects devices in the substation layer to devices at the top layer. Geographic information data of the substation location can be entered in the model, if available, and the substation can be placed at the appropriate location if a GPS map is available at the top network level. The substation model and its interface are illustrated in Figure 5.37 to Figure 5.39. An example substation configuration is illustrated in Figure 5.40.

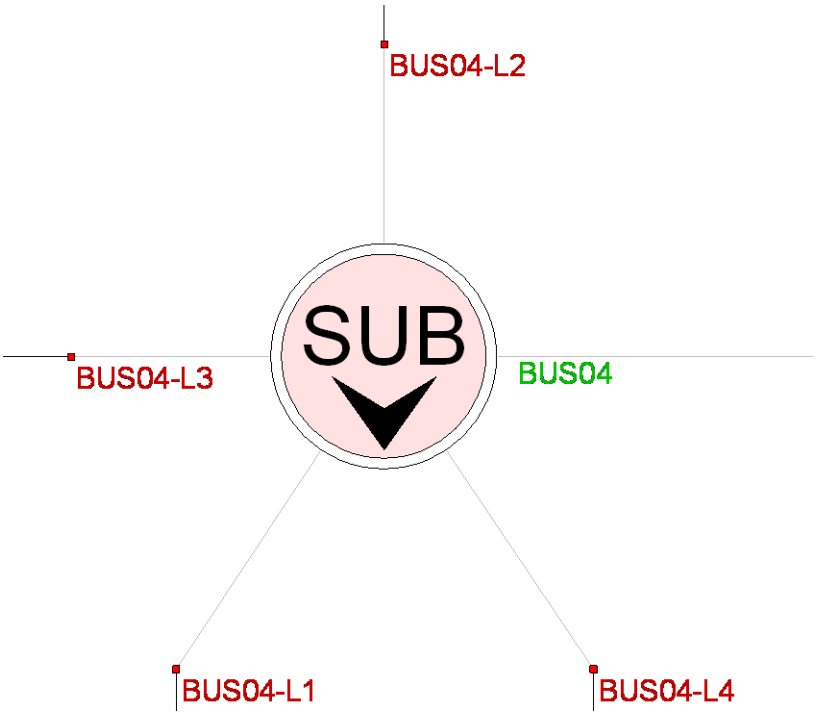


Figure 5.37. Substation Interface Model.

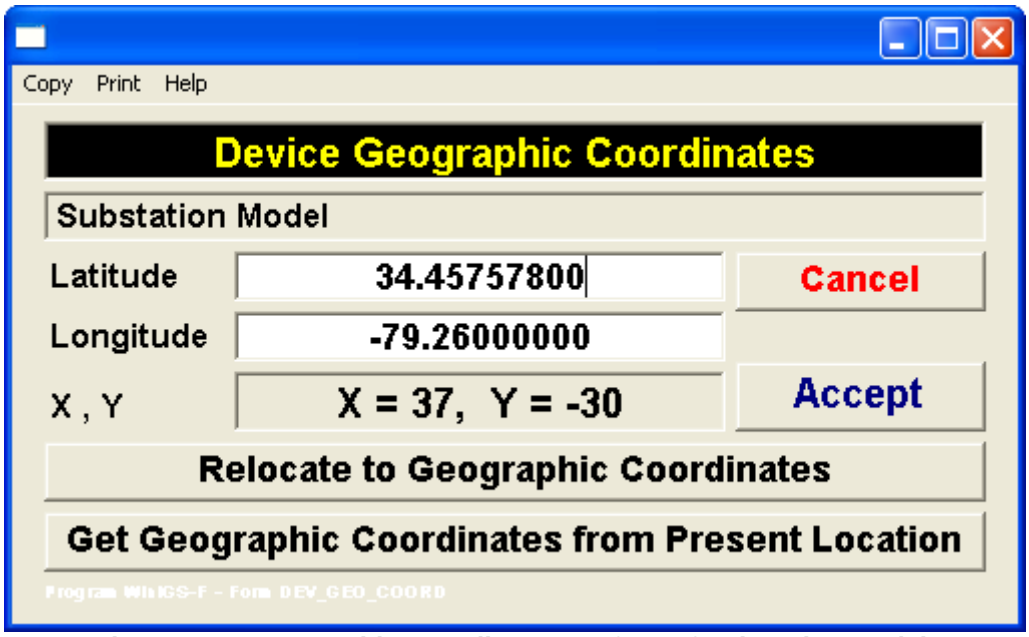


Figure 5.38. Geographic Coordinate Interface of Substation Model.

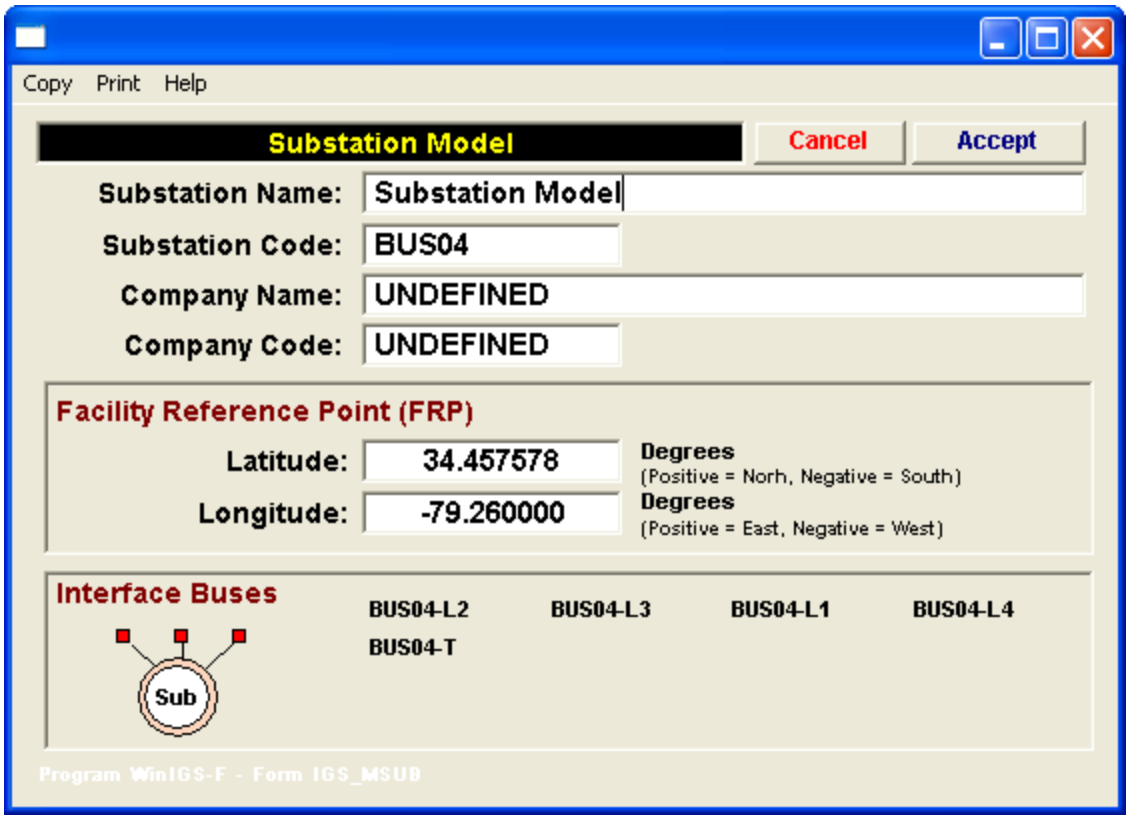


Figure 5.39. Substation Model Data.

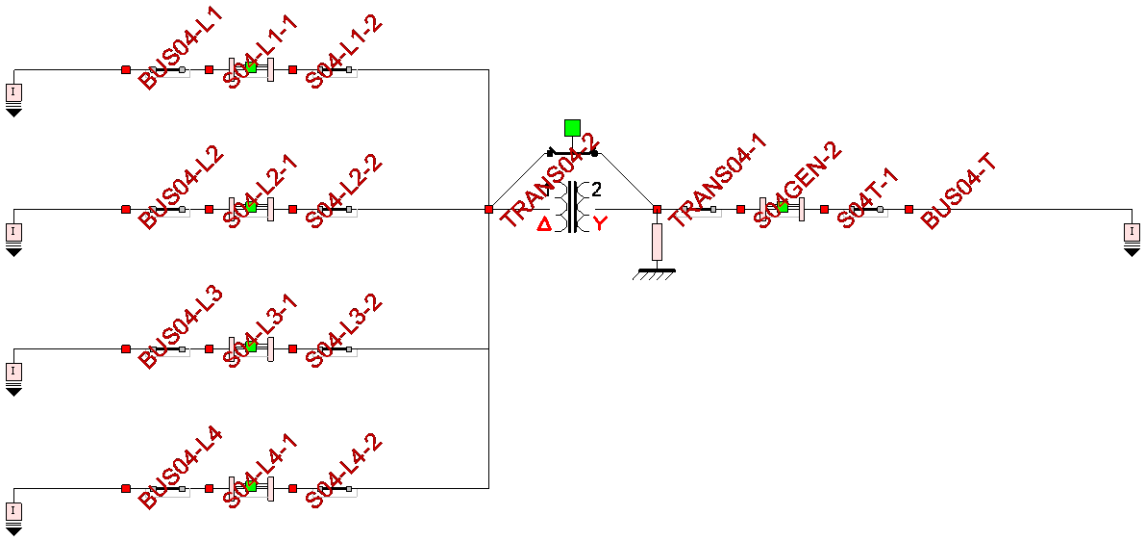


Figure 5.40. Example Substation Configuration. The Arrow Symbol is the Interface to the Network.

Network Model

A typical example of a small system containing most of the devices described in this section, as well as the load and generator models described in previous sections is illustrated in Figure 5.41.

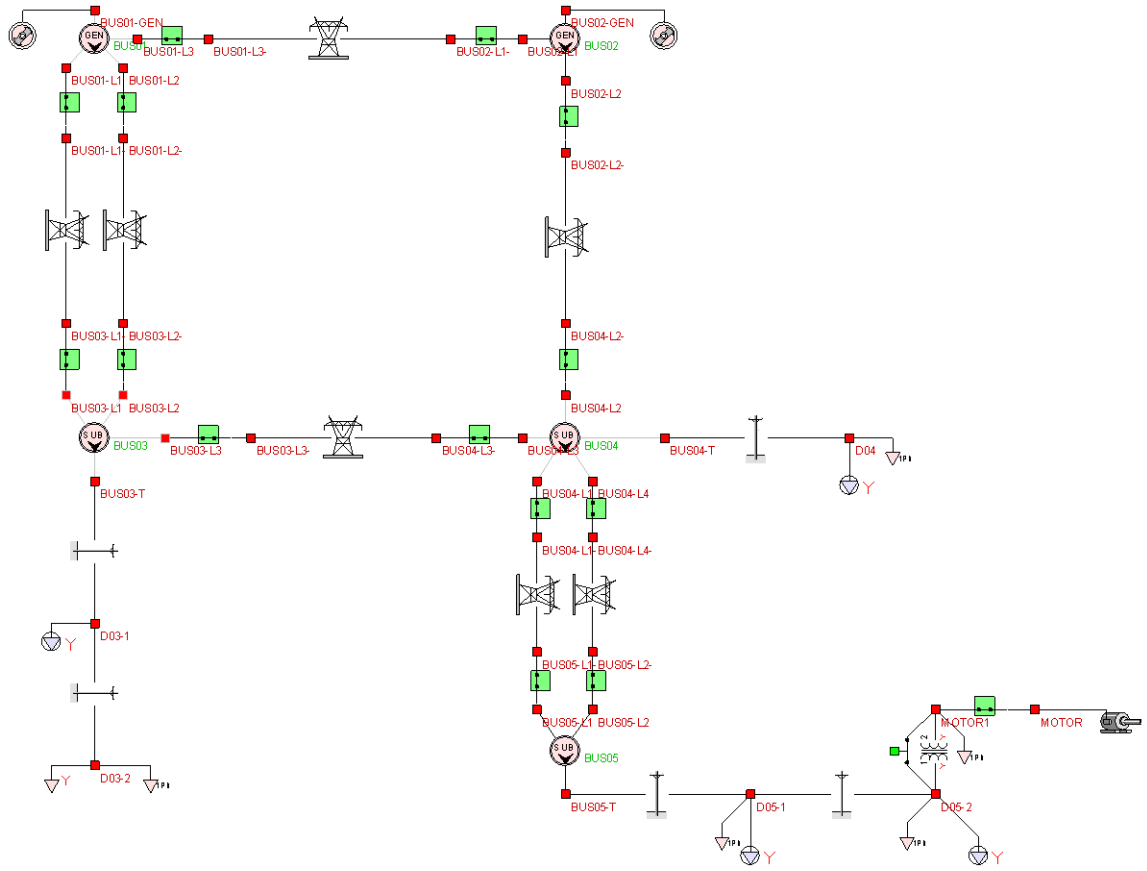


Figure 5.41. One Line Diagram of a Small Electric Power System.

6. Design Criteria

The dynamics of the system, consisting of generator response, load dynamics and VAR support devices leads to the phenomenon of not instantaneous recovery of the voltage following the clearance of a disturbance. The rate of voltage recovery depends on the parameters of the load, the parameters of the transmission system, the parameters of the generators and the exciter and the parameters (type – dynamic/static and quantity) of the VAR support devices. An example response is shown in Figure 6.1. The slow recovery of the voltage may have secondary unintended effects. Specifically large motors are equipped with protection systems that protect them against a variety of abnormal conditions.

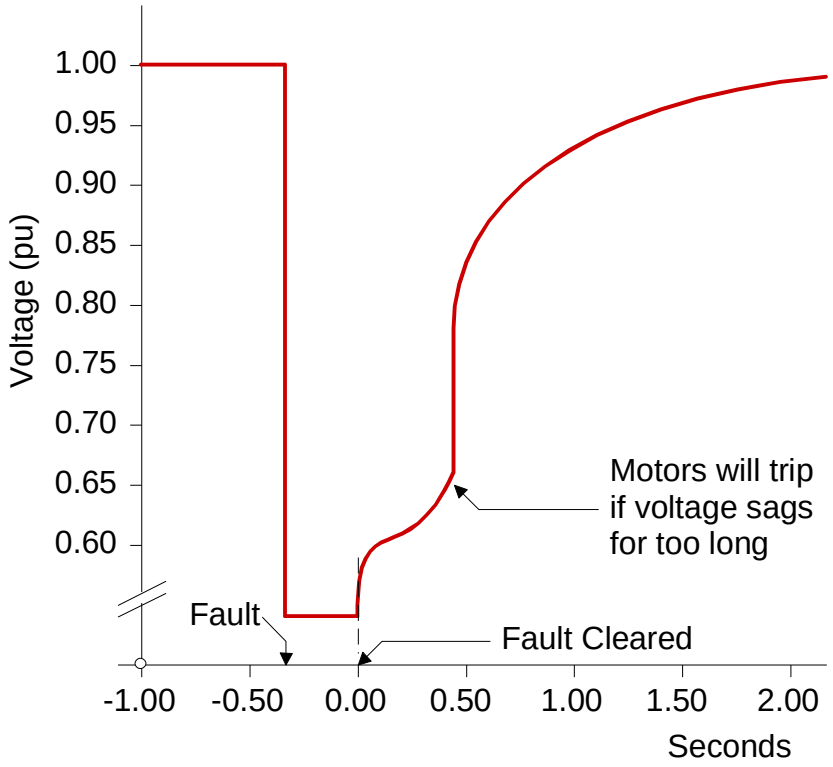


Figure 6.1. Illustration of Design Criteria for Voltage Recovery.

One abnormal condition is low voltage for a prolonged period of time. In this case, motors overheat because tend to operate at higher currents and lower speeds. Furthermore low voltage prevents motors from reaching rated speed on starting or causes them to loose speed and draw heavy overloads. While the overload protection will eventually detect this condition, in many installations the low voltage may jeopardize production or affect electronic or digital controls, in which case the motor should be quickly disconnected. Protection from low voltage is a standard feature of AC motor controllers. The protective relay will trip instantaneously when the voltage drops below a certain value, like 50% to 70% of rated voltage. If immediate loss of the motor is not acceptable, for example in manufacturing plants, a time-delay undervoltage relay is preferred [65]. This also helps avoiding motor tripping on momentary voltage dips. In any case motors

should be disconnected when severe low voltage conditions persist for more than a few seconds [66].

Therefore, in general settings of motor protective systems are such that may trip the electric motor in case of the voltage remaining below a specified threshold for a pre-specified period of time. A review of present practices indicates that the protective device settings can be as strict as follows: trip the motor of the voltage remains below 90% of nominal for a period of 30 cycles.

7. Optimal Placing of Voltage Control Devices

Introduction

The fast voltage recovery can be assisted by devices that respond fast in providing reactive power support to the system during the recovery period. The existing dynamic VAR support devices include:

1. Thyristor-controlled reactors (TCR)
2. Thyristor-switched capacitors (TSC)
3. Fixed-capacitor-thyristor-controlled reactor type VAr Compensators (FC-TCR),
4. Thyristor-switched capacitor-thyristor-controlled reactor type VAr compensators (TSC-TCR)
5. Unidirectional power switched VAr compensators
6. Hybrid converter TCR VAr compensators
7. Three phase synchronous solid-state VAr compensators (SSVC)
8. Multilevel voltage source inverter (VSI) VAr compensators
9. Synchronous generators
10. Superconducting DynVAR

A detailed overview of dynamic VAR source designs is presented in Appendix C.

Contingencies

The selection of the optimal mix of static and dynamic VAR sources should yield a system that will provide voltage regulation for the normal operating conditions of the system and all credible contingencies. Contingencies mainly include systems faults that result in line outages and loss of generation. Such faults may be symmetric or asymmetric. Furthermore, more detailed contingencies can be considered, like specific breaker operation or disoperation, protective relaying operation or disoperation and so on. In this report we will not go into detail on specific types of contingencies and we will mainly concentrate on system short circuits and line outages. However, the work performed during this project and the models developed have laid the foundation for easily modeling very detailed type of system contingencies, both symmetric and asymmetric.

Dynamic VAR Source Modeling

Here we concentrate on the implementation of a generic model of a static VAR system (SVC), since they constitute the major representative of voltage support devices in practical power systems. The system model is either a thyristor-controlled reactor (TCR) or a thyristor-switched capacitor (TSC) or a combination of a TCS in parallel with TSC modules. The implementation is based on reference [44] and more details can be found there. Here we will concentrate on the implementation of a TCR in parallel with fixed capacitor banks, i.e. TCR-FC SVC configuration as illustrated in Figure 7.1. For simplicity the filter is not considered at this stage.

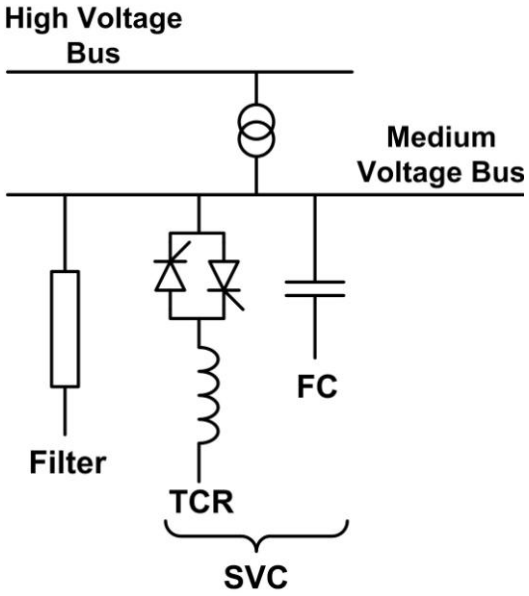


Figure 7.1. Illustration of TCR-FC SVC Configuration.

The basic elements of a TCR are a reactor in series with a bidirectional thyristor switch. The thyristors conduct on alternate half-cycles of the supply voltage frequency depending on the firing angle α, which is measured from a zero crossing of voltage. Full conductance is obtained with a firing angle of 90^0. The current is essentially reactive and sinusoidal. Partial conduction is obtained with firing angles between 90^0 and 180^0. Firing angles between 0^0 and 90^0 are not allowed as they produce asymmetrical currents with a DC component [44].

The conductance angle σ is related to a by $\sigma = 2(\pi - \alpha)$. The instantaneous current is given by:

$$i(t) = \begin{cases} \frac{\sqrt{2}V}{X_L}(\cos\alpha - \cos\omega t), & \alpha < \omega t < \alpha + \sigma \\ 0 & ,\alpha + \sigma < \omega t < \alpha + \pi \end{cases} \qquad (7.1)$$

By applying Fourier analysis, the RMS value of the fundamental component I_1 of the TCR current can be expressed as:

$$I_1 = \frac{V}{X_L}\frac{\sigma - \sin\sigma}{\pi} \qquad (7.2)$$

where I_1 and V are RMS values, and X_L is the reactance of the reactor at foundamental frequency.

The effect of increasing α (i.e. decreasing σ) is to reduce the fundamental component I_1. This is equivalent to increasing the effective inductance of the reactor. In effect, as far as the fundamental frequency current component is concerned, the TCR is a controllable susceptance. The effective susceptance as a function of α is:

$$B(\alpha) = \frac{I_1}{V} = \frac{\sigma - \sin\sigma}{\pi X_L} = \frac{2(\pi - \alpha) + \sin 2\alpha}{\pi X_L} \qquad (7.3)$$

The maximum value of the effective susceptance is at full conduction ($\alpha = 90^0, \sigma = 180^0$), and it is equal to $1/X_L$; the minimum value is zero, obtained with $\alpha = 180^0$ or $\sigma = 0^0$. This susceptance control principle is known as phase control. The susceptance is switched into the system for a controllable fraction of every half cycle. The variation in susceptance as well as the TCR current is smooth or continuous.

The TCR requires a control system which determines the firing instants, ie. the firing angle α, measured from the last zero crossing of the voltage. In some designs the control system respond to a signal that directly represents susceptance. In others the control responds to error signals such as voltage deviation. The result is a steady state V/I characteristic which can be described by:

$$V = V_{ref.} + X_{SL} I_1 \qquad (7.4)$$

where X_{SL} is the slope reactance determined by the control system gain.

The system voltage control characteristic can be extended into the capacitive region by adding in parallel fixed or switched capacitor banks, as illustrated in Figure 7.1.

For three phase systems the single phase legs described above can be connected either in wye, or in delta. Delta connection is preferable because of balanced conditions all triple harmonics generated by the TCR circulate within the closed delta and are therefore absent from the line currents.

A proportional-integral controller is used to provide the firing angles α or equivalently the conductance angles σ. The inputs of the controller are the actual voltage across the SVS and a voltage reference value, as illustrated in Figure 7.2. For a three phase system usually all single phase SVSs are controlled by the same controller, although each single phase leg can be also controlled independently by its own controller. In the case of a single controller the sensed voltage can be either one particular phase voltage, or the line to line voltage of two phases or preferably the positive sequence voltage value.

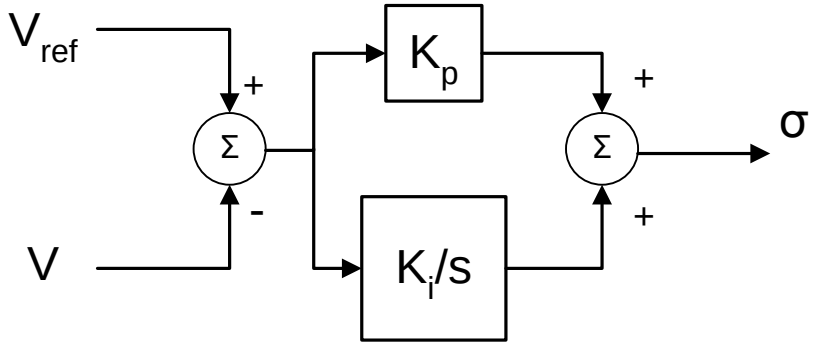


Figure 7.2. Schematic of SVS PI Control Scheme.

Steady State Model

The equations for the steady state model are:
The equations for the quasi steady state dynamic model are:

Thyristor-controller reactor

$$
\begin{aligned}
&I_{1r} = 0 \\
&I_{1i} = B \cdot V \\
&I_{2r} = -I_{1r} \\
&I_{2i} = -I_{1i} \\
&\sigma = 2(\pi - \alpha) \\
&0 = B - \frac{2}{X_L} + \frac{2\alpha}{\pi X_L} - \frac{1}{\pi X_L}\sin(2\alpha) \\
&0 = V^2 - (V_{1r} - V_{2r})^2 - (V_{1i} - V_{2i})^2
\end{aligned}
\qquad (7.5)
$$

where the subscripts 1 and 2 denote the terminals of the system (phase and neutral respectively) and the subscripts r and i denote real and imaginary parts.
The state variable of the system are defined as:

$$X_{TCR} = \begin{bmatrix} V_{1r} & V_{1i} & V_{2r} & V_{2i} & \alpha & B & V \end{bmatrix}^T$$

and the through variables are:

$$I_{TCR} = \begin{bmatrix} I_{1r} & I_{1i} & I_{2r} & I_{2i} & \sigma & 0 & 0 \end{bmatrix}^T$$

PI Controller

$$
\begin{aligned}
&\sigma = x + K_p(V_{ref} - V) \\
&0 = K_i(V_{ref} - V)
\end{aligned}
\quad \Rightarrow \; \sigma = x \qquad (7.6)
$$

The state variable of the system are defined as:

$$X_{PI} = \begin{bmatrix} x \end{bmatrix}^T$$

and the through variables are:

$$I_{PI} = \begin{bmatrix} \sigma \end{bmatrix}^T$$

and there is also a shared state with the TCR, V .

Fixed Capacitor

$$\tilde{I}_C = \tilde{Y}_C(\tilde{V}_1 - \tilde{V}_2) \qquad (7.7)$$

where

$C = \dfrac{Q_R}{V_R^2 \omega}$ and $\tilde{Y}_C = j\omega C = jY_C$, with Q_R the rated capacitor bank power and V_R the voltage rating..

TCR-FC SVC System

By combining the above sets of equations, assuming that the total current is the sum of the two parallel branches we get the set of equations for the SVS system:

$$
\begin{aligned}
&\tilde{I}_{SVS1} = \tilde{Y}_C(\tilde{V}_1 - \tilde{V}_2) + jB \cdot V \\
&\tilde{I}_{SVS2} = -\tilde{I}_{SVS1} \\
&0 = K_i(V_{ref} - V)
\end{aligned}
$$

$$0 = x + K_p\left(V_{ref} - V\right) - 2(\pi - \alpha) \tag{7.8}$$

$$0 = B - \frac{2}{X_L} + \frac{2\alpha}{\pi X_L} - \frac{1}{\pi X_L}\sin(2\alpha)$$

$$0 = V^2 - \left(V_{1r} - V_{2r}\right)^2 - \left(V_{1i} - V_{2i}\right)^2$$

The state variable of the system are defined as:

$$X_{SVS} = \left[\tilde{V}_1 \quad \tilde{V}_2 \quad x \quad \alpha \quad B \quad V\right]^T$$

and the through variables are:

$$I_{SVS} = \left[\tilde{I}_{SVS1} \quad \tilde{I}_{SVS2} \quad 0 \quad 0 \quad 0 \quad 0\right]^T$$

The three phase system is constructed by connecting three single phase systems either in wye, or preferably in delta, usually under the same controller, or using independent controls.

Dynamic Model

Since the dynamic analysis of interest is a quasi steady state type of analysis the dynamic models are the same as the steady state models. The additional dynamics included involve the dynamics of the SVS controller that controls the firing angles in order to maintain the bus voltage at a specific reference value. This is simply modeled via a PI controller with a time delay. The dynamic response time of a TCR is approximately half the period of the input voltage, therefore 5ms to 10ms at 60Hz frequency, but some additional delays may be introduced by measurement and control circuits. The dynamic response time of the TSC is about one period of the input voltage, therefore again at 60Hz about 16ms. Again delays may be introduced by the control or measurement circuits. For a combination SVS the response time is about the same as the TSC time, therefore about one period of the fundamental at 60Hz. Such delays are modeled with the value of the $1/K_i$ parameter of the PI controller.

The equations for the quasi steady state dynamic model are:

Thyristor-controller reactor

$$I_{1r} = 0$$

$$I_{1i} = B \cdot V$$

$$I_{2r} = -I_{1r}$$

$$I_{2i} = -I_{1i} \tag{7.9}$$

$$\sigma = 2(\pi - \alpha)$$

$$0 = B - \frac{2}{X_L} + \frac{2\alpha}{\pi X_L} - \frac{1}{\pi X_L}\sin(2\alpha)$$

$$0 = V^2 - \left(V_{1r} - V_{2r}\right)^2 - \left(V_{1i} - V_{2i}\right)^2$$

where the subscripts 1 and 2 denote the terminals of the system (phase and neutral respectively) and the subscripts r and i denote real and imaginary parts.

The state variable of the system are defined as:

$$X_{TCR} = \left[V_{1r} \quad V_{1i} \quad V_{2r} \quad V_{2i} \quad \alpha \quad B \quad V\right]^T$$

and the through variables are:

$$I_{TCR} = \begin{bmatrix} I_{1r} & I_{1i} & I_{2r} & I_{2i} & \sigma & 0 & 0 \end{bmatrix}^T$$

PI Controller

$$\begin{aligned} \sigma &= x + K_p\left(V_{ref} - V\right) \\ \frac{dx}{dt} &= K_i\left(V_{ref} - V\right) \end{aligned} \tag{7.10}$$

The state variable of the system are defined as:

$$X_{PI} = \begin{bmatrix} x \end{bmatrix}^T$$

and the through variables are:

$$I_{PI} = \begin{bmatrix} \sigma \end{bmatrix}^T$$

and there is also a shared state with the TCR, V .

Fixed Capacitor

$$\tilde{I}_C = \tilde{Y}_C\left(\tilde{V}_1 - \tilde{V}_2\right) \tag{7.11}$$

where

$C = \frac{Q_R}{V_R^2 \omega}$ and $\tilde{Y}_C = j\omega C = jY_C$, with Q_R the rated capacitor bank power and V_R the voltage rating..

TCR-FC SVC System

By combining the above sets of equations, assuming that the total current is the sum of the two parallel branches we get the set of equations for the SVS system:

$$\begin{aligned} \tilde{I}_{SVS1} &= \tilde{Y}_C\left(\tilde{V}_1 - \tilde{V}_2\right) + jB \cdot V \\ \tilde{I}_{SVS2} &= -\tilde{I}_{SVS1} \\ \frac{dx}{dt} &= K_i\left(V_{ref} - V\right) \\ 0 &= x + K_p\left(V_{ref} - V\right) - 2(\pi - \alpha) \\ 0 &= B - \frac{2}{X_L} + \frac{2\alpha}{\pi X_L} - \frac{1}{\pi X_L}\sin(2\alpha) \\ 0 &= V^2 - \left(V_{1r} - V_{2r}\right)^2 - \left(V_{1i} - V_{2i}\right)^2 \end{aligned} \tag{7.12}$$

The state variable of the system are defined as:

$$X_{SVS} = \begin{bmatrix} \tilde{V}_1 & \tilde{V}_2 & x & \alpha & B & V \end{bmatrix}^T$$

and the through variables are:

$$I_{SVS} = \begin{bmatrix} \tilde{I}_{SVS1} & \tilde{I}_{SVS2} & 0 & 0 & 0 & 0 \end{bmatrix}^T$$

The three phase system is constructed by connecting three single phase systems either in wye, or preferably in delta, usually under the same controller, or using independent controls.

Static VAR Source Modeling

In addition there are VAR support devices that cannot respond within the period of interest. For example mechanically switch capacitor banks provide reactive power support, but they can not respond within the time frame of the desired voltage recovery. The reason is that their switching depends on mechanical switches that have a relatively long response time. In the static VAR sources are fixed, and thus constantly connected to the grid, then they can respond very fast, but their existence will also affect the steady state system behavior. Therefore, static VAR sources are usually placed in an electric power grid based on steady state criteria (like e.g. leveling the system voltage profile, minimizing system losses, increase loadability limits etc) It is important to note that in general static VAR support devices are relatively low cost while the dynamic VAR support devices are of relative high cost. Therefore the issue of designing the system to provide dynamic VAR support and fast voltage recovery at minimal cost arises. We propose to address these problems via an optimization procedure that accounts for the technical characteristics of dynamic and static VAR sources, their cost and the requirements for fast voltage recovery. The optimization problem is described in a following section.

Shunt capacitors are the static VAR sources considered in this work. The mathematical model is presented next:

Steady State Model

The steady state model is the standard linear capacitor (reactor) model of specific capacitance (inductance) and therefore of specific impedance. The equivalent Y-leg capacitance or inductance is computed based on the provided nominal operating conditions, i.e. rated voltage V_R and rated reactive power Q_R. Note that it is assumed that Q_R has a negative value for inductors and positive for capacitors.

$C = \frac{Q_R}{V_R^2 \omega}$ and $L = -\frac{V_R^2}{Q_R \omega}$

The equivalent Y-leg impedance is computed as

$\tilde{Y}_S = j\omega C$ for capacitor banks and $\tilde{Y}_S = \frac{1}{j\omega L}$ for reactors.

For wye connection:

$$\begin{aligned}
\tilde{I}_A &= \tilde{Y}_S \cdot \left(\tilde{V}_A - \tilde{V}_N\right) \\
\tilde{I}_B &= \tilde{Y}_S \cdot \left(\tilde{V}_B - \tilde{V}_N\right) \\
\tilde{I}_C &= \tilde{Y}_S \cdot \left(\tilde{V}_C - \tilde{V}_N\right) \\
\tilde{I}_N &= -\tilde{Y}_S \cdot \left(\tilde{V}_A + \tilde{V}_B + \tilde{V}_C - 3\tilde{V}_N\right)
\end{aligned} \qquad (7.13)$$

where $\tilde{V}_A$, $\tilde{V}_B$, $\tilde{V}_C$, $\tilde{V}_N$ are the voltages at the bank terminals, and $\tilde{I}_A$, $\tilde{I}_B$, $\tilde{I}_C$, $\tilde{I}_N$ the phase and neutral currents the bank absorbs from the network.

For delta connection:

$$\tilde{I}_A = \frac{\tilde{Y}_S}{3} \cdot \left(2\tilde{V}_A - \tilde{V}_B - \tilde{V}_C\right)$$
$$\tilde{I}_B = \frac{\tilde{Y}_S}{3} \cdot \left(2\tilde{V}_B - \tilde{V}_A - \tilde{V}_C\right) \qquad (7.14)$$
$$\tilde{I}_C = \frac{\tilde{Y}_S}{3} \cdot \left(2\tilde{V}_C - \tilde{V}_A - \tilde{V}_B\right)$$

where $\tilde{V}_A$, $\tilde{V}_B$, $\tilde{V}_C$ are the voltages at the bank terminals, and $\tilde{I}_A$, $\tilde{I}_B$, $\tilde{I}_C$ the phase currents the bank absorbs from the network.

Dynamic Model

Since the type of analysis of interest is quasi steady state analysis that assumes sinusoidal steady state network conditions the model of the capacitor or inductor bank for this type of analysis is the same as the steady state model. No dynamics are included, since the capacitor dynamics are very fast to be considered for this type of analysis.

User Interface

The user interface of the 3-phase capacitor or inductor bank mode is illustrated in Figure 7.3. The rated voltage level and the rated reactive power is provided by the user, along with the connection type.

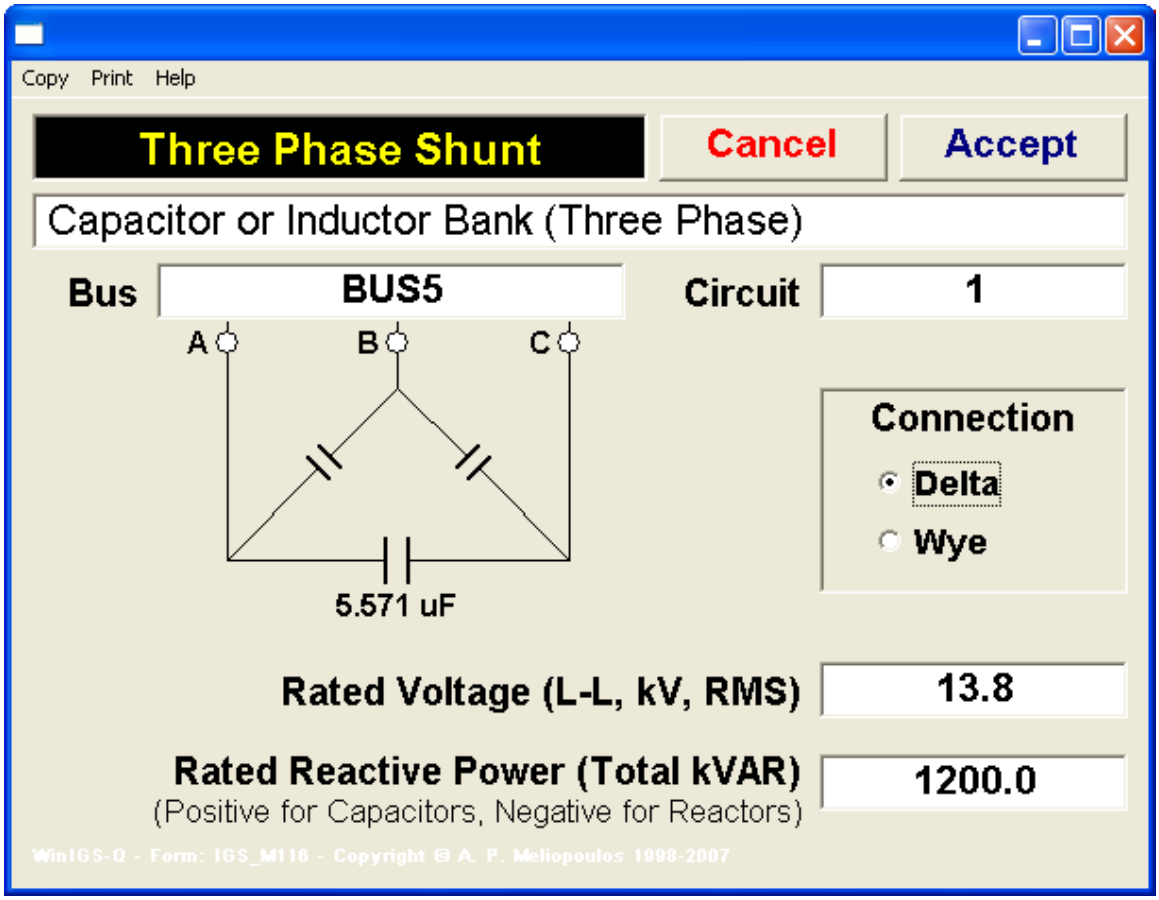


Figure 7.3. User Interface of Three-Phase Capacitor or Inductor Bank Model.

Optimization Problem

The overall optimization methodology consists of three main parts: a) determination of the optimal location for reactive support, b) computation of amount of support, and c) determination of the optimal mix of static and dynamic support.

A set of feasible locations for reactive support can be determined based on the system topology and the physical constraints of the system under study. Such a procedure selects a small number of system buses where support can actually be installed and is based on system data, utility practices and preferences and experience. Then, the best candidate locations are selected based on sensitivity analysis. Static sensitivity analysis can be used to determine locations based on steady-state performance criteria. Trajectory sensitivity analysis methods can be applied to determine locations based on dynamic criteria and also to illustrate optimal operation and control strategies for such devices during voltage recovery or other transient phenomena. A methodology for efficient computation of static and dynamic sensitivities is currently under development and implementation. Since the results of sensitivity analysis depend on the system configuration, the system operating point (mainly determined by the load level), the performance criteria and the disturbances into consideration, some prescreening has to be performed in advance in such a way that the most common system operating states are considered and the most important disturbances are studied, for the desired performance criteria (e.g. voltage recovery criteria). Sensitivity analysis, in particular dynamic trajectory sensitivities, can be also used to determine the optimal mix of static and dynamic support, based on voltage recovery criteria, once the amount of total compensation for a location is determined.

The amount of reactive support can be generally computed by the solution of an optimization problem. The problem can be formulated as follows:

Given:

A particular power system comprising of generating units, transmission network, electric loads with specific load composition and an expected daily variations (mainly peak, shoulder and valley load levels);

A number of candidate buses for reactive source placement (computed via sensitivity analysis);

Capacitor modules of capacity Q_c MVAr, operating at specific voltage level, at cost $C_c(Q_c)$ (consisting of operating cost and installation cost);

Dynamic VAR sources of capacity $Q_{D,\min}$, $Q_{D,\max}$, operating at specific voltage level, at cost $C_D(Q_{D,\min}, Q_{D,\max})$ (consisting of operating cost and installation cost);

Voltage limits and voltage recovery criteria;

Compute:

The optimal selection of Q_i's for each candidate bus, i, where $Q_i = \sum Q_c$, and of $(Q_{D,\min}, Q_{D,\max})_i$ that minimizes the total cost, observes the voltage limits and meets the voltage recovery criteria.

The above problem is a nonlinear optimization problem. Due to the dynamic nature of the problem dynamic programming [67] is the first solution approach that is being currently considered, in combination with sensitivity analysis. The approach is illustrated in Figure 7.4.

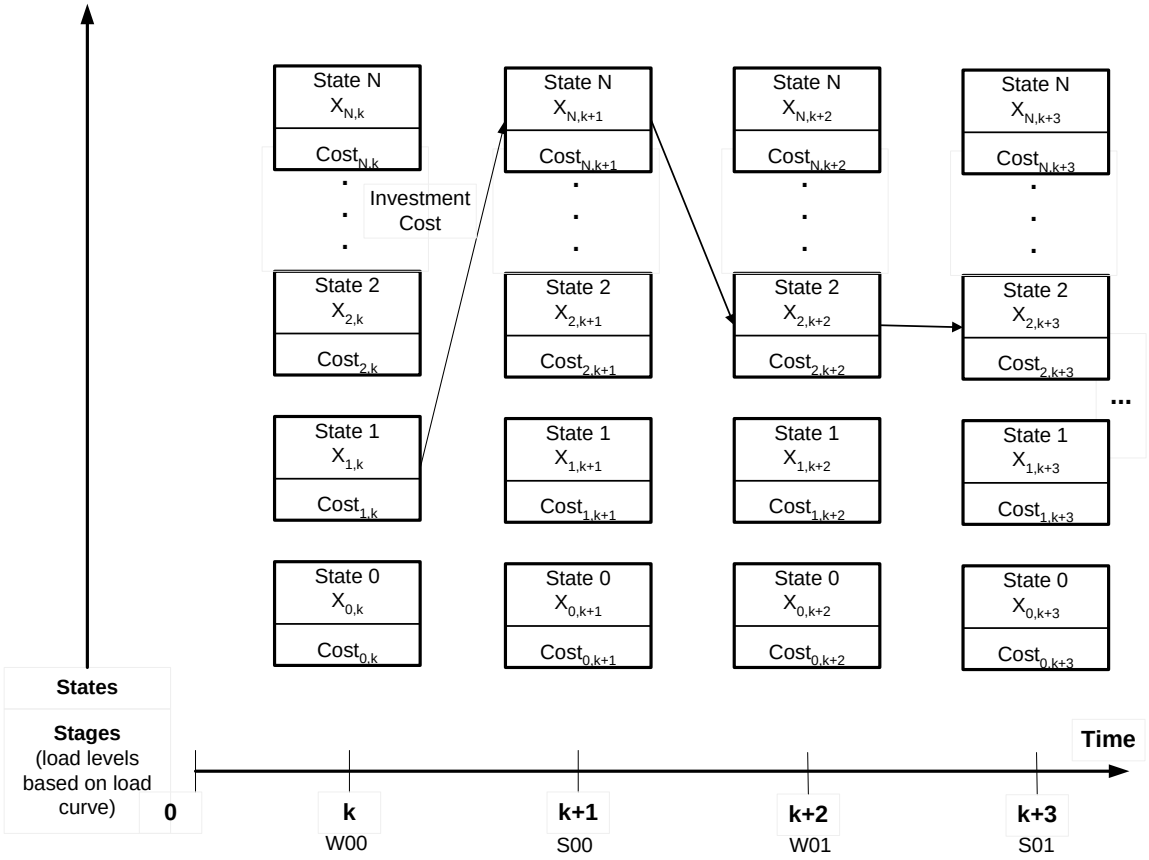


Figure 7.4. Block Diagram of the Successive Dynamic Programming Procedure

A planning time period is defined for the study. Depending on the actual objectives, this period can be a single day, a month or be defined in terms of years. When installation of new VAr sources is considered, years is the time period of interest. When operation of existing sources is of interest shorter periods of time, such as a day or several hours should be the total study period. The study period is divided into smaller periods of time, which comprise the stages of the problem. Expected load variations for these stages should be available, such as daily load curves, for a single day period, or load growth for periods of few years. The non-conforming load model described earlier in this report is used to more realistically represent such load variations. Therefore a representative load level and basic system power configuration is defined for each stage. In the example of Figure 7.4, the total period of study is defined as being two years and each year is subdivided into winder period and summer period. The winter and summer peak loads can be used as representative load levels and operating conditions at each stage of the problem. Transitions from stage to stage include expected load variations (via the non-conforming load model) and other expected system configuration changes (change in load composition, commissioning of new substation, generating units, transmission lines, etc).

For each stage of the problem a series of states is defined based on VAr source additions. The state 0 is the base case with no VAr source additions. The state 1 is the new state after the addition of a VAr source module at some location in the system. Note that we are assuming that VAr sources are added in specific, discrete module sizes. Thus state 2 is the state after the addition of a VAr module at a second location and so until theoretically all N possible location and module combinations are considered (up to a certain level of modules per location). When this exhaustive search is completed for the current state, the best location in terms of some defined objective function is selected. This objective function includes static performance measures, installation cost as well as dynamic performance measures (like voltage recovery criteria) under, in theory again, all possible system contingencies. Starting from this last state a transition is performed to the next stage of the problem. There the procedure is repeated assuming the new operating conditions and system configuration (having included the VAr source addition from the previous stage) and taking again into consideration all possible candidate locations and contingencies. A new VAr source addition is then defined and the problem moves to the next stage, and this procedure keeps going until the end of the study period is reached. Note that after the end of the study period is reached a path of VAr source additions at each stage during the study period is defined. This path is the optimal path.

Solution Method

Conceptually, the above method can be applied in a way that will consider all possible states at every stage. This approach makes the problem computationally intractable, even theoretically, because of the huge number of possible states. For example if one considers possibility of adding VAR sources at n_{VS} buses at up to m_{VS} different sizes per location (including no addition), then the number of possible states per stage will be ${m_{VS}}^{n_{VS}}$. Even for a very small test system of 10 possible locations with two possible additions per locations (i.e. three states per location: 0 additions, 1 addition, 2 additions) the total number of possible combinations will be $3^{10} = 59049$ states per stage!! This makes the problem practically intractable. If in addition all possible contingencies are to be considered at each state, say up to level 2 the number of contingencies per state will be approximately $(n_L + n_G)^2$ where n_L is the number of circuits in the system and n_G is the number of units in the system. For even a small system like the one above the product of this number and the total number of states, which indicates the number of simulations needed will be humongous.

However one does not need to take this brute force approach (and cannot take it in practice). The method of successive dynamic programming has been developed to address the dimensionality problem. Specifically, the basic idea of successive dynamic programming is to limit the number of states at every stage to a very small number. The small number of the states is selected with sensitivity methods that guarantee that these states will provide the states that will be part of the optimal solution. For this problem, the states are defined in terms of the most effective additions of dynamic or static VAR sources, and each state includes the most critical contingencies. Therefore small number of states is defined around the iterate of the system trajectory (defined with the sequence

of decisions to add static/dynamic VAR sources to the various system buses). The pass among all the problem stages is repeated successively, until the computed series of optimal states has converged to a unique path (sequence of optimal states through the problem stages).

Referring again to Figure 7.4, for each stage of the problem a series of states is defined based on VAr source additions. Only the first few best candidate locations are considered, based on static and dynamic sensitivity analysis. Single additions per location are considered at this time. The state 0 is the base case with no VAr source additions. The state 1 is the new state after the addition of a VAr source module at some location in the system. Note that we are assuming that VAr sources are added in specific, discrete module sizes. Furthermore, at this time we are only assuming one module to be placed at each location at each state. When this procedure is complete for the few selected locations for the current state, the best location in terms of some defined objective function is selected. This objective function includes static performance measures, installation cost as well as dynamic performance measures (like voltage recovery time) under a few specific system critical contingencies, selected via sensitivity methods again. Starting from this last state a transition is performed to the next stage of the problem. There the procedure is repeated assuming the new operating conditions and system configuration (having included the VAr source addition from the previous stage) and taking again into consideration specific, selected candidate locations and contingencies. A new VAr source addition is then defined and the problem moves to the next stage, and this procedure keeps going until the end of the study period is reached. Note that after the end of the study period is reached a path of VAr source additions at each stage during the study period is defined. However, this path might not be optimal, due to the fact that only a small subset of locations and contingencies were considered and also only one addition per location per stage was assumed. Therefore the procedure is repeated successively, starting form the first state of the path computed during the first iterate.

Again if one considers the possibility of adding VAR sources at n_{VS} location at up to m_{VS} different sizes per location (including no addition), then the number of possible states per stage will be ${m_{VS}}^{n_{VS}}$. If now n_{VS} is only the 2 most favorable possible locations, selected via sensitivity analysis with two possible additions per locations (i.e. three states per location: 0 additions, 1 addition, 2 additions) the total number of possible combinations will be $3^2 = 9$ states per stage!! This makes the problem very tractable in practice. If in addition only the two or three most important first level contingencies are to be considered at each state, chosen via sensitivity based contingency screening approximately then the number of computations per state also stays within low and tractable values.

The transition from state to state is based on the transition equation:

$$Cost^*(X_{i,k+1}) = OperCost(X_{i,k+1}) + \min_j \left[Cost^*(X_{j,k}) + T(X_{j,k} \to X_{i,k+1}) \right] \qquad (7.15)$$

Only transitions (forward) that add VAR sources are allowed

A state, Si, at stage Tk is feasible only if:
The static optimization problem has a solution.
It meets dynamic voltage recovery criteria.
A penalty function is applied to the cost function, for states that do not satisfy the performance criteria, based on the deviation of these criteria. These criteria involve:

Steady state voltage magnitude at load buses (of interest):

This can be expressed by utilizing a voltage index defined as

$$J_V = \sum_{k=1}^{N} w_k \left(\frac{V_k - V_{k,mean}}{V_{k,step}} \right)^{2n},$$

where

w_k : weighting factor, $0 < w_k < 1$,

$V_{k,mean}$: nominal bus voltage value (typically 1.0 p.u.),

(it is in general the mean value in the desired range, i.e. $\frac{1}{2}\left(V_k^{\max} + V_k^{\min}\right)$),

$V_{k,step}$: voltage deviation tolerance (i.e. $\frac{1}{2}\left(V_k^{\max} - V_k^{\min}\right)$),

V_k : actual voltage magnitude at bus k,

n : positive integer parameter defining the exponent,

N : total number of buses of interest.

More details are provided in the next section of this chapter.

Voltage sag magnitude and duration below a predefined value, or equivalently, voltage recovery rate at certain load buses of interest.

This can be expressed by utilizing a functional of the form

$$J_{dip}(v(t)) = t_1 - t_2$$

where

t_1 : transition time at which the voltage fall below threshold ($v(t) < V^{\min}$),

t_2 : transition time at which the voltage recovers above threshold ($v(t) > V^{\min}$),

or more generally of the form

$$J_R(z(t)) = \int_{t_1}^{t_2} \left(z_{threshold} - z(t) \right) dt$$

$z(t)$: output of interest (scalar or vector), e.g. voltage at specific load bus(es),

$z_{threshold}$: threshold level for performance criteria, e.g. minimum acceptable voltage level,

t_1 : time at which the observation quantity of interest fall below threshold value,

t_2 : time at which the observation quantity of interest recovers above threshold.

More details are provided at the end of this chapter, in the section about trajectory sensitivity analysis.

The cost $C(X)$ of installing and operating VAr sources is assumed to depend on the type of VAr support device, the rated power, and the location of placement (included in the X vector representing specific VAr source addition).

Therefore the problem is a multi-objective optimization problem. A typical way of approaching the problem is by combining all the objectives in one composite objective. Thus, a typical expression of the objective function to be minimized would be a weighted sum of the above components:

$$J(X) = W_1 C(X) + W_2 \sum_{i=1}^{n} J_{V,i} + W_3 \sum_{i=1}^{n} J_{dip,i} + W_4 \sum_{i=1}^{n} J_{R,i}$$

where

W_j s : objective weights,

n s : total number of considered cases (base case plus selected contingencies).

This objective function is computed for all possible additions considered. Furthermore the components of the objective function may also provide valuable information about the type of VAr source additions. The value of the J_V component and its sensitivity with respect to a specific VAr addition reflects the improvement on steady state network conditions and therefore towards capacitor placement. The value of the J_R (or J_{dip}) component and its sensitivity with respect to a specific VAr addition reflects the improvement on dynamic behavior and therefore towards dynamic VAr source placement.

A flow diagram of the successive dynamic programming approach is presented in Figure 7.5.

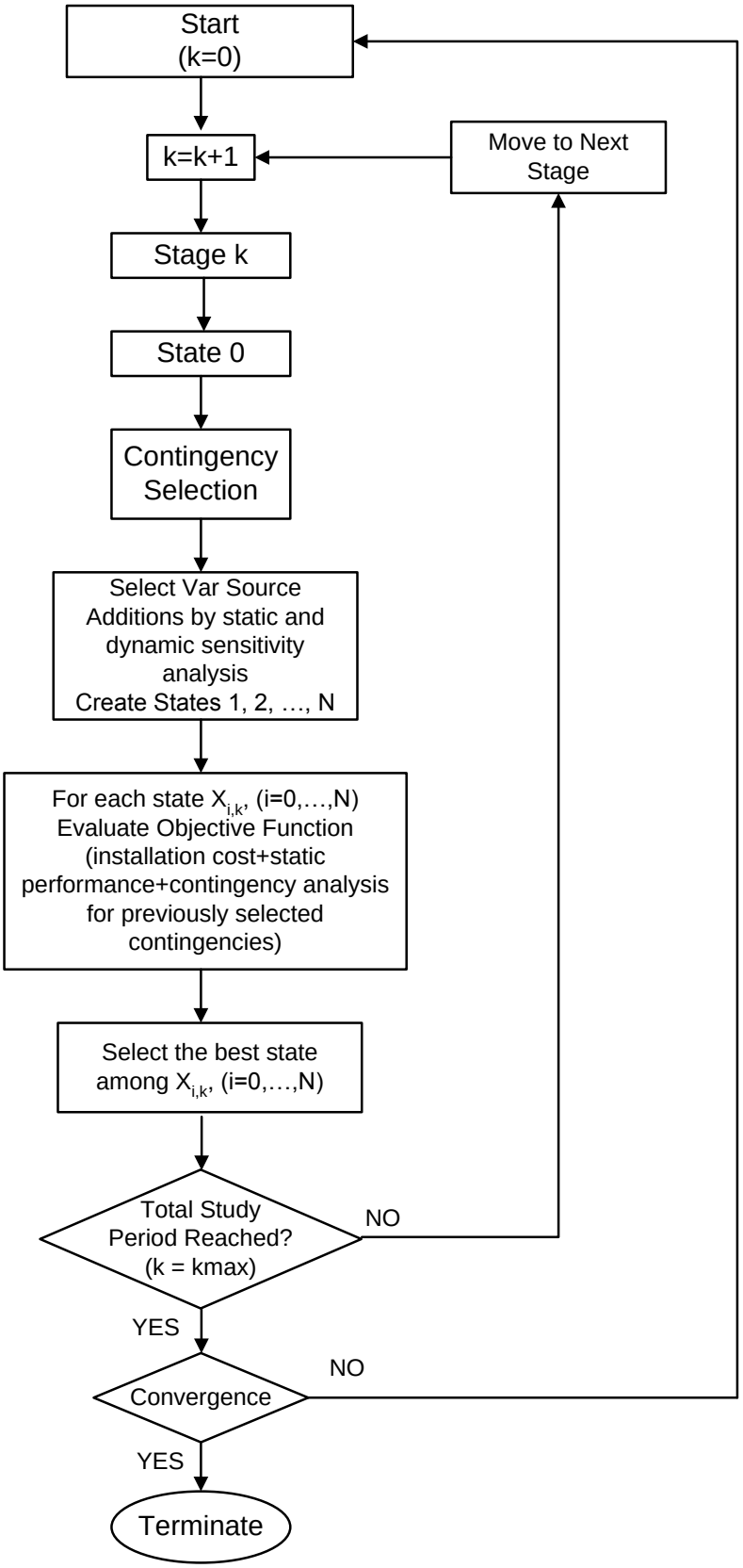


Figure 7.5. Flow Diagram of Proposed Successive Dynamic Programming Approach.

Contingency Selection

As shown earlier, it is of great importance to address the issue of contingencies. The optimal selection for the static and dynamic VAR sources should be such that the system performance/constraints are met for any credible contingency of the system. Therefore we describe below a procedure for selecting the credible contingencies and then the overall optimization problem is defined in the space of the selected contingencies.

One of the main computational issues in voltage recovery studies is the selection of simulation scenarios, to be studied. Clearly not all possibly contingencies and faults can be considered in a system, therefore contingency ranking and selection are of uttermost importance, to limit the analysis space. Specifically, the most critical contingencies, in terms of voltage problems, from all possible contingencies need to be identified and analyzed. For large scale systems, the process imposes a substantial computational burden. For this reason, there have been consistent efforts to invent fast contingency selection algorithms and subsequent contingency analysis. Significant developments in the area of contingency selection include (a) contingency ranking with performance indices (PI) [68], (b) local solutions based on concentric relaxation [69], (c) bounding methods [70], [71], etc. In addition, significant developments for contingency analysis include the introduction of the fast decoupled power flow [72], sparsity-oriented compensation method [73], sparse vector methods [74], partial refactorization [75], etc.

Much attention on this issue has been focused on subnetwork solutions which solve for a subset of state variables, using sparse vector methods. A typical application of subnetwork solutions to contingency selection is the bounding method [70], [71]. The subnetwork solution method had been also generalized with the zero mismatch approach [76], which is an iterative AC power flow solution method and is effective for both contingency screening and analysis.

Typical contingency selection methods consist of either ranking methods using a performance index (PI) or screening methods based on approximate power flow solutions. It is widely recognized that PI based methods are efficient but vulnerable to misrankings, while screening methods are more accurate but inefficient. It has been also identified that the inaccuracies of the PI based methods are mainly due to (a) nonlinearities of the system model [77], and (b) discontinuities of the system model arising from generator reactive power limits and regulator tap limits [78], [79].
A hybrid contingency selection method had been proposed in the past which takes advantage of the best features of the two approaches [78]. This method utilizes a procedure based on the concept of contingency stiffness index to identify ‘nonlinear’ contingencies and a performance index method to identify contingencies causing discontinuities. While the hybrid method performs very well, the computational burden is many times greater than pure PI based methods.

This section describes the development and implementation of contingency ranking and selection algorithms as part of a power system analysis program [80], [81], [82]. The implementation is based on PI-based methods and on the use of the quadratized power flow system model. Each contingency is modeled with the introduction of a contingency

or outage control variable. The ranking is based on the value of the sensitivity of the performance index with respect to the contingency control variable for each contingency. The computation of the sensitivities is performed using the very efficient co-state method. Moreover, the paper introduces some new concepts as a way for improving the accuracy of the PI-based contingency ranking methods. The basic concept is the use of state-linearization rather than performance-index-linearization with respect to the outage variable and it appears to provide more accurate results in contingency ranking and selection, at the expense of slightly increased computational time. However, with the appropriate use of sparsity techniques this increase can become minimal. The methodology implementation is demonstrated with two simple systems. The PI-contingency selection is implemented as part of a power system analysis program and it is used in combination with compensation-based contingency analysis method for steady state security assessment, and as a pre-filter for contingency ranking in power system dynamic voltage recovery analysis.

PI Methods for contingency ranking

PI-based contingency ranking methods reported in the literature are based on the evaluation of the PI gradient with respect to an outage. In [79]-[82] a rigorous definition of an outage has been proposed with the use of the outage (or contingency) control variable u_c that has the following property [79]-[82]:

$$u_c = \begin{cases} 1.0, & \text{if the component is in operation} \\ 0.0, & \text{if the component is outaged} \end{cases} \tag{7.16}$$

The outage control variable is used in the component modeling of a power system, as illustrated in Figure 7.6 and Figure 7.7.

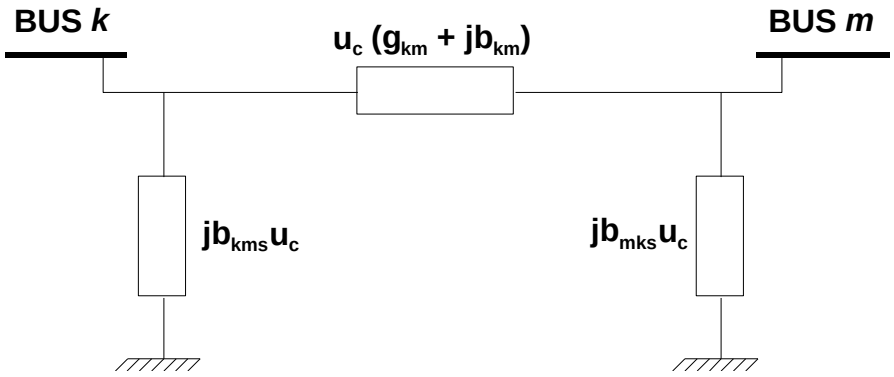


Figure 7.6. Circuit Outage Control Variable u_c.

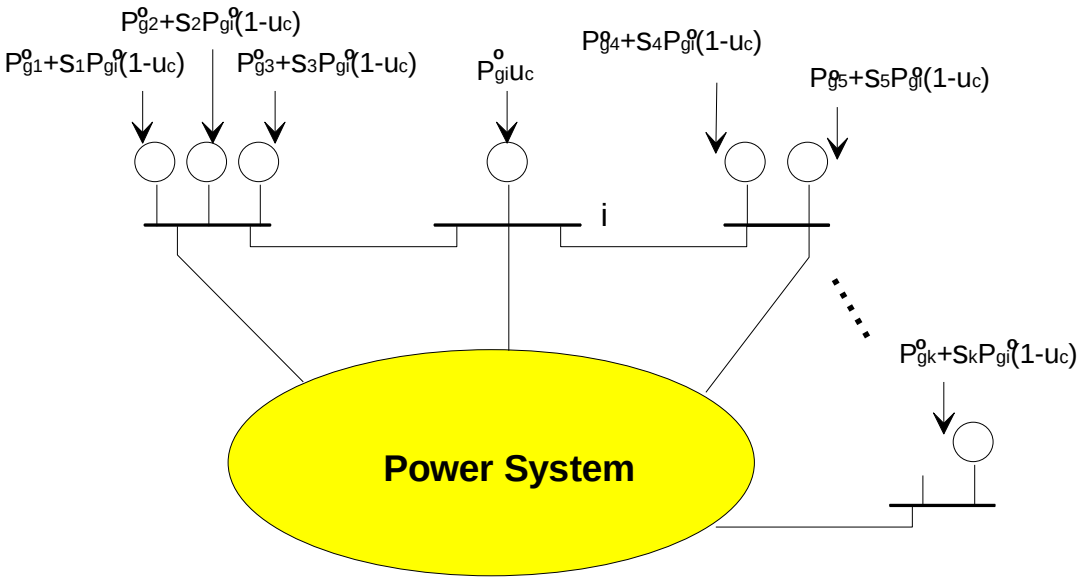


Figure 7.7. Generating Unit Outage Control Variable u_c.

Note that in the case of a generator outage the outage control variable not only affects the power produced by the outaged unit, but also indicates the re-dispatch of its produced power to the remaining units, via a re-dispatch algorithm (Figure 7.7 illustrates a linear re-dispatch, based on participation factors). The contingency control variable can not only model independent contingencies, like the ones indicated above, but can be also effectively used to model common mode contingencies, i.e., contingencies that are dependent upon each other. Such a situation is illustrated in Figure 7.8.

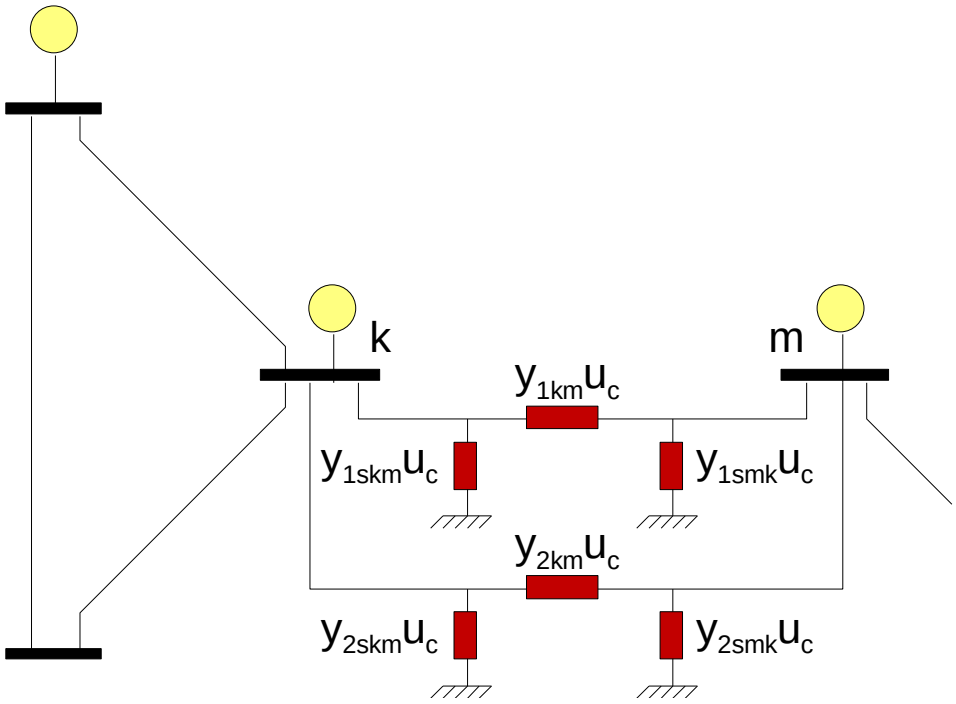


Figure 7.8. Representation of Common Mode Outages with Control Variable u_c.

Depending on the purpose of contingency selection, a variety of performance indices can be applied to it:

- *Circuit current-based index:*

$$J_C = \sum_j w_j \left(\frac{I_j}{I_{N,j}} \right)^{2n} , \tag{7.17}$$

where

w_j : weighting factor, $0 < w_j < 1$,

$I_{N,j}$: current-based thermal limit of the line,

I_j : magnitude of actual current through circuit j,

n : positive integer parameter defining the exponent.

- *Circuit power-based index:*

$$J_S = \sum_j w_j \left(\frac{S_j}{S_{N,j}} \right)^{2n} , \tag{7.18}$$

where

w_j : weighting factor, $0 < w_j < 1$,

$S_{N,j}$: power-based thermal limit of the line,

S_j : apparent power through circuit j,

n : positive integer parameter defining the exponent.

- *Voltage index:*

$$J_V = \sum_{k=1}^{N} w_k \left(\frac{V_k - V_{k,mean}}{V_{k,step}} \right)^{2n} , \tag{7.19}$$

where

w_k : weighting factor, $0 < w_k < 1$,

$V_{k,mean}$: nominal bus voltage value (typically 1.0 p.u.),

(it is in general the mean value in the desired range, i.e. $\frac{1}{2}\left(V_k^{\max} + V_k^{\min}\right)$),

$V_{k,step}$: voltage deviation tolerance (i.e. $\frac{1}{2}\left(V_k^{\max} - V_k^{\min}\right)$),

V_k : actual voltage magnitude at bus k,

n : positive integer parameter defining the exponent,

N : total number of PQ buses.

- *Generation reactive power index*:

$$J_Q = \sum_{j=1}^{L} w_j \left(\frac{Q_j - Q_{j,mean}}{Q_{j,step}} \right)^{2n}, \qquad (7.20)$$

where

w_j : weighting factor, $0 < w_j < 1$,

$Q_{j,mean}$: expected generated reactive power value,

This is the mean value is the allowable range for each generator, i.e., $\frac{1}{2}\left(Q_j^{\max} + Q_j^{\min}\right)$,

$Q_{j,step}$: reactive power deviation tolerance,

This is half of the allowable range, i.e., $\frac{1}{2}\left(Q_j^{\max} - Q_j^{\min}\right)$,

Q_j : actual reactive power generated by unit j,

n : positive integer parameter defining the exponent,

L : total number of generating units.

Several other performance indices can be defined. In this work voltage-based indices are mainly considered. By including the outage control variable in the system modeling the defined performance index J can be expressed as a function of the state vector and of the control variables, $J(x, u_c)$. The change of the performance index due to the contingency is:

$$\Delta J = J(x^{new}, u_c = 0.0) - J(x^0, u_c = 1.0), \qquad (7.21)$$

where x^0 is the initial state, prior to the contingency, x^{new} is the state after the contingency and the control variable u_c changes from 1.0 to 0.0, modeling the component outage. The first order approximation of the performance index variation is provided by the derivative of the PI with respect to the control variable:

$$\Delta J = \frac{dJ}{du_c} \cdot \Delta u_c = \frac{dJ}{du_c} \cdot (u_c - 1), \qquad (7.22)$$

and for a change in u_c from 1.0 to 0.0:

$$\Delta J = -\frac{dJ}{du_c}. \qquad (7.23)$$

It is therefore expected that the derivative of the performance index with respect to the outage control variable at the present operating point will provide a measure of the severity of a disturbance. Therefore, contingencies are ranked based on the values of $\frac{dJ}{du_c}$, which expresses the first order change of the performance index. The values of these derivatives can be calculated using the co-state method:

$$\frac{dJ}{du_c} = \frac{\partial J}{\partial u_c} - \hat{x}^T \cdot \frac{\partial g(x,u_c)}{\partial u_c}, \tag{7.24}$$

$$\hat{x}^T = \left[\frac{\partial J(x,u_c)}{\partial x}\right] \cdot \left[\frac{\partial g(x,u_c)}{\partial x}\right]^{-1}. \tag{7.25}$$

$J(x,u_c)$ is the performance index, $g(x,u_c)=0$ are the power flow equations, with the outage control variable incorporated in them, u_c is the vector of the control variables of interest, x is the state vector, $\hat{x}^T$ is the co-state vector.

Note that the performance index may depend explicitly on the control variables and it also depends implicitly on them through the power flow equations. The explicit dependence is captured by the partial derivative $\frac{\partial J}{\partial u_c}$ and the implicit by the term $\hat{x}^T \cdot \frac{\partial g(x,u_c)}{\partial u_c}$. Furthermore, the co-state vector is invariant for all contingencies, therefore it is pre-computed at the present operating condition, resulting in extremely fast computations, even for large scale power systems. After the co-state vector is computed the sensitivity of the performance index for each contingency is simply a vector-vector multiplication, with one of the vectors being very sparse.

The contingency ranking algorithm based on the co-state method is efficient and precise as a first order method. As a matter of fact the computational requirements are equivalent to one iteration of the power flow algorithm for the entire set of contingencies (cost of computing the co-state vector). However, for contingencies that trigger severe nonlinearities, the method may lead to misrankings. This is because the behavior of the performance index around the present operating point may be significantly different from the behavior as we move away from the current operating point. This issue has been addressed with the hybrid method which separates contingencies into those that trigger sever nonlinearities and those that do not. The former are processed with more accurate and computationally demanding contingency selection methods and the latter (which represent the majority of contingencies) are ranked with the above described PI based method. The processing of a small number of contingencies via selection methods adds to the computational burden. Therefore it is important to be able to use PI based methods on all contingencies. The following proposed method in this paper provides a promising approach towards this goal.

Higher Order State-Linearization PI-Based Contingency Ranking

The proposed state linearization approach is a variation of the PI-based contingency ranking algorithm. In this method, instead of linearizing the performance indices directly, the system states are linearized with respect to the contingency control variable; the performance index J is then calculated as follows:

$$J = J(x^0 + \frac{dx}{du_c}(u_c - 1), u_c), \tag{7.26}$$

where

x^0 : present operating condition,
x : system state vector,
u : contingency control variable.

The utilization of the linearized system states in calculating the system performance index provides higher order terms in Taylor's series. The unique potential of this method has been proven in some preliminary work by the authors described in [80], [82]. The state-linearization sensitivity method provides the traces of indices with curvature, which can follow the highly nonlinear variations of the original indices to some extent, while the PI-linearization method provides only the straight line. Therefore, the higher order sensitivity method is superior to the simple PI-linearization-based method.

The contingency selection is based on the computation of the performance index change due to a contingency and subsequent ranking of the contingencies on the basis of the change. Mathematically one can view the outage of a circuit as a reduction of the admittance of the circuit to zero. We use again the outage control variable, u_c, as illustrated in Figure 7.6 through Figure 7.8. Consider the performance index, J. The change of the performance index due to the contingency is:

$$\Delta J = J\left(x^{o} + \frac{dx}{du_c}(u_c - 1), u_c \right) - J\left(x^{o}, u_c = 1.0\right) \tag{7.27}$$

where x^o is the present operating condition. The sensitivity of the state with respect to the control variable can be easily computed as:

$$\frac{dx}{du_c} = -\left[\frac{\partial G(x,u)}{\partial x}\right]^{-1}\left[\frac{\partial G(x,u)}{\partial u_c}\right] \tag{7.28}$$

Note that $\frac{\partial G(x,u)}{\partial x}$ is the Jacobian of the system and therefore it is pre-computed at the present operating condition and remains invariant for all contingencies. Thus for each contingency we have to only compute the partial derivatives of the power flow equation G(x,u) with respect to the contingency control variable. This vector has only few nonzero entries and therefore the computations are extremely fast. Taking into account the sparsity of this vector can greatly improve the efficiency of the method. It should also be noted that $\frac{dx}{du_c}$ is a vector of the same size as the state vector each element of which is the derivative of the corresponding state with respect to the control variable. Once the new state is computed via this linear approximation, the calculation of the new value of the performance index is a straightforward operation.

The concept of the approach is illustrated graphically in Figure 7.9 and Figure 7.10 based on results obtained from the application of the method to a small test system. The first order analysis curve represents the PI-sensitivity linear curve after performing the linearization of the index with respect to the contingency control variable. The higher

order analysis curve is the state linearization curve with respect to the contingency control variable.

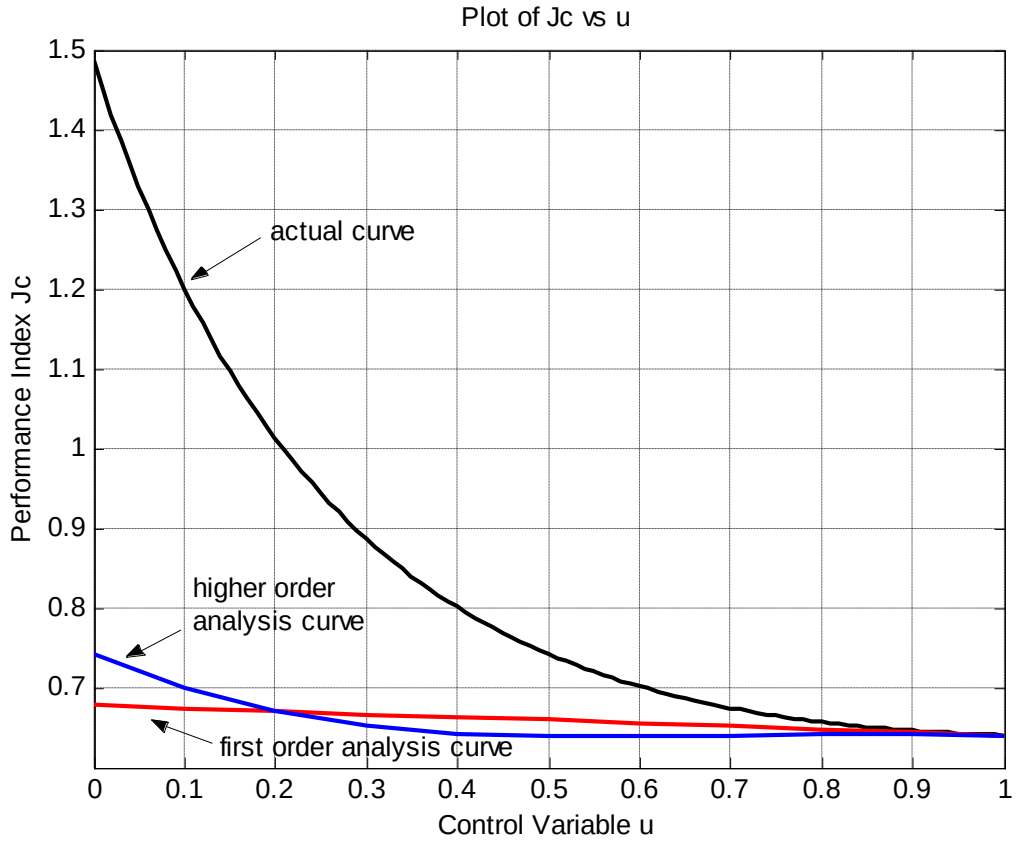


Figure 7.9. Plots of Circuit-Loading Index vs. the Contingency Control Variable u_c.

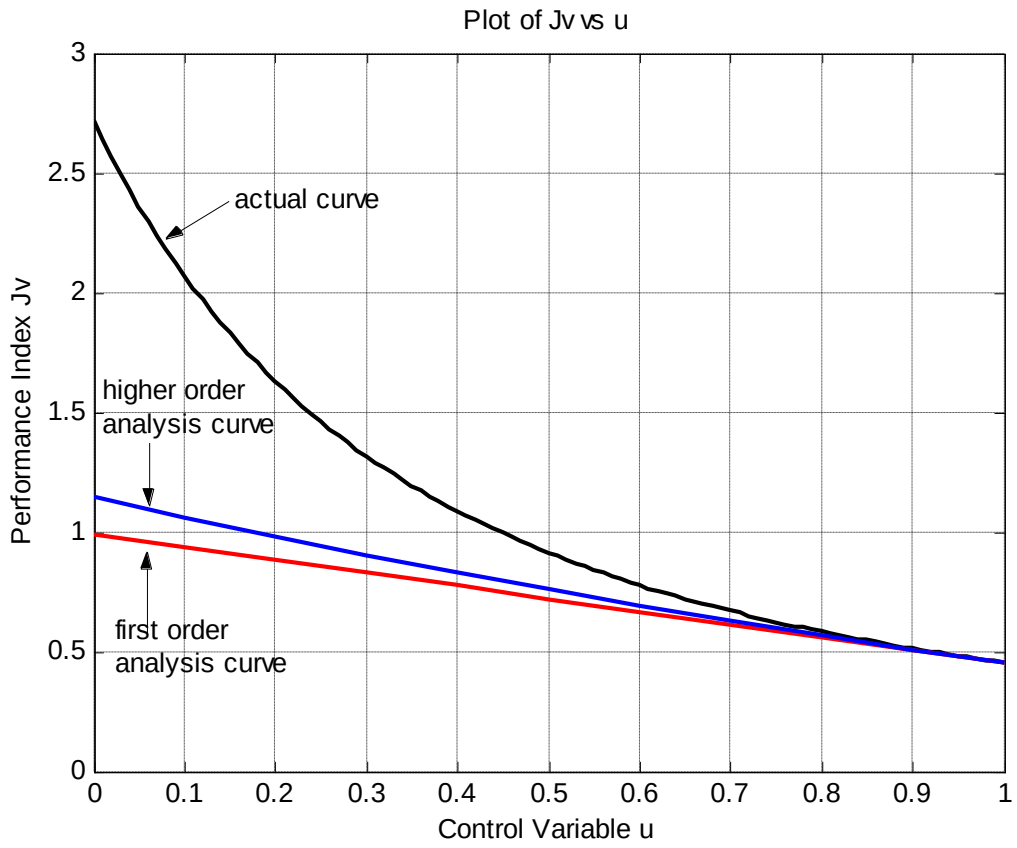


Figure 7.10. Plots of Voltage Index vs. the Contingency Control Variable u_c.

Static Sensitivity Analysis for Candidate Location Selection Using the Costate Method

Static sensitivity analysis is used to determine the best candidate locations of VAR source additions, based on steady state performance criteria and installation cost. The sensitivity of the defined objective function with respect to the addition of a specific VAR module at a specific system location can be efficiently computed using the costate method [78]-[82], in a similar way as the performance index sensitivity for contingency analysis is perform (described in the previous section).

More specifically, assume an objective function aiming to the leveling of the system voltage profile at selected load buses in the system, where voltage sensitive loads are connected.

$$J_V = \sum_{k=1}^{N} w_k \left(\frac{V_k - V_{k,mean}}{V_{k,step}} \right)^{2n}, \qquad (7.29)$$

where

w_k : weighting factor, $0 < w_k < 1$,

$V_{k,mean}$: nominal bus voltage value (typically 1.0 p.u.),

(it is in general the mean value in the desired range, i.e. $\frac{1}{2}\left(V_k^{\max} + V_k^{\min}\right)$),

$V_{k,step}$: voltage deviation tolerance (i.e. $\frac{1}{2}\left(V_k^{\max} - V_k^{\min}\right)$),

V_k : actual voltage magnitude at bus k,

n : positive integer parameter defining the exponent,

N : total number of PQ buses.

Several other performance indices can be defined, based on the desired performance and cost criteria. By including a control parameter Q_i defining the addition of a VAR support device of rating Q at location i in the system model the defined performance index J can be expressed as a function of the state vector and of the control variables, $J(x, Q_i)$. The change of the performance index due to the addition is:

$$\Delta J = J(x^{new}, Q_i) - J(x^0, Q_i = 0.0), \tag{7.30}$$

where x^0 is the initial state, prior to the addition, x^{new} is the state after the addition and the control variable Q_i changes from 0.0 to some specific value Q_i, modeling the additional VAR support component (either capacitor module, or any type of dynamic source).

Objective Function First Order Sensitivity Analysis for Candidate Location Selection

The first order approximation of the objective function (OF) variation is provided by the derivative of the OF with respect to the control variable:

$$\Delta J = \frac{dJ}{dQ_i} \cdot \Delta Q_i, \tag{7.31}$$

and for a change in the control parameter from 0.0 to a value Q_i:

$$\Delta J = -\frac{dJ}{dQ_i} Q_i. \tag{7.32}$$

The value of Q_i represents the specific minimum module values of reactive support that are added each time.

It is therefore expected that the derivative of the objective function with respect to the control parameter Q_i at the present operating point will provide a measure of the improvement achieved by the addition. Therefore, candidate locations are ranked based on the values of $\frac{dJ}{dQ_i}$, which expresses the first order change of the performance index. The values of these derivatives can be calculated using the co-state method:

$$\frac{dJ}{dQ_i} = \frac{\partial J}{\partial Q_i} - \hat{x}^T \cdot \frac{\partial g(x, Q_i)}{\partial Q_i}, \tag{7.33}$$

$$\hat{x}^T = \left[\frac{\partial J(x, Q_i)}{\partial x}\right] \cdot \left[\frac{\partial g(x, Q_i)}{\partial x}\right]^{-1}. \tag{7.34}$$

$J(x, Q_i)$ is the performance index, $g(x, Q_i) = 0$ are the power flow equations, with the control parameter Q_i incorporated in them, x is the state vector, $\hat{x}^T$ is the co-state vector.

Note that the objective function may depend explicitly on the control parameters and it also depends implicitly on them through the power flow equations. The explicit dependence is captured by the partial derivative $\frac{\partial J}{\partial Q_i}$ and the implicit by the term $\hat{x}^T \cdot \frac{\partial g(x, Q_i)}{\partial Q_i}$. Furthermore, the co-state vector is invariant for all addition in all possible candidate locations, therefore it is pre-computed at the present operating condition, resulting in extremely fast computations, even for large scale power systems. After the co-state vector is computed the sensitivity of the objective function for each addition is simply a vector-vector multiplication, with one of the vectors being very sparse.

The location selection algorithm based on objective function sensitivity and the co-state method is efficient and precise as a first order method. As a matter of fact the computational requirements are equivalent to one iteration of the power flow algorithm for the entire set of candidate locations (cost of computing the co-state vector). However, if severe nonlinearities are present, the method may lead to misrankings. This is because the behavior of the objective function around the present operating point may be significantly different from the behavior as we move away from the current operating point. This issue can be addressed with the hybrid method which separates the set of possible additions into those that trigger sever nonlinearities and those that do not. The former are processed with more accurate and computationally demanding selection methods and the latter (which represent the majority) are ranked with the above described method. The processing of a small number of contingencies via selection methods adds to the computational burden. Therefore it is important to be able to use PI based methods on all cases. The following proposed method in this section provides a promising approach towards this goal.

Higher Order State-Sensitivity Analysis for Candidate Location Selection

As in the contingency selection case, the proposed state linearization approach is again a variation of the objective function-based location selection algorithm. In this method, instead of linearizing the objective function directly, the system states are linearized with respect to the VAR module addition control parameter; the objective function J is then calculated as follows:

$$J = J(x^0 + \frac{dx}{dQ_i}\Delta Q_i, Q_i), \tag{7.35}$$

where

x^0 : present operating condition,
x : system state vector,
Q_i : reactive support control parameter.

The utilization of the linearized system states in calculating the system objective function provides higher order terms in Taylor's series. The unique potential of this method has been proven in some preliminary work by the authors described in [80], [82]. The state-linearization sensitivity method provides the traces of objective function with curvature, which can follow the highly nonlinear variations of the original objective functions to some extent, while the OF-linearization method provides only the straight line. Therefore, the higher order sensitivity method is superior to the simple OF-linearization-based method.

The location selection is based on the computation of the objective function improvement due to a reactive support module addition and subsequent ranking of the candidate locations on the basis of this change. Consider the objective function, J. The change of J due to the addition is:

$$\Delta J = J\left(x^{o} + \frac{dx}{dQ_i}\Delta Q_i, Q_i\right) - J\left(x^{o}, Q_i = 0.0\right) \tag{7.36}$$

where x^o is the present operating condition. The sensitivity of the state with respect to the control parameter can be easily computed as:

$$\frac{dx}{dQ_i} = -\left[\frac{\partial G(x, Q_i)}{\partial x}\right]^{-1}\left[\frac{\partial G(x, Q_i)}{\partial Q_i}\right] \tag{7.37}$$

Note that $\frac{\partial G(x, Q_i)}{\partial x}$ is the Jacobian of the system and therefore it is pre-computed at the present operating condition and remains invariant for all computations involving different locations. Thus for each possible location we have to only compute the partial derivatives of the power flow equation $G(x,Q_i)$ with respect to the reactive support control parameter. This vector has only few nonzero entries and therefore the computations are extremely fast. Taking into account the sparsity of this vector can greatly improve the efficiency of

the method. It should also be noted that $\frac{dx}{dQ_i}$ is a vector of the same size as the state vector each element of which is the derivative of the corresponding state with respect to the control parameter. Once the new state is computed via this linear approximation, the calculation of the new value of the objective function is a straightforward operation.

Trajectory Sensitivity Computation for Candidate Location Selection Using Quadratic Integration

Trajectory sensitivity analysis [8] is used to determine the best candidate locations of VAR source additions, based on dynamic performance criteria and installation cost. The sensitivity of the defined objective function J with respect to the addition of a specific VAR module at a specific system location is computed along the time trajectory of the dynamical system following a disturbance. This computation can be efficiently executed using again the costate method [78]-[82] at each simulation time step. Utilization of trajectory sensitivities can provide information about the best candidate locations for installing additional reactive support devices, considering criteria based on the system dynamic behavior, as well as information about the best way of operating existing VAR sources. The sensitivities may indicate that at specific instants of time it is more beneficial to inject reactive power at a specific location (where VAR sources exist), while at a later time injection at some other location may be more advantageous.

The dynamic simulation is being performed numerically using the some numerical integration technique. The value of the objective function J is also computed numerically along the simulation and its final value is obtain after the simulation is done. The numerical technique employed is the quadratic integration rule, which is more accurate and appears to have significant numerical advantages compared to other existing and commonly used techniques, while maintaining the basic desired properties. This numerical integration method is described in Appendix B. Application of the integration rule yields a set of algebraic equations to be solved at each time step. The numerical computation of the trajectory sensitivities is based on applying the costate method at each time step observing the set of algebraized system equations at each time step. Therefore the problem is converted to a static problem and the actual computation are similar to the ones described in the static sensitivity analysis section, where now each time step is assumed to be an operating point, around which the linearizations are performed. These computations are described next.

First a more theoretical approach is presented. The general form of the power system equations are as in (7.38)

$$\begin{aligned} 0 &= \frac{dx(t)}{dt} - f(x(t), y(t), t, u) \\ 0 &= g(x(t), y(t), t, u) \end{aligned} \tag{7.38}$$

where

$x(t)$: n-dimensional vector of dynamical states,
$y(t)$: m-dimensional vector of algebraic states,
u : p-dimensional vector of control variables
(in this case reactive support control parameters at possible system locations.
f : n-dimensional vector function of system dynamic equations,
g : m-dimensional vector function of system algebraic equations,

Assume a function $h(t,x,y,u)$, the sensitivity of which with respect to the controls, $\frac{dh}{du}$, is to be computed. Using the chain rule we have:

$$\frac{dh}{du} = \frac{\partial h}{\partial u} + \frac{\partial h}{\partial x} \cdot \frac{dx}{du} + \frac{\partial h}{\partial y} \cdot \frac{dy}{du}. \tag{7.39}$$

The values of $\frac{\partial h}{\partial u}$, $\frac{\partial h}{\partial x}$ and $\frac{\partial h}{\partial y}$ are computable analytically assuming the $h(t,x,y,u)$ is a known function. The only terms that require further computations are the trajectory sensitivities $x_u = \frac{dx}{du}$ and $y_u = \frac{dy}{du}$.

Differentiating (7.38) with respect to the control u we have:

$$\frac{dx(t)}{dt} = f(t,x,y,u)$$
$$0 = g(t,x,y,u)$$

$$\frac{d}{dt}\left(\frac{dx}{du}\right) = \frac{\partial f}{\partial u} + \frac{\partial f}{\partial x} \cdot \left(\frac{dx}{du}\right) + \frac{\partial f}{\partial y} \cdot \left(\frac{dy}{du}\right)$$

or

$$\frac{dx_u(t)}{dt} = \frac{\partial f}{\partial u} + \frac{\partial f}{\partial x} \cdot x_u(t) + \frac{\partial f}{\partial y} \cdot y_u(t) \tag{7.40}$$

and

$$0 = \frac{\partial g}{\partial u} + \frac{\partial g}{\partial x} \cdot \left(\frac{dx}{du}\right) + \frac{\partial g}{\partial y} \cdot \left(\frac{dy}{du}\right)$$

or

$$0 = \frac{\partial g}{\partial u} + \frac{\partial g}{\partial x} \cdot x_u(t) + \frac{\partial g}{\partial y} \cdot y_u(t) \tag{7.41}$$

Equations (7.40) and (7.41) form a system of linear differential algebraic equations (though time varying) in the trajectory sensitivities $x_u = \frac{dx}{du}$ and $y_u = \frac{dy}{du}$. x_u is the dynamical state of this system and y_u the algebraic.

One way of performing this computational procedure is:

Step 0: Initialize time, t=0, and variables $x(t), y(t), x_u(t), and\ y_u(t)$.

Step 1: Solve equation (7.38) for the interval (t,t+h) using quadratic integration.

Step 2: Solve equations (7.40) and (7.41) for the interval (t,t+h) using quadratic integration.

Step 3: Compute the sensitivity of the function h from:

$$\frac{dh}{du} = \frac{\partial h}{\partial u} + \frac{\partial h}{\partial x} \cdot x_u(t+h) + \frac{\partial h}{\partial y} \cdot y_u(t+h)$$

Step 4: Advance time t→t+h, and repeat process from step 1.

Equation (7.41) can be re-written as:

$$\frac{\partial g}{\partial y} \cdot y_u = -\frac{\partial g}{\partial u} - \frac{\partial g}{\partial x} \cdot x_u \Rightarrow y_u = -\left(\frac{\partial g}{\partial y}\right)^{-1} \frac{\partial g}{\partial u} - \left(\frac{\partial g}{\partial y}\right)^{-1} \frac{\partial g}{\partial x} \cdot x_u . \qquad (7.42)$$

Substituting (7.42) into (7.40) yields:

$$\dot{x}_u = \frac{\partial f}{\partial u} + \frac{\partial f}{\partial x} \cdot x_u + \frac{\partial f}{\partial y} \cdot \left[-\left(\frac{\partial g}{\partial y}\right)^{-1} \frac{\partial g}{\partial u} - \left(\frac{\partial g}{\partial y}\right)^{-1} \frac{\partial g}{\partial x} \cdot x_u \right]$$

or

$$\dot{x}_u = \frac{\partial f}{\partial u} + \frac{\partial f}{\partial x} \cdot x_u - \frac{\partial f}{\partial y}\left(\frac{\partial g}{\partial y}\right)^{-1} \frac{\partial g}{\partial u} - \frac{\partial f}{\partial y}\left(\frac{\partial g}{\partial y}\right)^{-1} \frac{\partial g}{\partial x} \cdot x_u \Rightarrow$$

$$\dot{x}_u = \left[\frac{\partial f}{\partial x} - \frac{\partial f}{\partial y}\left(\frac{\partial g}{\partial y}\right)^{-1} \frac{\partial g}{\partial x} \right] \cdot x_u - \frac{\partial f}{\partial y}\left(\frac{\partial g}{\partial y}\right)^{-1} \frac{\partial g}{\partial u} + \frac{\partial f}{\partial u}$$

Therefore the trajectory sensitivities can be computed by the equations:

$$\begin{aligned} \dot{x}_u &= \left[\frac{\partial f}{\partial x} - \frac{\partial f}{\partial y}\left(\frac{\partial g}{\partial y}\right)^{-1} \frac{\partial g}{\partial x} \right] \cdot x_u - \frac{\partial f}{\partial y}\left(\frac{\partial g}{\partial y}\right)^{-1} \frac{\partial g}{\partial u} + \frac{\partial f}{\partial u} \\ y_u &= -\left(\frac{\partial g}{\partial y}\right)^{-1} \left[\frac{\partial g}{\partial u} + \frac{\partial g}{\partial x} \cdot x_u \right] \end{aligned} \tag{7.43}$$

where:

$\frac{\partial f}{\partial x}$: nxn Jacobian matrix of partial derivatives of f wrt x,
$\frac{\partial f}{\partial y}$: nxm Jacobian matrix of partial derivatives of f wrt y,
$\frac{\partial f}{\partial u}$: nxp matrix of partial derivatives of f wrt controls u,
$\frac{\partial g}{\partial x}$: mxn Jacobian matrix of partial derivatives of g wrt x,
$\frac{\partial g}{\partial y}$: mxm Jacobian matrix of partial derivatives of g wrt y,
$\frac{\partial g}{\partial u}$: mxp matrix of partial derivatives of g wrt controls u,
x_u : nxp matrix of trajectory sensitivities of dynamic states wrt controls,
y_u : mxp matrix of trajectory sensitivities of dynamic states wrt controls.

Equations (7.43) are of the form:

$$\begin{aligned} \dot{x}_u &= A(t) \cdot x_u + B(t) \\ y_u &= C(t) \cdot x_u + D(t) \end{aligned}$$

with

$A = \frac{\partial f}{\partial x} - \frac{\partial f}{\partial y}\left(\frac{\partial g}{\partial y}\right)^{-1} \frac{\partial g}{\partial x}$: nxn matrix,
$B = -\frac{\partial f}{\partial y}\left(\frac{\partial g}{\partial y}\right)^{-1} \frac{\partial g}{\partial u} + \frac{\partial f}{\partial u}$: nxp matrix,
$C = -\left(\frac{\partial g}{\partial y}\right)^{-1} \frac{\partial g}{\partial x}$: mxn matrix,
$D = -\left(\frac{\partial g}{\partial y}\right)^{-1} \frac{\partial g}{\partial u}$: mxp matrix.

Note that if the control is a scalar quantity (p=1) the dimensionality of the equations is considerably reduced.

The above computation of the trajectory sensitivity can be modified and simplified if the costate method is employed, as explained at beginning of this section. More specifically: Consider again the general nonlinear system of differential algebraic equations describing the power system behavior, as in (7.38):

$$\begin{aligned} \frac{dx(t)}{dt} &= f(t,x,y,u) \\ 0 &= g(t,x,y,u) \end{aligned} \tag{7.44}$$

where:

$x(t)$: n-dimensional vector of dynamical states,
$y(t)$: m-dimensional vector of algebraic states,
u : p-dimensional vector of control variables,
f : n-dimensional vector function,
g : m-dimensional vector function.

To compute the solution of (7.44) through time equations (7.44) are solved numerically using some numerical integration rule. We assume that an implicit integration rule is used and in particular the quadratic integration rule. Therefore, at each time step from $t-h$ to t, the differential equations are replaced by a set of discrete difference equations and the algebraic equations $g(t,x,y,u)$ are appended to this set. Therefore, at each time step a set of algebraic equations:

$$0 = G(X,u) \tag{7.45}$$

is solved, where the new state vector X, of dimension N, contains all the unknown states, both differential and algebraic, at the time step from $t-h$ to t.

Assume a function $h(t,x,y,u)$, the sensitivity of which with respect to the controls, $\frac{dh}{du}$, is to be computed, at each time step, along the solution trajectory. Using the chain rule we have:

$$\frac{dh}{du} = \frac{\partial h}{\partial u} + \frac{\partial h}{\partial X} \cdot \frac{dX}{du}. \tag{7.46}$$

Differentiating (7.45) with respect to u we get, at each time step:

$$0 = \frac{\partial G}{\partial u} + \frac{\partial G}{\partial X} \cdot \frac{\partial X}{\partial u} \tag{7.47}$$

or

$$\frac{\partial X}{\partial u} = -\left(\frac{\partial G}{\partial X}\right)^{-1} \cdot \frac{\partial G}{\partial u}. \tag{7.48}$$

Substituting (7.48) into (7.46) we get:

$$\frac{dh}{du} = \frac{\partial h}{\partial u} - \frac{\partial h}{\partial X} \cdot \left(\frac{\partial G}{\partial X}\right)^{-1} \cdot \frac{\partial G}{\partial u}. \tag{7.49}$$

By defining the costate vector $\hat{X}^T = \frac{\partial h}{\partial X} \cdot \left(\frac{\partial G}{\partial X}\right)^{-1}$ (N-dimensional), (7.49) can be re-written as:

$$\frac{dh}{du} = \frac{\partial h}{\partial u} - \hat{X}^T \cdot \frac{\partial G}{\partial u}. \tag{7.50}$$

The costate vector is independent of the control parameter u and needs to be computed at each time step. However, its computation is quite straightforward when an implicit numerical integration scheme is used for the solution of the differential-algebraic system, as is usually the case. More specifically:

$$\hat{X}^T = \frac{\partial h}{\partial X} \cdot \left(\frac{\partial G}{\partial X}\right)^{-1} \Rightarrow \hat{X}^T \left(\frac{\partial G}{\partial X}\right) = \frac{\partial h}{\partial X} \tag{7.51}$$

The costate vector can be computed from the solution of the above system, where:

$\hat{X}^T$: N-dimensional row state vector,

$\frac{\partial h}{\partial X}$: N-dimensional row vector of the partial derivatives of h with respect to X ,

$\frac{\partial G}{\partial X}$: NxN Jacobian matrix of the system (7.45).

Note that $\frac{\partial G}{\partial X}$ has been already computed and factored as part of the solution of (7.45) at each simulation step and therefore it is readily available after (7.45) is solved, therefore solution of (7.51) only needs a backward and forward substitution (slightly modified because of the row instead of column vectors). Therefore, computation of the costate vector does not impose significant additional cost at each time step.

Once the costate vector is computed the computation of the sensitivity $\frac{dh}{du}$ is quite straightforward and very fast for any control u. The costate vector is the same irrespectively of the control. Therefore, for a scalar u we have $\frac{dh}{du} = \frac{\partial h}{\partial u} - \hat{X}^T \cdot \frac{\partial G}{\partial u}$, where $\frac{\partial h}{\partial u}$ is a scalar value easily computable and $\frac{\partial G}{\partial u}$ is an N-dimensional vector of the partial of the algebraic equations at each time step with respect to the control. Thus the sensitivity can be computed by only a vector vector multiplication at linear cost with respect to the system dimensionality. This inexpensive procedure is the only one that is repeated for all the controls. Furthermore, $\frac{\partial G}{\partial u}$ is a very sparse vector with constant number of non-zero elements, therefore, in practice the cost is not linear in terms of the system dimensionality, but it is constant and independent of the system dimensionality. This is an extremely important property. Thus, the total cost of computing the sensitivities of some quantity with respect to all the system controls is mainly defined by the cost of computing the costate vector at each step, which is the cost of a backward and forward substitution. Nevertheless, this cost is minor compared to the cost of solving the nonlinear system of equations at each time step, resulting from the numerical integration. Thus sensitivities along the solution trajectory are computed at minor additional cost, along with the system simulation.

For the study and mitigation of voltage recovery phenomena the control parameters u consist of additional VAR support of rating Q placed at candidate location i, therefore denoted as Q_i. Thus the control vector u is defined as:

$$u = \begin{bmatrix} Q_1 & Q_2 & \dots & Q_i & \dots & Q_p \end{bmatrix}^T$$

where

p : number of candidate locations considered.

In this case the function $h(t, x, y, u)$ is defined as a system performance objective function that is to be minimized. This will be denoted as J. A possible definition of J can be related to the duration of a voltage dip at a specific load bus. In this case:

$$J_{dip}(v(t)) = t_1 - t_2 \qquad (7.52)$$

where

t_1 : transition time at which the voltage fall below threshold ($v(t) < V^{\min}$),

t_2 : transition time at which the voltage recovers above threshold ($v(t) > V^{\min}$).

A more general performance objective function that takes into account both the duration and magnitude of the voltage dip can be defined via the area of the voltage curve and the threshold, during the time that the voltage is below the threshold value. This is illustrated

in Figure 7.11. Mathematically such a function is defined is (7.53). A more general assumption is made here, that the quantities under consideration can be any defined system quantities, not just specific voltage magnitudes, but also some other functions or combinations of the voltages. Such quantities are generally defined as $z(t)$. Therefore:

$$J(z(t)) = \int_{t_1}^{t_2} \left(z_{threshold} - z(t)\right) dt \qquad (7.53)$$

$z(t)$: output of interest (scalar or vector), e.g. voltage at specific load bus(es),

$z_{threshold}$: threshold level for performance criteria, e.g. minimum acceptable voltage level,

t_1 : time at which the observation quantity of interest fall below threshold value,

t_2 : time at which the observation quantity of interest recovers above threshold.

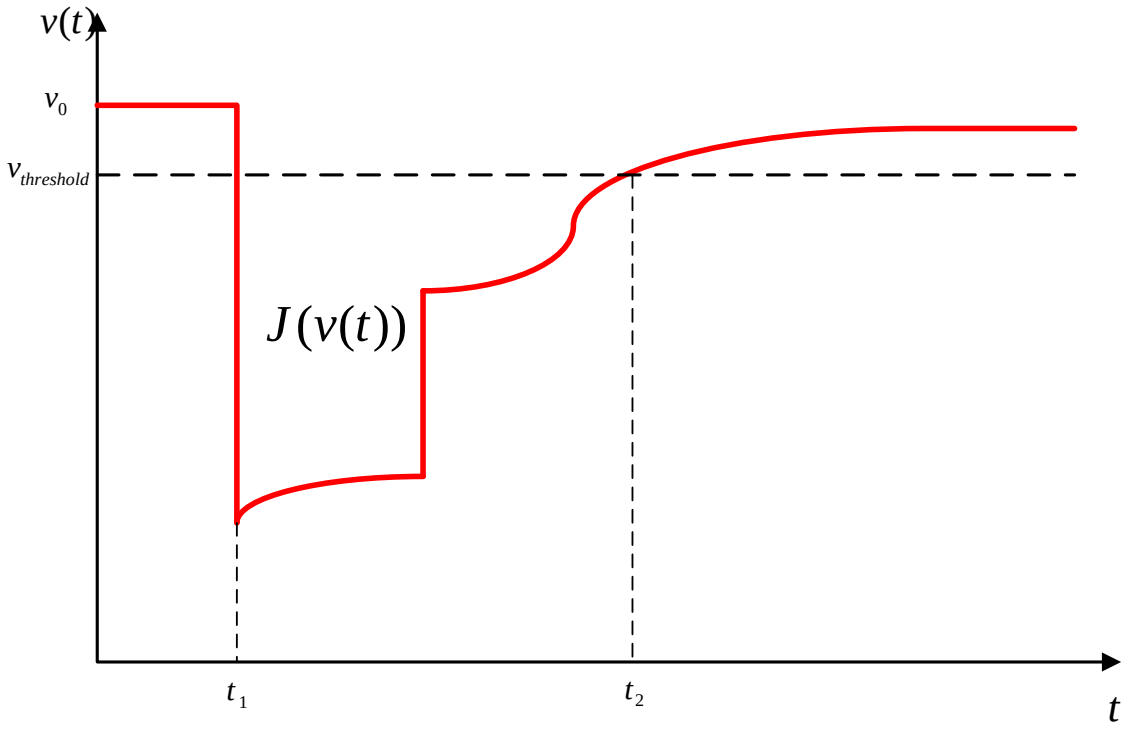


Figure 7.11. Illustration of voltage recovery and defined performance objective function.

The value of $J(z(t))$ is computed numerically along the system simulation, using again the quadratic integration rule, and it is know when the simulation has been completed. The sensitivity of $J(z(t))$ with respect to the controls u, $\frac{dJ}{du}$ is also computed numerically along the simulation using the costate method, as explained earlier. The final value of the sensitivity is also computed after the simulation has been completed based on the fact that:

$$\frac{dJ(z(t))}{du} = \frac{d}{du}\int_{t_1}^{t_2} \left(z_{threshold} - z(t)\right) dt = \int_{t_1}^{t_2} \frac{d}{du}\left(z_{threshold} - z(t)\right) dt = -\int_{t_1}^{t_2} \frac{dz(t)}{du} dt \qquad (7.54)$$

Therefore numerically the sensitivity value $\frac{dJ(z(t))}{du}$ is computed as a summation of sensitivity values computed at each simulation step.

8. Example Results

Power System Modeling and Simulation of Voltage Recovery

Introduction

The modeling and simulation tools developed are demonstrated for both steady state and transient operation in the simple power system shown in Figure 8.1. The system consists of two generating units at two different generator substations, connected to the rest of the grid via step-up transformers. Apart from the generating substation there are three main high voltage transmission substations. Note that the system is represented using physically-based, three phase modeling, as described throughout the report. Each substation configuration is explicitly represented, using the breaker oriented modeling approach, as illustrated in Figure 8.2 and Figure 8.3. The breakers and switches are represented and the system transformers are included in the substation models.

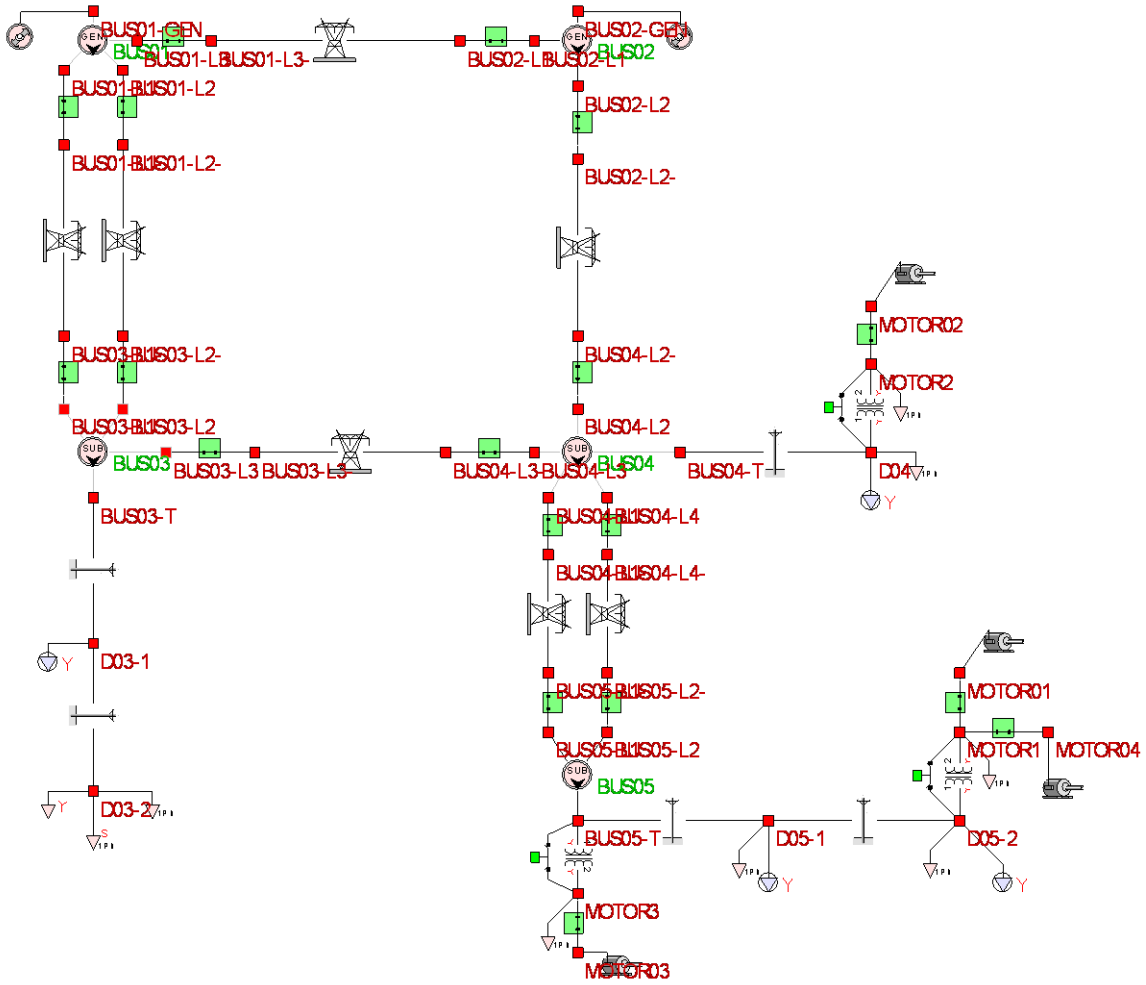


Figure 8.1. One-Line Diagram of Three Phase Model of Test System.

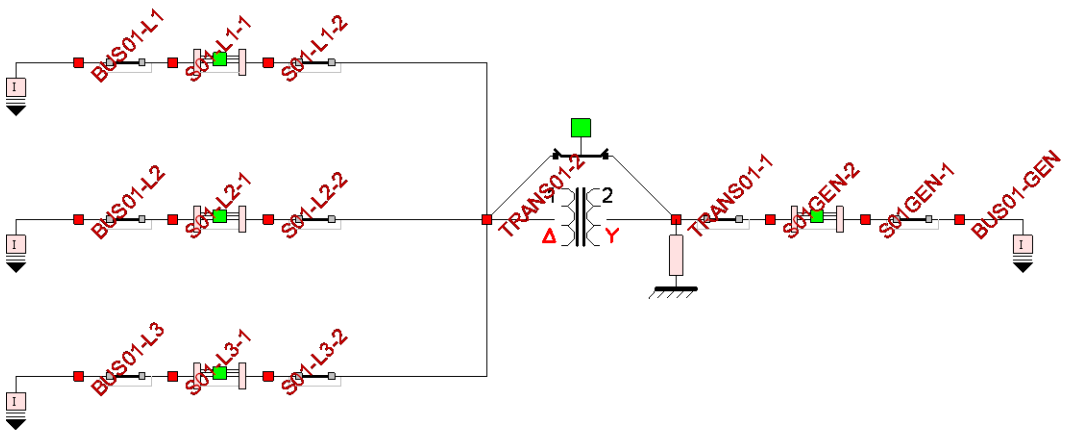


Figure 8.2. One-Line Diagram of Generating Substation Configuration.

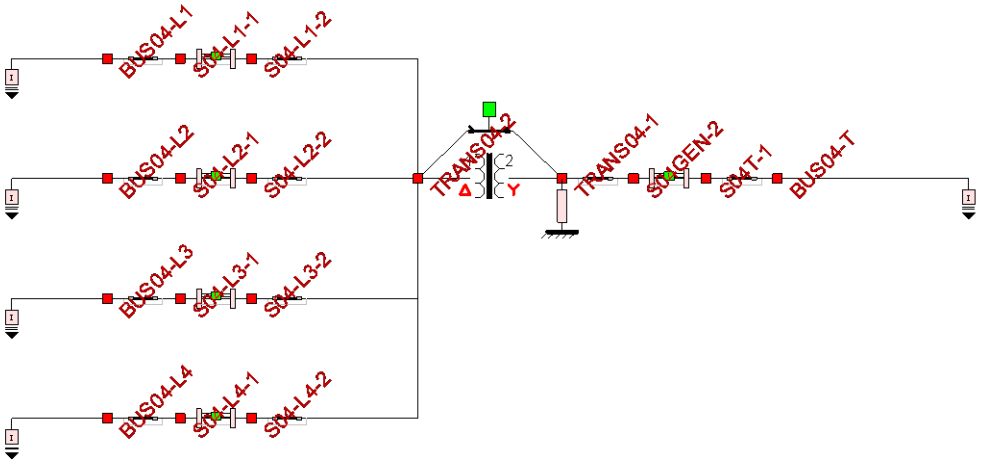


Figure 8.3. One Line Diagram of Distribution Substation Configuration.

The system also includes models of part of the medium voltage distribution level feeders. Distribution lines are modeled up to certain level and single phase loads, both constant impedance and power are also included, to introduce load imbalance. Induction motors are also connected, via a step down transformers at the ends of the distribution feeders at load buses. Four different motors are used, each of a different NEMA design, and their operation is compared. Furthermore, the motor model estimation procedure is demonstrated for the estimation of the rotor parameters for each one of the motors. The slip-torque characteristic is generated using some specific parameters and then these curves are used as input to the estimation algorithm. The estimated values are compared with the actual values, which in this artificial example are known.

Motor Model Estimation

The motors are rated at 1 MVA. Their stator electrical parameters are: $r_s = 0.01$, $x_s = 0.06$, $x_m = 3.5$, $g_m = 0$. All values are in p.u. at the motor ratings (1 MVA, 13.8 kV). The rotor parameters are used to test the estimation procedure. The slip-torque

characteristics of each motor are generated and are provided to the model estimator. These nominal slip-torque characteristics are presented in for each motor.

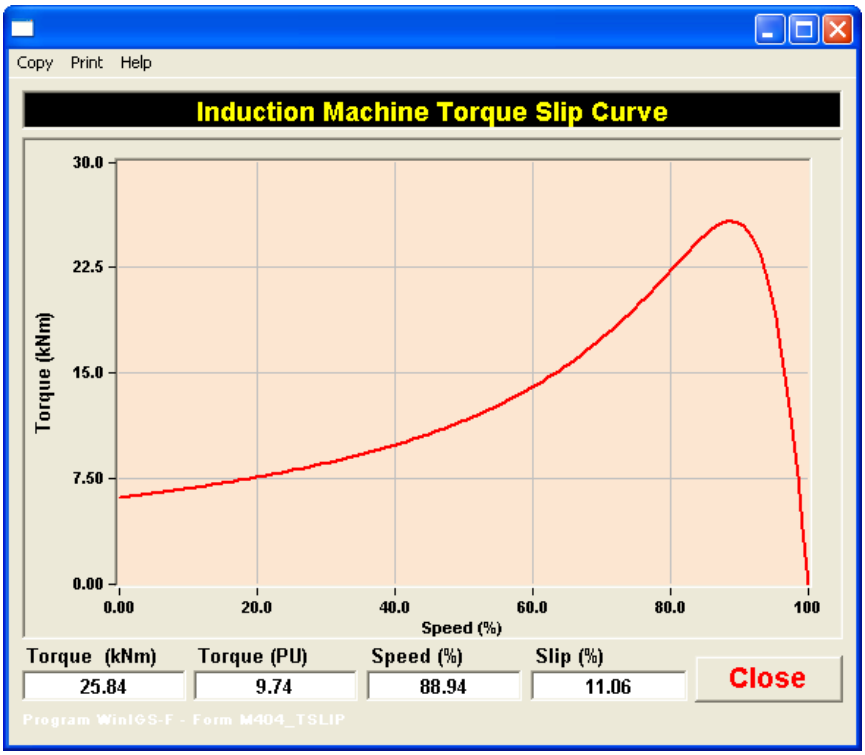


Figure 8.4. Nominal Slip-Torque Characteristic of Design A Induction Motor.

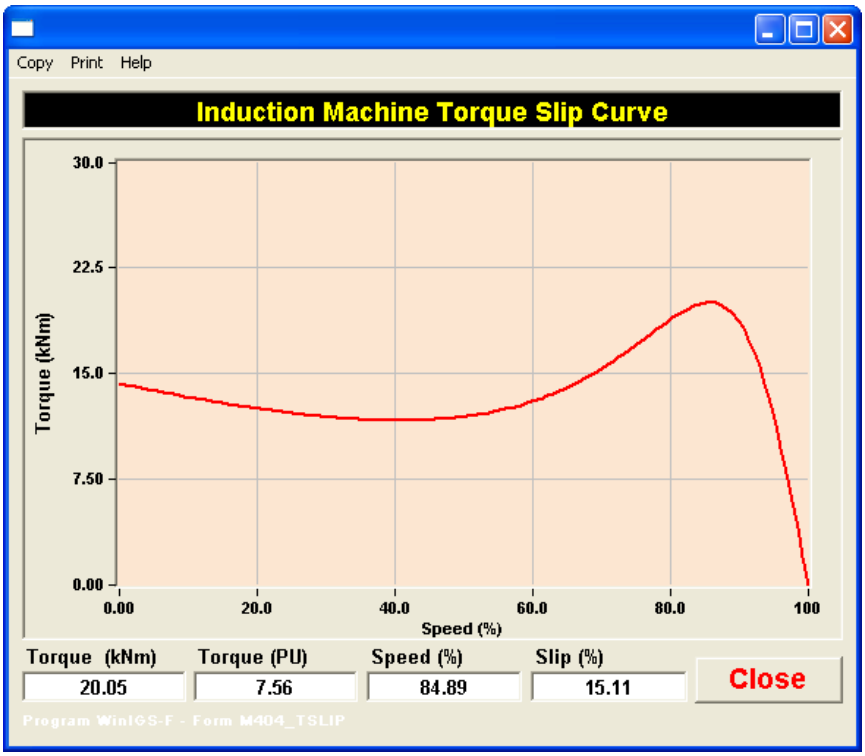


Figure 8.5. Nominal Slip-Torque Characteristic of Design B Induction Motor.

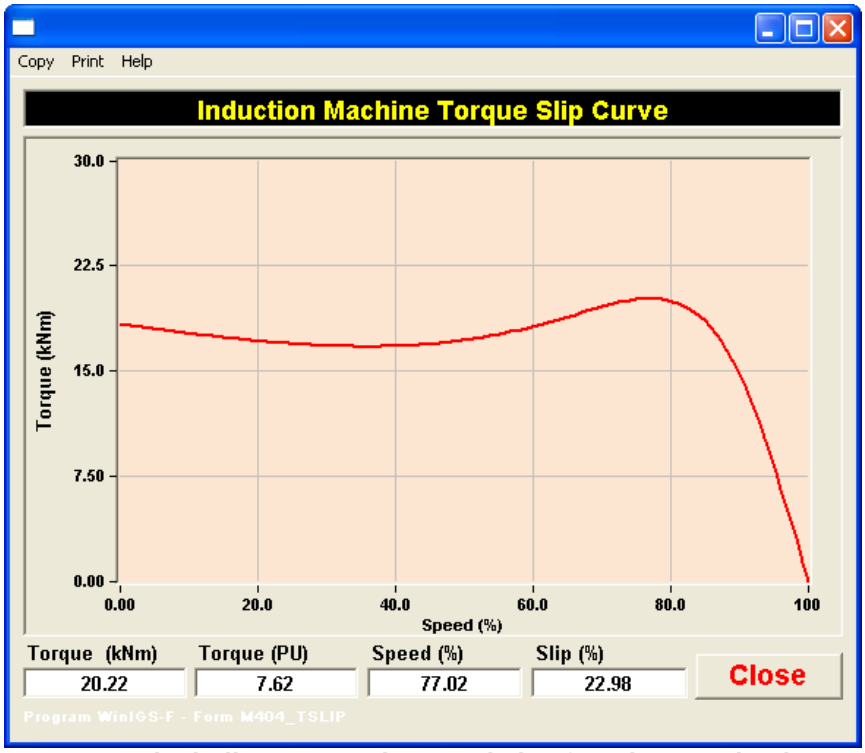


Figure 8.6. Nominal Slip-Torque Characteristic of Design C Induction Motor.

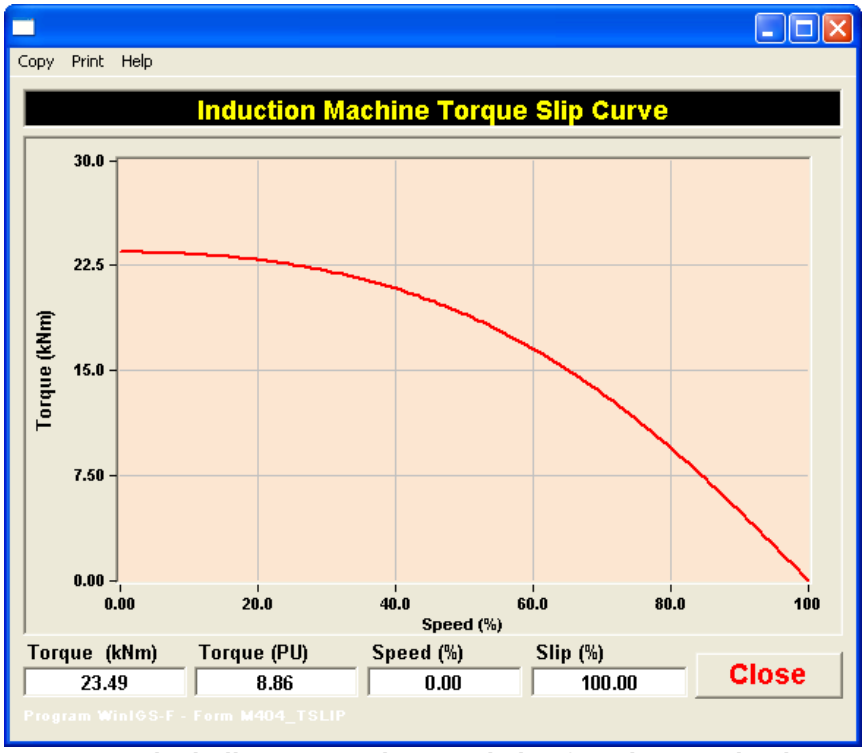


Figure 8.7. Nominal Slip-Torque Characteristic of Design D Induction Motor.

The estimated values are compared with the actual values used to generate the characteristics. A constant rotor parameter model is used for type A and D motors, while a slip-dependent model is used for type B and C motors. The initial value for all the parameters, for both the two-parameter model and the five-parameter model, was set to 0.01pu. The actual parameter values along with the estimation results are presented in Table 8-1 through Table 8-4. The tables also show the number of Newton iterations required, the execution time and the absolute maximum deviation between the estimated and actual slip-torque curve. Figure 8.8 though Figure 8.11 show the deviation between the actual and estimated slip torque characteristic, for each motor type. This would be the only measure of the estimation error, if the parameter values where not known in advance.

TABLE 8-1 ESTIMATION RESULTS FOR DESIGN A MOTOR

Param.	Actual Value (pu)	Estimated Value (pu)	# Iter.	Exec. Time (s)	Max. Torque Dev. (pu)
r_r	0.01	0.01			
x_r	0.03	0.03	4	0.05	3.05e-5

TABLE 8-2 ESTIMATION RESULTS FOR DESIGN B MOTOR

Param.	Actual Value (pu)	Estimated Value (pu)	# Iter.	Exec. Time (s)	Max. Torque Dev. (pu)
α	0.02	0.02			
β	-0.03	-0.03			
γ	0.05	0.05	5	0.16	4.13e-4
δ	0.06	0.06			
ε	-0.01	-0.01			

TABLE 8-3 ESTIMATION RESULTS FOR DESIGN B MOTOR

Param.	Actual Value (pu)	Estimated Value (pu)	# Iter.	Exec. Time (s)	Max. Torque Dev. (pu)
α	0.03	0.03			
β	-0.03	-0.03			
γ	0.06	0.06	5	0.08	8.95e-4
δ	0.06	0.06			
ε	-0.01	-0.01			

Simple Gauss-Newton and G-N with line search failed to converge.
Levenberg-Marquardt trust region algorithm was used.

TABLE 8-4 ESTIMATION RESULTS FOR DESIGN D MOTOR

Param.	Actual Value (pu)	Estimated Value (pu)	# Iter.	Exec. Time (s)	Max. Torque Dev. (pu)
r_r	0.1	0.1			
x_r	0.04	0.04	6	0.08	3.29e-4

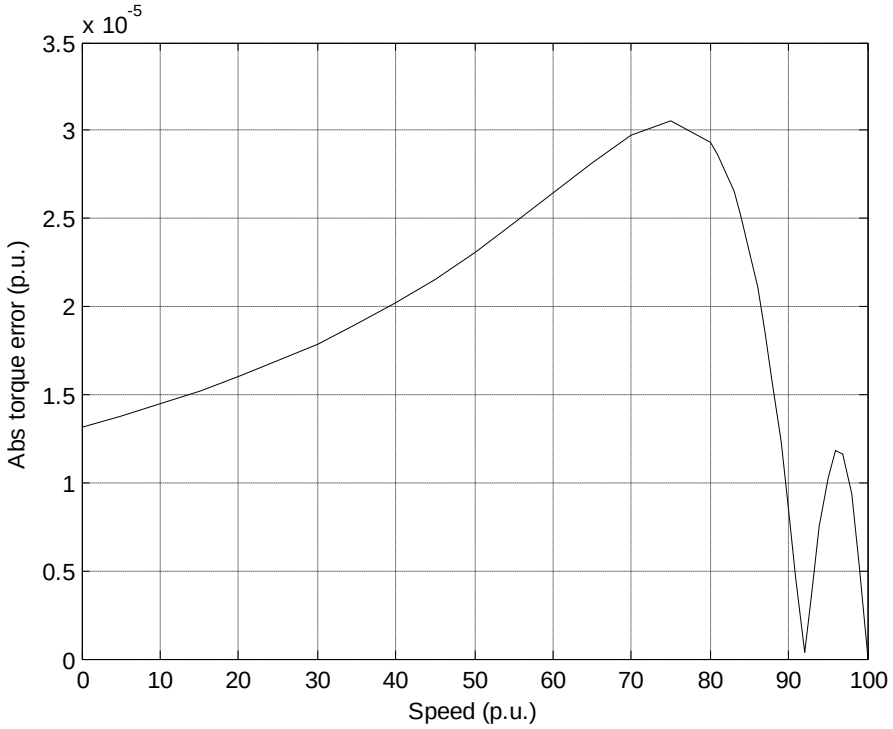


Figure 8.8. Error Between Actual and Estimated Slip-Torque Characteristic, for Design A Motor.

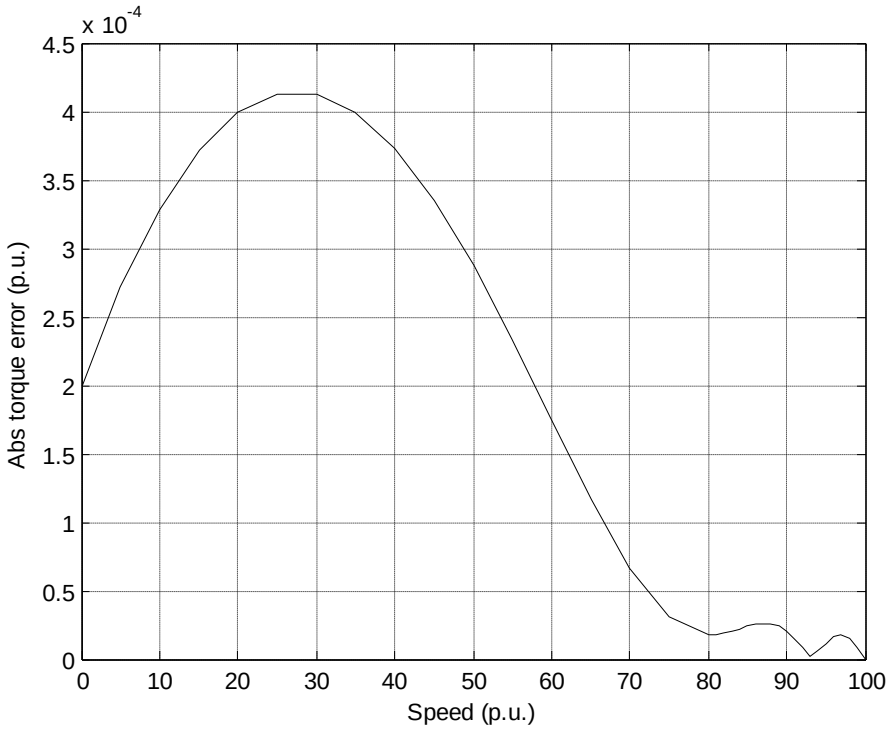


Figure 8.9. Error Between Actual and Estimated Slip-Torque Characteristic, for Design B Motor.

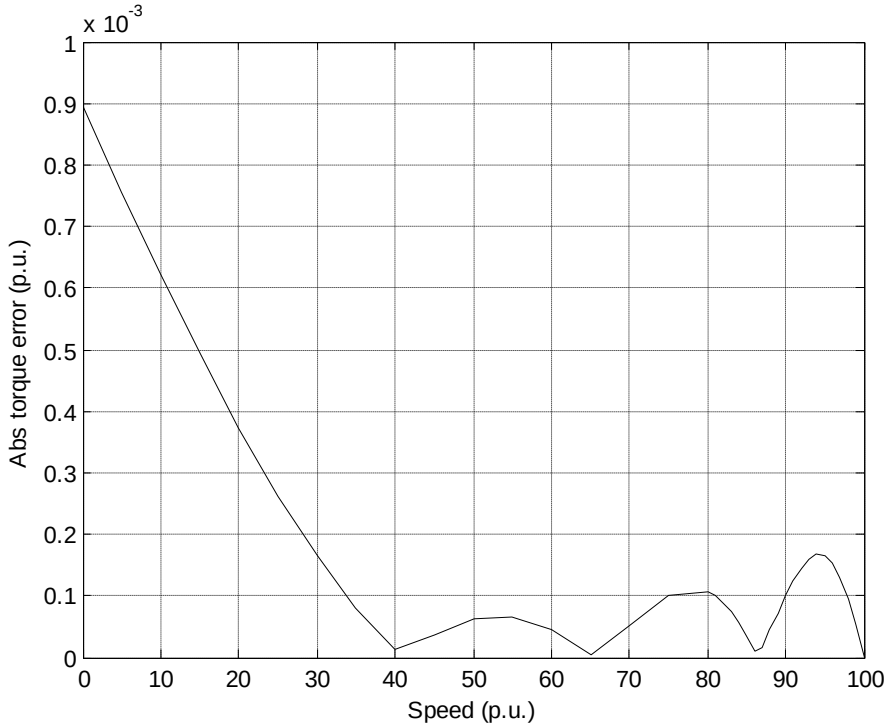


Figure 8.10. Error Between Actual and Estimated Slip-Torque Characteristic, for Design C Motor.

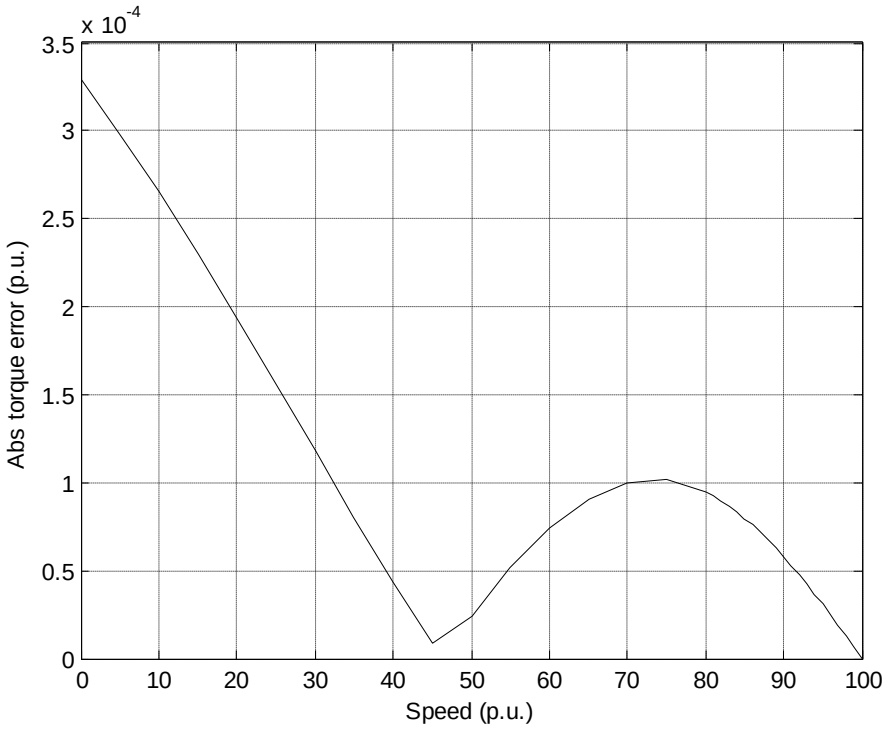


Figure 8.11. Error Between Actual and Estimated Slip-Torque Characteristic, for Design D Motor.

In all cases the estimation algorithm provided practically exact values of the model parameters. For the motors A, B and D the simple Gauss-Newton based algorithm without global convergence strategy was enough. In the case of motor C, the simple Gauss-Newton algorithm and the line search failed to provide the solution, therefore the trust region algorithm was employed, as a global convergence strategy, along with the Gauss-Newton solution process to provide a result. The convergence of the algorithm for the type C motor is illustrated in Figure 8.12. The objective function tolerance was set to 10^{-4}. The actual value achieved at the 5th iteration was 1.25e-6.

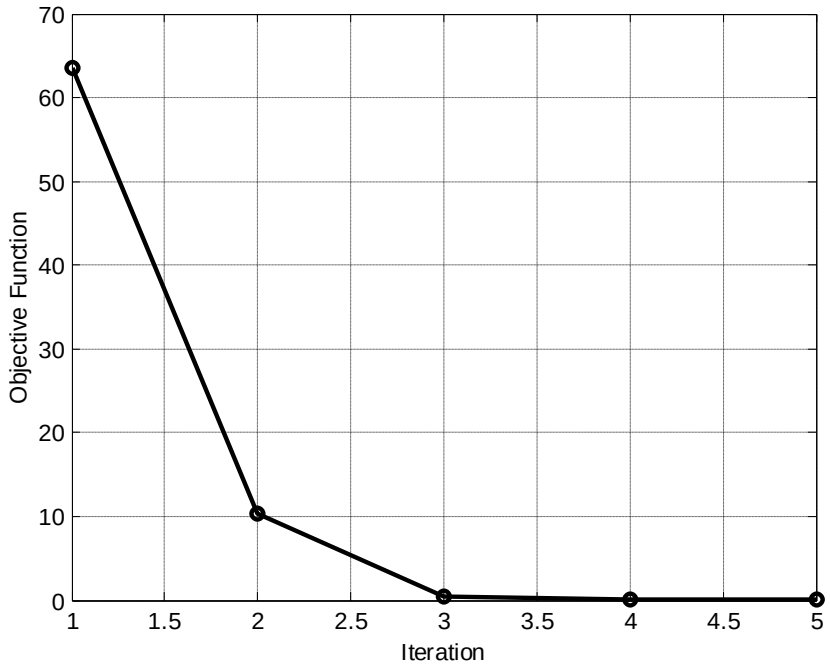


Figure 8.12. Convergence of iterative estimation process for design C motor.

Steady State Analysis

The steady state analysis results for four different motor types are illustrated in Figure 8.13 through Figure 8.16. The motors are operating at torque equilibrium mode and they all have the same load torque that depends quadratically on speed:

$T_m = 0.5 + 0.5 \cdot \omega + 0.2 \cdot \omega^2$

with

T_m : mechanical load torque in p.u.,

ω : mechanical speed in p.u.

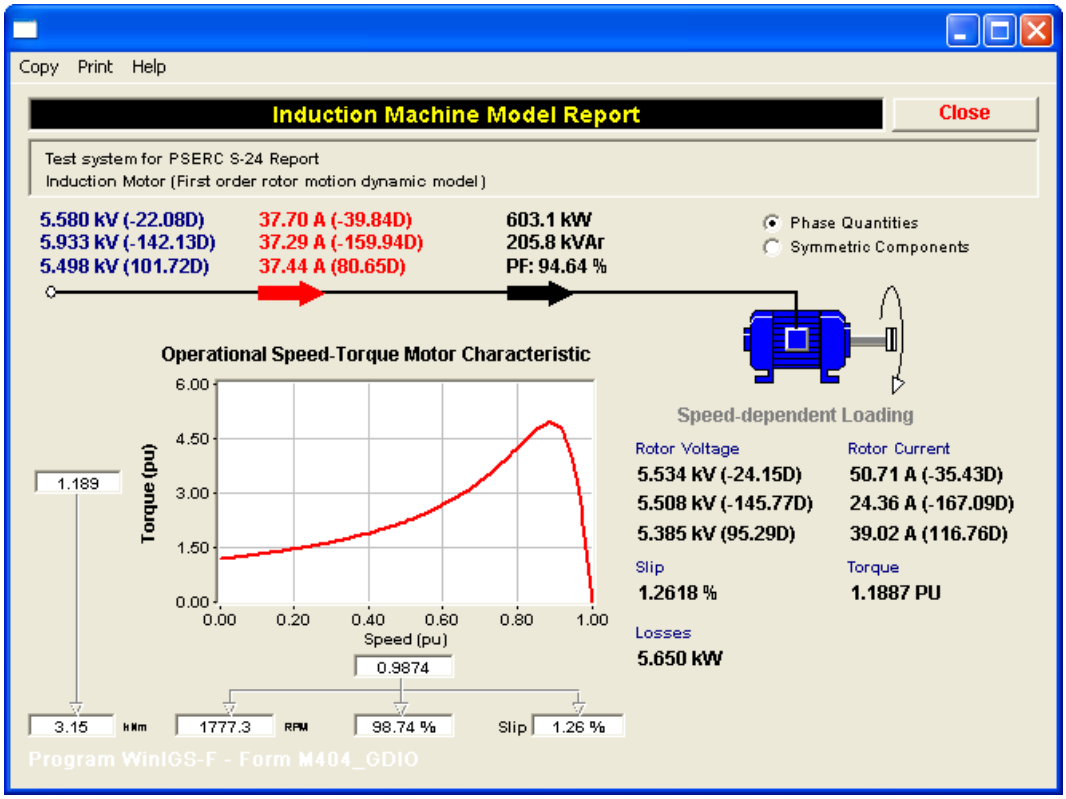


Figure 8.13. Steady state analysis results for NEMA class A motor.

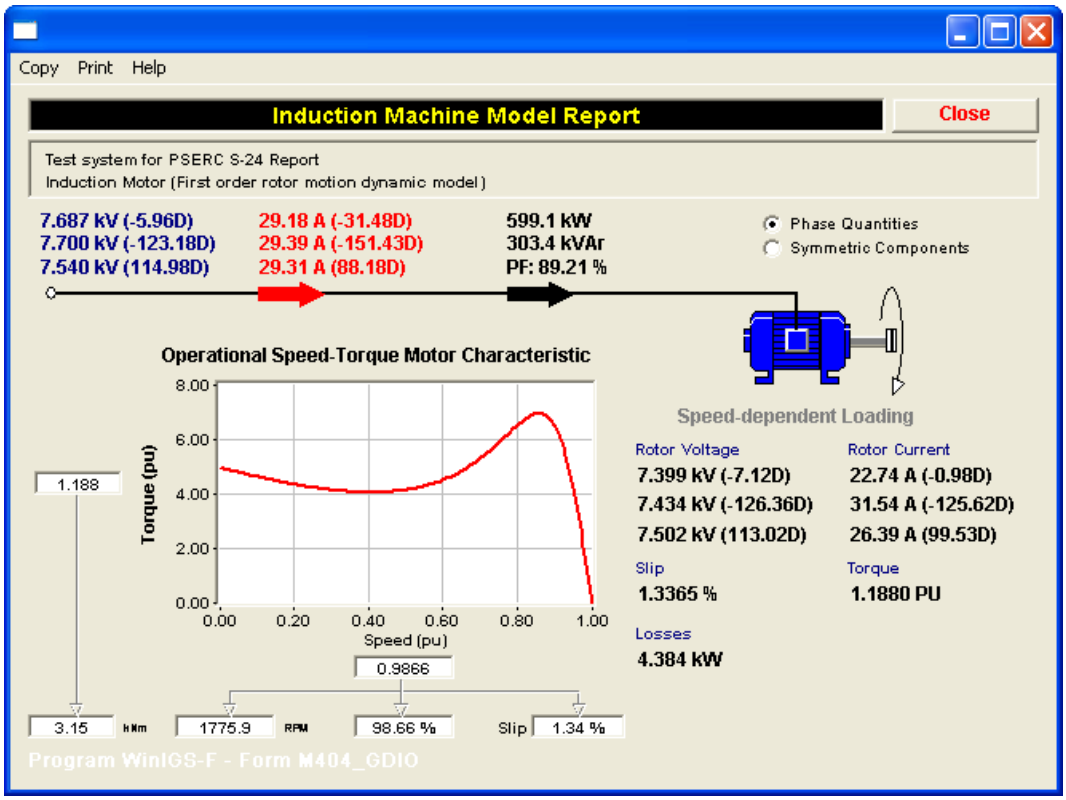


Figure 8.14. Steady State Analysis Results for NEMA Class B Motor.

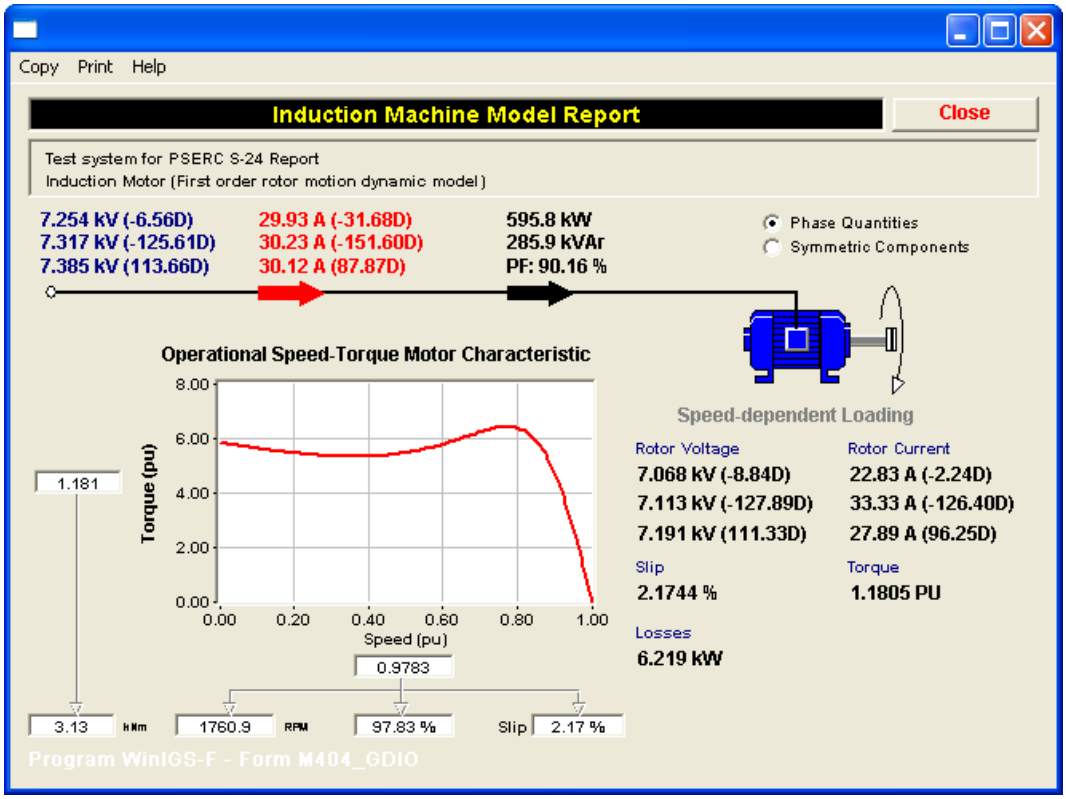


Figure 8.15. Steady State Analysis Results for NEMA Class C Motor.

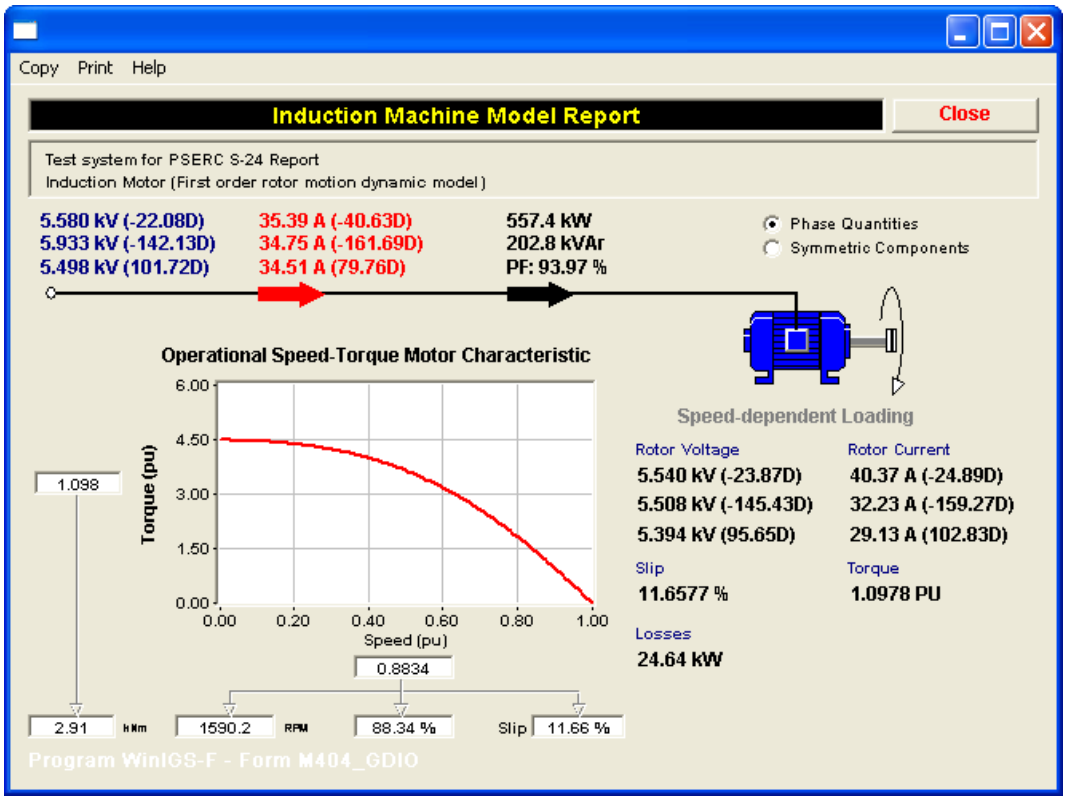


Figure 8.16. Steady State Analysis Results for NEMA Class D Motor.

The model output provides information about the terminal voltage of the motor, the absorbed current and power per phase as well as the motor speed, internal voltages, losses and the produced mechanical torque. It also provides graphically the operating slip-torque characteristic of the motor at the current operating point.

It is interesting to notice the different behavior of the four different motors. Design A motor operates with the smallest slip value and the best power factor. Design D has a similarly high power factor, but operates at reduced speed, at a slip value of more than 11%. Design D also produces the lower torque, compared to design A, although their terminal voltage is the same, and also has significantly higher losses compared to all other designs. Design B has the least amount of losses, but operates at the worse power factor. Of course, the operating point of each motor also depends on the network bus it is connected to.

Additional network quantities are presented in the reporting Figures below. Note in Figure 8.21 the low voltage profile of the system, especially at the load areas.

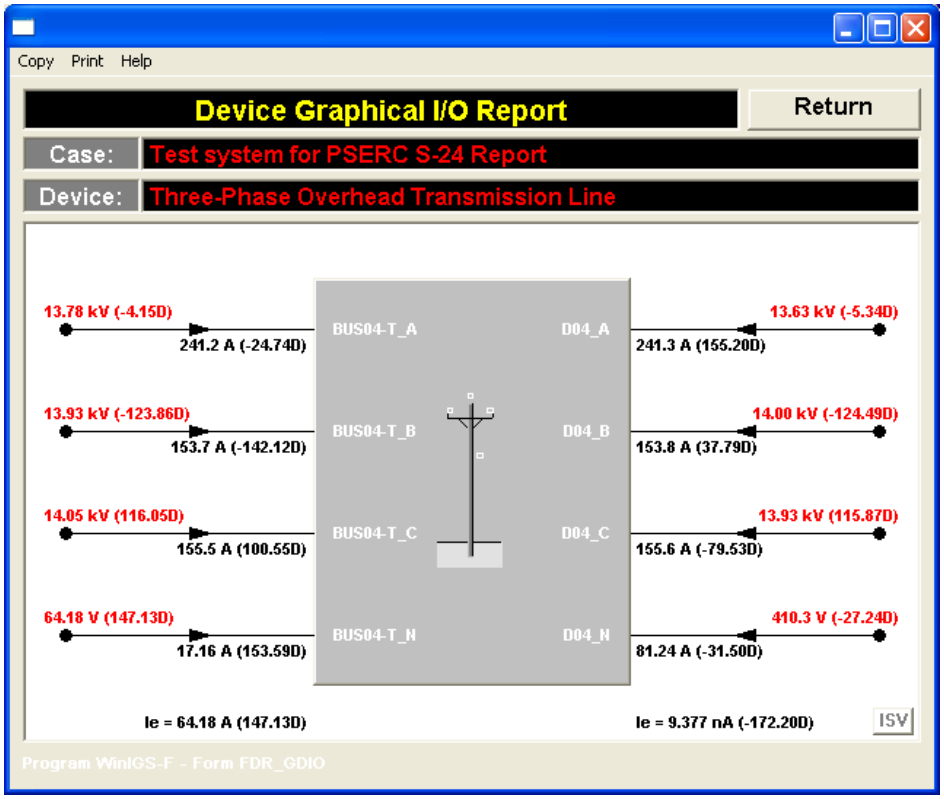


Figure 8.17. Voltage and Current Values at the Terminals of a Distribution Line. Notice the Significant Imbalance Among the Phases.

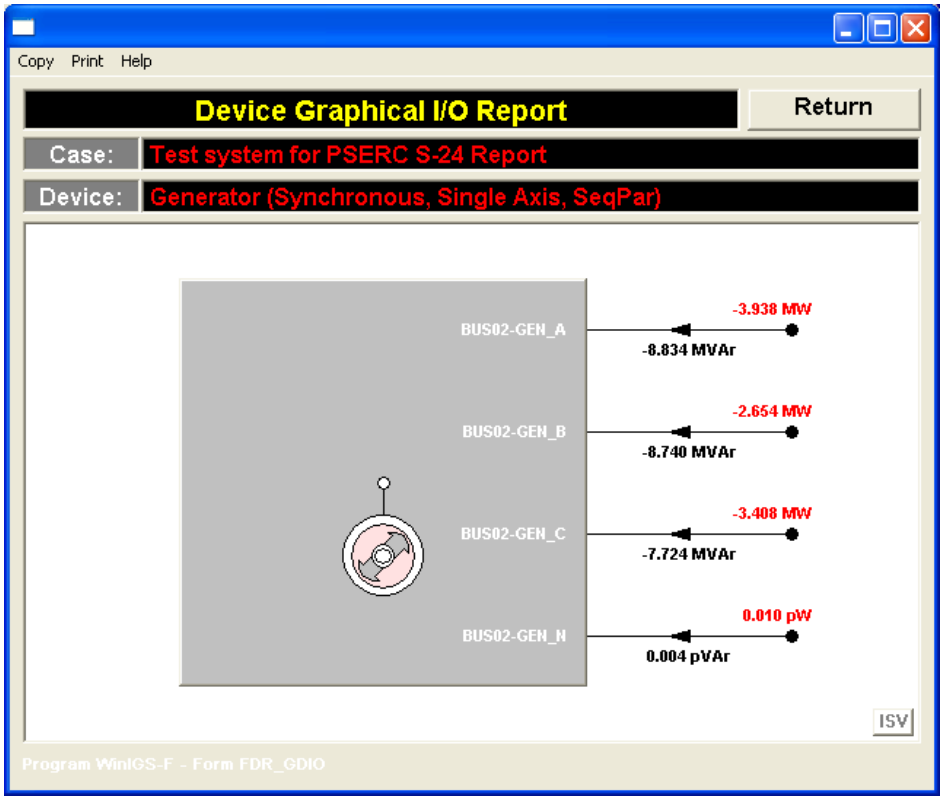


Figure 8.18. Active and Reactive Power Production of Second Generating Unit.

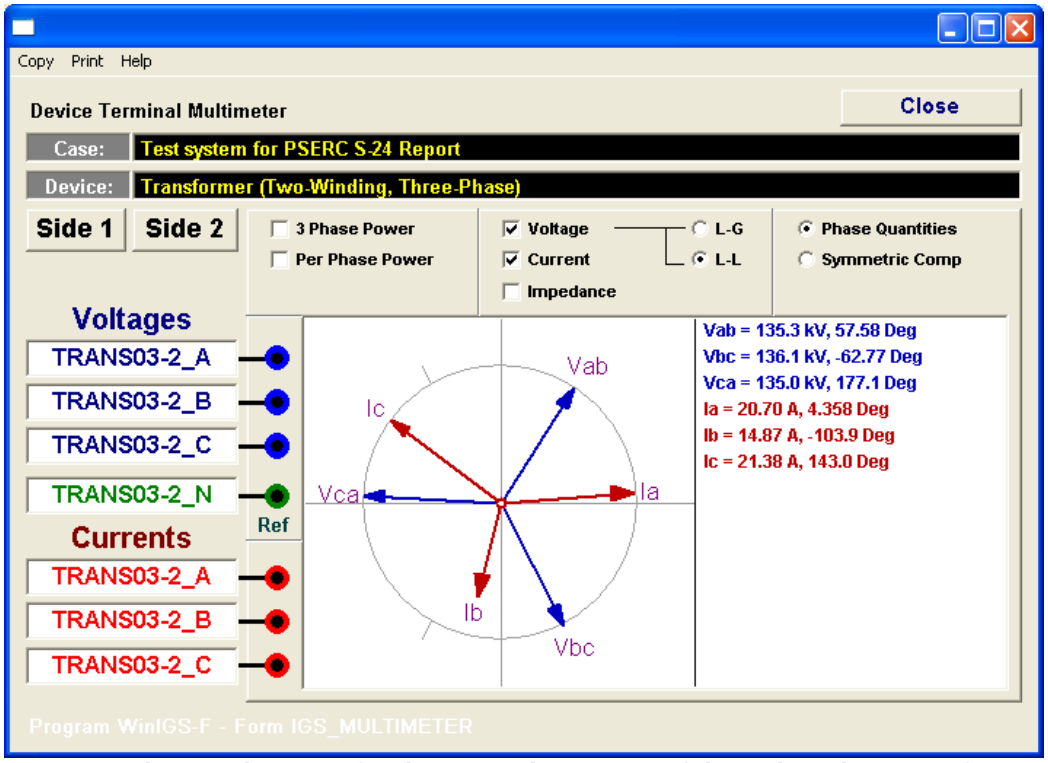


Figure 8.19. Phasor Diagram of Voltages and Currents of the Substation Transformer at BUS03. Note again the system imbalance.

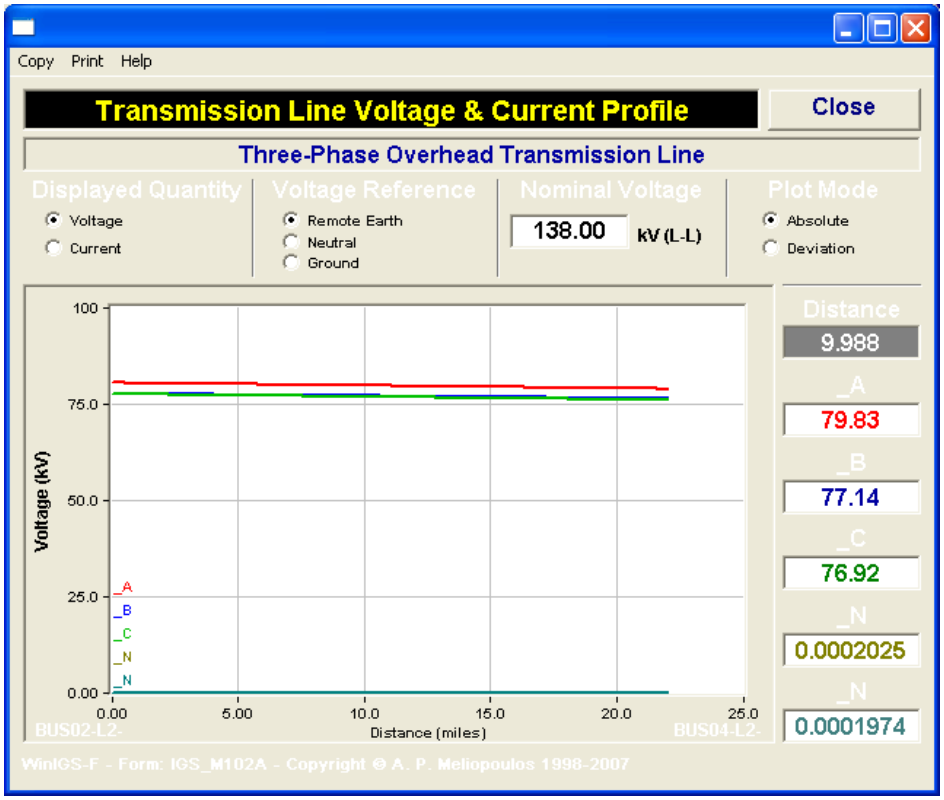


Figure 8.20. Voltage Profile Along a System Transmission Line.

Bus Voltage – Min = 0.702p.u. Max = 1.012p.u.

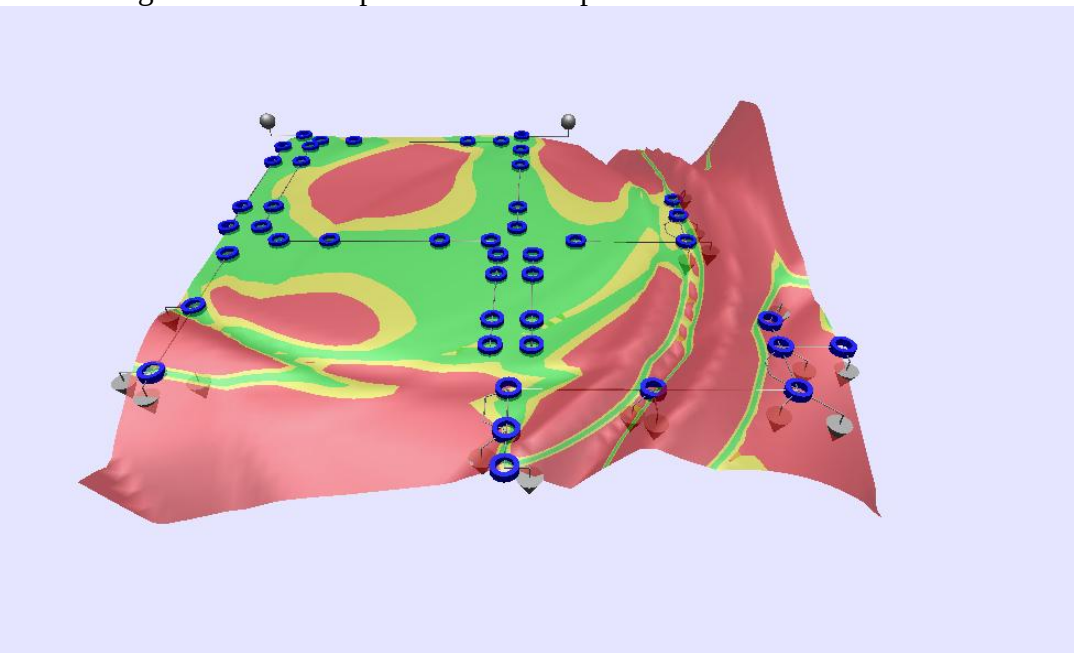


Figure 8.21. Surface Plot of System Voltage Profile (positive sequence). Green color indicates normal voltage, yellow deviations up to ±5% and red deviations above ±5%.

Simple sensitivity analysis among the high voltage substations reveals that the system voltage profile (voltage index defined earlier) is most sensitive to VAr support placement

at BUS05 and BUS04. Placing an equal amount of reactive support at the high side of each one of these substations significantly improves the system voltage profile.

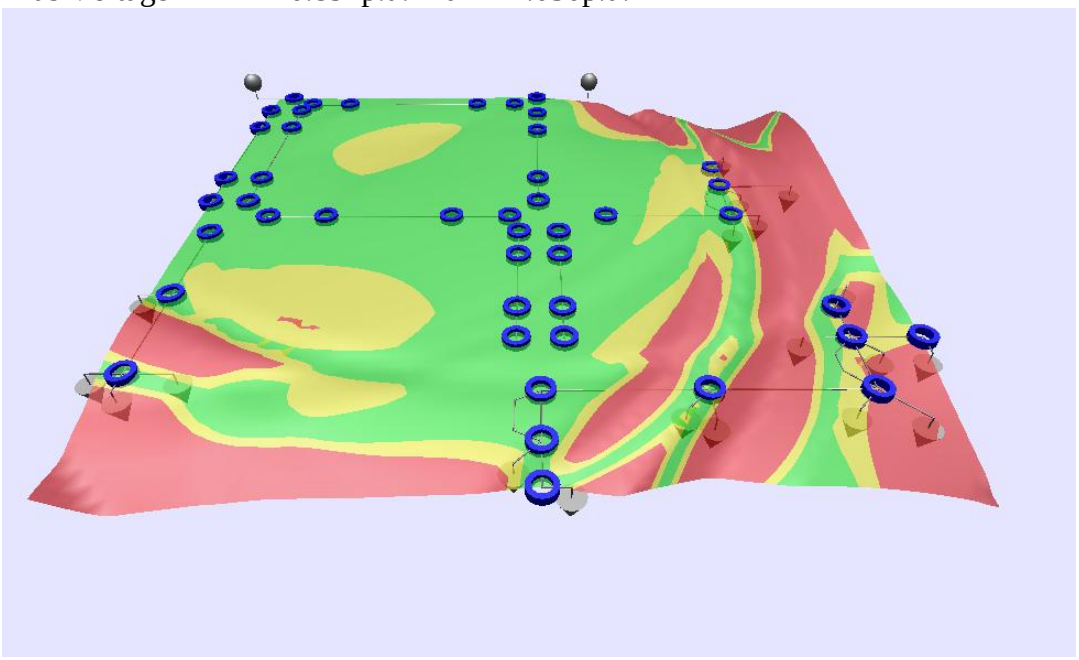


Figure 8.22. Surface Plot of System Voltage Profile (positive sequence), after application of capacitive support.

Quasi Steady State Analysis

Results from dynamic analysis are presented next. First, a line to line fault, between phases A and B is applied to the system at the line BUS03-L3 – BUS04-L3 very close to the BUS03 terminal. The fault is cleared after 300ms by removing the line. A quasi-steady-state analysis is performed, assuming that the network is operating under sinusoidal steady-state conditions. The motor inertia constants are set as follows:
Motor 1 (design A) 0.5 sec (moment of inertia of 28.14 kg.m2);
Motor 2 (design B) 1.0 sec (moment of inertia of 56.29 kg.m2);
Motor 3 (design C) 0.05 sec (moment of inertia of 2.81 kg.m2);
Motor 4 (desing D) 0.5 sec (moment of inertia of 28.14 kg.m2).

Simulation results with emphasis in monitoring the voltage recovery at the induction motor terminals are presented in Figure 8.23 to Figure 8.27. Note that because of the delta-wye transformers between the fault location and the monitoring buses, the faulted phases at the load buses may not necessarily appear to be the same as at the fault location.

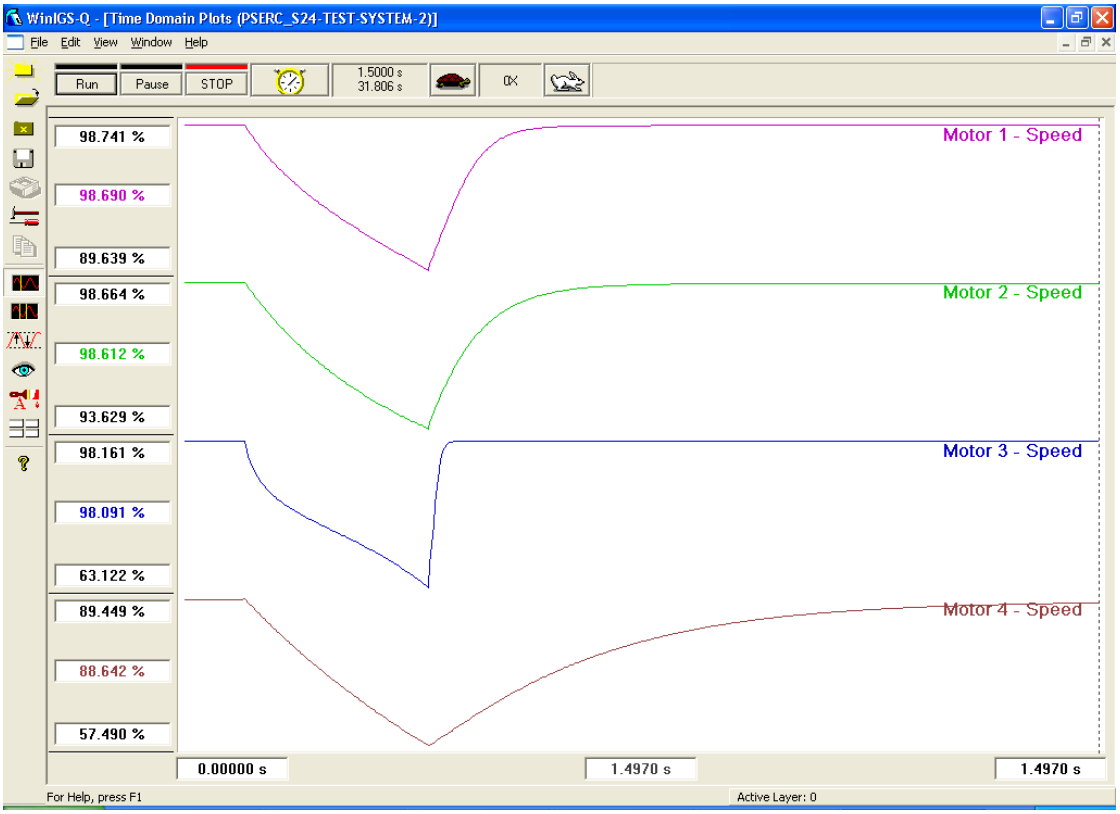


Figure 8.23. Motor Speeds After Line to Line Fault, cleared by Line Removal.

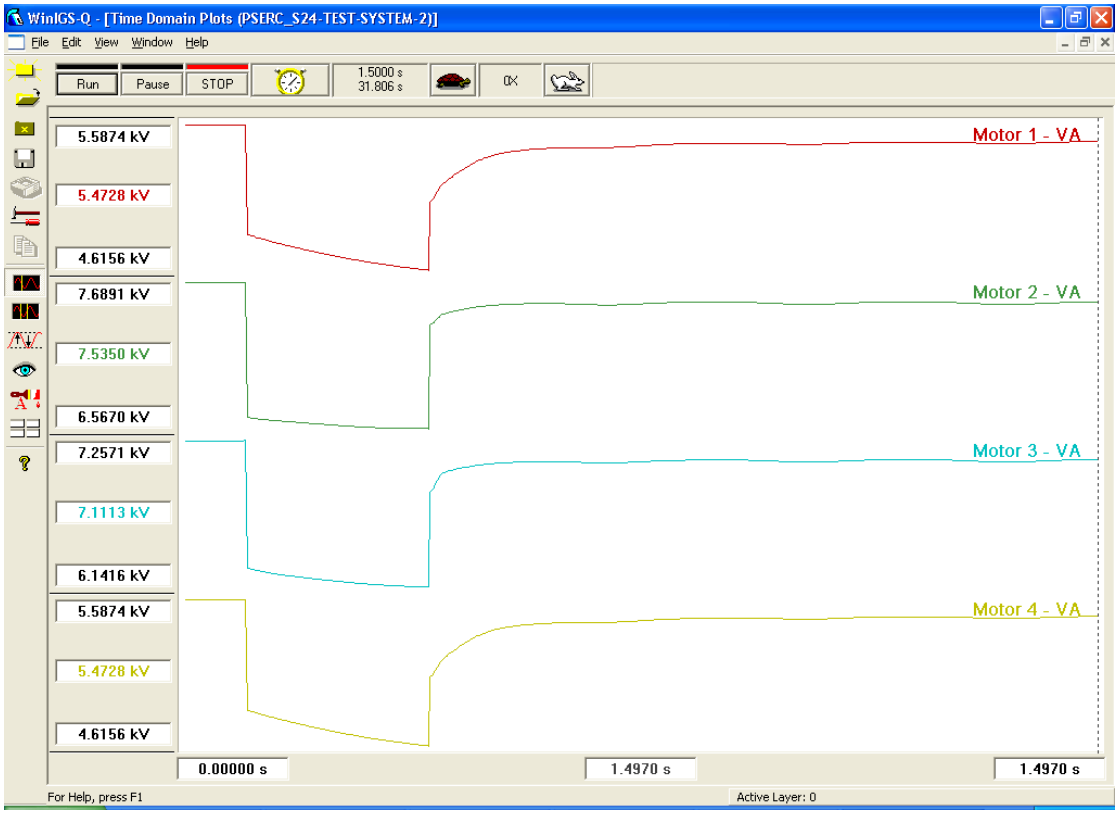


Figure 8.24. Voltage Recovery of Phase A at the Induction Motor Terminal Buses.

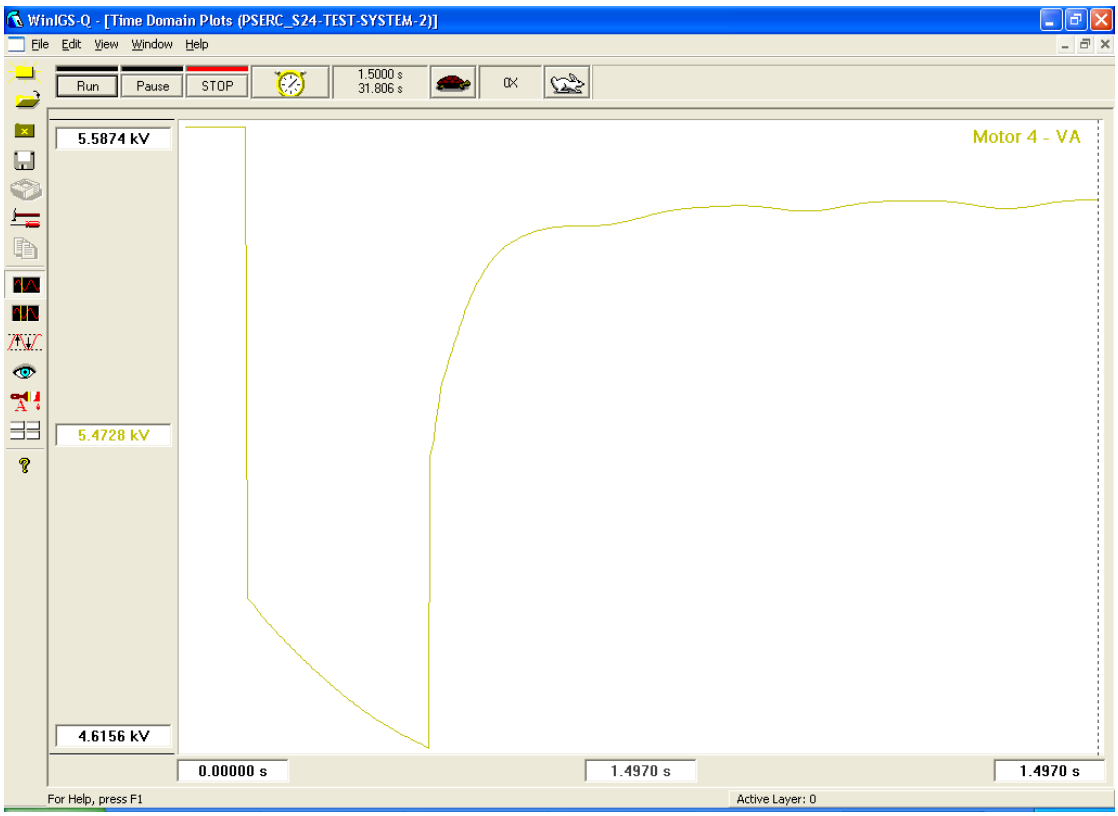


Figure 8.25. Voltage Recovery of Phase C at Induction Motor 4 Terminal Bus.

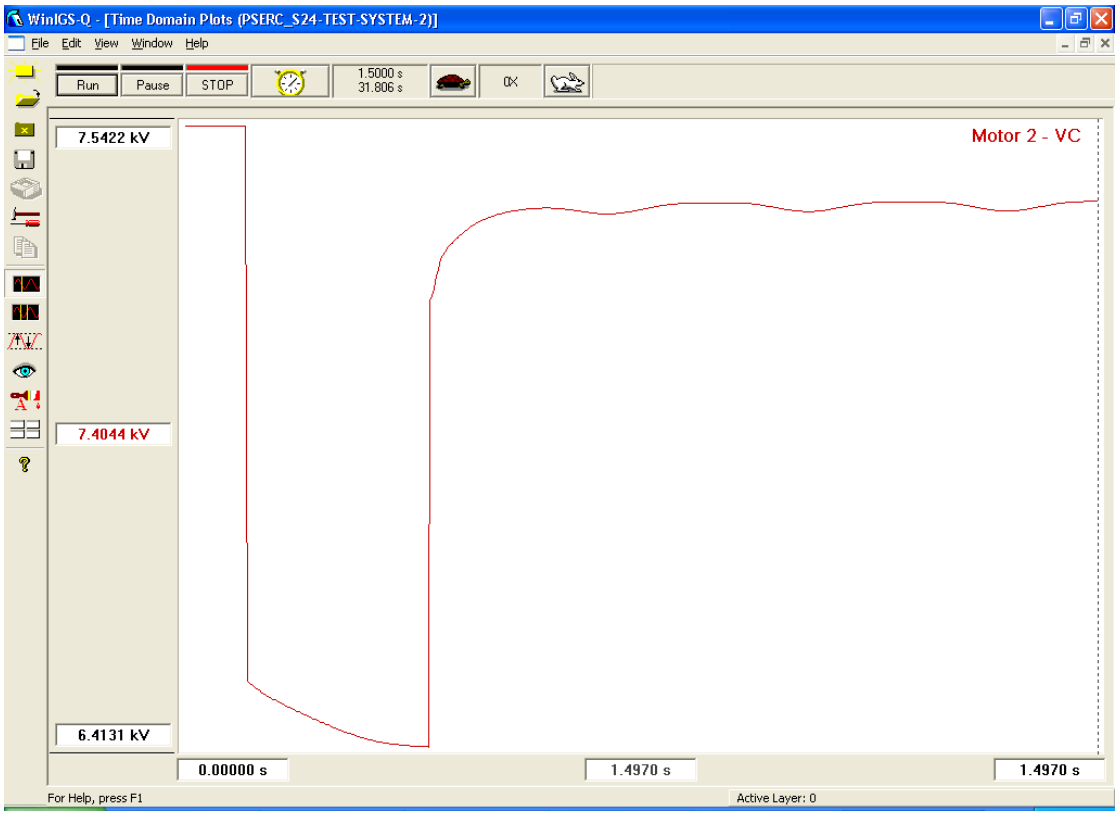


Figure 8.26. Voltage Recovery of Phase C at Induction Motor 2 Terminal Bus.

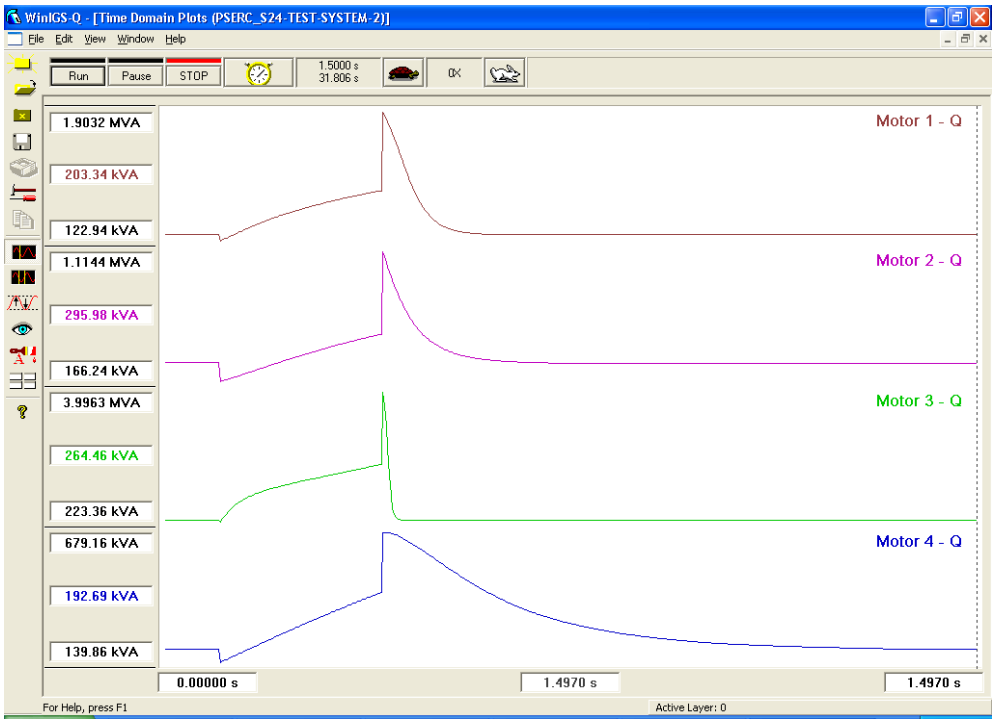


Figure 8.27. Induction Motor Reactive Power Absorption during Fault and Post-Fault Period.

Next, a three phase fault is applied to the system at the same line BUS03-L3 – BUS04-L3 very close to the BUS03 terminal. The fault is cleared after 300ms by removing the line. The dynamic simulation results from this test case are presented in Figure 8.28 to Figure 8.33.

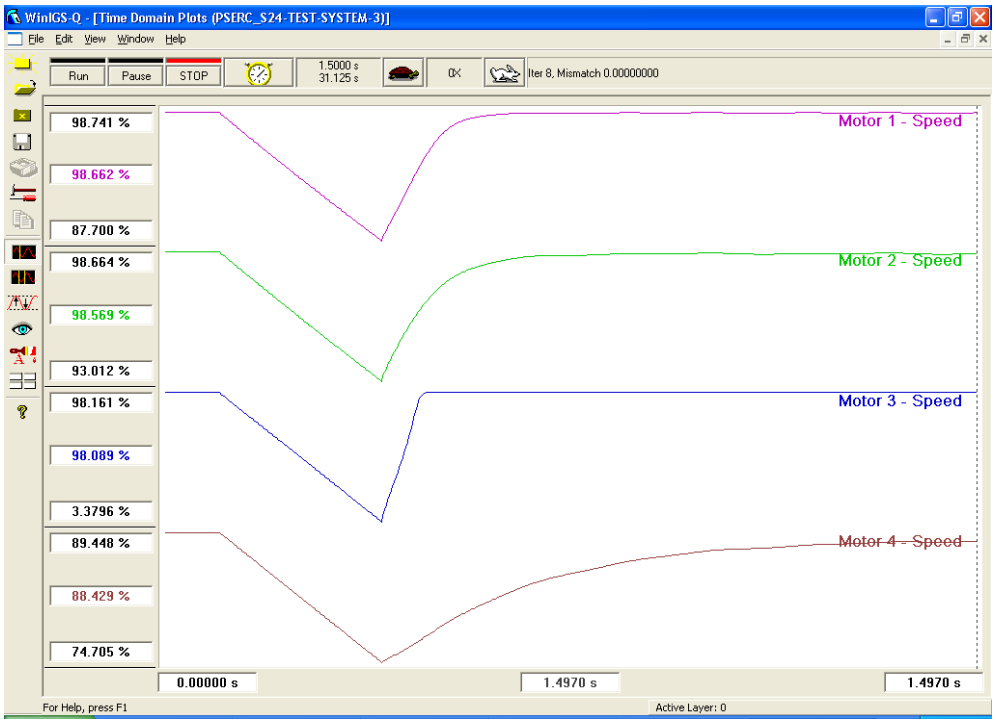


Figure 8.28. Motor Speeds After Three Phase Fault, cleared by Line Removal.

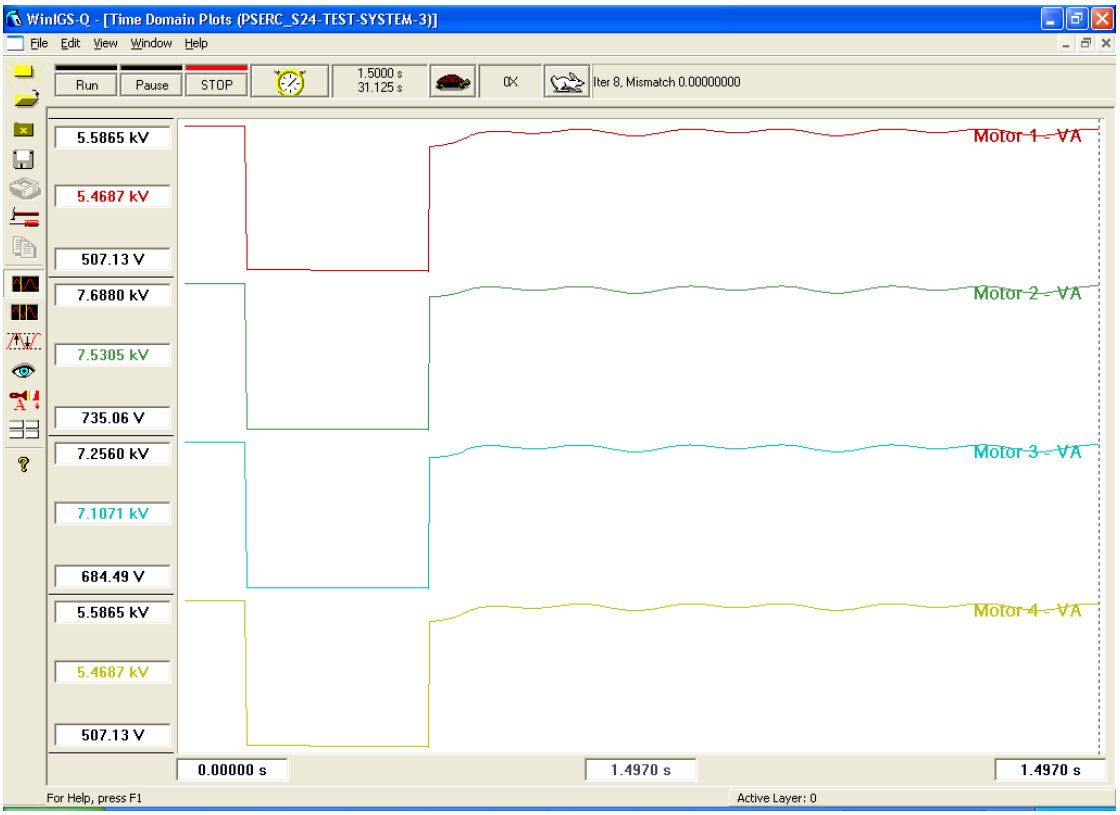


Figure 8.29. Voltage Recovery of Phase A at the Induction Motor Terminal Buses.

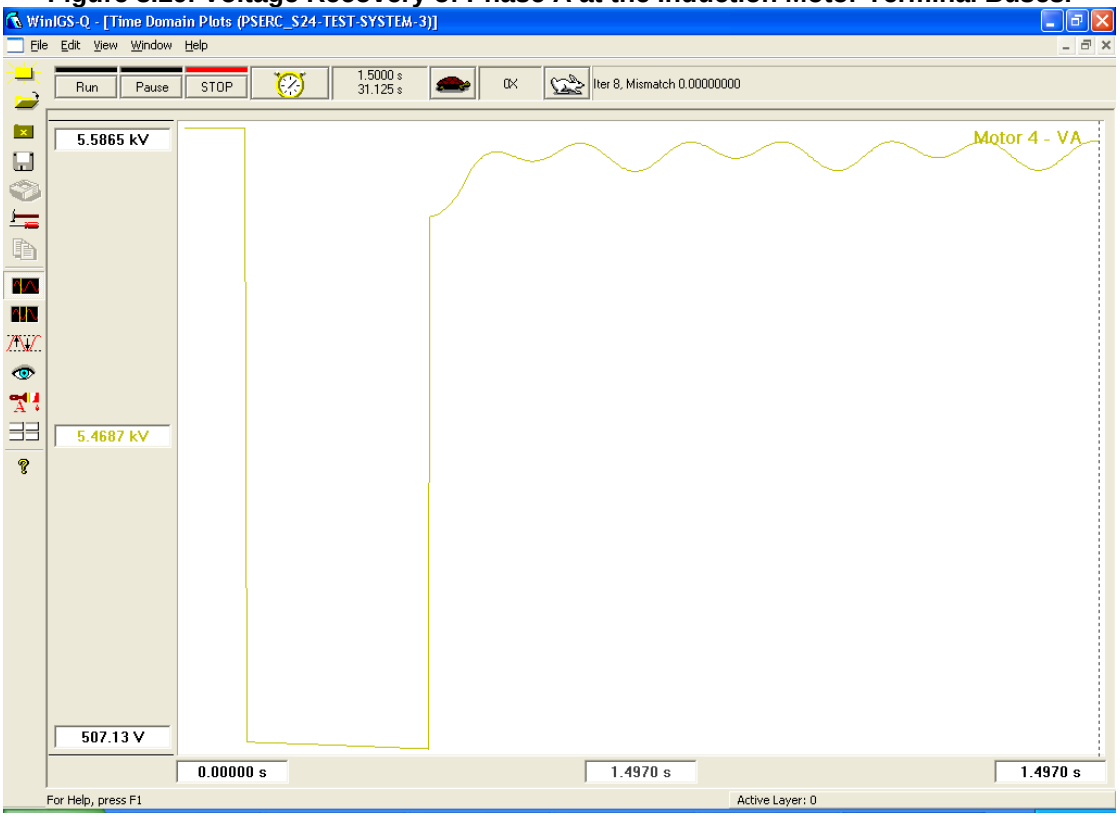


Figure 8.30. Voltage Recovery of Phase A at Induction Motor 4 Terminal Bus.

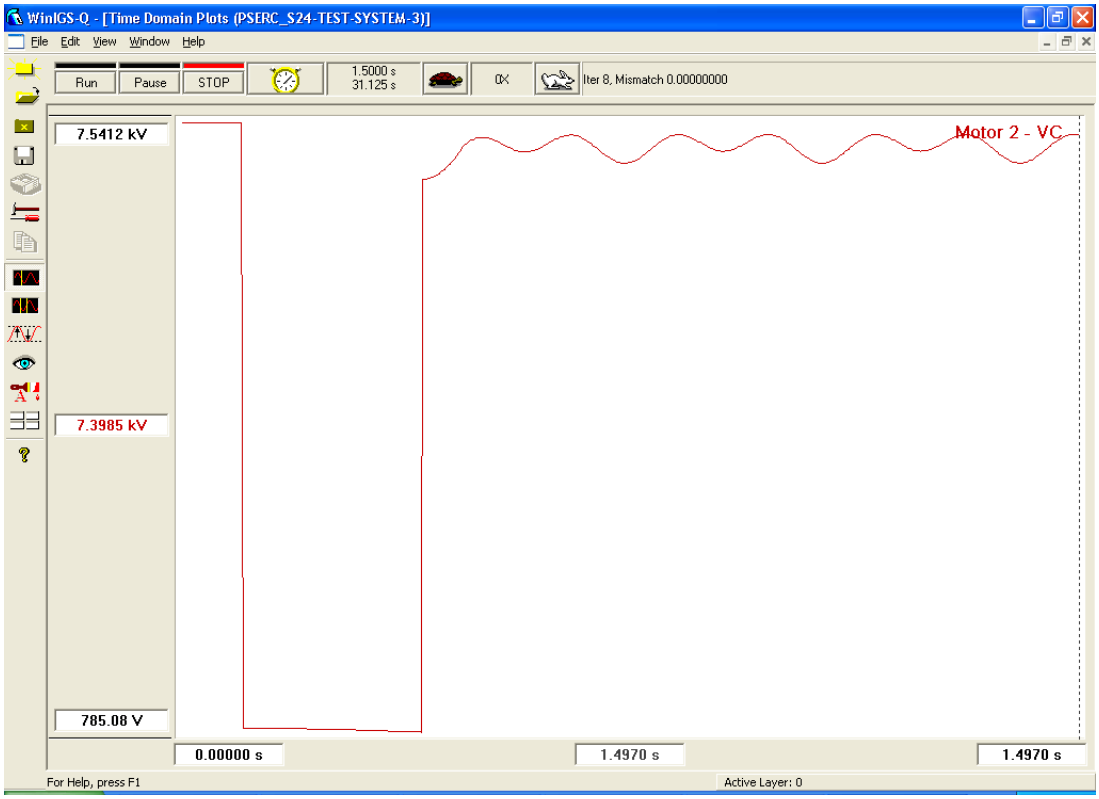


Figure 8.31. Voltage Recovery of Phase C at Induction Motor 2 Terminal Bus.

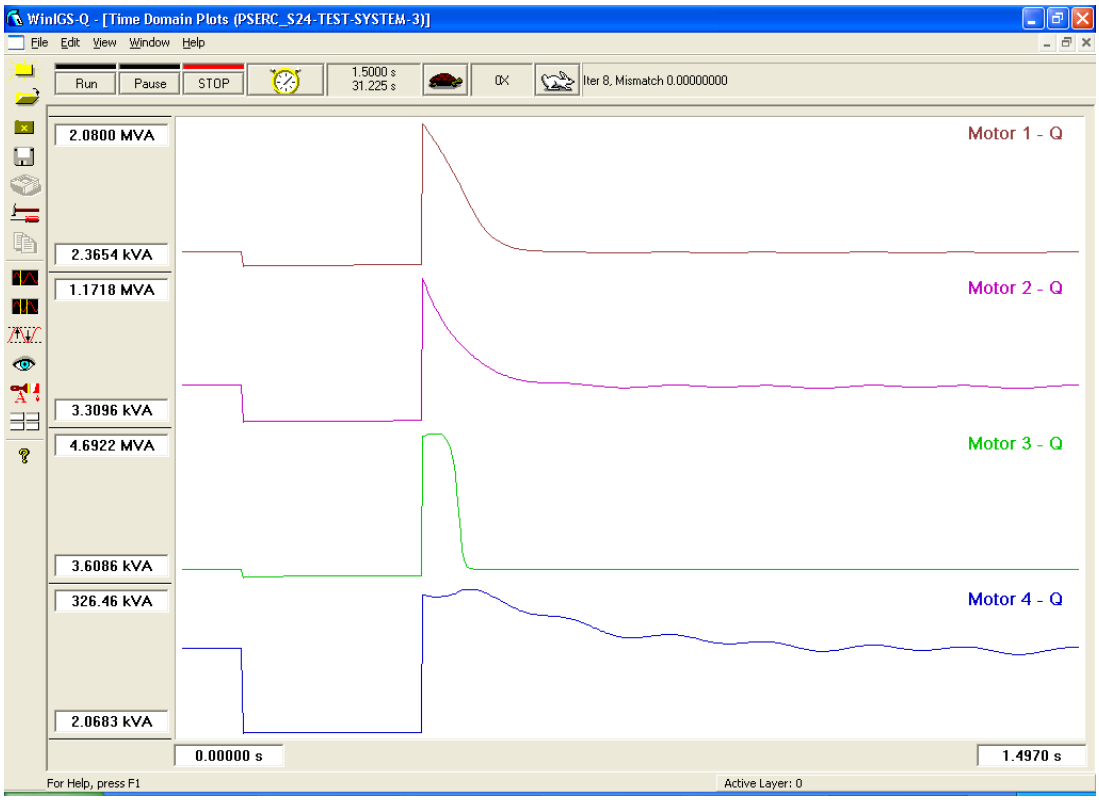


Figure 8.32. Induction Motor Reactive Power Absorption during Fault and Post-Fault Period.

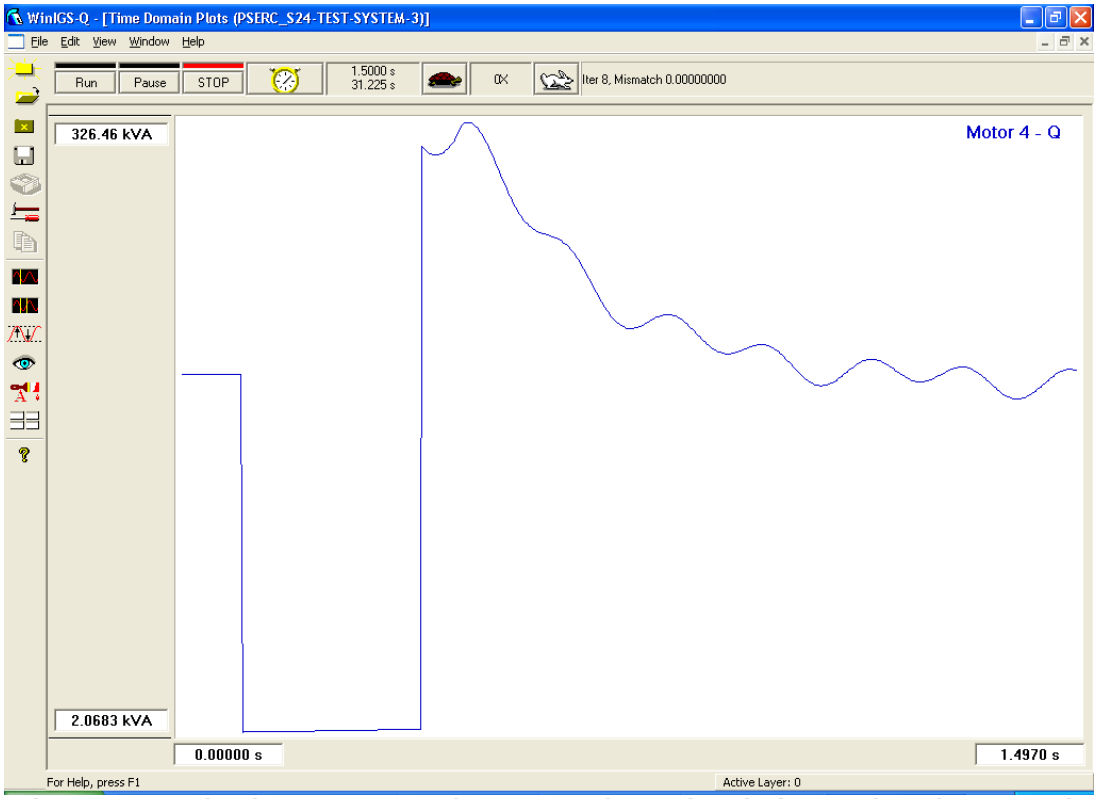


Figure 8.33. Induction Motor Reactive Power Absorption during Fault and Post-Fault Period, for Motor 4.

Finally, a line to line fault is considered again at the same line BUS03-L3 – BUS04-L3 very close to the BUS03 terminal. The fault is cleared after 300ms by removing the line. However, now motors 3 and 4 are disconnected after a specific time following the fault, when their speed fell below a certain value; the motors are reconnected to the system following the fault clearance. In particular, Motor 3 disconnects at 0.2 seconds after the fault and reconnects 0.05 seconds following the fault clearance and Motor 4 trips 0.15 seconds after the fault and reconnects 0.3 seconds after the fault is cleared. The dynamic simulation results from this test case are presented in Figure 8.34 to Figure 8.36.

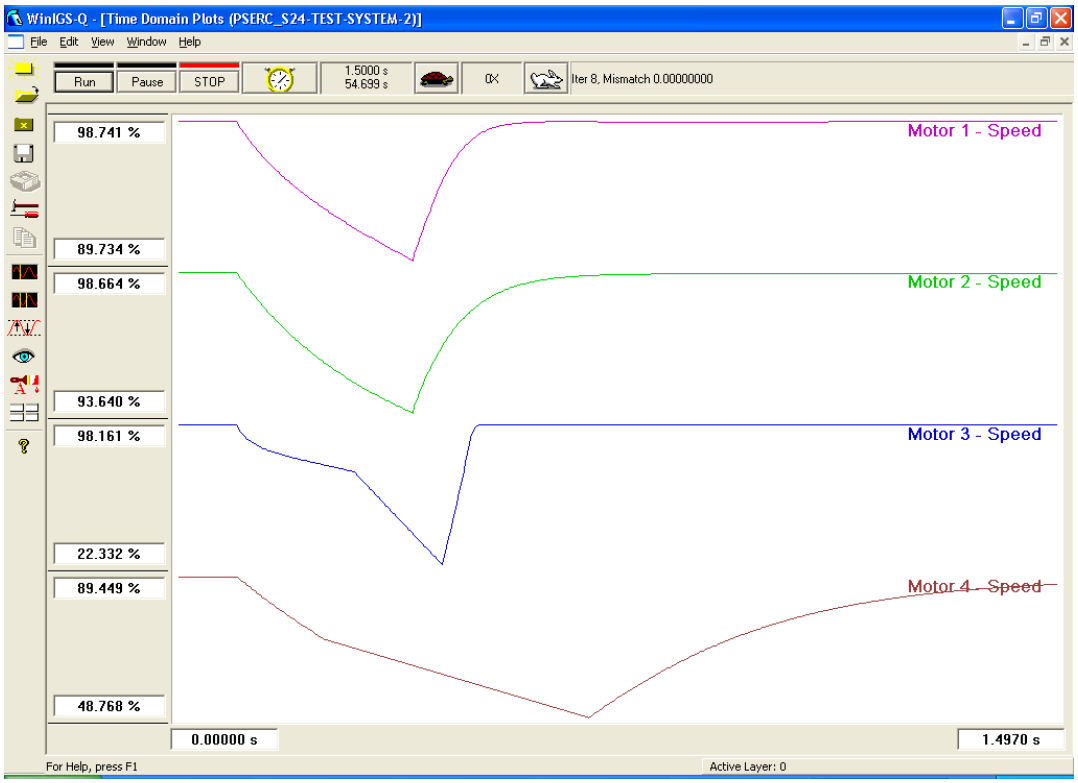


Figure 8.34. Motor Speeds After Three Phase Fault, cleared by Line Removal, with Motor Tripping and Reconnection.

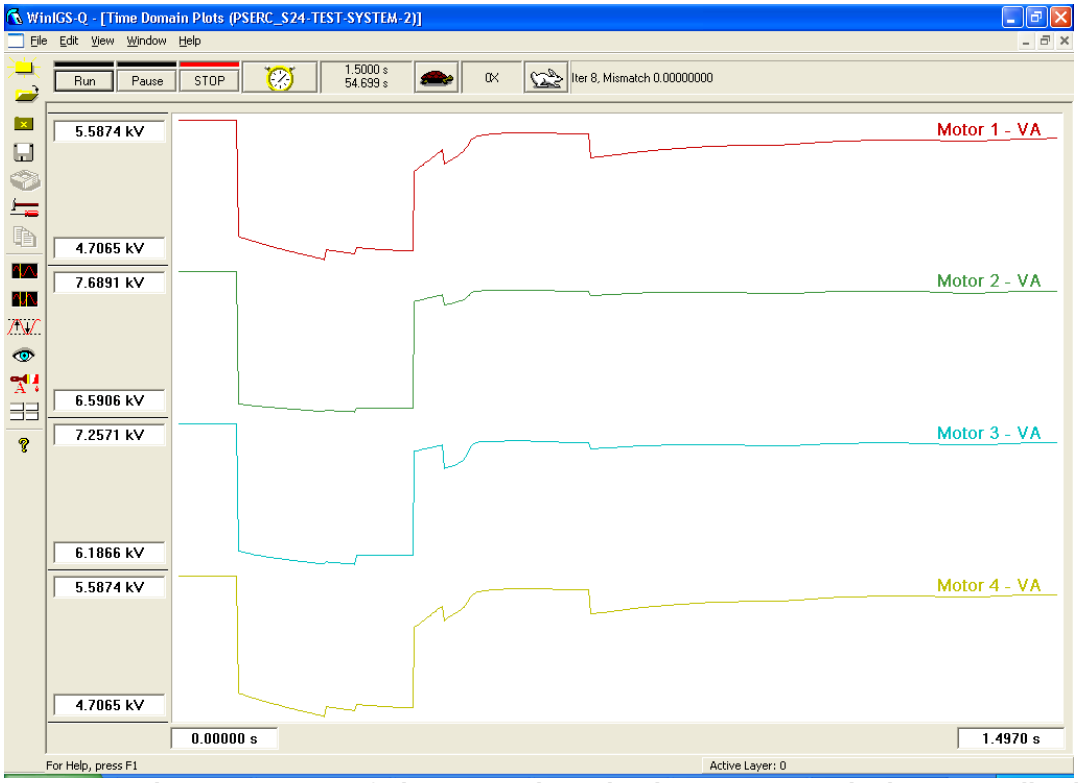


Figure 8.35. Voltage Recovery of Phase A at the Induction Motor Terminal Buses Following a Line to Line fault, with Motor Tripping and Reconnection.

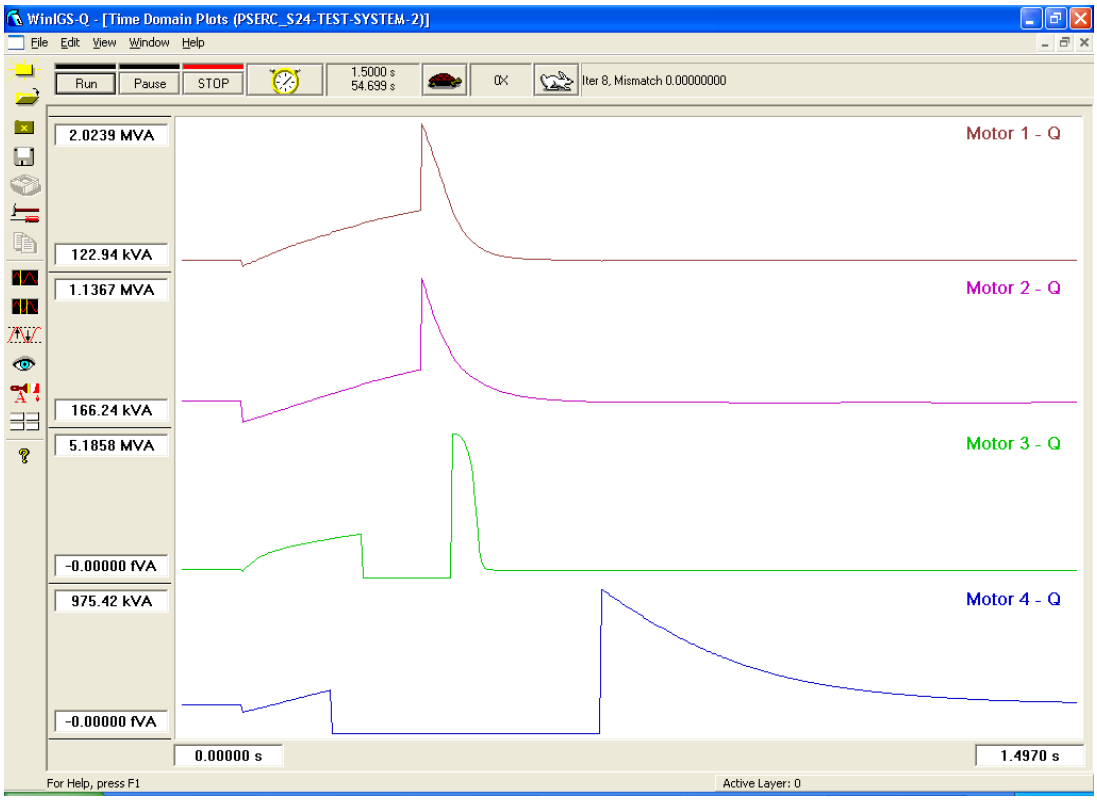


Figure 8.36. Induction Motor Reactive Power Absorption during Fault and Post-Fault Period, Following a Line to Line fault, with Motor Tripping and Reconnection.

Optimization of VAr sources

The second part of results involves a step by step demonstration of the application of successive dynamic programming for the optimal allocation of VAr sources. The system that is being used for the study is a three phase version of the IEEE 24-Bus Reliability Test System (RTS-24), presented in Figure 8.37. The data for the system, in the form of positive sequence equivalent network are available from [83]. The three phase model was obtained by assuming some specific line configuration and trying to match the positive sequence model of each line, to the branch circuit parameters provided in [83]. Small asymmetries are introduced in the system due to the transmission line structure. No single phase loads are included, therefore no significant imbalances exist. A portion (50%) of the static constant power load is replaced by induction motors of the same rating and of design A, at some of the system load buses. A total number of four stages will be considered, representing a two year period of time. Each year is divided into winter time and summer time, with different peak load at each time. The peak loading conditions are the only ones assumed for this example, and it is expected that they are representative of the system behavior. Furthermore the nonconforming static load model is used to represent the load growth and variations between the time stages of the problem.

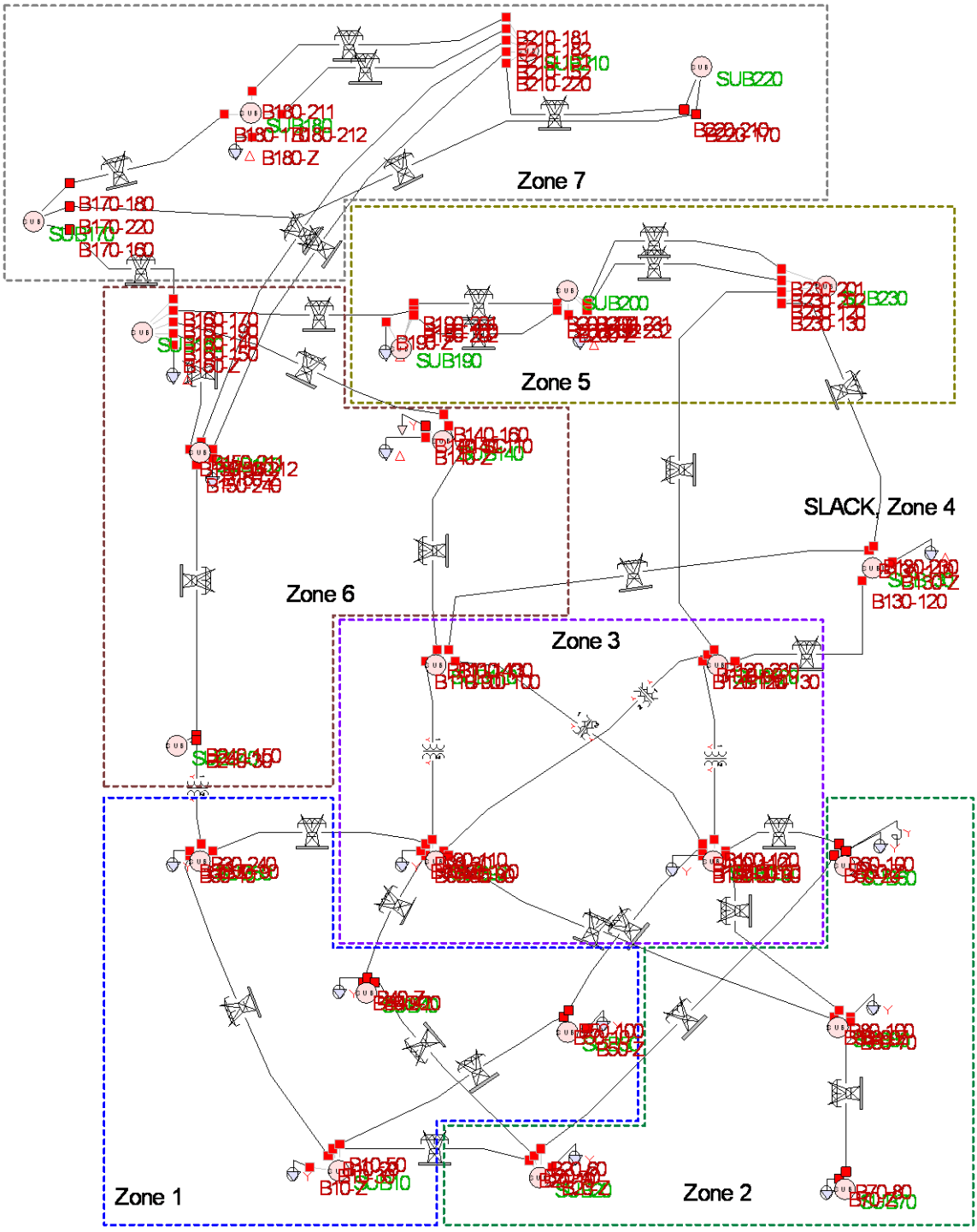


Figure 8.37. Three Phase Model of the IEEE 24-Bus RTS.

VAr support modules are assumed to be connected to the system at increments of 500 kVAr. Their cost is defined as an installation and operating cost depending quadratically on the rated power of the unit, plus a contant cost that depends on the installation location. Location cost is arbitrary defined based on the system zones, shown in Figure

8.37. Installation and operating cost is also arbitrary defined and is assumed approximately 500$/kVAr. A quadratic relation is assumed of the form:

$C(X) = 0.01 \cdot X^2 + 500 \cdot X + C_L(X)$,

where

X : is the amount of reactive support in kVAr,

$C(X)$: is the cost of installation and operation in $,

$C_L(X)$: is the additional installation cost depending on location.

The location cost is assumed to depend linearly on X and is defined as:

Zone 1: 150 $/kVAr
Zone 2: 200 $/kVAr
Zone 3: 100 $/kVAr
Zone 4: 50 $/kVAr
Zone 5: 120 $/kVAr
Zone 6: 90 $/kVAr
Zone 7: 90 $/kVAr

Only load buses are considered for VAr support installation, since there is no point in placing VAr sources at generating stations.

The voltage index defined in (7.19) is used as part of the objective function to represent static performance, as also explained earlier. This performance index is also used for the contingency selection.

$$J_V = \sum_{k=1}^{N} w_k \left(\frac{V_k - V_{k,mean}}{V_{k,step}} \right)^{2n},$$

where

w_k : weighting factor, $0 < w_k < 1$,

$V_{k,mean}$: nominal bus voltage value (typically 1.0 p.u.),

(it is in general the mean value in the desired range, i.e. $\frac{1}{2}\left(V_k^{\max} + V_k^{\min}\right)$),

$V_{k,step}$: voltage deviation tolerance (i.e. $\frac{1}{2}\left(V_k^{\max} - V_k^{\min}\right)$),

V_k : actual voltage magnitude at bus k,

n : positive integer parameter defining the exponent (2 in this case),

N : total number of load buses of interest
(buses where motor loads are connected in this case).

The functional (7.53) is used as part of the objective function to represent dynamic performance. Voltage sag magnitude and duration at the load buses of interest (in this case where motors are connected) are being monitored.

$$J_R(v(t)) = \int_{t_1}^{t_2} \left(V^{\min} - v(t)\right) dt$$

$v(t)$: output of interest e.g. voltage at specific load bus(es),

$V^{\min}$: threshold level for performance criteria, e.g. minimum acceptable voltage level,

t_1 : time at which the voltage quantity of interest fall below threshold value,

t_2 : time at which the voltage quantity of interest recovers above threshold.

Furthermore, a penalty factor is assigned to the objective function for states that under some of the selected contingencies do not satisfy voltage recovery criteria, based on the functional of the form (7.52)

$$J_{dip}(v(t)) = t_1 - t_2$$

where

t_1 : transition time at which the voltage fall below threshold ($v(t) < V^{\min}$),

t_2 : transition time at which the voltage recovers above threshold ($v(t) > V^{\min}$),

The criterion used is the voltage remaining below 80% of nominal for a period of more than 30 cycles

A weight is assigned at each component of the objective function, so that no component has an overwhelming effect on it, apart from the penalty factor. The weights are chosen in such a way that the objective function values are normalized.

Circuit contingencies are only considered in the form of line outages after three phase faults. The base case screening of circuit contingencies, based on the voltage index is illustrated in Table 8-5 for the two proposed sensitivity analysis methods. The two most important contingencies are the outage of lines connecting buses 20 and 60 of zone 2 and buses 60 and 100. This second circuit is indeed an underground cable circuit. Therefore these two contingencies will only be considered, both for steady state analysis and dynamic analysis assuming three phase faults cleared by the line (cable) removal from the system.

TABLE 8-5 PERFORMANCE INDEX CHANGE AND RANKING RESULTS FOR THE VOLTAGE INDEX FOR THE IEEE 24-BUS RELIABILITY TEST SYSTEM.

Outaged Branch	J(u=1)	J(u=0)	Actual ΔJ	Nonlinear Approach Ranking	ΔJ = -dJ/du	Proposed Index Linearization Ranking	State Linearization Analysis ΔJ	Proposed State Linearization Ranking
60_100 C	25.41	3306.22	3280.81	1	-243.87	39	120.99	1
20_60	25.41	133.82	108.41	2	30.72	1	49.99	2
100_110 T	25.41	63.10	37.69	3	16.73	2	24.95	3
150_240	25.41	58.58	33.17	4	0.00	19	1.65	8
50_100	25.41	55.57	30.16	5	7.48	5	8.68	6
100_120 T	25.41	50.63	25.22	6	12.98	3	19.67	4
80_100	25.41	48.74	23.33	7	10.20	4	12.24	5
10_50	25.41	39.40	13.98	8	4.12	6	4.55	7
240_30 T	25.41	37.04	11.63	9	-1.33	31	-0.90	32
110_140	25.41	30.62	5.21	10	1.08	7	1.18	9
30_90	25.41	28.41	3.00	11	0.88	8	1.10	10

Starting from this base case and assuming the above mentioned contingencies the two most favorable VAr source additions are determined, based on sensitivity analysis. These locations are BUS60 and BUS100, and 500 kVAr are added to each one of them, creating two new system states, at this first stage of the problem. Therefore, the first stage has three states:

State 0: Base case (with no additions of VAr sources);

State 1: Addition 1 of 500 kVAr at BUS60 at a cost of $C(X_{1,1}) = 0.01 \cdot 500^2 + 500 \cdot 500 + 200 \cdot 500 = 352{,}500\$$

State 2: Addition 1 of 500 kVAr at BUS100 at a cost of $C(X_{2,1}) = 0.01 \cdot 500^2 + 500 \cdot 500 + 100 \cdot 500 = 302{,}500\$$

The normalized objective function value is computed for each state. The cost above is part of the objective function; the rest of the components are evaluated based on the static and dynamic performance for each state under base case and contingencies. The normalized values of the objective function are shown along with each state in Figure 8.38. The best state of stage 1 is picked to be State 2, i.e. addition of 500 kVAr at BUS 100.

The problem is then moved to the next stage. The new system base case is considered under stage 2 conditions, but with the addition of the VAr source at BUS100, as resulted from the computations of the previous stage. The procedure is repeated again in this stage. Contingency ranking is performed again and the two most critical contingencies are selected. Furthermore, assuming these contingencies the two most favorable locations for installation of VAr support are selected creating two new states for the second stage of the problem.

State 0: Base case (with no additions of VAr sources);

State 1: Addition 1 of 500 kVAr at BUS100 at a cost of $C(X_{2,1}) = 0.01 \cdot 500^2 + 500 \cdot 500 + 100 \cdot 500 = 302{,}500\$$

State 2: Addition 1 of 500 kVAr at BUS80 at a cost of $C(X_{1,1}) = 0.01 \cdot 500^2 + 500 \cdot 500 + 200 \cdot 500 = 352{,}500\$$

The normalized objective function value is computed for each state. The cost above is part of the objective function; the rest of the components are evaluated based on the static and dynamic performance for each state under base case and contingencies. The best state of stage 2 is picked to be again State 2, i.e. addition of another 500 kVAr at BUS 100. The problem then moves to the next stage. The first iterate of the problem is shown in Figure 8.38. The solution after the first iterate is to add 1 MVAr of reactive support at system BUS100: 500 kVAr at stage one and another 500 kVAr at stage 2. The total cost will be 605 k$, based on the assumed cost values. The voltage profile and the voltage recovery rate is within desired specifications for the selected contingencies.

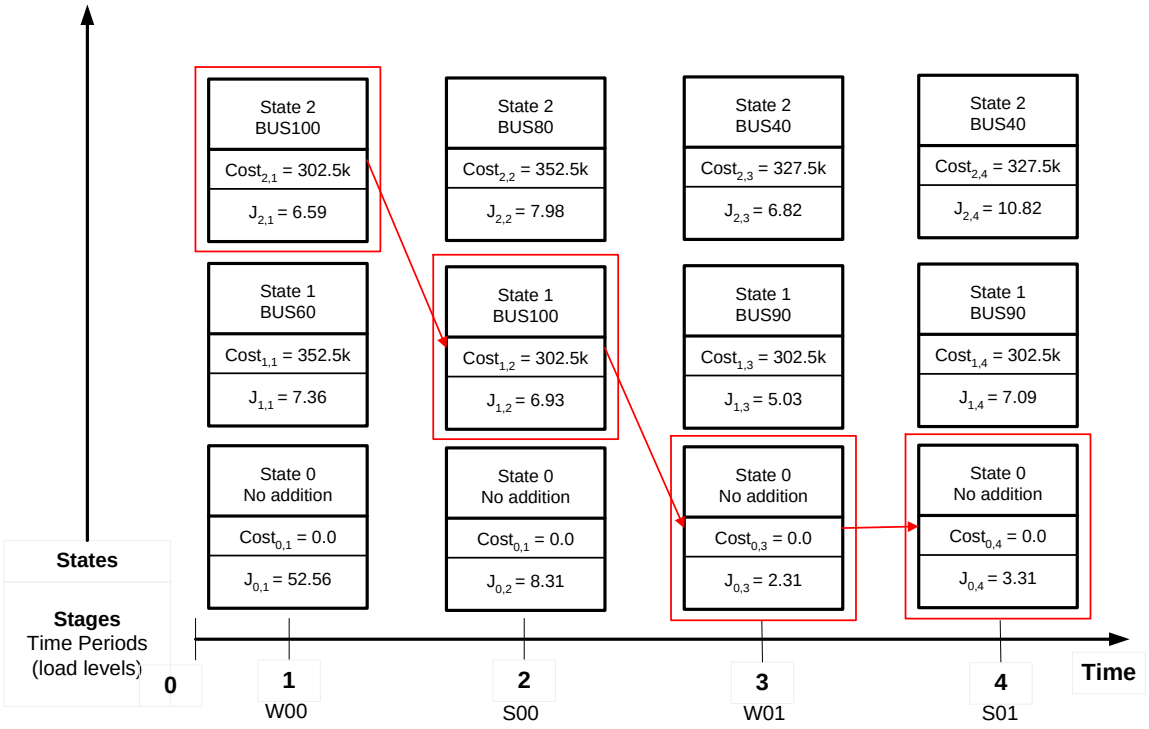


Figure 8.38. First Iterate of Successive Dynamic Programming.

The procedure is then repeated for the next iterate. State 2 of stage 1 is assumed to be the new first base case at stage 1. Sensitivity analysis is performed around this state to select the most important contingencies and candidate locations for VAR support. And the procedure is the same as described earlier. However, due to the small system size and low loading level and the small number of candidate locations, no additional VAr support devices are required and the second iterate provides the same results are above. Systems of more realistic sizes need to be considered to better evaluate the methodology performance.

9. Future Research Directions

The present research project resulted in techniques that select the optimal mix of static and reactive power sources to meet specific design criteria. The design criteria ensure that there will be no load interruption by action of protective relaying due to voltage recovery phenomena. The methodology uses dynamic load models which are defined by physical considerations such as percentage of induction motor loads and percentage of other static and dynamic loads. In real time, the composition of the electric load model is determined by the actions of the customers (who are connected and who are not). In addition the exact parameters of the dynamics of the loads may not be known. Considering these facts, we expect two important extensions of this project:

As a first extension of this project will be the ability to determine the dynamics of the electric load on line. For this purpose, one can use waveform recordings of load response during a disturbance, for example a voltage dip. The recorded waveforms during a disturbance can be utilized to provide the parameter of the real time dynamic load model. We propose that the dynamic load model developed in this project to be utilized. The parameters of this model can be identified by fitting the recorded waveform data during the disturbance to the dynamic load model. This procedure will provide the parameters of a dynamic load model that best fits the actual response of the system. Since the present reality is that disturbance recorders and relays with oscillography are plentiful in a substation, the proposed approach could be implemented in real time utilizing the existing infrastructure.

The second extension will be to further develop the prototype software into production grade software capable of dealing with very large systems. This step will be straightforward from the existing software. As a first step will be the application of the methodology using the software on a very large system. The major task (and time consuming) will be the development of the dynamic load models for such a system. This will involve manpower from a participating company, preferably PSERC member. This application will provide a better feeling of performance of the methodology in terms of execution times, what computational procedures can be improved, etc. Considering the importance of the voltage recovery phenomena, it appears that pursuing this goal will be worthwhile.

References

[1] IEEE Std. 493 2007, IEEE Recommended Practices for the Design of Reliable Industrial and Commercial Power Systems.

[2] Z. Feng, V. Ajjarapu, D.J. Maratukulam A comprehensive approach for preventive and corrective control to mitigate voltage collapse ", IEEE Transactions on Power Systems,Volume:15, Issue:2, Pages:791– 797, May 2000.

[3] A. P. Sakis Meliopoulos and George J. Cokkinides, "A Virtual Environment for Protective Relaying Evaluation and Testing", *IEEE Transactions of Power Systems*, Vol. 19, No. 1, pp. 104-111, February, 2004.

[4] A. P. Sakis Meliopoulos, George. J. Cokkinides and Thomas J. Overbye, "Component Monitoring and Dynamic Loading Visualization from Real Time Power Flow Model Data", *Proceedings of the 37st Annual Hawaii International Conference on System Sciences*, p. 58 (pp. 1-6), Big Island, Hawaii, January 5-8, 2004.

[5] Yuan Zhou and V. Ajjarapu "A Novel Approach to Trace Time Domain Trajectories of Power Systems in Multiple Time Scales" Accepted for publication in IEEE transactions on Power Systems, 2004.

[6] J. McCalley, R. Kumar, N. Elia, V. Ajjarapu, V. Vittal, H. Liu, L. Jin, O. Volij, W. Shang "Planning of reconfigurable power systems," presented at the NSF Workshop on Electric Power Networks Efficiency and Security, July 12-13, 2004, University of Puerto Rico, Mayaguez, available at the PSerc web site, located at http://www.pserc.org/ecow/get/publicatio/2004public/.

[7] T.B. Nguyen, M.A. Pai and I.A. Hiskens, "Sensitivity approaches for direct computation of critical clearing time", *International Journal of Electrical Power and Energy Systems*, Vol. 24, 2002, pp. 337-343.

[8] I.A. Hiskens and M.A. Pai, "Trajectory sensitivity analysis of hybrid systems", *IEEE Transactions on Circuits and Systems I: Fundamental Theory and Applications*, Vol. 47, No. 2, February 2000, pp. 204-220.

[9] V. Donde and I.A. Hiskens, "Guaranteeing dynamic performance in nonlinear non-smooth power systems", *Proceedings of the IFAC Symposium on Nonlinear Control Systems NOLCOS'04*, Stuttgart, Germany, September 2004.

[10] V. Donde and I.A. Hiskens, "Shooting for border collision bifurcations in hybrid systems", *Proceedings of the 42nd IEEE Conference on Decision and Control*, Maui, HI, December 2003, pp. 5514-5519.

[11] I.A. Hiskens and B. Gong, "Voltage Stability Enhancement via Model Predictive Control of Load", *Proceedings of the Symposium on Bulk Power System Dynamics and Control VI*, Cortina d'Ampezzo, Italy, September 2004.

[12] I.A. Hiskens, M.A. Pai and T. Nguyen, "Dynamic contingency analysis studies for interarea transfers", *Proceedings of 13th Power Systems Computation Conference*, Trondheim, Norway, June 1999.

[13] M. H. J. Bollen, "Voltage recovery after unbalanced and balanced voltage dips in three-phase systems," *IEEE Trans. on Power Systems*, vol. 18, issue 4, Oct. 2003, pp. 1376-1381.

[14] B. R. Williams, W. R. Schmus and D. C. Dawson, "Transmission voltage recovery delayed by stalled air conditioner compressors," *IEEE Trans. on Power Systems*, vol. 7, no. 3, Aug. 1992, pp. 1173-1181.
[15] L. Y. Taylor, and S. -M. Hsu, "Transmission voltage recovery following a fault event in the Metro Atlanta area," *Proceedings of the 2000 IEEE-PES Summer Meeting*, July 16-20, 2000, pp. 537-542.
[16] T. Sun, Z. Chen and F. Blaabjerg, "Voltage recovery of grid-connected wind turbines after a short-circuit fault," *Proceedings of the 29th Annual Conference of the IEEE Industrial Electronics Society (IECON '03)*, vol. 3, Nov. 2-6, 2003, pp. 2723-2728.
[17] T. Sun, Z. Chen and F. Blaabjerg, "Voltage recovery of grid-connected wind turbines with DFIG after a short-circuit fault," *Proceedings of the 35th Annual IEEE Power Electronics Specialists Conference (PESC '04)*, vol. 3, June 20-25, 2004, pp. 1991-1997.
[18] L. Haijun and H. W. Renzhen, "Preventing of transient voltage instability due to induction motor loads by static condenser," *Proceedings of the 1994 IEEE Conference on Industrial Technology*, Dec. 5-9, 1994, pp. 827-831.
[19] E. Hammad and M. Z. El-Sadek, "Prevention of transient voltage instabilities due to induction motor loads by static VAR compensators," *IEEE Trans. on Power Systems*, vol. 4, no. 3, Aug. 1989, pp. 1182-1190.
[20] I.A. Hamzah and J. A. Yasin, "Static VAR compensators (SVC) required to solve the problem of delayed voltage recovery following faults in the power system of the Saudi electricity company, western region (SEC-WR)," *Proceedings of the 2003 IEEE PowerTech Conference*, vol. 4, Bologna, Italy, June 23-26, 2003.
[21] F. P. de Mello, and J. W. Feltes, "Voltage oscillatory instability caused by induction motor loads," *IEEE Trans. on Power Systems*, vol. 11, no. 3, Aug. 1996, pp. 1279-1285.
[22] N. Martins, S. Gomes Jr., R. M. Henriques, C. B. Gomes, A. de Andrade Barbosa, and A. C. B. Martins, "Impact of induction motor loads in system loadability margins and damping of inter-area modes," *Proceedings of the 2003 IEEE-PES General Meeting*, Toronto, Canada, July 13-17, 2003.
[23] J. Undrill, A. Renno, and G. Drobnjak, "Dynamics of a large induction motor load system," *Proceedings of the 2003 IEEE-PES General Meeting*, Toronto, Canada, July 13-17, 2003.
[24] K. Morison, H. Hamadani, and L. Wang, "Practical issues in load modeling for voltage stability studies," *Proceedings of the 2003 IEEE-PES General Meeting*, Toronto, Canada, July 13-17, 2003.
[25] K. Tomiyama, S. Ueoka, T. Takano, I. Iyoda, K. Matsuno, K. Temma, and J. J. Paserba, "Modeling of Load During and After System Faults Based on Actual Field Data," *Proceedings of the 2003 IEEE-PES General Meeting*, Toronto, Canada, July 13-17, 2003.
[26] R. Navarro, O. Samuelsson, and S. Lindahi, "Automatic determination of parameters in dynamic load models from normal operation data," *Proceedings of the 2003 IEEE-PES General Meeting*, Toronto, Canada, July 13-17, 2003.

[27] R. Navarro, O. Samuelsson, and S. Lindahi, "Influence of normalization in dynamics reactive load models," *IEEE Trans. on Power Systems*, vol. 18, issue 2, May 2003, pp. 972-973.
[28] C. –J. Lin, A. Y. –T. Chen, C. –Y. Chiou, C. –H. Huang, H. –D. Chiang, J. –C. Wang and L. Fekih-Ahmed, "Dynamic load models in power systems using the measurement approach," *IEEE Trans. on Power Systems*, vol. 8, issue 1, Feb. 1993, pp. 309-315.
[29] D. J. Hill, "Nonlinear dynamic load models with recovery for voltage stability studies," ," *IEEE Trans. on Power Systems*, vol. 8, no. 1, Feb. 1993, pp. 166-176.
[30] D. Karlsson and D. J. Hill, "Modelling and identification of nonlinear dynamic loads in power systems," *IEEE Trans. on Power Systems*, vol. 9, no. 1, Feb. 1994, pp. 157-166.
[31] P. Sakis Meliopoulos, Wenzhong Gao, Shengyuan Li, G. J. Cokkinides and Roger Dougal, "Quadratized induction machine model for power flow analysis," *Proceedings of the Second IASTED International Conference*, *EuroPES*, Crete, Greece, pp 194-199, June 25-28, 2002.
[32] G. K. Stefopoulos and A. P. Meliopoulos, "Quadratized Three-Phase Induction Motor Model for Steady-State and Dynamic Analysis," in *Proc. of the 38th North America Power Symposium*, Carbondale, IL, USA, Sept. 17-19, 2006, pp. 79-89.
[33] G. K. Stefopoulos and A. P. Meliopoulos, "Numerical Parameter Estimation Procedure for Three Phase Induction Motor Models," *Proceedings of the 2007 PowerTech Conference*, Lausanne, Switzerland, July 1-5, 2007.
[34] G. K. Stefopoulos and A. P. Meliopoulos, "Induction motor load dynamics: Impact on voltage recovery phenomena," presented at the *2005-2006 IEEE PES T&D Conference and Exposition*, Dallas, TX, May 21-26, 2006.
[35] P. Meliopoulos, G. J. Cokkinides, and G. K. Stefopoulos, "Voltage stability and voltage recovery: Effects of electric load dynamics," presented at the *2006 IEEE International Symposium on Circuits and Systems*, Island of Kos, Greece, May 21-24, 2006.
[36] A. P. Meliopoulos, G. J. Cokkinides, and G. K. Stefopoulos, "Voltage stability and voltage recovery: load dynamics and dynamic VAr sources," presented at the *2006 IEEE PES General Meeting*, Montréal, Quebec, Canada, June 18-29, 2006.
[37] A. P. Meliopoulos, G. J. Cokkinides, and G. K. Stefopoulos, "Voltage Stability and Voltage Recovery: Load Dynamics and Dynamic VAR Sources," *Proceedings of the 2006 IEEE PES Power Systems Conference and Exposition (PSCE 2006)*, Atlanta, GA, USA, Oct. 29-Nov. 1, 2006, pp. 124-131.
[38] G. K. Stefopoulos, A. P. Meliopoulos, and G. J. Cokkinides, "Voltage-Load Dynamics: Modeling and Control," in Proceedings of the 2007 iREP Symposium on Bulk Power System Dynamics and Control – VII (iREP 2007), Charleston, SC, USA, Aug. 19-24, 2007.
[39] P. Sakis Meliopoulos, G. J. Cokkinides, and G. K. Stefopoulos, "Symbolic integration of dynamical systems by collocation methods," *Proceedings of the 2005 IEEE-PES General Meeting*, San Francisco, CA, June 12-16, 2005, pp. 2387-2392.
[40] A. P. Sakis Meliopoulos, G. J. Cokkinides, and G. K. Stefopoulos, "Quadratic integration method," *Proceedings of the 8th Int. Conference on Power System Transients (IPST 05)*, Montréal, Canada, June 19-23, 2005.

[41] G. K. Stefopoulos, G. J. Cokkinides, and A. P. Meliopoulos, "Expert symbolic transient simulator based on quadratic integration method," *presented at the 13th International Conference on Intelligent System Application to Power Systems (ISAP 2005)*, Washington DC, Nov. 6-10, 2005.

[42] A. P. Meliopoulos, G. J. Cokkinides, and G. K. Stefopoulos, "Improved numerical integration method for power/power electronic systems based on three-point collocation," *presented at the 44th IEEE Conference on Decision and Control (CDC 2005)*, Seville, Spain, Dec 12-15, 2005.

[43] A. P. Meliopoulos, G. J. Cokkinides, and G. K. Stefopoulos, "Symbolic Integration of Dynamical Systems by Collocation Methods," *Proceedings of the 2006 IEEE PES Power Systems Conference and Exposition (PSCE 2006)*, Atlanta, GA, USA, Oct. 29-Nov. 1, 2006, pp. 362-367.

[44] P. Kundur, *Power System Stability and Control*. New York: McGraw-Hill, 1994.

[45] G. K. Stefopoulos, A. P. Sakis Meliopoulos, and G. J. Cokkinides, "Probabilistic power flow with non-conforming electric loads," *Proceedings of the 8th International Conference on Probabilistic Methods Applied to Power Systems (PMAPS 2004)*, Ames, IA, Sept. 12-16, 2004, pp. 525-531.

[46] Z. Zhang, G. E. Dawson, and T. R. Eastham, "Evaluation of dynamic parameters and performance of deep-bar induction machines," *Proeedings of the IEEE-IAS Annual Meeting*, 1993, pp. 62-66.

[47] S. I. Moon and A. Keyhani, "Estimation of induction machine parameters from standstill time domain data," *Proceedings of the IEEE-IAS Annual Meeting*, 1993, pp. 336-342.

[48] J. R. Willis, G. J. Brock, and J. S. Edmonds, "Derivation of induction motor models form standstill frequency response tests," *IEEE Transactions on Energy Conversion*, vol. 4, pp. 608-615, Dec. 1989.

[49] T. A. Lipo and A. Consoli, "Modeling and simulation of induction motors with saturable leakage reactances," *IEEE Transactions on Ind. Applications*, vol. IA-21, pp. 180-189, Jan./Feb. 1984.

[50] A. Keyani and H. Tsai, "IGSPICE simulation of induction machines with saturable inductances," *IEEE Trans. Energy Conversion*, vol. 4, pp. 118-125, Mar. 1989.

[51] L. Zai, C. L. de Marco, and T. A. Lipo, "An extended Kalman filter approach to rotor time constant measurement in PWM induction motor drives," *IEEE Transactions on Ind. Applications*, vol. 28, pp. 96-104, Jan./Feb. 1992.

[52] J. Holtz and T. Thim, "Identification of the machine parameters in a vector controlled induction motor drive," *IEEE Transactions on Ind. Applications*, vol. 27, pp. 1111-1118, Nov./Dec., 1991.

[53] J. A. de Koch, F. S. van der Merwe, and H. J. Vermeuler, "Induction motor parameter estimation through and output error technique," presented at the *IEEE-PES Winter Meeting*, Columbus, OH, 1993, Paper 93-WM 01909 EC.

[54] P. Pillay, R. Nolan, and T. Haque, "Application of genetic algorithm to motor parameter determination for transient torque calculations," *IEEE Transactions on Ind. Applications*, vol. 33, no 5, pp. 1273-1282, Sept./Oct. 1997.

[55] T. Phumiphak and C. Chat-uthai, "Estimation of induction motor parameters based on field test coupled with genetic algorithm," in *Proceedings of the International Conference on Power System Technology 2002 (PowerCon 2002)*, pp. 1199-1203.

[56] H. Weatherford and C. W. Brice, "Estimation of induction motor parameters by a genetic algorithm," *Proceedings of the 2003 Annual Pulp and Paper Industry Technical Conference*, pp. 21-28.
[57] P. Nangsue, P. Pillay, S. Conry, "Evolutionary algorithms for induction motor parameter determinations," *IEEE Transactions on Energy Conversion*, vol. 14, no 3, pp. 447-453, Sept./1999.
[58] B. K. Johnson and J. R. Willis, "Tailoring induction motor analytical models to fit known motor performance characteristics and satisfy particular study needs," *IEEE Transactions on Power Systems*, vol. 6, no 3, pp. 959-965, Aug. 1991.
[59] J. Pedra and F. Corcoles, "Estimation of induction motor double-cage model parameters from manufacturer data," *IEEE Transactions on Energy Conversion*, vol. 19, no 2, June 2004.
[60] M. Cirrincione, M. Pucci, G. Cirrincione, and G-A Capolino, "A new experimental application of least squares techniques for the estimation of the induction motor parameters," *IEEE Transactions on Ind. Applications*, vol. 39, no 5, pp. 1247-1256, Sept./Oct. 2003.
[61] P. Ju, E. Handschin, Z. N. Wei, U. Schluecking, "Sequential parameter estimation of a simplified induction motor load model," *IEEE Transactions on Power Systems*, vol. 11, no 1, pp. 319-324, Feb. 1996.
[62] J. E. Dennis, Jr., R. B. Schnabel, *Numerical methods for unconstrained optimization and nonlinear equations*. SIAM 1996.
[63] P. W. Sauer, M. A. Pai, *Power System Dynamics and Stability*.
[64] P. M. Anderson, A. A. Fouad, *Power System Control and Stability*, IEEE Press, 2003.
[65] S. H. Horowitz, A. G. Phadke, *Power System Relaying*, 2nd Edition, RSP Press, 2000.
[66] ABB – *Protective Relaying Theory and Applications*, edited by W. A. Elmore, Marcel Dekker Inc., New York, 1994.
[67] D. P. Bertsekas, *Dynamic Programming and Optimal Control, volumes 1 and 2*, Athena Scientific.
[68] G.C. Ejebe and B. F. Wollenberg, "Automatic Contingency Selection," *IEEE Trans. on Power Apparatus and Systems*, vol. PAS-98, No. 1, pp. 92–104, Jan./Feb. 1979.
[69] J. Zaborszky, F.W. Whang and Prasad, "Fast contingency evaluation using concentric relaxation," *IEEE Trans. on Power Apparatus and Systems*, vol. PAS-99, No. 1, pp. 28–36, Jan./Feb. 1980.
[70] V. Brandwajn, "Efficient bounding method for linear contingency analysis," *IEEE Trans. on Power Systems*, vol. PWRS-3, No. 1, pp. 38–43, Feb. 1988.
[71] V. Brandwajn and M. G. Lauby, "Complete bounding for ac contingency analysis," *IEEE Trans. on Power Systems*, vol. PWRS-4, No. 2, pp. 724–729, May 1990.
[72] B Stott and O. Alsac, "Fast Decoupled Power Flow," *IEEE Trans. on Power Apparatus and Systems*, vol. PAS-93, No. 3, pp. 859–869, May/June 1974.
[73] O. Alsac, B. Stott and M. F. Tinney, "Sparsity-oriented Compensation Mathods for Modified Network Solutions," *IEEE Trans. on Power Apparatus and Systems*, vol. PAS-102, No. 5, pp. 1050–1060, May 1983.
[74] W. F. Tinney, V. Brandwajn and S. M. Chan, "Sparse vector method," *IEEE Trans. on Power Apparatus and Systems*, vol. PAS-104, No. 2, pp. 295–301, Feb. 1985.

[75] S. M. Chan and V. Brandwajn, "Partial matrix refactorization," *IEEE Trans. on Power Systems*, vol. PWRS-1, No. 1, pp. 193–200, Feb. 1986.
[76] R. Bacher and W. F. Tinney, "Faster local power solutions: The zero mismatch approach," *IEEE Trans. on Power Systems*, vol. PWRS-4, No. 4, pp. 1345–1354, Feb. 1989.
[77] G. Irisarri, A. M. Sasson and D. Levner, "Automatic Contingency Selection for On-Line Security Analysis – Real Time Tests," *IEEE Trans. on Power Apparatus and Systems*, vol. PAS-98, No. 5, pp. 1552–1559, Sept./Oct. 1979.
[78] A. P. Sakis Meliopoulos and C. Cheng, "A hybrid contingency selection method," in *Proceedings of the 10th Power System Computation Conference*, Graz, Austria, Aug. 1990, pp. 605–612.
[79] A. P. Sakis Meliopoulos, Carol S. Cheng, Feng Xia, "Performance Evaluation of Static Security Analysis Methods," *IEEE Trans. on Power Systems*, vol. 9, No. 3, pp. 1441–1449, Aug. 1994.
[80] Sun Wook Kang, A. P. Meliopoulos, "Contingency Selection via Quadratized Power Flow Sensitivity Analysis," in Proceedings of the IEEE 2002 Power Engineering Society Summer Meeting, vol.3, pp.1494-1499.
[81] George Stefopoulos, Fang Yang and A. P. Sakis Meliopoulos, "An Improved Contingency Ranking Method," in *Proceedings of the 35th Annual North American Power Symposium*, Oct. 20-21, 2003, Rolla, MO.
[82] G. K. Stefopoulos, F. Yang, G. J. Cokkinides, and A. P. Meliopoulos, "Advanced contingency selection methodology," presented at the *37th North American Power Symposium (NAPS 2005)*, Ames, IA, Oct. 23-25, 2005.
[83] IEEE Committee Report, "IEEE Reliability Test System," *IEEE Trans. Power Apparatus and Systems*, vol. PAS-98, No. 6, pp. 2047–2054, Nov./Dec. 1979.
[84] L.Gyugyi, "Reactive power generation and control by thyristor circuits," *IEEE Transactions on Industrial Applications*, vol. 15, no 5, pp. 521-532, Sept./Oct. 1979.
[85] L.Gyugyi, "Fundamentals of thyristor-controlled static var compensators in electric power system applications," presented at the *1987 Symposium on Application of Static Car Systems for System Dynamic Performance*, IEEE Publication no 7TH0187-5-PWR.
[86] L.Gyugyi, "Power electronics in electric utilities: static var compensators," *Proceedings of the IEEE*, vol. 76, no 4, pp. 483-494, April 1988.
[87] J. Dixon, C. Maffrand, L. Moran, "New topology for harmonic-free, dynamic var compensator using unidirectional power switches," *IEEE Publication*, no 0-7803-4489-8, pp. 835-839, 1998.
[88] M. Manjrekar, V. Venkataramanan, "Control strategies for a hybrid static reactive compensator," *IEEE CCECE*, Bozeman, pp. 834-837, 1996.
[89] L. Moran, P. Ziogas, G. Joos, "Analysis and design of a three-phase synchronous solid-state var compensator," *IEEE Transactions Industrial Application*, vol. 25, no 4, pp. 598-608, 1989.
[90] N. Choi, Y. Jung, H. Liu, G. Cho, "A high voltage large capacity dynamic var compensator using multilevel voltage source inverter," *23rd IEEE Power Electronics Specialists Conference*, vol. 1, pp. 538-545, 1992.
[91] W. Sweet, "Adrenaline for the grid: Novel superconduction device provides essentail voltage support," *IEEE Spectrium*, vol. 42, no 1, pp. 44-47, Jan. 2006.

[92] S. Kalsi, K. Weeber, H. Takesue, C. Lewis, H. Neumueuller, R. Blaugher, "Development status of rotating machines employing superconducting field windings," *Proceedings of the IEEE*, vol. 92, no 10, pp. 1688-1704, Oct. 2004.

Appendix A: Quadratized Three-Phase Power System Modeling and Analysis

Introduction

Because of the importance of the system modeling and simulation, both static and dynamic, as one of the basic analysis tools in power systems, many attempts have been made to improve the efficiency and accuracy of modeling and solution techniques. These attempts range from different formulations of the power flow or dynamic simulation problem to advanced sparsity methods and shortcuts for repeat solutions or even to attempts to obtain a direct non-iterative solution to the problem. In this section a method of reformulating the power system mathematical modeling in a way that will improve the efficiency of the solution method is presented. In this context it was observed in the early 70's that expressing the bus voltage phasors in Cartesian coordinates results in a formulation of the system model that is less complex, since trigonometric functions are absent. Going one step further, an improved idea is not only to use Cartesian coordinates for the phasor expressions, but also to "quadratize" the sytem equations, i.e., to express the equations as a set of equations with order no greater than two. It turns out that this can be achieved very easily with the introduction of additional state variables as needed. The advantage of this formulation is that the resulting system model equations are either linear or quadratic. Application of Newton's method is ideally suitable to quadratic equations. This results in the quadratized power flow (QPF) formulation, for steady state analysis, or mode generally in the quadratized power system modeling for both steady state and dynamic analysis.

When network equations are considered, the traditional power flow model consists of the power balance equations at each bus of the system. Power flow equations are expressed in the polar coordinates in terms of the systems states (bus voltage magnitudes and angles). Therefore, trigonometric terms exist in the formulated power flow equations. In addition, induction machine load are very complicated and contain very high-order terms resulting from the complex load model. Consequently, the highest order of the equations in this traditional formulation is more than two.

Quadratic system modeling, however, is set up based on applying the Kirchhoff's current law at each bus. In addition, the complex states variables are expressed in Cartesian coordinates. As a result, the system equations are quadratized as a set of equations that are linear or quadratic with order no more than two. Also trigonometric terms are absent, which makes the power flow equations less complex. Such a quadratic formulation of system model provides superior performance in two aspects: (a) faster convergence, (b) ability to model complex load characteristics, classes of loads such as interruptible load, critical load, etc, and in general complex devices without increasing the degree of nonlinearity of the whole system to more than two.

Three phase power system modeling, with emphasis on network modeling, is another important issue that is being considered in this work. Typically electric networks are modeled as single phase equivalents, using the positive sequence network of the system.

This basic structure implies the following assumptions: (1) the system operates under balanced three phase conditions, and (2) the power system is a symmetric three phase system which is fully described by its positive sequence network. Although most of the times this is quite true in transmission network analysis, in many cases these assumptions introduce deviations between the physical system and the mathematical model.

An actual power transmission system operates near balanced conditions. The imbalance may be small or large depending on the design of the system. As an example, Figure A.1 illustrates the three phase voltages and currents on an actual system. Note for example a significant difference in the currents of Phases A and B of transmission line to EDIC UEI-7 and to VOLNEY. The voltage in this case has also a significant difference between these two phases. Furthermore, the imbalances become a very important issue, when distribution feeders are modeled for distribution system analysis. The existence of single phase loads at the distribution level makes the system operate under unbalanced conditions and therefore full three phase analysis is highly desired in these cases. Since most of the voltage problems may appear at the distribution level, close to load centers and mainly affect sensitive loads at load centers the ability of modeling and performing analysis at the distribution level is highly desired.

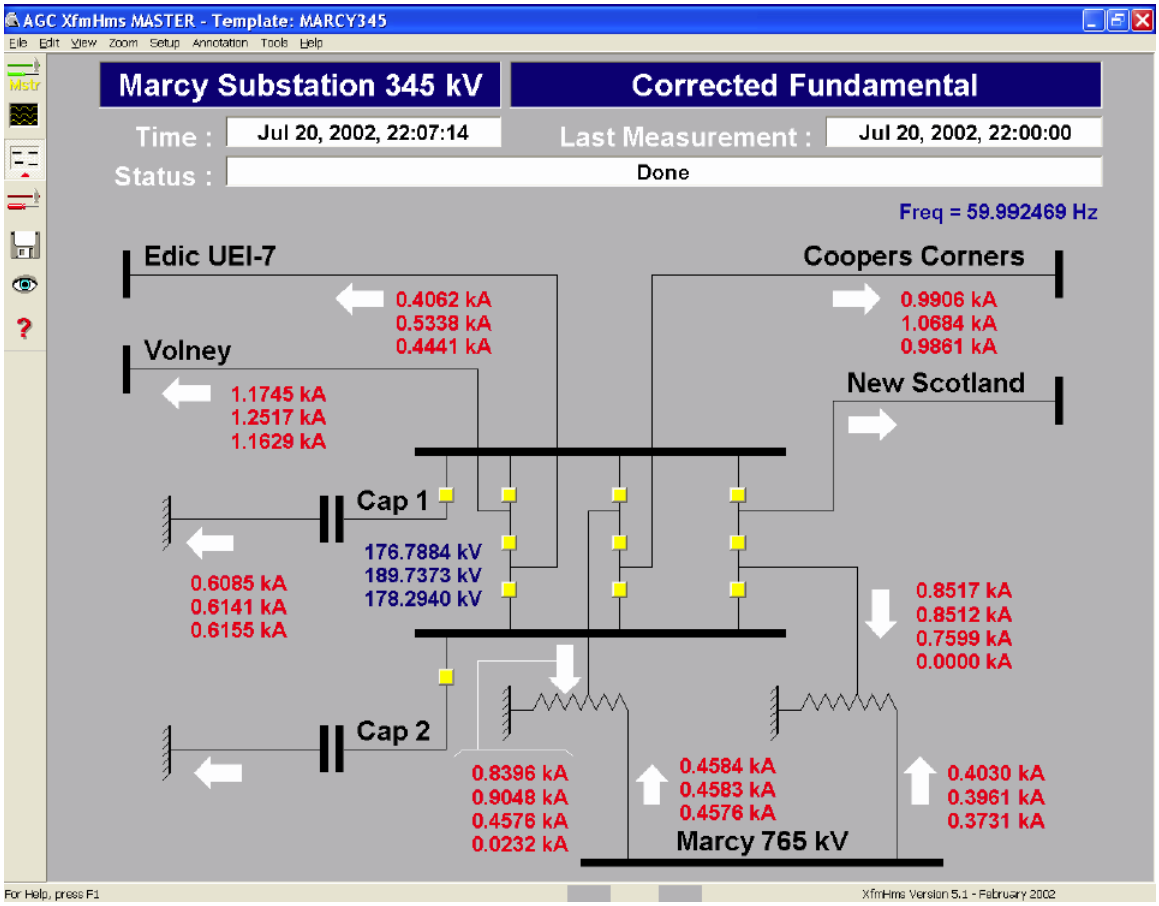


Figure A.1. Actual three phase voltages and currents in MARCY 345 kV substation, at NYPA.

Moreover, an actual power transmission system is never symmetric. While some power system elements are designed to be near symmetric, transmission lines are never symmetric. The impedance of any phase is different than the impedance of any other phase. In many cases, this imbalance can be corrected with transposition, however, because of cost many lines are not transposed. The asymmetry may be small or large depending on the design of the system. One power system component that contributes to the asymmetry is the three phase untransposed line. As an example, Figure A.2 illustrates an actual three phase line configuration.

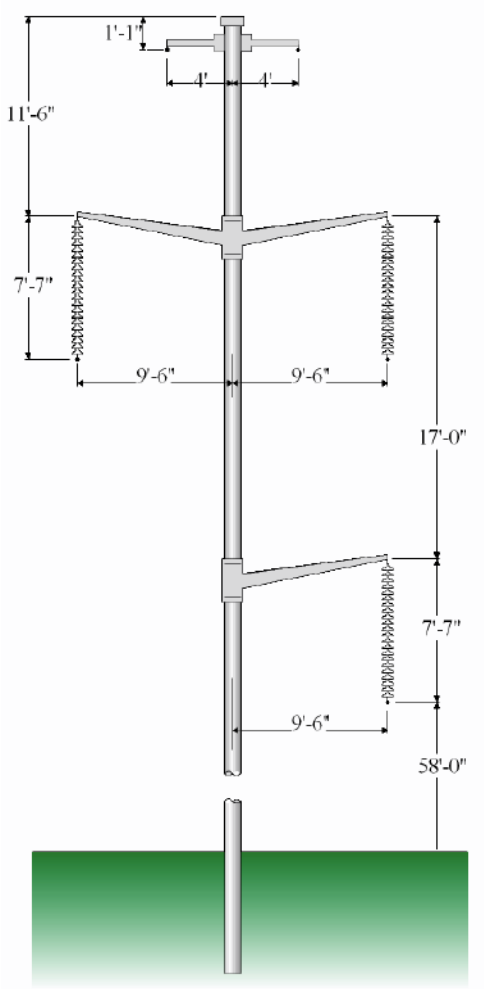


Figure A.2. Typical transmission line construction.

For the purpose of quantifying the asymmetry of this line, two asymmetry metrics are defined:

$$S_1 = \frac{1}{2}\frac{|z_{\max} - z_{\min}|}{|z_1|} \quad \text{(A.1)}$$

$$S_2 = \frac{1}{2}\frac{|y_{\max} - y_{\min}|}{|y_1|} \quad \text{(A.2)}$$

where z_1 is the positive sequence series impedance of the line, z_{max} and z_{min} are the max and min series impedances of the individual phases, y_1 is the positive sequence shunt admittance of the line, y_{max} and y_{min} are the max and min shunt admittances of the individual phases. The above indices provide, in a quantitative manner, the level of asymmetry among phases of a transmission line. As a numerical example, these metrics have been computed for the line of Figure A.2 and are presented in Figure A.3. Note that the asymmetry is in the order of 5 to 6%.

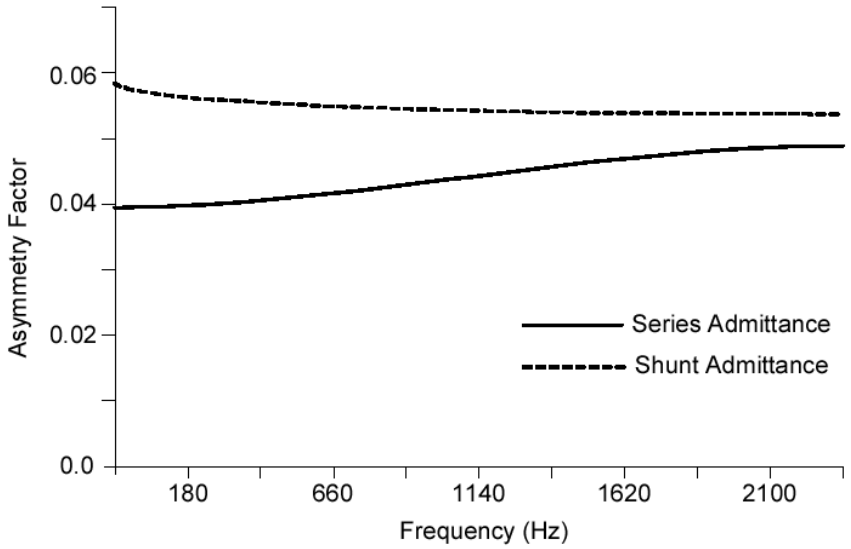


Figure A.3. Line Asymmetry Indices (Line of Figure A.2).

For these reasons three phase modeling has been adopted in this report. Three phase models of the various system components have been described in the main part of the report.

Quadratic Three Phase Modeling: Steady State Analysis

In general, at a bus, there may be generation, loads (various types of loads), circuits, shunt devices, etc. The general bus of a system with several connected components is illustrated in Figure A.4. While the circuits and shunt terms are linear elements, the loads and generation may operate in such a way that imposes nonlinearities. Common loads models are: (a) three phase and single phase constant power load, (b) three phase and single phase constant impedance load and (c) induction motor loads. Common operating modes of generating units for steady state analysis are: (a) constant voltage, constant real power operation, (b) constant real power constant power factor operation. The new quadratic modeling approach consists of writing the Kirchoff's current law at each bus of the system. The models of loads and generators are expressed in terms of their terminal current and additional equations in additional internal state variables that define their operating mode. The additional equations may be nonlinear, but of order no higher than two. This can be achieved without any approximations (therefore only the mathematical formulation is different, the physical models are the same) by introducing additional state variables. The resulting set of equations is consistent, i.e., the number of equations equals

the number of unknowns. In addition, the set of equations are linear or quadratic in terms of the state variables. These equations are solved via Newton's method. The proposed model has two advantages: (a) the resulting model is more accurate than usual models without increasing the complexity of the equations and (b) the convergence characteristics of the proposed model are superior to conventional methods.

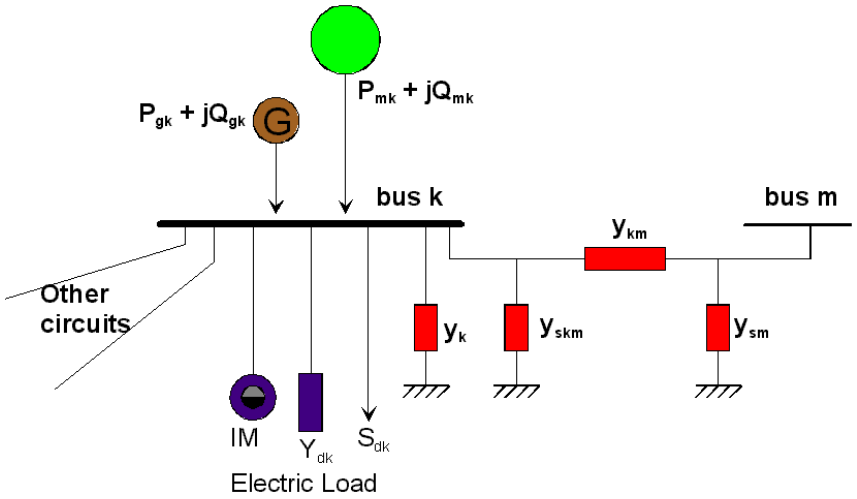


Figure A.4. General power system bus.

As discussed above each component of the system can be represented with an appropriate set of linear or quadratic equations. By expressing the voltage and current phasors with their Cartesian coordinates (i.e., $\tilde{I} = I_r + I_i$ and $\tilde{V} = V_r + V_i$) the following general form is obtained for any power system component:

$$\begin{bmatrix} I_r^k \\ I_i^k \\ 0 \end{bmatrix} = y_{eq\_real}^k \begin{bmatrix} V_r^k \\ V_i^k \\ y^k \end{bmatrix} + \begin{bmatrix} x^{kT} f_{eq\_real1}^k x^k \\ x^{kT} f_{eq\_real2}^k x^k \\ \cdots \end{bmatrix} - b_{eq\_real}^k \qquad \text{(A.3)}$$

where: $x^k = \begin{bmatrix} V_r^k \\ V_i^k \\ y^k \end{bmatrix}$

and $y_{eq\_real}^k$, $b_{eq\_real}^k$, and $f_{eq\_real}^k$ are matrices with appropriate dimensions.

Application of Kirchoff's current law at each bus of the system, like bus k of Figure A.4, eliminates the left hand side, current variables and results in a quadratic set of equations for the whole system of the form:

$$\begin{bmatrix} 0 \\ 0 \\ 0 \end{bmatrix} = Y_{eq\_real} \begin{bmatrix} V_r \\ V_i \\ y \end{bmatrix} + \begin{bmatrix} x^T F_{eq\_real1} x \\ x^T F_{eq\_real2} x \\ \cdots \end{bmatrix} - B_{eq\_real} \qquad \text{(A.4)}$$

Quadratic Three Phase Modeling: Dynamic Analysis

Note that this form is also directly applicable to dynamic component modeling, after the differential equations have been converted to algebraic equations using some numerical integration rule. In our case the quadratic integration rule is assumed, as presented in Appendix B. For this case, the following conventions have been used to construct the generalized algebraic.quadratized component form of each model:

The general model consists of differential and algebraic equations of the form:

$$\begin{aligned} \frac{dx(t)}{dt} &= f(x(t),t) \\ 0 &= g(x(t),y(t),t) \end{aligned} \qquad \text{(A.5)}$$

where $x(t)$ and $y(t)$ denote the dynamic and algebraic states respectively. Note that via the quadratization process f and g are at most quadratic.

After applying the quadratic integration rule at the interval $[t-h,t]$ the differential equations become algebraic equations involving the values of the dynamical states at times $t-h$, t, and at the midpoint of the interval t_m. The compact expression of the rule is:

$$\begin{aligned} &\frac{h}{24} f\left(t,x(t)\right) + x_m - \frac{h}{3} f\left(t_m,x_m\right) = x(t-h) + \frac{5h}{24} f\left(t-h,x(t-h)\right) \\ &x(t) - \frac{h}{6} f\left(t,x(t)\right) - \frac{2h}{3} f\left(t_m,x_m\right) = x(t-h) + \frac{h}{6} f\left(t-h,x(t-h)\right) \end{aligned} \qquad \text{(A.6)}$$

The algebraic equations are appended to the algebrized differential equations at times t and t_m and this results in a consistent set of equations (equal number of equations and unknowns). The unknowns are the values of the states (dynamic x and algebraic y) at times t and t_m. The values at $t-h$ are known values from the previous time step. These equations are solved for the unknown quantities at each time step.

For the construction and solution of the network equations the resulting set of algebraic equations for each component need to be written in an algebraic companion form. This form contains the equations for the through variables of the model (in our case terminal currents) along with the additional model equations. The equations of the through variables are referred to as external or interface equations, while the rest model equations are internal. The through variables are not unknowns, but are just used as a means of connecting the device to the rest of the network. They are eliminated after the application of the connectivity constraints (in our case Kirchoff's current law). The generalized component companion form, at each time step $[t-h,t]$ has the general form:

$$\begin{bmatrix} I \\ 0 \end{bmatrix} = A \cdot X + \begin{bmatrix} X^T F_1 X \\ ... \\ X^T F_n X \end{bmatrix} - b, \qquad \text{(A.7)}$$

where
I denotes the through variables
X denotes the total state vector
A is the coefficient matrix for the linear terms
F_i is the coefficient matrix for the quadratic terms for each equation i
n is the total number of equations and also unknowns
b is the vector of past history terms and constant or state independent terms (e.g. inputs)

The ordering of the model equations is as follows:
The equations are separated into two main groups: equations at time t and equations at time t_m. Equations at time t are listed first, followed by equations at time t_m.
First, the external equations (terminal currents) are listed. Then, the algebraic equations resulting from discretizing the differential equations by applying the quadratic integration rule from time $t-h$ to time t. Finally the remaining internal algebraic equations at time t; the linear equations go first and the nonlinear (quadratic) next. The further ordering of the internal equations (and equations) is arbitrary and it is done in a way so that the resulting equations have diagonal dominance. The same ordering is used for the second group of equations, at time t_m. The external equations at time t_m are first, followed by the discretized differential equations after integrating from $t-h$ to time t_m, and then followed by the internal algebraic equations at time t_m.

The ordering of the total state vector X, follows the equation ordering and is as follows:
It should be noted again that since application of the quadratic integration yields the values of the states at times t and t_m, each state variable exists at two time instants in the state vector. The ordering used in the state vector assumes two groups of variable: each variable at time t is first, followed by the variables at time t_m in the same order. The terminal device voltages v are called external states, since they interface the device with the rest of the network and they are states shared by other devices as well (connected to the same nodes). Other variables can also be external states. These variables, at time t, appear first in the state vector in correspondence with the equations for the though variables. The rest of the states are referred to as internal device states. They correspond to equations with zero left-hand-side. The dynamic states, at time t, are listed next, followed by the algebraic states at time t, first the linear and then the nonlinear. Then the group of variables at time t_m follows with the same ordering.

For implementation reasons it preferable to convert all the differential equations to linear equations of the very simple form:

$\frac{dx(t)}{dt} = x'(t)$, (where $x'(t)$ is part of the internal states and can be either linear or nonlinear) and move all the nonlinearities to the algebraic equations. Therefore, based on the ordering and grouping described above in compact matrix notation the model () can be put in the general form:

$$i(t) = A_1(t)v(t) + A_2(t)x(t) + A_3(t)y(t) + A_4(t)z(t) \quad \text{[external equations]}$$

$$0 = \frac{dx(t)}{dt} + B_1(t)v(t) + B_2(t)x(t) + B_3(t)y(t) + B_4(t)z(t) \quad \text{[differential equations]}$$

$$0 = C_1(t)v(t) + C_2(t)x(t) + C_3(t)y(t) + C_4(t)z(t) \quad \text{[linear internal equations]}$$

$$0 = q(v(t), x(t), y(t), z(t), t) \quad \text{[nonlinear internal equations]}$$

where

$v(t)$ are the external states,

$x(t)$ are the internal dynamic states,

$y(t)$ are the internal linear algebraic states, and

$z(t)$ are the internal nonlinear algebraic states.

The coefficient matrices A_1 to A_4, B_1 to B_4, C_1 to C_4 can be constant or time varying in the general case (like for example when the system configuration is changing, there are discrete switchings in the system or there exist limits). Equations q are the system nonlinear equations.

Therefore, after applying the quadratic integration rule the differential equations become algebraic and the state vector at each time step is [assuming i external equations (and states), k internal dynamic equations (and states), j internal algebraic linear equations (and corresponding states) and l internal algebraic nonlinear equations (and corresponding states)]:

$$X = \left[X^T(t) \quad X^T(t_m)\right]^T$$

with $X(t) = \left[v^T(t) \quad x^T(t) \quad y^T(t) \quad z^T(t)\right]^T$ and $X(t_m) = \left[v^T(t_m) \quad x^T(t_m) \quad y^T(t_m) \quad z^T(t_m)\right]^T$ where

$$v(t) = \left[v_1(t) \quad ... \quad v_i(t)\right]^T$$

$$x(t) = \left[x_1(t) \quad ... \quad x_k(t)\right]^T$$

$$y(t) = \left[y_1(t) \quad ... \quad y_j(t)\right]^T$$

$$z(t) = \left[z_1(t) \quad ... \quad z_l(t)\right]^T$$

$$v(t_m) = \begin{bmatrix} v_1(t_m) & \dots & v_i(t_m) \end{bmatrix}^T$$
$$x(t_m) = \begin{bmatrix} x_1(t_m) & \dots & x_k(t_m) \end{bmatrix}^T$$
$$y(t_m) = \begin{bmatrix} y_1(t_m) & \dots & y_j(t_m) \end{bmatrix}^T$$
$$z(t_m) = \begin{bmatrix} z_1(t_m) & \dots & z_l(t_m) \end{bmatrix}^T$$

and the equations in quadratic form are:

$$\begin{bmatrix} i_1(t) \\ \dots \\ i_i(t) \\ 0 \\ \dots \\ 0 \\ i_1(t_m) \\ \dots \\ i_i(t_m) \\ 0 \\ \dots \\ 0 \end{bmatrix} = A \cdot \begin{bmatrix} v(t) \\ x(t) \\ y(t) \\ z(t) \\ v(t_m) \\ x(t_m) \\ y(t_m) \\ z(t_m) \end{bmatrix} + \begin{bmatrix} X^T F_1 X \\ \dots \\ X^T F_n X \end{bmatrix} - b$$

External states: $v_1(t),\dots,v_i(t),v_1(t_m),\dots,v_i(t_m)$

Internal dynamical states: $x_1(t),\dots,x_k(t),x_1(t_m),\dots,x_k(t_m)$

Internal linear algebraic states: $y_1(t),\dots,y_j(t),y_1(t_m),\dots,y_j(t_m)$

Internal nonlinear algebraic states: $z_1(t),\dots,z_l(t),z_1(t_m),\dots,z_l(t_m)$

Through variables: $i_1(t),\dots,i_i(t),i_1(t_m),\dots,i_i(t_m)$

Solution Method

The solution method is the same, for both steady state or dynamic analysis. The network solution is obtained with application of Newton's method to a quadratized form of the network equations. The quadratized network equations are generated as follows. Consider the general form of equations for any model of the system (linear or nonlinear). Note that this form includes two major sets of equation, which are named external equations or current equations and internal equations respectively. The electric currents at the terminals of the component appear only in the external equations. Similarly, the device states consist of two variable sets: external states (i.e., bus voltage $\tilde{V}^k = V_r^k + jV_i^k$) and internal state variables y^k (if any). The set of equations is consistent in the sense that the number of external states and the number of internal states equal the number of external and internal equations respectively.

The entire network equations are obtained by application of the connectivity constraints among the system components, i.e., Kirchoff's current law at each system bus. Specifically, Kirchoff's current law applied to all buses of the system yields:

$$\sum_k A^k \tilde{I}^k = 0, \tag{A.8}$$

where $\tilde{I}^k = I_r^k + jI_i^k$ is the device k bus current injections, and A^k is a component incidence matrix with:

$$\{A_{ij}^k\} = \begin{cases} 1, \text{ if bus j of device k is connected to bus i} \\ 0, \qquad \text{otherwise} \end{cases} \tag{A.9}$$

All the internal equations from all devices should be added to the above equation, yielding the following set of equations:

$$\begin{cases} \sum_k A^k \tilde{I}^k = 0 \\ [\text{internal equations of all devices}] \end{cases} \tag{A.10}$$

Let $\tilde{V} = V_r + jV_i$ be the vector of all bus voltage phasors. Then, the following relationship hold:

$$\tilde{V}^k = (A^k)^T \tilde{V}, \tag{A.11}$$

where $\tilde{V}^k$ is device k bus voltage.

Equations (A.11) can be separated into two sets of real equations by expressing the voltages and currents with their Cartesian coordinates. Then the device currents can be eliminated with the use of equations (A.8). This procedure will yield a set of equations in terms of the voltage variables and the internal device state variables. If all the state variables are represented with the vector x, then the equations can be written in the following form:

$$G(x) = Y_{real} x + \begin{bmatrix} x^T f_1 x \\ x^T f_2 x \\ \cdots \end{bmatrix} - B_{real} = 0, \tag{A.12}$$

where x is the vector of all the state variables and Y_{real}, f, B_{real} are matrices with appropriate dimensions. The simultaneous solution of these equations is obtained via Newton's method as described next.

Equation (A.12) is solved using Newton's method. Specifically, the solution is given by the following algorithm:

$$x^{v+1} = x^{v} - J_G^{-1}\left\{ Y_{real}x^{v} + \begin{bmatrix} x^{vT} f_1 x^{v} \\ x^{vT} f_2 x^{v} \\ \cdots \end{bmatrix} - B_{real} \right\} \tag{A.13}$$

where v is the iteration step number; J_G is the Jacobian matrix of the function $G(x)$ in equation (A.12). In particular, the Jacobian matrix takes the following form:

$$J_G = Y_{real} + \begin{bmatrix} x^{vT}\left(f_1 + f_1^{T}\right) \\ x^{vT}\left(f_2 + f_2^{T}\right) \\ \cdots \end{bmatrix} \tag{A.14}$$

It is important to note that Newton's method is ideally suited for solution of quadratic equations.

Appendix B: Quadratic Integration Method

Introduction

This section of the proposal describes a new proposed approach for power system time domain simulation. The new methodology, referred to as quadratic integration method, is based on the following two innovations: (a) the nonlinear system-model equations (nonlinear differential or differential-algebraic equations) are reformulated to a fully equivalent system of linear differential and quadratic algebraic equations, by introducing additional state variables and algebraic equations, and (b) the system model equations are integrated using a numerical integration scheme that assumes that the system states vary quadratically within an integration time step, as functions of time (quadratic integration). As a comparison, in the trapezoidal rule it is assumed that the system functions/states vary linearly throughout a time step.

This basic concept in the derivation of the quadratic integration method is illustrated in Figure B.9.5. Note that within an integration time step of length h, defined by the interval $[t-h,t]$, the two end points, $x(t-h)$, $x(t)$, and the midpoint $x(t_m) = x(t-h/2)$ fully define the quadratic function in the interval $[t-h,t]$. This quadratic function is integrated in the time interval $[t-h,t]$ resulting in a set of algebraic equations for this integration step. The solution of the equations is obtained via Newton's method, in the general, nonlinear system case, or via a direct solution in the linear case. Note that by virtue of the first step of quadratization the resulting algebraic equations are either linear or quadratic. The proposed method demonstrates improved convergence characteristics of the iterative solution algorithm. It is an implicit numerical integration method (it can be easily observed that it makes use of information at the unknown point $x(t)$) and therefore demonstrates the desired advanced numerical stability properties compared to explicit methods. It is also fourth order accurate and therefore much more precise compared to all the traditionally used methods in power system applications. Furthermore, the proposed method does not suffer from the numerical oscillation problem, contrary to the trapezoidal rule.

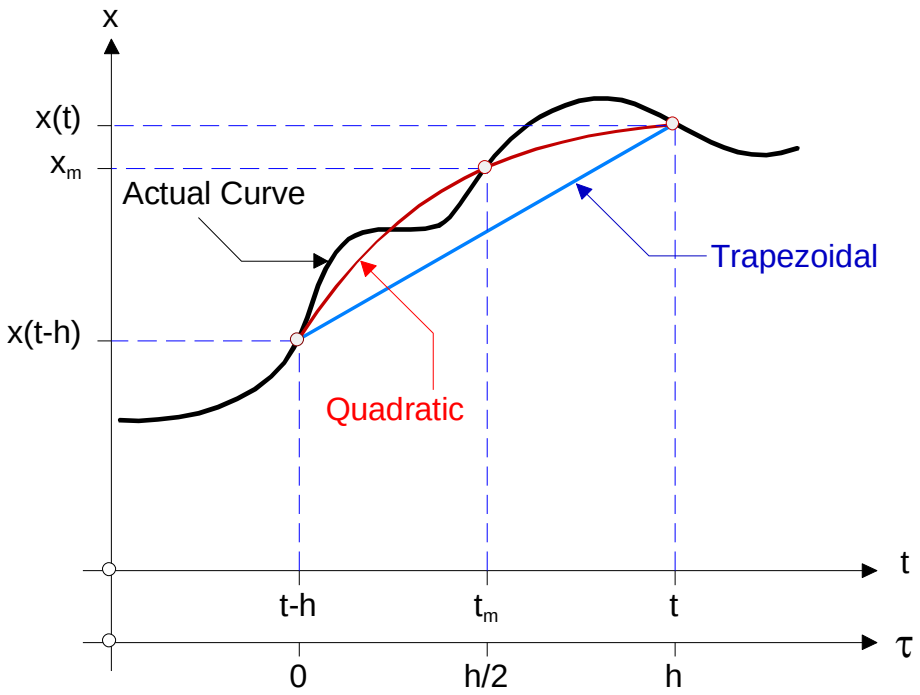


Figure B.9.5. Illustration of the Quadratic Integration Method - Basic Assumption. Description of Quadratic Integration Method

Description of Quadratic Integration Method

This section presents the key features of the quadratic integration method. The method is based on two innovations: First, the nonlinear system-model equations (nonlinear differential or differential-algebraic equations) are reformulated to a fully equivalent system of linear differential and quadratic algebraic equations, by introducing additional state variables and additional algebraic equations. This step aims in reducing the nonlinearity of the system to at most quadratic in an attempt to improve the efficiency of the solution algorithm, as well as facilitate the method implementation, especially for large complex models. It is independent of the integration method and thus can be applied in combination with any numerical integration rule. Second, the system model equations are integrated using the implicit numerical scheme that was conceptually described in the introductory section of this chapter.

The quadratic integration method belongs to the category of implicit, one-step, Runge-Kutta methods. More specifically it is an implicit Runge-Kutta method based on collocation and it can be alternative derived based on the collocation theory. The basic idea is to choose a function from a simple space, like the polynomial space, and a set of collocation points, and require that the function satisfy the given problem equations at the collocation points [21]-[23]. The method has three collocation points, at $x(t-h)$, $x_m = x(t_m)$, and $x(t)$. It uses the Lobatto quadrature rules and is a member of the Lobatto-methods family. Any Lobatto method with s collocation points has an order of accuracy of $2s-2$, and therefore the method is order four accurate [21]-[23].
Assuming the general nonlinear, non-autonomous dynamical system:

$$\dot{x} = f(t, x) \tag{B.1}$$

the algebraic equations at each integration step of length h, resulting from the quadratic integration method, are:

$$\begin{aligned} x_m - \frac{h}{3} f(t_m, x_m) + \frac{h}{24} f(t, x(t)) &= x(t-h) + \frac{5h}{24} f(t-h, x(t-h)) \\ x(t) - \frac{2h}{3} f(t_m, x_m) - \frac{h}{6} f(t, x(t)) &= x(t-h) + \frac{h}{6} f(t-h, x(t-h)) \end{aligned} \tag{B.2}$$

Solution of the system, via Newton's method in practice, yields the value of the state vector $x(t)$. Note that the value at the midpoint, x_m, is simply an intermediate result and it is discarded at the end of the calculations at each step. For the special case of a linear system,

$$\dot{x} = Ax + Bu\,, \tag{B.3}$$

the algebraic equations at each time step become:

$$\begin{bmatrix} \frac{h}{24}A & I - \frac{h}{3}A \\ I - \frac{h}{6}A & -\frac{2h}{3}A \end{bmatrix} \cdot \begin{bmatrix} x(t) \\ x_m \end{bmatrix} = \begin{bmatrix} \left(I + \frac{5h}{24}A\right) \\ \left(I + \frac{h}{6}A\right) \end{bmatrix} \cdot x(t-h) + \begin{bmatrix} -\frac{h}{24}B & \frac{5h}{24}B & \frac{h}{3}B \\ \frac{h}{6}B & \frac{h}{6}B & \frac{2h}{3}B \end{bmatrix} \cdot \begin{bmatrix} u(t) \\ u(t-h) \\ u_m \end{bmatrix}, \tag{B.4}$$

where I is the identity matrix of proper dimension and h the length of the integration step.

The proposed integration approach has the following advantages: (a) improved accuracy and numerical stability, and (b) free of fictitious numerical oscillations. Details about the numerical properties of the method are discussed next.

Numerical properties

The basic numerical stability properties of a numerical integration method are studied using the first order test equation:

$$\dot{x} = ax. \tag{B.5}$$

Applying the quadratic integration method yields at each time step:

$$\begin{bmatrix} x(t) \\ x_m \end{bmatrix} = \begin{bmatrix} \left(\frac{12 + 6ah + a^2h^2}{12 - 6ah + a^2h^2}\right) \\ \left(\frac{12 - 0.5a^2h^2}{12 - 6ah + a^2h^2}\right) \end{bmatrix} x(t-h) \tag{B.6}$$

and therefore:

$$x(t) = \frac{12 + 6ah + a^2h^2}{12 - 6ah + a^2h^2} \cdot x(t-h)\,, \tag{B.7}$$

where h is the integration step. Setting $z = ah$ yields the characteristic polynomial for the method:

$$R(z) = \frac{z^2 + 6z + 12}{z^2 - 6z + 12} \qquad \text{(B.8)}$$

Note that the eigenvalue a of the system can be complex, so z is in general a complex number.

The region of absolute stability is given by the set of values z such that $|R(z)| \le 1$. A method is called A-stable if the region of absolute stability in the complex z-plane contains the entire left half plane. This means that independently of the step size $h > 0$, a stable eigenvalue a of the original continuous time system, with $\mathrm{Re}(a) < 0$, will be still represented as a stable mode in the discrete time system, and thus the discrete system mimics accurately the behavior of the original system, in terms of stability. Note that for $\mathrm{Re}(z) < 0$ it follows that $|R(z)| \le 1$. Therefore, the proposed method is A-stable.

Furthermore, the absolute stability region is exactly the left-hand half complex plane. This property is called strict A-stability. If the dynamical system under study includes an unstable mode, then, irrespectively of the integration step-size, this mode will remain unstable in the descretized system. This is not the case for other methods, for example, the backward Euler, or the BDF linear multi-step methods, where the numerical stability domain extends in the right-hand plane, where $\mathrm{Re}(z) > 0$. In this case, if the real dynamical system includes an unstable mode, this mode could appear as stable for some step size, in the discrete system.

Comparing the quadratic and the trapezoidal integration methods the following hold:

1. Both the trapezoidal method and the quadratic integration method are strictly A-stable. The characteristic polynomial for the trapezoidal method is $R(z) = \frac{2+z}{2-z}$, and it holds that $R(z) \le 1$ in the whole left-hand complex plane, i.e., $\mathrm{Re}(z) < 0$.
2. The trapezoidal method is second order accurate. The quadratic integration is a fourth order method. Therefore, in terms of accuracy, quadratic integration is much preferable. This however, comes with the drawback of additional computational expense.
3. It has been observed in applications that the trapezoidal method can provide an oscillatory solution even for systems that have exponential solutions as the simple test equation above. This is apparent if one considers the term $R(z) = \frac{2+z}{2-z}$ for a physically stable system. Note that it is possible to select the integration time step ($z = ah$), so that this term is negative (for example any real value for z, with $z < -2$). This can occur when larger integration steps are selected. In this case the solution will be oscillatory, oscillating around the true solution of the problem. In the case of the quadratic integration, the corresponding term $R(z) = \frac{z^2 + 6z + 12}{z^2 - 6z + 12}$ can

never be negative as long as $\mathrm{Re}(z)$ is negative, i.e. as long as the physical system is stable. Therefore, it appears that this method is free of such fictitious oscillations. This can be a very nice characteristic in many applications. The behavior of the quadratic integration method in terms of this issue is still under investigation and will be part of the future work associated with this research.

As described, the proposed quadratic integration method is a one-step implicit Runge-Kutta method based on collocation. The trapezoidal integration method can be also viewed as a member of this category; however, trapezoidal rule uses two collocation points, while the proposed method uses three. This provides a great advantage in terms of accuracy. As every numerical integration method, the quadratic integration directly converts the system of differential equations to a set of algebraic equations, at each integration step. The formulation of these equations is straightforward and the procedure can also be automated. This can facilitate the process in more complicated models. However, the number of algebraic equations of the quadratic integration scheme is double compared to that of the trapezoidal rule, due to the additional collocation point. The end-result is increased computational effort compared to the trapezoidal method per iteration (approximately double when sparsity techniques are used). Nonetheless, the improved method accuracy (order four, compared to order two of the trapezoidal method) allows the use of larger time-steps, so that the total computational effort becomes less than that of trapezoidal integration, while the accuracy remains significantly higher. The trade-off between accuracy and computational speed applies also to higher order implicit Runge-Kutta methods. As the number of collocation points, and thus the order, increase, the computational effort also increases. It appears that the quadratic integration method achieves a good balance between accuracy and computational speed.

The proposed method also appears to possess better numerical properties and be more accurate when compared to linear, multi-step methods commonly used in power system transient analysis. The use of such methods is usually restricted to order two accurate methods. Detailed comparison of the quadratic integration and linear, multi-step methods used will be reported in future work of this research.

Appendix C: Review of VAR Sources and Models

Introduction

This Appendix presents a literature review of currently available reactive power compensator designs. The objective of the review is to give a general overview of VAR compensator strategies in order to provide background in designing and implementing a dynamic VAR source model for power networks. The Appendix is organized as follows. In the first section a literature survey is presented which documents the available technologies for Dynamic VAR compensators. Then in the second section the effects of harmonics are discussed and harmonic models are presented. Models for the steady state operation follow in the third section and finally dynamic operation models of the most common designs of VAR compensators are presented.

Literature Survey

Thyristor-Controlled Reactor (TCR)

A thyristor controlled reactor (Figure C.1) consists of a fixed inductor and a bidirectional thyristor switch. In order to meet the required blocking voltage levels at a given power rating many thyristors are connected in series [84], [85]. The thyristor switch is turned on via a gate pulse fired simultaneously to all thyristors with the same polarity, which will block instantaneously after the ac current crosses zero. The current in the inductor is controlled from maximum to zero through firing delay angle control (α), which is the closure of the thyristor switch delayed with respect to the applied voltage per half cycle [86]. This means current conduction intervals can be controlled and modulated. The draw-back of the firing delay angle control is the generation of harmonics due to the non-sinusoidal current waveform. However, in a three-phase system, if three TCRs are delta connected and are under balanced conditions the triplen harmonic currents only circulate in the TCR system and never enter the power network. The other harmonics generated can be filtered and reduced by multipulse and multibank circuits.

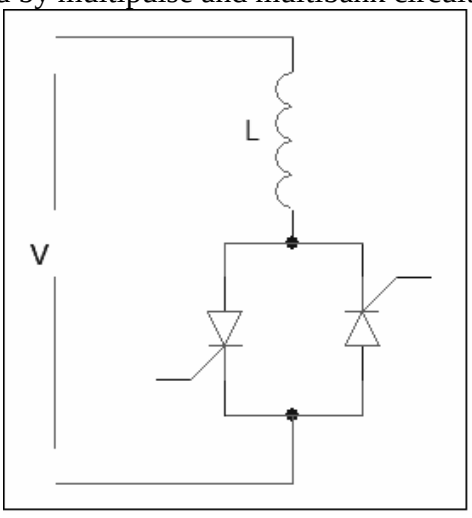


Figure C.1. Thyristor-Controlled Reactor.

Thyristor-Switched Capacitor (TSC)

A thyristor controlled capacitor (Figure C.2) is very similar to a TCR. It consists of a bidirectional thyristor, a capacitor and a surge current limiting inductor [84]. Normally, the TSC is connected to (switched in) the ac voltage source. It is disconnected (switched out) at current zero by former removal of the gate drive to the thyristor switch. Usually, the capacitor is discharged after disconnection and the reconnection of the capacitor is implemented at the residual voltage between zero and peak, which introduced transient disturbances [85]. The disturbances can be minimized if the thyristor switch is turned on at the instances when the residual capacitor voltage and the applied voltage are equal.

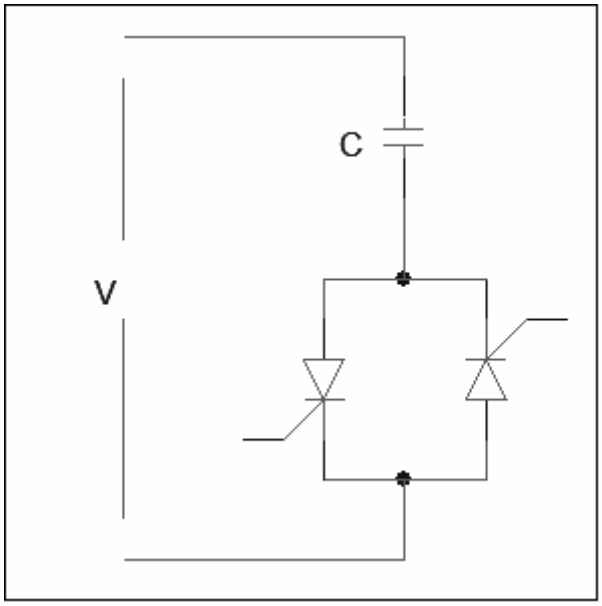


Figure C.2. Thyristor-Switched Capacitor.

Fixed-Capacitor-Thyristor-Controlled Reactor Type VAr Compensator (FC-TCR)

The arrangement of FC-TCR (Figure C.3) is a TCR connected in parallel with a fixed capacitor. The current in the TCR is modulated via firing delay angle control and the fixed capacitor is the representation of a filter network that has the capability of generating the VARs needed [85]. The variable var output is achieved through the opposition of VAR generation by the capacitor and var absorption by the TCR. The control of the FC-TCR has four functions, synchronous timing, firing angle conversion, computation of reactor current, and thyristor firing pulse generation [86]. By controlling the four functions, maximum capacitive var generation is achieve when the TCR is off (angle = 90 deg), and to decrease the var output the current in the TCR is increased by decreasing the delay angle. The losses in a FC-TCR is high due to the indirect generation of zero var output (via cancellation), therefore it is disadvantageous in power transmission systems. Since this compensator only uses one single capacitor for reactive storage, the output current and voltages will have significant harmonics and the range of the vars provided will be limited as well.

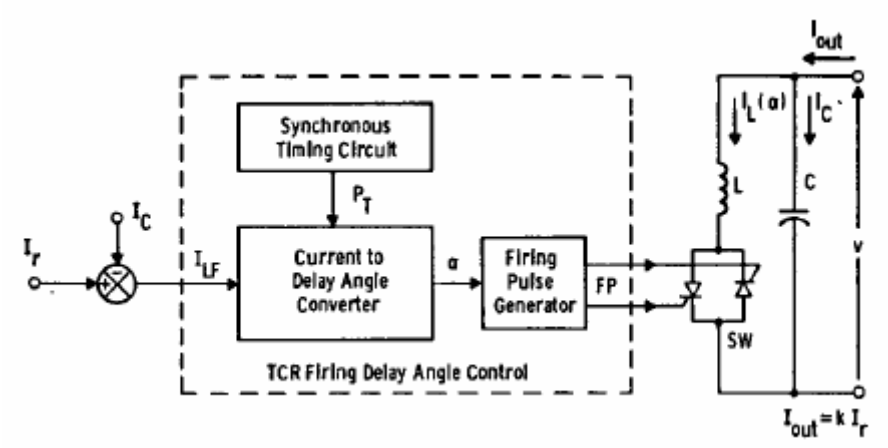


Figure C.3. Fixed-Capacitor Thyristor-Controlled Reactor.

Thyristor-Switched Capacitor-Thyristor-Controlled Reactor Type VAr Compensator (TSC-TCR)

The arrangement of TSC-TCR (Figure C.4) is n TSC branches and one TCR branch, all connected in parallel. The number of branches is determined by various transmission system requirements such as operating voltage, current rating, cost, etc. The operation of the TSC-TCR is similar to FC-TCR, except the capacitive var generation is achieved via n intervals each ranging from zero to Var(max)/n. Depending on the requirement of the power system each TSC branch can be activated by turning on the thyristor switches for each branch and the summation of the TSC and TCR branch produces the total var output of the generator [86]. The control for the TSC-TCR requires three functions, determining the number of TSC branches, transient free control of switching, and firing delay angle control. The power loss of the TSC-TCR is zero at zero var output, but increases as more TSC branches are switched on [86]. This is advantageous in dynamic compensation applications that do no require high average var output. It also provides better range of reactive power by selecting different values of capacitors and branch switching.

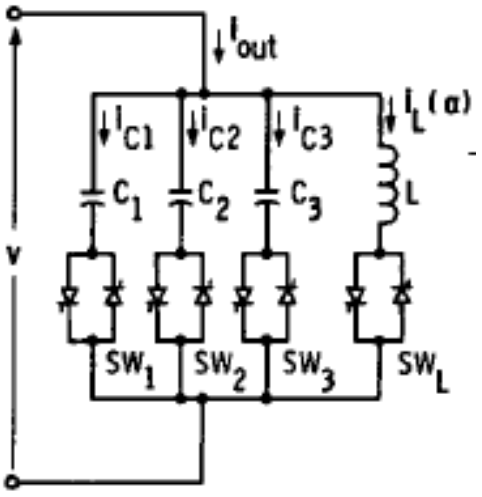


Figure C.4. Thyristor Controlled Reactor-Thyristor Switched Capacitor.

Unidirectional Power Switched Var Compensator

The unidirectional power switched var generator (Figure C.5) differs from the other generators in that it only uses capacitors. It does not generate harmonics, it is cheaper, compensates reactive power cycle by cycle, no forced switches, and no in rush issues. The layout is a binary chain of capacitor branches with unidirectionally controlled switches, which consist of one thyristor and one anti-parallel diode [87]. All of the thyristors are connected in a wye configuration and are controlled through a common cathode connection. Each branch has a unique capacitor value determined by the requirements of the power network. To connect each branch, a firing pulse is applied to the thyristor gate only when the main supply reaches maximum negative voltage to insure a soft connection. After a cycle is completed, the capacitor voltage will reach negative maximum, and the thyristor will block, unless a new firing pulse is applied [87]. Therefore, both the connection and disconnection of each branch will be soft and distortion free. In addition, if the firing pulses and negative maximum voltage is adjusted properly, the generator will be harmonic free and in rush current free.

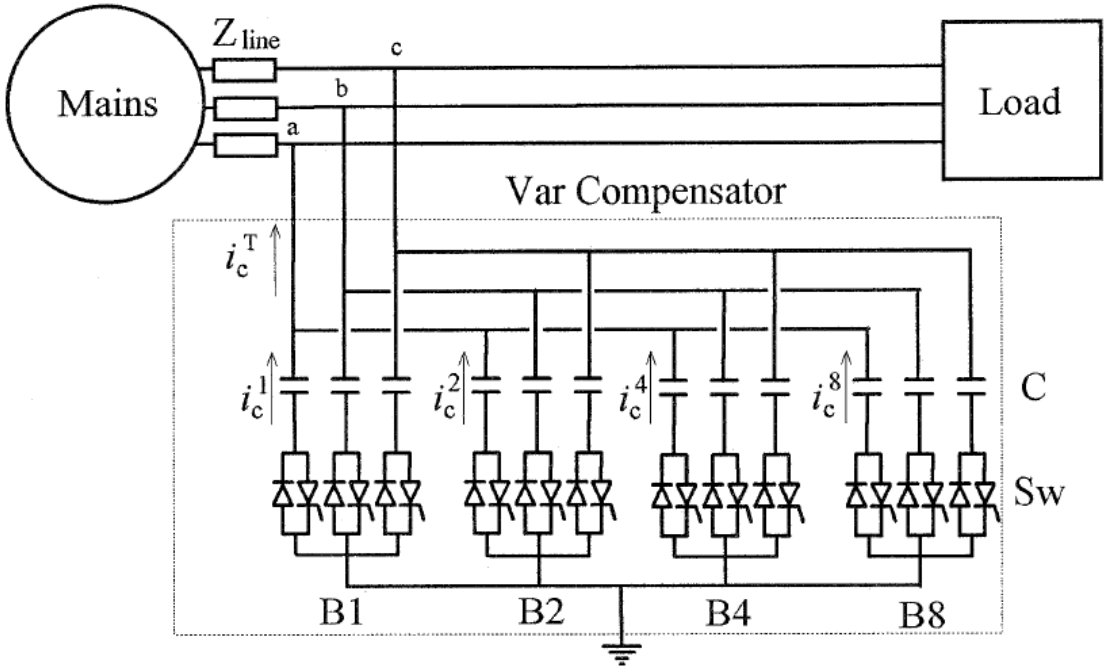


Figure C.5. Unidiretionally power switched compensator.

Hybrid Converter TCR Var Compensator

The topology of the hybrid generator (Figure C.6) is a TCR SVC in series with a converter. The addition of the converter provides sinusoidal injection current into the transmission line through the transformer. By choosing the firing angle of the TCR carefully, the fundamental voltage of the TCR and the transmission line will be the same and there by eliminating the fundamental components to the converter, which implies a small power rating on the converter [88]. Therefore, through the control of both the converter and the TCR, the injection current will be purely sinusoidal and harmonic free. A proportional integral (P-I) controller is used in order to correct the modeling and errors and parameter uncertainties [88]. Although the P-I controller provides the necessary

filtering of the unwanted harmonic content via synchronous rotating reference frame, it is time consuming (slow) and operates mostly under static conditions. During dynamic conditions (i.e. during switching) the system will not be able to guarantee harmonic free sinusoidal reactive current.

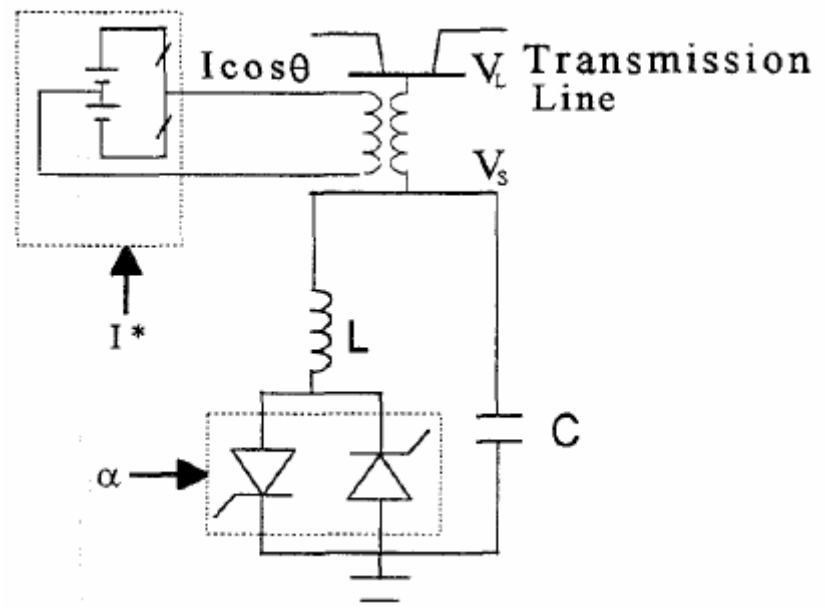


Figure C.6. Hybrid Thyristor Controlled Reactor.

Three Phase Synchronous Solid-State Var Compensator (SSVC)

The topology of the solid-state compensator is shown in Figure C.7. The major component of the SSVC is the three phase pulsewidth-modulated (PWM) force commuted inverter connected to the ac mains through a low-pass filter. The filter is used to minimize the injection of current harmonics into the power network. The dc side is connected to a dc supply and the capacitor is used to carry the input ripple current and provides the reactive storage [89]. The percentage of real and reactive power can be controlled by varying alpha. To increase the amplitude of Vao1, a small direct current must circulate through the dc capacitor so that Vdc will increase until Vao1 reaches the requested value. In the same way, if it is necessary to decrease the amplitude of Vao1, then a small negative current must flow through the dc capacitor [89]. Although this SSVC minimized harmonic current, it does so by PWM wave-shaping switching patterns, which have a slow response time. The slow response time implies that during high frequency applications where reactive power demand changes quickly (dynamic), the SSVC will not be able to provide harmonic free reactive power consistently.

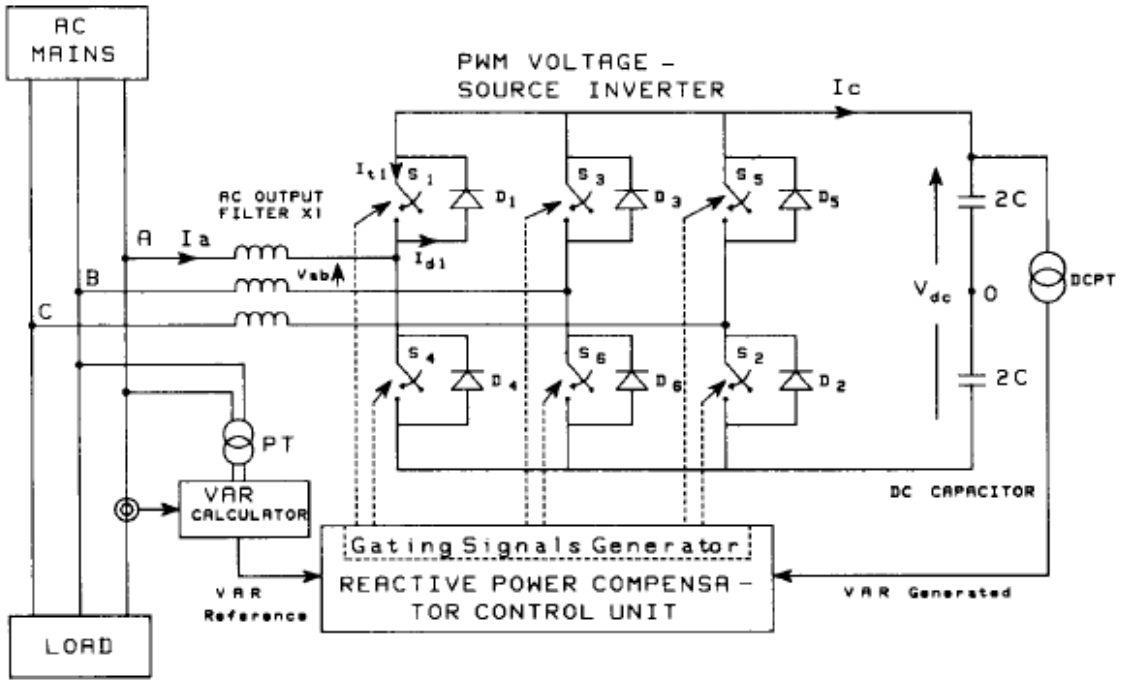


Figure C.7. Solid-State VAR Compensator.

Multilevel Voltage Source Inverter (VSI) Var Compensator

The arrangement of the inverter compensator (Figure C.8) consists of a multilevel PWM inverter with a set of reactors connected in series with a capacitor tank, a load, and the ac mains [90]. The VSI controls the amplitude and phase of the output phase voltage. Within the inverter, each of the active switches' voltage is clamped via diodes to only one capacitor voltage. In addition, due to the circuit structure of the inverter, the PWM generates low amounts of harmonics in the current. A programmed PWM can be used to eliminate unwanted harmonics (filtering) and reduction of current harmonics [90]. The adjustment of the output reactive power is made by varying the phase angle of the inverter. By using the inverter, the filter size can be smaller and the bulky transformer to provide the input voltage at the ac side of inverter is completely eliminated. The inverter is used as a multiplexer to select a dc voltage to generate a waveform as sinusoidal as possible. This implies it only approximates sinusoids and harmonics will remain due to the switching functions.

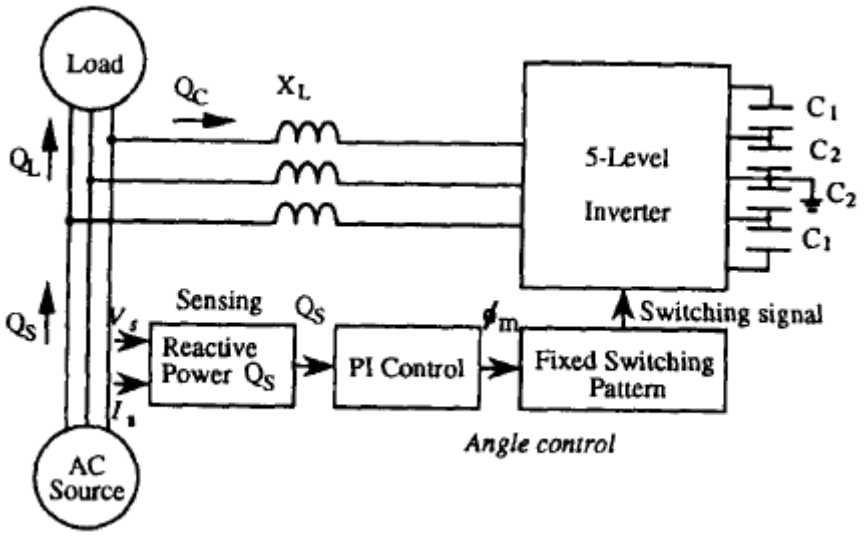


Figure C.8. Multilevel Voltage Source Inverter.

Synchronous Machine

A synchronous machine (Figure C.9) is an ac machine whose speed under steady-state conditions is proportional to the frequency of the current in its armature. The magnetic field created by the armature currents rotates at the same speed as that created by field current on the rotor (rotating at synchronous speed). Typically, alternating current flows in the armature winding and dc excitation is supplied to the field winding. The armature winding on the stator is usually a three-phase winding, and the field winding is on the rotor. The dc power needed for excitation is usually one to few percent of the rating of the synchronous machine and is typically supplied through slip rings from a dc generator called an exciter. The source of the energy for the field windings can be any conventional dc power supply, including batteries, solar converters, dc generators, and electronic power supplies. In the case of synchronous machines, the excitation source is often mounted on the same shaft as the synchronous machine itself. The exciter most commonly used is an ac machine, in which the exciter is a conventional synchronous machine of the same configuration as the main machine; the alternating output is rectified and applied to the field winding of the main machine. Normally in large central generating plants, excitation is supplied via a brush-slip-ring system. However, this system requires considerable maintenance and upkeep, therefore, for most cases a rotating-rectifier exciter is used. This exciter has the reverse configuration of the conventional synchronous machine, with the field on the stator and the armature on the rotor. The output of the voltage generated in the exciter armature is rectified and applied directly to the main field circuit, eliminating the need for slip rings (Figure C.10).

To produce reactive power, the three-phase induced electromotive forces (EMFs) e1, e2, and e3 of the synchronous rotating machines are in phase with the system voltages v1, v2, and v3 [84]. Therefore, by controlling the excitation of the machine, E, reactive power can be controlled. Hence, if the amplitude of E is above V then the current is leading (capacitive), and if E is below V then the current is lagging (inductive). Of course, the system requires a small amount of real power to compensate for internal

losses of the machine. A synchronous machine is typically characterized by its phasor diagram (Figure C.11) and its capability curve (Figure C.12). It gives the maximum reactive-power loadings corresponding to various power loadings with operation at rated voltage. In any synchronous machine, armature heating is the limiting factor in the region from unity to rated power factor. A synchronous condenser is essentially a synchronous motor running idle (without a load) with an overexcited field. In the case of superconducting synchronous condenser, which uses superconducting materials for windings, the losses are nearly zero and the synchronous reactance is significantly lower than conventional machines [91]. These two features allow the superconducting machine to response almost instantaneously to changes in voltage [92]. In addition, because of the low operating temperature of the machine, the rated power factor can be lowered to generate more reactive power in comparison to conventional condensers.

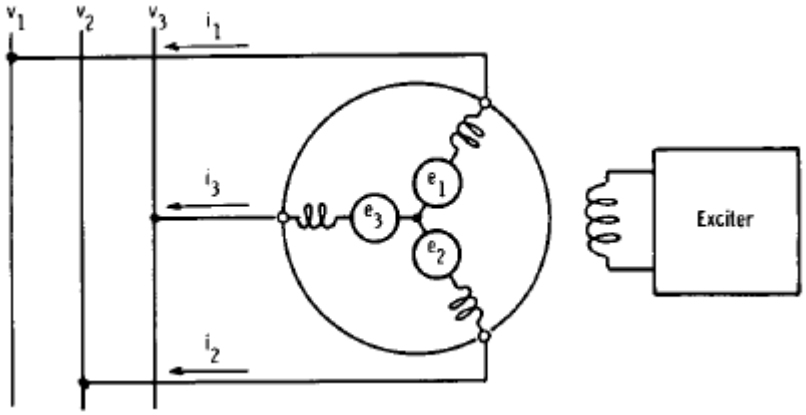


Figure C.9. Synchronous Machine.

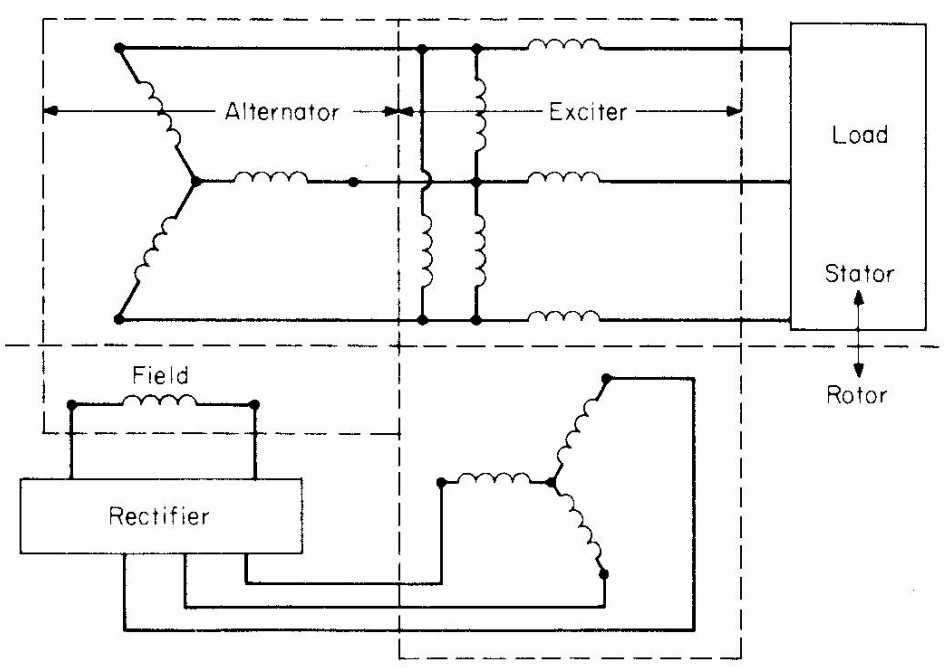


Figure C.10. Schematic of Self-Excited Rotating-Rectifier.

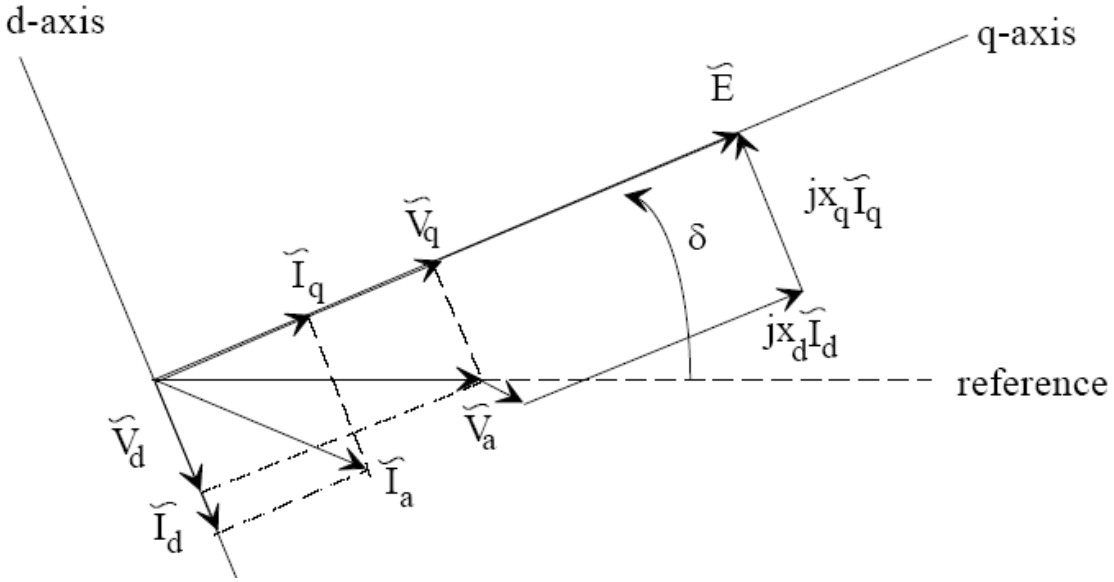


Figure C.11. Phasor Diagram of a Synchronous Machine in Steady-State.

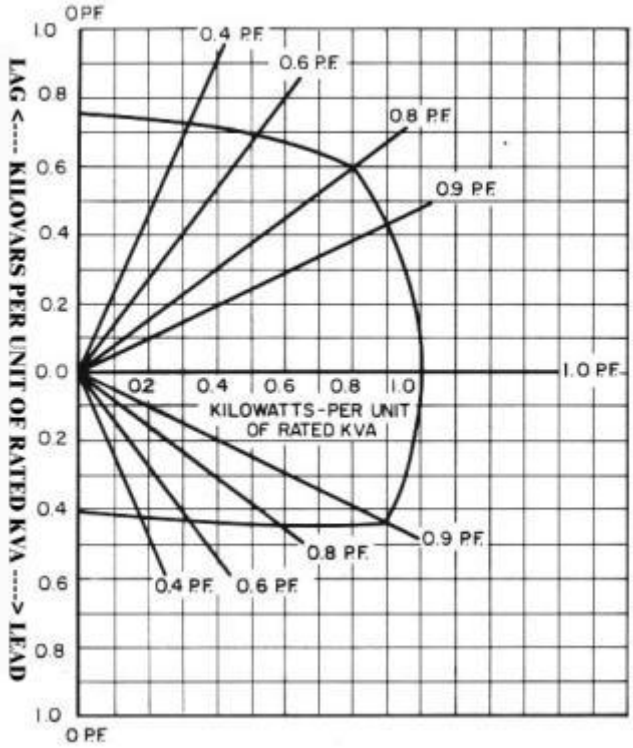


Figure C.12. Typical Capability Curve of a Synchronous Machine.

The general diagram in Figure C.13 shows various synchronous machine excitation subsystems. These subsystems may include a terminal voltage transducer and load compensator, excitation control elements, an exciter, and, in many instances, a power system stabilizer.

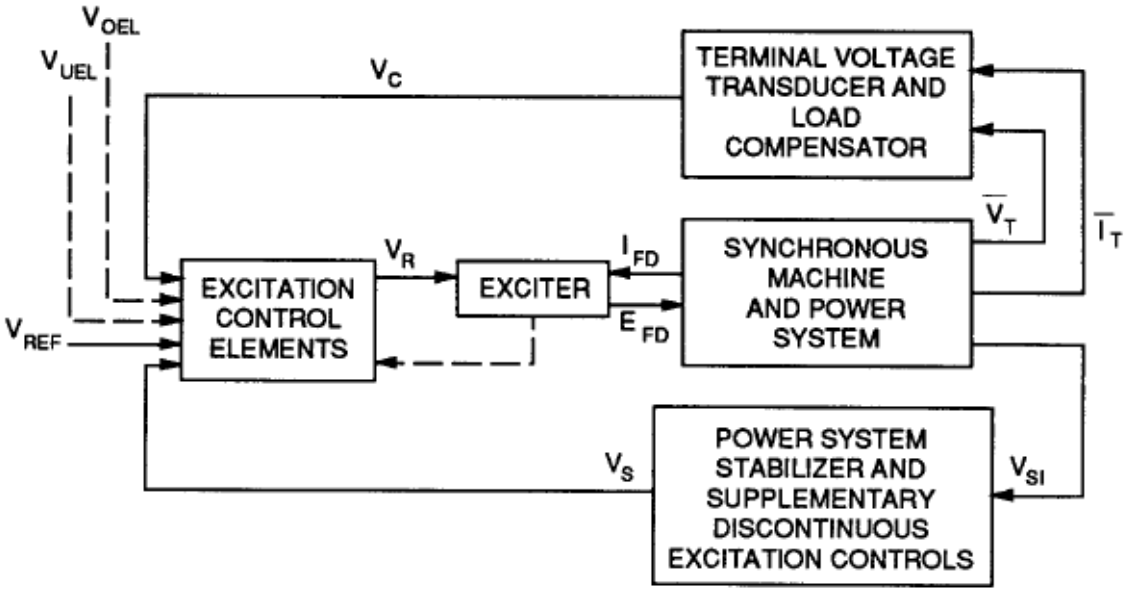


Figure C.13. Functional Diagram of Synchronous Machine Excitation System.

There are three distinct types of excitation systems:
1) Type DC excitation systems, which utilize a direct current generator with a commutator as the source of excitation system power.
2) Type AC excitation systems, which use an alternator and either stationary or rotating rectifiers to produce the direct current needed for the synchronous machine field.
3) Type ST excitation systems, in which the excitation power is supplied through transformers or auxiliary generator windings and rectifiers.

Type DC – Direct Current Commutator Excitation Systems

Few type DC exciters are now being produced, having been superseded by type AC and ST systems. There are, however, many such systems still in service. Therefore, they must still be considered.

Type DC1A

This model, described by the block diagram of Figure C.14, is used to represent field controlled dc commutator exciters with continuously acting voltage regulators (especially the direct-acting rheostatic, rotating amplifier, and magnetic amplifier types).

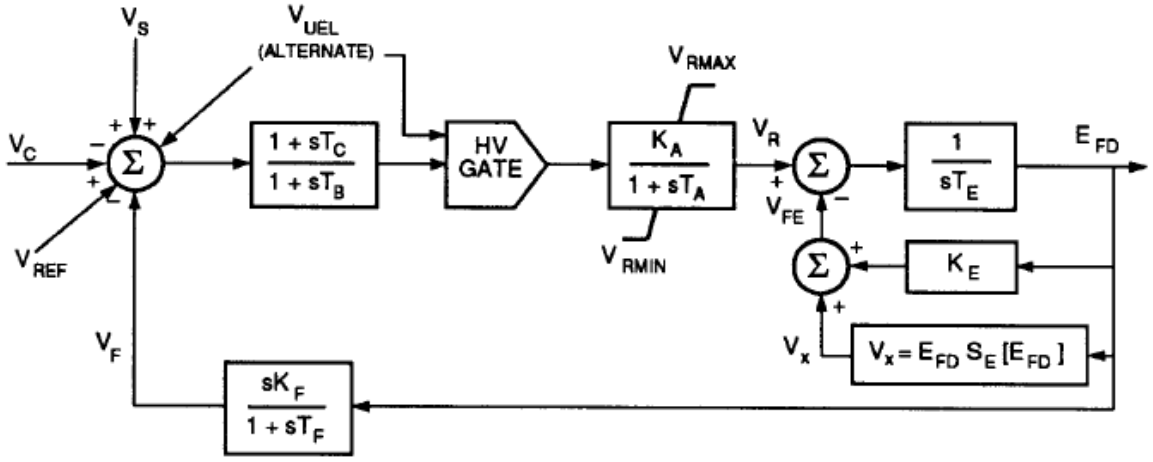


Figure C.14. Type DC1A DC Commutator Exciter.

The principal input to this model is the output, *V*C, from the terminal voltage transducer and load compensator model described above. At the summing junction, terminal voltage transducer output, *V*C, is subtracted from the set point reference, *V*REF. The stabilizing feedback, *V*F, is subtracted, and the power system stabilizing signal, *V*S, is added to produce an error voltage. In the steady-state, these last two signals are zero, leaving only the terminal voltage error signal. The resulting signal is amplified in the regulator. The major time constant, *T*A, and gain, *K*A, associated with the voltage regulator are shown incorporating nonwindup limits typical of limitations. These voltage regulators utilize power sources that are essentially unaffected by brief transients on the synchronous machine or auxiliaries buses. The time constants, *T*B and *T*C, may be used to model equivalent time constants inherent in the voltage regulator; but these time constants are frequently small enough to be neglected, and provision should be made for zero input data. The voltage regulator output, *V*R, is used to control the exciter, which may be either separately-excited or self-excited. When a self-excited shunt field is used, the value of *K*E reflects the setting of the shunt field rheostat. In some instances, the resulting value of *K*E can be negative, and allowance should be made for this. Most of these exciters utilize self-excited shunt fields with the voltage regulator operating in a mode commonly termed buck-boost. The majority of station operators manually track the voltage regulator by periodically trimming the rheostat set point so as to zero the voltage regulator output. This may be simulated by selecting the value of *K*E such that initial conditions are satisfied with *V*R = 0. In some programs, if *K*E is not provided, it is automatically calculated by the program for self-excitation. If a value for *K*E is provided, the program should not recalculate *K*E because a fixed rheostat setting is implied. For such systems, the rheostat is frequently fixed at a value that would produce self-excitation near rated conditions. Systems with fixed field rheostat settings are in widespread use on units that are remotely controlled. A value of *K*E = 1 is used to represent a separately excited exciter. The term *S*E[*E*FD] is a nonlinear function with a value defined at any chosen *E*FD. The output of this saturation block, *V*X, is the product of the input, *E*FD, and the value of the nonlinear function, *S*E[*E*FD], at this exciter voltage. A signal derived from field voltage is normally used to provide excitation system stabilization, *V*F, via the rate feedback with gain, *K*F, and time constant, *T*F.

Type DC2A

The model shown in Figure C.15 is used to represent field controlled dc commutator exciters with continuously acting voltage regulators having supplies obtained from the generator or auxiliaries bus. It differs from the type DC1A model only in the voltage regulator output limits, which are now proportional to terminal voltage, *V*T.

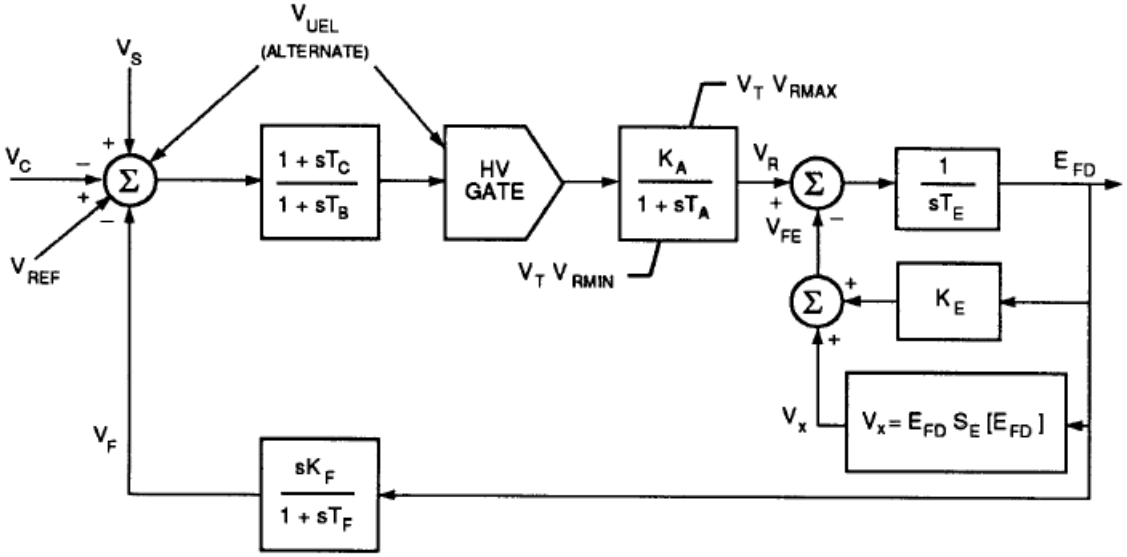


Figure C.15. Type DC2A DC Commutator Exciter With Bus-Fed Regulator.

Type DC3A

The systems discussed in the previous sections are representative of the first generation of high gain, fast-acting excitation sources. The type DC3A model is used to represent older systems, in particular those dc commutator exciters with noncontinuously acting regulators that were commonly used before the development of the continuously acting varieties. These systems respond at basically two different rates, depending upon the magnitude of voltage error. For small errors, adjustment is made periodically with a signal to a motor-operated rheostat. Larger errors cause resistors to be quickly shorted or inserted and a strong forcing signal to be applied to the exciter. Continuous motion of the motor operated rheostat occurs for these larger error signals, even though it is bypassed by contactor action. Figure C.16 illustrates this control action.

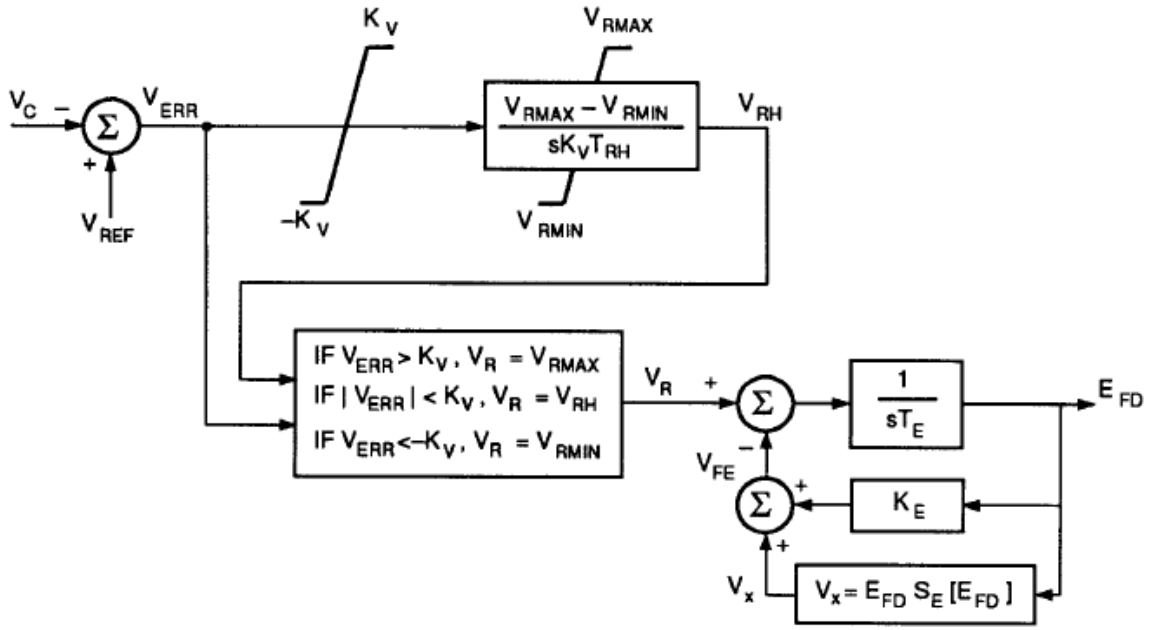


Figure C.16. Type DC3A DC Commutator Exciter With Noncontinuously Acting Regulators.

Depending upon the magnitude of voltage error, *V*REF - *V*C, different regulator modes come into play. If the voltage error is larger than the fast raise/lower contact setting, *K*V (typically 5%), *V*RMAX or *V*RMIN is applied to the exciter, depending upon the sign of the voltage error. For an absolute value of voltage error less than *K*V, the exciter input equals the rheostat setting, *V*RH. The rheostat setting is notched up and down, depending upon the sign of the error. The travel time representing continuous motion of the rheostat drive motor is *T*RH. A nonwindup limit is shown around this block to represent the fact that, when the rheostat reaches either limit, it is ready to come off the limit immediately when the input signal reverses. Additional refinements, such as dead band for small errors, have been considered, but were not deemed justified for the relatively few older machines using these voltage regulators. The model assumes that the quick raise/lower limits are the same as the rheostat limits. It does not account for time constant changes in the exciter field as a result of changes in field resistance (as a result of rheostat movement and operation of quick action contacts).

Type AC – Alternator Supplied Rectifier Excitation Systems

These excitation systems use an ac alternator and either stationary or rotating rectifiers to produce the direct current needed for the generator field. Loading effects on such exciters are significant, and the use of generator field current as an input to the models allows these effects to be represented accurately. These systems do not allow the supply of negative field current, and only the type AC4A model allows negative field voltage forcing.

Type AC1A

The model shown in Figure C.17 represents the field controlled alternator-rectifier excitation systems designated as type AC1A. These excitation systems consist of an alternator main exciter with noncontrolled rectifiers. The exciter does not employ self excitation, and the voltage regulator power is taken from a source that is not affected by

external transients. The diode characteristic in the exciter output imposes a lower limit of zero on the exciter output voltage, as shown in Figure C.17.

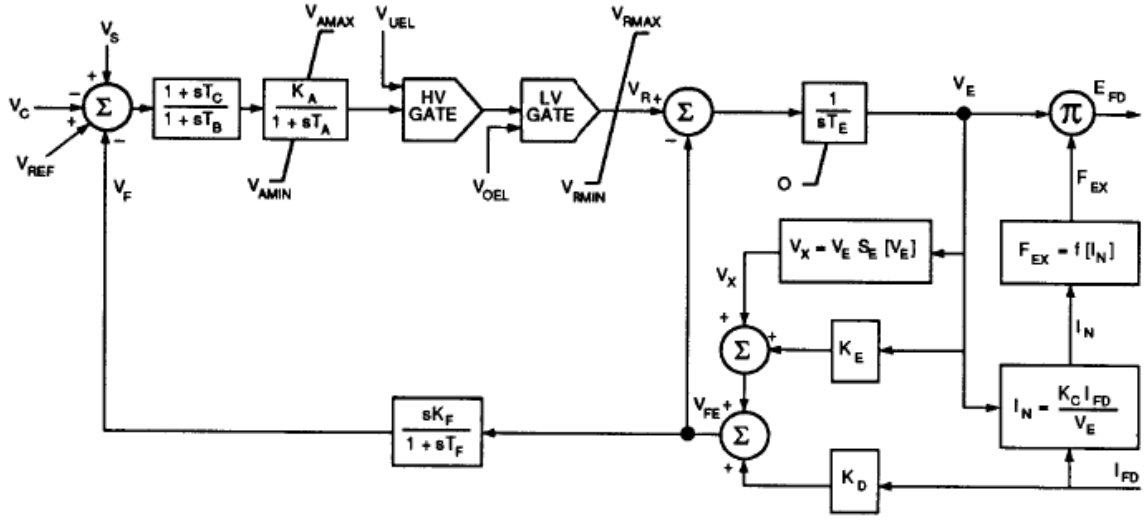


Figure C.17. Type AC1A Alternator-Rectifier Excitation System With Noncontrolled Rectifiers and Feedback From Exciter Field Current.

For large power system stability studies, the exciter alternator synchronous machine can be represented by the simplified model shown in Figure C.17. The demagnetizing effect of load current, *I*FD, on the exciter alternator output voltage, *V*E, is accounted for in the feedback path that includes the constant, *K*D. This constant is a function of the exciter alternator synchronous and transient reactances.

Exciter output voltage drop due to rectifier regulation is simulated by inclusion of the constant, *K*C (which is a function of commutating reactance) and the rectifier regulation curve, *F*EX. In the model, a signal, *V*FE, proportional to exciter field current is derived from the summation of signals from exciter output voltage, *V*E, multiplied by *K*E + *S*E [*V*E] represents saturation and *I*FD multiplied by the demagnetization term, *K*D. The exciter field current signal, *V*FE, is used as the input to the excitation system stabilizing block with output, *V*F.

Type AC2A

The model shown in Figure C.18, designated as type AC2A, represents a high initial response field controlled alternator rectifier excitation system. The alternator main exciter is used with noncontrolled rectifiers. The type AC2A model is similar to that of type AC1A except for the inclusion of exciter time constant compensation and exciter field current limiting elements.

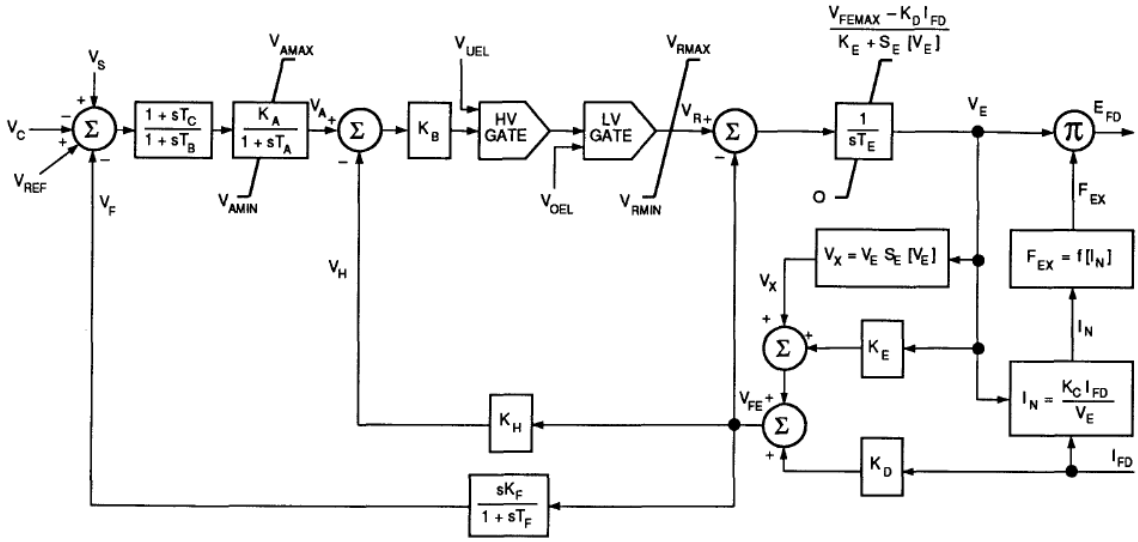


Figure C.18. Type AC2A High Initial Response Alternator-Rectifier Excitation System With Noncontrolled Rectifiers and Feedback From Exciter Field Current.

The exciter time constant compensation consists essentially of a direct negative feedback, *V*H, around the exciter field time constant, reducing its effective value and thereby increasing the small signal response bandwidth of the excitation system. The time constant is reduced by a factor proportional to the product of gains, *K*B and *K*H, of the compensation loop and is normally more than an order of magnitude lower than the time constant without compensation. To obtain high initial response with this system, a very high forcing voltage, *V*RMAX, is applied to the exciter field. A limiter sensing exciter field current serves to allow high forcing but limits the current. By limiting the exciter field current, exciter output voltage, *E*E, is limited to a selected value that is usually determined by the specified excitation system nominal response. Although this limit is realized physically by a feedback loop, the time constants associated with the loop can be extremely small and can cause computational problems. For this reason, the limiter is shown in the model as a positive limit on exciter voltage back of commutating reactance, which is in turn a function of generator field current. For small limiter loop time constants, this has the same effect, but it circumvents the computational problem associated with the high gain, low time constant loop.

Type AC3A

The model shown in Figure C.19 represents the field controlled alternator-rectifier excitation systems designated as type AC3A. These excitation systems include an alternator main exciter with noncontrolled rectifiers. The exciter employs self-excitation and the voltage regulator power is derived from the exciter output voltage. Therefore, this system has an additional nonlinearity, simulated by the use of a multiplier whose inputs are the voltage regulator command signal, *V*A, and the exciter output voltage, *V*FD, times *K*R.

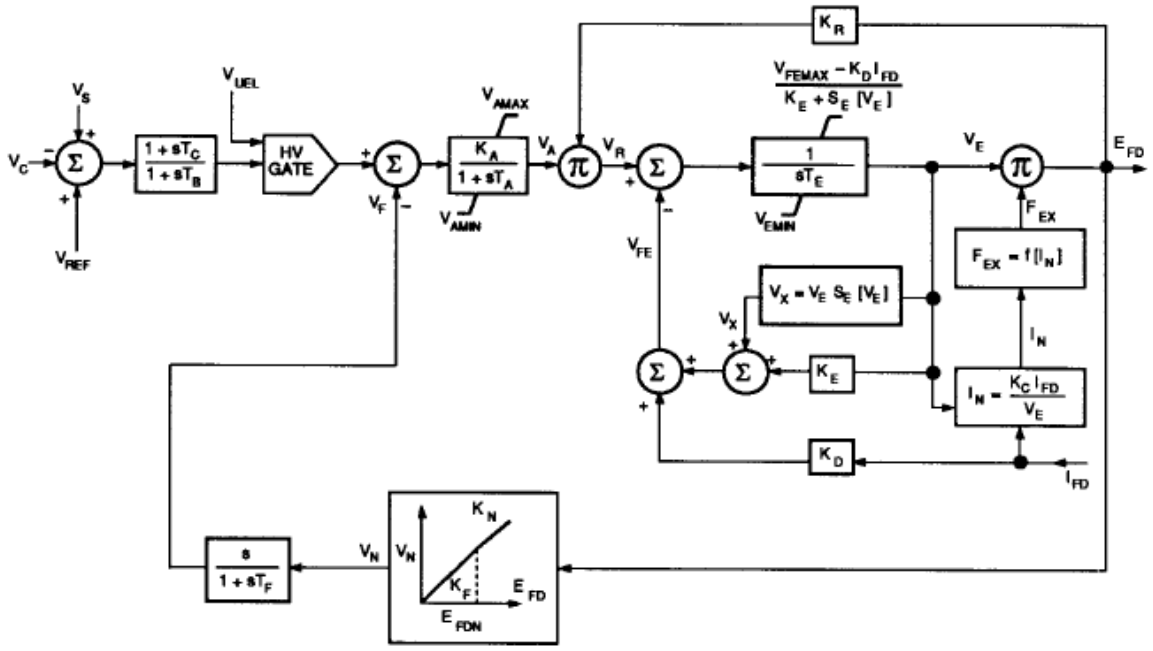


Figure C.19. Type AC3A Alternator-Rectifier Exciter With Alternator Field Current Limiter.

For large power system stability studies, the exciter alternator synchronous machine model is simplified. The demagnetizing effect of load current, *I*FD, on the dynamics of the exciter alternator output voltage, *V*E, is accounted for. The feedback path includes the constant, *K*D, which is a function of the exciter alternator synchronous and transient reactances. Exciter output voltage drop due to rectifier regulation is simulated by inclusion of the constant, *K*C, (which is a function of commutating reactance) and the regulation curve, *F*EX. In the model, a signal, *V*FE, proportional to exciter field current is derived from the summation of signals from exciter output voltage, *V*E, multiplied by *K*E + *S*E [*V*E], (where *S*E [*V*E] represents saturation) and *I*FD multiplied by the demagnetization term, *K*D. The excitation system stabilizer also has a nonlinear characteristic. The gain is *K*F with exciter output voltage less than *E*FDN. When exciter output exceeds *E*FDN, the value of this gain becomes *K*N. The limits on *V*E are used to represent the effects of feedback limiter operation.

Type AC4A

The type AC4A alternator supplied controlled rectifier system illustrated in Figure C.20 is quite different from the other type AC systems. This high initial response excitation system utilizes a full thyristor bridge in the exciter output circuit.

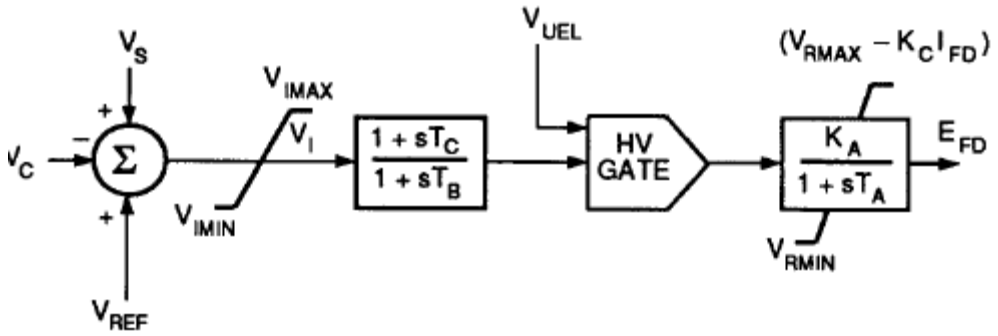


Figure C.20. Type AC4A Alternator Supplied Controlled-Rectifier Exciter.

The voltage regulator controls the firing of the thyristor bridges. The exciter alternator uses an independent voltage regulator to control its output voltage to a constant value. These effects are not modeled; however, transient loading effects on the exciter alternator are included. The loading effects can be accounted for by using the exciter load current and commutating reactance to modify excitation limits. The excitation system stabilization is frequently accomplished in thyristor systems by a series lag-lead network rather than through rate feedback. The time constants, *T*B and *T*C, allow simulation of this control function. The overall equivalent gain and the time constant associated with the regulator and/or firings of the thyristors are simulated by *K*A and *T*A, respectively.

Type AC5A

The model shown in Figure C.21 designated as type AC5A, is a simplified model for brushless excitation systems. The regulator is supplied from a source, such as a permanent magnet generator, that is not affected by system disturbances.

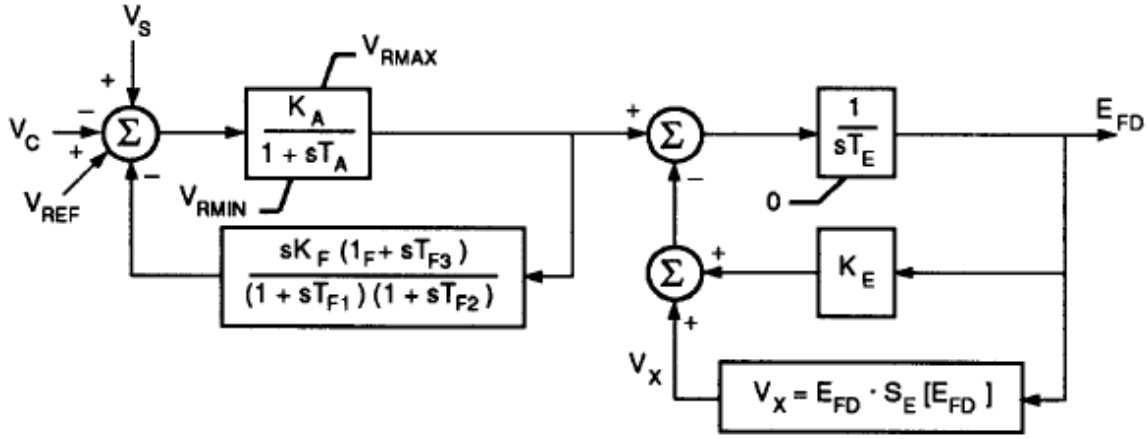


Figure C.21. Type AC5A Simplified Rotating Rectifier Excitation System Representation.

Unlike other ac models, this model uses loaded rather than open circuit exciter saturation data in the same way as it is used for the dc models. Because the model has been widely implemented by the industry, it is sometimes used to represent other types of systems when either detailed data for them are not available or simplified models are required.

Type AC6A

The model shown in Figure C.22 is used to represent field controlled alternator-rectifier excitation systems with system supplied electronic voltage regulators. The maximum output of the regulator, *V*R, is a function of terminal voltage, *V*T, and the model includes an exciter field current limiter. It is particularly suitable for representation of stationary diode systems.

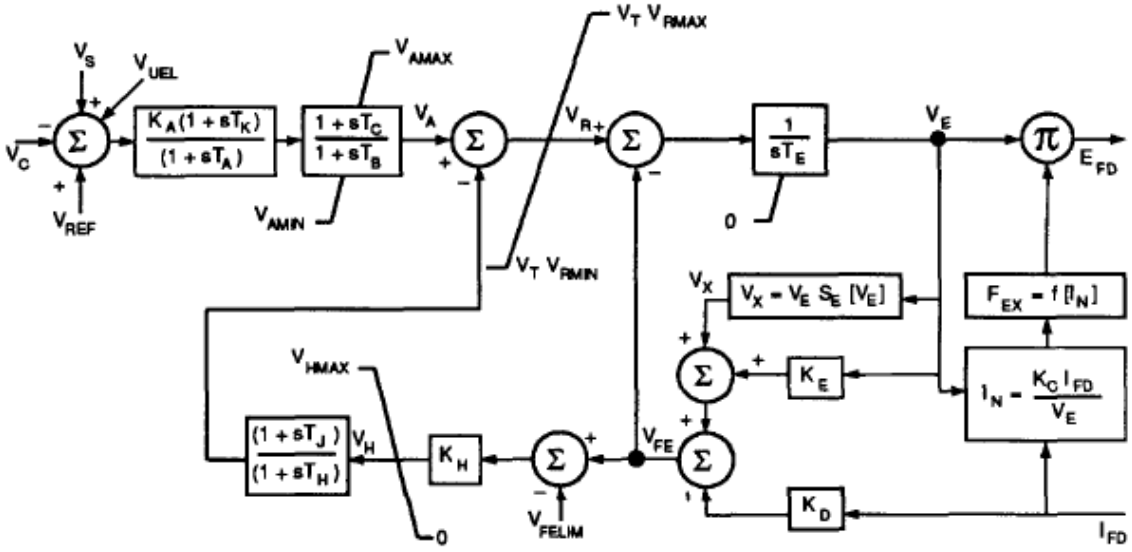


Figure C.22. Type AC6A Alternator-Rectifier Excitation System With Noncontrolled Rectifiers and System-Supplied Electronic Voltage Regulator.

Type ST – Static Excitation Systems

In these excitation systems, voltage (and also current in compounded systems) is transformed to an appropriate level. Rectifiers, either controlled or noncontrolled, provide the necessary direct current for the generator field. While many of these systems allow negative field voltage forcing, most do not supply negative field current. For specialized studies where negative field current must be accommodated, more detailed modeling is required.

For many of the static systems, exciter ceiling voltage is very high. For such systems, additional field current limiter circuits may be used to protect the exciter and the generator rotor. These frequently include both instantaneous and time delayed elements; however, only the instantaneous limits are included here, and these are shown only for the ST1A model.

Type ST1A

The computer model of the type ST1A potential-source controlled-rectifier exciter excitation system shown in Figure C.23 is intended to represent systems in which excitation power is supplied through a transformer from the generator terminals (or the unit auxiliaries bus) and is regulated by a controlled rectifier. The maximum exciter voltage available from such systems is directly related to the generator terminal voltage (except as noted below).

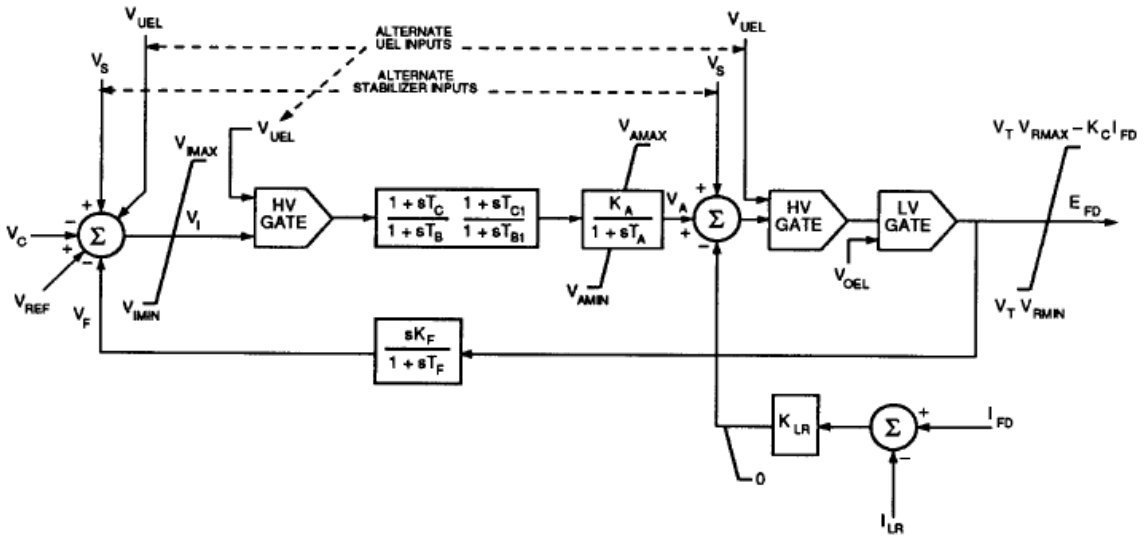


Figure C.23. Type ST1A Potential-Source Controlled-Rectifier Exciter.

In this type of system, the inherent exciter time constants are very small, and exciter stabilization may not be required. On the other hand, it may be desirable to reduce the transient gain of these systems for other reasons. The model shown is sufficiently versatile to represent transient gain reduction implemented either in the forward path via time constants, *T*B and *T*C (in which case *K*F would normally be set to zero), or in the feedback path by suitable choice of rate feedback parameters, *K*F and *T*F. Voltage regulator gain and any inherent excitation system time constant are represented by *K*A and *T*A, respectively. The time constants, *T*C1 and *T*B1, allow for the possibility of representing transient gain increase, with *T*C1 normally being greater than *T*B1.

The way in which the firing angle for the bridge rectifiers is derived affects the input output relationship, which is assumed to be linear in the model by choice of a simple gain, *K*A. For many systems, a truly linear relationship applies. In a few systems, the bridge relationship is not linearized, leaving this nominally linear gain a sinusoidal function, the amplitude of which may be dependent on the supply voltage. As the gain is normally set very high, a linearization of this characteristic is normally satisfactory for modeling purposes. The representation of the ceiling is the same whether the characteristic is linear or sinusoidal.

In many cases, the internal limits on *V*I can be neglected. The field voltage limits that are functions of both terminal voltage and synchronous machine field current should be modeled. The representation of the field voltage positive limit as a linear function of synchronous machine field current is possible because operation of the rectifier bridge in such systems is confined to the mode 1 region. The negative limit would have a similar current dependent characteristic, but the sign of the term could be either positive of negative depending upon whether constant firing angle or constant extinction angle is chosen for the limit. As field current is normally low under this condition, the term is not included in the model.

As a result of the very high forcing capability of these systems, a field current limiter is sometimes employed to protect the generator rotor and exciter. The limit start setting is defined by *I*LR, and the gain is represented by *K*LR. To permit this limit to be ignored, provision should be made to allow *K*LR to be set to zero. While, for the majority of these excitation systems, a fully controlled bridge is employed, the model is also applicable to systems in which only half of the bridge is controlled, in which case the negative field voltage ceiling is set to zero (*V*RMIN = 0).

Type ST2A

Some static systems utilize both current and voltage sources (generator terminal quantities) to comprise the power source. These compound-source rectifier excitation systems are designated type ST2A and are modeled as shown in Figure C.24. It is necessary to form a model of the exciter power source utilizing a phasor combination of terminal voltage, *V*T, and terminal current, *I*T. Rectifier loading and commutation effects are accounted for. *E*FDMAX represents the limit on the exciter voltage due to saturation of the magnetic components. The regulator controls the exciter output through controlled saturation of the power transformer components. *T*E is a time constant associated with the inductance of the control windings.

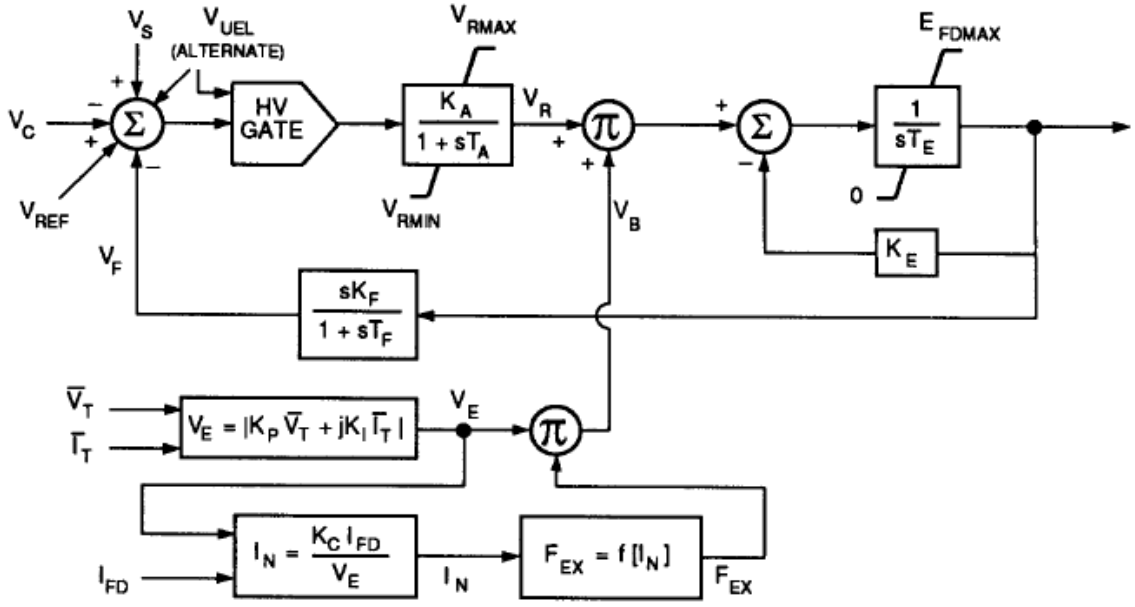


Figure C.24. Type ST2A Compound-Source Rectifier Exciter.

Type ST3A

Some static systems utilize a field voltage control loop to linearize the exciter control characteristic as shown in Figure C.25. This also makes the output independent of supply source variations until supply limitations are reached.

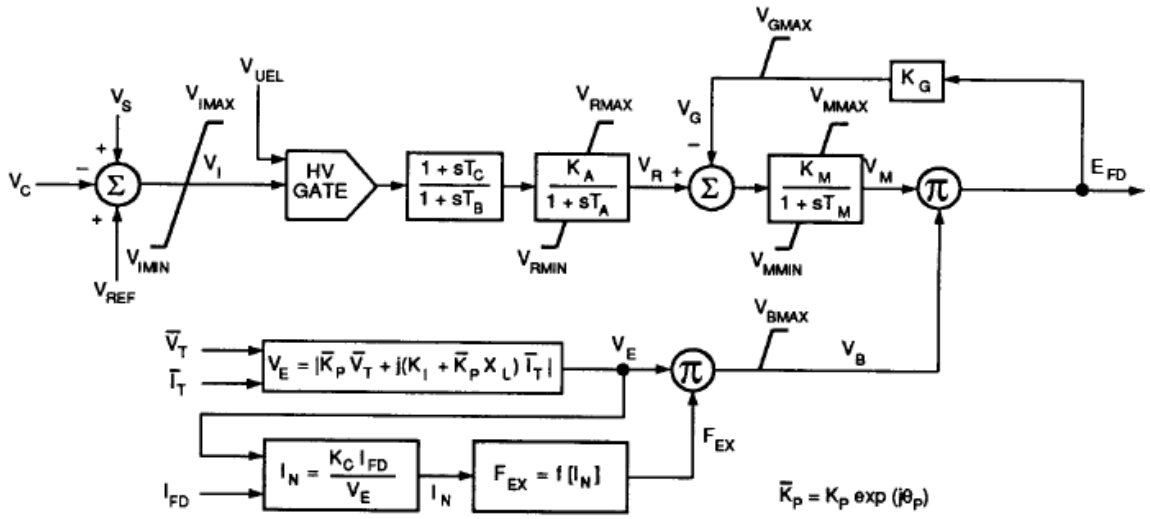


Figure C.25. Type ST3A Potential or Compound-Source Controlled-Rectifier Exciter With Field Voltage Control Loop.

These systems utilize a variety of controlled rectifier designs: full thyristor complements or hybrid bridges in either series or shunt configurations. The power source may consist of only a potential source, either fed from the machine terminals or from internal windings. Some designs may have compound power sources utilizing both machine potential and current. These power sources are represented as phasor combinations of machine terminal current and voltage and are accommodated by suitable parameters in the model shown.

The excitation system stabilizer for these systems is provided by a series lag-lead element in the voltage regulator, represented by the time constants, *T*B and *T*C. The inner loop field voltage regulator is comprised of the gains, *K*M and *K*G, and the time constant *T*M. This loop has a wide bandwidth compared with the upper limit of 3 Hz for the models described in this standard. The time constant, *T*M, may be increased for study purposes, eliminating the need for excessively short computing increments while still retaining the required accuracy at 3 Hz. Rectifier loading and commutation effects are accounted for. The *V*BMAX limit is determined by the saturation level of power components.

Converters

As discussed in previous section, nearly most of the exciters require a converter (rectifier) to convert AC to DC for the field excitation. There are numerous designs for three-phase rectifiers, therefore only an example will be discussed. Figure C.26 shows a six valve converter design. The electronics switches in general are constructed from stacks of devices such as thyristors, GTOs, etc. depending on the design and the intended application. Because the DC output is generated with pulses, there will be significant harmonics which are typically contained within the converter by harmonic filters.

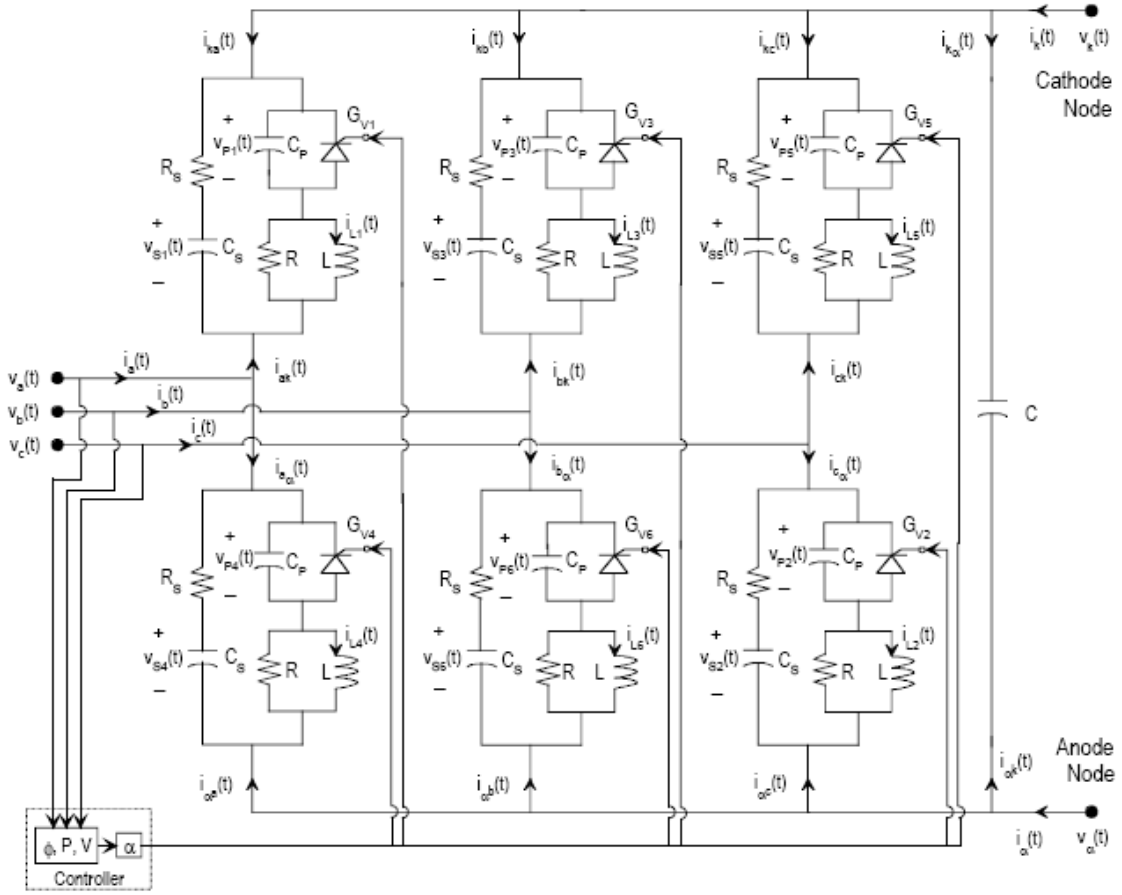


Figure C.26. Topology of a Six-Pulse Converter.

Harmonics

The previously presented designs of reactive compensator all have a common drawback in relations to the entire power network. The compensators inject and amplify harmonics into the supply network, which can cause heating of induction motors, transformers and capacitors and overloading of neutrals. This section presents a background on the effects of harmonics on different loads.

Generally, traditional household equipment like incandescent lights and stoves are not affected by harmonics, however, today's high tech electronics using advanced power electronics are not immune to the distortions in supply power. However, the most important loads are induction motors and their responses to harmonics are of utmost priority. Harmonics overheat the windings in the motor, causing accelerated degradation of insulation and loss of life. Additionally, harmonics cause higher currents which causes additional heating. For other equipment that only operate with accurate voltage waveforms (thyristors), they can malfunction in presence of harmonics.

The impedance of the power system at low frequencies is determined by the inductive impedance of transformers and the transmission lines, and at high frequencies, it is determined by capacitive impedance from power factor correction capacitors

(compensators). Therefore, at an intermediate range of frequencies where the capacitive and inductive effects combine to form very high impedance, a small harmonic current can be amplified to a high harmonic voltage (resonance).

In relation to compensators, there're a couple of techniques to correct for harmonics. One is to use a harmonic filter consisting of an inductor, resistor and capacitor to absorb the harmonic current before it propagates into the network. In the case of harmonic amplification, a detuning inductor connected in series with the compensator can be used to prevent the compensator from drawing too much harmonic currents.

Thyristor-Controlled Reactor (TCR)

The harmonics generated are a direct result of the firing delay control of the thyristors. These harmonics can be characterized with the following model with reference to Figure 1.

$$I_{LH}(a) = \frac{V}{\omega L}\frac{4}{\pi}\left(\frac{\sin a\cos(na) - n\cos a\sin(na)}{n(n^2-1)}\right) \qquad \text{(C.1)}$$

where n=2k+1, k=1,2,3,…are the harmonic numbers.

Thyristor-Switched Capacitor (TSC)

There are almost no harmonics generated because of the way the TSC is switched in and switched out.

Fixed Capacitor-Thyristor Controlled Reactor (FC-TCR)

The harmonics generated are the same as those of the TCR.

Thyristor Controlled Reactor-Thyristor Switched Capacitor (TCR-TSC)

The harmonics generated are the same as those of the TCR.

Unidirectionally Switched

The compensator is free of harmonics if the firing pulses and negative maximum voltage is adjusted properly.

Hybrid Thyristor Controlled Reactor

Although the TCR portion of the compensator produces harmonics as described by A.2.1, they are isolated from the transmission system by the controlled current source in series with the TCR. Therefore, there is essentially no harmonic injection into the system.

Three Phase Synchronous Solid State SVC

Typically, the harmonics produced in the compensator is filtered by the output filter, however, the model with reference to Figure 7 for the output voltage harmonics produced by the compensator is:

$$V_{ao1} = \frac{4V_{dc}}{\sqrt{2}2\pi}\left\{2\sum_{j=1}^{n+1}(-1)^{j+1}\cos(a_j) - 1\right\}, \qquad \text{(C.2)}$$

where Vdc is the voltage on the DC supply side, αj the angle of switching patterns of the PWM, and n is the harmonic number. In addition, the apparent power needed by the output filter is given by

$$S_f = X_1 I_{a1}^2 (1 + THD_i^2), \quad \text{(C.3)}$$

where Ia1 is the fundamental current and THD the total harmonic distortion in current.

Multilevel Voltage Source Inverter (VSI)

The harmonics associated with the VSI depends on the selection of number of levels in the inverter. The equation governing the voltage harmonic coefficients with reference to Figure 8 is

$$V_l = \frac{4v_2}{n\pi}\{\cos(na_1) - \cos(na_2) + \cos(na_3) + ...\}, \quad \text{(C.4)}$$

where v2 is the DC voltage on the capacitors, and alphas are the PWM switching angles for each level, and n is the harmonic number.

Synchronous Machine

The harmonics produced are results from two phenomena: Electrical windings in both the rotor and stator are not "infinitely" distributed about the airgap circumference but are grouped in discrete bundles known as phase belts, and the magnetic surfaces of both the rotor and stator are non-uniform and consist of alternate magnetic and non-magnetic regions as a result of slot/tooth construction or salient-pole construction. The equations governing the mmf of both single phase and three phase machines are

$$m_{\phi_n} = \frac{2M_m S_{pm}}{\pi}\left[\frac{1}{n}K_{pn}K_{dn}\cos(nx - \omega t) + \frac{1}{n}K_{pn}K_{dn}\cos(nx + \omega t)\right], \text{ for n = 1,3,5,…} \quad \text{(C.5)}$$

$$m_{3\phi_n} = \frac{6M_m S_{pm}}{\pi}\left[\frac{1}{n}K_{pn}K_{dn}\cos(nx - \omega t)\right], \text{ for n = 1,7,13,…} \quad \text{(C.6)}$$

$$m_{3\phi_n} = \frac{6M_m S_{pm}}{\pi}\left[\frac{1}{n}K_{pn}K_{dn}\cos(nx + \omega t)\right], \text{ for n = 5,11,17,…} \quad \text{(C.7)}$$

where

$M_m = \sqrt{2}IT = \max mmf$,

$S_{pm} = S/P/M$ = number of coils per phase per pole,

$a = \frac{180}{S} = $ electrical degrees,

$K_p = \cos\frac{na}{2} = $ pitch factor,

$K_d = \frac{\sin(aS_{pm}/2)}{S_{pm}(\sin a/2)} = $ distribution factor,

x = position along the airgap,
w = angular frequency of machine,
t = time,
n = harmonic number.

Steady-State Operation

This section presents the static models of the most common types of VAR source designs.

Thyristor-Controlled Reactor (TCR)

The TCR uses input voltage, V, and control angle, α, to produce the shifted current. The fundamental current amplitude with reference to Figure C.1 is described by

$$I_F(a) = \frac{V}{\omega L}\left(1 - \frac{2}{\pi}a - \frac{1}{\pi}\sin(2a)\right) \quad \text{(C.8)}$$

where ω=angular frequency of source.

Thyristor-Switched Capacitor (TSC)

The TSC model has input voltage, V, and the output current magnitude with reference to Figure C.2 of Appendix C is described by

$$I = V\frac{n^2}{n^2 - 1}\omega C \quad \text{(C.9)}$$

where ω=angular frequency and

$$n = \frac{1}{\sqrt{\omega^2 LC}} \quad \text{(C.10)}$$

Fixed Capacitor-Thyristor Controlled Reactor (FC-TCR)

The mathematical models for each of the branches are same as those of the TCR, and the total current injected with reference to Figure C.3 being

$$I_T = \sum_{i=1}^{n} i_i \,, \quad \text{(C.11)}$$

where n = number of branches.

Thyristor Controlled Reactor-Thyristor Switched Capacitor (TCR-TSC)

The mathematical models for each of the branches are same as those of the TCR and TSC, and the total current injected with reference to and Figure C.4 being

$$I_T = \sum_{i=1}^{n} i_i \quad \text{(C.12)}$$

where n = number of branches.

Unidirectional Switched

The mathematical model for the current in each branch with reference to Figure C.5 is described by

$$i = C \cdot V \cdot \sin(\omega t) \quad \text{(C.13)}$$

where V = source voltage.

Hybrid Thyristor Controlled Reactor

The governing equations for this Var compensator are the same as those of the TCR with the exception of the controlled current source with reference to Figure C.6 which injects

$$i = I\cos(\theta). \quad \text{(C.14)}$$

Three Phase Synchronous Solid State SVC

The apparent power between the ac mains and SSVC with reference to Figure C.7 is described by

$$S = \frac{V_{an}V_{ao1}}{X_1}\sin(a) - j\left\{\frac{V_{an}V_{ao1}}{X_1}\cos(a) - \frac{V_{an}^2}{X_1}\right\}, \quad \text{(C.15)}$$

where, Van =line to neutral ac voltage, Vao1 =output voltage, α =delay angle, and X1 =output resistance element. Therefore, the injected fundamental current magnitude is described by

$$I = \frac{V_{ao1}}{X_1}\sin(a) - j\left\{\frac{V_{ao1}}{X_1}\cos(a) - \frac{V_{an}}{X_1}\right\}. \quad \text{(C.16)}$$

Multilevel Voltage Source Inverter (VSI)

The per phase output real and reactive power with reference to Figure C.8 are described by

$$P = \frac{V_s V_L}{X_L}\sin(\phi_m), \qquad Q = \frac{V_s \cdot (V_L\cos(\phi_m) - V_s)}{X_L}, \quad \text{(C.17)}$$

therefore the magnitude of real and reactive current injections are described by

$$I_{real} = \frac{V_L}{X_L}\sin(\phi_m), \qquad I_{imag} = \frac{V_L\cos(\phi_m) - V_s}{X_L}, \quad \text{(C.18)}$$

where , Vs =source voltage, VL =output voltage, , and Φm =control phase angle of the PWM.

Synchronous Machine

The per phase output real and reactive power with reference to Figure C.11 are approximately described by

$$P = \frac{V_t E_f}{X_S + R_a}\sin(\delta), \qquad Q = \frac{V_t(E_f\cos(\delta) - V_t)}{X_s + R_a}, \quad \text{(C.19)}$$

therefore the magnitude of real and reactive current injections are described by

$$I_{real} = \frac{E_f}{X_S + R_a}\sin(\delta), \qquad I_{imag} = \frac{E_f\cos(\delta) - V_t}{X_s + R_a}, \quad \text{(C.20)}$$

where, Vt =source voltage, Ef =excitation voltage, Xs=synchronous reactance, and Ra =armature resistance.

Project Publications

[1] G. K. Stefopoulos and A. P. Meliopoulos, "Induction motor load dynamics: Impact on voltage recovery phenomena," presented at the *2005-2006 IEEE PES T&D Conference and Exposition*, Dallas, TX, May 21-26, 2006.

[2] P. Meliopoulos, G. J. Cokkinides, and G. K. Stefopoulos, "Voltage stability and voltage recovery: Effects of electric load dynamics," presented at the *2006 IEEE International Symposium on Circuits and Systems*, Island of Kos, Greece, May 21-24, 2006.

[3] A. P. Meliopoulos, G. J. Cokkinides, and G. K. Stefopoulos, "Voltage stability and voltage recovery: load dynamics and dynamic VAr sources," presented at the *2006 IEEE PES General Meeting*, Montréal, Quebec, Canada, June 18-29, 2006.

[4] G. K. Stefopoulos and A. P. Meliopoulos, "Quadratized Three-Phase Induction Motor Model for Steady-State and Dynamic Analysis," in *Proc. of the 38th North America Power Symposium*, Carbondale, IL, USA, Sept. 17-19, 2006, pp. 79-89.

[5] A. P. Meliopoulos, G. J. Cokkinides, and G. K. Stefopoulos, "Voltage Stability and Voltage Recovery: Load Dynamics and Dynamic VAR Sources," *Proceedings of the 2006 IEEE PES Power Systems Conference and Exposition (PSCE 2006)*, Atlanta, GA, USA, Oct. 29-Nov. 1, 2006, pp. 124-131.

[6] G. K. Stefopoulos and A. P. Meliopoulos, "Numerical Parameter Estimation Procedure for Three Phase Induction Motor Models," *Proceedings of the 2007 PowerTech Conference*, Lausanne, Switzerland, July 1-5, 2007.

[7] G. K. Stefopoulos, A. P. Meliopoulos, and G. J. Cokkinides, "Voltage-Load Dynamics: Modeling and Control," in Proceedings of the 2007 iREP Symposium on Bulk Power System Dynamics and Control – VII (iREP 2007), Charleston, SC, USA, Aug. 19-24, 2007.